Department of Civil Engineering
Faculty of Science and Engineering

Anisotropic Characterisation of Reinforced Sand

Alaa H. J. Al-Rkaby

This thesis is presented for the degree of
Doctor of Philosophy
of
Curtin University

February 2018

Declaration

To the best of my knowledge and belief this thesis contains no previously published by any other person except where due acknowledgement has been made.

This thesis contains no material which has been accepted for the award of any other degree or diploma in any university.

Signature: 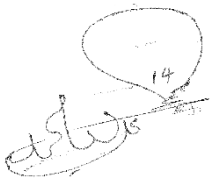

Date : 6 / 2 / 2018

Abstract

Anisotropic three-dimensional stress state, unequal principal stresses, are induced within the soil elements of most geostructures. This complex state includes different directions of principal stress α, different values of the intermediate principal stress parameter b and/or cyclic rotation of the principal stress direction. Soil reinforcement, which is commonly used worldwide, can be implemented in many structures. Therefore, investigating the anisotropic characterisation of reinforced sand is important so that solid designs and analyses of reinforced geostructures can be achieved.

A large-scale hollow cylinder torsional shear apparatus HCA was used in this research to investigate sand that was reinforced with planar reinforcements (geogrid and geotextile) and with a three-dimensional reinforcement (geocell). Furthermore, the effect of adding clay to sand on the anisotropic characteristics of unreinforced and reinforced samples was investigated. Three main types of stress path were performed on reinforced sand and mixed sand-clay: monotonic shearing with different directions of principal stress, monotonic shearing with different intermediate principal stress parameters, and cyclic rotation of the principal stress direction.

Sand reinforced with geogrid and geotextile planar reinforcements demonstrated significantly improved performance (compared with unreinforced sand) when α = 0–30°; and this improvement increased considerably as the number of reinforcement layers increased up to six layers. The rate of improvement increased more slowly with further layers. However, for α = 60–90°, the performance of planar reinforcements was much lower and, thus, the differences in the peak deviator stress due to anisotropy were 50.4 and 47.7% for six-layer geogrid- and six-layer geotextile-reinforced sand, respectively. Geocell reinforcement provided the greatest improvement, and the improvement was significant even at α = 60–90°, although the difference in peak deviator stress remained clear at 25.3%. Adding clay improved the performance of reinforced sand: the differences in the peak deviator stress decreased to 29.4–37.3% for six layers of planar reinforcement and to 16.4% for geocell reinforcement. This is attributed to the fact that clay provides bonding and cushioning effects, which limit poor interlocking in any plane.

Increasing b decreased peak deviator stress at all values of α, and this decrease was lower for reinforced mixed sand-clay than reinforced clean sand. The combination of largest value of b (1.0) and the range of α = 60–90° caused the lowest deviator stress in reinforced samples. Furthermore, when b = 1.0, the minimum deviator stress occurred at α = 90° instead of α = 60°, which occurred when b = 0.2.

This low performance of reinforcement layers is linked to the fact that the conditions of α = 60–90° and b = 1.0 are characterised by increasing stresses that are applied horizontally. For α = 60–90°, the principal stress tends to rotate close to the horizontal direction where the layers of planar reinforcement are embedded. Moreover, samples under such conditions enter an extension mode where horizontal stresses, circumferential σ_θ and radial σ_r stresses, become larger than axial stress σ_z, resulting in less sand-reinforcement interaction and, thus, the tensile strength of the reinforcement cannot be mobilised sufficiently. A similar mechanism, of increasing horizontal stress at the expense of vertical stress, occurred when b increased to 1.0. However, three-dimensional geocell reinforcement provides all-around confinement by its connected walls, which reduces the effect of increasing horizontal stresses.

Rotation of the principal stress direction caused failure of sand and mixed sand samples due to inducing dramatic axial, radial, circumferential and shear strains during the first cycle at α = 50°, despite the fact that the magnitude of deviator stress was kept constant at 110 kPa. However, reinforced samples sustained this continuous rotation of principal stress even though significant strains were induced. The least amounts of these strains were observed for samples reinforced with geocell, in which the volumetric strain was half that of geogrid. Significant amounts of these strains, particularly at the first few cycles, were plastic strains, although the applied stresses returned, at the end of each single cycle, to their initial state (before rotation). In general, with increasing cycles of rotation, strains became more stable. All of the induced strains changed in oscillation mode, indicating variation in the performance of the reinforcements that can be attributed to variation in the applied stresses during rotation, where the test mode was subsequently changed from extension to compression.

During the continuous rotation of principal stress, some densification and sand-reinforcement interaction occurred, resulting in increased shear modulus. However, such densification caused less dissipation of energy and, consequently, decreased the damping ratio.

Furthermore, monotonic and cyclic loading tests conducted on cemented sand prepared with an anisotropic bed inclined at α to the horizontal revealed that adding cement significantly decreased the directional dependency of bearing pressure and settlement.

The results of this thesis are imperative for improving the performance of reinforced soil and related structures, efficiently designing geostructures, decreasing deformation, reducing costs and decreasing the frequency of required maintenance.

Publications

The following publication have resulted from this research.

1. Al-Rkaby, A. H., Chegenizadeh, A., & Nikraz, H. R. (2016). Directional-dependence in the mechanical characteristics of sand: a review. *International Journal of Geotechnical Engineering*, *10*(5), 499-509.

2. Al-Rkaby, A. H., Chegenizadeh, A., & Nikraz, H. R. (2017). Anisotropic strength of large scale geogrid-reinforced sand: Experimental study. *Soils and Foundations*, *57*(4), 557-574.

3. Al-Rkaby, A. H., Chegenizadeh, A., & Nikraz, H. R. (2017). Cyclic behavior of reinforced sand under principal stress rotation. *Journal of Rock Mechanics and Geotechnical Engineering*, *9*(4), 585-598.

4. Al-Rkaby, A. H., Nikraz, H. R., & Chegenizadeh, A. (2017). Stress and Deformation Characteristics of Nonwoven Geotextile Reinforced Sand under Different Directions of Principal Stress. *International Journal of Geosynthetics and Ground Engineering*, *3*(4), 34.

5. Al-Rkaby, A. H., Nikraz, H. R., & Chegenizadeh, A. (2017). Effect of anisotropy on the bearing capacity and deformation of sand. *Australian Geomechanics Journal*, *52*(3), 53-63.

6. Al-Rkaby, A. H., Chegenizadeh, A., & Nikraz, H. R. (2017). An experimental study on the cyclic settlement of sand and cemented sand under different inclinations of the bedding angle and loading amplitudes. *European Journal of Environmental and Civil Engineering*, 1-16.

7. Al-Rkaby, A. H., Chegenizadeh, A., & Nikraz, H. R. (2017). Anisotropic Shear Strength of Sand Containing Plastic Fine Materials. *World Academy of Science, Engineering and Technology, International Journal of Geotechnical and geological Engineering*, *11*(3), 210-213.

8. Al-Rkaby, A. H., Chegenizadeh, A., & Nikraz, H. R. (2017). Anisotropic Shear Strength of Sand Containing Plastic Fine Materials. *Proceedings of the19th International Conference on Ground Improvement Methods for Stabilization of Different Soils (ICGIMSDS 2017)* (pp. 112-115). Rome, Italy.

9. Al-Rkaby, A. H., Chegenizadeh, A., & Nikraz, H. R. (2017). Effect of clay content on the response of reinforced sand to anisotropic conditions. *Proceedings of the 3rd International Conference on Ground Improvement and Ground Control (ICGI2017)* (pp. 278-288). Hangzhou, China.

10. Al-Rkaby, A. H., Chegenizadeh, A., & Nikraz, H. R. (2017). Directional Dependence in the Strength and Deformation of Sand Containing Clay. *Proceedings of One Curtin International Postgraduate Conference(OCPC)* (pp. 31-35). Sarawak, Malaysia.

11. Al-Rkaby, A. H., Chegenizadeh, A., & Nikraz, H. R. (2018). Directional Dependence of the Stress-Strain Behavior of Reinforced Sand. The International Conference on Geogrids, Geotechnical Engineering and Test Methods (ICGGETM), Jun 3–4 2018, New York, USA. (Accepted)

Acknowledgements

O Allah, send blessings upon Muhammad and the Household of Muhammad. Praise be to Allah Almighty, prophet Mohammed and his holy family “Ahlul Bayt”. This research has been completed under their benediction.

I am deeply indebted to my supervisor, Prof. H. Nikraz, for his continuous and consistent advice, support, guidance, assistance and regular meetings throughout my research. I am also thankful to my co-supervisor, Dr. A. Chegenizadeh, for his efforts, support and valuable advice. In particular, I would like to extend my gratitude to the chairperson of the thesis committee, associate Professor Prabir Sarker.

I would like to convey my gratitude to the Department of Civil Engineering at Curtin University for providing a pleasant research environment, with specific thanks to Dr. Andrew Whyte, Sucy Leong, Frankie Sia and Cheryl Cheng. I sincerely thank the staff of the Geomechanics Laboratory: Mark Whittaker, Darren Isaac and Mirzet Sehic, whose participation in carrying out experiments and providing technical support was greatly appreciated. I would like to thank Kirsty Balog for performing the long task of reading through my manuscript and making this thesis more readable in a very short time.

I would like to express my deepest love to my parents, brothers and sisters, and the rest of the family, for their sincere prayers, which have kept me on the path to success. I record my sincere and affectionate gratitude to my grandma, who passed away very peacefully in my absence.

Sincere thanks and great appreciation to my beloved wife and sons for their support during my study. In closing, thesis is dedicated to prophet “Mohammed” and his holy family “Ahlul Bayt”.

Table of Contents

List of Figures

List of Tables

List of Notations and Abbreviations

Symbol	Unit	Description
α	°	The angle between the major principal stress or load and the symmetry axis, i.e., the normal axis on the bedding plane.
b	dimensionless	Intermediate principal stress parameter
D_r	%	Relative density
e	dimensionless	Void ratio
D_o	mm	Outer diameter of hollow cylinder specimen
D_i	mm	Inner diameter of hollow cylinder specimen
H	mm	Soil specimen height
p'	kPa	Mean effective stress
σ_1	kPa	Major principal stress
σ_2	kPa	Intermediate principal stress
σ_3	kPa	Minor principal stress
$\emptyset$	°	Friction angle
q	kPa	Deviator stress
q_p	kPa	Peak deviator stress
α_c	°	Direction of principal stress during consolidation
ε_z	%	Axial strain
ε_r	%	Radial strain
ε_θ	%	Circumferential strain
$\gamma_{z\theta}$	%	Shear strain
ε_1	%	Major principal strain
ε_2	%	Intermediate principal strain
ε_3	%	Minor principal strain
ε_q	%	Deviator strain
ε_v	%	Volumetric strain

C	kPa	Cohesion of soil
u	mm	Depth of the reinforcement below the applied load
$B_{footing}$	mm	Footing width
B_{cell}	mm	Width of the geocell layer
$q_{unconfined}$	kPa	Unconfined compressive strength
q_f	kPa	Deviator stress at failure
F	%	Fine content
γ_d	kN/m^3	Dry unit weight of soil
C_u	dimensionless	Coefficient of uniformity
C_c	dimensionless	Coefficient of curvature
D_{30}, D_{60}	mm	The sizes such that 30% and 60% of the particles are smaller than those sizes, respectively
D_{50}	mm	Medium particle size
G_s	dimensionless	Specific gravity
e_{max}	dimensionless	Maximum void ratio
e_{min}	dimensionless	Minimum void ratio
T	kN/m	Tensile force of geosynthetics
W	kN	Axial load
M_T	kN.m	Torque
p_i	kPa	Inner pressure
p_o	kPa	Outer pressure
Δv	mm^3	Change of the cell volume
v	mm^3	Sample volume
d_{ri}	mm	Inner radial deformation
d_{ro}	mm	Outer radial deformation
r_o	mm	Outer radius of hollow cylinder specimen
r_i	mm	Inner radius of hollow cylinder specimen
ω	dimensionless	Angular deformaion
OPC		Ordinary Portland cement

q_s	kPa	Static pressure in the loading tests
q_c	kPa	Cyclic pressure in the loading tests
θ	°	Inclination of the mobilized plane with the major principal stress
q/p'	dimensionless	Stress ratio
σ_z	kPa	Axial stress
σ_θ	kPa	Circumferential stress
σ_r	kPa	Radial stress
$\tau_{z\theta}$	kPa	Shear stress
N_c	dimensionless	Number of rotation cycles in the rotational shear tests
N	dimensionless	Number of cycles in the loading tests
$(I.R)_{\varepsilon v}$	%	Decrease in the variation of ε_v with α by inclusion of reinforcement
G	MPa	Shear modulus
G_1, G_n	MPa	Shear modulus obtained from the first cycle and the subsequent cycles respectively.
G_n/G_1	dimensionless	Normalized shear modulus
λ	%	Damping ratio
ΔW	mm	The energy dissipated in one cycle
W	mm	The largest strain energy stored during one cycle
q_b	kPa	Bearing pressure of sand or cemented sand
$(q_b)_u$	kPa	Ultimate bearing capacity
S/B	dimensionless	Settlement ratio, settlement/ footing width

Abbreviation	**Description**
PP	Polypropylene
PET	Polyester
PA	Polyamide
PE	Polyethylene

HDPE	High density polyethylene
LDPE	Low density polyethylene
VLDPE	Very low density polyethylene
PVC	Polyvinyl chloride
CPE	Chlorinated polyethylene
CSPE	Chlorosul phonated polyethylene
PCP	Pressure control panel
LVDTs	Linear variable differential transformer
PVCs	Pressure /volume controllers
HPS	Hydraulic power system
SEM	Scanning electron microscope image
EDS	Energy Dispersive Spectroscopy

Chapter 1
Introduction

1.1 Background

Anisotropy refers to directional dependence in the mechanical characteristics of geomaterials. According to many researchers, it is one of the most important parameters, if not *the* most important, that influences soil behaviour (P. Guo & Stolle, 2005; X. Li & Dafalias, 2002, 2004; Matsuoka, 1974; Matsuoka & Geka, 1983; Nemat-Nasser, 1980, 2000; Oda, 1972a, 1993; Radjai & Azéma, 2009; Rothenburg & Bathurst, 1989; Wrzesiński & Lechowicz, 2013).

In most geotechnical structures, soil elements are subjected to complex anisotropic conditions with different directions of principal stress α, unequal principal stresses $\sigma_1 \neq \sigma_2 \neq \sigma_3$ and cyclic rotation of the principal stress axes. Therefore, soil's response to loading will reflect its inherent anisotropic structure and, consequently, will depend on the orientation and continuous rotation of the principal stresses and the intermediate principal stress parameter imposed by many structures. Anisotropic soils are affected by the discrete nature of their particles and their spatial arrangement. Contact between particles tends to concentrate in the direction of an applied load, while their long axes tend to align horizontally, i.e., perpendicular to the major principal stress axis (X. Li & Yu, 2009; Parkin, Gerrard, & Willoughby, 1968; Seyedi Hosseininia, 2012a; L. Yang, Li, Yu, & Wanatowski, 2016). Consequently, most soils, even those comprised of spherical particles, exhibit significant changes in their behaviour when subjected to loads with different directions (Haruyama, 1981; Kallstenius & Bergau, 1961; L. Yang et al., 2016).

In many structures, the aforementioned anisotropic conditions are well recognised in situ. For example, loading on shallow foundations can induce principal stresses with different directions α depending on the distance from the footing centre, and different values of the intermediate principal stress parameter b , which describes the value of intermediate principal stress relative to the minor and major principal stresses (Equation 1.1), depending on the depth of the loading and the distance from the centre, as illustrated simply in Figure 1.1(Leroueil & Hight, 2003).

$$b = (\sigma_2 - \sigma_3) / (\sigma_1 - \sigma_3) \quad (1.1)$$

where σ_1, σ_2 and σ_3 are the major, intermediate and minor principal stresses. Similar variation can be observed in the embankments in Figure 1.2 (Xiong, Guo, Cai, & Yang, 2016), where the direction of principal stress within the soil varies from one point to another depending on the distance from the loading centre. In these two examples, static loading induces different fixed directions. Soil elements are under moving loads in Figure 1.3 (Lekarp & Dawson, 1998); however, they are subjected to gradual and cyclic rotation of the principal stress direction. This means that soil elements can be subjected to a given fixed inclined direction of principal stress under a monotonic load, or continuous cyclic rotation of the principal stress direction under a moving load. Consequently, anisotropic stress states have significant impacts on many structures.

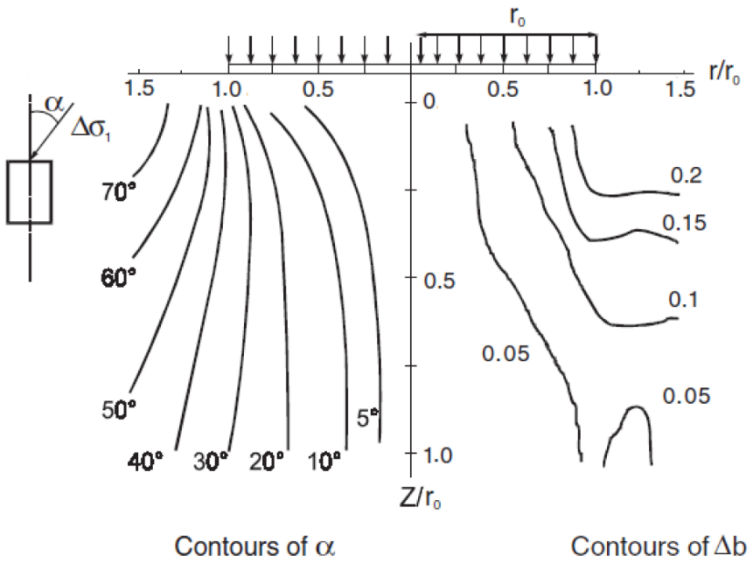

Figure 1.1 Description of stress state beneath footing (Leroueil & Hight, 2003)

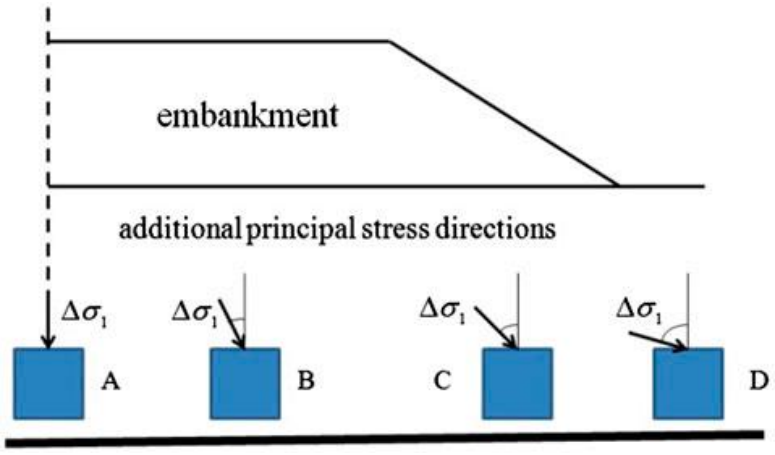

Figure 1.2 Variation of principal stress direction beneath the embankment (Xiong et al., 2016)

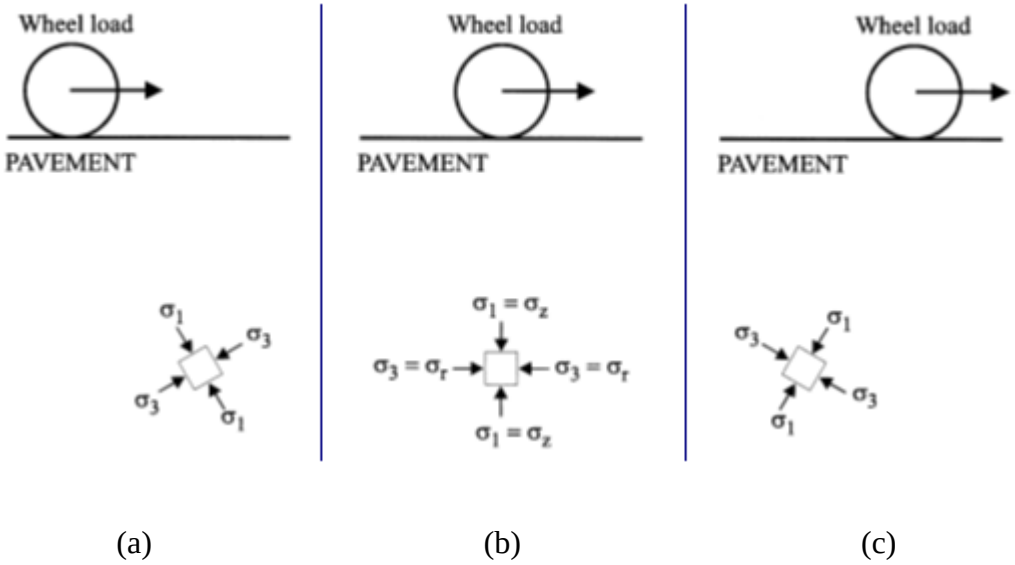

Figure 1.3 Stress states of soil element (a) before it was subjected directly to moving wheel load, (b) located along the wheel load center, and (c) after it was subjected directly to moving wheel load (Lekarp & Dawson, 1998)

Many of these structures may be implemented using soil reinforcing, which has become a viable geotechnical engineering technique for improving soil strength and deformation properties in many geostructures, such as foundations, railways, pavements, airfields and embankments. A wide range of materials, such as cement and geosynthetics, have been used for reinforcing soil. Reinforcement with artificial cement is still an important technique in many geotechnical applications. Furthermore,

many cities in the world lie on geological deposits that exhibit crossbedding with different levels of cementation (e.g. Bassendean and Safety Bay sands in Perth, Australia). However, there are few studies on the effects of anisotropic conditions on cemented sand (e.g. Eghbali & Fakharian, 2014; Gao & Zhao, 2012; Salehzadeh, Hassanlourad, Procter, & Merrifield, 2008).

The last few decades have seen tremendous growth in the use of polymeric materials called *geosynthetics*, such as geogrids, geotextiles and geocells, as alternatives to conventional engineering methods. Several factors have made the use of geosynthetics attractive in foundation engineering, such as their cost and time savings, storability, ease of handling and installation, reliability, simplicity, and adaptability to different site conditions. The concept of reinforcing soil with natural fibres or reed mats is many thousands of years old. It was first used in the Ziggurat of Ur, which was built by ancient Sumerians 3000 years ago in Mesopotamia. It was also used in the Great Wall of China. However, the use of metallic and polymeric materials is more recent, and was conceived by Vidal in the 1960s. Extensive studies have investigated the behaviour of reinforced soil, and the majority of these studies suggest that reinforced soil outperforms unreinforced soil in terms of increased strength, as well as decreased settlement and lateral deformation (Bathurst & Karpurapu, 1993; Das & Omar, 1994; Haeri, Noorzad, & Oskoorouchi, 2000; Latha & Murthy, 2006; Nguyen, Yang, Lee, Wu, & Tsai, 2013; Shukla & Yin, 2006 among others). Other studies have investigated the effect of adding sand-clay mixtures on soil interfacial and bonding properties (Abdi, Sadrnejad, & Arjomand, 2009; Naeini & Gholampoor, 2014; Naeini, Khalaj, & Izadi, 2013). Although great research efforts have been made into soil reinforcement, a review of the literature reveals that the effects of anisotropy in reinforced soil have not yet been addressed.

In conclusion, anisotropic effects may contribute to the overestimation of strength, unsafe design, deterioration, short lifespan and high maintenance costs of structures. Awareness of these issues has prompted many studies over recent decades. However, to date, no comprehensive study has investigated the performance of reinforced soils under such anisotropic conditions. A knowledge gap exists regarding the influences of principal stress direction, intermediate principal stress parameters and cyclic rotation of principal stress direction on the characteristics of reinforced sand.

1.2 Research Objectives

In summary of what has been described thus far, ***i)*** the profound effects of anisotropy on soil behaviour have long been recognised in clay and clean-sand soils and ***ii)*** reinforcement is widely used in many geotechnical applications. However, the effects of anisotropic conditions on the characterisation of reinforced sand are not yet fully understood, despite being equally important.

Prompted by this lack of studies, this thesis contributes original research that aims to establish a clear picture of the effect of anisotropic conditions on the characterisation of reinforced sand. Principally, a sophisticated, advanced, large-scale, hollow cylinder apparatus (HCA) is employed. To accomplish this main aim, the following specific objectives were addressed:

1. Investigation of the effect of different directions of principal stress α and intermediate principal stress parameter b on the characterisation of sand and sand reinforced with geosynthetics (geogrids, geotextiles and geocells), through a monotonic torsional shear experimental program.

2. Investigation of the effect of different directions of principal stress α on the characterisation of sand with different contents of plastic fines (kaolinite), through a monotonic torsional shear experimental program.

3. Investigation of the effect of different directions of principal stress α and the intermediate principal stress parameter b on the characterisation of a selected sand-clay mixture reinforced with geosynthetics (geogrids, geotextiles and geocells), through a monotonic torsional shear experimental program.

4. Investigation of the effect of cyclic continuous rotation of the principal stress direction on the characterisation of sand reinforced with geosynthetics (geogrids, geotextiles and geocells), through a cyclic rotational experimental program.

5. Investigation of the effect of cyclic continuous rotation of principal stress direction on the characterisation of a selected sand-clay mixture reinforced with geosynthetics (geogrids, geotextiles and geocells), through a cyclic rotational experimental program.

6. Investigation of the bearing pressure and deformation characteristics of sand reinforced with cement, using a lab model with static and cyclic loading tests.

1.3 Significance

The present study provides significant knowledge regarding the characterisation of reinforced soil under anisotropic conditions. It will use an advanced HCA in experiments that replicate field stress states. This knowledge has important applications in a wide range of structures involving various directions of principal stress, different intermediate principal stress parameters and cyclic rotation of principal stress (e.g. foundations, embankments, airfields, roads and railways), as explained previously in Figures 1.1-1.3.

The findings of this study may improve the performance of roads and railways, which are crucial in all countries for the transport of commodities, freight and passengers. Each year, many new highways and railways are built, and the maintenance of old ones can cost hundreds of millions of dollars. Moreover, such maintenance operations also cause disruptions to highways and railways, resulting in transport delays. Therefore, investigation of the characterisation of reinforced sand subjected to anisotropic conditions is imperative for improving the performance of reinforced soil and related structures, efficiently designing geostructures, decreasing deformation, reducing costs and decreasing the frequency of required maintenance.

Furthermore, the outcomes of this study, along with existing studies on unreinforced soils, can be used as a base for developing and crystallising some tools for modelling the anisotropic characterisation of reinforced soils. In conclusion, introducing the parameters of α, b and cyclic rotation of α into geotechnical engineering models of the performance of reinforced soils is a crucial step toward improving design guidelines and guaranteeing the safe design of geostructures.

1.4 Thesis Outline

This thesis has been organised into the following nine chapters:

Chapter 1 gives an introduction to this study and defines its aims, objectives and significance.

Chapter 2 reviews the literature pertinent to this work. It begins with a summary of anisotropy and its effects on soil and geostructures. It then reviews studies that have investigated anisotropic effects using laboratory-based tilted-sample techniques in

conventional triaxial tests, direct shear tests and loading tests. Studies using HCA and those related to the effect of principal stress direction, intermediate principal stress parameters and the cyclic rotation of principal stress direction are also reviewed. Then, the use of geosynthetics in soil reinforcement, its pros and cons, raw materials, manufacturing types and functions are reviewed, as are existing studies on geogrids, geotextiles and geocells. This chapter also presents a general review of cement reinforcement and the effects of the addition of fine material (clay and silt) on the characterisation of sand and reinforced sand.

Chapter 3 describes the materials used in this research (sand, geogrid, geotextile, geocell, kaolinite and cement) and their physical characteristics. It also introduces a detailed description of the large-scale hollow cylinder apparatus system (HCA), the applied loads, torque and stresses used, test controls and sample preparation. Description of the small laboratory model of cemented sand is also presented in this chapter. Details of the testing program using HCA for monotonic torsional tests or cyclic rotational tests on sand and sand-clay mixtures reinforced with different geosynthetics, are presented. The loading tests performed on the cemented sand laboratory model are also described.

Chapter 4 presents and discusses the results of drained monotonic torsional tests performed on sand and sand reinforced with different numbers of planar geo-inclusion layers (geogrids and geotextiles) as well as three-dimensional geo-inclusions (geocells), considering different directions of principal stress α.

Chapter 5 focuses on the effect of different kaolinite contents on the characterisation of sand under different directions of principal stress α throughout a series of drained monotonic torsional tests. Results for a selected sand-clay mixture reinforced with geogrids, geotextiles and geocells, under different directions of principal stress α, are also described in this chapter.

Chapter 6 contains the combined effect of different values of the intermediate principal stress parameter b and principal stress direction α on the characterisation of a selected mixture of sand-clay reinforced with geocells or various numbers of geogrid and geotextile layers, throughout a series of drained monotonic torsional tests.

Chapter 7 investigates the effect of cyclic rotation of the principal stress direction on the characterisation of sand and sand reinforced with various layers of geogrid. The effect of the stress ratio on the characterisation of sand and geogrid-reinforced sand under cyclic rotation is also presented. This chapter also describes the effect of cyclic rotation on the characterisation of sand reinforced with the other geosynthetics: geotextiles and geocells. The investigation of cyclic rotation effects on a sand-clay mixture reinforced with three types of geo-inclusions are also discussed.

Chapter 8 presents the results of monotonic and cyclic loading tests performed on cemented sand in a bedding plane set at various inclines. The bearing pressure and cyclic settlement characteristics are also presented in this chapter.

Chapter 9 summarises the main outcomes of this thesis and proposes directions for future work.

Chapter 2

Background and Literature Review

2.1 Introduction

Conventionally, soil is assumed to have isotropic characteristics, although experiments demonstrate that it can also have anisotropic properties. This approach does not stem from a lack of awareness of the anisotropic nature of soil and its significant effect on soil strength and deformation. Rather, the isotropic assumption provides simplicity, while the anisotropic testing apparatus is complex, and most geotechnical laboratories have limited availability of such facilities. Moreover, fines content that is present in sand, or is added to improve its behaviour, can have significant effects and, thus, could also affect the anisotropic response of sand; although there are very few studies that consider this issue.

Reinforced soil is widely used in many geotechnical applications, such as footings, embankments and pavements, in which multiaxial loading and rotation in the principal stress direction are common features. As a consequence, the response of reinforced soil to such anisotropic stress states should be taken into account, particularly as anisotropy may be the reason for significant differences between the calculated and experimentally-modelled bearing capacities that are often observed (C. Huang & Tatsuoka, 1990). However, the effects of the principal stress direction, intermediate principal stress parameters, and the cyclic rotation of principal stress axes have yet to be investigated.

Based on the aforementioned issues, this chapter is heavily weighted towards the discussion of these issues and the factors that contribute to variations in soil behaviour. The chapter has been organised as follows. Section 2.2 will firstly delve into soil anisotropy, its dependence on load direction and some related situations in this field. This section focuses on the effect of anisotropy on soil behaviour, which is reflected by: **a)** the dependence on the fixed direction of loading, which has been determined through tests conducted on tilted samples and hollow cylinder samples; **b)** dependence on the continuous cyclic rotation of the principal stress direction; and **c)** dependence on the intermediate principal stress parameter. Then, Section 2.3 reviews the types,

benefits and functions of reinforcement, and focuses on relevant research into geogrids, geotextiles and geocells on the behaviour of soil. Further, reinforcement by artificial cement is also reviewed. Section 2.4 introduces the effect of addition of fines to sand behaviour under conventional conditions, and its mechanism of performance. The structure of this chapter is illustrated in Figure 2.1.

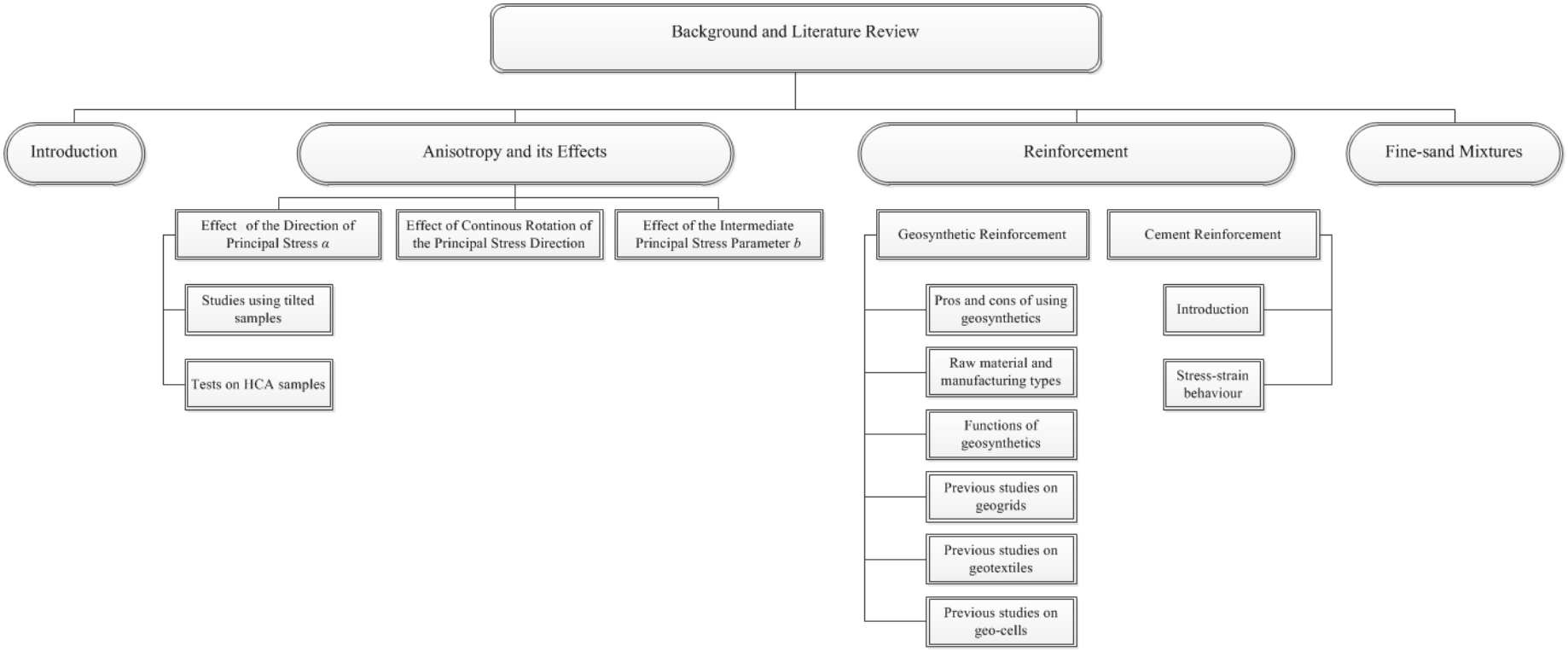

Figure 2.1 Structure of background and literature review

2.2 Anisotropy and its Effects

Anisotropy is a well-known feature of most natural materials and is considered one of the most important issues affecting soil behaviour. It refers to directionally-dependent variation in the behaviour, characteristics and responses of materials.

Interest in soil mechanics has shifted to the anisotropic behaviour of soils due to the fact that most geotechnical engineering applications induce complex stress states within soil that comprise various directions of principal stress α, various intermediate principal stress parameters b, and cyclic rotation of principal stress direction, as explained in Chapter One (Figures 1.1-1.3). These conditions result in significant differences in soil characteristics and can lead to significant uncertainties and problems in geotechnical constructions, if ignored. For example, the characteristics of shear strength along a rupture surface change from one position to another based on variation in the direction of the principal stress (Figure 1.1). Thus, it is inappropriate to generalise a particular shear strength across multiple positions because this can lead to over- or under-estimation of bearing capacity. This renders anisotropy an important feature to be considered in design, in order to avoid potential future problems.

Anisotropy is strongly linked to *soil fabric*, which is described as the spatial arrangement of soil particles, particle geometry (shape and size), alignment and voids (Al Hattamleh, Muhunthan, & Shalabi, 2009; Oda, 1972b; Zeghal & Tsigginos, 2015). The arrangement of contacts and the preferred alignment of particles—in which their longest sides tend to align horizontally—are the main contributors to inherent anisotropy. Moreover, the arrangement of soil particles changes continuously during shearing by sliding, moving, redistribution, breakage, and the creation and breaking of contacts, resulting in further induced anisotropy.

Fabric anisotropy was investigated systematically by numerous researchers, especially between the 1960s and 1980s, and attention was focused on the packing structure and orientation of cohesionless soil (Arthur & Assadi, 1977; Arthur & Menzies, 1972; Arthur & Phillips, 1975; Casagrande, 1944; Iwasaki & Tatsuoka, 1977; Oda, 1972a, 1972b; Oda, Koishikawa, & Higuchi, 1978; Parkin et al., 1968; Yamada & Ishihara, 1979, 1981).

Some attempts have been made to investigate the alignment of sand particles. For example, Oda (1972b) and Oda et al. (1978) investigated several types of sand and found that soils composed of elongated particles showed clear preferred alignment, while there was less or no preferred alignment for soils composed mainly of spherical particles. Moreover, Z. Yang, Li, and Yang (2008) investigated the alignment of particles by impregnating epoxy through samples that were prepared in two ways—dry deposition and moist tamping—and then cut slides to take scanning electron microscopy (SEM) images. They found that the former method gives a higher preferred alignment than the latter for vertical sections, while horizontal sections did not show a clear preferred alignment for either method.

Although this indicates that the alignment of particles in a preferred stable position contributes in the anisotropy of materials, many studies have reported a certain level of anisotropy for soils that have less-preferred alignment, such as those composed of spherical particles. This is related to the complex fabric of soil and the changes that occur during shearing which induce further anisotropy where contacts intensify along the load direction. X. Li and Yu (2009) reported that the contact normal has more effects on anisotropy than particle shape, and that the principal direction of normal anisotropy is aligned with the direction of load. For example, Kallstenius and Bergau (1961) and Haruyama (1981) reported variation in the contacts of glass balls between the horizontal and vertical planes, which resulted in a clear anisotropic stress ratio during shearing with different directions of radial shear stress. More recently, the difference in stress ratio due to anisotropy of glass beds was reported to be 34% by Y. Yang, Fei, Yu, Ooi, and Rotter (2015) and 17% by L. Yang et al. (2016). The difference can be attributed to many reasons, including the material type, relative density, test conditions, etc. The point is that even spherical particles can produce an anisotropic response.

As mentioned before, the role of the soil fabric in anisotropic response is not limited to the initial fabric but also includes the changes that occur during shearing, i.e., rearrangement. Oda, Kazama, and Konishi (1998) and Seyedi Hosseininia (2012b) reported that once shearing commences, granular particles tend to stacked to form microstructural columns that support the applied load. These microstructures intensify

in the direction of loading, resulting in more contacts compared with other directions (Fonseca, O'Sullivan, Coop, & Lee, 2013; Seyedi Hosseininia, 2012b, 2013). As the long dimension of the particles align horizontally, microstructures are generated under vertical load with great width and, consequently, exhibit greater stability compared with structures created under horizontal loading, whose width and stability are low.

The investigation of anisotropy requires complex and advanced apparatuses that are not generally available in most labs, which makes researchers reluctant to investigate the effect of anisotropy on soil (P. Guo, 2008). This consistent with Miura, Miura, and Toki (1986), who stated that the lack of available apparatus resulted in studies being restricted to investigating very limited paths of stress.

As anisotropy involves changes in behaviour according to the direction of applied loads, its effect can consequently be reflected by:

a) The effect of the principal stress direction α, (Section 2.2.1)
b) The effect of the cyclic rotation of principal stress axes, (Section 2.2.2), and
c) The effect of the intermediate principal stress parameter b, (Section 2.2.3).

These sections review the existing literature on the effect of anisotropy on stress-strain characteristics. We give greater focus to drained conditions in our work, as the research of this thesis was performed under such conditions.

2.2.1 Effect of the Direction of Principal Stress α

Most studies that have investigated the effect of load direction on the anisotropic characterisation of soil have been conducted, in general, by:

i. Preparing samples in bedding planes with different angles α and testing these tilted samples using conventional triaxial, direct shear or loading tests. This method produces samples with various orientations of bedding plane.
ii. Preparing samples the normal way, i.e. in a horizontal bedding plane, and subjecting these samples to inclined principal stresses. Conditions of inclined principal stress can be conducted using a true triaxial apparatus and/or a hollow cylinderical triaxial apparatus (HCA).

In this review, we have unified the inclination angle α (Figure 2.2) for all studies, because some researchers defined α as the angle between the bedding plane and the loading direction, while others consider it as the angle between the loading direction and vertical. In this thesis, α is expressed as the angle between the major principal stress or load and the symmetry axis, i.e., the normal axis on the bedding plane.

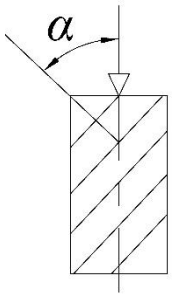

Figure 2.2a Definition of the angle α in tilted samples

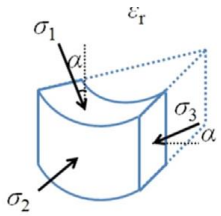

Figure 2.2b Definition of the angle of the principal stress direction α in HCA

2.2.1.1 Studies using tilted samples

Tilted samples have been used as a technique to overcome the lack of apparatus with which to study the anisotropic characteristics of soil. With this technique, different angles between the inclined bedding plane and the applied vertical load can be produced. Usually, these samples are tested using conventional triaxial, direct shear, or loading tests.

In 1972, Arthur and Menzies prepared cubical tilted samples of sand (porosity of 34%) with α = 0°, 50°, 60°, 70° and 90°, and reported σ_1 / σ_3 of 4.34, 4.3, 4.1, 4.0 and 3.9, respectively. At same time, Oda (1972b) made a great effort to investigate the anisotropic stress-strain characteristics of elongated and spherical sand particles. It was found that elongated sand particles exhibited significant decreases in deviator stress from a maximum value of 340 kPa achieved at α = 0° to 322, 295 and 280 kPa at α = 30°, 60° and 90°, respectively. Spherical sand particles also exhibited a certain level of directional dependence, where the σ_1 / σ_3 decreased from 340 kPa at α = 0°, to 322, 295 and 280 kPa at α = 30°, 60° and 90°, respectively. Anisotropic response was not limited to the strength, but also to the deformation characteristics. Both spherical

and elongated sand particles showed anisotropic deformation, where the axial strain at the peaks increased by almost two times as α changed from 0° to 90°, this was associated with a significant decrease in the expansion of volumetric strain.

Studies using triaxial tests (Arthur & Menzies, 1972; Arthur & Phillips, 1975; Oda, 1972b; Oda et al., 1978) showed that the minimum stress ratio occurred at α = 90°. However, Oda et al. (1978) found that plane strain tests produced minimum stress ratios in the range of α = 60–75°. Furthermore, most studies showed a clear decrease in dilation strain with increasing α.

The use of a conventional triaxial apparatus for testing samples fabricated with various bedding plane inclination angles may cause distortion in the samples if the preferential deformation direction is coincident with the tilted bedding plane (P. Guo, 2008). However, this technique has still been used until recently. For example, Azami, Pietruszczak, and Guo (2010) investigated the anisotropic behaviour of crushed limestone (0.15–2.0 mm particle size) prepared with horizontal and vertical bedding angles of α = 0° and 90°, and tested with a triaxial apparatus. They found clear directional dependence of deviator stress, as shown in Figure 2.3.

Direct shear tests have also been employed to investigate the anisotropic behaviour of soil by preparing samples on bedding planes with different inclinations, although such tests have less uniform stresses and less homogenous deformation than triaxial tests (P. Guo, 2008; Tong, Fu, Zhou, & Dafalias, 2014). Mahmood and Mitchell (1974) investigated the anisotropic behaviour of a silty-fine sand consisting of crushed basalt, and reported that there was clear anisotropic strength. They mentioned that soil under tamping or vibration compaction has no preferred alignment, i.e., where particles arrange themselves in a way that resists the compaction force. However, many other studies have reported significant anisotropic characteristics for samples subject to tamping or compaction.

Recently, a modified direct shear mould (60 × 60 × 45 mm) that can be opened from the side was used by P. Guo (2008) to test different soils with various inclinations of bedding plane. For dense crushed limestone and Ottawa sand, the maximum friction angle occurred when the bedding plane was vertical to the shearing direction, and the

minimum occurred when the bedding plane was inclined at 60–75° from vertical. The differences between the friction angles obtained at α = 0° and those obtained at α = 60 were 12° and 4° for crushed limestone and Ottawa sand, respectively. A similar trend was observed by Azami et al. (2010), who found that shear stress of crushed limestone under normal stress of 50 kPa varied from the largest value of 83 kPa to the smallest one of 54 kPa as α increased from 0° to 60° (Figure 2.4). This decrease was associated with a decreasing friction angle from 55.6° at α = 0° to 43.64° at α = 60° and 46.2° at α = 90° (Figure 2.5). Although the cohesion was slight, it exhibited a steady decrease from 4.4 kPa at α = 0° to 2.5 kPa at α = 90°. In contrast to previous studies such as Oda (1972b), a slight anisotropic effect on glass beads was observed by P. Guo (2008), where only a 1° difference between the maximum and minimum friction angles was reported.

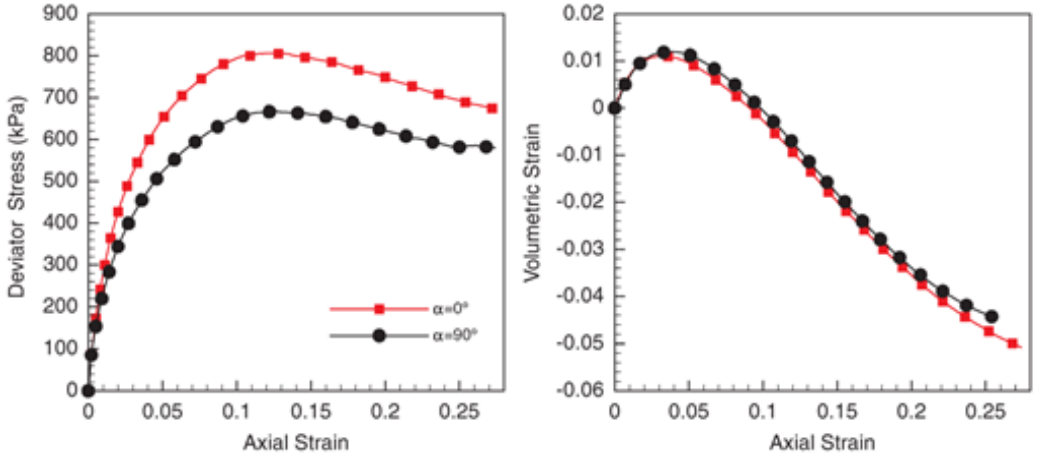

(a) (b)

Figure 2.3 Variation of (a) deviator stress with axial strain and (b) volumetric strain with axial strain for vertical and horizontal bedding plane directions (Azami et al., 2010)

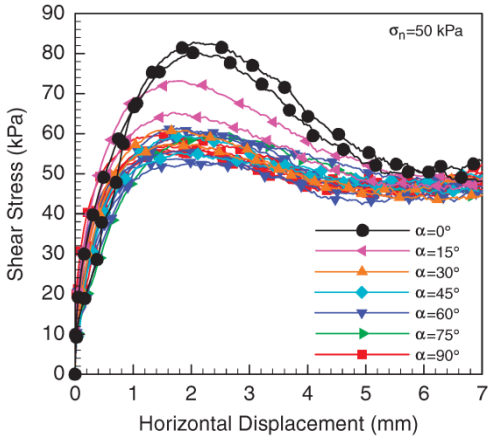

Figure 2.4 Shear stress-horizontal displacement relation for limestone under different bedding plane angles (Azami et al., 2010)

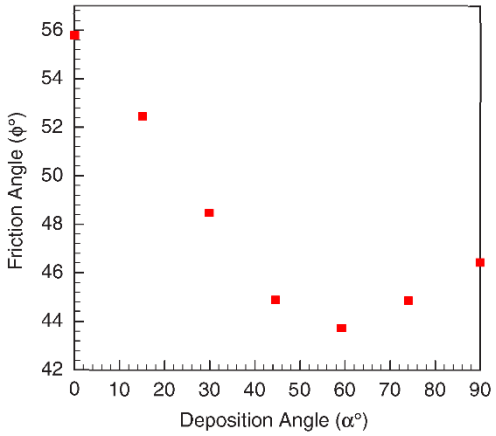

Figure 2.5 Variation of angle of internal friction with α (Azami et al., 2010)

The symmetrical assumption of the relationship between shear strength and shear plane inclination angle in P. Guo (2008)'s work was the reason to consider only half of the full domain of the bedding plane angle α. Therefore, this point was addressed by Tong et al. (2014). Figure 2.6 illustrates the results for three soils: Fujian sand, featuring rounded and moderately-elongated particles (D_r = 49%); mica sand, composed of flaky particles (D_r = 62%); and glass beads (D_r = 65%). When samples were subjected to shearing from right to left (case 1), the peak friction angle for all types of soils decreased steadily from a maximum value at α = 0° until α = 60–75°, then increased slightly. Some difference were observed under the opposite direction of load, from left to right (case 2), where α increased from 0° to 15–30°, resulting in an initial increase in the friction angle of Fujian and mica sand, before decreases with further increases in α. In contrast to P. Guo (2008), the anisotropic friction angle of glass beads was clear, and this may be attributed, as mentioned previously, to the effect of contact normal and also to the fact that the shape of the particles were not absolutely spherical.

Moreover, it was observed that the residual shear strength obtained by Tong et al. (2014) was not affected by bedding angle inclination. This supports the anisotropic critical state theory (ACST) presented by X. Li and Dafalias (2011) and Fu and Dafalias (2011), in which soil fabric changes, rearranges and reaches a critical state

where soil characterisations become unaffected by the initial fabric of the soil. Despite the strengths of the study by Tong et al. (2014), the small sample size used is a major concern.

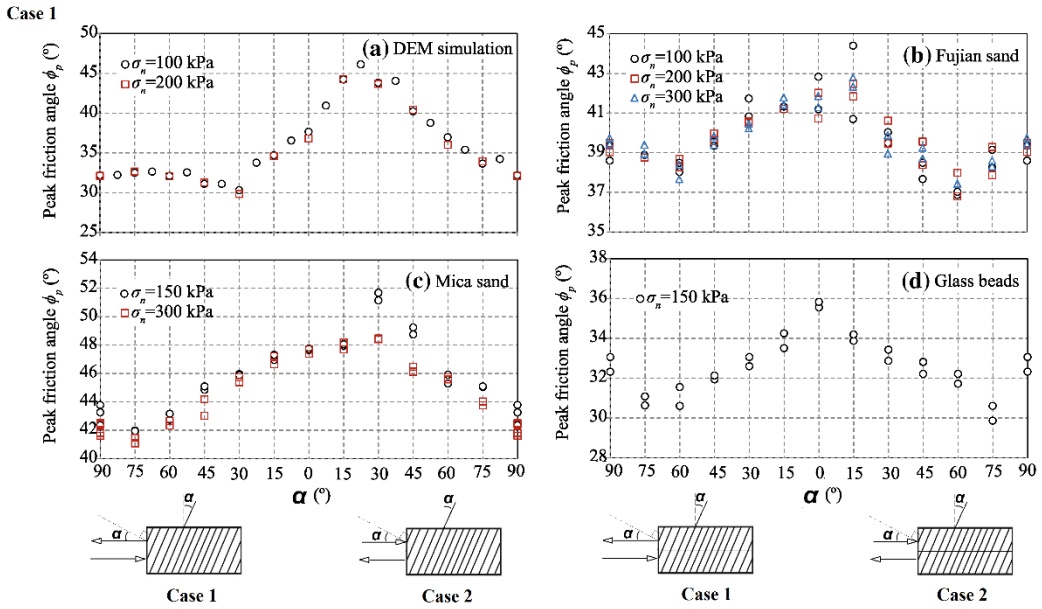

Figure 2.6 The relationship between the bedding plane inclination angle and the peak friction angle for (a) DEM simulation, (b) Fujian sand, (c) mica sand, and (d) glass sand (Tong et al., 2014)

Neglecting anisotropic effects could lead to underestimation of bearing capacity by approximately 50% when an inclined load is applied on a footing resting over such material (Siddiquee et al., 2001). Therefore, in addition to the triaxial and direct shear tests, some studies have been conducted on small-scale laboratory footing models to investigate directional dependence on the bearing capacity of anisotropic materials. Oda and Koishikawa (1979) used a mould of 300 × 70 × 200 mm to prepare samples of dense sand (D_r = 90%) with various bedding plane inclinations. Load was applied on a footing of 30 mm width placed on the foundation soil. Clear directional dependence was observed, with ultimate bearing pressures of 284, 240 and 186 kPa for α = 0, 45 and 90°. However, the difference in the residual strength was slight due to the anisotropic critical state.

Similar effects were also recently presented by Azami et al. (2010), Kawamura, Miura, and Yokohama (2010), and Kawamura and Miura (2014). For example, Figure 2.7

shows the variation in bearing pressure of crushed limestone samples (e = 0.6) for different inclination angles, where the differences in strength due to inherent anisotropy were 23.4% (Azami et al., 2010). Deformation was also influenced by a fabric tilted bedding plane, where the formation of the wedge is nearly symmetrical for α = 0° but is rotated when α = 55° (Kawamura & Miura, 2014; Kawamura et al., 2010).

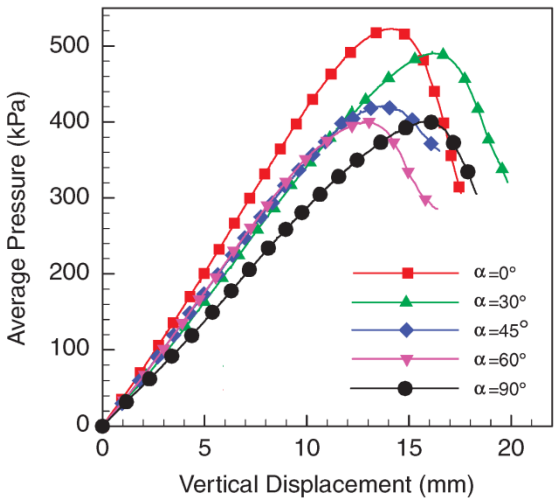

Figure 2.7 Load-axial displacement response of scaled footing tests for different inclination angles (Azami et al., 2010)

2.2.1.2. Tests on HCA samples

Using a conventional triaxial apparatus to test inclined bedding plane samples may produce a non-uniform stress inside the sample (Lade, Rodriguez, & Van Dyck, 2014; Saada, 1970). A hollow cylinder apparatus (HCA), on the other hand, provides a very advanced and valuable way to perform a wide range of tests which simulate in situ conditions under various directions of principal stress, continuous rotation of the principal stress, and different intermediate principal stresses, among others. With this device, the three principal stresses can be individually controlled by varying the applied stresses and torque. Consequently, the intermediate principal stress and principal stress direction can follow the targeted path. Details of this device are included in Chapter Three.

Most previous studies have used small-scale samples. For example, Miura et al. (1986) used a hollow cylindrical apparatus, with outer D_o and inner D_i diameters of 50 and 30 mm, respectively, and height H of 200 mm, to investigate the anisotropic behaviour of Toyoura sand (D_r = 82%, p' = 98 kPa, b = 0.5) in terms of strength-deformation characteristics. This sand is important in many critical projects such as nuclear power plants and large petrol tanks. Results showed that variation in the principal stress direction resulted in an anisotropic strength of the sand. The ultimate ratio of (σ_1 - σ_3) / (σ_1 + σ_3) dropped rapidly from its maximum value of 0.90 at α = 0° to 0.87, 0.81, 0.77 and 0.73 for α = 15, 30, 45 and 60°, respectively, followed by somewhat of an increase to 0.74 and 0.76 for α = 75 and 90°, respectively. The lowest strength, near bedding or α = 60°, was related to the fact that a horizontally-preferred alignment of particles results in easy deformation of the horizontal bedding plane. This is also related to the coincidence between the Matsuoka mobilised plane and the direction of the applied principal stress. A similar trend was observed by Symes, Gens, and Hight (1988) and Tong, Yu, Zhang, and Zhang (2008), although Symes et al. (1988) only considered the limited range of α = 0–45°.

SEM images presented by Z. Yang et al. (2008) indicated that most soil particles tend to align at 70–80° compared to the horizontal axis, and this produces the poorest resistance plane against sliding along such inclination. This was used by Xiong et al. (2016) to explain their findings, in which minimum strength occurred at 70° with an approximately 31.2% difference in peak deviator stress q_p.

This variation in the developed peak stress ratio results in clear directional dependency of shear strength. In their study of Nevada sand (e = 0.57) under b = 0.5, Lade et al. (2014) found that the friction angle of sand, $Ø$, was 53, 46.25, 42.5, 38.75 and 45° for α = 0, 22.5, 45, 67.5 and 90°, respectively. This means that the difference between the maximum and minimum friction angles due to anisotropy was about 14.25°. Therefore, the friction angle used to represent overall strength can result in unsafe geotechnical designs, even when a safety factor is incorporated.

Sand in a loose state (e = 0.71) can also exhibit a certain level of anisotropy. Sayao (1989) found that the ratio of (σ_1 / σ_3) decreased gradually from 3.48 at α = 0° to 2.6 at α = 55°, and was associated with increasing contractive volumetric strain. A similar

trend was observed for shear strain (ε_1 - ε_3), which increased from 0.8 to 4.0% as α increased from 0 to 55°. These results indicate that increasing contraction due to increasing α can result in a significant decrease in effective stress under undrained conditions, thus increasing susceptibility to liquefaction.

More recently, L. Yang et al. (2016) conducted a comprehensive study on Leighton sand. Several points need to be mentioned. Firstly, it was observed that medium and dense states of sand showed almost the same degree of anisotropy as shown in Figures 2.8 and 2.9, in which deviator stress decreased at a low rate from 0–30° and then more rapidly until 60°, followed by a slight increase. Secondly, consistent with previous studies (e.g. Oda, 1972b; Tong et al., 2014 among others), a clear anisotropic response of glass beads to α was reported, noting that the deviator stress was smaller and the volume compressibility larger than for dense sand. The inherent anisotropy of sand can take the form of ***(i)*** preferred orientation of longitudinal or flaky particles, and ***(ii)*** preferred orientation of unit vectors normal to the contact plane (Oda & Iwashita, 1999). Thus, the anisotropic behaviour of glass beads is likely to be related to ***(ii)***. They also reported that the effect of pre-shearing on anisotropic strength was almost same as that of non-pre-sheared samples. Deformation variation was analogous to the variation of deviator stress with α. For example, the expansion volumetric strain of dense sand at 10% deviator strain ε_q decreased from 2.1% at α = 0° to 2.0, 1.26 and 0.32% for α = 15, 30° and 60°, respectively, then increased to 0.4–0.5% for α = 75° and 90°. Similar directionally-dependent deformation was observed for pre-sheared medium-density sand, but with lesser dilation and higher contraction than that of dense sand.

The aforementioned studies conducted hollow cylinder tests under conditions where b was held constant at approximately 0.5; however, Cai (2010); Cai, Yu, Wanatowski, and Li (2012) investigated anisotropic effects with b varied from 0.0 to 1.0 ($b = \sin^2\alpha$). This simultaneous variation of b and α resulted in a combination of effects and, thus, the real effect of principal stress direction could not be separated. However, the stress trend was similar to that of studies using constant b. In contrast to L. Yang et al. (2016), there were no clear trends in deformation behaviour in terms of increasing or decreasing dilation or contraction with increasing values of α. This may be linked to

b not being held constant for all values of α considered. A similar trend was observed recently by Romiani, Razeghi, and Keykha (2015), who investigated the effect of α on Firoozkuh sand (D_r = 50%) under various values of *b* ($b = \sin^2\alpha$) and found that the friction angle varied from 35° to 23° as α increased from 0° to 90°.

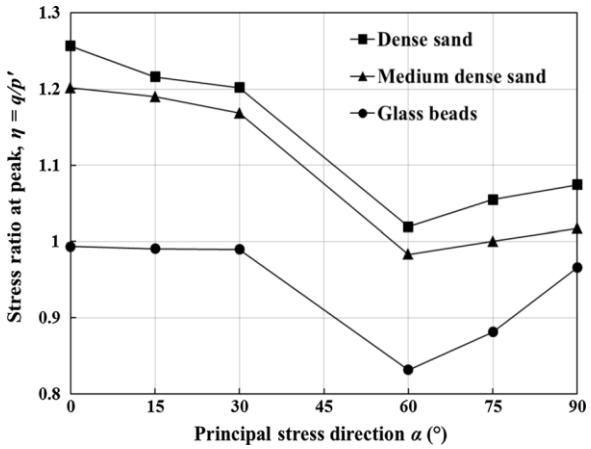

Figure 2.8 Comparison of the peak stress ratios of dense sand, medium-density sand and glass beads under different principal stress directions (L. Yang et al., 2016)

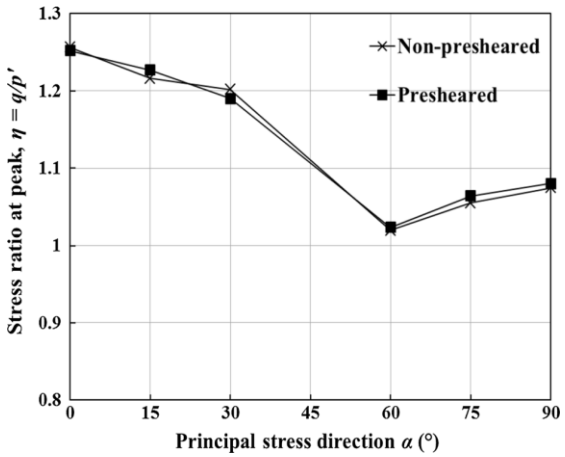

Figure 2.9 Comparison of the peak stress ratios of pre-sheared and sheared dense sand (L. Yang et al., 2016)

In real-life geostructures, particularly in urban areas, soil is subjected to anisotropic consolidation, i.e., $\sigma_1 / \sigma_3 \neq 1$, due to adjacent structural loads or preloading, or due to principal stresses with different directions. The aforementioned studies were conducted under isotropic consolidation. However, some research has been carried out to investigate the effect of principal stress direction on sand that is consolidated

anisotropically. For example, Razeghi and Romiani (2015) investigated the effect of α on two types of samples: 1) samples consolidated anisotropically under $\sigma_1 / \sigma_3 = 2$ with directions of principal stress during consolidation, α_c, being 0° and 45°, and 2) samples consolidated isotopically, i.e., $\sigma_1 / \sigma_3 = 1.0$. Both types were then sheared under α = 0°, 15°, 30°, 45° and 60°. Figure 2.10a shows that anisotropically consolidated samples had larger deviator stresses than those consolidated isotropically, noting that the general trend was similar. Larger deviator stress owing to the densification of samples occurred under larger stress ratios for anisotropic consolidation. For samples consolidated anisotropically but under α_c = 45°, larger deviator stress occurred at α = 45° instead of 0°. This may be because consolidation under conditions of α_c = 45° and $\sigma_1 / \sigma_3 = 2$ can produce greater densification along such a direction and, consequently, such a plane exhibits greater resistance when sheared compared with other directions. Further, slight differences in deviator stress were observed due to variation in α_c (Figure 2.10b). Deformation characteristics were similar to those observed in the above-mentioned studies, where expansion volumetric strain dominated the behaviour and such expansion decreased significantly as α increased.

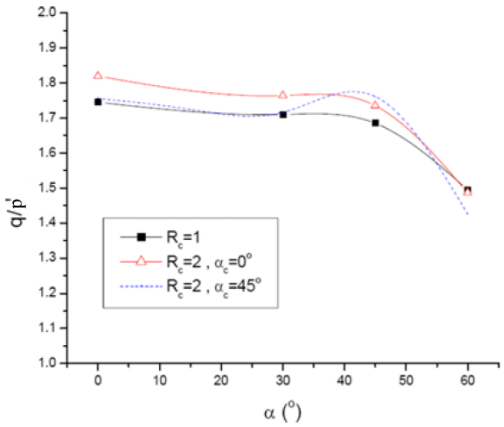

Figure 2.10a Variation of peak q / p' along α (Razeghi and Romiani, 2015)

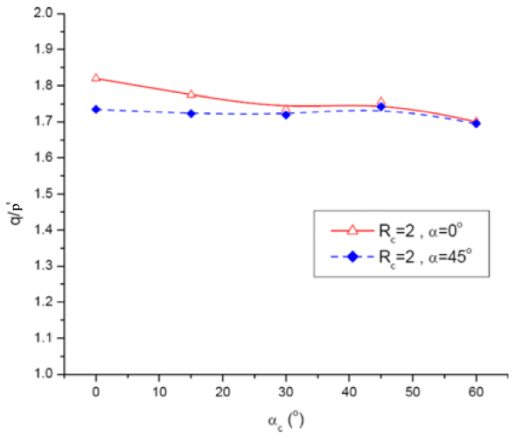

Figure 2.10b Variation of peak q / p' along α_c (Razeghi and Romiani, 2015)

In general, the findings of HCA experiments agree with those based on the use of tilted samples (e.g. Arthur & Assadi, 1977; Arthur & Menzies, 1972; Arthur & Phillips, 1975; Oda, 1972b; Oda et al., 1978). This section focuses on the drained behaviour of

soils, as the research presented in this thesis was performed under such conditions. On the other hand, most past studies have investigated undrained behaviour (e.g Aghajani & Salehzadeh, 2015; Bahadori, Ghalandarzadeh, & Towhata, 2008; Kumruzzaman & Yin, 2010b; Nakata, Hyodo, Murata, & Yasufuku, 1998; Uthayakumar, 1996; Yoshimine & Ishihara, 1998; Yoshimine, Ishihara, & Vargas, 1998; Yoshimine, Ozay, Sezen, & Ansal, 1999). For example, Kumruzzaman and Yin (2010b) investigated the undrained shear strength of soil consisting of silt and sand which was compacted to 16.77 kN/m^3 under different α and constant b = 0.5. They reported an approximately 14° difference in friction angles with variation of α from 2° to 90°. Maximum strength was achieved at α = 2° while the minimum occurred at 90°. Similar trends were recently reported by Aghajani and Salehzadeh (2015), who investigated the undrained anisotropic behaviour of carbonate sand (D_r = 20%). Ultimate strength for both anisotropic- and isotropic-consolidated samples under a mean principal stress of 100 kPa depended on the direction of principal stress, as shown in Figure 2.11. Moreover, maximum strength was obtained at α = 0, similar to the above-mentioned studies; however, the minimum strength was achieved at 30°, in contrast to most investigations. This may be related to particle breakage occurring under shearing.

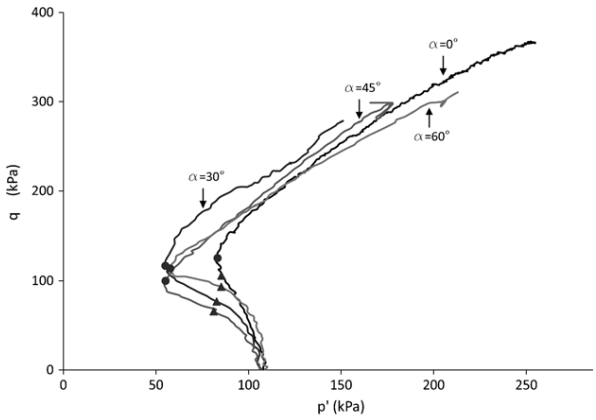

Figure 2.11a Effective stress path for samples tested under isotropic consolidation and various values of α (Aghajani and Salehzadeh, 2015)

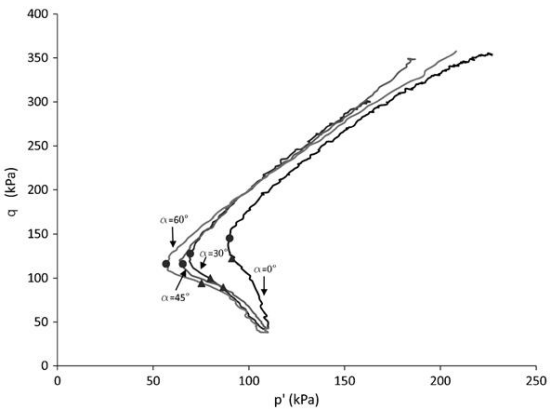

Figure 2.11b Effective stress path for samples tested under anisotropic consolidation and various values of α (Aghajani and Salehzadeh, 2015)

2.2.2. Effect of Continuous Rotation of the Principal Stress Direction

In Section 2.2.1, the anisotropic effect was investigated with a fixed, inclined, direction of principal stress. This condition simulates soil elements in different locations relative to a specific monotonic load in real-life structures. However, many geotechnical applications, as explained in Chapter One, involve continuous rotation of the principal stress axes for specific soil elements. This cyclic rotation is well recognised in pavement, railway and airfield systems due to the presence of moving loads. Many studies have reported that gradual deformation accumulation of the subsoil induced by cyclic rotation can be a considerable source of settlement in many geostructures.

Sayao (1989) investigated the effects of forward and backward rotation under σ_1 / σ_3 = 2.0 and b = 2.0 on loose sand (D_r = 20%). During the tests, the direction of principal stress rotated from 0° to 60° then decreased to 0°, before being rotated to -60° and finally returning to 60°. Several observations can be summarised as follows: most of the volumetric strain ε_v or shear strain ε_1 - ε_3 occurred during the first stage of rotation between 0–60°. For other ranges, strains still accumulated, but at a lower rate, and did not recover to zero after α returned to its initial direction. This indicates that a significant amount of plastic strain was induced due to the cyclic rotation. However, shear strain showed some reduction for the backward rotation, but still did not recover to zero.

Larger relative density results in lower amounts of induced strains (Cai, 2010; Sayao, 1989; Wijewickreme, 1990). For example, increasing relative density from 30% to 50% and then 70% led to decreases in the accumulated volumetric strain ε_v from 4.25% to 0.15% and 0.05%, respectively (Wijewickreme, 1990). Further, it was reported that there was a significant effect of σ_1 / σ_3 on deformation behaviour during the rotation of principal stress, as shown in Figure 2.12 (Wijewickreme & Vaid, 1993).

Recently, Cai et al. (2012) and Cai (2010) investigated the rotation of principal stress (0–90°) on sand, considering q / p' of 0.5–0.875. Both dense and medium states of sand exhibited a significant number of strain components. Axial, radial and circumferential strains, ε_z, ε_r, and ε_θ, accumulated initially at a low rate then increased obviously as α

rotated further. However, shear strain $\gamma_{z\theta}$ accumulated significantly from the beginning of the rotation until reaching its maximum value, then it decreased with further rotation of α. The maximum shear strain occurred at different α depending on the D_r and q / p'. Aside from axial strain, all other strain components were in contractive forms. The rotation of the principal direction induced contractive volumetric strain ε_v and this strain was larger for larger values of the stress ratio q / p'. However, under $q / p' = 0.875$, i.e., q = 175 kPa, the volumetric strain of dense samples started to dilate when α approached 60°. This is linked to the fact that samples under such values of q / p' and α approach a failure state that is observed under monotonic shear test. As mentioned in Section 2.2.1, the drawback of Cai's work is the variation of b during the tests, where $b = \sin^2\alpha$, which means that the induced strains cannot be solely due to the effect of the rotation of the principal stress direction.

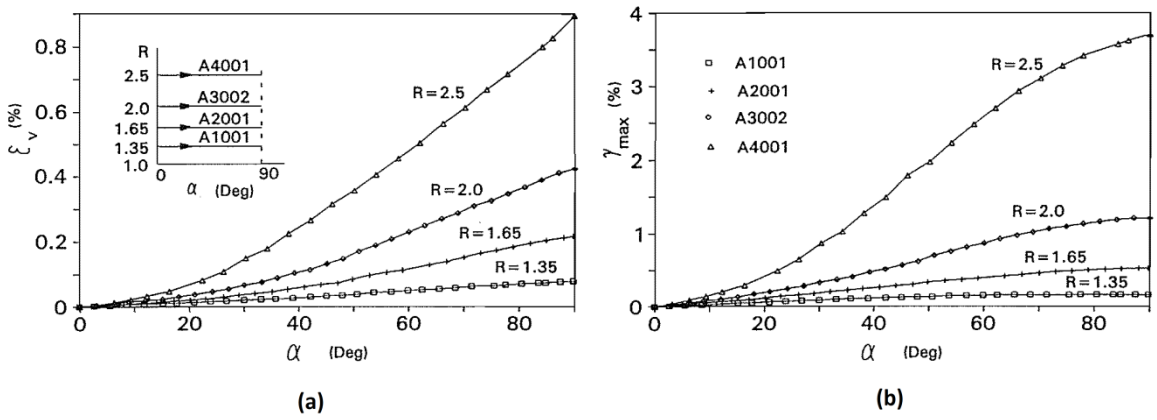

Figure 2.12 Induced deformation: (a) volumetric strain and (b) shear strain due to principal stress rotation under different stress ratios (Wijewickreme & Vaid, 1993)

The aforementioned studies investigated the effect of rotation of the principal stress direction while the magnitude of deviator stress was held constant. However, in many real cases, rotation of principal stress axes and increasing loading can occur synchronously and, thus, this combination effect has also been investigated by some researchers. For example, Figure 2.13 shows results for samples that were subjected to simultaneous rotation and increasing stress ratio until reaching $\sigma_1 / \sigma_3 = 2$ at α = 0° (for A0), 30° (for A30), 45° (for A45), 60° (for A60) and 90° (for A90), then rotated further until reaching 90° (Wijewickreme & Vaid, 1993). It was observed that samples reached the targeted stress ratio ($\sigma_1 / \sigma_3 = 2$) before completing the rotation, i.e. A30,

A45 and A60 exhibited almost same volumetric and shear strains particularly after α = 45°. However, A90, which reached $\sigma_1 / \sigma_3 = 2$ at 90°, showed less volumetric and shear strains. This indicates two points: 1) reaching the targeted stress ratio then completing rotation resulted in stress path-independent deformation behaviour and 2) reaching the targeted σ_1 / σ_3 early resulted in larger induced strains than when most rotation occurred with a value of σ_1 / σ_3 that was less than the targeted value.

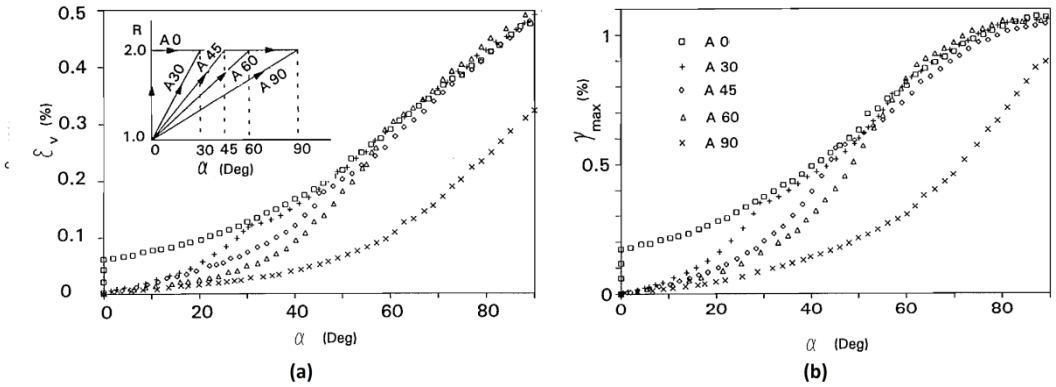

Figure 2.13 Induced deformation under a combination of rotation and increase of principal stress: (a) volumetric strain and (b) shear strain (Wijewickreme & Vaid, 1993)

Samples under the combination of effects presented by Wijewickreme and Vaid (1993) did not reach failure due to the fact that σ_1 / σ_3 only increased to 2.0 before stopping. However, Cai et al. (2012) and Cai (2010) conducted a series of such combination tests, where the deviator stress increased continuously until failure. It was found that dense samples failed when the condition reached q = 205 kPa and α = 83–84°, while medium sand failed under q = 192 kPa and α = 79°. During this combination of rotation and increase of deviator stress, all strains except shear developed at very low rates until α = 60°, then increased dramatically. For example, the induced axial, circumferential, radial and shear strains at the end of the tests were 1.43, 0.4, 1.041 and 1.41%, respectively.

In real-life geotechnical structures, subsoil is subjected to multiple cycles of rotation of the principal stress direction. However, previous studies have been limited to one or two cycles of rotation, and the range of rotation is also limited within specific domains of α. Several studies have been conducted under cyclic rotation of principal

stress, such as Tong et al. (2008), Tong, Zhang, Yu, and Zhang (2010) and Xiong et al. (2016). These studies reported that cyclic rotation of the principal stress axes resulted in significant accumulated strain components ε_z, ε_r, ε_θ and $\gamma_{z\theta}$ that changed in a sinusoidal mode with various amplitudes. Irrespective of the number of cycles or the stress ratio, axial strain ε_z was dilative while the radial ε_r and circumferential ε_θ strains were contractive. Figure 2.14a shows the variation of strain components according to the number of cycles rotation (Yu, Yang, Li, & Wanatowski, 2016). Most of these induced strains and their largest amplitudes occurred during the first few cycles, compared with subsequent cycles where some stabilisation of strains occurred, noting that these strains did not recover completely, indicating the occurrence of plastic deformation. For example, the induced strains at the twentieth cycle were only 10% of those induced during the first cycle (Xiong et al., 2016). The reduction in the amplitudes of strain with increasing numbers of cycles indicates that the samples became stronger and stiffer as sand particles were rearranged during the rotation of the principal stress direction to sustain the cyclic rotation. For example, Xiong et al. (2016) reported that relative density increased from 61 % before testing to around 70.35% after 20 cycles of rotation. Within the range of α = 45–135°, there was a larger tendency to develop strains, and this is agreed with the results of monotonic tests, which revealed that soil became weakened and approached failure within this range of principal stress directions. It is important to mention that the effect of the stress ratio q / p' is not limited to the amount of strain, but also to the oscillation of strains, where larger q / p' values produce larger amplitudes, particularly at the first few cycles. Moreover, increasing q / p' to a certain level—0.7 by Tong et al. (2008) and Tong et al. (2010) and 0.994 by Yu et al. (2016)—resulted in shifting the shear strain $\gamma_{z\theta}$ totally to the dilation form. Tong et al. (2008) and Tong et al. (2010) did not report any failure of sand subjected to cyclic rotation of principal stress axes, even under q / p' = 0.99. This is in contrast to Yu et al. (2016) findings, where cyclic rotation under q / p' = 0.95 resulted in dramatic increases in the strain components, resulting in sample failure during the second cycle (Figure 2.14b), while under $q / p' > 1.0$, failure took place during the first cycle at α = 48°.

Cyclic rotation resulted in considerable amounts of contractive volumetric strain ε_v, particularly during the first few cycles, then it continued to develop but with a lower

rate and with low variation along α (Tong et al., 2008; Tong et al., 2010; Xiong et al., 2016; Yu et al., 2016). After 50 cycles, the ε_v developed due to cyclic rotation under $q / p' = 0.93$ was four times the volumetric strain when $q / p' = 0.6$ (Yu et al., 2016), as shown in Figure 2.15. A similar trend was observed by Tong et al. (2010), although their results implied that relative density has more affect than stress ratio. For example, the volumetric strain ε_v of medium-dense sand ($D_r = 50\%$) due to rotation under $q / p' = 0.693$ was larger than that of dense samples ($D_r = 70\%$), although it was subjected to a larger stress ratio, $q / p' = 0.866$ (Tong et al., 2010). This is likely related with the tendency of medium-dense sand to contract more than dense sand.

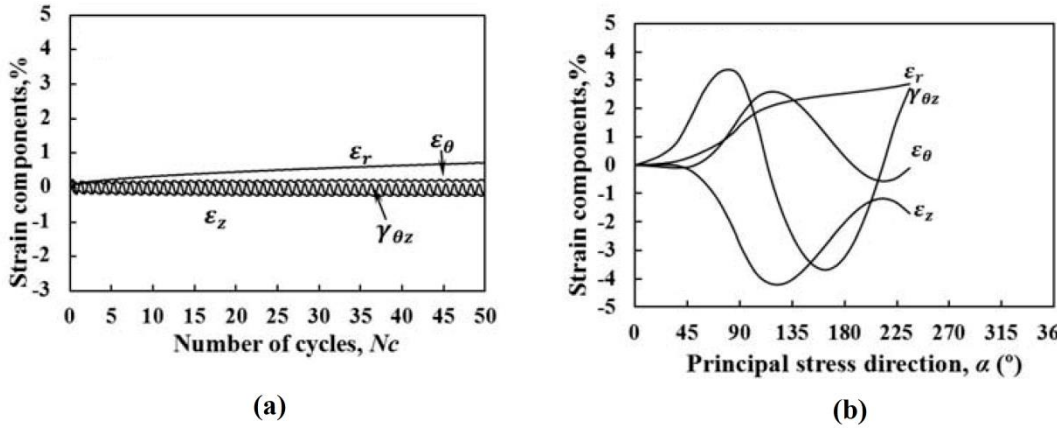

Figure 2.14 Development of strain components under cyclic shear rotation for dense sand: (a) $q / p' = 0.6$ and (b) $q / p' = 0.95$ (Yu et al., 2016)

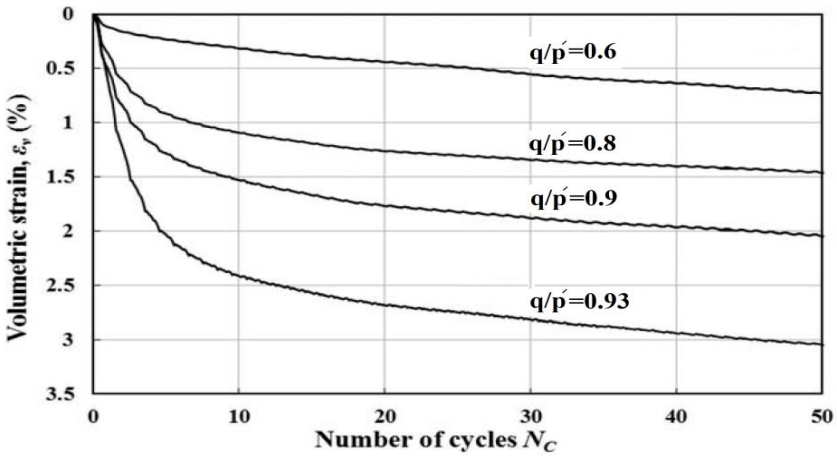

Figure 2.15 Development of the volumetric strain with number of cycles for test with different q / p'(Yu et al., 2016)

Cyclic rotation of principal stress axes was also investigated in samples that consolidated anisotropically under inclined principal stress directions of α_c = 0, 45 and 90° (Xiong et al., 2016). This means that the rotation began from α_c= 0, 45 and 90°. When rotation began from 0° or 45°, sand exhibited similar trends to that observed by Tong et al. (2010) and Yu et al. (2016). However, when the principal stress direction started cyclic rotation from 90°, some difference occurred—axial strain changed to being contractive, while circumferential strain became dilative.

Limited numerical studies have been conducted on these issues. For example, X. Li, Yang, and Yu (2016) investigated the deformation behaviour of dense soil (e = 0.645) under b = 0.5 and q / p'= 0.5, 0.6, 0.7 and 0.9. They reported that ε_θ, ε_z, and $\gamma_{z\theta}$ changed cyclically and induced a significant amount of plastic strain. Both ε_θ and ε_r were contractive for all q / p'values, while shear strain changed sinusoidally from dilation to contraction. However, in contrast to the experimental results, axial strain for q / p'= 0.5 was induced in the contractive mode during the first few cycles, then began to move to dilation. For larger q / p'values, amplitudes of ε_θ, ε_z and $\gamma_{z\theta}$ become very wide, associated with a dramatic increase in the radial strain. Moreover, expansive axial strain still accumulated even after 50 cycles, while circumferential strain tended to decrease with increasing numbers of cycles N_c. Strain trajectories were open in the first cycle due to the sliding, rearrangement and extensive induced deformation that led to plastic strain, then it changed to an approximately closed circular shape (Figure 2.16). Similar trends were observed for all values of q / p', however, larger values resulted in larger strain paths. This rotation was associated with considerable increases in induced contractive volumetric strain where volumetric strains ε_v were 3.3, 3.9, 4.5 and 5.4 % for q / p'= 0.5, 0.6, 0.7 and 0.9, respectively, after N_c = 50.

Dynamic properties during cyclic rotation have received very little attention. The determination of shear modulus G and damping ratio λ values is possible by plotting the hysteresis loop curves (Figure 2.17). The available results show that hysteric loops, i.e., the relationship between shear strain and shear stress, become closer to each other after the first cycle due to decreasing accumulated shear strain. Consequently, significant increases in the shear modulus were reported with increasing numbers of cycles N_c, mainly during the first few cycles. Moreover, the hysteric loops were open

during the first few cycles, indicating that plastic deformation developed in the samples; however, with increasing numbers of rotational cycles, they tended to form closed loops. For example, under $q / p' = 0.866$, the shear modulus of sand ($D_r = 70\%$) normalised to that of the first cycle G_n / G_1 was 1.22 at $N_c = 2$, 1.39 at $N_c = 10$ and 1.45 at $N_c = 17$ (Tong et al., 2008). Similar trends were observed by Tong et al. (2010), noting that larger stress ratios produced larger ratios of G_n / G_1, but with lower values of the shear modulus, where the G_n / G_1 of dense sand under $q / p' = 0.866$ and 0.994 was 1.28 and 1.5, respectively, after 17 cycles of rotation. For a lower relative density sand ($D_r = 50\%$) tested under $q / p' = 0.693$, it was found that G_n / G_1 increased to 1.32 after 17 cycles of rotation (Tong et al., 2008). This increase in the shear modulus of the subsequent cycle, relative to the previous one, is due to the densification that has occurred due to the rearrangement of sand particles. This explanation can be inferred through comparing the G_n / G_1 of $D_r = 50$ % with that when $D_r = 70$ %, where the G_n / G_1 of medium density sand was larger, although samples were subjected to lower stress ratios than dense samples were. This indicates that cyclic rotation has a greater effect on the densification of samples of lower density. However, no studies were found regarding the effect of principal stress rotation on the damping ratio.

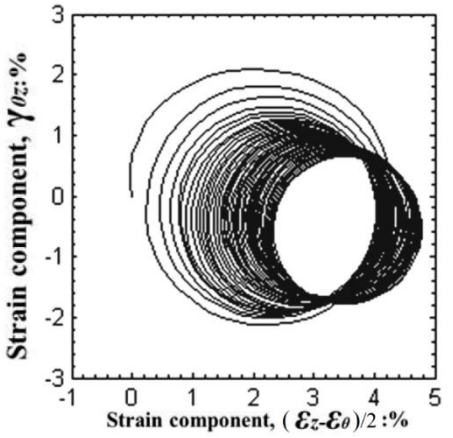

Figure 2.16 Strain trajectory at q / p' = 0.9 (X. Li et al., 2016)

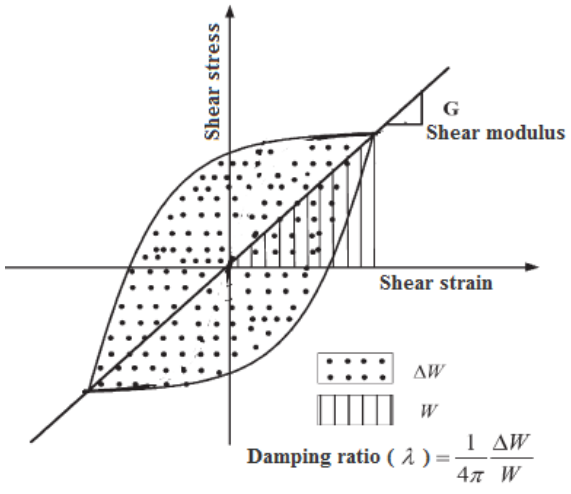

Figure 2.17 Hysteretic shear stress–strain relationship for estimating shear modulus and material damping ratio

2.2.3 Effect of the Intermediate Principal Stress Parameter

Despite the three-dimensional stress condition of most geotechnical problems in field, determination of the design parameters depends mainly on standard laboratory tests and field tests, such as the conventional triaxial test, which does not consider the effect of the intermediate principal stress σ_2. This disregard is related to the limited availability of the advanced apparatus, and also to the complexity of duplicating such in-situ 3D stress conditions in tests. Tastan (2009) stated that intermediate principal stress effects should be considered in offshore foundations subjected to wave loads, multi-stage construction embankments, pavements under moving loads, foundations subjected to earthquakes and any soil element located far from the load centre.

As per α, intermediate principal stress has a crucial effect on soil behaviour. This effect stems from that fact that most soils have an anisotropic nature, and thus, any applied stress in a direction other than the usual vertical one can produce a variation in soil behaviour. The effect of the intermediate principal stress direction σ_2 is often represented by intermediate principal stress parameter b, which describes the value of intermediate principal stress relative to the minor and major principal stresses, as explained in the Equation 1.1.

The value of b ranges from zero (when the intermediate principal stress and minor stress are equal, i.e., $\sigma_2 = \sigma_3$) to 1.0 (when the intermediate principal stress is equal to the major principal stress, i.e., $\sigma_2 = \sigma_1$). Conventional devices cannot perform tests under different values of b as they are limited to 0.0 for conventional triaxial compression tests, 1.0 for extension tests and 0.2–0.4 for plane strain tests. Therefore, HCA offers a great opportunity to investigate this issue.

Many studies have been conducted to investigate the effect of b on the stress-strain characterisation of soils in monotonic tests. In general, peak deviator stress decreases with increasing b, as shown in Figure 2.18 (L. Yang et al., 2016). Furthermore, as b increases to 0.2 (Kumruzzaman & Yin, 2010b), 0.4 (Kandasami & Murthy, 2015), and 0.5 (L. Yang et al., 2016), the internal friction angle $Ø$ of sand increases and then decreases with further increases of b. However, the study of Shi, Zhu, Chiu, and Liu (2010) on coarse-grained soil reported a different trend, where maximum strength

deviator stress occurred when b = 1.0, while the minimum occurred when b = 0. Furthermore, they found that the friction angle increased as b increased to 1.0. The effect of b also depends on the direction of principal stress α. Lade et al. (2014) demonstrated that the Ø values of samples under α = 0° increased as b increased to 0.75, then decreased. When α was 22.5–90°, however, Ø increased as b increased to 0.25–0.5, then decreased for larger values of b. The difference in Ø, for example, between α = 0° and 67.5° under b = 0.75 reached 25°. Depending on the project, this significant variation could result in an unsafe design/analysis.

Kandasami and Murthy (2014) found that b values of 0–0.6 had an insignificant effect on deviator stresses in critical states, while a clear effect was observed when b was greater than 0.6. They ascribed the effect of b on deviator stress prior to the critical stage to the inherent anisotropy of soil particles, which have a propensity to align themselves horizontally. However, this preferred alignment, i.e. the initial fabric, was disturbed after the critical state. This agrees somewhat with Sayao (1989) and Sayao and Vaid (1996) who found that after shear strain of 1–1.4%, the variation of b between 0.3–0.8 has no effect on the stress ratio. However, a different trend was reported by Romiani et al. (2015), who found a clear effect of b on Firoozkuh sand, even at a large deviator strain.

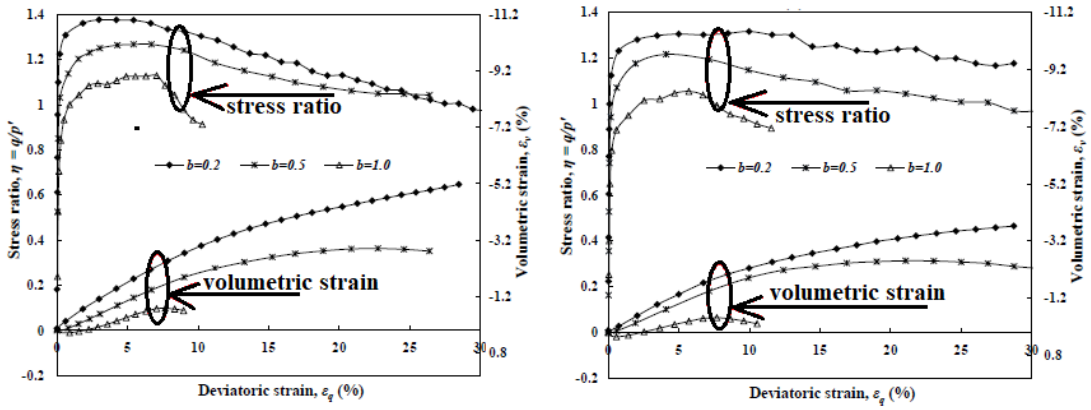

Figure 2.18 Stress-strain relationships for tests where b = 0, 0.2, 0.5 and 1.0 for (a) α = 0° and (b) α = 15° (L. Yang et al., 2016)

Friction angle was observed to increase with b up to a certain level before dropping with further increases in b. This is related to the fact that increasing b, i.e. increasing σ_2, provides extra confinement to sample that results in increased internal friction. However, with further increases in σ_2, sliding and rotation can occur, inducing large strains and thus decreasing the friction angle. Regarding the effect of b on the induced strain components, samples under α = 0–30° exhibited expansive volumetric strain when b = 0.2 and 0.5, while under b = 1.0, contractive strain occurred initially followed by slight dilation (L. Yang et al., 2016). For α = 60–90°, samples exhibited contractive volumetric strain for all values of b and such contractive strain increased dramatically as b approached 1.0. Figure 2.18 shows the typical effect of b on sand tested under α = 0° and 15°.

Numerically, D. Yang (2014) reported a similar trend to that of previous experimental studies (e.g. Arthur, Chua, & Dunstan, 1977; Lade & Duncan, 1973; Yamada & Ishihara, 1979). By using discrete element method DEM, he found that peak q / p' decreased continuously with increasing b. For example, peak q / p' of dense sand decreased from 0.94 to 0.77 as b increased from 0.0 to 1.0. However, it was found that b had an insignificant effect on the deformation of dense sand, while volumetric strain of loose sand generally decreased with increasing b. The friction angle of dense sand increased as b increased until reaching a maximum value at around b = 0.5, then decreased as b increased to 1.0, constituting a difference of 5°.

In addition to these monotonic tests, the effect of intermediate principal stress parameter b has also been investigated under the rotation of principal stress. M. Jiang, Li, and Yang (2013) reported that b has a clear influence on the deformation of granular soil (D_r = 53%) induced under rotation conditions of principal stress where α = -70–70°. Dense sand exhibited dilative axial strain for all b values and the largest amount took place when b = 1.0 (Tong et al., 2010; L. Yang et al., 2016). Circumferential strain under b = 0.1 and 0.5 increased as N_c increased, while under b = 1.0, it decreased after the first cycle (Tong et al., 2010). However, L. Yang et al. (2016) found a slight effect of b on circumferential strain. Radial or intermediate strain changed from expansive to contractive with increasing b values from 0–0.1 to 0.25–0.5 then developed dramatically in contractive form for b = 1.0 (Shi et al., 2010; Tong

et al., 2010). This changing of ε_r from expansion to contraction as b increases from 0.1 to 0.5 indicates that plane strain conditions occur within this range of b. Similar extensive accumulated radial strain was observed under b = 0.5 and 1.0 by Yu et al. (2016), but they did not report any shifting from dilation to contraction. Volumetric strain was induced significantly during cyclic rotation under all b values, noting that larger values resulted in larger volumetric strains (Tong et al., 2010; Yu et al., 2016). Most of this volumetric strain accumulated during the first few cycles for all b values. Tong et al. (2010) demonstrated that the rate of increasing volumetric strain after N_c = 10 was slight, while Yu et al. (2016) reported that the increasing rate kept accumulating significantly even at an advanced number of cycles. Figure 2.19a depicts the accumulated volumetric strain with increasing numbers of cycles for different values of b (Yu et al., 2016). In general, a similar effect was observed for samples with lower density (D_r = 50%), although the difference due to the effect of b was lower (Tong et al., 2010).

Regarding hysteretic loops of shear stress-strain relationships, L. Yang (2013) and L. Yang et al. (2016) found that the loops were closer to each other when b = 0.2, compared with other values. Larger b values resulted in larger sizes of the first several loops. In general, this is consistent with the findings of Tong et al. (2010). Moreover, increasing b resulted in increasing shear modules ratios G_n / G_1 for different stress ratios and relative density. For instance, after 20 cycles of rotation at q/p'=0.99, G_{20} / G_1 was 1.31, 1.5 and 1.88 for b = 0.1, 0.5 and 1.0, respectively (Tong et al., 2010). The results of L. Yang et al. (2016) imply a similar trend.

Consistent with previous experimental studies, X. Li et al. (2016) used discrete element method DEM to numerically investigate the deformation behaviour of dense soil under different values of b. They reported that sand under b = 1.0 failed upon stress rotation. After 30 cycles of rotation, samples under b = 0 and 0.5 were sustained despite the significant induced contractive volumetric strain, ε_v = 4.0% for b = 0.5 and 3.05% for b = 0.0 (Figure 2.19b).

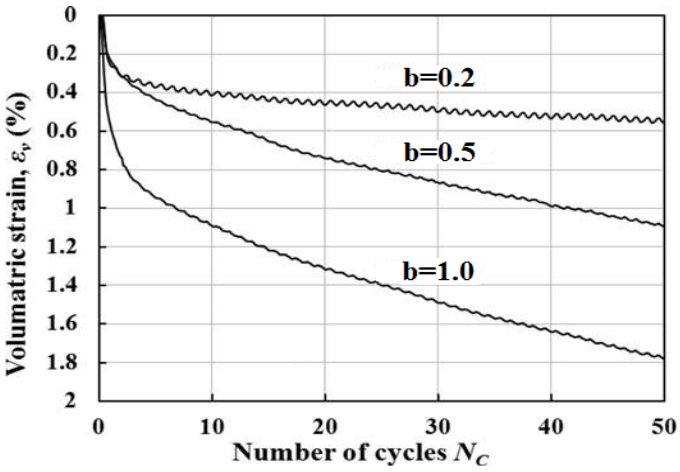

Figure 2.19a Development of the volumetric strain with number of cycles under different values of *b* (X. Li et al., 2016)

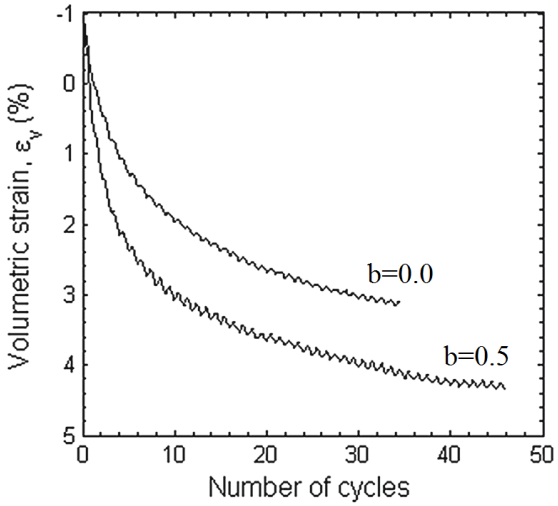

Figure 2.19b The effect of *b* value on the development of volumetric strain (X. Li et al., 2016)

2.3 Reinforcement

Different types of reinforcement, such as cement and geosynthetics, are used in a variety of applications to improve soil bearing capacity, deformation and shear strength. Geosynthetic reinforcement is an innovation of modern soil reinforcement methods, although it dates to ancient times. The first known use of geosynthetic-reinforced soil was about 3000 years ago in the Ziggurat of Ur in the civilization of Mesopotamia. Geosynthetics are available in a wide range of types; for example, geogrids, geotextiles, fibre, geocells, etc.

Cemented soils occur when granular deposits are artificially or naturally bonded together with small amounts of cement at the contact point between sand grains. Cement stabilisation is a widely-used, effective and rapid method of producing artificially-cemented sand and improving the bearing capacity of weak soil. On the other hand, naturally-cemented soils are widespread in many geological environments. In many countries such as Australia, there are extensive areas of cemented superficial formations, such as the Bassendean and Safety Bay sands. Calcium carbonate, silica, silt, clay, gypsum and iron oxides are the most common cements in such formations.

In the next sections, the literature review focuses on the behaviour of sand reinforced by geogrids, geotextiles and geocells. The benefits, types, functions and stress-strain and deformation behaviours of geosynthetics are summarised. Moreover, the performance of cemented sand under loading tests and triaxial tests will also be reviewed.

2.3.1 Geosynthetic Reinforcement

It is well known that soil exhibits good resistance against shear and compression forces, but only very weakly resists tension. Accordingly, tensile elements have been utilised to overcome this weakness (Haeri et al., 2000; Kim, Oh, & Cho, 2010).

Geosynthetics refers to synthetic materials used as an integral part of soil and rock to form a composite construction material, i.e., reinforced soil with high compressive and tensile strength (Shukla, 2012).

In most geotechnical applications of raft foundations, slopes, bridge abutments and retaining walls, reinforcement layers are coupled to the soil as a tensile member by providing confinement, interlocking, adhesion or friction, which consequently increases shear strength, resists applied tensile stress, and eliminates induced deformations. Moreover, reinforcement is suitable for sustaining earthquakes or other vibration sources that can induce severe differential settlement due to their flexible nature (Shukla, Sivakugan, & Das, 2009).

2.3.1.1 Pros and cons of using geosynthetics

Economic and technical advantages are the reasons why geosynthetic materials are widely used in both temporary and permanent constructions. Moreover, their flexibility renders them suitable for sustaining earthquakes or other vibration sources that could induce severe differential settlement (Shukla et al., 2009). Some of the advantages of using geosynthetic reinforcement are listed below:

a) Saving of time and cost (Abdi et al., 2009; Naeini & Gholampoor, 2014; Tafreshi & Asakereh, 2007). For example, the readiness of use of the reinforcement results in increased construction speed. Further, with reinforcement, steep slopes can be achieved, and thus, there are significant reductions in the land areas required for infrastructure (e.g., slopes, roads, railways) and fewer fillings and excavations are required. This technique of soil stabilisation also results in minimal wear and tear for the equipment used (Shukla, 2012).

b) Negligible corrosion and long-term durability with only slight degradation due to chemical and biological conditions.

c) Extension of pavement structure service life by reducing the different types of distress (X. Yang et al., 2012).

d) Reliability, simplicity and adaptability to different site conditions, even those with unsuitable soil, i.e., poor or soft soil (Abdi et al., 2009; Naeini & Gholampoor, 2014). For example, controlling and checking the quality of geosynthetics in factories results in minimum variation in their specifications. Moreover, the quality of reinforced soil is more homogeneous compared with other stabilisation methods, such as chemical stabilisation, which needs high quality control for mixing, placement and curing.

e) Their small volume and light weight make them easy to store and handle. This allows them to be installed rapidly and easily with minimum control, even by unskilled workers.

As with any method, however, some there are also some disadvantages (Jewell, 1996).

a) Durability and very long-term performance is still under investigation. Moreover, no specific codes and standards exist due to its novelty.

b) Storage, handling and installation must be performed carefully to avoid the possibility of damage.

2.3.1.2 Raw material and manufacturing types

There are many products of geosynthetics such as geogrids, geotextiles, geonets, geomembranes, geofoams and geocomposites, among others. Most of these are made from polymeric materials although some products are fabricated using wool, jute, silk or cotton. A wide range of polymers are used for the manufacture of such products, such as polypropylene (PP), polyester (PET), polyamide (PA), polyethylene (PE). Geogrids are formed from PP, PET and high-density polyethylene (HDPE). Geomembranes are formed from a wider range of polymers type, including HDPE, PP, low-density polyethylene (LDPE), very low-density polyethylene (VLDPE), polyvinyl chloride (PVC), chlorinated polyethylene (CPE) and chlorosulphonated polyethylene (CSPE) (Shukla, 2012).

For less critical or non-critical structures or permanent works, geosynthetics are manufactured using PP due to its high economic benefits and great resistance to chemical and pH conditions. However, this type shows poor performance under long-term applied stress because it accumulates large creep deformations. Therefore, in projects with critical conditions, PE is increasingly being employed due to its low cost, high resistance to chemical attachment or reaction, and excellent resistance to creep deformation in long-term service. HDPE is used extensively to fabricate geogrid and geomembrane reinforcements (Shukla, 2012).

Although there is a wide range of raw materials used for geosynthetics, their manufacturing consists of two main steps: ***1)*** production of linear elements such as

yarn, filaments and fibres; and ***2)*** combining these elements to form different types of planar fabric (Jewell, 1996; Shukla, 2012). Several types of linear elements can be summarised as follows (Shukla, 2012):

a) *Filaments fibres*: Polymers that are melted, spun or extruded through special moulds and extended longitudinally. When this product is cut into short pieces of 20–100 mm length, they are called *staple fibres*. Single filaments or multi-fine filaments can be used to produce yarn that is called *monofilament yarn* and *multifilament yarn*, respectively. Moreover, *spun yarn* can also be produced using interlaced staple fibres.

b) *Slit films*: Extruded polymer films that are slitted and extended to form flat strip fibres with widths of 1–3 mm. Yarn made from this type is called *slit film yarn*.

c) *Strands*: Bundles of strip fibres used to form *fibrillated yarn*.

As aforementioned, there are a wide range of reinforcement products; however, the most commonly available types of geosynthetics are summarised below:

i) *Geotextile*: Flexible sheets of two main types (Jewell, 1996; Shukla, 2012):

− Woven geotextile: Manufactured by a weaving process of two parallel linear elements set in perpendicular form to make a planar form.

− Nonwoven geotextile: Formed from linear elements randomly arranged and bonded together by partial melting (thermally), needle punching (mechanically) or chemically.

There are also other types of geotextiles such as knitted geotextiles and stitch-bonded geotextiles.

ii) *Geogrids*: Similar to woven geotextiles, they use linear elements such as yarns that are intersected in a perpendicular fashion and connected in joints to form a grid. In other types, polymer sheets are heated and stretched to form geogrids. Moreover, two main types of extruded geogrids can be described based on the direction of stretching during production:

− Uniaxial geogrids are perforated sheets stretched longitudinally. Most of the tensile strength of this type is occurs along its longitudinal direction.

− Biaxial geogrids have close, or almost similar, tensile strengths in both directions.

iii) *Geomembranes*: Produced by extrusion of a melted polymer to form a planner sheet. Moreover, different types of geotextile can be coated by polymers or asphalt to form reinforced geomembranes. The most common manufacturing method is by *calendaring*, where heated rollers pass the heated polymer to form a geomembrane with thickness ranging from 0.25–7.5 mm (Shukla, 2012).

iv) *Geocells*: Manufactured by welding or stitching planner geosynthetic sheets to form cellular nets (Shukla, 2012).

Figure 2.20 shows some types and forms of geosynthetics.

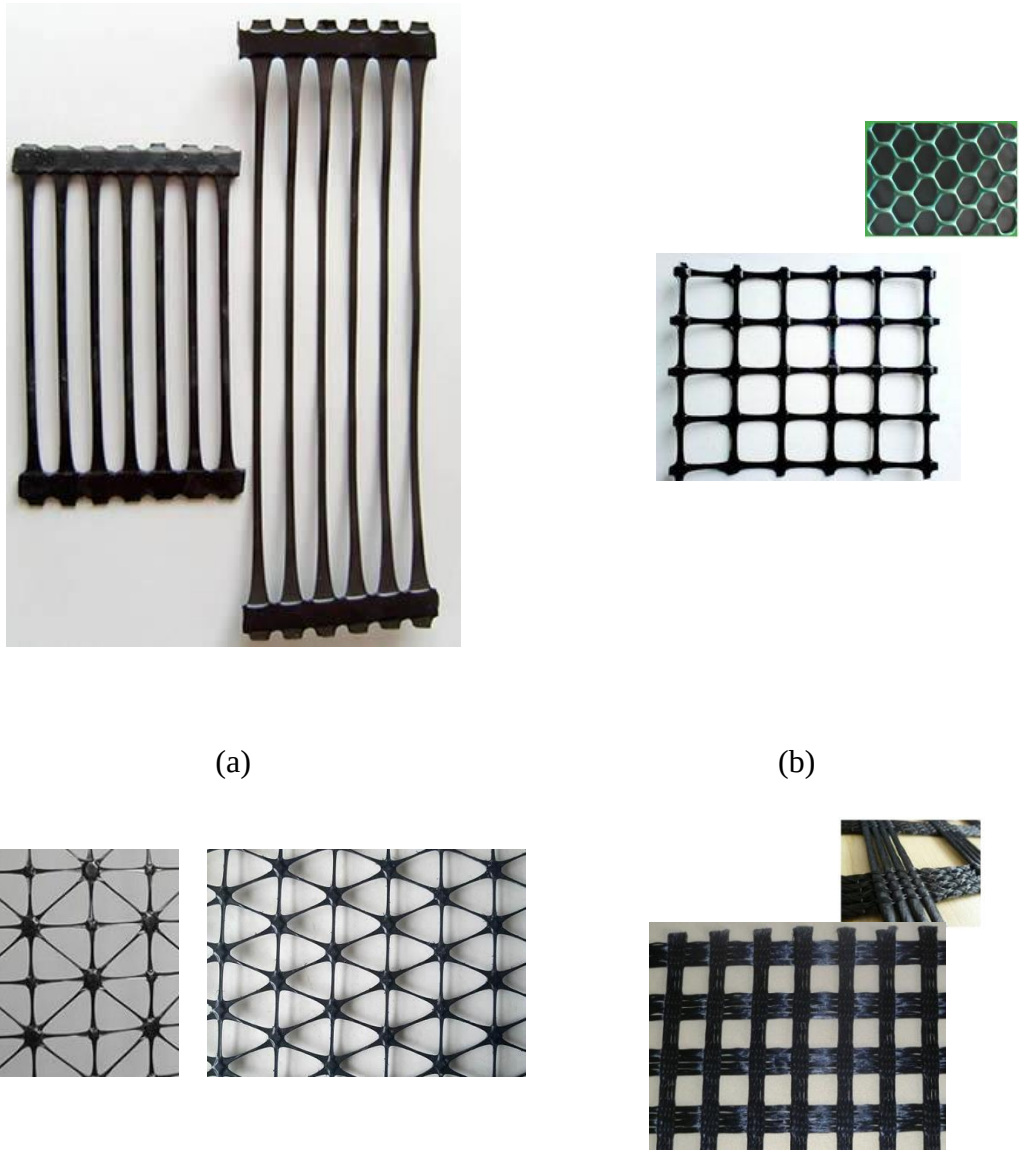

(a) (b)

(c) (d)

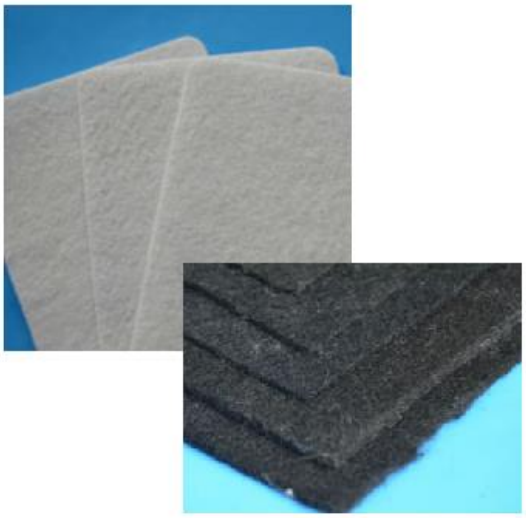

(e) (f)

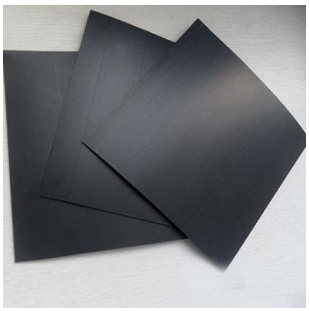

(g) (h)

Figure 2.20 Some types and forms of geosynthetics: (a) uniaxial geogrid, (b) biaxial geogrid, (c) triaxial geogrid, (d) knitted geogrid, (e) nonwoven geotextile, (f) woven geotextile, (g) geomembrane and (h) geocell.

2.3.1.3 Functions of geosynthetics

The improvement obtained by reinforcement depends mainly on the geosynthetic material's properties and its interaction/interlocking with the soil. The selection of the reinforcement type depends mainly on its tensile strength, stress-elongation characteristics and bonding with the soil. Further, some reinforcement elements can exhibit continuous creep or deformation over time under an applied load, and thus,

deformation should be expected over the service life. This should be considered in most geotechnical applications, particularly in abutments and retaining walls, where settlement and movement are major design considerations (Jewell, 1996). For example, if the required function of the geosynthetic is separation, then puncture resistance is more important than tensile strength, while for reinforcement functions, there should be sufficient strength to sustain the designed load within allowable deformation specifications. This required tensile strength of reinforcement varies based on the type of application. It is in the range of 3–15 kN/m for walls or steep slopes and 30–150 kN/m for embankments over soft soil. Moreover, the allowable maximum tensile strain of reinforcement is 1–2% for bridge abutments, 3–5% for steep slopes and 4–8% for embankments on soft soil (Jewell, 1996).

The major applications of geosynthetics are summarised below:

a) *Fluid barrier*

Movement of water and capillary rise results in differential movement in underlying layers of soil along with degradation in the stiffness of pavement. Therefore, undersealing is one of the purposes of using geosynthetics—to hinder infiltration and movement of moisture into pavement structures, and consequently, avoid damage to them (Mounes, Karim, Mahrez, & Khodaii, 2011).

b) *Cushioning*

Geosynthetics can act as cushions to absorb and relieve stresses applied to pavement structures and, consequently, prevent and delay induced cracks, such as reflecting cracks. During 44 months of field observations of reinforced pavement, Maurer and Malasheskie (1989) reported a significant improvement in pavement response in terms of retarding the amount of cracks and their rate of progress. This means that reinforcement layers work to dissipate the strain energy of cracks and, thus, using geosynthetics as interlayers can prevent cracks from accumulating, developing and passing through a structure (Mounes et al., 2011). This function is also important for damping the dynamic loads induced in many structures; such as in shore protection, where reinforcement works to isolate a structure's base from seismic loads (Shukla, 2012).

c) *Separation*

In sites with soft soil, geosynthetics can be laid on the surface before filling with good quality soil (e.g. granular soil), to prevent movement of particles from the upper layer through the soft bottom layer. In other words, its function is to prevent the intermixing of dissimilar layers, which could reduce the thickness of the good quality layer (Jewell, 1996; Koerner, 1986; Ling, 2003). Under applied loads, tensile cracks usually develop at the base of the granular fill layer and subsequently expand and shrink in pavement under cyclic load. Therefore, without a geosynthetic layer as a separator, the lower soft soil will be pumped up inside these cracks, resulting in degradation and significant damage. This function renders geosynthetics suitable for use in most constructions on soft soil, particularly unpaved and paved roads, railways, preparation of storage areas (Jewell, 1996). Even if the required function of geosynthetics in such cases is separation, geotextiles should have sufficient tensile strength to avoid tears, punctures or bursts under local concentrations of applied stress, particularly when the bottom layer could become deformed under compaction (Ling, 2003). Furthermore, the mobilised tensile strength of separator geosynthetics gives them an associated role as reinforcement layers (Jewell, 1996).

d) *Reinforcement*

A main function of geosynthetics is reinforcement. The inclusion of geosynthetics within soil produces a composite with a greater ability to sustain applied stresses, as compared to regular soil. The mobilised tensile strength of geosynthetics can improve stress support and decrease the transmission of stresses to underlying soil (Jewell, 1996; Shukla, 2016; Shukla & Yin, 2006). This tensile membrane action requires a local deformation to mobilise the tensile strength of the reinforcement layers. In general, reinforcement increases the shear resistance of a composite and simultaneously decreases the induced shear force that should be supported by soil. Furthermore, reinforcements provide lower post-peak strength reduction, improved ductility and improved resistance to static liquefaction when compared with unreinforced sand (Naeini & Gholampoor, 2014).

It is of benefit to mention that geosynthetics can be used temporarily and permanently as follows (Jewell, 1996). In constructions over soft soil, reinforcement is used to improve short-term stability during the critical construction and consolidation stages. After that, the bearing capacity of soft soil is increased due to the occurrence of consolidation and, thus, there is no more need for the reinforcement. Alternatively, it can be used permanently to decrease differential settlement in road foundations and embankments, in addition to reducing the lateral stress induced against a gravity retaining wall's back. Furthermore, geosynthetics are used to maintain stability throughout the life of many structures such as bridge abutments, vertical walls and steep slopes. The benefits of geotextiles can be doubled by combining their separation and reinforcement functions—they can simultaneously prevent the intermixing of poor and good quality soil while increasing the bearing capacity of the soil.

Lateral deformation within soil, induced by applied loads, can be transferred to the reinforcement layers by the interlocking of soil particles and geosynthetics, which consequently mobilises the tensile strength of geosynthetics. This mobilisation of tensile strength provides significant restraint and produces an extra confining stress along the horizontal direction, i.e., less lateral expansion and greater strength of the composite material. Based on this concept, under the same value of major principal stress σ_1, a reinforced sample exhibits larger confining pressure ($\sigma_3 + \sigma_{resulted\ from\ lateral\ restraint}$) compared with that for unreinforced soil, only σ_3 (Shukla et al., 2009). Three mechanisms have been reported for planar reinforced soil: sliding soil particles along the reinforcement layers, the anchorage pullout of reinforcement layers from the soil, and the membrane effect (Jewell, 1996; Koerner, 1986). The first two mechanisms can sustain a planar applied load, while a membrane effect mobilised under deformation can sustain both normal and planar loads. Furthermore, the mechanism of geosynthetic improvement based on the tensioned membrane can be summarised as ***i)*** restraint of the lateral deformation of soil, ***ii)*** provision of confinement (confining stress) that increases shear strength and stiffness, and ***iii)*** improvement of the load distribution to the subgrade layer, and decreasing of its shear stress (Giroud & Han, 2004; Pokharel, Han, Leshchinsky, Parsons, & Halahmi, 2010; X. Yang et al., 2012).

Moreover, Shukla (2002) and Shukla and Yin (2006) reported some other roles of geosynthetics that are related to the aforementioned mechanisms:

a) *Shear stress reduction effect of reinforcement*, where geosynthetics decrease the transition of shear stresses from overlying soil to underlying soft soil. This effect changes the failure mode from local to general and, consequently, increases the bearing capacity of foundations and eliminates or decreases rutting.

b) *Confinement or slab effect of reinforcement layers* by redistributing the applied load as a result of the soil restraint provided by reinforcement layers. This effect is a function of the friction between reinforcement and soil layers.

c) *Membrane effect*, where deformed reinforcement has a membrane force which resists the applied stress and, consequently, affords axial support to the upper soil layer subjected to loading. This type of support can divided into the *normal stress membrane effect* and the *interfacial shear stress membrane effect* (Espinoza & Bray, 1995). The former type of effect requires an anchorage for the reinforcement edges, while the latter does not.

d) *Interlocking effect*, in which soil particles are interlocked through the apertures of geogrids. This helps to transfer the applied or induced stress from soil to geogrid, i.e. induces passive resistance against the transverse ribs of the geogrid (Shukla et al., 2009).

There are many other functions and usages of geosynthetics such as for protection, absorption, interlayers, containment, insulation and screening.

2.3.1.4 Previous studies on geogrids

Studies performed to investigate the behaviour of geogrid-reinforced soil report significant improvements and benefits, such as delays and decreases in rutting development (Kinney, Abbott, & Schuler, 1998; Moghaddas-Nejad & Small, 1996), decreased induced settlement under footings, decreased need for thick granular layers under footings (Shukla, 2016), decreased thickness required for base layers (Cancelli & Montanelli, 1999; Montanelli, Zhao, & Rimoldi, 1997) and increased projected

service life of roads (Al-Qadi, Brandon, & Bhutta, 1997; Cancelli & Montanelli, 1999).

Higuchi, Ishihara, Tsukamoto, and Masuo (1998) investigated the strength and deformation response of dense sand (D_r = 90%) reinforced by two types of geogrid, Types A and B, that had tensile strengths of 69.6 kN/m and 61.7 kN/m, respectively. This difference in the tensile strength was found to be associated with no improvement in samples reinforced with three and six layers, where σ_1 / σ_3 increased to 11 and 20, respectively, compared with σ_1 / σ_3 = 5 for unreinforced samples. However, with 11 layers, σ_1 / σ_3 became 54 for the first type of geogrid (Type A), compared with 95 for Type B. The difference in improvement due to variation in the tensile strength of the geogrid was observed clearly by Futaki, Suzuki, and Yamato (1990), who used geogrids with large differences in tensile strength. It was found that the σ_1 / σ_3 value of sand (D_r = 50%) reinforced with five layers of geogrid increased from 3.25 to 21 as the tensile strength of the geogrid increased from 60 to 180 kPa (Futaki et al., 1990). The improved strength also depended on the pitches size, where σ_1 / σ_3 increased from 6.3 to 8.2, 10.7 and 10.6 as the pitches decreased in size from 200 to 150, 100 and 50, respectively (Futaki et al., 1990).

Figure 2.21 showed the relationship between the deviator stress and strain of large-scale samples of crushed limestone (d_{50} = 5 mm) reinforced with geogrids (X. Chen, Jia, & Zhang, 2017). It clear that the improvement increased as the spacing between layers decreased; where q increased by about 81.0, 152.3 and 251.0 % for geogrid spacings of 200, 150 and 100 mm, respectively. Furthermore, they reported that the critical state line was shifted upward when a geogrid was used.

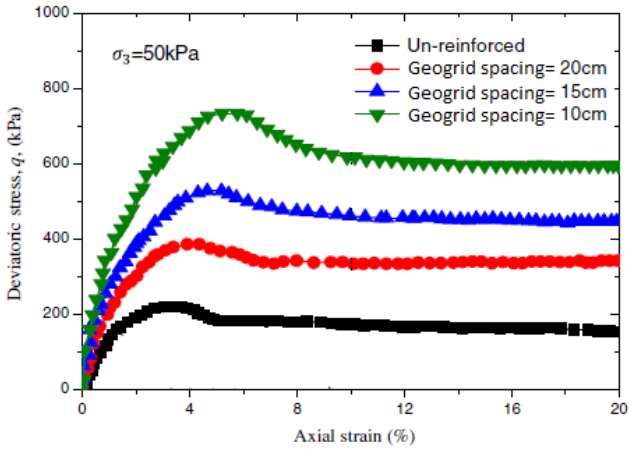

Figure 2.21 Deviator stress-axial strain relationship of reinforced crushed limestone (X. Chen et al., 2017)

Reinforced samples exhibited larger strains at failure compared with unreinforced samples. Axial strain increased from 0.9% for unreinforced samples to 4–6% for ones reinforced with eleven layers of geogrid (Higuchi et al., 1998). Moreover, geogrid restrains expansion strain significantly, which decreased from 3% for unreinforced samples to 1.25% for reinforced samples (with 100 mm spacing) (X. Chen et al., 2017). The induced strain in the geogrid was zero at the edges while it increased to a maximum at the centre (Futaki et al., 1990).

Maximum shear stress is induced significantly near the interfacial area where reinforcement layers are placed and decreases with distance. This can cause the failure along the interface (Jewell & Wroth, 1987; Milligan, Earl, & Bush, 1990; Sridharan, Murthy, Bindumadhava, & Revanasiddappa, 1991). Therefore, many researchers have investigated the interfacial characterisation of reinforced sand using laboratory model loading tests and/or direct shear tests. Abdi et al. (2009) investigated the possibility of improving geogrid-reinforced kaolinite by including a thin layer of sand around the geogrid layer. Reinforcing clay resulted in a slight improvement, while significant improvement was observed when a geogrid was embedded in such a thin sand layer. As shown in Figure 2.22 and Table 2.1, a 10 mm thick sand layer provided the optimum improvement. This thickness increased the peak shear stress of reinforced clay under a normal stress of 75 kPa by 65%, in addition to improving the cohesion and friction angle significantly. This indicates that geogrids with clay were not mobilised during the tests due to their low efficiency in restraining the sliding of

particles with much smaller sizes than the geogrid apertures. This is in agreement with Bergado, Chai, Abiera, Alfaro, and Balasubramaniam (1993), who found that the strength of soil depends on the geogrid opening size. The effect of particle size on the overall restraining ability of geogrids was also reported by Touahamia, Sivakumar, and McKelvey (2002).

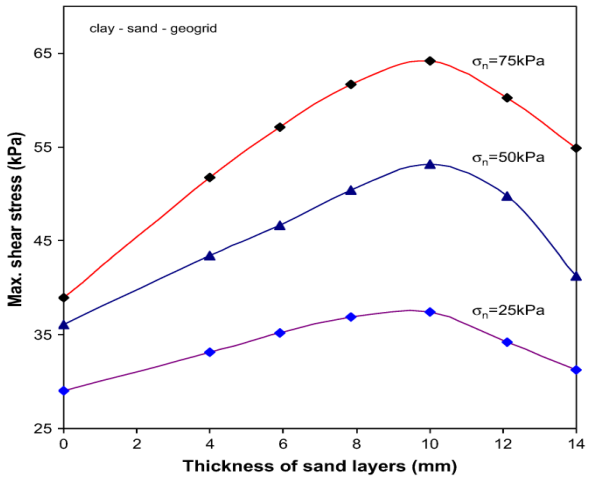

Figure 2.22 Maximum shear stress-thickness relationship of sand layers for clay-sand-geogrid samples (Abdi et al, 2009)

Table 2.1 Strength parameters of clay, sand and clay-sand-geogrid

Sample type	Ø (°)		C (kPa)	
	Unreinforced	Reinforced	Unreinforced	Reinforced
Clay	10	7.9	23.2	28.8
Clay-4 mm sand layer	15.5	23	14.5	20.8
Clay-6 mm sand layer	16.8	24.1	15.9	23.5
Clay-8 mm sand layer	17.3	26.4	16.3	23.6
Clay-10 mm sand layer	19.9	28.4	18.5	24.5
Clay-12 mm sand layer	25.8	26.4	17.4	22.3
Clay-14 mm sand layer	28	25.3	17.5	18.9
sand	33.7	36.1	12.1	12

Soil-geogrid interface strength is not solely attributed to the shear resistance between sand particles and grid surfaces, but also to the passive resistance provided by the transverse ribs. This contribution of passive resistance by transverse ribs was well defined recently by Z. Wang, Jacobs, Ziegler, and Yang (2017), who reported that geogrids with transverse members outperformed those that did not. This agrees well

with results obtained from pullout tests (Bergado et al., 1993; Jewell, 1990; Palmeira, 2004) and direct shear tests (Bergado et al. (1993). However, Lopes (2002) found only a low amount of passive resistance produced by the transverse members of geogrids.

Geogrids also improve soil behaviour under cyclic loading. Without reinforcement, increasing numbers of load cycles can cause degradation and damage in base coarse layers, leading to lower angles of load distribution, increased transformed vertical loads to the bottom layers of soil, and larger deformations (Giroud & Han, 2004). For reinforced soil, however, repeated loads mobilise the tensile strength of geogrids and improve the deformation response of soil. It can reduce the lateral movement of soil and therefore decrease rutting in pavement. Furthermore, reinforcement plays a clear role in improving the flexural characterisation of base layers of soil under footings, which is accompanied by increases in the load distribution angle (Abu-Farsakh & Chen, 2011; Giroud & Han, 2004). In other words, it leads to increases in the safety factor of the bearing capacity due to decreasing the normal stress transmitted to the subgrade or deeper layers under footings. Figure 2.23a shows that geogrid reinforced samples (properties of geogrids are illustrated in Table 2.2) exhibited better performance than unreinforced sample (Abu-Farsakh & Chen, 2011). Furthermore, Figure 2.23b illustrates that the sample reinforced with a geogrid placed at the upper one-third shows a lower amount of accumulated permanent strain than samples with a geogrid placed in the middle (Abu-Farsakh & Chen, 2011). This agrees well with the observations obtained using pressure cells, which revealed that reinforcement decreased transmitted stresses significantly. Using cyclic plate loading tests, for example, Qian, Han, Pokharel, and Parsons (2010) reported that the transmitted vertical stress decreased to about half its value when no geogrid was used. Furthermore, Abu-Farsakh and Chen (2011) reported that with geogrid reinforcement placed in the upper one-third, only 60 kPa of normal stress was transmitted under the centreline of the loading after 30,000 cycles, compared with 175 kPa for unreinforced soil. This redistribution of the applied stress led to decreases in the permanent deformation of weak subgrade soil (75% sand and 25% kaolinite) reinforced with two types of geogrid under cyclic load by 29.3% compared with unreinforced soil (Qian et al., 2010).

As mentioned in Section 2.3.1.3, it is necessary to create adequate interaction between soil and embedded reinforcement layers to mobilise its tensile strength. In the field, this interlocking can be achieved during compaction when particles penetrate and project through geogrid holes (Abu-Farsakh & Chen, 2011). Therefore, this interlocking can be weak when a geogrid is placed between two layers of crushed limestone with smooth, hard surfaces. Abu-Farsakh and Chen (2011) suggested that applying a prime coat on the surface before placing the geogrid would give good results.

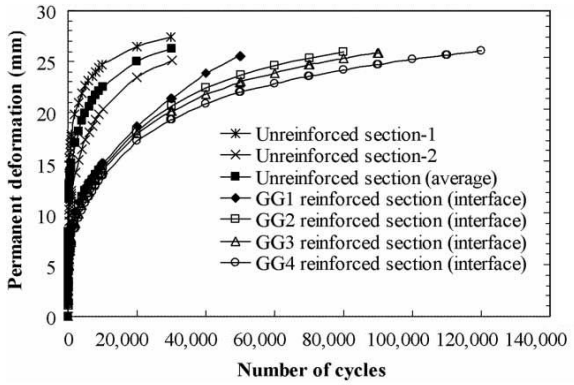

Figure 2.23a Permanent deformation—number of load cycles for different types of geogrids embedded at the interface between subgrade and base layers (Abu-Farsakh & Chen, 2011)

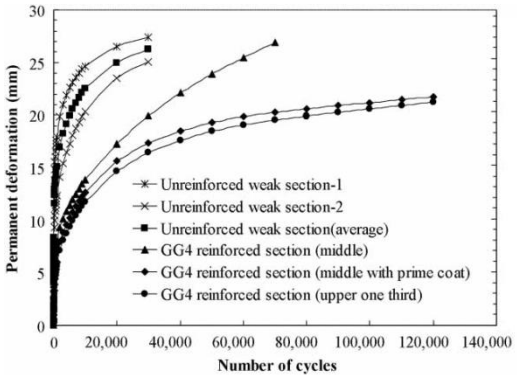

Figure 2.23b Permanent deformation—number of load cycles for GG4 (see Table 2.2) embedded at middle and upper one third of base layer (Abu-Farsakh & Chen, 2011)

Table 2.2 Properties of geogrids used by Abu-Farsakh and Chen (2011) and Abu-Farsakh, Souci, Voyiadjis, and Chen (2011)

Reinforcement	Aperture shape	Tensile strength (kN/m at 2% strain)	Aperture size (mm)
GG [a]	Rectangular	7.3 × 7.3	25.4 × 25.4
GG1 [a, b]	Rectangular	4.1 × 6.6	25 × 33
GG2 [a, b]	Rectangular	6.0 × 9.0	25 × 33
GG3 [a, b]	Triangular	8.6	40 × 40 × 40
GG4 [a, b]	Triangular	9.5	40 × 40 × 40

[a] used only by Abu-Farsakh et al. (2011)
[b] used only by Abu-Farsakh and Chen (2011)

It should be mentioned that loads applied during plate load tests are a vertical concentrated type, while in real situations, soil elements are subjected to various conditions and loading types, e.g. moving wheel loads, that cause multiple stress paths of compression-extension-compression, continuous rotation of principal stress direction, and various combinations of radial, axial and shear stresses. Under such conditions, a series of movements, slides and rearrangements of soil particles occurs, resulting in dramatic degradation of pavement or/and soil layers. This degradation causes a significant reduction in the strength of reinforced materials and a high amount of induced plastic deformation. In other words, moving wheel loads have much greater negative effects on pavement compared with cyclic plate load tests (Abu-Farsakh & Chen, 2011; Q. Chen & Abu-Farsakh, 2010; X. Yang et al., 2012).

Repeated-load triaxial tests were used to investigate the behaviour of crushed limestone while considering factors such as the arrangement, tensile strength and the geometry of the geogrid (Abu-Farsakh et al., 2011). The five types of reinforcement used in their study are shown in Table 2.2. Reinforcement was placed as a single layer at the middle or at the upper one-third, and as two layers at one-third from the top and bottom. It was found that induced permanent deformation was reduced significantly due to the confinement effect of the geogrid, which restricted the sliding and rotation of particles. After 10,000 cycles, permanent strain reached around 2.95% for unreinforced and 1.24–1.6% for reinforced sand. The largest induced strain of reinforced sand was achieved (yielded) for GG1, while the lowest amount of plastic strain was achieved for GG4. Double layers exhibited significant improvement, where the reduction in permanent strain was 20% larger than for a single layer at the middle or in the upper one-third.

Naeini et al. (2013) studied the effects of fines content (0–45%) on the interface shear strength of geogrid-reinforced sand. For all contents of fines, they observed that reinforced samples showed greater shear strength compared with unreinforced samples. The shear strength of reinforced and unreinforced sand decreased as silt content was increased to 35%, then strength increased slightly. Adding fines to geogrid-reinforced sand resulted in a lower post-peak loss of strength, indicating that the behaviour changed to being more ductile. However, as silt content increased, the

benefit of reinforcement decreased. For example, C_{reinf} ./ $C_{unreinf}$ and $Ø_{reinf.}$ / $Ø_{unreinf}$ were 11.2 and 1.06, respectively, for clean sand, while they became 3.5 and 1.03 respectively with 10% silt. There are limited studies about the effects of fine material on the behaviour of reinforced sand. However, the effects of fines on the stress-strain characteristics of sand are discussed generally in Section 2.4.

2.3.1.5 Previous studies on geotextiles

As mentioned previously in Section 2.3.13, the interaction between geosynthetics and geo-materials is affected mainly by ***a)*** the interaction mechanism between the reinforcement and the soils, and ***b)*** the physical and mechanical properties of the soils and geosynthetics (Tuna & Altun, 2012). Due to the fact that geotextile layers have a greater surface area than geogrids (i.e., greater interface between the soil and the geotextile) and do not have apertures, reinforcing thus depends mainly on the interface characteristics.

In general, it has been found that increasing the number of layers, i.e., reducing reinforcement spacing, increases the strength of soil (Chandrasekaran, Broms, & Wong, 1989; Haeri et al., 2000; Latha & Murthy, 2006; Nguyen et al., 2013; Nouri, Nechnech, Lamri, & Lopes, 2016; Tafreshi & Asakereh, 2007), as shown, for example, in Figure 2.24 (Chandrasekaran et al., 1989). Nguyen et al. (2013) reported that geotextiles have significant effects when placed at a spacing ratio, i.e., geotextile spacing divided by sample diameter, of 1.1–1.3. This agrees with Gray and Al-Refeai (1986), who demonstrated that increasing the spacing ratio to more than 1.0 results in geotextiles having insignificant effects on the behaviour of reinforced samples. Further, as confining pressure increased, the strength of reinforced sand increased while the improvement ratio q_{reinf} / $q_{unreinf}$ decreased (Haeri et al., 2000; Nguyen et al., 2013), as shown in Figure 2.25 (Haeri et al., 2000). Increased strength is attributed to larger confining pressure mobilising greater tensile strain. However, the decrease in the improvement ratio is related to the fact that larger confining pressures lead to lesser interaction between the reinforcement layers and the soil (Haeri et al., 2000; Tafreshi & Asakereh, 2007). This can also be explained as the larger confining pressure causing densification of the pure sand, as sand particles are easily moved, while the inclusion of geotextiles can resist this tendency.

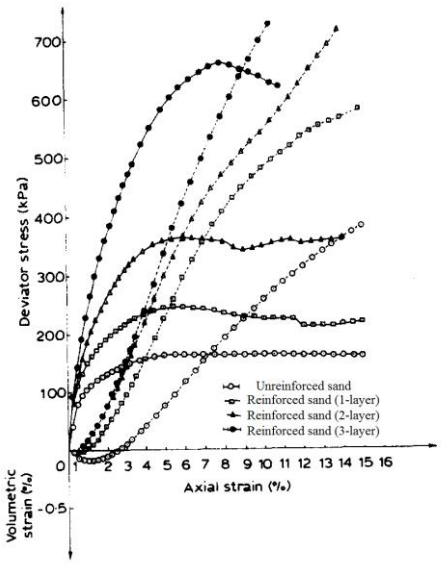

Figure 2.24 Deviator stress and volumetric strain versus axial strain of reinforced samples (Chandrasekaran et al., 1989)

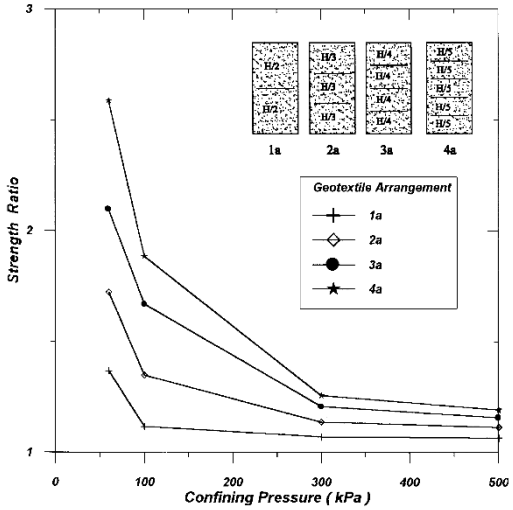

Figure 2.25 Strength ratio for reinforced samples (geotextiles of T = 8.4 kN/m) under different confining pressures (Haeri et al., 2000)

Several researchers have reported that geotextiles have significant effects at larger strain levels, while there is no clear enhancement at low strains (Haeri et al., 2000; Nguyen et al., 2013; Nouri et al., 2016; Tafreshi & Asakereh, 2007). This is similar to what was reported for geogrid reinforcement, where geosynthetics require a certain amount of strain or stress to be mobilised and act as tensile membranes. For example, Tafreshi and Asakereh (2007) found that $(q_p)_{reinf} / (q_p)_{unreinf}$ for four layers of reinforced sand increased from 1.28 at an axial strain (ε_z) of 3% to 3.31 at ε_z = 15%. Figure 2.26 explains a similar trend where $(q_p)_{reinf} / (q_p)_{unreinf}$ increased as the axial strain and number of geotextile layers increased (Nouri et al., 2016).

Inclusion of geotextiles increases the axial strain at failure, changing soil to be more ductile, and reducing the loss of post-peak strength (Chandrasekaran et al., 1989; Haeri et al., 2000; Nguyen et al., 2013; Nouri et al., 2016; Tafreshi & Asakereh, 2007). Tafreshi and Asakereh (2007) reported that there are no signs of failure or shear bands even after 20% axial strain. Furthermore, an important effort was made by Nguyen et al. (2013) to measure the plastic strain accumulated in geotextiles during shearing using a high resolution digital camera. Geotextiles were marked with grids, then

several images were taken of them before they were imbedded in the soil (before deformation) and after completing the test (after occurrence of deformation). Plastic deformation was computed by determining the number of pixels between two adjacent points along the grid before and after deformation. It is notable that such a method helps to measure only the residual strain due to plastic deformation but not the whole mobilised strain during loading. Nguyen et al.'s observation was consistent with and confirmed the previous findings where the plastic strain induced within the geotextile increased with increasing numbers of reinforcement layers and increasing confining pressure. However, the increasing rate of induced strain decreased with increasing confining pressure, and this can explain the observed decrease in $q_{reinf} / q_{unreinf}$. For example, the tensile strains induced in the transverse direction of three layers of geotextile were 42% and 90% under σ_3 = 50 and 200 kPa, respectively. For the longitudinal direction, the induced tensile strain increased slightly from 25% to 29% as σ_3 increased from 50 to 200 kPa.

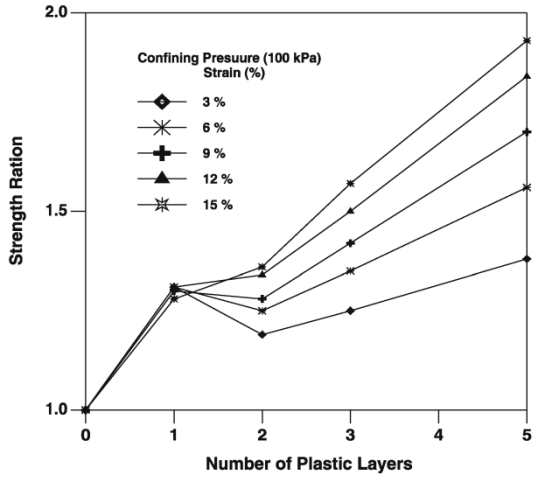

Figure 2.26 Strength ratio of reinforced samples with different numbers of geotextile layers under various strain level (Nouri et al., 2016)

On the other hand, Haeri et al. (2000) tested samples reinforced with geotextiles of different tensile strengths. They found that the geotextile with greater tensile strength and elongation provided the maximum improvement. The observed improvement in the shear strength of sand could not be totally attributed to the tensile strength of the reinforcement, due to the fact that polyester film gave the maximum improvement despite having lower tensile strength than woven geotextiles (Latha & Murthy, 2006).

This can be explained based on the observation of scanning electronic microscope images that showed that sand particles penetrated the surface of the polyester film, made clear indentations, and were housed inside these indents (Latha & Murthy, 2006). This resulted in increased friction of the interface. To confirm this effect on the strength of reinforced samples, further tests were conducted using rice flour as a matrix instead of sand, because it does not cause scratches, penetrations and indentions to the surface of polyester. The results showed that without these aforementioned indents, samples reinforced with polyester film exhibited less deviator stress than those reinforced with geotextiles (Latha & Murthy, 2006).

Reinforcement provides significant improvement of apparent cohesion and friction angle for whole reinforced samples (Latha & Murthy, 2006; Nouri et al., 2016). For example, Latha and Murthy (2006) found that the cohesion increased from zero to about 316 kPa with eight layers, while the friction angle increased from 42° for sand to about approximately 44.7° for three and four layers and to 47.5° for eight layers. This partially agrees with Nguyen et al. (2013), who observed significant increases in apparent cohesion while there was no effect of reinforcement on friction angle. On the other hand, the interfacial friction angle has also been investigated by many researchers such as Anubhav and Basudhar (2013), who found that geotextile inclusion decreased the interfacial friction angle from 46° to 40° for sand with angular particles, and from 36° to 35° for sand with rounded particles. Similar results for interfacial friction angles were reported more recently by Afzali-Nejad, Lashkari, and Shourijeh (2017).

Regarding volumetric strain, Nouri et al. (2016) reported a significant restraint of the dilation volumetric strain of dense sand during drained triaxial tests. As the number of reinforcement layers increased, samples exhibited more contractive and less dilative behaviour. This behaviour agrees with many studies, such as Consoli, Montardo, Prietto, and Pasa (2002) and Michalowski and Čermák (2003). However, some studies, such as Chandrasekaran et al. (1989) as shown in Figure 2.24 and Nguyen et al. (2013), reported a different trend, in which the dilation increased with increasing reinforcing layers. Further, Nouri et al. (2016) reported that reinforced samples exhibited the largest compressive response at axial strain less than 7.5% (Figure 2.27),

then they tended to dilate. They interpreted this compressive strain as a consequence of decreases in the thickness of the geotextile layers. We think that this reported compression strain is larger than expected. Indeed, the thickness of the geotextile layers was too thin (0.2 mm) and, even if we assume most of this thickness was compressed under loading, this amount is very little compared with the total compressive strain (9%).

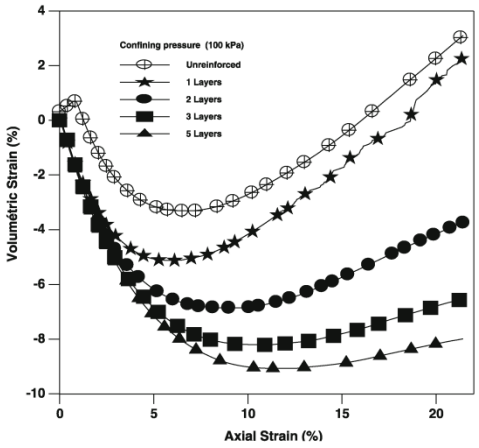

Figure 2.27 Volumetric strain versus axial strain of reinforced sand (Nouri et al., 2016)

Some dynamic properties of geotextile-reinforced sand using cyclic triaxial tests were investigated by Naeini and Gholampoor (2014). Figure 2.28a shows that increasing the number of geotextile layers increases the axial modulus of samples. Furthermore, similar to the aforementioned trend for many studies using monotonic testing, the axial modulus increased with increases in confining pressure, although the rate of increase decreased. Under cyclic load, reinforcement resulted in decreases in strength under constant applied stress and this consequently lead to decreases in cyclic ductility, as represented by the area enclosed within the hysteresis loop (Figure 2.28b). However, the damping ratio computed for such a hysteresis loop seems to not have been affected by either the number or arrangement of the geotextile layers (Naeini & Gholampoor, 2014). This is because the damping ratio is a function of the loading velocity (Ravishankar, Sitharam, & Govindaraju, 2005) which is constant in their results (f = 6 Hz).

Similar to what was mentioned in Section 2.3.1.4, placing geotextile layers near the load surface gives the best reinforcement performance (Naeini & Gholampoor, 2014). Similar recommendations were made by Tafreshi and Asakereh (2007), who concluded that there is an insignificant effect of reinforcement layers placed at great depths underground. This can be observed clearly in Figure 2.28a, where increases in the embedded depth (from the surface) decrease the shear modulus. This trend occurs because the effect of the applied load or its frequency is greatest near the surface (top and bottom) (Naeini & Gholampoor, 2014).

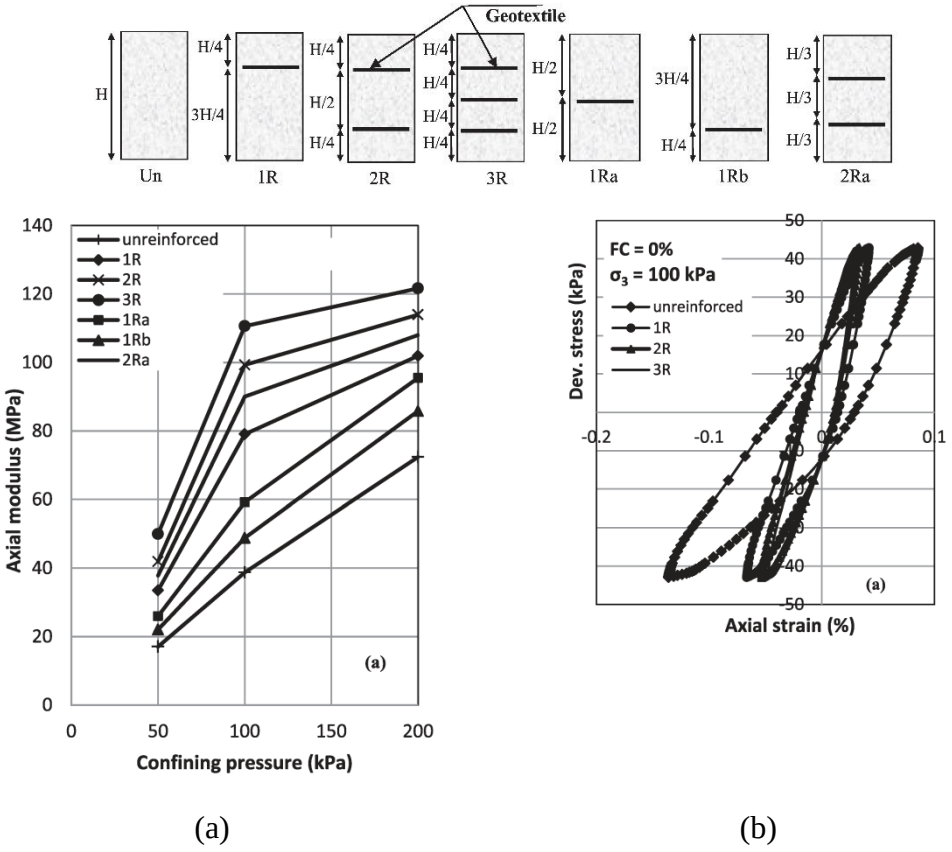

(a) (b)

Figure 2.28 (a) Axial modulus versus confining pressure for reinforced samples with different arrangements, and (b) effect of geotextile layers on cyclic ductility (Naeini & Gholampoor, 2014)

2.3.1.6 Previous studies on geocells

The latest advancement in soil reinforcement is to provide three-dimensional confinement using geocell mattresses. This geosynthetic material was developed by the US Army Corps of Engineers in the 1970s, and can be described as a three-

dimensional polymeric cellular network interconnected by joints. It is often fabricated from HDPE sheets or other materials and welded together ultrasonically to give an open-cell structure for containing soil (Rajagopal, Krishnaswamy, & Latha, 1999)

Geocell materials come in a collapsed form, such as a foldable three-dimensional geometry, and form a honeycomb shape after being stretched and filled with soil to cover an area of about 2.44 × and 6.6 m (X. Yang et al., 2012). In pavement construction, geocells are put on the geotextile that is laid first (to separate the infill material from the soft soil). This type of geosynthetic confines the soil within its pockets and produces a highly stiffened foundation mattress which reduces lateral movement, intercepts the potential failure plane, distributes applied loads deeper to a wider area, and consequently, increases the bearing capacity (Dash, Krishnaswamy, & Rajagopal, 2001; Han, Yang, Leshchinsky, & Parsons, 2008). Therefore, it is used below the high contact pressure areas of footings, pavements, grade crossings and transitions. It is also used in the applications of track and pipe excavation to provide a stiffened mat to support narrow fills over compressible soil (Bathurst & Karpurapu, 1993). It can also be used in many other applications, such as slopes, erosion control and the ballasted foundations of railways (Leshchinsky & Ling, 2012).

Compared with other types of geosynthetics, geocells have not been well investigated (X. Yang et al., 2012). To study the effects of geocells on the behaviour of soils, geocells are mainly fabricated by stitching or gluing different fabrics into single or multi-cylinder shapes. Two main points need to be noted regarding the fabrication of geocells. Firstly, seam tensile strength is very important in geocells, where often this strength is much lower than the tensile strength of the parent material and, thus, samples can fail due to ruptures occurring in the joint (i.e., seam). Second, the elongation required to mobilise the ultimate tensile strength has an effect on the stress-strain relationship of the geocell reinforced sand.

Rajagopal et al. (1999) investigated the effects of the stiffness of geocells fabricated from different materials on the overall behaviour of sand (D_r = 55%). Table 2.3 illustrates the tensile and seam strengths of the geosynthetics used. They found that geocells made from woven geotextile exhibited larger deviator stress than those made from nonwoven geotextile (Figure 2.29), although the woven geotextile had lower

seam tensile strength. This is attributed as above-mentioned elongation characteristics of the fabric materials, where a 10% axial strain can mobilise a seam tensile strength of 7.5–8 kPa for a woven geotextile, compared with only 0.5 kPa for a nonwoven one. This means that woven geotextiles can be mobilised under low strain and, consequently, provide significant improvement to the sample strength. Similar trends were observed by Latha and Murthy (2007), where the strength of sand increased by 113% and 360% when reinforced with polyester geocells (tensile seam strength = 4.6 kN/m) and geotextile geocells (tensile seam strength = 3.7 kN/m), respectively. Furthermore, it was reported that the failure occurring in unreinforced sand could be observed clearly, while reinforced sand did not fail even when the test was terminated at 15% axial strain (R. Chen, Huang, & Huang, 2013). Evidently, the induced tensile strain mobilises the confining strength to prevent soil failure.

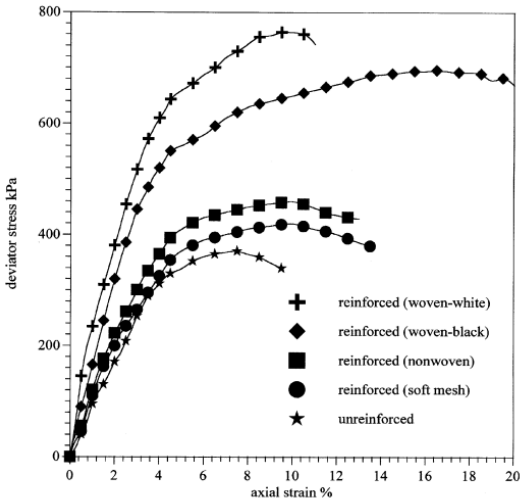

Figure 2.29 Stress-strain relationships for sand with different types of geocells (Rajagopal et al., 1999)

The effects of the length, number and shape of cells have been investigated by several researchers. Regarding the length of the cells, plastic bottles were used by Ram Rathan Lal and Mandal (2013) as cellular reinforcement, with different heights used to improve the behaviour of fly ash samples. It was found that the deviator stress of samples (under a confining pressure of 100 kPa) reinforced by a single geocell (placed at the middle) with 10, 20, 30 and 50 mm heights increased by 24, 36, 49.6 and 57%, respectively. This improvement increased to 38, 48, 53 and 57%, respectively, when

two layers of geocell with the same previous heights were used instead of a single layer and placed at one-third of the sample depth. However, for two layers players at the top and bottom, the improvement decreased to 1.6, 4.5, 13.2, and 14.8%, respectively. This trend is similar to that observed by Khedkar and Mandal (2009), who investigated the deviator stress of sand reinforced by aluminium cells with different depths (Figure 2.30). Such increases in cell length resulted in reductions in the transmission of loads from footings into the soil by distributing them over a vast area (Dash et al., 2001).

The shape, size and arrangement of cells also affect the behaviour of geocell reinforced sand. It was found that increasing the number of cells increases the deviator stress, as shown in Figure 2.31 (Rajagopal et al., 1999) and Figure 2.32 (R. Chen et al., 2013). This is because the confinement offered by cells per unit soil volume increases as the number of cells increases. Further, circular geocells gave greater strength than hexagonal ones, as they can be expanded more easily (Figure 2.33a) (R. Chen et al., 2013). The results revealed that reinforcement by multi-circular cells provided the greatest improvement, in contrast to multi-rectangular cells which exhibited the lowest strength (R. Chen et al., 2013). The largest improvement of strength for three-circle cells occurred rapidly after 10% axial strain.

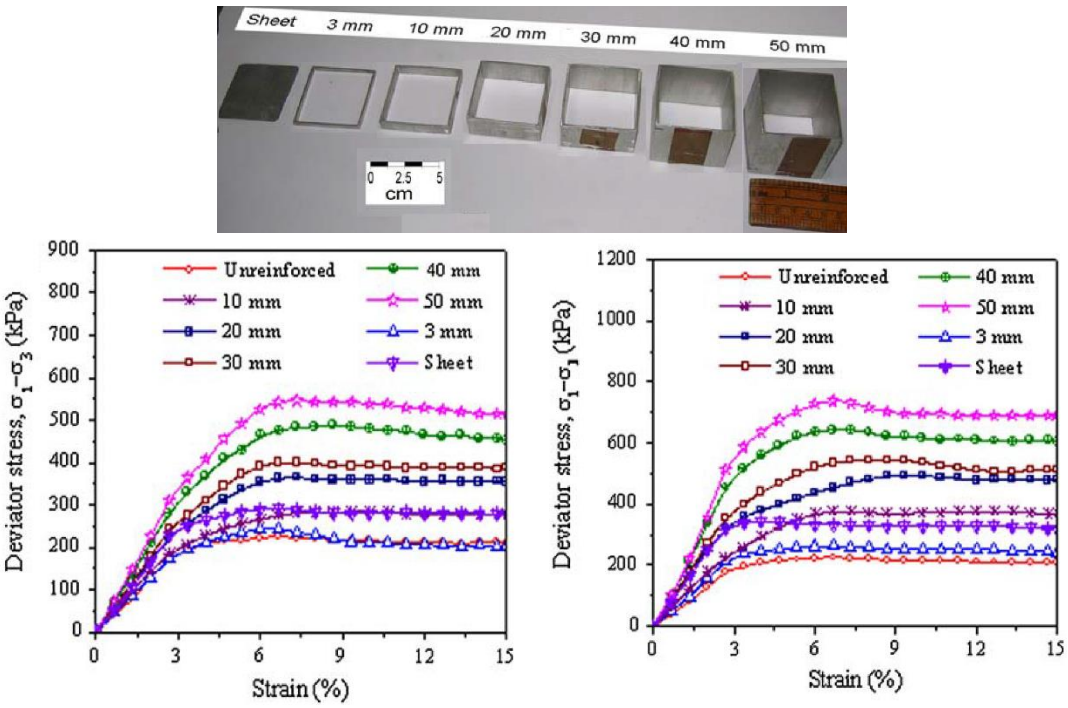

Figure 2.30a Stress-strain relationships for a single layer of geocell reinforcement (Khedkar and Mandal, 2009)

Figure 2.30b Stress-strain relationships for a double layer of geocell reinforcement (Khedkar and Mandal, 2009)

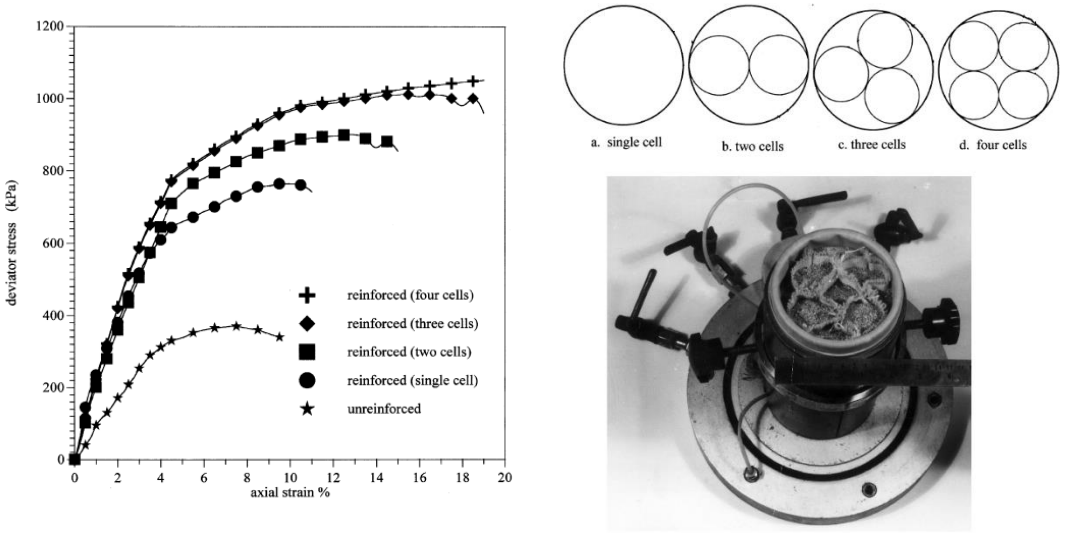

Figure 2.31 Stress-strain relationships for sand with different configurations of geocells (Rajagopal et al., 1999)

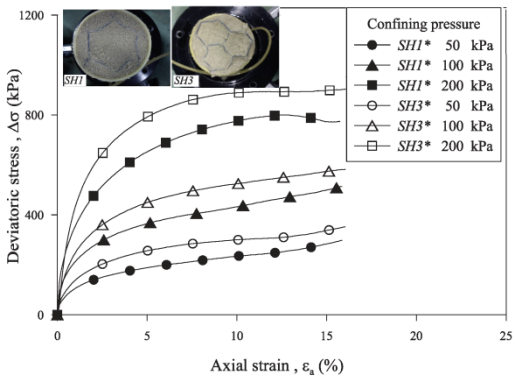

(a)

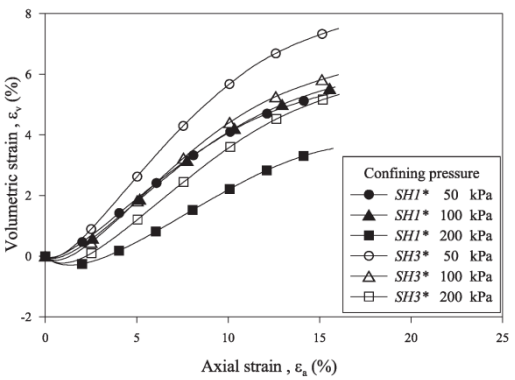

(b)

Figure 2.32 Results of samples reinforced with different numbers of cells (a) deviator stress-strain, and (b) volumetric-axial strain (R. Chen et al., 2013)

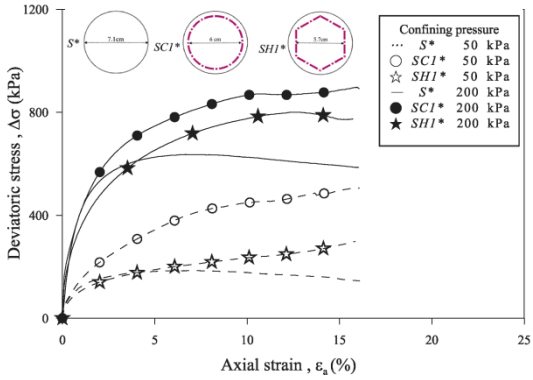

(a)

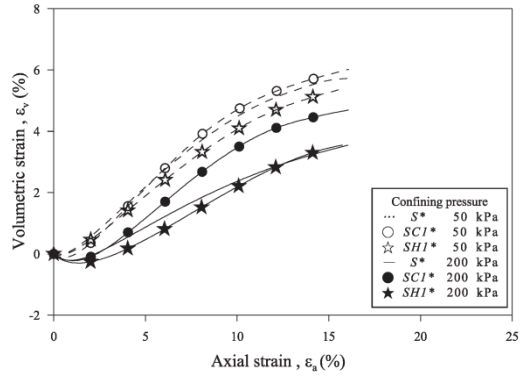

(b)

Figure 2.33 Results of samples reinforced with different shapes of cell (a) deviator stress-strain, and (b) volumetric- axial strain (R. Chen et al., 2013)

In general, the friction angle of sand is not changed significantly by reinforcement with geocells, while substantial cohesion has been reported (Bathurst & Karpurapu, 1993; R. Chen et al., 2013; Rajagopal et al., 1999). This trend is clear in Table 2.3, which summarises the results obtained by Rajagopal et al. (1999). However, Khedkar and Mandal (2009) reported that friction angle increased significantly, from 31.5° for unreinforced sand to about 37.2° and 41.7° for reinforced sand, with single and double geocells (50 mm depth), respectively. Mali and Singh (2015) demonstrated that geocells with high tensile strength (12 kN/m) exhibited increases in the friction angle, while geocells with low tensile strength (2 kN/m) caused an insignificant difference. Further, a combination of fibre and geocells increased the friction angle by 2–3° (Mali

& Singh, 2015). This improvement is attributed to the same mechanism of planar reinforcement, where the lateral spreading, i.e. expansion volumetric strain, caused under external static or cyclic loads will be reduced due to the confinement provided by the cells (Bathurst & Karpurapu, 1993). In contrast with previous studies, reported that geocell reinforcement did not provide restraint of volumetric expansion strain, as shown in Figures 2.32b and 2.33b.

Table 2.3 Properties of geocells and strength parameters of reinforced samples

Reinforcement	Tensile strength (kN/m)	Seam strength (kN/m)	*Ø* (°)	*C* (kPa)
Unreinforced	———	———	40.5	0
Woven geotextile (white): single cell	65	8	39.2	98.9
Woven geotextile (white): two cells			39.2	134.9
Woven geotextile (white): three cells			39.0	159.2
Woven geotextile (white): four cells			39.0	169.1
Woven geotextile (black): single cell	54.5	7.5	40.5	77.1
Nonwoven geotextile: single cell	9	9	40.9	17.3
Mesh reinforcement: single cell	1	1	40.5	11.0

Comparing with planar reinforcements such as geogrids and geotextiles, it was reported that the strength of sand reinforced with a planar reinforcement layer was larger than that of sand reinforced with geocell reinforcement (Lal, Sankar, & Chandrakaran, 2017; Latha & Murthy, 2007; Mali & Singh, 2015). This is related to the joints of the geocells being weaker than the strength of parent fabric itself, where the tensile strength of planar geotextile can be mobilised to its ultimate value under loading, while geocells are likely to fail at the weakest welding joint. For example, the seam strength for geocells fabricated from geotextile, was only 3.7 kN/m, compared with a 51 kN/m tensile strength for the parent geotextile (Latha & Murthy, 2007). Therefore, high-quality welding, as used for readymade geocells, can produce high

welding tensile resistance. The aforementioned significant improvement in strength-strain provided by geocells, although having low tensile strength, renders geocells the most efficient type of reinforcement (Lal et al., 2017; Latha & Murthy, 2007; Mali & Singh, 2015). This trend is different when soil under footings undergoes shear failure, where planar layers will be subjected to downward settlement such that most tensile strength cannot be mobilised (Yetimoglu, Wu, & Saglamer, 1994). However, passive and friction resistance developing along the walls of cells acts as beams or mattresses to support the footing (Dash et al., 2001). Therefore, soil reinforced with geocells provides greater bearing capacity than soil with other reinforcement types.

Many studies have investigated the bearing capacity of soil reinforced with geocells and have reported significant improvements (Dash, 2010; Dash et al., 2001; Han et al., 2008; Leshchinsky & Ling, 2012; Pokharel et al., 2010). For example, Han et al. (2008) demonstrated that geocells can increase the bearing capacity of sand (D_r = 70%) by 65% while decreasing settlement. They reported that axial and horizontal displacement of reinforced sand decreased by 2.5 times compared with unreinforced samples. Moreover, a laboratory model of an embankment reinforced with single and double layers of geocells sustained a maximum stress of 575–625 kPa, compared with 175 kPa for the unreinforced model. Additionally, lateral deformation was decreased by 41–79% (Leshchinsky & Ling, 2012). The embedded depth u of the geocell beneath a footing prevents the direct contact of the footing base with the geocell walls. Therefore, this embedded depth helps to distribute the footing pressure more uniformly over the geocells so that early buckling of the geocells is prevented (Gurbuz & Mertol, 2012). Maximum improvement can be achieved when the depth u of the reinforcement below the applied load equals 20% of the footing width, $B_{footing}$ (Yoon, Heo, & Kim, 2008). However, when $u/B_{footing}$ = 1.0, soil behaves as if unreinforced, and the geocells have no effect (Tafreshi & Dawson, 2010a, 2010b; Yoon et al., 2008). Furthermore, increasing the length and/or the width of geocells under a footing increases the area over which the load is distributed (Dash et al., 2001). For example, it was reported that bearing capacity increased as the width increased up to B_{cell} / $B_{footing}$ = 2–4, after which the improvement becomes marginal (Dash et al., 2001; Sireesh, Sitharam, & Dash, 2009; Tafreshi & Dawson, 2010a, 2010b; Yoon et al., 2008). However, Gurbuz and Mertol (2012) demonstrated that increases in bearing capacity

are still significant until $B_{cell} / B_{footing} = 8.2$. Similar to the results obtained using planar reinforcement, i.e., geogrid and geotextile, increasing the distance between geocell layers (in the case of double layers) reduces the bearing capacity. For example, Gurbuz and Mertol (2012) demonstrated that improvement in the ratio of q_{reinf} / q_{un} decreased from 4–4.2 to about 3.76–3.84 as the ratio of vertical distance between the two geocell layers to the footing width increased from 0.142 to 1.42. This may be because the reinforcement is effective in the stress influence zone.

Most of the geocells used in the field have elliptical shapes. Experimental plate loading tests show that soil reinforced with circular geocells exhibit larger bearing capacity and less settlement than elliptical geocells (Pokharel et al., 2010). Elliptical geocells become circular under loading and this is also accompanied by a tendency for sand particles to move and lift outside the pocket, which may cause sudden failure (Pokharel et al., 2010). Therefore, increasing the interlocking at the interface between the geocell sand the infill can reduce the possibility for geocells to uplift and, consequently, increase the bearing capacity. Pokharel et al. (2010) conducted loading tests on two cases of geocell-reinforced samples. After placing a geocell layer at the centre of the test box, soil was poured inside the pockets for the unconfined case, and inside and outside the pockets for the confined case. Unconfined geocells suffered from rupture along the weld lines. However, for confined geocells, minimal lateral expansion took place and failure occurred due to uplifting of the geocell and escape of soil from the bottom of the geocells. Despite the failure along the welds, the bearing capacity of unconfined geocells was larger than that of confined ones. Pokharel et al. (2010) attributed this to associated lateral expansion that increases the area, allowing more load to be applied (Pokharel et al., 2010). However, we think it is because the larger lateral deformation in the unconfined case leads to very significant mobilisation of the geocells' tensile strength. Leshchinsky and Ling (2012) observed some rupturing at seams under monotonic loading when using a single layer, while no tearing was observed when double layers were used, although there was some bending. Passive and frictional resistance that develops at the interface of the interconnected geocell provides great anchorage from both sides of the loaded area (Dash et al., 2001). It was observed that geocells still provide support to soil even if the soil inside the cellular undergoes shear failure where the mechanism of the geocell layer is similar to

that of the beam (Dash et al., 2001). The entire geocell mattress acted as a single entity (Dash et al., 2001).

Under cyclic load, slight bending and some superficial scraping was observed for single and double layers of geocells used to reinforce laboratory models of embankments (Leshchinsky & Ling, 2012). Furthermore, the induced axial deformation under such cyclic loads were reduced by 52% and 48% for single and double geocell layers, respectively, compared with unreinforced soil. However, moving loads can cause more severe failures than cyclic loads. For example, X. Yang et al. (2012) observed that geocells failed due to cell bursting (where breakage occurred in the geocell joints) under wheel loads, resulting in soil escaping laterally by being squeezed out. They found that the performance of a 15 cm layer of geocell-reinforced sand is equivalent to that of a 15 cm layer of high quality unreinforced aggregate.

2.3.2 Cement Stabilisation

2.3.2.1 Introduction

Cement reinforcement has been used widely for many years as a common soil stabilisation method for a variety of applications in geotechnical engineering. This is because it is a very effective and quick way to improve bearing capacity, deformation behaviour, soil shear strength and workability. Generally, increasing the cement content results in a stronger, stiffer and more brittle material.

The behaviour of cemented soil has received considerable attention due to the realisation that natural, cemented sand is found in many countries, and because artificially-cemented soil is increasingly used in engineering applications. Its overall stress-strain and volumetric behaviour is usually required to be known for most design and construction works. This can be studied in terms of 1) the deviator stress, 2) the stress ratio versus axial strain and volumetric strain, and/or 3) the shear strain versus axial stress. These can be derived from plate load tests, unconfined compressive tests or triaxial tests. These properties mainly depend on the void ratio, the nature of the soil particles, and the cement content.

2.3.2.2 Stress-strain behaviour

Most studies report significant improvement in soil strength even with small amounts of cement. Increasing the cement content results in increased size and thickness of the bonds between particles (Marri, Wanatowski, & Yu, 2012). Moreover, increasing the cement content not only surrounds particles and bonds them together, but also fills voids as inclusions. This improvement in bonding results in increased unconfined compression strength, as shown in Figure 2.34 and 2.35 (Sariosseiri & Muhunthan, 2009) and Figure 2.36 (Marri, Uddin, & Wanatowski, 2014). Furthermore, decreasing the void ratio increases the soil strength, as the number of contacts between cemented sand particles are increased (Clough, Sitar, Bachus, & Rad, 1981; Consoli, Cruz, Floss, & Festugato, 2010; Consoli, Rotta, & Prietto, 2006; J. Huang & Airey, 1998).

Schnaid, Prietto, and Consoli (2001) found that unconfined compression strength $q_{unconfined}$ for 5% Portland cemented silty sand increased to 1168 kPa, compared with zero for untreated samples, as illustrated in Table 2.4. A similar trend was found by Sariosseiri and Muhunthan (2009), who reported that samples treated with 5–10% cement showed significant strength (Figure 2.34 and 2.35) while untreated samples and samples treated with 2.5% cement failed after being soaked in water. Gypsum has also been used as a cementing agent in different percentages, with significant improvements in unconfined strength achieved, as shown in Figure 2.37 (J. Huang & Airey, 1998).

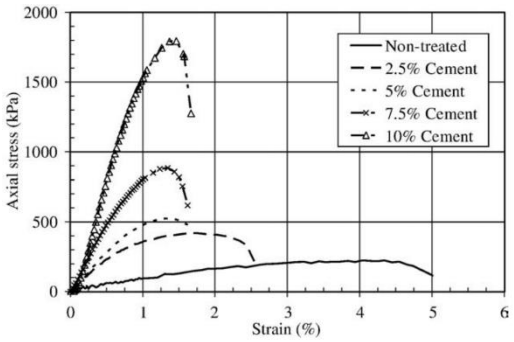

Figure 2.34 Effect of cement content on unconfined compressive strength (unsoaked) (Sariosseiri and Muhunthan, 2009)

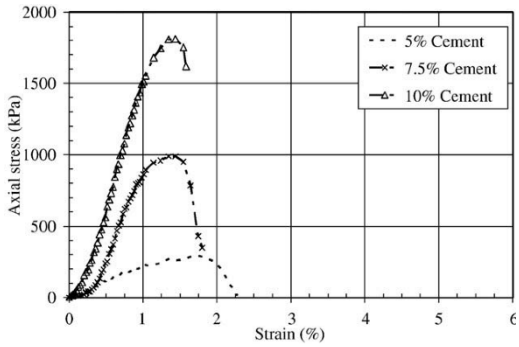

Figure 2.35 Effect of cement content on unconfined compressive strength (soaked) (Sariosseiri and Muhunthan, 2009)

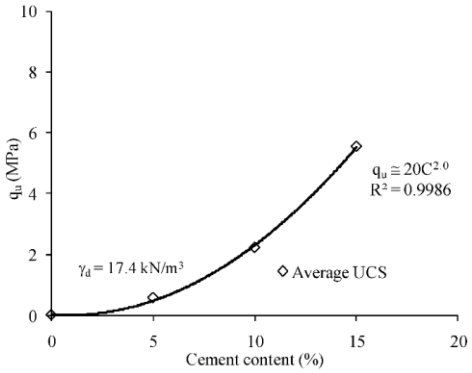

Figure 2.36 Effect of cement content on unconfined compressive strength (Marri et al., 2014)

Table 2.4 Shear strength parameters of sand-cement mixtures

Author (s)	Cement (%)	$q_{unconfined}$ (kPa)	q_f (kPa)	C (kPa)	$Ø$ (°)
Schnaid et al. (2001)	0	0	212	9.9	35
	1	305	510.2	56.7	41
	3	737	729.1	137.6	44
	5	1168	1355.7	276.7	39
Consoli, Vendruscolo, Fonini, and Dalla Rosa (2009)	0	-----	-----	0	36.7
	1	-----	-----	19.5	30
	4	-----	-----	84	39
	7	-----	-----	146.5	52
	10	-----	-----	328	48.5
Marri et al. (2012)	0	-----	2363	9.9	32.4
	5	-----	3800	56.7	40.6
	10	-----	8484	137.6	52.4
	15	-----	11124	276.7	56.6

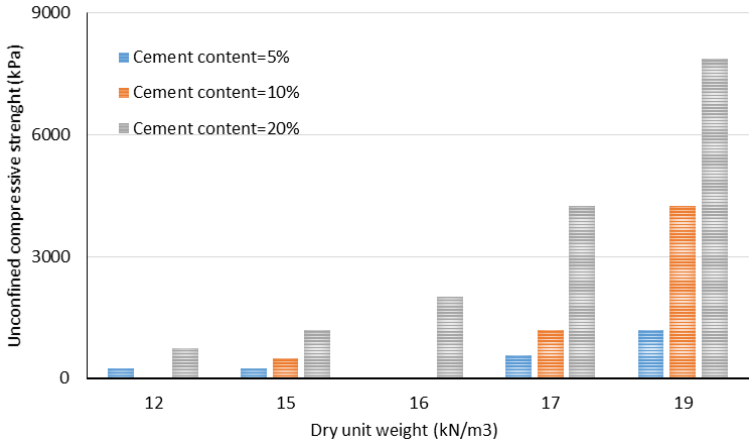

Figure 2.37 Effect of cement content on unconfined compressive strength

In addition to unconfined compressive tests, triaxial tests have been employed to investigate the behaviour of cemented soil. Schnaid et al. (2001) reported significant improvements in deviator stress at failure q_f and strength parameters for silty sand reinforced with 1, 3 and 5% cement, as shown in Table 2.3. Similar results were reported by several researchers such as Consoli et al. (2009), Marri et al. (2012), Rios, Da Fonseca, and Baudet (2014) and Rios, Ramos, Da Fonseca, Cruz, and Rodrigues (2017). For example, Consoli et al. (2009) reported that increasing cement content to 10% resulted in increased deviator stress by approximately 560% (Figure 2.38), while Rios et al. (2014) found that addition of 2–4% and 5–7% cement can increase the deviator stress five- and ten-fold, respectively.

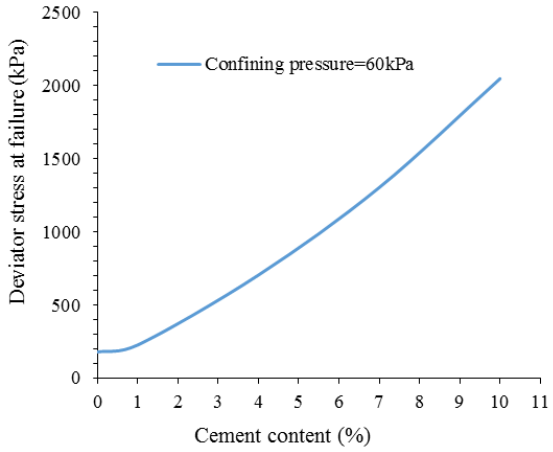

Figure 2.38 Effect of cement content on deviator stress (Consoli et al., 2009)

There is no general consensus regarding the correlation between friction angle and cement content. For example, Clough, Kuck, and Kasali (1979), Clough et al. (1981), Clough, Iwabuchi, Rad, and Kuppusamy (1989), Acar and El-Tahir (1986), Rad and Tumay (1986), O'Rourke and Crespo (1988), and Juran and Riccobono (1991) reported that uncemented and cemented samples have similar friction angles. However, Schnaid et al. (2001), Consoli et al. (2009) and Marri et al. (2012) found that although there is no correlation between friction angle and cement content, the average value of cemented samples is larger than that of untreated samples. For instance, the friction angle with 1% cement was less than that of clean sand, and the friction angle increased further with up to 10% cement.

However, most of the experimental studies report that increasing the cement content results in increased cohesion. Saxena and Lastrico (1978) suggested that at low axial strains (< 1%), the cohesion caused by the cement bonding between particles provides the major component of the strength. The cohesive shear strength vanishes at around 1% strain and, at the same time, the frictional strength becomes dominant. J. Huang and Airey (1998) demonstrated that the contributions of inter-particle friction and particle interlocking to the behaviour of soil are relatively more important at high densities, while the contribution of cementation is relatively more important at low densities. It appears that at high densities in artificially-cemented material, a significant proportion of the cement fills in voids and does not contribute significantly to inter-particle bonding. Thus, the effectiveness of a given proportion of cement decreases as the density increase.

Regarding deformation behaviour, cemented samples subjected to drained triaxial tests demonstrated linear and stiff stress-strain behaviour until the peak, then increasingly plastic strain until failure (Schnaid et al., 2001). This trend corresponds with decreasing axial strain at failure, clear initial compression strain followed by significant dilative strain, and a change in behaviour from ductile to brittle (Marri et al., 2012; Schnaid et al., 2001). Maximum dilation took place immediately after the peak deviator stress and corresponded with the initiation of bond breakage (Consoli et al., 2009; Da Fonseca, Rios, Amaral, & Panico, 2013; Marri et al., 2012; Schnaid et al., 2001). This observed dilative behaviour means that there is rearrangement of the particles, which is only possible after cementation breakage, and thus, the destruction of bonding likely began prior to peak deviator stress (Menéndez, Zhu, & Wong, 1996).

Dos Santos, Consoli, and Baudet (2010) and Lee, Hong, Choi, and Lee (2010) mentioned that larger stresses are necessary to yield cementitious bonds between particles. This is consistent with Saxena and Lastrico (1978), who reported that a very high confining stress can break cementitious bonds. The yield of cemented sand is approached when the bonds created by the cementing agent gradually break, after which the stresses will be carried by the new, destructed (uncemented) matrix of the host grains and broken cement (Coop & Atkinson, 1993; Hamidi & Haeri, 2008).

The deformation of cemented soil induced under cyclic load was investigated by Da Fonseca et al. (2013) using cyclic drained and undrained triaxial tests. They reported that there was no plastic strain in samples with more than 7% cement content under low cyclic stress (5–45 kPa) (Figure 2.39). However, untreated sand suffered from plastic creep strain, in which a significant and increasing amount of permanent deformation took place with increasing numbers of cycles. Samples with 2% cement exhibited lower induced strain until 20,000 cycles, at which time, dramatic plastic strain occurred. This is linked to the role of cementation bonds that resist the development of plastic strain until a certain number of cycles, after which the bonds degrade and breakage results in rapidly accumulated strain. Therefore, the deformations of both untreated and 2% cemented sand become almost identical after 500,000 cycles. Under high cyclic stress, all cemented samples, even those with 7% cement content, exhibited cyclic plastic deformation after 30,000 cycles.

The load-settlement characteristics of cemented sand layers were investigated by Consoli, Vendruscolo, and Prietto (2003) using plate load tests. Cemented sand layers (7% cement content) were constructed over residual soil. They observed that for settlement equal to or less than 8 mm, the bearing load of cemented sand was 98 kN, compared with only 20 kN for the uncemented residual layer. With increasing settlement, an abrupt decrease in the bearing load was observed for the cemented sand layer, which approached that of the untreated layer. This sharp decrease is attributed to tension fissures starting on the bottom of the cemented sand layer, and the gaps induced in the layers.

Despite the extensive studies on cemented sand, there is a lack of studies that have investigated combined fabric and bonding (Gao & Zhao, 2012). The available studies investigating anisotropic effects on cemented sand have focused on fine materials used as cementing agents, such as clay and silt. Eghbali and Fakharian (2014) investigated the effect of principal stress rotation on cemented sand (0, 1.5, 3 and 5%). Undrained triaxial tests were carried out on samples (D_r = 10–15%) under compression conditions of α = 0° and b = 0, and under extension conditions of α = 90° and b = 1.0. Clear anisotropic behaviour was represented by the significant difference between the deviator stresses observed at α = 0° and α = 90°. For clean sand, the peak deviator stress was 174 kPa under α = 0°, while it was only 41 kPa under α = 90°. Adding

cement contents of 1.5, 3 and 5% resulted in increases in peak deviator stress to 650, 1000 and 1080 kPa, respectively, under α = 0°. However, under α = 90°, it became 280–310 kPa for all cement contents.

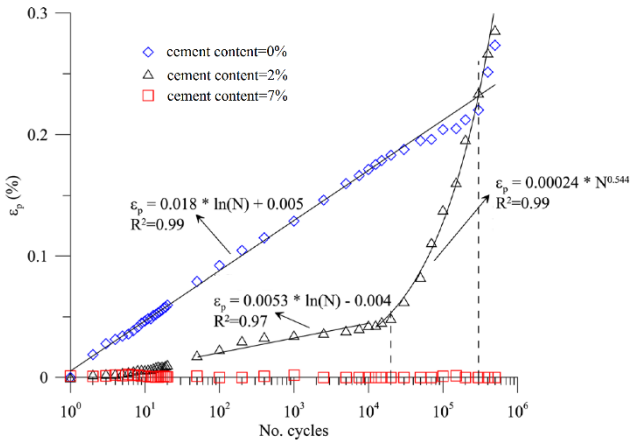

Figure 2.39 Development of plastic strain with increasing numbers of load cycles for cemented sand (Da Fonseca et al., 2013)

2.4 Fine-sand Mixtures

Mixtures of fine material (such as clay and silt) and coarse aggregate (such as sand and gravel) occur widely in nature in many countries, including Australia. Artificial mixtures are also widely used in geotechnical practice; for example, to reduce settlement after construction. Although many researchers have investigated the behaviour of such mixtures, most studies have focused either on the properties of the coarse components (H. Chen & Wan, 2004; Coli, Boldini, Bandini, & Lopes, 2012; Y. Li, Huang, Chan, & Chen, 2013; Lindquist & Goodman, 1994; Medley, 2004; Medley & Lindquist, 1995; Wen-Jie, Qiang, & Rui-Lin, 2011; Xu, Hu, & Tan, 2007) or on the compression and shear strength of fine materials (Cabalar, 2011; Georgiannou, Burland, & Hight, 1990; Kumar & Wood, 1999; Skempton, 1985; Vallejo, 2001; Vallejo & Mawby, 2000). There are very limited studies on the anisotropic behaviour of sand-fine mixtures or on reinforced mixtures. In other words, soil mechanics research has focused mainly on clean soils, while silty or clayey sands have been assumed to behave like clean sand. However, awareness of the significant

effect of fines content on the behaviour of sand has encouraged researchers to investigate this issue.

The strength of a mixture depends on the amount of fines and the way they are distributed within the sand. Mollins (1996) reported that strength is a function of the relative volumes of the mixture. Strength is governed by the sand matrix for high sand content mixtures, by the fines matrix for high fines content mixtures; or by a combination of both. For a small amount of clay, the behaviour of the mixture is controlled by the sand, which forms a continuous skeleton structure to sustain the applied stress, while the small amount of fines fills the voids (Mollins, 1996). Increasing the fines content causes the behaviour of the mixture to be controlled by the fines instead of the sand. For a certain percentage of clay, i.e. 7–8% as reported by Mollins (1996) and Georgiannou (1988), clay becomes concentrated on the surfaces of sand particles and at their contacts, forming bridges and bonds Fei (2016) demonstrated that such bridges lead to a stable force chain that sustains the applied load. Generally, it was reported that increasing the clay content increases the brittleness and decreases the shearing angle (Mollins, 1996; Shafiee, Tavakoli, & Jafari, 2008). However, there are some studies that have reported an opposite trend, such as Çabalar and Mustafa (2015) who reported decreasing shear strength as the sand amount increases. This conflict reflects the variable roles of sand and clay in carrying loads (Fei, 2016).

Mollins (1996) performed drained triaxial tests on sand containing different percentages of bentonite. It was found that adding 5 or 10% clay resulted in greater strength than that of clean sand, whereas when the clay content was increased to 20%, the strength was lower. A different trend, however, was found by Carraro, Prezzi, and Salgado (2009), where the strength of sand decreased due to addition of 2, 5 and 10% clay. For large contents of clay, sand exists as inclusions within the fine matrix, in which there are no contacts between sand particles and, thus, compressive volumetric strain dominates during shearing. With more shearing, more interactions will occur, resulting in closer packing and dilation. This means that the mixture will shear like a fines material until sufficient compressive volumetric strain occurs that brings sand particles into closer proximity.

The effect of non-plastic fine content was also investigated by several researchers including Salgado, Bandini, and Karim (2000), who performed drained tests on loose and dense samples of Ottawa sand with different silt contents (0–20%). Loose mixtures have greater deviator stresses than clean, loose sand, where the increasing ratio reached 23.45% for a 20% silt content under 400 kPa confining pressure. Similar findings were reported by Carraro et al. (2009), where the peak deviator stress of sand increased by 16.1% when mixed with 15% silt. Regarding the dense state, a similar trend of increasing peak deviator stress was observed, noting that there was a considerable post-peak loss compared with the loose state (Carraro et al., 2009; Salgado et al., 2000). In contrast, Hsiao, Phan, Hsieh, and Kuo (2015) reported a decrease in deviator stress and friction angle with increasing silt contents of up to 50%, which then increased to be almost similar to that of clean sand. They explained this based on Thevanayagam, Shenthan, Mohan, and Liang (2002) study, where reduction in strength occurred when sand particles were the primary contributor to the mixture's shear strength with silt having a secondary role. However, when strength began increasing, fines start to dominate the behaviour while sand particles dispersed and contributed to a secondary reinforcement role. Strength improvement was associated with increasing compressive volumetric strain in a loose state, and expansion strain for a dense state (Carraro et al., 2009; Salgado et al., 2000). However, under undrained triaxial testing, residual strength decreased considerably with increasing silt content, reaching a minimum at a fines content of F = 30%. It then started to increase steadily with increasing fines content but remained weaker than clean sand (Naeini & Baziar, 2004). For example, at a confining pressure of 500 kPa, the residual strength decreased from 231 kPa for clean sand to 142 kPa for 30% fines content, then increased to 200 kPa for a 100% fines content.

Comparing the results of sand-clay/silt mixtures at the same density (dense state) revealed that silt content increases strength, in contrast to sand-clay mixtures which were weaker (Carraro et al., 2009). They attributed that to the larger dilation strain that is associated with adding silt, and consequently leads to mobilisation of stress at larger strains. However, adding clay decreases friction between particles and consequently decreases strength.

Table 2.5 shows the strength parameters of sand containing 5, 10 and 15% clay, according to a direct shear test by Dafalla (2013). Generally, increasing the clay content increases cohesion and decreases the friction angle. A similar trend was also found more recently, using drained triaxial tests, by Phan, Hsiao, and Nguyen (2016). In this study, fine material not only mobilised cohesive strength but also took advantage of slipping between the aggregate particles, i.e., it facilitated slipping between coarse particles. This improvement in cohesion properties was clearly reflected as a significant component of the unconfined compression strength and tensile strength, as shown in Figure 2.40 (X. Jiang, Cui, & Ge, 2015).

Table 2.5 Shear strength parameters of various clay-sand mixtures

Clay content (%)	γ_d (kN/m^3)	C (kPa)	$\emptyset$ (°)
0	16.3	0	43
5	17.3	12	40.7
10	17. 7	15	39.4
15	18.0	26	41
100	12.0	114	38.7

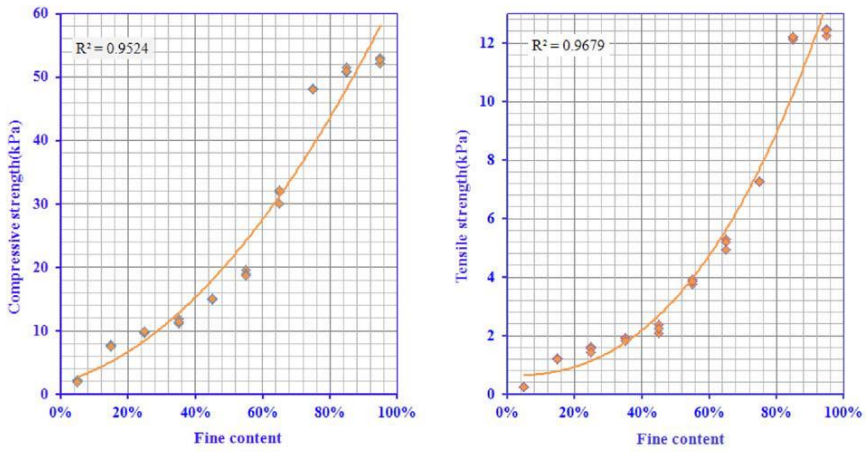

(a) (b)

Figure 2.40 Relationship between (a) compressive strength and fines content and (b) tensile strength and fines content (X. Jiang et al., 2015)

As mentioned in the previous sections, studies on reinforced mixtures are limited. For example, Naeini and Gholampoor (2014) investigated the dynamic properties of reinforced sand with geotextiles and considered the effect of different percentages of silt (0, 20, 30, 35, 40 and 50%). For all numbers of geotextile layers and arrangements, increasing silt in the range of 0–35% caused increases in axial strain (Figure 2.41) and, consequently, decreases in the shear modulus, as shown in Figure 2.42. Increasing the number of reinforcement layers resulted in increases in the axial modulus of different mixtures. With a silt content of more than 35%, the axial modulus started to increase. This threshold is similar to that observed by Lade, Liggio, and Yamamuro (1998) and Das and Sobhan (2013). Within this range, silt plays a secondary role in the transfer of contact forces as it decreases the contact between sand particles, resulting in decreases in the shear strength and axial modulus of the mixture. Their results show that silt content has no effect on the damping ratio under different silt contents and confining pressures, which was approximately 19–19.5% (Figure 2.43).

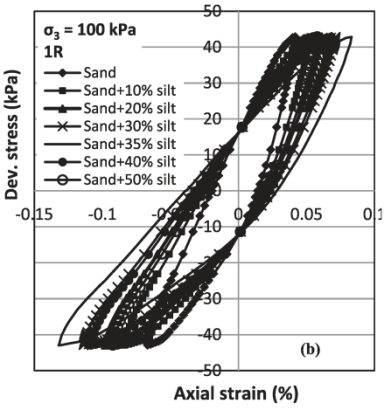

Figure 2.41 Hysteresis loops for reinforced sand-silt mixtures (Naeini and Gholampoor, 2014)

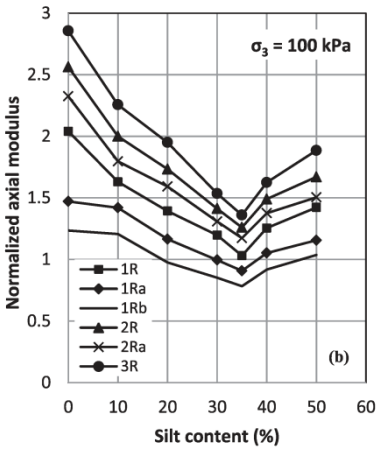

Figure 2.42 Effect of silt content on axial modulus (Naeini and Gholampoor, 2014)

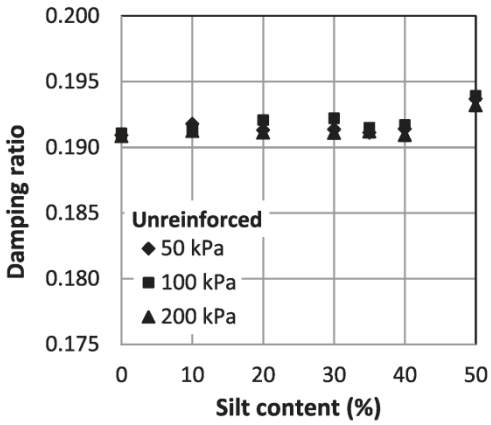

Figure 2.43 Effect of silt content on damping ratio (Naeini and Gholampoor, 2014)

The effect of silt contents of 0–45% on the interfacial strength characteristics of geogrid-reinforced sand was investigated by Naeini et al. (2013) using large-scale direct shear tests. It was found that increasing the silt content resulted in decreases in the interfacial shear strength of reinforced mixtures. This was attributed to the great difference between aperture size and the average particle size (Naeini et al., 2013). Minimum strength occurred at F = 35%. For example, the interfacial shear strength increased due to geogrid reinforcement by 21% for clean sand and by 12.3% for sand containing 35% silt (Naeini et al., 2013). This agrees with Juran, Knochenmus, Acar, and Arman (1988), who reported that mixtures with high silt contents required geogrids with smaller aperture sizes to achieve effective reinforcing. This decrease in strength is related to the role of silt located between and around particles acting as a lubricant, allowing the easy rotation and sliding of particles and, consequently, decreased strength. Both Naeini et al. (2013) and Infante, Martinez, Arrua, and Eberhardt (2016) found that unreinforced and reinforced sand-silt mixtures exhibited greater cohesion than clean sand samples, while there were insignificant differences in friction parameters.

Studies on the effect of fines content on the anisotropic behaviour of sand are rare and limited to a few research groups. For example, Nakase and Kamei (1983) found significant differences between the compression and extension strength of sand mixed with different percentages of fines, using a conventional triaxial device. They reported that the ratios of shear strength obtained from compression tests, as compared to those

obtained from extension tests, were 1.9, 1.53, 1.37 and 1.311 for sand mixed with fine contents (clay and silt) of 38.6, 52.6, 65.9 and 83.9% respectively. Tests by HCA under different values of α (2–90°) revealed a similar significant anisotropic response of compacted samples comprised of 52% fines (clay and silt), 47% sand and 1% gravel, where the difference in the stress ratio at failure q/p, due to increases in the principal stress direction α from 2 to 90°, reached 38.7% and was associated with a 34% reduction in the friction angle (Kumruzzaman & Yin, 2010a, 2010b). Such reductions in strength were also reported recently by Keyhani and Haeri (2013) for samples of sand mixed with different percentages of silt. For example, increasing α from 20 to 80° resulted in a decrease in the deviator stress, at 1.0% shear strain, by 42.8%. In addition, several studies found that pure fines, such as clay, exhibit considerable variation in strength and deformation behaviour according to the principal stress direction.

Chapter 3

Materials, Testing Apparatus and Methods

3.1 Introduction

This chapter describes the testing apparatus employed in this study, as well as the testing materials, procedures and programs used. A variety of laboratory apparatus are used to study the stress-strain and strength behaviours of soil, but most of them do not simulate in-situ conditions. This study used a hollow cylinder apparatus, which is capable of replicating real conditions by individually controlling the axial load, torque and inner and outer pressures. Different types of loading conditions can be tested, such as different directions of principal stress that are kept constant throughout the tests, testing under cyclic rotation of the principal stress direction, and testing under different values of the intermediate principal stress parameter. This allows the study of anisotropic effects on the mechanical properties of sample materials; an aspect that cannot be tested with conventional devices.

3.2 Materials

3.2.1 Sand

In the current study, Perth sand was chosen for investigation. This sand is commonly used under foundations and as a base material for roads. It is characterised as poorly-graded sand (SP) based on the unified classification system, and has a mean particle size of 0.6 mm. Measurement of specific gravity, maximum void ratio, minimum void ratio and particle size distribution were performed according to the standards ASTM D854 (2014), ASTM D4254 (2016), ASTM D4253 (2016) and ASTM D422 (2007), respectively. The physical properties are illustrated in Table 3.1. The particle size distribution, photograph, and scanning electronic microscope (SEM) image of the Perth sand used are shown in Figures 3.1a, 3.1b and 3.1c, respectively.

Table 3.1 Physical properties of Perth sand

Description	Value
Coefficient of uniformity, C_u	1.5
Coefficient of curvature, C_c	1.04
D_{30} (mm)	0.5
Medium grain size, D_{50} (mm)	0.6
D_{60} (mm)	0.603
Maximum void ratio, e_{max}	0.826
Minimum void ratio, e_{min}	0.549
Specific gravity, G_s	2.65
Sphericity	0.63
USCS classification	SP
Friction angle of used sand, $\emptyset$ (°)	40.1
Cohesion of the used sand, C (kPa)	0.0

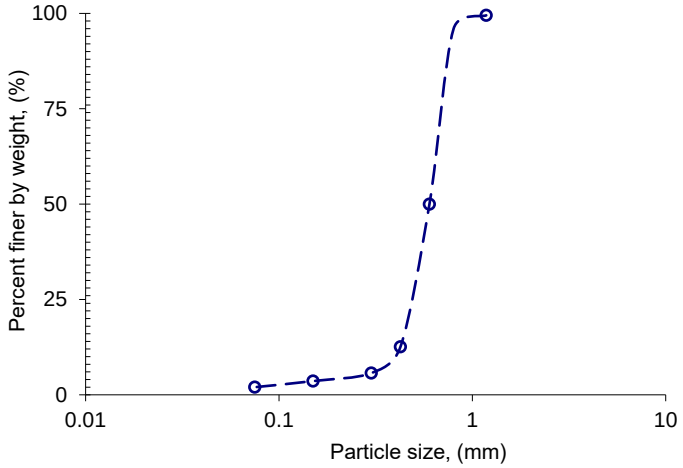

(a)

(b)

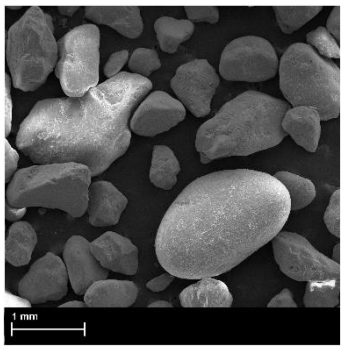

(c)

Figure 3.1 Characteristics of Perth sand: (a) particle size distribution, (b) photograph, and (c) typical SEM image

3.2.2 Kaolinite

Kaolinite was used in this study and was supplied by Sibelco, a local provider in Western Australia. This clay is known commercially as *Prestige NY*, and is composed of 93% kaolinite and 7% quartz. The particle size distribution, photograph and SEM image are shown in Figures 3.2a, 3.2b and 3.2c, respectively. It is classified as highly plastic soil group with a 58% liquid limit and 31% plastic limit (ASTM D4318, 2017), and specific gravity of 2.68 (ASTM D854, 2014).

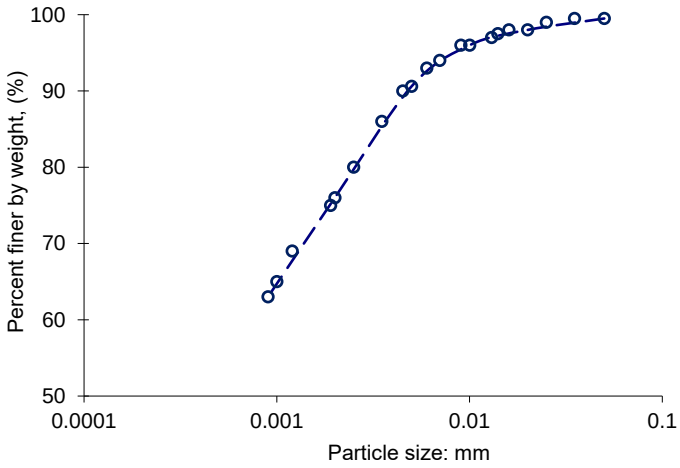

(a)

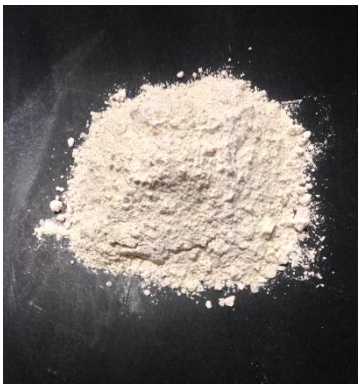

(b)

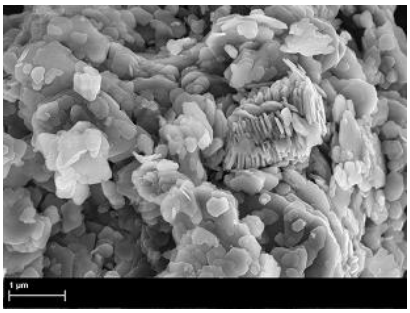

(c)

Figure 3.2 Features of the kaolinite used in this study: (a) particle size distribution, (b) photograph, and (c) typical SEM image

3.2.3 Geogrid

A high-density polyethylene geogrid (Figure 3.3a) was employed as one of the reinforcements for this study. The average mesh size was 8 × 6 mm and its mass per unit area was 728 g/m^2. The tensile properties of the tested geogrid (ASTM D6637/D6637M, 2015) in terms of the load-elongation relationship are shown in Figure 3.3b. The ultimate tensile strengths were 9.8 and 6.15 kN/m in the longitudinal and transverse directions, respectively.

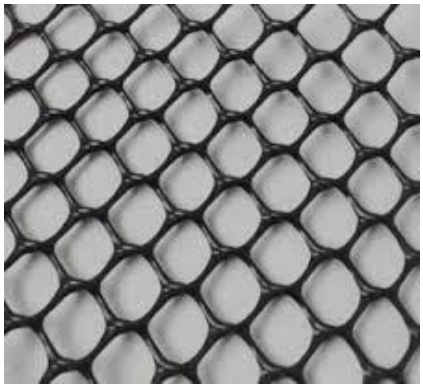

Figure 3.3a CE121 Geogrid used in this study.

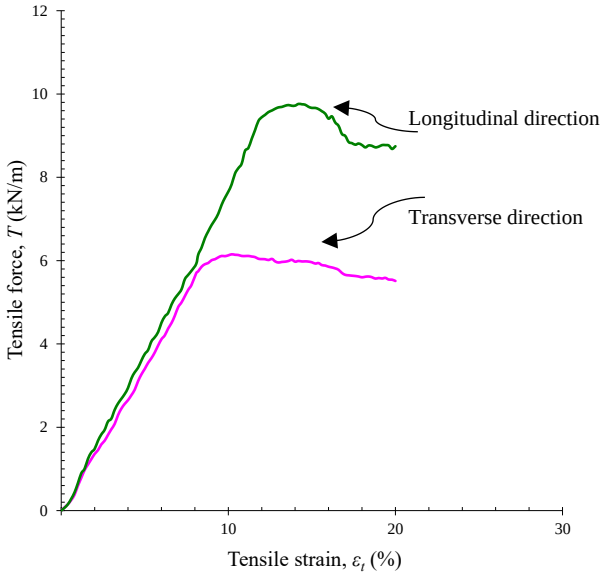

Figure 3.3b Tensile force-elongation response of geogrid

3.2.4 Geotextile

Nonwoven sheets were used in this study as a geotextile reinforcement (Figure 3.4a). The average thickness of the sheets was 1.61 mm and the unit mass per area was 200 g/m^2. The load-elongation relationship of the geotextile used is shown in Figure 3.4b, as obtained from a wide-width test carried out in accordance with ASTM D4595 (2017). The ultimate tensile forces per unit width in the longitudinal and transverse directions were 9.41 and 8.04 kN/m, respectively.

Figure 3.4a Nonwoven geotextile used in this study

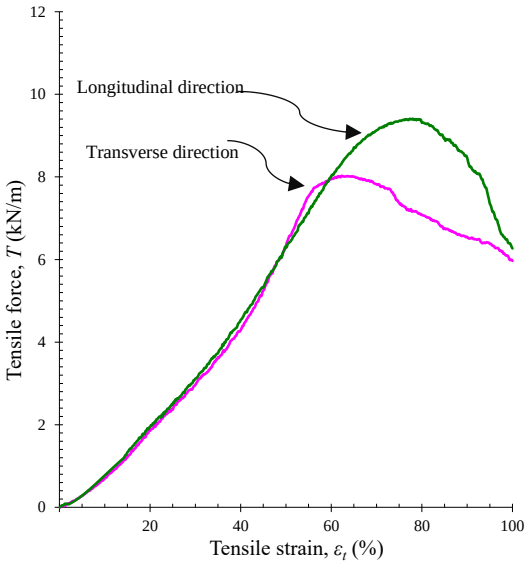

Figure 3.4b Tensile force-elongation response of nonwoven geotextile

3.2.5 Geocell

Geocell (Figure 3.5a) was made by hand using the nonwoven geotextile described above. Therefore, the tensile properties of the tested geocell (in the longitudinal and transverse directions) are also presented in Figure 3.4b. Geotextile sheets were folded and stitched to make cylindrical shapes with average diameters of 75 mm. The tensile strength of the joint was tested (perpendicular to the direction of stitches) as described by Cancelli, Rimoldi, and Montanelli (1993). Its tearing tensile strength was 8.4 kN/m, and the stress-strain relationship is shown in Figure 3.5b.

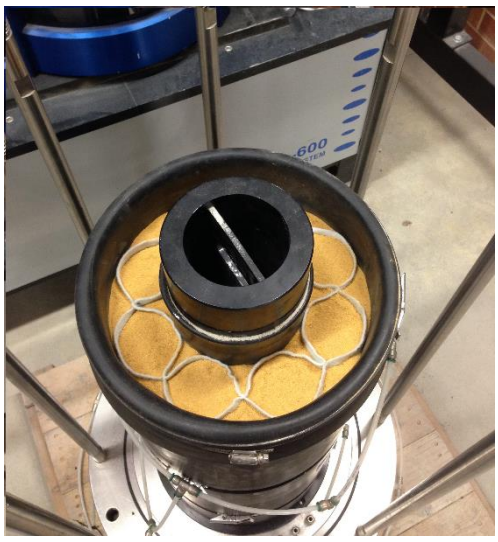

Figure 3.5a Geocell used in this study

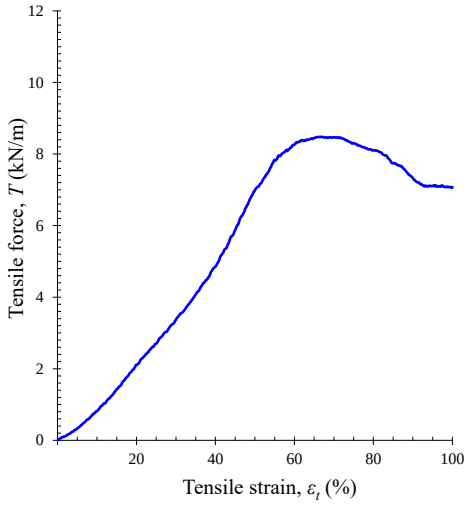

Figure 3.5b Tensile force-elongation response of geocell seam

3.2.6 Cement

The cement which was utilised in this research was ordinary Portland cement (OPC). This type of cement is commonly used in Perth's infrastructure. Its chemical and physical properties are listed in Table 3.2.

Table 3.2 Chemical and physical properties of ordinary Portland cement (OPC) (Swan Cement material Safety data Sheets, 2012)

Parameter	Value
CaO	63.7%
SiO2	20.4%
Al2O3	5.4%
Fe2O3	2.8%
MgO	1.3%
SO3	2.7%
Na2O equivalent	0.5%
Chloride	0.01%
Compressive strength	
3 days	38 MPa
7 days	50 MPa
28 days	63 MPa
Initial setting time	110 minutes
Final setting time	170 minutes

3.3 Tests Using Large Hollow Cylinder Apparatus (HCA)

3.3.1 Description of HCA

The device used in the present study was a large dynamic hollow cylinder apparatus (HCA). This device is sophisticated and offers the opportunity to investigate large-scale samples under a variety of stress and strain paths that simulate field conditions, and cannot be performed using conventional triaxial devices. This device can

accommodate solid samples with diameters of 300 mm, and hollow samples with outer and inner diameters of 300 and 150 mm, respectively. The height of the solid and hollow cylinders was 600 mm. These large-scale samples can provide representative and reliable tests, especially for reinforced soil samples, as smaller-sized samples may not demonstrate the real interactions between the reinforcement and the soil. The limitations of using small-scale samples were reported by Latha and Murthy (2006) and Tafreshi and Asakereh (2007), who used samples of 38 mm diameter and suggested that large-scale triaxial tests should be used for reinforced samples.

A photo and schematic diagram of the device are presented in Figures 3.6a and 3.6b. The HCA can subject test samples to individually-controlled axial loads W, torques M_T and inner p_i and outer p_o pressures (Figure 3.6c). The induced components of the stresses acting within the soil element are also shown in Figure 3.6c (L. Guo, Chen, Wang, Cai, & Deng, 2016). This means that the major σ_1, intermediate σ_2 and minor σ_3 principal stresses can be also independently controlled, and consequently, conditions of different directions of principal stresses α, different intermediate principal stress parameter b and cyclic rotation of principal stress direction can be achieved. Conventional triaxial tests can be carried out under either compression conditions (α = 0° and b = 0.0) or extension conditions (α = 90° and b = 1.0), while the HCA can investigate the full range of b = 0.0–1.0 and α = 0–90°. The HCA's capability of independent control of the parameters presents a great opportunity to investigate the anisotropic stress-strain characteristics of soil and, hence, the directionally-dependent characteristics of geomaterials.

The HCA consisted of several main parts: a steel frame, pressure control panel (PCP), hydraulic power system (HPS), controller (SCON) and computer with CATS software. The frame was made from stainless steel and included an axial actuator of 300 kN capacity, a torque actuator of 1000 Nm capacity and was supported by steel threaded columns fixed into a base table (100 × 100 cm area × 80 cm height). The pressure control cabinet was made from metal and consisted of three pressure volume controllers (PVCs) for the inner, outer and back pressures, in addition to a 20,000 ml capacity water reservoir. Each PVC has transducers and a linear variable differential transformer (LVDT) that are connected to the SCON with an analog interface. Moreover, there were sighting tubes in the front of the panel allowing observation of

the amount of water in the water circuit. The above-mentioned PVCs received commands from the software to operate the motors. They sent back readings of induced pressures and deformation to the software, which would then calculate test parameters and create new commands for transmission to the PVCs. This control of a synchronised circuit of commands and readings made it possible to perform advanced tests investigating anisotropic behaviour under wide range of stress/strain paths.

The hydraulic power system (HPS) mainly consisted of pressure and return lines, a high-pressure filter, an output pressure gauge, accumulator motors and a heat exchanger. The system was operated on either a low or high pressure setting based on the required output pressure. Moreover, the HPS is provided with a sensor that relieves overpressure and protects the system, in addition to temperature and fluid level sensors.

The controller (SCON) and CATS software is the "brain" of the HCA system. The incorporation of the SCON and CATS software into the HCA allows the operation, monitoring and control of every feature of the system and, thus, allows the anisotropic investigation to be greatly simplified. The SCON is highly developed and supplies 16-bit resolution and an analogue anti-alias filter for high and low frequencies. This thus generates a very precise and stable signal measurement and control system. Eight separate output channels can be controlled independently and simultaneously. Moreover, the SCON is capable of accommodating 24 signal inputs. This system allows the user to select the appropriate testing parameters and phases, combine a number of inputs and, also, define user inputs as a function of other inputs. This includes the ability to define and calculate 20 parameters such as the principal strains $\varepsilon_{1,2,3}$ and stresses $\sigma_{1,2,3}$, deviator stress q and strain ε_q, volumetric strain ε_v, principal stress direction α and the intermediate principal stress parameter b. Moreover, a watchdog timer and remote interlock are provided with this system for easy and safe operation and testing.

As a consequence, with this valuable device, it is possible to extend the stress/strain path to simulate field conditions with different fixed directions of principal stress, continuous rotation of the principal stress direction and various magnitudes of the intermediate principal stress parameter. Contrary to conventional triaxial tests, the

HCA allows investigation of the anisotropic behaviour of samples under a wider range of stress paths and general stress states.

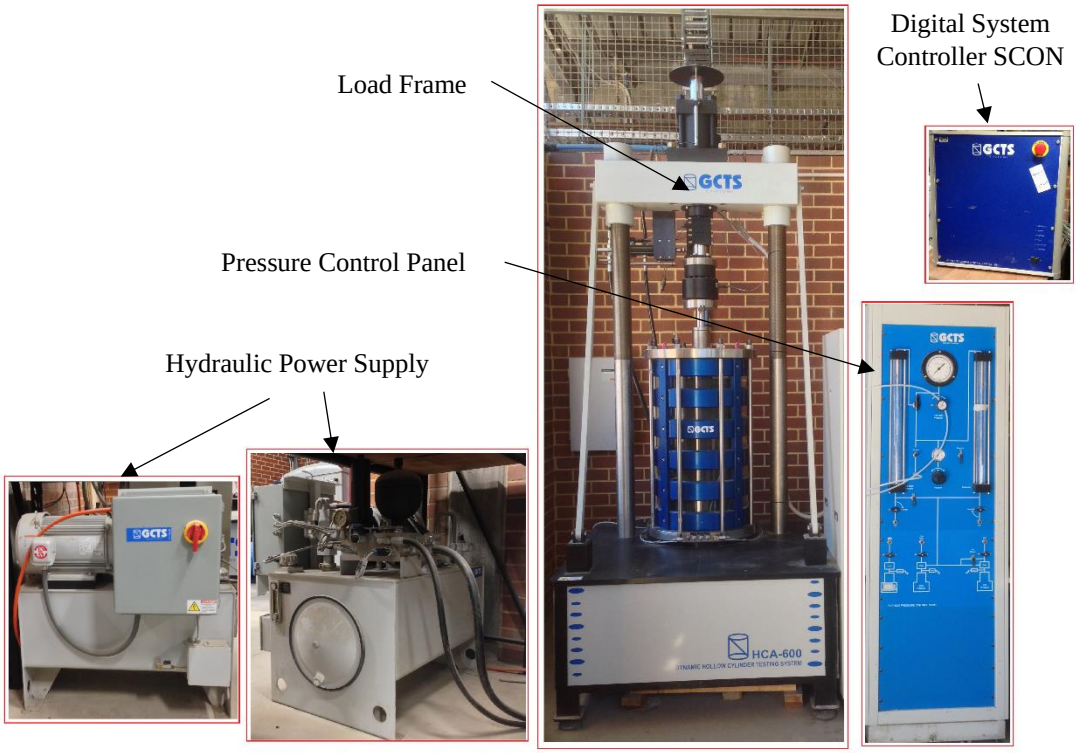

Figure 3.6a Large hollow cylinder apparatus used in this study

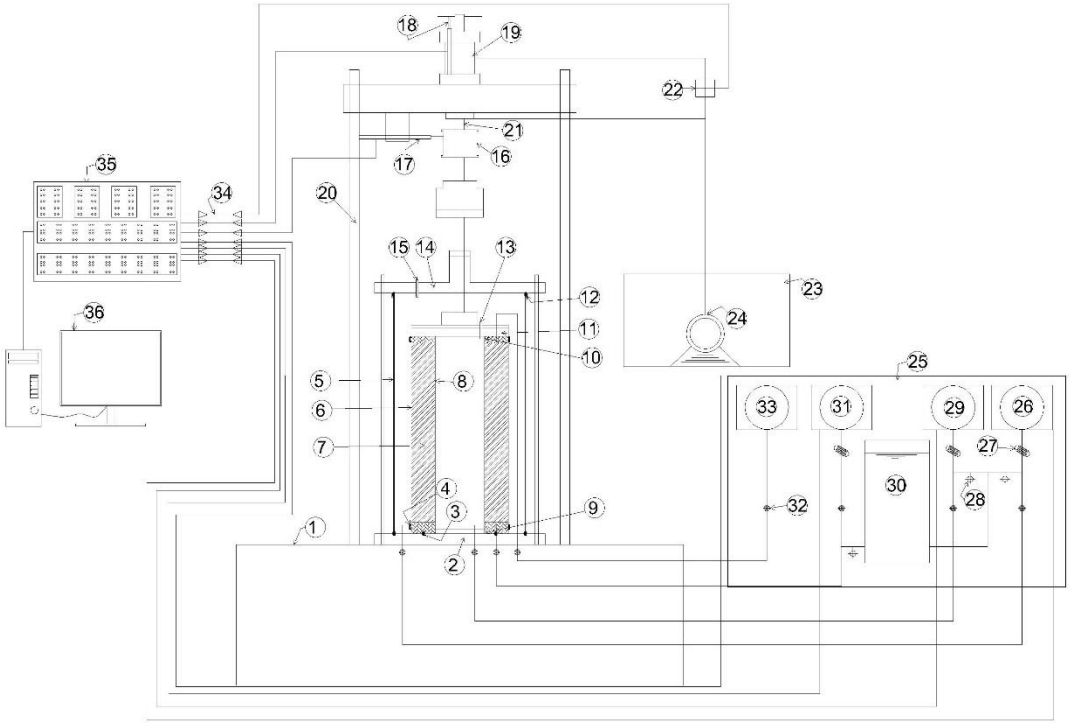

1	Table	10	lower cap with porous stone	19	Double-acting actuator	28	Automatic three-way valve
2	Base plate	11	Upper cap	20	Steel threaded columns	29	Cell pressure/volume controller
3	Base O-ring	12	Cell O-ring	21	Spline shaft	30	Water reservoir
4	Bottom steel clamp ring	13	Inner cell vent	22	Axial load servo valve	31	Back pressure/volume controller
5	Cell wall	14	Cell cap	23	Hydraulic power system	32	Manual ball valve
6	Outer membrane	15	Cell vent	24	Hydraulic pump	33	Top pore pressure
7	Sand specimen	16	Axial load/torque cell	25	Pressure control cabinet	34	Signals from/to sensors
8	Inner membrane	17	Horizontal LVDT	26	Cell pressure/volume controller	35	SCON 2000 controller
9	Pedestal base with porous stone	18	Vertical LVDT	27	Pressure transducer	36	Computer with CATS software

Figure 3.6b Schematic diagram of the HCA

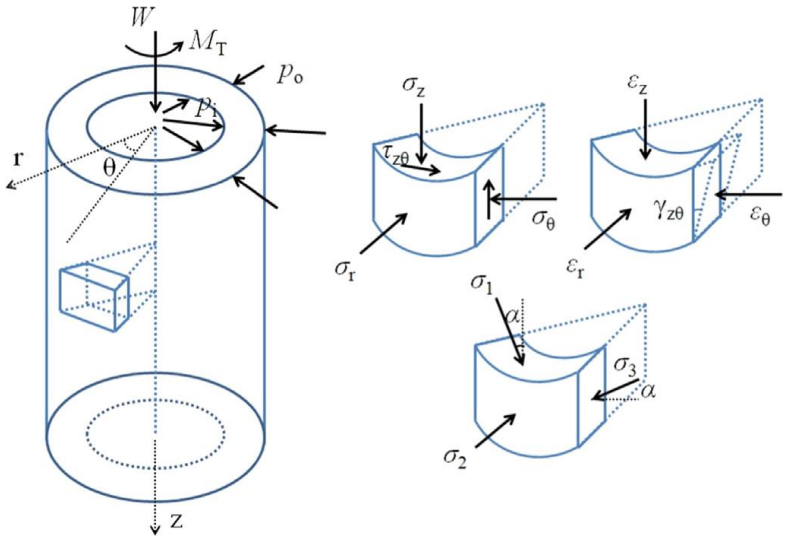

Figure 3.6c Stress state of hollow cylinder specimens

3.3.2 Deformation

The strains considered in this study, i.e. volumetric ε_v and deviator strains ε_q, are calculated automatically using CATS software based on the deformations measured by the various sensors and transducers. Volumetric and/or deviator strains are functions of the axial ε_z, circumferential ε_θ, radial ε_r and shear strains $\gamma_{z\theta}$. Therefore, it is beneficial to explain these strains and deformations.

Volumetric strain ε_v can be calculated using Equation 3.1 based on the volume change of inner and outer cells Δv relative to the sample volume v that were measured simultaneously using transducers connected to the pressure/volume controllers (PVCs) (Hight, Gens, & Symes, 1983). The CATS software receives and records these measurements via the analogue interface.

Volumetric strain: $\varepsilon_v = \Delta v / v$ (3.1)

Deviator strain ε_q is measured by CATS software using Equation 3.2. It is a function of the major, intermediate and minor strains ε_1, ε_2 and ε_3 which are also calculated by the software, based on Equations 3.3a-c.

Deviator strain: $\varepsilon_q = [2/9 \{ (\varepsilon_1 - \varepsilon_2)^2 + (\varepsilon_1 - \varepsilon_3)^2 + (\varepsilon_2 - \varepsilon_3)^2 \}]^{1/2}$ (3.2)

Major principal strain: $\varepsilon_1 = (\varepsilon_z + \varepsilon_\theta) / 2 + [(\varepsilon_z - \varepsilon_\theta)^2 / 4 + (\gamma_{z\theta})^2 / 4]^{1/2}$ (3.3a)

Minor principal strain: $\varepsilon_3 = (\varepsilon_z + \varepsilon_\theta) / 2 - [(\varepsilon_z - \varepsilon_\theta)^2 / 4 + (\gamma_{z\theta})^2 / 4]^{1/2}$ (3.3b)

Intermediate principal strain: $\varepsilon_2 = \varepsilon_r$ (3.3c)

Axial strain is calculated using the axial deformation, which is measured precisely and accurately using a deformation sensor (LVDT) placed on the actuator to control its axial movement.

The CATS software can also calculate the values of ε_θ and ε_r using Equations 3.4 and 3.5, respectively, depending on the values of the inner and outer radial deformations (d_{ri}, d_{ro}) that were calculated simultaneously from the inner and outer volume changes.

Circumferential strain: $\varepsilon_\theta = (d_{ro} + d_{ri}) / (r_o + r_i)$ (3.4)

Radial strain: $\varepsilon_r = (d_{ro} - d_{ri}) / (r_o + r_i)$ (3.5)

Moreover, the angular deformation sensor that controls the torsional actuator is used to measure the angular deformation ω and, consequently, calculate the shear strain according to Equation 3.6.

Shear strain: $\gamma_{z\theta} = 2\omega (r_o^3 - r_i^3) / [3H (r_o^2 - r_i^2)]$ (3.6)

Similar procedures and equations have also been used by several studies such as Hight et al. (1983), Kumruzzaman and Yin (2010a, 2010b), and L. Yang et al. (2016).

3.3.3 Applied Load, Torque and Pressures

During the tests, the applied axial load, torque and inner and outer pressures were all controlled and monitored by the SCON. Axial load was applied by an axial actuator of 300 kN capacity, according to commands received from the CATS software. Control and measurements were performed based on the axial deformation and load feedback, using the transducers and analogue output control connected to the servo valve.

Furthermore, the HCA has the ability to apply torque on the tested sample via a torque actuator of 1000 Nm capacity. Similar to the axial load actuator, angular deformation and torque are used to control the test via the analogue output connected to the torsional actuator servo valve. This angular deformation is measured by an angular deformation gauge.

The outer, inner and back pressures could be applied and monitored using the three main PVCs that were supplemented by a number of transducers and LVDTs, as mentioned in Section 3.3.1. The process of applying and controlling the inner and outer pressure was performed by the CATS software via the SCON, which was connected to all of these sensors. During operation, each piston was commanded to push or pull water by individually rotating steeping motors forward or backwards. As a consequence, the inner, outer and back pressures were increased or decreased based on the piston motion. All operations were monitored and controlled automatically by the CATS software via the SCON to ensure that the tests followed the intended path.

Several functions are available in the CATS software to perform hollow cylinder tests or other tests, such as saturation, consolidation, universal, static loading and dynamic loading stages.

For the saturation stage, the outer, inner and back pressure analogue outputs were selected. Then, the cell pressures (inner and outer) were ramped up in increments simultaneously with a ramp-up of the back pressure, taking care to avoid disturbance or over-consolidation. After each increment, Skempton's *B*-value was calculated to check whether it reached a value considered sufficient for sample saturation. At any increment, if a sample reached the required Skempton's *B*-value, the test would skip subsequent incremental increases of back and cell pressure and advance to the next stage (consolidation); otherwise, it would continue increasing incrementally until final specific values of back and cell pressure were obtained. However, if it failed to reach the required saturation at the end of the test, the software prompted the user to choose the stage that should be followed next. This process was carried out by applying different values of back pressure while keeping a constant initial effective stress of 30 kPa for about 12 hours to obtain a Skempton's B-value greater than 0.95. The amount of water required for saturation was 3814146 mL.

The HCA offers two consolidation conditions: isotropic and anisotropic. In the isotropic case, the effective consolidating stress was reached by applying uniform cell pressure. In anisotropic consolidation, however, the effective axial and consolidation stresses were applied to samples using cell pressures and an axial actuator. In the present study, specimens were consolidated isotropically by ramping the effective confining pressure (outer and inner) up to 100 kPa. This means that during tests, equal inner and outer cell pressures were applied all around to achieve the isotropic consolidation condition. During the consolidation stage, the duration and final stresses were monitored and controlled by the SCON and CATS software via the PVCs and sensors, as mentioned previously. The volume changes during the saturation and consolidation processes were very small, typically less than 0.019%, where void ratio e before and after consolidation was 0.6321 and 0.6319 respectively. The shearing stage was being executed automatically using the universal stage set.

In the shearing stage, independent control of axial load, torque and inner and outer pressures was implemented during tests to achieve the targeted stress path. This control process was performed based on the feedback, commands and readings that were sent and received simultaneously from the CATS software and the actuators and motors via the analogue output and input that was connected to the PVCs, LVDTs and other valves and sensors. The stress path that was used in this study is presented in Section 3.5 –Testing Program.

This system is similar to the principles used by Hight et al. (1983), Naughton and O'Kelly (2001) and O'Kelly and Naughton (2005), although Hight et al. (1983) maintained equal inner and outer pressures during shearing.

3.3.4 Controlling the Tests

Control of the process was necessary to keep the test running on the targeted stress path. A description of the test control process was given in Sections 3.3.1 and 3.3.3 and will be summarised again here. The stress paths of the tests included saturation inputs, such as the required Skempton's B-value, consolidation information, such as the isotropic or anisotropic condition, and shearing information, such as required mean effective stress p', required principal stress direction α and required intermediate principal stress parameter b. All this information was input before executing the tests.

Once a test began, the SCON transmitted the required initial commands to separately and independently apply axial load, torque and inner and outer stresses via the analogue output connected to the transducers, LVDTs, valves and sensors, so that the required conditions for the test were achieved. Simultaneously, the induced deformations and pressures were measured by these instruments and sent back to the CATS software via the SCON. These were recorded and used to calculate the required test parameters and all relevant strains and stresses acting on the hollow cylinder sample, such as the strains mentioned in Equations 3.1-3.6. These computed stresses and strains were analysed and used by the CATS software to create new commands to maintain the test on the required stress path and, subsequently, such commands were sent to the controllers via the SCON. Therefore, the pressures, axial load and torque were varied to achieve the targeted test conditions and parameters, such as maintaining constant values of p' and b and the specific constant α. Naughton and O'Kelly (2001); O'Kelly and Naughton (2005), Kumruzzaman and Yin (2010a, 2010b) and GCTS (2016) have reported similar principles of control.

3.3.5 HCA Sample Preparation

Large-scale hollow samples have the advantage of providing better representations of reinforced samples than conventional tests; however, handling such large samples is very difficult and requires more precision, people, time and facilities. Moreover, safety is an important consideration when handling such a device. For example, the weight of the cell (before filling with water) is about 330 kg and most of the other parts are also heavy.

Because HCAs are different from convention triaxial devices, a series of photographs of the various stages of sample preparation and their installation in the HCA are included in Figure 3.7. Firstly, the base was cleaned carefully to remove any dust or sand that could cause later problems such as leakage, then an O-ring was placed in the groove and lubricated with silicon grease (Figure 3.7a). Before fastening the pedestal to the base plate, the inner membrane was fixed to the pedestal. The pedestal was comprised of top and bottom parts (Figures 3.7b). The top part contained eight porous stone disks of 50 mm diameter to allow saturation. The top part of the pedestal had eight stainless steel blades (2 × 0.5 × 70 mm) that prevented the samples from slipping

under torque. The inner membrane (Figure 3.7c) was fixed inside the top part of the pedestal by inserting it, folding it around the inner pedestal perimeter, mounting an O-ring around it and then fastening it to the bottom part of the pedestal with four nuts (Figure 3.7d). It should be noted that double O-rings lubricated with silicon grease were placed between these two parts of the pedestal. Subsequently, this pedestal was fixed on the chamber base plate (Figure 3.7e) followed by mounting the inner split mould (Figure 3.7f) inside the inner membrane. One half was inserted and then adjusted, then the other half was inserted and, finally, the separator piece was inserted between these two parts (Figure 3.7g). This separator piece was important during the preparation of samples as it provided full contact between the membrane and the inner mould. Moreover, removing this piece first, after completing soil pouring, made removing the other components of the inner mould much easier; otherwise, it became very difficult to extrude the mould due to the lateral bushing of the soil, which could result in soil disturbance. The outer membrane was installed around the pedestal and tightened carefully with a stainless-steel clamping ring (Figure 3.7h). The installation of the inner and outer membranes was not easy due to their size and thickness; thus, great care was taken during installation of the membrane to prevent collapse of the sample due to the large amount of soil used and to prevent leakage during testing. The outer split mould was then erected and tightened with three stainless steel clamping rings (Figure 3.7i). The upper end of the outer membrane was folded around the upper perimeter of the outer mould and secured by a stainless-steel clamping ring.

In small samples, it is common to stretch the membrane to release any creases; however, this is very difficult to do in large-scale samples due to the thickness and size of the membrane. Therefore, it was confirmed that there were no creases before setting the outer mould. Vacuum pressure was then applied to attach the membrane to the mould before pouring the soil. Subsequently, sand was poured inside the hollow assembly in several layers with little tamping. The required amount for each layer was calculated and prepared in advance to achieve and maintain a relative density of approximately 70%. For reinforced samples, geogrid and geotextile layers were cut as hollow planes (Figure 3.7j) with diameters slightly larger than that of the inner mould and slightly smaller than that of the outer membrane, and then placed in different layers (mainly in the form of 2, 3, 4, 5 and 6 layers) after levelling each layer of soil

(Figure 3.7k). For geocell reinforcement, geocells were fabricated from the geotextile materials in the form of multi connected cells and then installed between the membranes before pouring soil inside them (Figures 3.7j and k). When soil reached the final marked level (Figures 3.7l), the bottom part of the top base was placed on soil, which consisted of porous stone and blades similar to that in the upper part of the pedestal (Figure 3.7m). The inner mould was then removed by first grabbing the separator piece before removing its two parts (Figure 3.7n), as explained previously. After that, the loading base was placed and fastened on the porous stone part (Figure 3.7o). A rocket rod was connected temporarily with a loading piston that was fixed on the loading base (Figure 3.7o). The folded outer membrane was then slipped over the top base and tightened by a stainless-steel clamping ring. Subsequently, the outer mould was removed (Figure 3.7p) and samples left under a vacuum pressure of 25 kPa to maintain soil stability when removing the outer mould.

The next step was very important. The chamber was lifted by a forklift and then lowered carefully so that all the rods of the base frame were inserted into the holes of the top base of the chamber (Figure 3.7q). It was important to avoid any knocks to the samples during installation that could cause sample failure or soil disturbance. The rocket rod helped alignment during the above step to minimise this concern (Figure 3.7r). After bringing the chamber down and installing it, the top nuts were fastened on the cell rods (Figure 3.7s). Subsequently, the prepared cell and chamber were lifted and installed in the loading frame with precise care, then pushed gently to connect the loading piston to the piston of the axial actuator and torque actuator (Figures 3.7t and u). Finally, the outer cell was filled with water, making the system ready for testing. In this large-scale apparatus, which required at least three people and a forklift to prepare, safety was maintained as the most important issue.

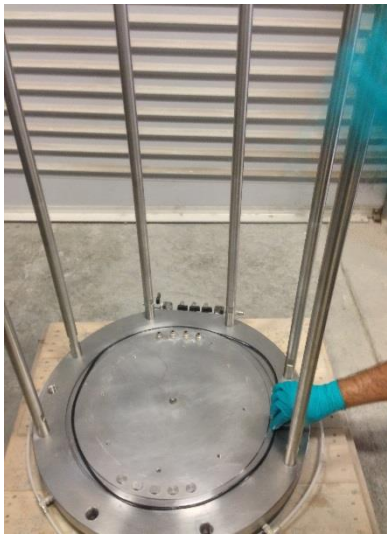

a. Cleaning the base of chamber and placing the O-ring

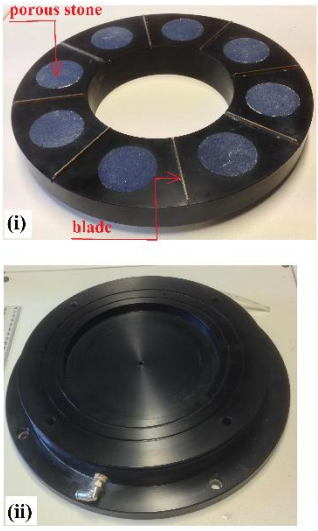

b. Upper and bottom parts of the pedestal

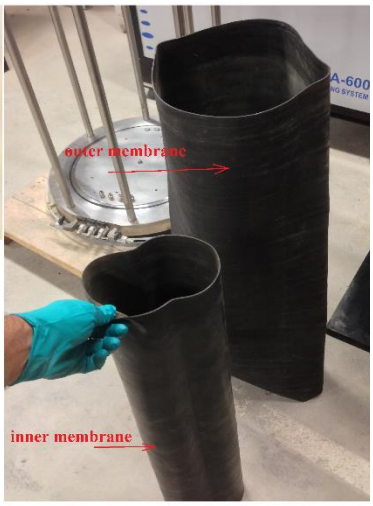

c. Outer and inner membranes

d. Fixing the inner membrane inside the porous stone compartment and fastening them on the base of the pedestal

e. Seating the pedestal base (with porous stone part and inner membrane) on the base of the chamber and securing with bolts

f. Inner split mould assembly

g. Erecting the inner split mould assembly inside the inner membrane

h. Fastening the outer membrane outside the pedestal using a clamping ring

i. Fixing the outer split mould with a clamping ring and assembling it on the base pedestal. Connecting the vacuum pipe to the outer mould.

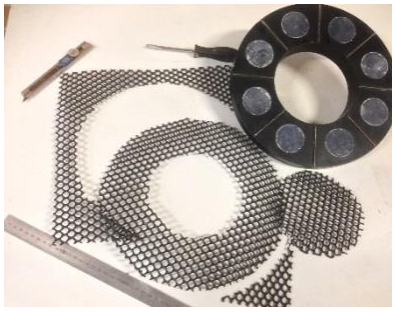

Geogrid

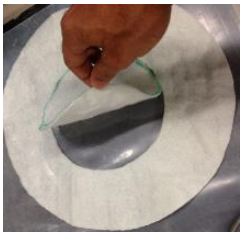

Geotextile

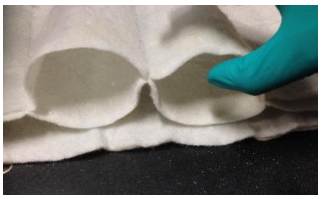

Geocell

j. Preparation of the reinforcements

Geogrid-reinforced sample

Geotextile-reinforced sample

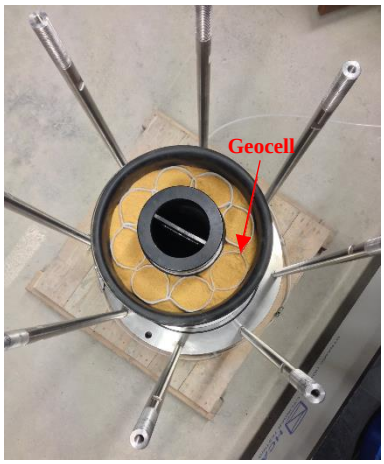

Geocell-reinforced sample

k. Placing soil within the hollow cylinder mould

l. Prepared unreinforced/reinforced sand

m. Seating the top porous stone gently on the top of the specimen

n. Remove the inner split mould after applying a vacuum through the prepared sample

o. Installing the top cap and tightening the porous stone cover. Positioning the rocket rod at the top of the cap, which was necessary for easy installation of the cell chamber (using a forklift) to avoid any knocks to the side and top of the sample

p. Removing the outer split mould

q. Bringing down the cell chamber using a forklift

r. Alignment by the rocket bar

s. Tightening the cell chamber on the prepared sample

t. Using a forklift to lift and set the sample up in the hollow cylinder apparatus

u. Connecting the prepared sample to the axial load and torque actuators

Figure 3.7 General procedures of sample preparation and installation

3.4 Small-scale Loading Tests on Cemented Sand

In addition to the main work on geosynthetics using the large HCA, a series of small-scale model tests were carried out to examine how settlement and load-carrying capacity vary as a function of the bedding plane angle. Sand and cemented sand were used for preparing the samples. These model tests were planned as a static loading test series and a cyclic loading test series.

3.4.1 Sample Preparation

The amount of sand and Portland cement required was determined in advance based on the selected relative density (D_r = 70%) and the volume of each layer. Cement was added to the sand at proportions of 3, 5 and 7% by weight, and blended until a uniform colour was obtained. Then, the water was added to the mixture and blended until homogenised. In order to prepare compacted samples, the mould was divided into several layers. The amount of cemented sand required for each layer was poured into the mould and tamped, and the surface was levelled with a thin steel plate. Some photographs of the various stages of sample preparation are included in Figure 3.8*a-l*.

In order to investigate the fundamental behaviour of anisotropic load-carrying capacity and settlement, samples were prepared with different inclination angles of the bedding plane α. A steel mould (length = 500 mm, width = 400 mm, depth = 400 mm) was fabricated with a removable top and front sides, as shown in Figure 3.8k, so that these two sides could be rejoined gradually at different heights corresponding to the material level during material placement. This is consistent with previous studies such as Oda and Koishikawa (1979), who used a mould with dimensions of 70 × 300 × 200 mm filled with anisotropic sand to support a strip footing of $B_{footing}$ = 30 mm. Similarly, Azami et al. (2010) conducted loading tests on a footing of 57 mm resting on anisotropic sand in a mould with dimensions of 350 × 500 × 200 mm.

The procedure of preparing the samples with initial anisotropy (Figure 3.8k) consisted of removing the front and top sides and then placing the mould on a fabricated tilting base in order to obtain a selected inclination angle relative to horizontal (0°, 15°, 30°, 45°, 60°, 75° and 90°). The material was then placed as a layer inside the tilting mould and after the material had reached the required level, the removable parts were rejoined

gradually according to the material level so that the material remained inside the mould. After a sequence in which sand or cemented sand was placed and the removable parts rejoined, a fully covered mould was obtained and then rotated gently to the horizontal position. The blending and compaction of the samples took less than 60 minutes, which was shorter than the initial setting time (110 minutes, Table 3.2). Since the curing time is out of the scope the present study, the period of 14 days was chosen as an enough curing time without an unnecessarily prolonged waiting time. In this manner, samples were prepared with an inclined bedding angle to investigate anisotropic settlement-load response. It is of benefit to mention that although mixing could prevent particles obtaining their preferred alignment, the layered soil still had inclined layers.

(a) Sand

(b) The mass of cement is determined

(c) Cement is added to the sand

(d) Sand-cement is thoroughly mixed by hand

(e) Sand (0% cement)

(f) The mixture (7% cement) after the hand mixing

(g) Sand and cement are added to the mixing bowl

(h) After mixing has begun, water is added

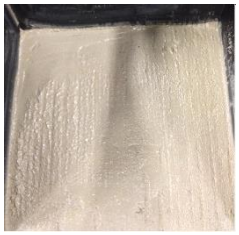

(i) Cemented sand is placed into the mould, compacted, and then levelled

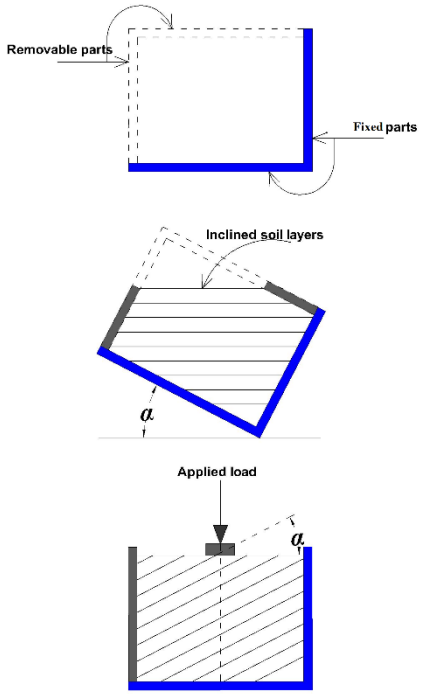

(k) Experimental procedure to make an anisotropic bed that inclined at α to the horizontal

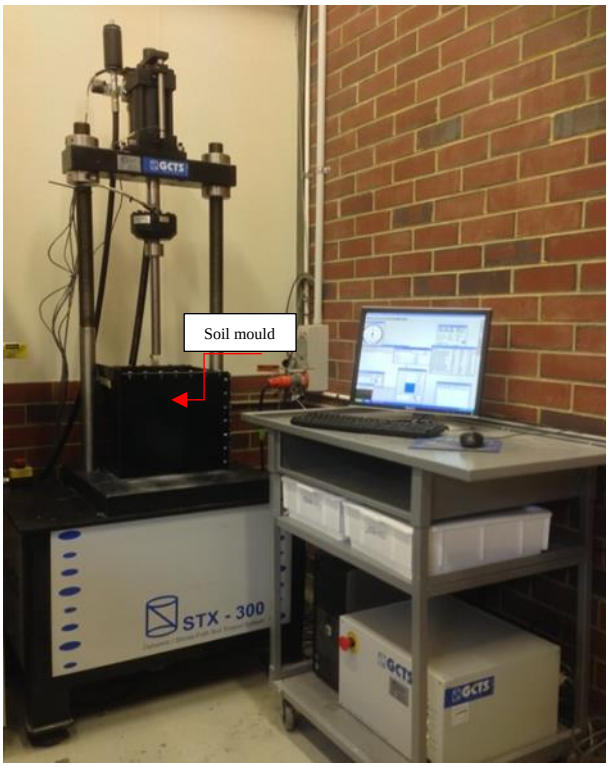

(*l*) View of load testing apparatus

Figure 3.8 General procedures of preparation of cemented sand

3.4.2 Tests

After preparing the anisotropic bed, an STX-300 machine (illustrated in Figure 3.8*l*) was used to perform loading tests on model rigid footings fabricated from steel, with a thickness of 25 mm and dimensions of 50 × 350 mm. A rough base condition for the footing was made by cementing a thin layer of sand using epoxy. For monotonic loading tests, vertical load was applied in equal increments and each increment was maintained until the induced settlement no longer changed significantly.

Regarding cyclic loading tests, an initial static pressure q_s with a desired factor of safety equal to three ($F.S. = (q_b)_u / q_s$) was first applied gradually at a rate of 1.0 kPa/sec, where $(q_b)_u$ is the ultimate bearing pressure obtained from the monotonic series. This initial static pressure q_s was maintained at a constant level until settlement took place or the settlement rate became negligible. In the second stage, sinusoidal cyclic loads with a range of different amplitudes in the form of a percentage of the ultimate bearing capacity ($q_c / (q_b)_u$ = 10%, 20% and 30%) were superimposed on a sustained static load, thereby providing an intensity of pressure varying between $q_{min.} = q_s$ and $q_{max.} = q_s + q_c$ (Figure 3.9). Cycles of this sinusoidal load were continued until excessive settlement occurred or the rate of settlement became insignificant. Many studies have pointed out that these amplitudes are appropriate for simulating the stress caused by traffic loads and vibrating machines resting on foundations, (e.g. Tafreshi and Dawson, 2012; Asakereh et al., 2013, among others).

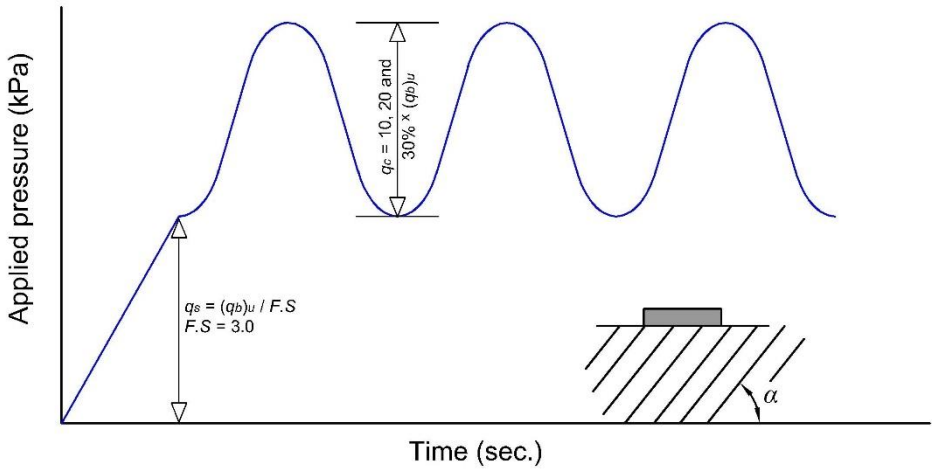

Figure 3.9 Cyclic loading sequence on the anisotropic model footing

3.5 Testing Program

The testing program primarily included an extensive series of large-scale hollow cylinder drained triaxial tests on sand, reinforced sand, a sand-clay mixture and a reinforced mixture. Moreover, series of loading tests were also performed on cemented sand.

Hollow cylinder tests were performed using two different types of tests: ***1)*** monotonic tests under different directions of principal stress α (Figure 3.10); and **2)** cyclic rotational shear tests (Figure 3.11). In the first type of test, drained hollow cylinder triaxial tests were performed under different values of principal stress directions α of 0, 15, 30, 60, 75 and 90°, while the mean effective stress p' and intermediate principal stress parameter b were kept constant at 100 kPa and 0.5, respectively. Tests were conducted under strain control mode at a slow rate of 0.05% per minute to allow time for the water to drain. During the tests, principal stresses were applied in a particular direction α, and this was associated with increases in deviator stress q until failure.

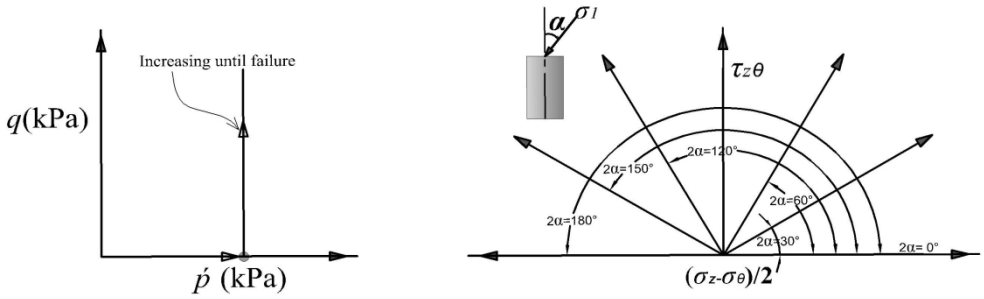

Figure 3.10 Stress paths for monotonic tests with fixed principal stress directions

However, for the second type of test, samples were subjected to continuous rotation of the principal stress direction for sixty cycles at a rotation rate of 2° per minute while the deviator stress magnitude was kept constant (Figure 3.11). Initially, samples were subjected to monotonic shear stress to reach the required stress ratio q / p', and then the principal stresses started rotating counter clockwise from A to B, C and then D before returning back again to A. A rotation of the principal stress direction from A to A

represents one cycle. This type of test was conducted using stress control mode, where all principal stresses σ_1, σ_2, σ_3 were constant during cyclic rotation.

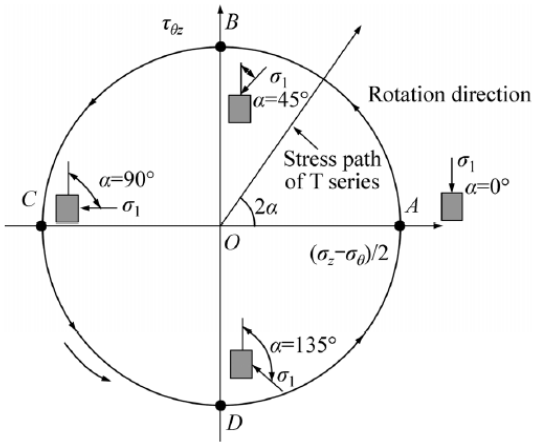

Figure 3.11 Typical stress paths in deviator space for rotational shear tests (Yan, Zhou, Gong, & Cao, 2015)

Regarding loading tests on small-scaled cemented sand, as mentioned in Section 3.4.2, monotonic loading tests were performed by applying a static axial load to investigate bearing pressure-settlement characterisation with an inclined bedding plane. Cyclic loading tests were also conducted on small-scaled cemented sand samples, as explained in Figure 3.9, which shows the typical time history of initial static and cyclic loading on the footing.

To make it easy to follow and compare, the research program can be divided into four main parts. Three parts involved hollow cylinder torsional tests, while the fourth involved scaled loading tests. These parts are explained below, with an outline depicted in Figure 3.14.

3.5.1 Part One: Monotonic Tests on Sand and Reinforced Sand Using the HCA under Various Directions of Principal Stress α

In this part, approximately 96 large-scale hollow cylinder samples were tested based on the stress path shown in Figure 3.10. This part can be divided into two series.

Series I: Tests on clean sand

To investigate the effect of different directions of principal stress on the characterisation of stress-strain and volumetric strain in sand, samples of clean sand were prepared with a relative density of about 70%, and tested under a monotonic drained torsional test. During all tests, the mean effective stress p' and intermediate principal stress parameter b were kept constant at 100 kPa and 0.5, respectively. However, these tests were performed under different principal stress directions α of 0, 15, 30, 60, 75 and 90°. This means that during tests, samples were subjected to increases in deviator stress until failure, while α was held constant at certain values.

Series II: Tests on reinforced clean sand

In this series, monotonic hollow cylinder tests were carried out on samples reinforced with different types and arrangements of geosynthetics, and considering six directions of principal stress α: 0, 15, 30, 60, 75 and 90°. Three types of geosynthetic reinforcement were used in these samples: geogrid, geotextile and geocell. Regarding the planar reinforcement of geogrid and geotextile, samples were arranged with two, three, four, five, six, nine and twelve layers, representing reinforcement spacings of *H/3*, *H/4*, *H/5*, *H/6*, *H/7*, *H/10* and *H/13*, respectively, where H is the total height of the sample. Geocell was used in a form of multi connected cells. Samples that were reinforced with each of these different types and arrangements were tested under different directions of principal stress α, as mentioned above, while the mean effective principal stress p' and intermediate principal stress parameter b were kept constant at 100 kPa and 0.5, respectively.

Comparing the results of this series with the previous one can provide some insight into the effect of anisotropy, i.e. directional dependence, on reinforced sand and the extent to which reinforcement can reduce this effect.

3.5.2 Part Two: Monotonic Tests on Sand-clay Mixtures and Reinforced Mixtures Using HCA under Various Directions of Principal Stress α

In this part, about 44 large-scale hollow cylinder samples were tested based on the stress path shown in Figure 3.10. This part was divided into two series of tests.

Series I: Tests on the sand-clay mixture

The effect of different percentages of kaolinite on the shear strength and deformation characteristics of sand under anisotropic conditions was investigated in this series. Drained torsional tests were performed on sand mixed with fines content F, kaolinite content 5, 10, 15 and 20%, under constant p' and b, and various directions of principal stress direction α, similar to as was mentioned previously. The findings of this series can be compared with the findings of Series I (in Section 3.5.1) to get an idea about the role of fines on the behaviour of sand under anisotropic conditions.

Series II: Tests on the reinforced sand-clay mixture

This series is an extension of Series II in Section 3.5.1, where fine F was added to the reinforced sand. In these tests, the percentage of fine that produced maximum strength in term of peak deviator stress q_p in Series I (above) was added to reinforced samples in this series. The types of reinforcement (geogrid, geotextile, geocell) and test conditions (p' = 100 kPa, b = 0.5) employed in this section were similar to those used in Section 3.5.1. However, to eliminate the huge number of tests that would be required to test all possible combinations, only three and six layers of planar reinforcement were considered, and only four values of α were chosen: 0, 30, 60 and 90°.

The results of Sections 3.5.1 and 3.5.2 give insights regarding several points:

a) The effect of anisotropy on clean sand;

b) The effect of fines on sand behaviour under anisotropic conditions, and the extent to which fines reduce or increase anisotropic strength and deformation.

c) The anisotropic strength and deformation of sand reinforced with different types and forms of geosynthetic reinforcements.

d) The anisotropic characteristics of the combination of sand, clay and reinforcement.

3.5.3 Part Three: Monotonic Tests Using the HCA under Various Values of α and Intermediate Principal Stress Parameter b

In Sections 3.5.1 and 3.5.2, the tests were carried out under a constant intermediate principal stress parameter b of 0.5. In this part, the tests were extended to include intermediate principal stress parameter b of 0.2 and 1.0, to investigate their effect on sand, reinforced sand, the sand-clay mixture and the reinforced mixture. Therefore, more than 64 large-scale hollow cylinder tests were carried out based on the stress path shown in Figure 3.10. These were divided into four test series, as follows.

Series I: Tests on clean sand

Hollow cylinder torsional tests were carried out in this series on sand under intermediate principal stress parameter values b of 0.2 and 1.0 (tests with b = 0.5 were already carried out in Section 3.5.1). For each value of b, tests were conducted considering several values of α, 0, 30, 60 and 90°, while p' was held constant at 100 kPa (similar to the previous series). Therefore, the results of this series provide information about the effect of intermediate principal stress parameter b on the strength and deformation of sand under every single value of principal stress direction α.

Series II: Tests on the sand-clay mixture

Sand mixed with optimum clay content (obtained from Series I in Section 3.5.2) was tested under the different values of b (0.2 and 1.0). For each b value, four values of principal stress direction α (0, 30, 60 and 90°) were considered, while p' was kept constant.

Series III: Tests on reinforced clean sand

In Section 3.5.1, extensive tests were performed on reinforced sand considering only b = 0.5. Therefore, in this series, conditions of b = 0.2 and 1.0 were investigated by testing sand reinforced with selected reinforcements: six layers of geogrid, six layers of geotextile, as well as geocell. Moreover, each case was tested considering principal stress directions α of 0, 30, 60 and 90°.

Series IV: Tests on the reinforced sand-clay mixture

In this series, samples of sand containing the optimum percentage of clay and reinforced with six layers of planar reinforcements (geogrid; geotextile) and geocell were tested under b = 0.2 and 1.0. The effect of intermediate principal stress parameter b was investigated at different values of α: 0, 30, 60 and 90°.

3.5.4 Part Four: Cyclic Rotational Shear Tests Using HCA

Eighteen large-scale cyclic rotational shear tests were conducted in this part. In Sections 3.5.1–3.5.3, samples were sheared monotonically under a targeted direction of principal stress α that was kept constant during tests, while deviator stress q was increased continuously. For example, for α = 30, samples were subjected to increasing deviator stress until failure, while α was kept constant at 30°. However, the test path in this part was different—the deviator stress q was kept constant at a given stress ratio q / p' during the test, while the direction of principal stress α rotated continuously from 0° to 180° for 60 cycles as shown in Figure 3.11. Tests in this part are divided into several series:

Series I: Cyclic rotational shear tests on clean sand

In this series, rotational cyclic tests were performed on dense sand of 70% relative density, for 60 cycles. This type of test was conducted under different constant stress ratios q / p' of 0.69, 0.9 and 1.1, where q = 69, 90 and 110 kPa. During this test, p' and b were held constant at 100 kPa and 0.5, respectively.

Series II: Tests on reinforced sand

The effect of cyclic rotational shear was investigated on sand reinforced with two, three, four, five and six layers of geogrid. These tests were carried out considering the effect of different stress ratios q / p' (0.69, 0.9 and 1.1). Rotational tests were also carried out on samples reinforced with six layers of geotextile and with geocell under a selected stress ratio q / p' of 1.1. Similar to the above series, D_r, p' and b were 70%, 100 kPa and 0.5, respectively.

The results of these tests demonstrate the anisotropic deformation characteristics of reinforced samples, with different types and selective forms of reinforcements,

subjected to cyclic rotation of the principal stress axes at different effective stress ratios.

Series III: Tests on sand-clay mixture

Sand mixed with the optimum clay content was tested for 60 cycles of rotational shear (0–180°) with a q / p' of 1.1, and constant values of p' and b of 100 kPa and 0.5, respectively.

Series IV: Tests on reinforced sand-clay mixture

In this series, samples containing optimum clay content and reinforced with six layers of planar reinforcements (geogrid, geotextile) and with geocell were tested under continuous rotation of the principal stress directions for 60 cycles with a stress ratio q / p' of 1.1. Similar to the previous series, tests were conducted under constant p' and b.

3.5.5 Part Five: Scaled Model Tests – "Loading Tests"

In this series, anisotropy was investigated by preparing samples with bedding plane inclination angles of 0, 15, 30, 45, 60, 75 and 90°. For each of these angles, cement contents of 0, 3, 5 and 7% were considered. Static loading and cyclic loading tests were performed on these samples. For cyclic loading tests, three different amplitudes were considered: 10, 20 and 30% (Figure 3.9). These tests demonstrate the effect of the anisotropy of sand on settlement-carrying loading, as well as cyclic settlement. It provides insight into the role of cementation in eliminating the anisotropic effect.

3.6 Reliability and Repeatability of Test Results

In order to validate the reliability of the hollow cylinder apparatus test results, preliminary experiments were performed on dense sand (D_r = 70%) using the HCA and a conventional triaxial apparatus. Three tests were carried out using the conventional triaxial device under constant σ_3 values of 100, 150 and 200 kPa. Two tests were performed also using the HCA: one under a constant σ_3 value of 100 kPa, and the other under a constant mean effective stress p' of 100 kPa. It should be mentioned that the samples were tested under b=0.0 (triaxial compression test). From Figure 3.12, it can be observed that very good agreement was obtained from both apparatuses. The average stress ratio at failure q / p' was 1.265 with only 2.4%

deviation. Moreover, the repeatability of the test findings was verified by performing repeated tests on clean sand under two different directions of principal stress, α = 0 and 60°, as shown in Figure 3.13. The results of these repeated tests exhibited good agreement.

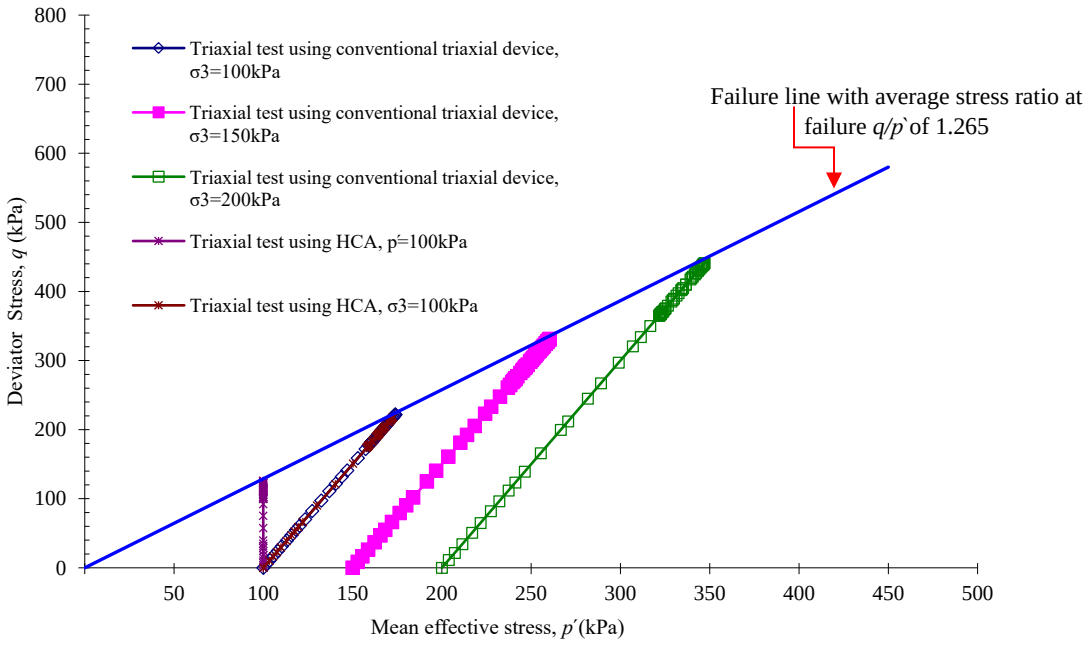

Figure 3.12 The stress paths of triaxial compression tests obtained from the HCA and conventional triaxial testing devices

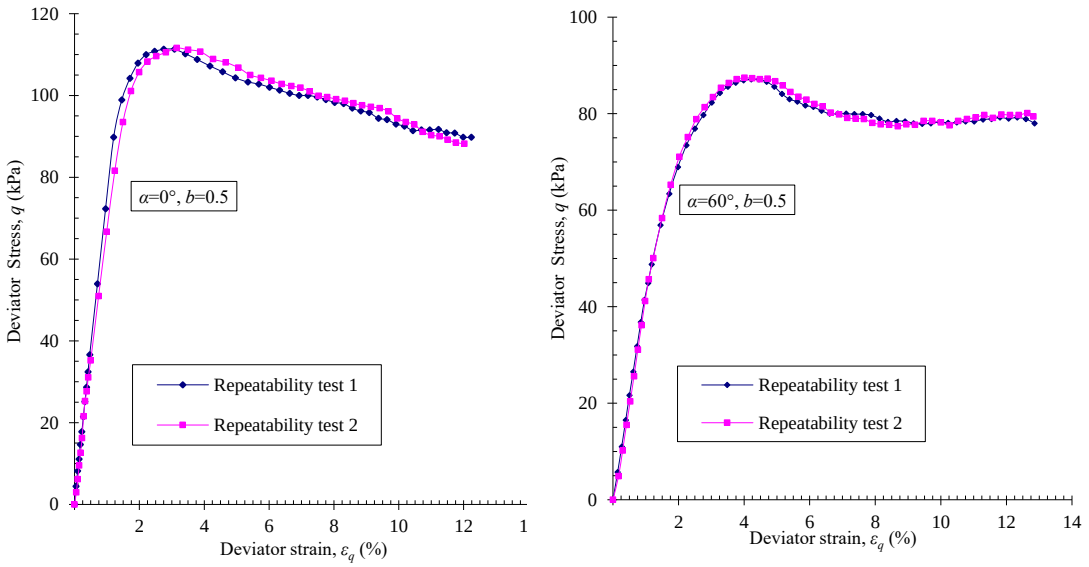

Figure 3.13 Deviator stress-strain of the repeat tests: (a) under α = 0° and (b) under α = 60°

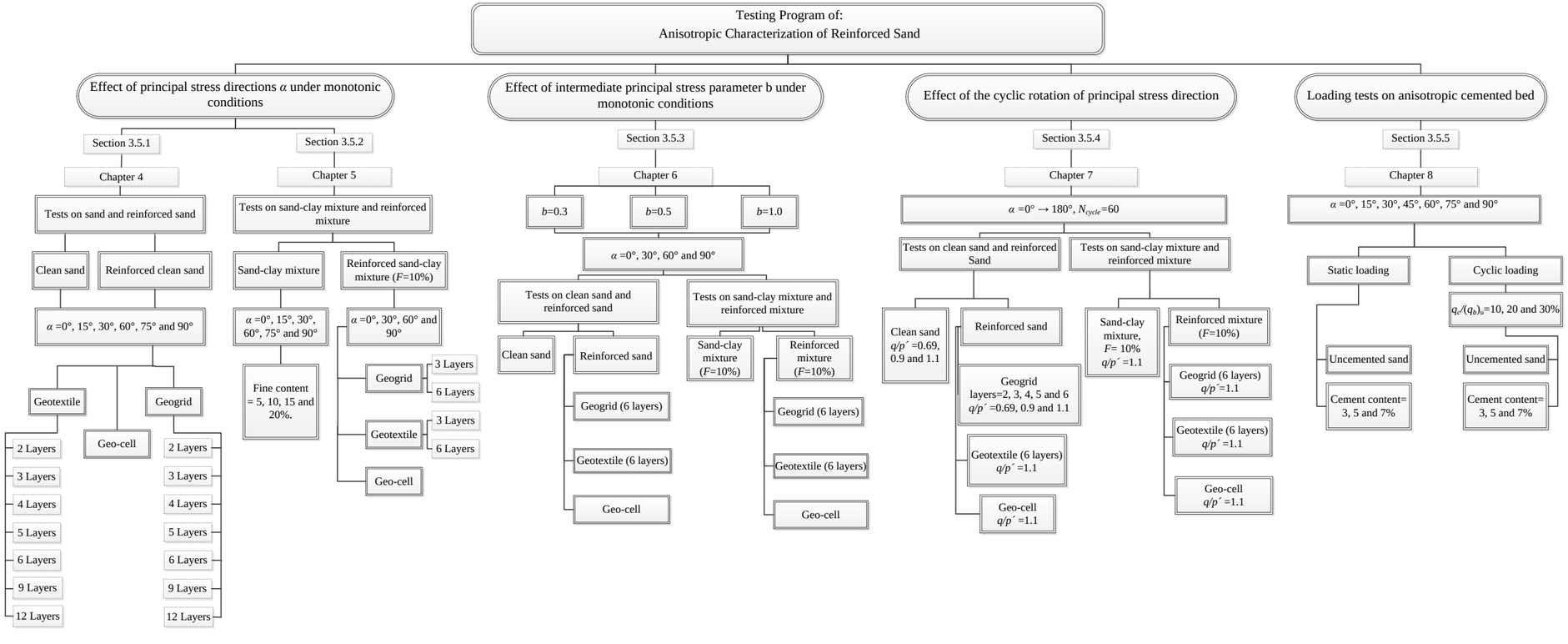

Figure 3.14 Flow chart of the testing program

Chapter 4

Monotonic Hollow Cylinder Tests on Reinforced Sand under Various Directions of Principal Stress

4.1 Introduction

In recent decades, there has been widespread use of geosynthetics to enhance the shear strength and deformation characteristics of geomaterials. However, no information is available in the literature regarding the anisotropic characteristics of reinforced soil in relation to the direction of principal stress. Moreover, there is little information on the drained behaviour of clean sand.

The effects of the direction of principal stress α on the stress-strain and deformation characteristics of sand and reinforced sand are investigated in this chapter. Table 4.1 shows the monotonic tests series conducted on unreinforced and reinforced sand. There are two testing sections illustrated in this table; the former one includes three series of tests on geogrid-, geotextile- and geocell-reinforced sand. Tests were carried out, as detailed in Chapter 3, by shearing samples with the major principal stress direction fixed at a given value, as shown in Figure 4.1.

Table 4.1 Summary of the conditions and parameters of the tests performed on reinforced and unreinforced sand under different directions of principal stress

Test Series	Reinforcement type	Arrangement of geosynthetics	Relative density, D_r (%)	Mean effective stress, p'	Intermediate principal stress parameter, b	Principal stress direction, α (°)
Series I Unreinforced sand	-----	-----	70.1-70.7	100	0.5	0, 15, 30, 60, 75 and 90°
Series II Reinforced sand	Geogrid	2, 3, 4, 5, 6, 9 and 12 layers	69.91-70.4	100	0.5	0, 15, 30, 60, 75 and 90°
	Geotextile	2, 3, 4, 5, 6, 9 and 12 layers	70.2-70.3	100	0.5	0, 15, 30, 60, 75 and 90°
	Geocell	geocells	69.3-70.6	100	0.5	0, 15, 30, 60, 75 and 90°

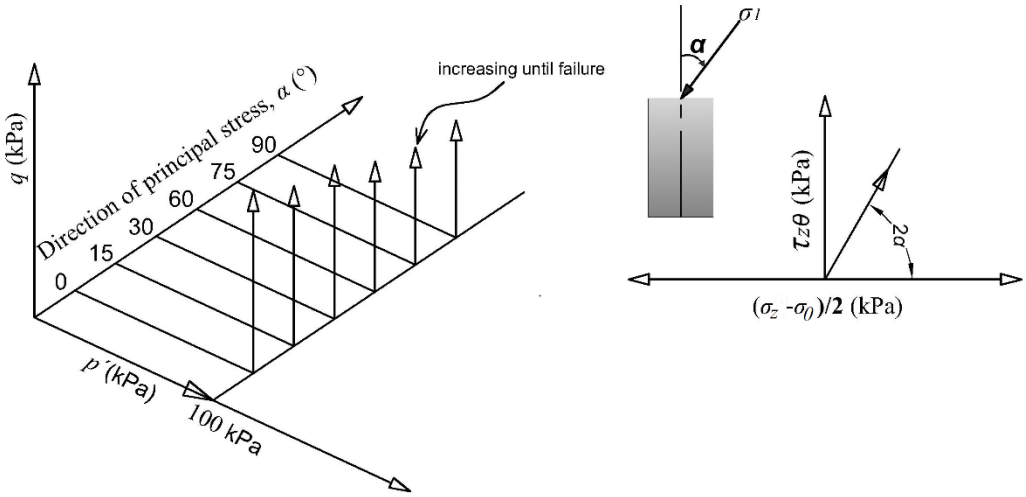

Figure 4.1 Stress paths for monotonic tests with fixed principal stress directions

4.2 Unreinforced Clean Sand

4.2.1 Strength Characteristics

The results of the tests outlined in Table 4.1 and described in Section 3.5.1 (Chapter 3) are presented in Figures 4.2a and b. These figures show the deviator stress q vs. deviator strain ε_q, where ε_q is calculated according to Equation 3.2, while q is based on the following equation:

$$\text{Deviator stress: } q = [1/2\{ (\sigma_1 - \sigma_2)^2 + (\sigma_2 - \sigma_3)^2 + (\sigma_3 - \sigma_1)^2 \}]^{1/2} \qquad (4.1)$$

There was a clear directional dependence of strength, where the deviator stress q varied significantly based on the principal stress direction α. This change in strength indicates that this material is anisotropic. Figure 4.2a shows the relationship between the deviator stress and deviator strain of sand under different directions of principal stress. It demonstrates that deviator stress q increased with deviator strain ε_q until reaching a peak, and then decreased, and the peaks of deviator stress q_p decreased with increasing α. Moreover, it can be seen that for α = 60–90°, the loss of post-peak

strength was lower than for α = 0–30°. At high deviator strain levels, deviator stresses for different values of α approached each other.

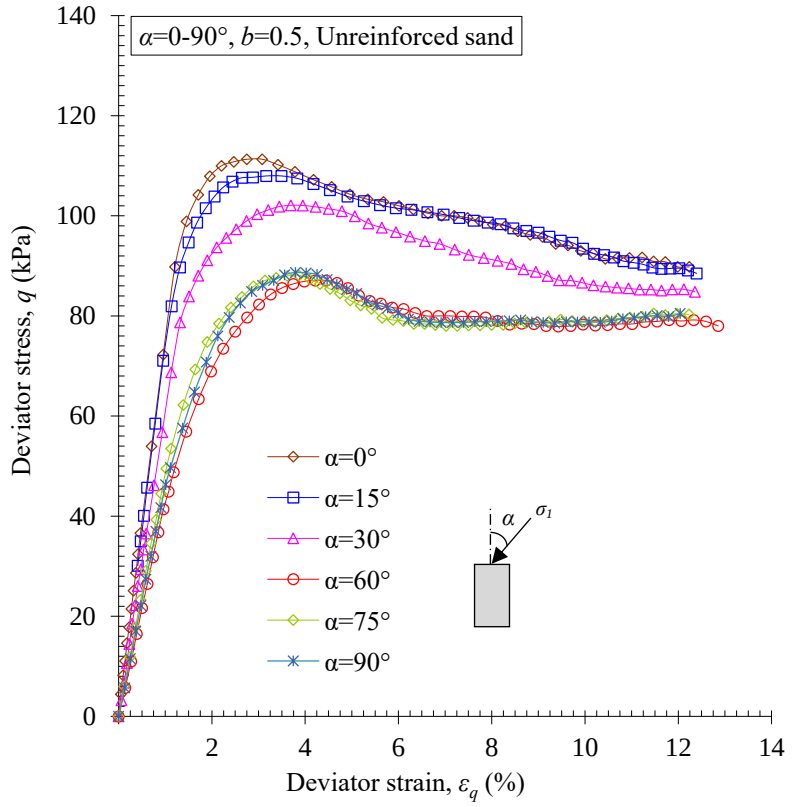

(a)

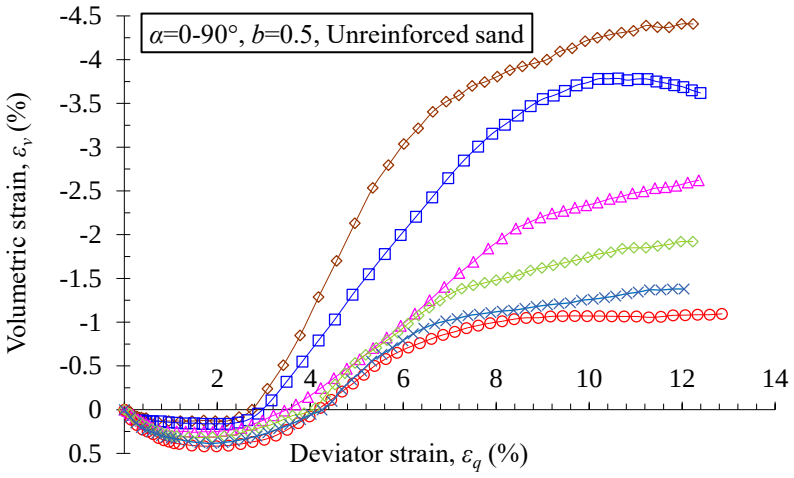

(b)

Figure 4.2 Relationships between (a) deviator stress and deviator strain and (b) volumetric strain and deviator strain (for unreinforced sand).

Figure 4.3 demonstrates the variation in peak deviator stress q_p with α. Deviator stress decreased moderately from its largest value of 111.3 kPa at α = 0° to 108.0 and 102.2 kPa for α = 15 and 30°. It then dropped rapidly to a minimum value of 87 kPa at α = 60°, before reverting slightly to 88 and 88.5 kPa at 75 and 90°, respectively. This variation in strength due to anisotropy produced a maximum difference of around 21.8% between the deviator stresses at α = 0 and 60°, at which the maximum and minimum strengths were attained, respectively.

This difference ratio in the peak deviator stress (Δq_p), which is defined in Equation 4.2, was used to represent the effect of directional dependence.

$$\Delta q_p = [(q_{p\,\alpha=0°}) - (q_{p\,\alpha})] / q_{p\,\alpha=0°} \quad (4.2)$$

Here, $q_{p\,\alpha=0°}$ and $q_{p\,\alpha}$ are the peak deviator stresses for sand at α = 0°, 15°, 30°, 60°, 75° or 90°. This trend, of the variation of deviator stress with α, is consistent with that observed by Miura et al. (1986), Cai et al. (2012) and Lade et al. (2014). The friction angles for these figures were computed with the assumption that cohesion is insignificant for sand soil.

As the inclination of the major principal stress α is a function to $\tau_{z\theta}$ and (σ_z - σ_θ), most of the failure surfaces obtained from torsional tests can be plotted simply in a space of (σ_z - σ_θ) / 2p' and $\tau_{z\theta}$ / p', which clearly describes the stress state of samples (Kumruzzaman & Yin, 2010b; Nishimura, Minh, & Jardine, 2007). This is important to determine whether or not the samples show any anisotropic behaviour. Figure 4.4 shows the failure envelope for tests on unreinforced sand. This failure surface represents the relation between (σ_z - σ_θ) /2p' and $\tau_{z\theta}$ / p' at the peak state and it was obtained by connecting the failure points of tests conducted under values of α ranging from 0–90°. For comparison, the assumed isotropic envelope was plotted as dashed lines in this figure. It is clear that the solid failure envelope of tested sand was not circular—the points have different radii from the origin, which is because of the anisotropic effect. This asymmetry generally began after α = 30°, where the shaded area (in Figure 4.4) represents the anisotropy in strength due to variation in the direction of principal stress.

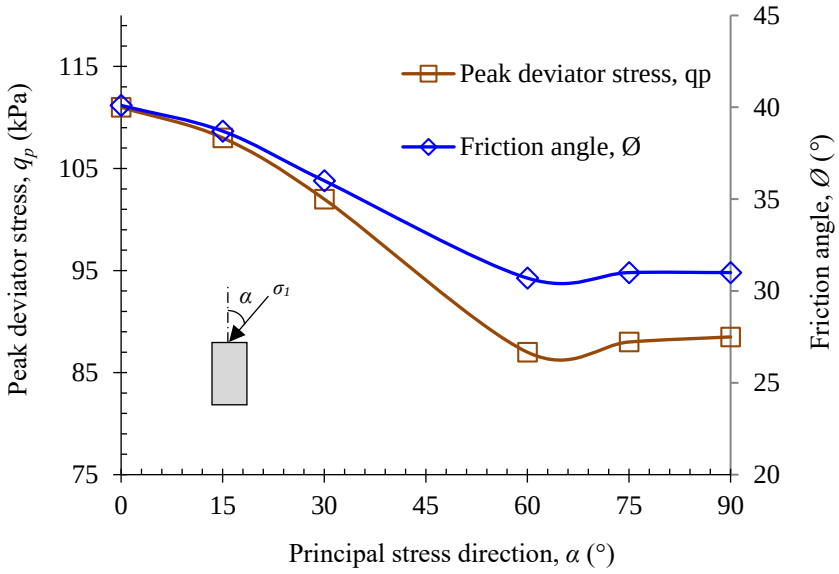

Figure 4.3 Peak deviator stress and friction angle of unreinforced sand at different directions of principal stress

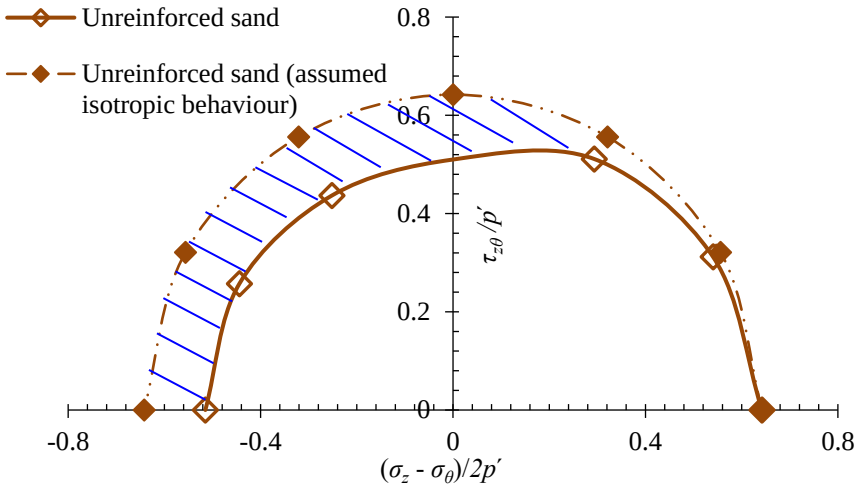

Figure 4.4 Failure envelopes for unreinforced sand in the $(\sigma_z - \sigma_\theta)/2p'$ vs. the $\tau_{z\theta}/p'$ spaces

This behaviour is related to inherent anisotropy and can be explained in conjunction with the mobilised plane or maximum obliquity plane presented by Matsuoka (1974). This plane can be produced at an inclination of θ to the major principal stress, which in turn makes an angle α relative to the vertical axis. The maximum obliquity plane

angle θ is 45^o - $\emptyset$ / 2 relative to the major principal stress (Figure 4.5) and, consequently, the mobilised plane is α + (45^o - $\emptyset$ / 2) relative to the vertical and (45^o + $\emptyset$ / 2) – α relative to the bedding plane, where $\emptyset$ is the angle of internal friction of the material used. When α = 60°, the friction angle was 30.7° (Figure 4.3) and, thus, the mobilised plane was coincident with bedding plane. The particles tended to aligned horizontally in a form where their longest dimensions become parallel to the horizontal plane. This can produce very poor interlocking between particles resulting in easy sliding. Accordingly, the bedding plane is considered the weakest plane. As a consequence, coincidence of the maximum obliquity plane and bedding plane resulted in the lowest strength. This weak interlocking between sand particles in the bedding plane caused by preferred horizontal alignment has also been reported by Oda and Koishikawa (1979) and Miura et al. (1986).

Scanning electron microscope (SEM) image was made of the sand used in this study to determine the sphericity of its particles, which is a good indicator of its dimensional properties. Zheng and Hryciw (2015) and Hryciw, Zheng, and Shetler (2016) defined sphericity as the particle length-to-width ratio (Figure 4.6). Therefore, the mean value of this ratio was measured based on many particles, although calculation is difficult due to their irregular shapes. The mean sphericity was calculated as 0.63 (Table 3.1), which indicates that the particles are clearly long in shape.

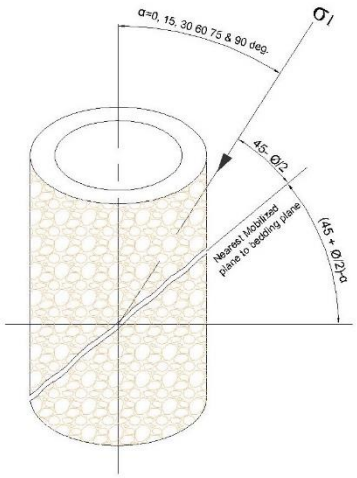

Figure 4.5 Schematic explanation of maximum stress obliquity plane

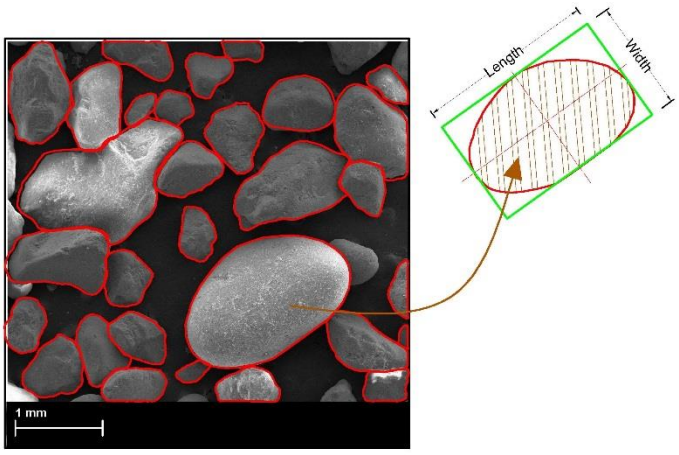

Figure 4.6 Typical SEM image of the sand used as samples

Moreover, the variation in deviator stress can also be interpreted as a reflection of fabric evolution during shearing, where the preferred contact normal and preferred alignment of particles can contribute to the anisotropic effect. The decrease in strength can be attributed to the lower stability of the induced microstructure during loading. Here, continuous chains of contact normal are formed in columnar microstructures once shearing starts. These have a tendency to become aligned along the major principal stress direction in order to transfer the applied load (Oda et al., 1998; Sazzad & Suzuki, 2010; Seyedi Hosseininia, 2012b). This is accompanied by the rotation and rearrangement of particles undergoing loading and, thus, some of these columns collapse and new ones are formed. As mentioned in most of the literature, the longest dimensions of the particles align horizontally. Therefore, these columns are likely to be most stable when $\alpha = 0°$, where column width (*b col.1*) is equal to the longest particle dimension (l). Meanwhile, for $\alpha > 0°$, the column width (*b col.2*) is lower, as shown in Figure 4.7, resulting in lower stability (Seyedi Hosseininia, 2012b). For $\alpha = 90°$, for instance, the width of the columns becomes equal to the shortest particle dimension (w) due to preferred horizontal alignment. This results in the lowest stability and high deformation due to the strong tendency to rotate and collapse under torque produced by some eccentricity of forces (Seyedi Hosseininia, 2012b). In other words, particles under $\alpha > 0°$ are vulnerable to sliding, rotation and collapse due to the torque caused by force eccentricities in such columnar microstructures.

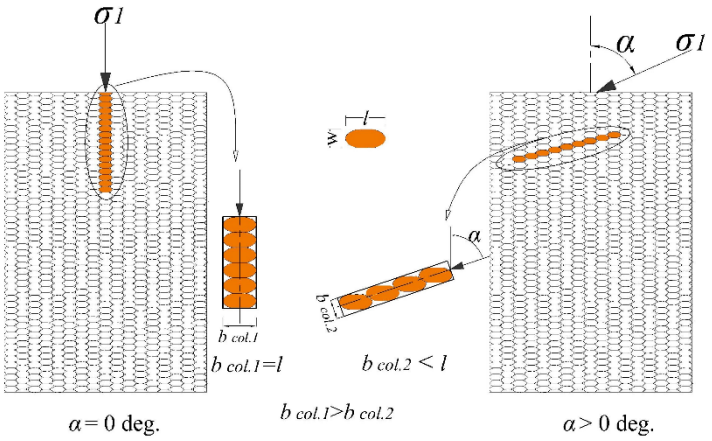

Figure 4.7 Simple explanation for columnar microstructures under inclined principal stress (concept from (Seyedi Hosseininia, 2012b))

The effect of anisotropy on the strength of sand presented in this work is consistent with previous studies conducted on small samples using hollow cylinder torsional tests or by numerical simulation, such as Cai et al. (2012); X. Li and Yu (2009); Tong et al. (2008); L. Yang et al. (2016); Y. Yang et al. (2015) among others, as shown in Figure 4.8. It is notable that soil type, particle shape and the boundary conditions of tests can cause some differences in the findings. For example, the intermediate principal stress parameter varied from 0.0 to 1.0 during every single test conducted by Cai et al. (2012), while it was held constant at 0.5 in L. Yang et al. (2016) study. Moreover, deviator stress was presented as (σ_1 - σ_3) in some studies such as Cai et al. (2012), while others such as L. Yang et al. (2016) and the present study presented it considering the three principal stresses (Equation 4.1) instead of only two.

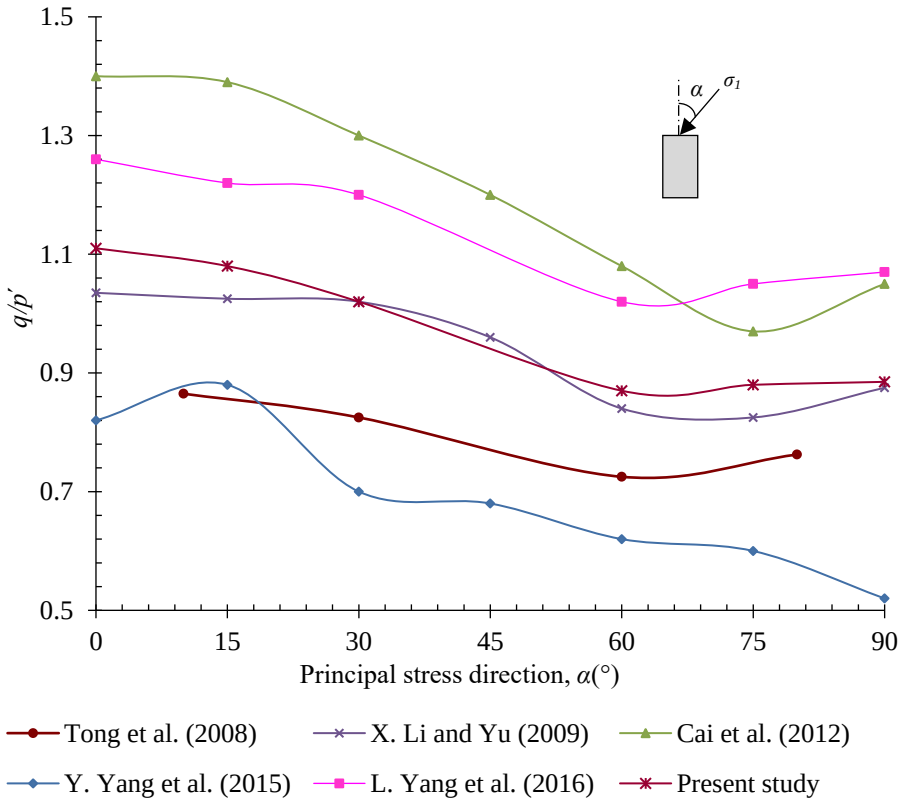

Figure 4.8 Maximum stress ratio (q / p) at different directions of major principal stress (α), and comparison with previous studies

4.2.2 Volumetric Strain Characteristics

The results showed that anisotropy influences not only strength characteristics but also deformation behaviour, as depicted in Figure 4.2b. This figure shows the volumetric-deviator strain relationship of sand tested under different directions of principal stress. The positive and negative signs of the strain refer to decreases (compression) and increases (expansion) in volume during shearing, respectively.

It is clear that the deviator strain ε_q at peak stress increases as α increases. For example, peak deviator stress q_p occurred at a deviator strain ε_q of 2.7–3.6% for α = 0–30°, while this range increased to 3.79–4.1% for α = 60–90°. During tests, sand exhibited an initial reduction in volume, and this compression behaviour was significant when $\alpha \geq$ 60°. For example, compressive volumetric strain ranged between 0.13% and 0.25% for α = 0–30°, while it increased for $\alpha \geq$ 60° to 0.32–0.42%. As deviator strain ε_q increased from 2.75–4.25%, volumetric strain transformed to dilative behaviour. Note

that such dilative volumetric strain generally reduced as α increased; it was 4.4, 3.62, 2.57, 1.08, 1.92 and 1.37% at α = 0, 15, 30, 60, 75 and 90°, respectively.

The induced compressive volumetric strain can be attributed to fabric evolution during shearing in terms of rearrangement, sliding, and rotation of particles which close some of the voids and gaps in the sand structure and, consequently, decrease the sample volume. The particular increase in compressive volumetric strain when $\alpha \geq 60°$ is related to what was explained in Section 4.2.1 regarding the weakest bedding plane and the mobilised plane in addition to the induced microstructural columns. When samples were subjected to shearing with α = 60°, the maximum obliquity plane was coincident with the weakest bedding plane, which was caused by the preferred alignment of particles. This coincidence results in maximum compression deformation due to the tendency of particles to slide, rotate and deform along the radial direction.

Moreover, the dilation is related to the behaviour of the induced columns that were mentioned in Section 4.2.1. These columnar microstructures can buckle under shearing with increases in deviator stress/strain, leading to increases in sample volume and a change in the trend from compression to expansion. The density of the induced columnar microstructures, i.e. the number per unit volume, was higher when $\alpha = 0^{\circ}$, relative to other inclinations (Seyedi Hosseininia, 2012b). This may be the cause of the higher expansion observed under the lower range of α. This is in accordance with Wan and Guo (2004), who observed that samples under α = 90° exhibited less dilative volumetric strain with fewer contact normals aligned in the horizontal plane than when α = 0°.

4.3 Reinforced Sand

In this section, the anisotropic strength and deformation of sand reinforced with three different types of reinforcements, geogrid, geotextile and geocell, are presented. All tests were conducted under constant b and p' values of 0.5 and 100 kPa, respectively, and various values of α of 0–90°. In practice, many reinforced geostructures such as earth abutment, steep slopes and walls are constructed with more than four layers of reinforcement. Twelve-layer configuration is chosen in this study to determine the number of the reinforcement layers $N_{reinf.}$ required to achieve the maximum strength of reinforced sand, after which the improvement becomes insignificant.

4.3.1 Geogrid Reinforcement

4.3.1.1 Strength characteristics

In order to investigate the anisotropic strength characteristics of geogrid-reinforced sand, a series of drained hollow cylinder tests were carried out on sand reinforced with two, three, four, five, six, nine and twelve layers of geogrid. Each reinforcement case was investigated at different directions of principal stress α of 0, 15, 30, 60, 75 and 90°.

Figures 4.9-4.14 show that soil strength increased considerably with increasing numbers of reinforcement layers, under all directions of principal stress α. For example, reinforced sand at α = 0° (i.e. with principal stress normal to the bedding plane), exhibited increases in peak deviator stress of 19.8, 63.0, 92.5, 107.2, 116.3, 118.1 and 123.2% with two, three, four, five, six, nine and twelve reinforcement layers, respectively. The rate of increase was greatest when the number of layers was increased from two to six, while the rate increased more slowly as the number of layers was increased from six to twelve. The peak deviator stresses q_p obtained from samples reinforced with different numbers of layers of geogrid, and tested under different directions of principal stress, are plotted in Figure 4.15.

These increases in strength agree well with previous studies conducted on reinforced soil using conventional triaxial compression tests, such as Latha and Murthy (2006, 2007) and Peng, Kotake, Tatsuoka, Hirakawa, and Tanaka (2000). The observed

improvement is attributed to the soil confinement mechanism provided by the reinforcement. Such confinement is dependent on the reinforcement type, reinforcement tensile strength, interfacial friction between the reinforcement and soil, the shear resistance of confined sand inside the reinforcement apertures, and the induced passive resistance.

However, the anisotropic response of reinforced sand to shearing under different directions of principal stress was clear. There were various amounts of improvement depending on α. Therefore, the findings can be divided into two trends: one for the range α = 0–30° and the other for α = 60–90°. Figure 4.16 depicts the variation in peak deviator stress q_p along the direction of principal stress α for different numbers of geogrid layers.

Geogrid-reinforced samples under conditions of $\alpha \leq 30°$ showed very significant increases in peak deviator stress q_p. Increasing the number of layers resulted in larger increases in q_p, while decreases in the variation of q_p occurred due to variation in α. For example, under α = 0°, 15° and 30°, unreinforced samples had q_p values of 111.3, 108.0 and 102.2 kPa, respectively; while in samples reinforced with two layers of geogrid, q_p increased to 133.8, 129. and 123.1 kPa. With six reinforcement layers, q increased greatly to 240.1, 238.9 and 240.6 kPa, respectively. This means that the difference ratio in deviator stress Δq caused by increasing α from 0° to 15° was slight (< 3.0%) with two reinforcement layers, and decreased significantly to 0.45, 0.9 and 0.06% with six, nine and twelve layers respectively. Similarly low values for the difference ratio in deviator stress Δq were reported for α = 30°, where Δq dropped from 8.1% for unreinforced sand to 0.26-1.1% for sample reinforced with 6 –12 layers of geogrid.

Compared with tests where $\alpha \leq 30°$, a different trend was reported for samples tested under conditions of $\alpha \geq 60°$, where sample behaviour was characterised by significant anisotropic responses. Samples reinforced with two, three, four, five, six, nine and twelve geogrid layers under α = 60° produced peak deviator stresses of 90.1, 95.2, 111.2, 116.3, 119.0, 120.9 and 123.8 kPa, respectively, compared with 87 kPa for unreinforced sand. This increase in q_p results in an improvement in strength of around

40.8% (for six layers) relative to unreinforced sand. In spite of this increase, there was a clear anisotropic effect. For example, the peak deviator stress of samples reinforced with six layers of geogrid was only 119.0 kPa at α = 60°, compared with 240.1 kPa at α = 0°, which constitutes a difference ratio Δq_p equal to 50.4%. Similar trends were observed at α = 75° and 90°, where the peak deviator stresses of six-layer reinforced samples were 39.5 and 36.7% higher, respectively, than those of unreinforced samples. Figure 4.17 presents a three-dimensional (3D) surface graph of the test results.

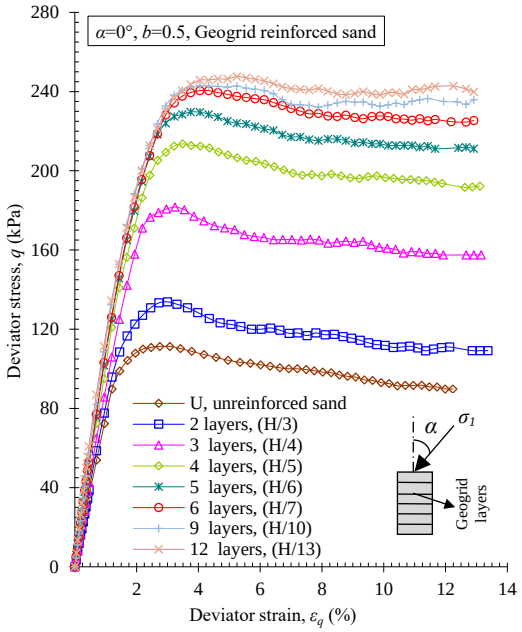

(a)

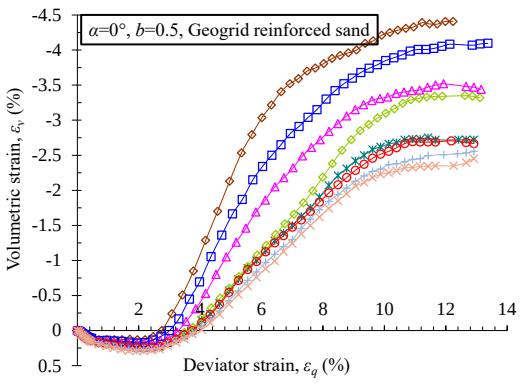

(b)

Figure 4.9 Relationships between (a) deviator stress and deviator strain; (b) volumetric strain and deviator strain (geogrid reinforced sand, α = 0°)

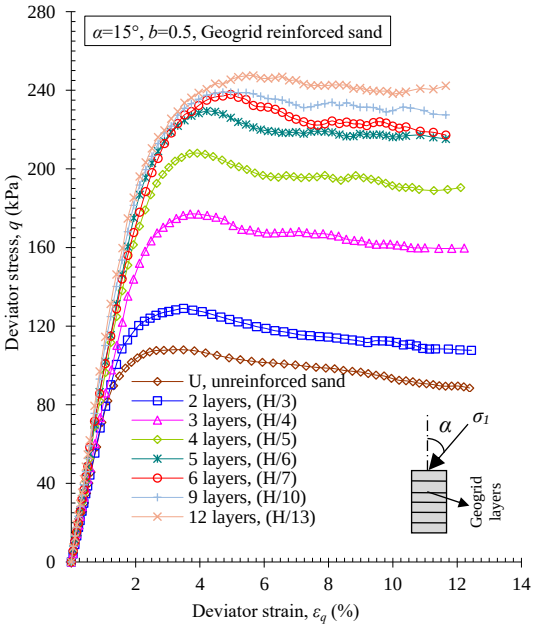

(a)

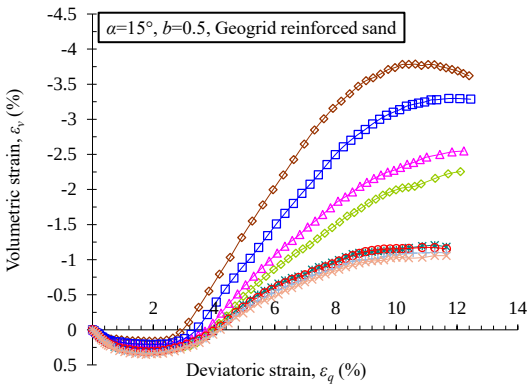

(b)

Figure 4.10 Relationships between (a) deviator stress and deviator strain; (b) volumetric strain and deviator strain (geogrid reinforced sand, α = 15°)

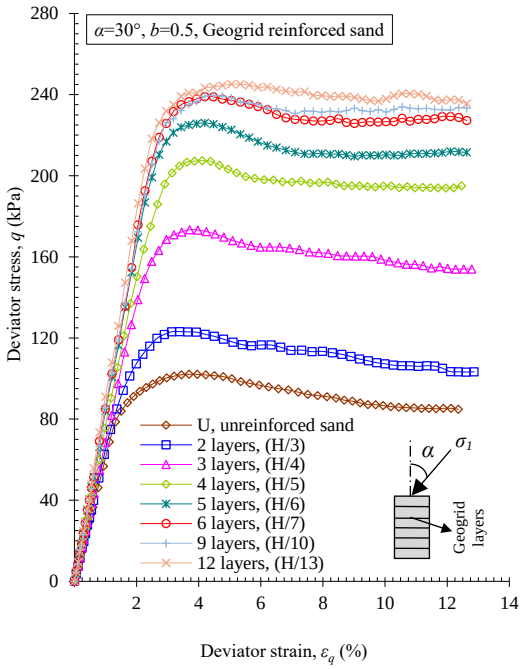

(a)

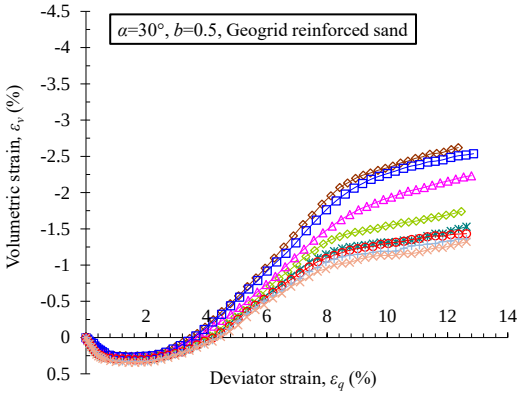

(b)

Figure 4.11 Relationships between (a) deviator stress and deviator strain; (b) volumetric strain and deviator strain (geogrid reinforced sand, α = 30°)

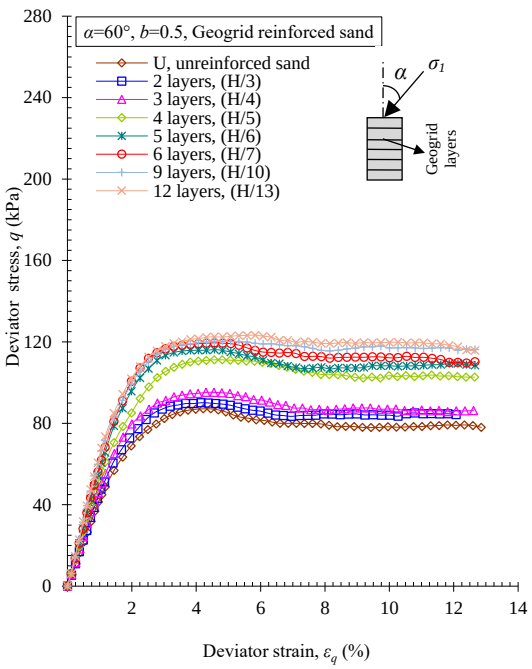

(a)

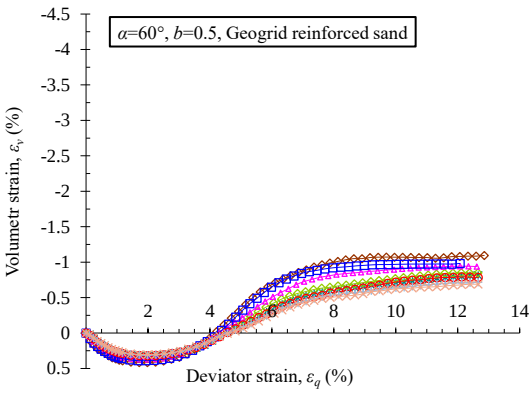

(b)

Figure 4.12 Relationships between (a) deviator stress and deviator strain; (b) volumetric strain and deviator strain (geogrid reinforced sand, α = 60°)

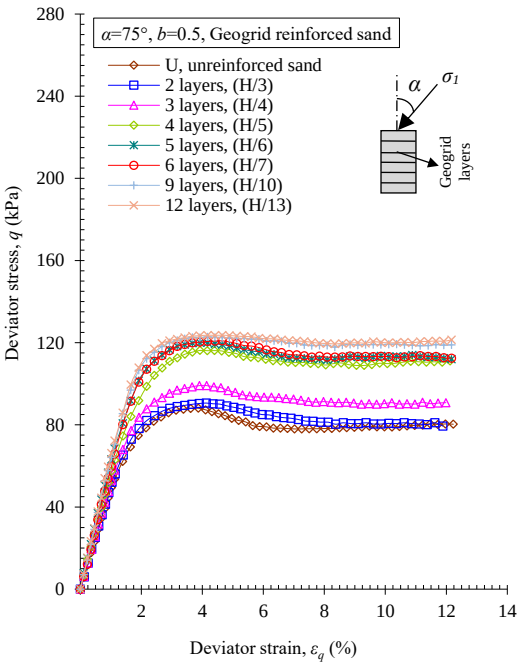

(a)

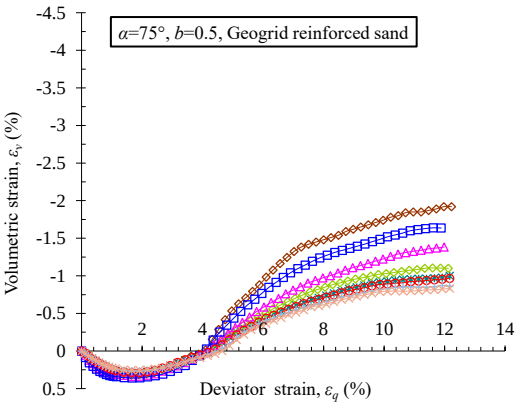

(b)

Figure 4.13 Relationships between (a) deviator stress and deviator strain; (b) volumetric strain and deviator strain (geogrid reinforced sand, α = 75°)

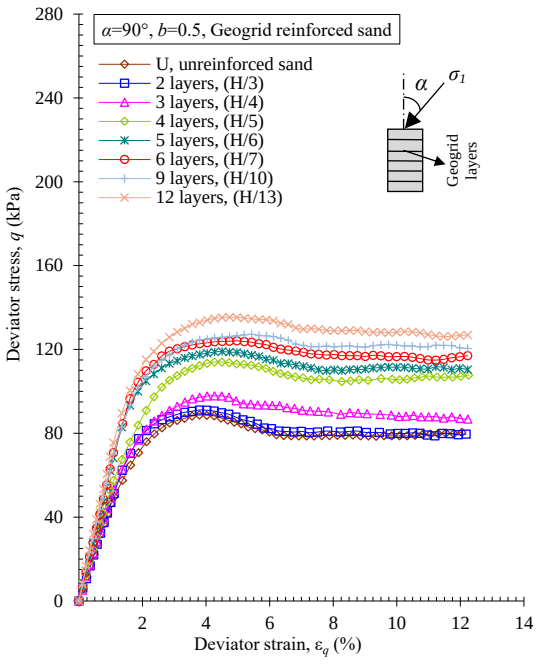

(a)

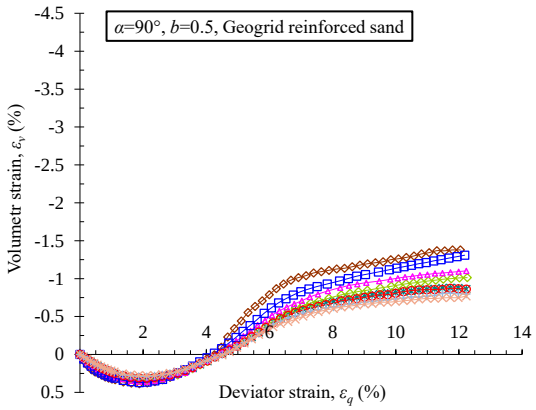

(b)

Figure 4.14 Relationships between (a) deviator stress and deviator strain; (b) volumetric strain and deviator strain (geogrid reinforced sand, α = 90°)

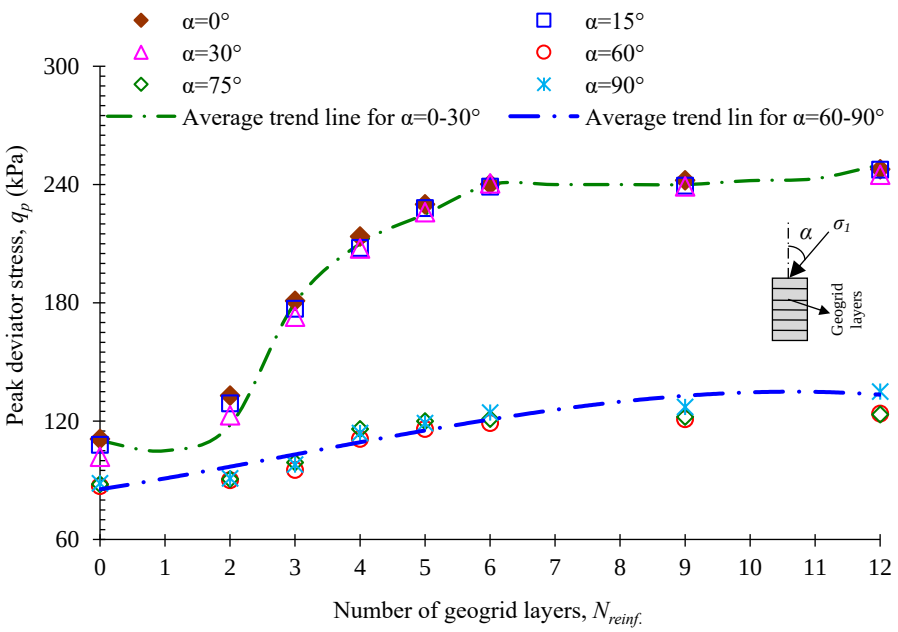

Figure 4.15 Peak deviator stress of reinforced samples with different numbers of geogrid layers under various directions of principal stress

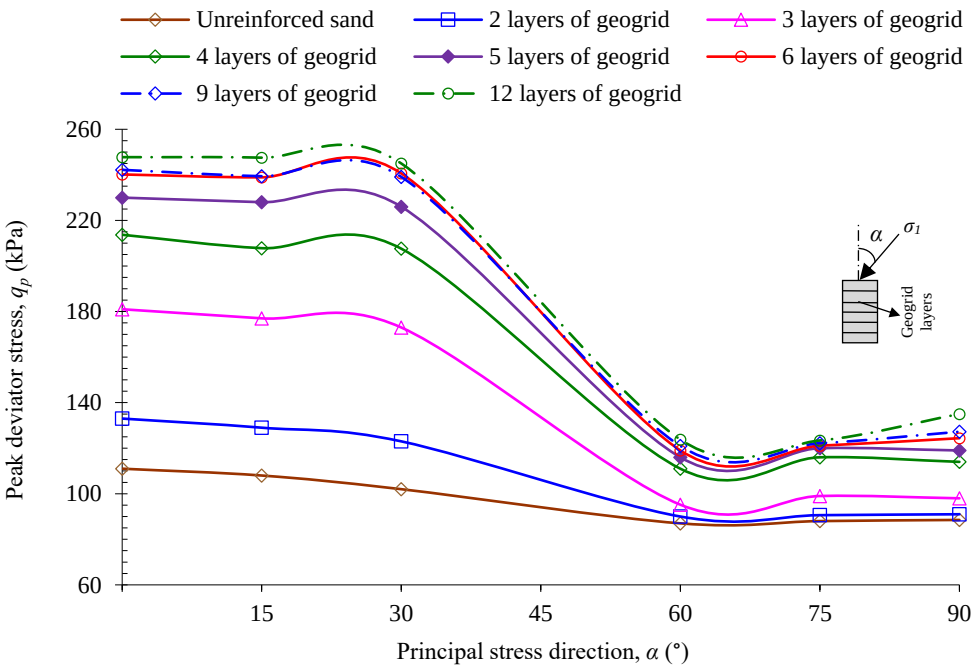

Figure 4.16 Relationship between the peak deviator stress q_p of reinforced samples and the direction of principal stress α

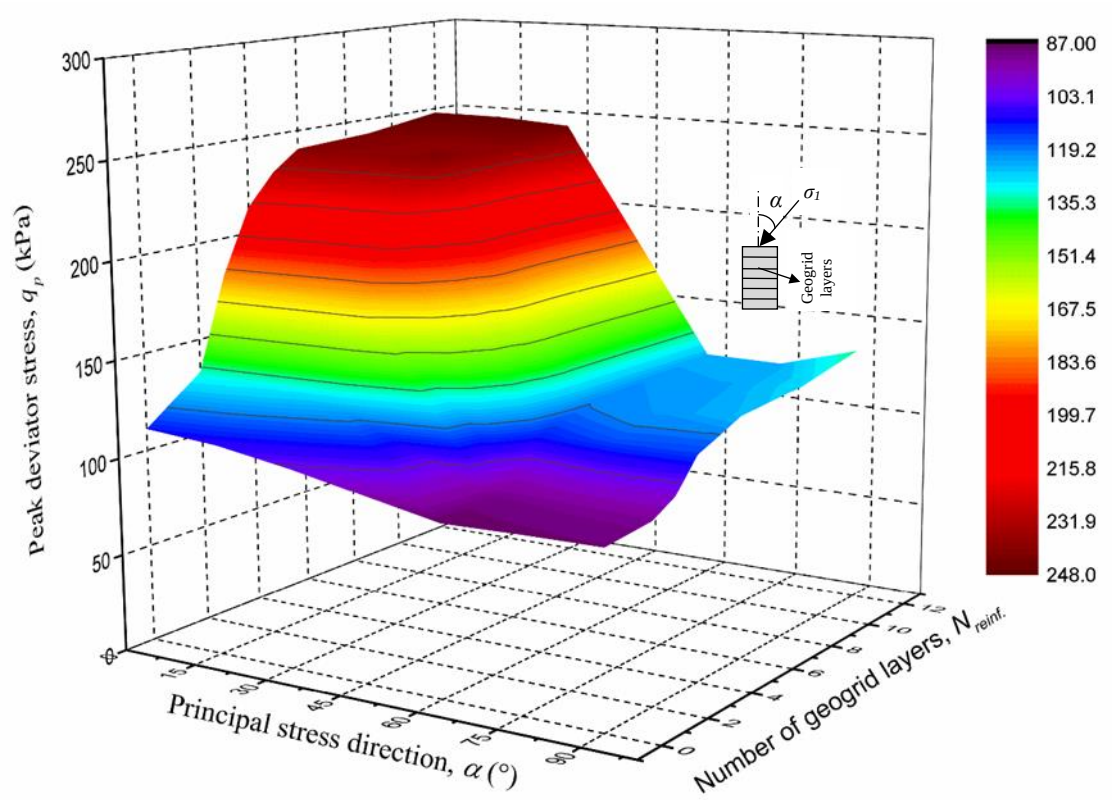

Figure 4.17 Composite α, $N_{reinf.}$, q_p values of the 3D failure surface for geogrid-reinforced sand

Most of the failure surface obtained for torsional tests can be plotted simply in a space of $(\sigma_z - \sigma_\theta) / 2p'$ and $\tau_{z\theta} / p'$, which clearly describes the stress state of samples. Accordingly, Figure 4.18a shows the failure envelope for tests on sand reinforced with two, three, four, five and six layers of geogrid. Furthermore, Figure 4.18b compares the failure envelopes for unreinforced sand and sand reinforced with six layers of geogrid. These failure surfaces were obtained by connecting the failure points of tests conducted under values of α ranging from 0–90°. For comparison, the assumed isotropic envelope was plotted as dashed lines in this figure. It is clear that the failure envelope of tested reinforced samples is asymmetrical—the points have different radii from the origin. This asymmetry generally began after α = 30°, where the shaded area (in Figure 4.18b) represents the anisotropy in strength due to variation in the principal stress direction.

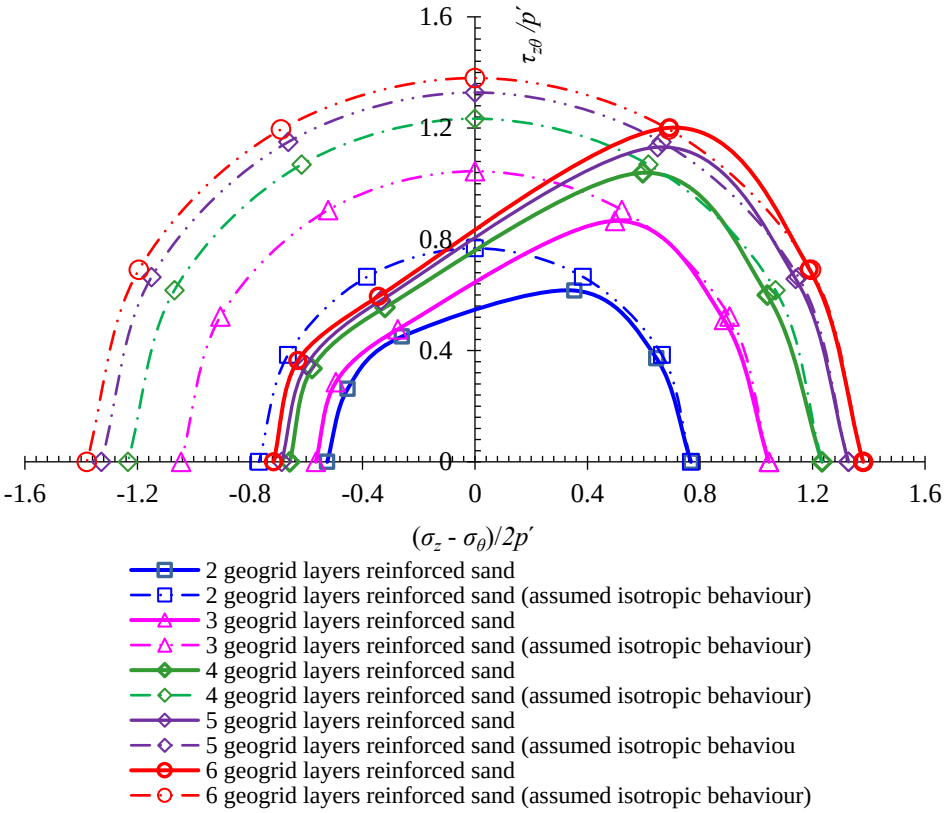

(a)

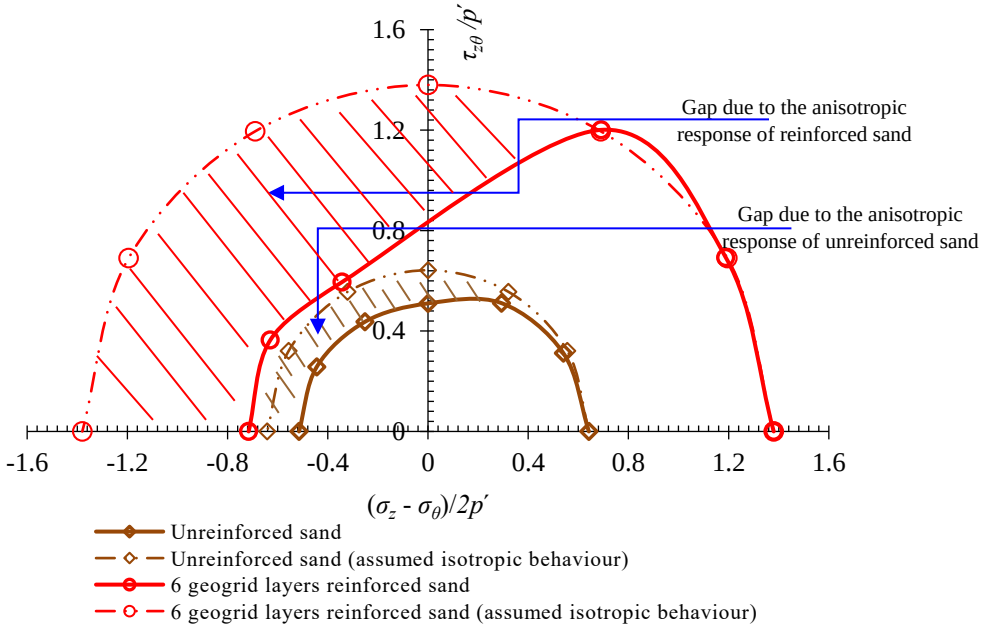

(b)

Figure 4.18 (a) Failure envelopes of geogrid-reinforced sand, and (b) comparison of the failure envelopes of unreinforced sand and six-layer geogrid-reinforced sand

The anisotropic effect on strength behaviour, particularly in the range of α = 60–90°, is related to the nature of the reinforcement layers. Their ability to resist shear decreases as the principal stress direction approaches that of the bedding plane, i.e., where the layers are embedded horizontally. This near coincidence between the maximum obliquity plane and the bedding plane occurred when α = 60–90°, as mentioned previously in Section 4.2.1. Consequently, less confinement is provided as little of the geogrid's tensile strength can be mobilised, compared to when load is applied vertically. Moreover, it is notable that tests under α = 0–30° were conducted in a mode similar to the compression condition ($\sigma_z > \sigma_r$), while it changed to the extension mode ($\sigma_r > \sigma_z$) for α = 60–90°. This indicates that under similar extension test conditions, the ability of geogrid layers to provide resistance is much less than when tests are conducted under compression. This is consistent with the results obtained by Habibi, Shafiee, and Jafari (2014).

4.3.1.2 Volumetric strain characteristics

Figures 4.9b-4.14b present the deformation results for sand reinforced with different numbers of geogrid layers, and tested under b = 0.5, p' = 100 kPa and different directions of principal stress α.

Compared with unreinforced samples, geogrid-reinforced samples exhibited larger deviator strains ε_q at failure. This increase in ε_q at failure was greater under conditions of $\alpha \leq 30°$ than when $\alpha \geq 60°$, due to the deviator stress developing significantly during the former compared with only slight increases occurring during the latter. For instance, the deviator strains corresponding to peak deviator stress under α = 0° were 2.7 and 5.2% for unreinforced sand and sand reinforced with twelve geogrid layers, respectively. Similar observations were reported for tests under other directions of principal stress where under α = 90°; for example, ε_q at peak strength increased from 4.0% for unreinforced specimens to 5.0% for sand with twelve layers of reinforcement.

Regarding the volumetric strain ε_v, a similar trend was observed to that of unreinforced sand where, as explained in Section 4.2.2, the volume of samples decreased initially before tending to expand. The amount of both compression and expansion strain depended on the principal stress direction α as well as the number of geogrid

reinforcement layers $N_{reinf.}$. As the principal stress direction α increased, compression volumetric strain $(\varepsilon_v)_{comp}$ increased while dilation or expansion volumetric strain $(\varepsilon_v)_{dil}$ decreased. This behaviour is linked to the low stability of incline-induced microstructures in addition to the preferred alignment of particles, which produces a poor interlocking plane. In other words, poor interlocking of particles along the horizontal plane results in easy deformation, as sand particles are vulnerable to sliding and rotation.

However, geogrid reinforcement contributed to significant reductions in the dilation amount compared with unreinforced sand. For example, at 12% deviator strain, the dilation volumetric strain $(\varepsilon_v)_{dil}$ of samples tested under $\alpha = 0°$ decreased from 4.4% for unreinforced sand to 4.0, 3.52, 3.35, 2.72, 2.71, 2.51 and 2.34% for sand reinforced with two, three, four, five, six, nine and twelve layers of geogrid, respectively. The amount of reduction in dilation due to reinforcement was also affected by the principal stress direction. For example, compared with unreinforced sand, sand with six layers of reinforcement had a lower $(\varepsilon_v)_{dil}$ value at $\varepsilon_q = 12\%$. The values for reinforced sand were 2.71% (at $\alpha = 0°$), 1.15% (at $\alpha = 15°$), 1.41% (at $\alpha = 30°$), 0.79% (at $\alpha = 60°$), 0.96% (at $\alpha = 75°$) and 0.86% (at $\alpha = 90°$), compared with 4.4, 3.62, 2.59, 1.08, 1.92 and 1.37% for unreinforced sand, respectively. Decreases in the variation of volumetric strain ε_v with α by inclusion of geotextile layers can be defined based on Equation 4.3, which describes the ratio of the amount of difference in ε_v at a given ε_q of reinforced sand relative to that of unreinforced sand:

$$(I.R)_{\varepsilon v} = [(\varepsilon_v)_{\alpha = 0°} - (\varepsilon_v)_{\alpha = 60°}]_{\text{reinforced}} / [(\varepsilon_v)_{\alpha = 0°} - (\varepsilon_v)_{\alpha = 60°}]_{\text{unreinforced}} \quad (4.3)$$

This ratio decreased from 90.9% to 57.8 and 50% with increasing geogrid layers from two to six and twelve respectively. The trend towards less dilative volumetric strain can be interpreted in terms of the mechanisms of soil-reinforcement interaction (Higuchi et al., 1998; Liu, Yang, & Nguyen, 2014; Nazzal, Abu-Farsakh, & Mohammad, 2007). When samples are subjected to loading, lateral stress will develop that is associated with lateral deformation. This induced stress and strain will be then transferred through the sand particles to the horizontally-embedded geogrid layers,

thus placing the planar layers under tension. Reinforcement mechanisms, caused by the interaction between soil and reinforcement, can include:

a) Shearing resistance produced by friction between particles and between particles and the geogrid surface.

b) Internal shear resistance induced by particles confined inside geogrid apertures.

c) Passive resistance induced along the transverse ribs due to the mobilisation of confinement, which corresponds to the transmission of applied stress from the particles to the reinforcement.

This interaction will mobilise the tensile strength of the tensioned membrane (geogrid), which resists the developing tensile stress and strain and, consequently, restrains and eliminates lateral deformation in the soil adjacent to the reinforcement layers. Therefore, this will decrease the tendency of soil to expand and increase its strength.

Increasing the number of reinforcement layers produced larger confinement, resulting in greater restriction of lateral strain due to an increased amount of soil particles being adjacent to geogrid layers. Decreasing dilation for reinforced soil agrees with the findings of Liu et al. (2014), Higuchi et al. (1998) and Peng et al. (2000).

Samples under $\alpha \geq 60°$ also exhibited low expansion strain, although the mobilisation of reinforcement in this range was much less than when $\alpha \leq 30°$. This lesser expansion is attributed to the larger compression strain that develops under $\alpha \geq 60°$ due to poor interlocking, and not to the role of reinforcement in restraining lateral deformation. In other words, as explained in the previous section, the near alignment between the mobilised plane and the poorly-interlocked bedding plane allows particles to slide easily along the horizontal direction. This consequently results in more compression than dilation when the principal stress direction is rotated to become near-horizontal, i.e. $\alpha \geq 60°$.

4.3.2 Geotextile Reinforcement

4.3.2.1 Strength characteristics

The deviator stress-strain characteristics of sand reinforced with two, three, four, five, six, nine and twelve layers, of nonwoven geotextile reinforcement, and tested under b = 0.5, p' = 100 and α = 0–90°, are presented in Figures 4.19a-4.24a.

In general, a similar trend was observed to that of geogrid-reinforced sand, with some differences that will be reported later (Section 4.3.4). The embedded geotextile layers resulted in significant increases in peak deviator stress q_p for all values of principal stress direction α. This improvement was clear, even with two layers of geotextile where the deviator stress under α = 0° increased from 111.3 kPa for unreinforced sand to 140.4 kPa, constituting of a 26.5% improvement in deviator stress (Figure 4.19). This improvement increased to 92.8, 116.9, 123.4, 127.6, 129.7 and 134.2% with three, four, five, six, nine and twelve reinforcement layers, respectively. The increase in peak deviator stress with increasing numbers of geotextile layers is plotted in Figure 4.25 for all directions of principal stress α. Notably, increases in peak deviator stress with more than six layers were minor. For example, peak deviator stress under α = 0–30° increased by 134.2–147.0% with the inclusion of twelve geogrid layers, compared with 127.6–141.1% with six layers.

Despite this improvement, geotextile-reinforced samples exhibited significant directional dependency, as represented by clear variation in peak deviator stress q_p corresponding to variation in the principal stress direction α. The variation of peak deviator stress along the principal stress direction α is summarised in Figure 4.26 for different numbers of geotextile layers. For instance, with two layers of geotextile, q_p was 140.4, 138.3, 134.5, 98.5, 100.8 and 106.8 kPa for α = 0, 15, 30, 60, 75 and 90°, respectively (Figures 4.19-4.26). The maximum difference ratio Δq_p relative to α = 0° was about 29.8% and took place at α = 60°.

With increasing numbers of layers, anisotropic effects became clearer (Figures 4.25 and 4.26). The reinforcement did not provide significant improvement in the range of α = 60–90° compared with the range α = 0–30°. For example, increasing reinforcement to six layers resulted in q_p values of 252.7, 248.5, 246.0, 132.1, 134.0 and 134.8 kPa

for α = 0, 15, 30, 60, 75 and 90°, respectively. This means that the improvement in peak deviator stress obtained by increasing the number of geotextile layers to six was 51.5–141.1% (depending on α) compared with only 13.2–31.8% in the case of two layers. Therefore, larger Δq_p values were reported with increasing numbers of geotextile layers; it increased from 29.8% for two layers to 46.7, 48.0, 47.5, 47.7, 47.4 and 47.8% for three, four, five, six, nine and twelve layers of geotextile, respectively. The 3D failure surface of geotextile-reinforced sand is presented in Figure 4.27 with a combination of N_{reinf}, α and q_p.

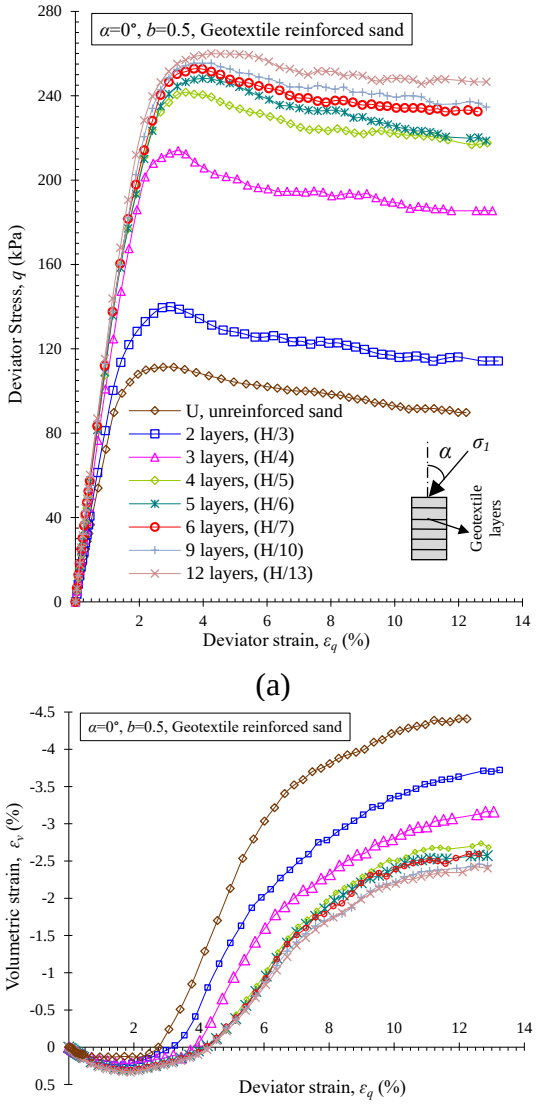

Figure 4.19 Relationships between (a) deviator stress and deviator strain and (b) volumetric strain and deviator strain (geotextile reinforced sand, α = 0°)

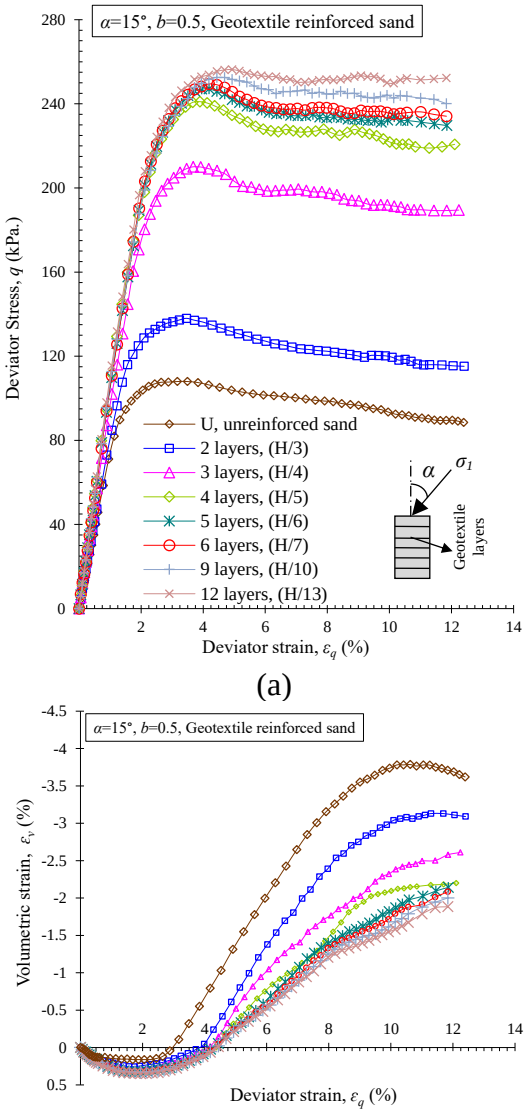

Figure 4.20 Relationships between (a) deviator stress and deviator strain and (b) volumetric strain and deviator strain (geotextile reinforced sand, α = 15°)

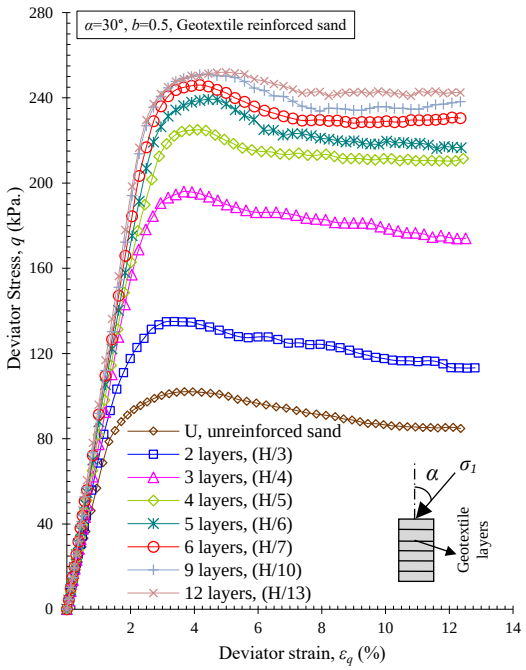

(a)

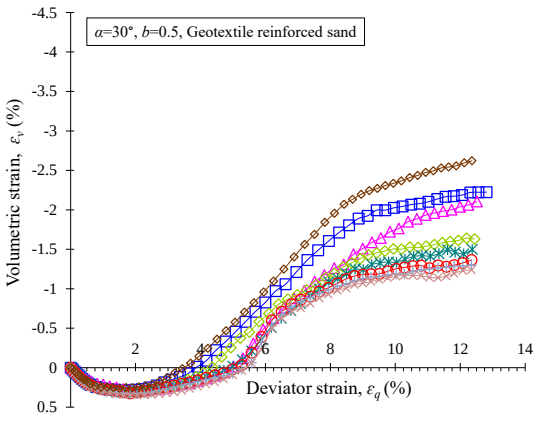

(b)

Figure 4.21 Relationships between (a) deviator stress and deviator strain and (b) volumetric strain and deviator strain (geotextile reinforced sand, α = 30°)

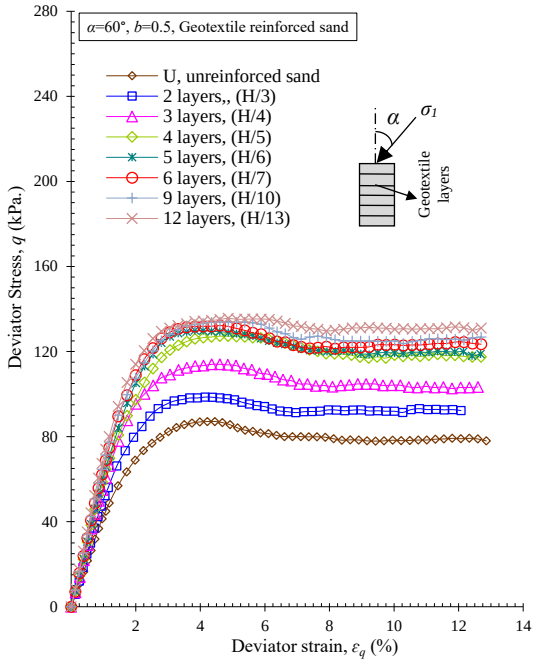

(a)

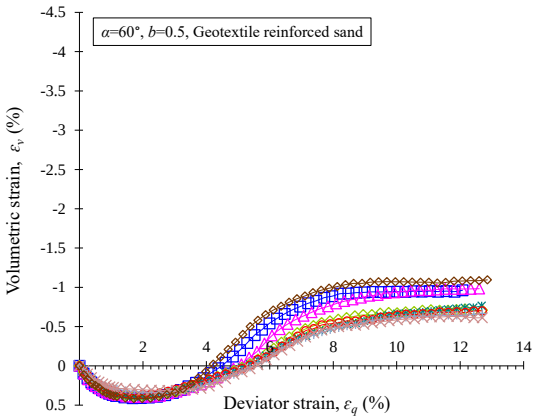

(b)

Figure 4.22 Relationships between (a) deviator stress and deviator strain and (b) volumetric strain and deviator strain (geotextile reinforced sand, α = 60°)

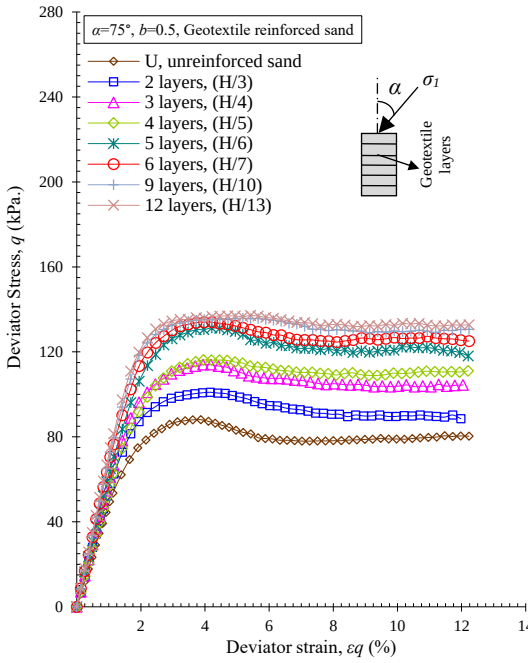

(a)

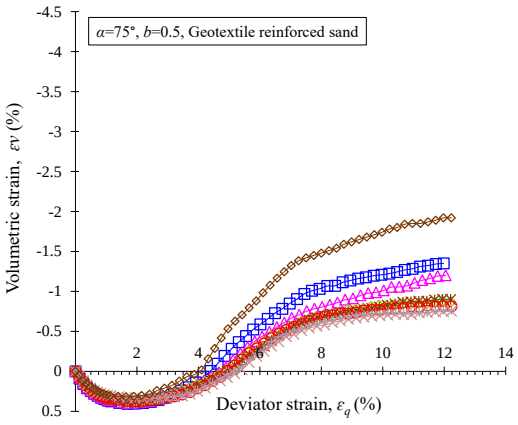

(b)

Figure 4.23 Relationships between (a) deviator stress and deviator strain and (b) volumetric strain and deviator strain (geotextile reinforced sand, α = 75°)

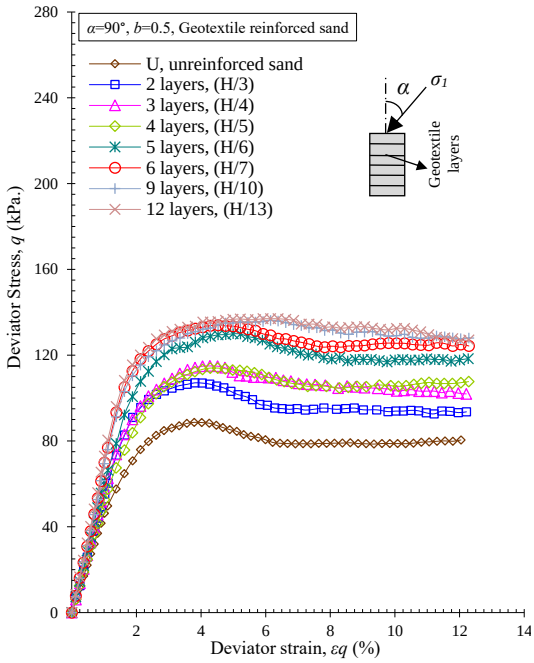

(a)

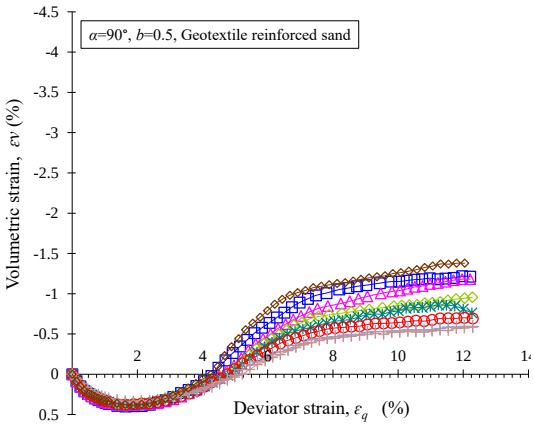

(b)

Figure 4.24 Relationships between (a) deviator stress and deviator strain and (b) volumetric strain and deviator strain (geotextile reinforced sand, α = 90°)

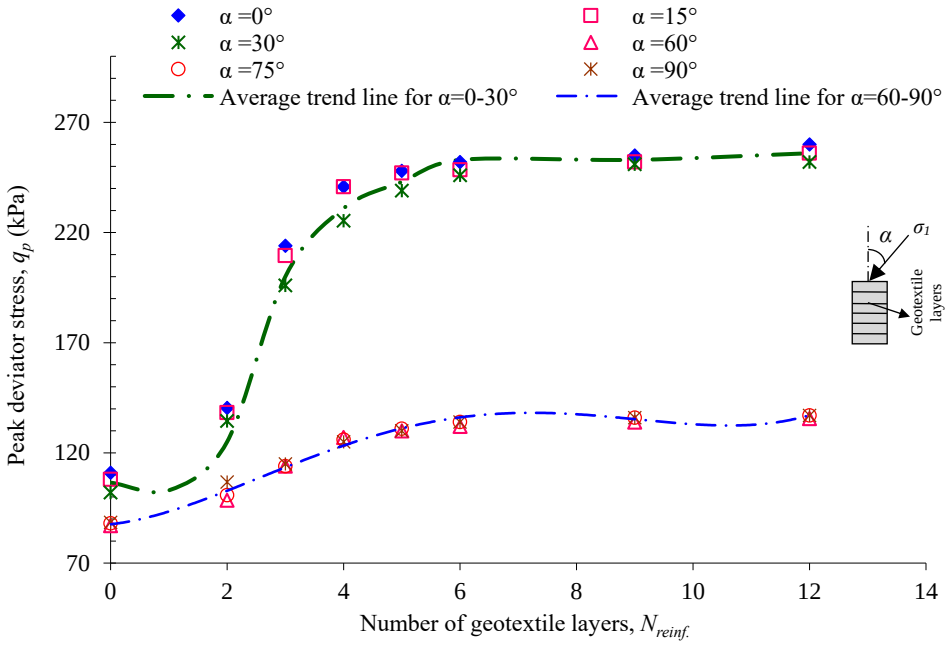

Figure 4.25 Peak deviator stresses of reinforced samples with different numbers of geotextile layers under various directions of principal stress

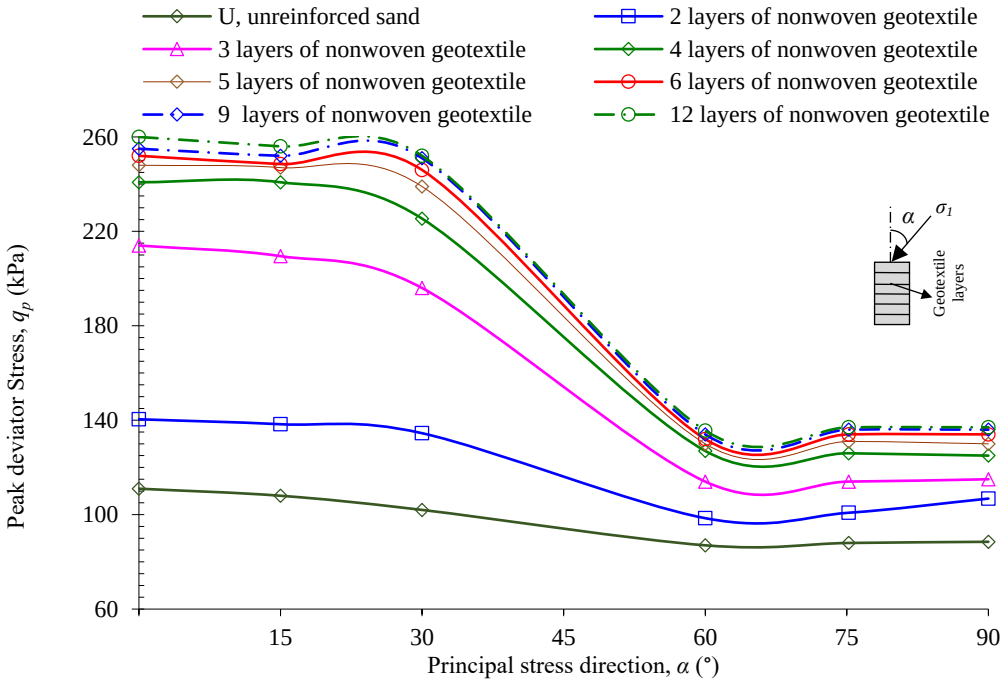

Figure 4.26 Relationship between the peak deviator stress q_p of geotextile-reinforced samples and direction of principal stress α

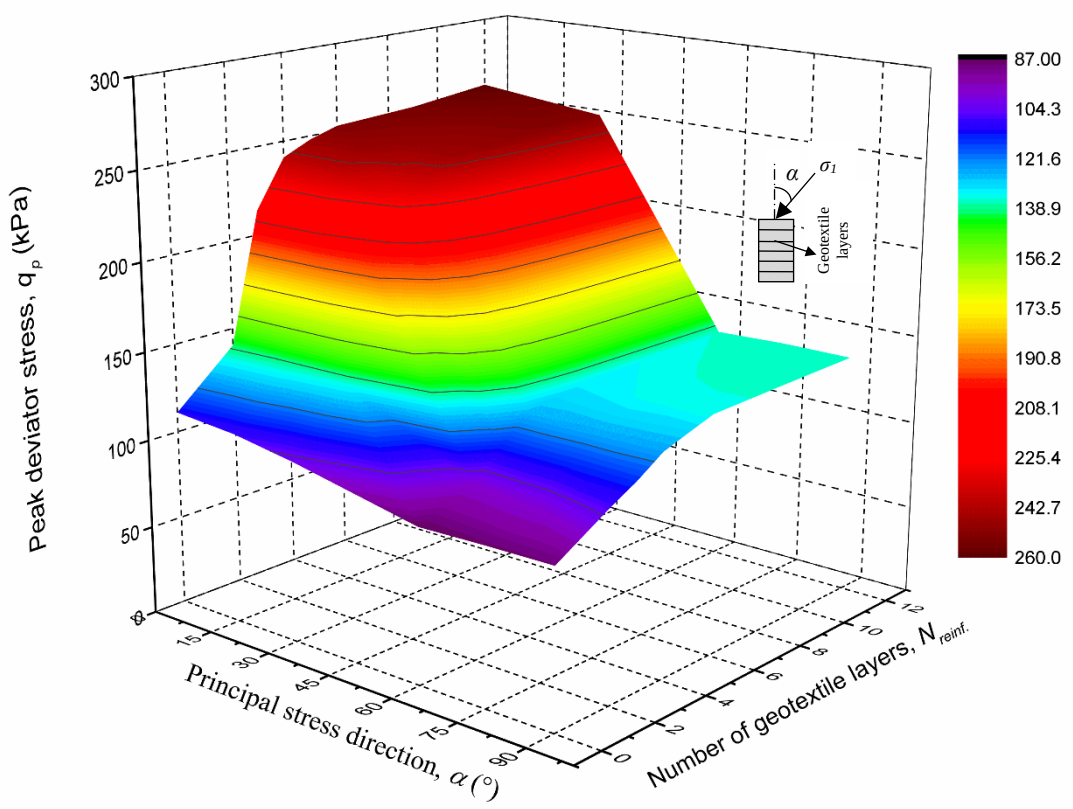

Figure 4.27 Composite α–$N_{reinf.}$ –q_p values of 3D failure surface for geotextile-reinforced sand

The anisotropic failure envelopes for samples reinforced with various numbers of geotextile layers are plotted in Figure 4.28. Each of these curves represents the failure surface, $(\sigma_z - \sigma_\theta) / 2p'$ versus $\tau_{z\theta} / p'$, for samples reinforced with a given number of reinforcement layers, and tested under different directions of principal stress, α = 0–90°. The initial parts of the failure envelopes (i.e., at α = 0–30°) of the reinforced samples are closer to (almost coincident with) the corresponding parts of the assumed isotropic envelopes. However, under α = 60–90° there is a large difference, indicating an anisotropic response of reinforced samples to the load direction.

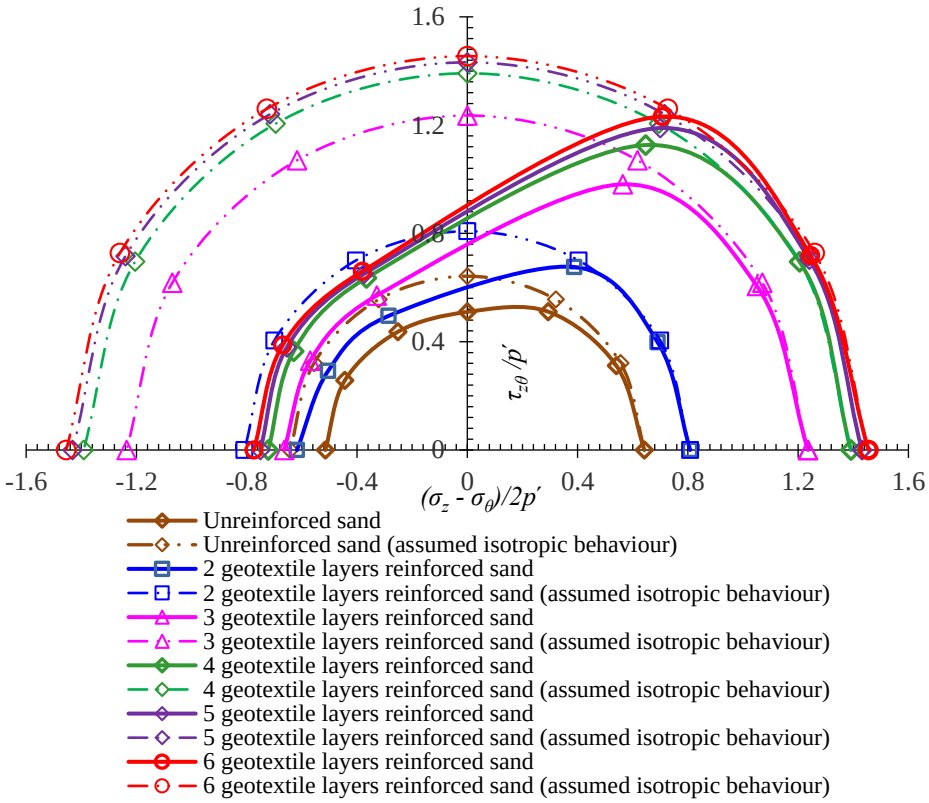

Figure 4.28 Comparison of the failure envelopes of unreinforced clean sand and 2, 3, 4, 5 and 6 geotextile layers reinforced sand

This significant variation of peak deviator stress q_p along the direction of principal stress α is due to variation in the geotextile's ability to provide resistance to the applied load depending on its direction. The condition of vertical major principal stress results in a tendency for sand to deform laterally. This induces tensile stress and strain that mobilises the mechanism of reinforcement as a tensioned membrane and, consequently, develops tensile strength that increases the sample's strength by providing extra confinement. As the principal stress direction rotates to approach the horizontal (α = 60–90°), the geotextile's ability to provide tensile strength becomes low, because the test conditions cannot mobilise the tensioned membrane, as mentioned in Sections 4.3.1.1 and 4.3.1.2.

The improvement of strength comes from the interaction and friction between planar layers and adjacent particles of sand, i.e. the first point in the mechanism mentioned in Section 4.3.1.2. Furthermore, a lot of sand particles were observed on both faces of the planner layers after completing the tests, i.e. where many sand particles were

hosted inside the geotextile fabric and provided more friction. As geotextiles do not have large enough apertures to allow for sand-strike through, there is no shear resistance of the confined particles or passive resistance.

4.3.2.2 Volumetric strain characteristics

The induced volumetric strains of the samples described in the above section (4.3.2.1) are discussed herein. Figures 4.19b-4.24b represent the relationship between volumetric strain ε_v and the corresponding deviator strain ε_q.

Increasing peaks of deviator stress in sand due to the confinement role provided by the embedded geotextile were associated with larger corresponding deviator strains compared with unreinforced sand. For example, the q_p of sand reinforced with six layers occurred at 4.8–5.7% for α = 0–90°, while it was 2.7–4.1% for unreinforced sand. This difference in ε_q (which corresponds to q_p), between reinforced and unreinforced sand, was slight when a small number of geotextile layers was used.

Similar to the unreinforced sand described in Section 4.2.2, nonwoven geotextile-reinforced samples initially exhibited compressive volumetric strain that was followed by expansion. This transformation from compressive to expansive behaviour occurred when deviator strain ε_q approached the range of 3.8–5.5%. These ranges depended on the number of reinforcement layers and α, with their lower limits corresponding to low values of α, and the upper limits corresponding to high values of α. Geotextile provided very significant confinement that led to decreases in the expansion deformation of samples that occurred simultaneously with observed improvements in strength, as reported in Section 4.3.2.1. For example, for α = 0°, the inclusion of six layers of geotextile caused the induced expansive volumetric strain at 12% deviator strain to decrease from 4.4% (for unreinforced sand) to 2.49%. In general, as the number of geotextile layers increased, the amount of reduction in volumetric strain increased. The reductions in dilative volumetric strain at 12% deviator strain were 17.3, 29.5, 39.3, 43.1, 43.2, 45.4 and 46.4% with two, three, four, five, six, nine and twelve reinforcement layers, respectively.

On the other hand, the variation in principal stress direction α resulted in conspicuous anisotropic volumetric strain. For example, the expansive volumetric strains $(\varepsilon_v)_{dil}$ of

samples reinforced with two geotextile layers (at 12% deviator strain) were 3.65, 3.11, 2.18, 0.96, 1.35, and 1.21%, corresponding to values of α of 0, 15, 30, 60, 75 and 90°, respectively. Although reinforcement with twelve layers resulted in minimal differences in volumetric strain ε_v with variation in α (compared with other numbers of geotextile layers) the differences are still very clear.

Decreases in the variation of volumetric strain ε_v, represented by $(I.R)_{\varepsilon v}$ based Equation 4.3 in Section 4.3.1.2, was 81% with two reinforcement layers and decreased to 63.9, 59.2, 54.7, 54.8, 53.0 and 52.1% as the number of geotextile layers increased to three, four, five, six, nine and twelve, respectively.

The decrease in the volumetric strain of sand reinforced with geotextile is attributed to the lateral restraint effect provided by the mobilised tensile strength of the planner sheet, which is a result of the interaction between sand particles and the geotextile surfaces. The large contact area of the planner sheet along the cross-sectional area of the sample, compared with that of geogrid, is the reason for the greater restraint provided. Furthermore, the particles hosted inside the geotextile fabric contribute to more effective interactions between the planner sheets and the adjacent soil. On the other hand, compressive volumetric strain was low compared with dilation strain, with the range of α = 60–90° showing the greatest amount of this compression strain. This is related to the preferred alignment of particles, which gives the horizontal direction the least resistance against deformation. Some increases in compression strain compared with unreinforced sand were observed under vertical loading (α = 0°), corresponding with increases in the number of reinforcement layers. This is probably related to the compressibility of the geotextile sheets embedded within the soil.

4.3.3 Geocell Reinforcement

4.3.3.1 Strength characteristics

In the previous sections (4.3.1 and 4.3.2), sand was reinforced with two-dimensional (2D) geo-inclusions, i.e. planar layers, which were embedded horizontally inside th samples. This section investigates the anisotropic characteristics of sand reinforced with geocells, which are a three-dimensional (3D) geo-inclusions. The deviator stress-strain relationships of samples reinforced with geocell and tested under various directions of principal stress (α = 0–90°) at b = 0.5 are presented in Figure 4.29.

Reinforcement with geocell provides the greatest improvement in the deviator stress of sand, compared with geogrid and geotextile, where peak deviator stress increased by 141.4% under α = 0°. Although the strength of sand reinforced with geocell is still dependent on the loading direction, this dependence is much lower than that for geogrid or geotextile (as will be discussed later). For example, Figure 4.30 explains that the peak deviator stress q_p of geocell-reinforced samples were 268.0, 264.7, 252.8, 202.0, 200.3 and 200.0 kPa for principal stress directions of α = 0, 15, 30, 60, 75 and 90°, respectively, consisting of an increasing ratio of 141.4–147.8% for α = 0–30° and 126.0–132.2% for α = 60–90°. This means that the difference between the maximum peak of deviator stress $(q_p)_{max}$ and the minimum peak $(q_p)_{min}$, was 25.3%; compared with 21.8, 50.0 and 47.8% for unreinforced sand, twelve-layer geogrid- and twelve-layer geotextile-reinforced sand, respectively.

Figure 4.31 shows that the failure envelope of geocell-reinforced sand exhibited lower anisotropy and was close to that of an assumed isotropic surface.

Geocell can provide a confinement effect, a tensioned membrane effect, and wider stress distribution. In planar reinforcement types such as geotextile and geogrid, reinforcement occurs primarily due to the confinement provided by the interfacial interaction. However, in geocell reinforcement, the reinforcement action is attributed mainly to the 3D confinement provided by the 3D structures of geocell. This all-around confinement is the reason for the significant increase in the strength of sand reinforced with geocell and its low anisotropy. Applied load induces lateral deformation of soil and this, in turn, imposes active pressure on the geocell wall, thus

allowing circumferential strain to develop on the membrane wall. Consequently, this will mobilise the tensile strength of the curved geocell, which will provide additional all-around confinement (Bathurst & Karpurapu, 1993; Gurbuz & Mertol, 2012; Yadav, Agnihotri, Priyadarshee, & Dhane, 2014). Under this additional confinement, sand particles will be brought closer to each other, corresponding with arrest of the lateral spreading of the sand. As a consequence, the lateral stability of reinforced samples will increase, creating a stiff composite material. A similar interpretation was presented by Pokharel (2010), who explained that hoop stress on the walls of geocell contributes significantly to the sustaining of applied loads.

The additional all-around confinement, as mentioned above, increases contact between sand particles and the wall membrane, inducing a frictional force that likely contributes to resistance against lateral strain in sand. As loads increase, better bonding between geocell and particles can be achieved due to increases in interlocking between particles, producing a composite mass that resists imposed loads (Yadav et al., 2014). It is of benefit to mention that such interlocking and friction along the vertical walls of geocell can provide a vertical confinement in addition to the lateral one. Pokharel (2010) reported that this vertical confinement works to prevent the soil from moving upward outside the loading area.

The significantly lower anisotropy observed when geocell was used, as compared to when other reinforcements were used, is attributed to the fact that geocell is placed vertically in a way that surrounds the soil, rather than horizontally like geogrid or geotextile. Therefore, confinement, frictional force and good interlocking between particles can be induced, even under inclined principal stresses. In other words, under inclined or horizontal loading, cells that are connected with each other mobilise tensile strength that resists the induced lateral strain, and consequently, provides all-around confinement that is similar to that which occurs when vertical load is applied. This confinement forms a stiff mattress that exhibits bending resistance, and contributes to the strength of reinforced sand. Moreover, by virtue of geocell's 3D structure that encloses soil, the walls of geocell contribute to resisting and delaying the initiation of the shear band and intercept the failure plane under all directions of principal stress. Zhou and Wen (2008) reported a similar role of geocell in intercepting failure planes.

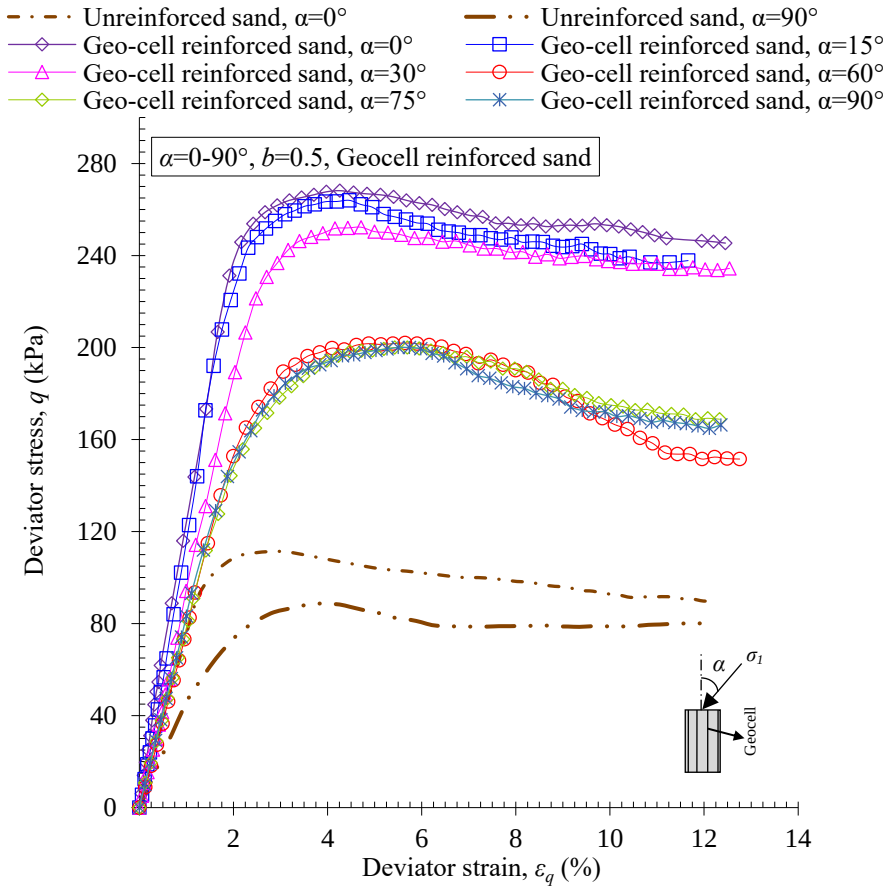

(a)

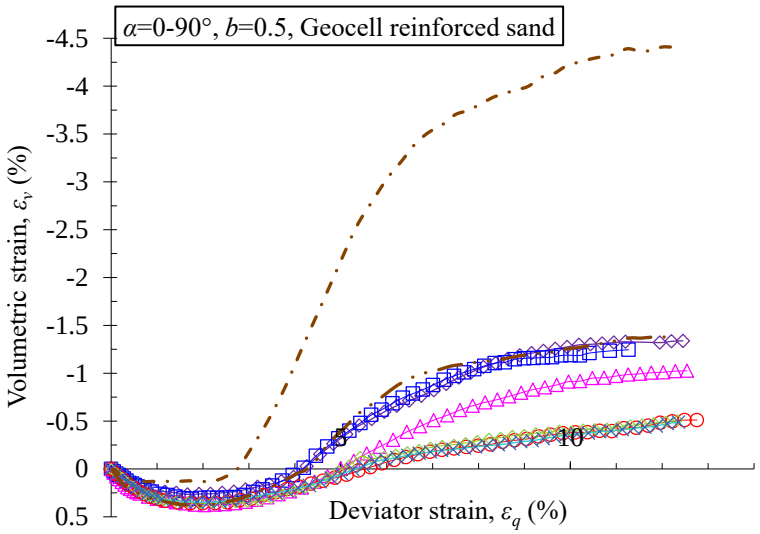

(b)

Figure 4.29 Relationships between (a) deviator stress and deviator strain; (b) volumetric strain and deviator strain (geocell-reinforced sand, α = 0–90°)

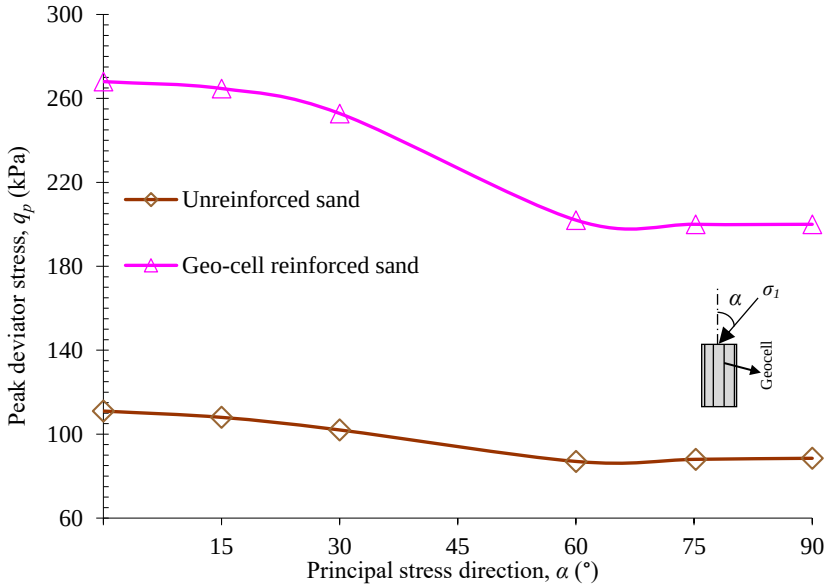

Figure 4.30 Relationship between the peak deviator stress q_p of reinforced samples with geocell and the direction of principal stress α

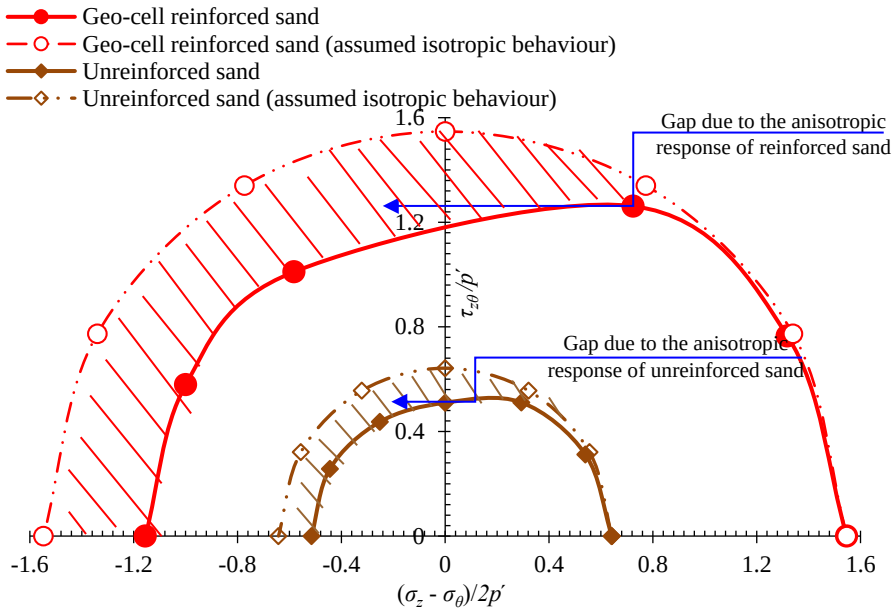

Figure 4.31 Comparison of the failure envelope of sand and geocell-reinforced sand

4.3.3.2 Volumetric strain characteristics

The relationships between the volumetric and deviator strains of sand reinforced with geocell are plotted in Figure 4.29b. In general, the volume of geocell-reinforced sand shows initial contractive behaviour before tending to expand when the deviator strain reaches a certain value. The transformation from compression to expansion occurs when the deviator strain reaches 4.19–5.5% (depending on α), where the deviator strain ε_q required to begin expansion strain increases as α increases.

The increases in the volumes of geocell-reinforced sand samples were significantly lower compared with unreinforced samples. The developed expansion volumetric strain ε_v of reinforced sand at 12% deviator strain reduced to 1.32, 1.24, 1.01, 0.48, 0.49 and 0.46% under conditions of α = 0, 15, 30, 60, 75 and 90°, respectively compared with 4.4, 3.62, 2.57, 1.08, 1.92 and 1.37% for unreinforced sand. These deformations formed reduction ratios of 55.5–70.0% for α = 0–90° as compared with unreinforced sand.

The general decrease in the developed expansive volumetric strain is related to the mechanism of geocell mentioned in Section 4.3.3.1. The mobilised tensile strength of geocell, which results from the pressure exerted by sand particles on the membrane wall, results in significant additional confinement and, as a result, lateral deformation will be significantly restricted. This confinement of the geocell occurs from all sides, such that it is not only characterised by interfacial confinement (as provided by planar geogrid and geotextile). Thus, it results in a decrease, to a certain level, of the effect of loading direction on deformation behaviour. Moreover, the stiff geocell-reinforced sand composite exhibited better resistance against the bending that is caused by an inclined load.

4.3.4 Comparison of the Performance of Sand and Sand Reinforced with 2D (Geogrid and Geotextile) and 3D (Geocell) Geo-inclusions under Different Directions of Principal Stress

In this section, some comparisons are presented to summarise the performance of samples reinforced with geogrid, geotextile and geocell and tested under different directions of principal stress. Figures 4.32-4.35 show the comparative deviator stress-strain relationships of reinforced soil under selected principal stress directions of α = 0, 30, 60 and 90°. As the planar reinforcements provide little improvement after more than six layers, this comparison considers only three and six layers of reinforcement.

Irrespective of reinforcement type, reinforced sand exhibited better performance than unreinforced sand at a given α in terms of improved peak deviator stress q and strain ε_q, as reported in the previous sections. Figures 4.32-4.35 show that geocell provides the greatest strength improvement at any strain level, while geogrid gives the minimum improvement for all values of α.

The variations of peak deviator stress q_p of reinforced sand along the direction of principal stress α are summarized in Figure 4.36. Further, Figure 4.37 compares the failure envelopes of sand and reinforced sand. For α = 0°, it was found that the peak deviator stress was 141.4% higher when geocell reinforcement was used, while it was 127.6% and 116.3% with six layers of geotextile and geogrid, respectively. A similar trend was observed under conditions of α = 30°. On the other hand, when α increased to a range of 60–90°, the trend was different. The benefit of geotextile and geogrid reinforcement, in terms of improving deviator stress, was low compared with conditions of α = 0–30°. For example, the q_p value of sand reinforced with six layers of geogrid and geotextile increased by only 36.7% and 51.8%, respectively, when α = 60°, and by 51.4% and 41.3%, respectively, under α = 90°. However, when 3D geo-inclusion was used, significant improvements were observed in comparison to geogrid and geotextile, even under conditions of α = 60–90°, although this benefit was lower than that when α = 0–30°. Table 4.2 shows the peak deviator stresses for sand reinforced with geogrid, geotextile and geocell and tested under various directions of principal stress.

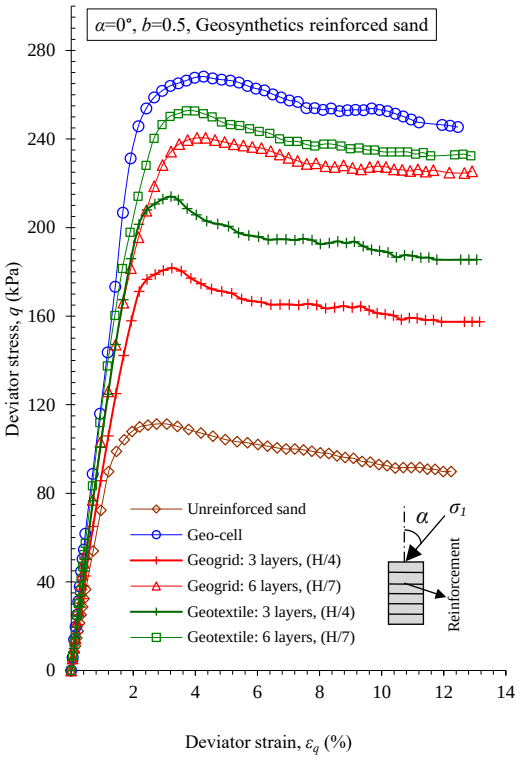

(a)

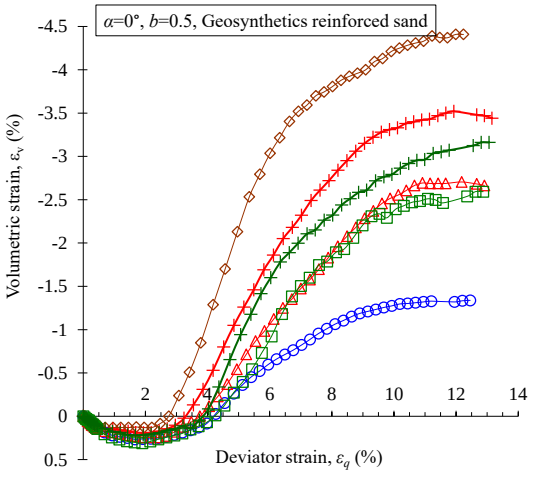

(b)

Figure 4.32 Comparison of (a) deviator stress vs. deviator strain; (b) volumetric strain vs. deviator strain of sand reinforced with different types of geosynthetic reinforcement (α = 0°)

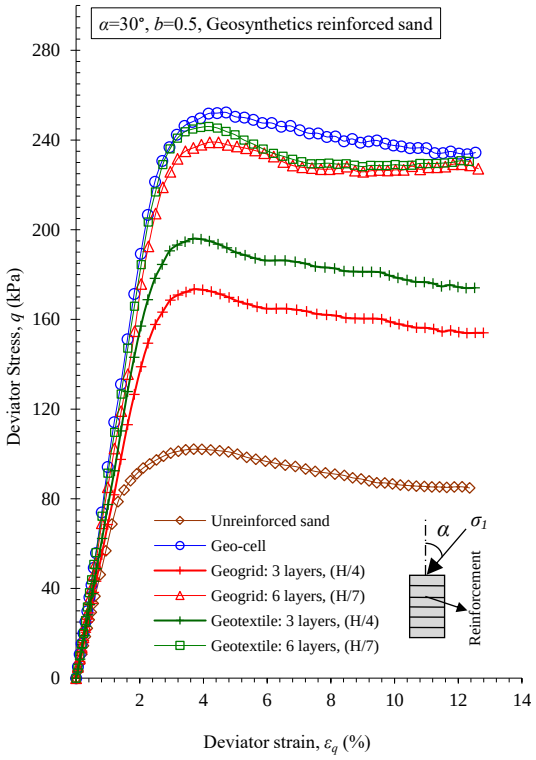

(a)

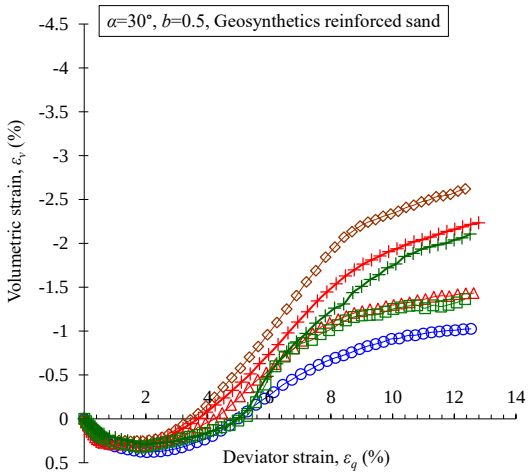

(b)

Figure 4.33 Comparison of (a) deviator stress vs. deviator strain; (b) volumetric strain vs. deviator strain of sand reinforced with different types of geosynthetic reinforcement (α = 30°)

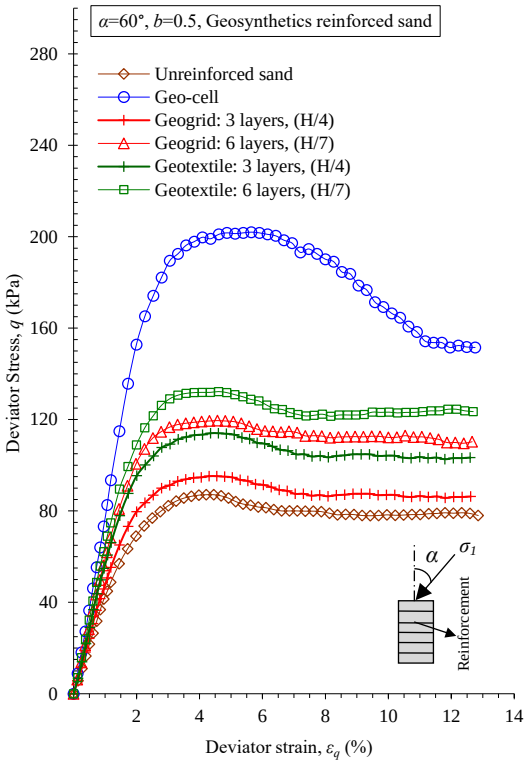

(a)

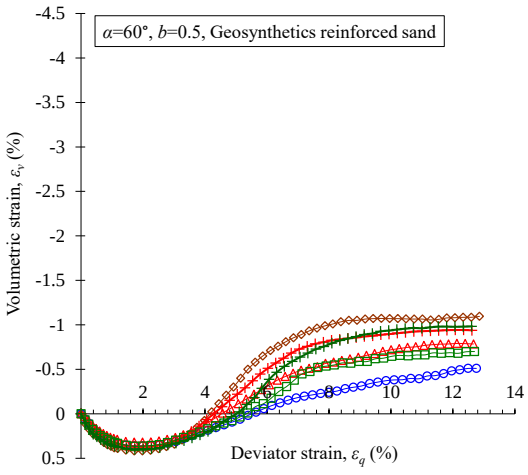

(b)

Figure 4.34 Comparison of (a) deviator stress vs. deviator strain; (b) volumetric strain vs. deviator strain of sand reinforced with different types of geosynthetic reinforcement (α = 60°)

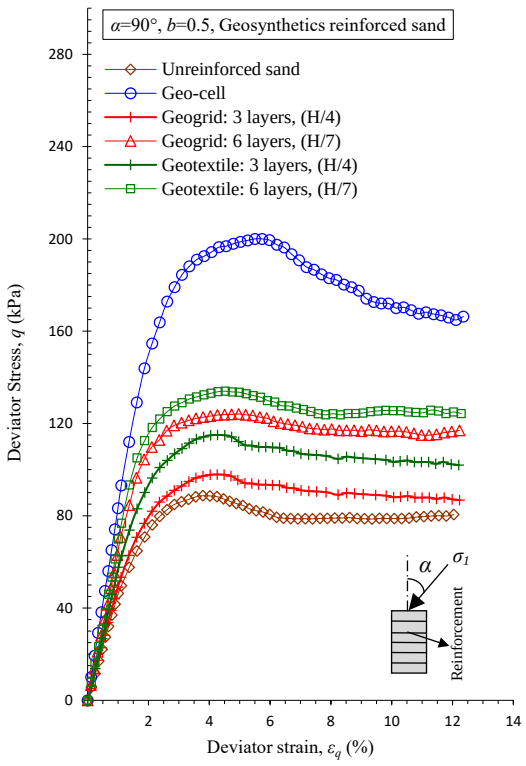

(a)

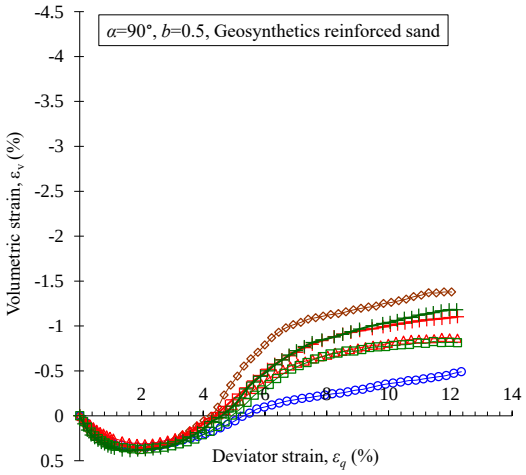

(b)

Figure 4.35 Comparison of (a) deviator stress vs. deviator strain; (b) volumetric strain vs. deviator strain of sand reinforced with different types of geosynthetic reinforcement (α = 90°)

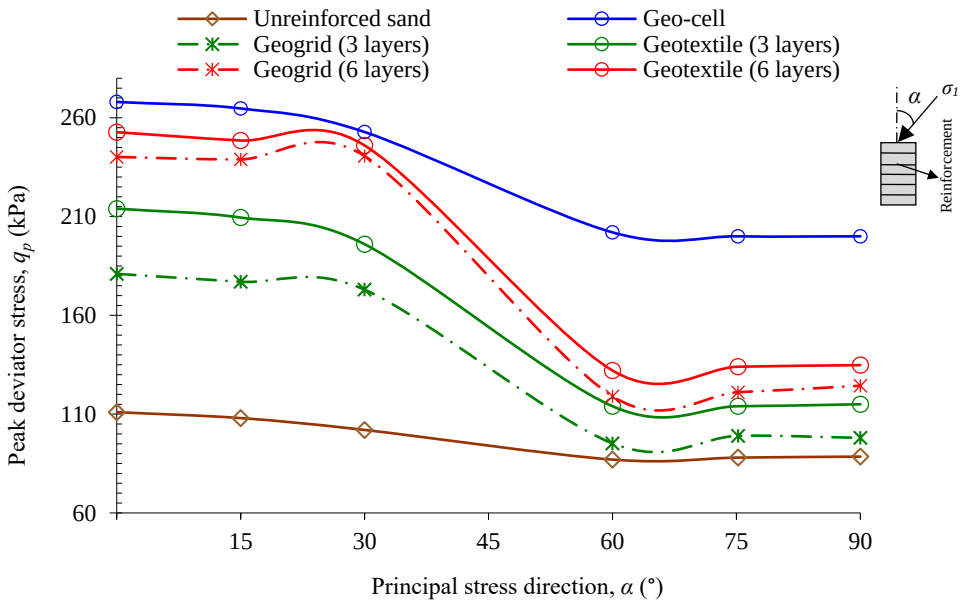

Figure 4.36 Comparison the variations of peak deviator stress q_p of samples reinforced with different types of geosynthetic reinforcement along the direction of principal stress α

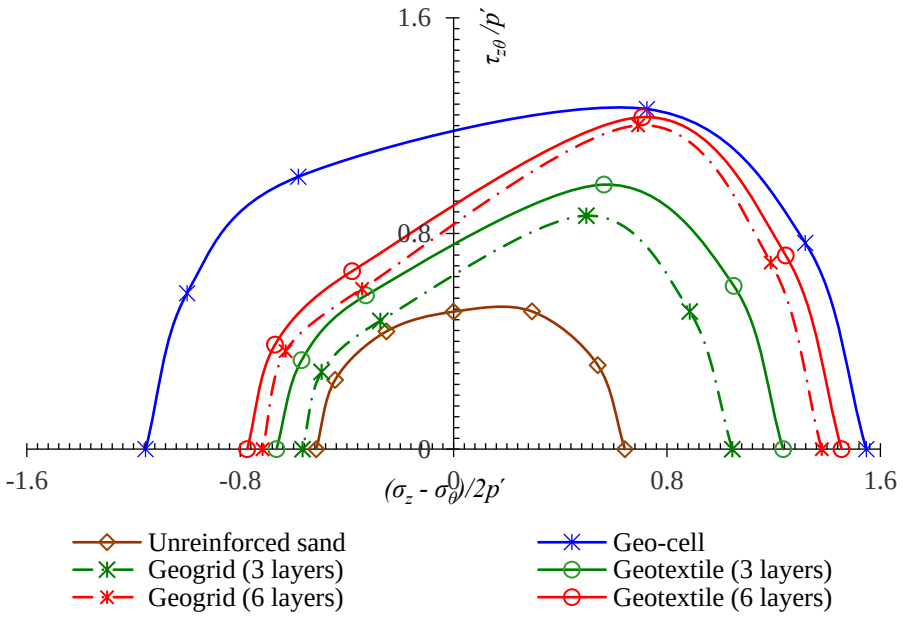

Figure 4.37 Comparison of the failure envelopes of sand and geocell-reinforced sand

Figures 4.32b-4.35b compare the volumetric strain responses of sand reinforced with different types of reinforcement and different layer configurations under various directions of principal stress α. For α = 0°, planar and cellular reinforcements effectively restrained expansive volumetric strain. Among geogrid and geotextile, geocell provided the greatest restriction of sample volume increase. For example, the reduction in expansive volumetric strain under α = 0° at a deviator strain ε_q of 12% was 38.3% and 43.2% for geogrid and geotextile (six layers), respectively, while it was 70.6% for geocell. However, as α increased, the volumetric strain observed with different reinforcements approached each other.

Planar reinforcements, i.e. geogrid and geotextile, depend mainly on the confinement effect produced by the tensioned membrane and its interfacial interaction between the layers and the adjacent soil. Geogrid can also exhibit some passive resistance along transverse ribs, and shear resistance of the particles confined in apertures. The better improvement exhibited by geotextiles can be attributed to the larger cross-sectional area of the geotextile layer that provides a larger interface compared with that of geogrid, which has many apertures. Furthermore, although both geotextile and geogrid have similar longitudinal tensile strengths (9.4–9.8 kN/m), geotextile has greater tensile strength along the transverse axis. The better improvement provided by geotextile is also linked to its better stress-elongation characteristics—where samples can sustain induced tensile stress even under large strains. On the other hand, geocell-reinforced sand exhibited the greatest confinement by virtue of its 3D form that provides all-around confinement by its tensioned wall (instead of that resulting from interfacial interaction) and, thus, it exhibited the maximum benefit. Moreover, geocell exhibited significant friction between its cell walls and sand particles, in addition to having bending resistance due to its behaviour as a stiff composite. As mentioned in Sections 4.3.2 and 4.3.3, there was little difference in the characterisation of reinforced sand when the number of layers was increased from six to twelve. It is noteworthy to mention that the amount of material used for twelve layers of planar reinforcement was about half that used for geocell reinforcement.

On the other hand, samples reinforced with geogrid or geotextile showed a significant anisotropic response to the direction of principal stress α, and this would be related to

what was mentioned in Sections 4.3.2 and 4.3.3 regarding the mechanism of planar reinforcement. Layers of such planar reinforcement were placed horizontally and, thus, their ability to resist shearing and the development of deformation becomes much lower when the principal stress is applied in a direction close to horizontal rather than vertically. This lesser ability would be linked to the fact that when α = 60°–90°, the samples were subjected to an extension mode in which the radial stress σ_r becomes greater than the axial stress σ_z and, thus, the tensile strength of the horizontal planar layers cannot be mobilised. However, geocell-reinforced sand can exhibit better performance even under inclined principal stress directions due to the tensioned wall of the reinforcement that encases the sheared soil. Under vertical load, the induced lateral deformation mobilises the tensile strength of the cells. This mobilised ability is still significant under inclined principal stresses where cells, which are connected to each other, will be mobilised because they are 3D structures rather than horizontal layers. This better performance occurs due to the bending resistance of the relatively stiff 3D composite that forms, and the improved interaction between the sand and cell walls.

Table 4.2 Summary of the peak deviator stresses of unreinforced and reinforced sand obtained under various α

Direction of principal stress, α (°)	Unreinforced sand	Geogrid reinforced sand		Geotextile reinforced sand		Geocell reinforced sand
		3 layers	6 layers	3 layers	6 layers	
	Peak deviator stress, q_p (kPa)					
0	111.3	181.0	240.1	214.0	252.7	268.0
15	108.0	177	238.9	209.5	248.5	264.7
30	102.2	173	240.6	196.2	246.0	252.8
60	87.0	95.2	119.0	114.1	132.1	202.0
75	88.0	99	121.1	114.3	134.0	200.3
90	88.5	98	124.3	115.1	134.8	200.0
	Difference in peak deviator stress, Δq_p (%)					
	21.8	47.4	50.4	46.7	47.7	25.3

Chapter 5

Monotonic Hollow Cylinder Tests on Reinforced and Unreinforced Mixed Sand-clay under Various Directions of Principal Stress

5.1 Introduction

This chapter presents and discusses the results obtained from testing program outlined in Section 3.5.2 in Chapter Three. The aim of this chapter is to 1) investigate the effects of clay content (kaolinite) and principal stress direction on the anisotropic stress-strain characteristics of sand, and 2) to examine to what extent the clay content can reduce the anisotropic effect. In addition, this chapter investigates the stress-strain anisotropy of sand-clay mixture reinforced with different types of geosynthetics and, explores their ability to decrease anisotropy and increase bonding.

The behaviour of sand containing various proportions of kaolinite and subjected to different directions of principal stress will be introduced first in Section 5.2. This will be followed by the behaviour of mixtures reinforced with geogrid, geotextile and geocell, in Sections 5.3–5.5. Finally, a summary of this chapter will be provided in Section 5.6.

Table 5.1 Summary of the conditions and parameters of the tests performed in this chapter

Test Series	Plastic fines content (kaolinite), F (%)	Arrangement of geosynthetics	Relative density, D_r (%)	Principal stress direction, α (°)	Intermediate principal stress parameter, b	Mean effective stress, p' kPa
Series I Unreinforced sand-clay mixture	5%	-----	69.9–70.1	0, 15, 30, 60, 75 and 90°	0.5	100
	10%	-----	70.1–70.2	0, 15, 30, 60, 75 and 90°	0.5	100
	15%	-----	70.0–70.3	0, 15, 30, 60, 75 and 90°	0.5	100
	20%	-----	69.9–70.3	0, 15, 30, 60, 75 and 90°	0.5	100
Series II Geogrid reinforced sand-clay mixture	10%	3 and 6 layers	69.8–70.1	0, 30, 60 and 90°	0.5	100
Series III Geotextile reinforced sand-clay mixture	10%	3 and 6 layers	70.1–70.2	0, 30, 60 and 90°	0.5	100
Series IV Geocell reinforced sand-clay mixture	10%	geocells	69.9–70.1	0, 30, 60 and 90°	0.5	100

5.2 Sand Containing Different Amounts of Plastic Fines (Kaolinite)

5.2.1 Strength Characteristics

In this part, the anisotropic behaviour of sand containing up to 20% plastic fines (kaolinite) was considered. The stress-strain relationships of sand with different kaolinite contents, under various directions of principal stress α, are presented in Figures 5.1a-5.6a.

The results reveal that fines content F significantly affects the stress-strain characteristics of sand. In general, the inclusion of clay in sand decreases its peak deviator stress q_p, depending on α.

Under α = 0–30°, adding fines changed the developed stress-strain relationship such that its slope was less steep than that observed for clean sand. The developed stress-strain relationships for different fines contents almost coincided with each other until before the peaks, then significant differences occurred where deviator stress decreased with increasing fine content, except for F = 10%. For example, under α = 0°, peak deviator stress q_p decreased from 111.3 kPa for clean sand to 100.6 kPa for 5% fines content and then increased to 106.2 kPa for 10% fines content before decreasing again to 98.4 and 94.2 kPa for F = 15 and 20%, respectively. This means that the maximum reduction in q_p (15.3%) occurred at F = 20%, while the minimum reduction of 4.5% occurred at F = 10%. A similar trend was reported for α = 15°, where the largest reduction due to adding fines content was 12.98% when F = 20%, while the lowest was 1.8% when F = 10%.

However, the trend for the range α = 30–90° was somewhat different. Samples with a fines content of 10% exhibited a slight increase in the peak deviator stress q_p compared with that of clean sand, while sand mixed with other fines contents showed similar reductions in strength. For example, an increase in q_p of 1.96–3.45% (depending on α) was achieved when adding 10% fines content, while 20% fines resulted in about 9.8–11.8 reduction in q_p.

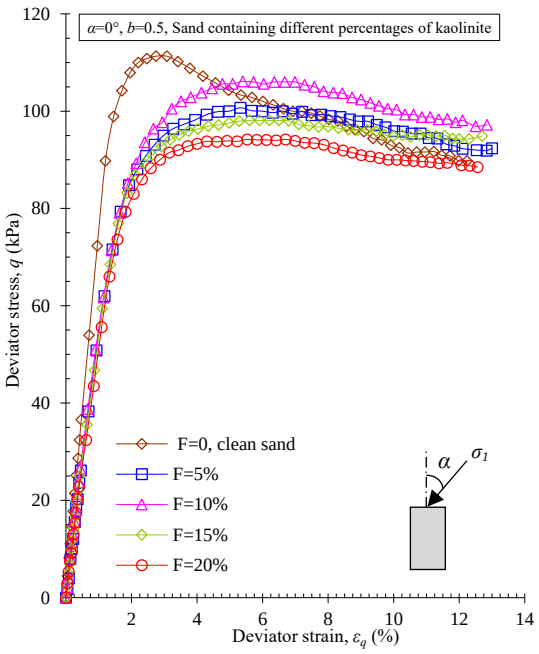

(a)

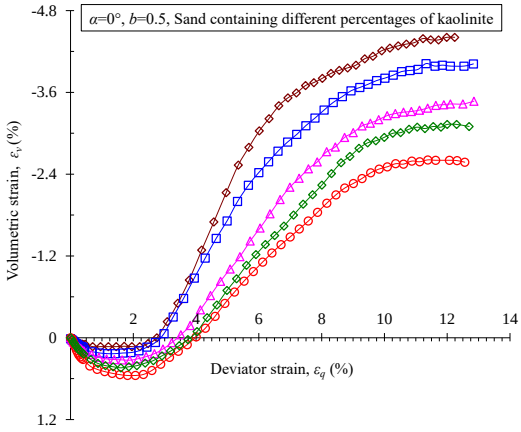

(b)

Figure 5.1 Relationships between (a) deviator stress and deviator strain; (b) volumetric strain and deviator strain (sand containing different clay contents, α = 0°)

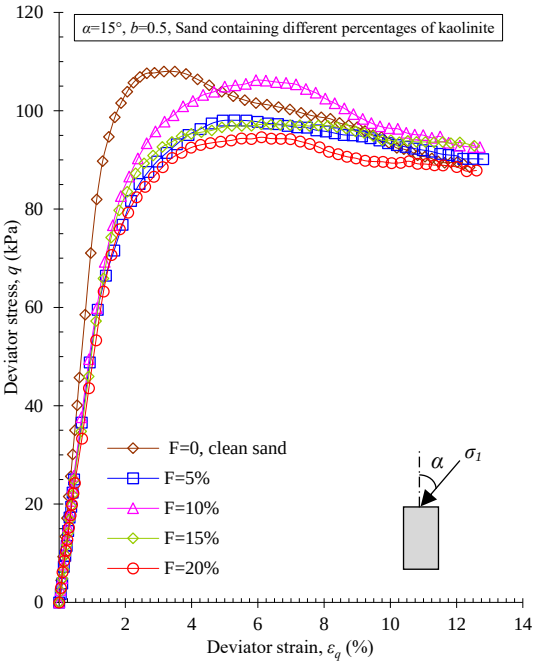

(a)

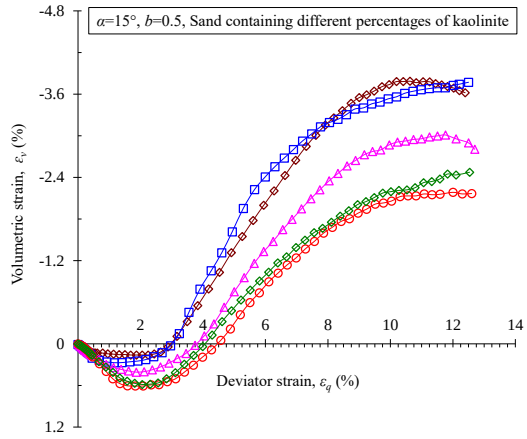

(b)

Figure 5.2 Relationships between (a) deviator stress and deviator strain; (b) volumetric strain and deviator strain (sand containing different clay contents, α = 15°)

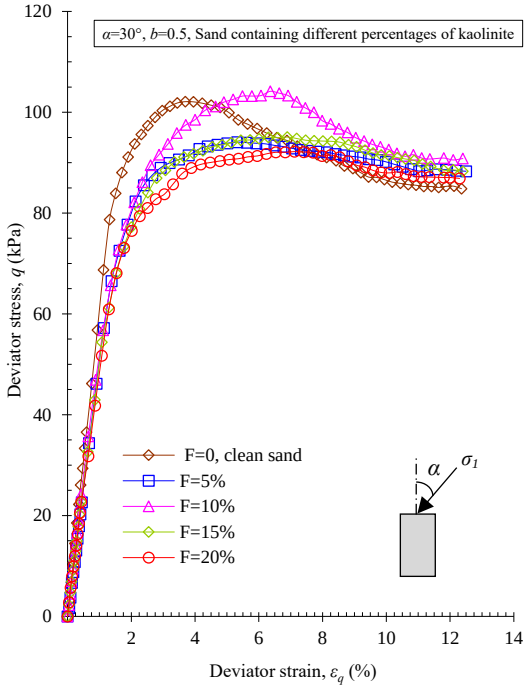

(a)

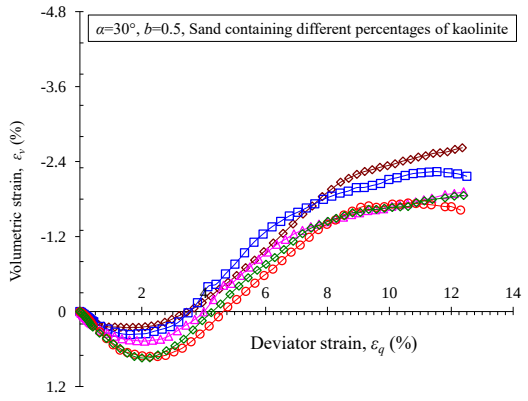

(b)

Figure 5.3 Relationships between (a) deviator stress and deviator strain; (b) volumetric strain and deviator strain (sand containing different clay contents, α = 30°)

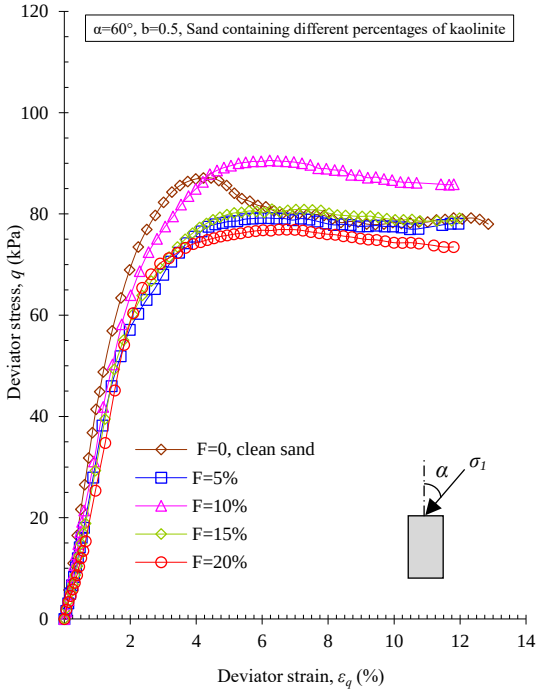

(a)

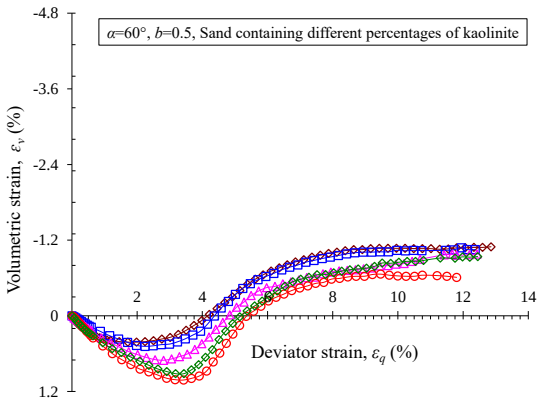

(b)

Figure 5.4 Relationships between (a) deviator stress and deviator strain; (b) volumetric strain and deviator strain (sand containing different clay contents, α = 60°)

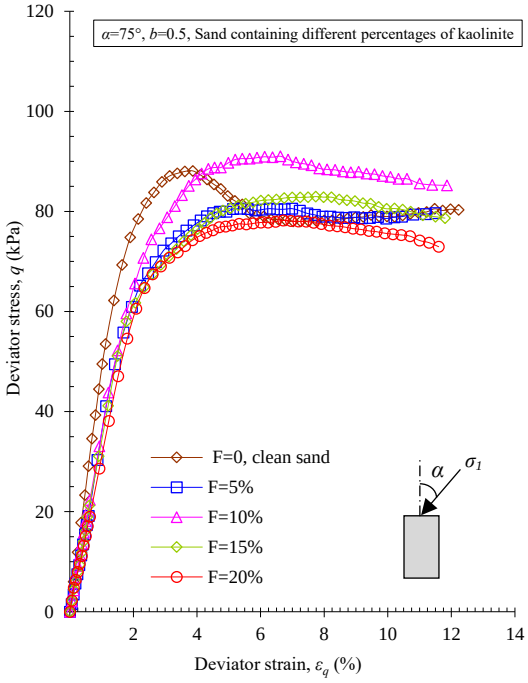

(a)

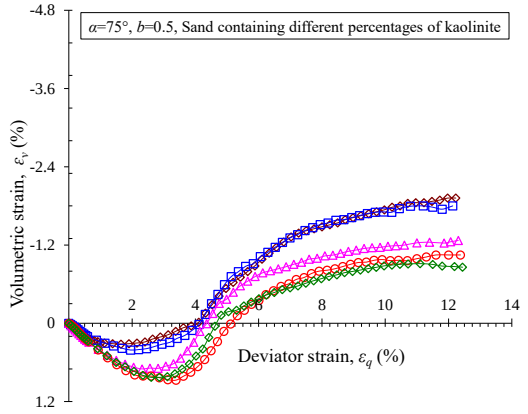

(b)

Figure 5.5 Relationships between (a) deviator stress and deviator strain; (b) volumetric strain and deviator strain (sand containing different clay contents, α = 75°)

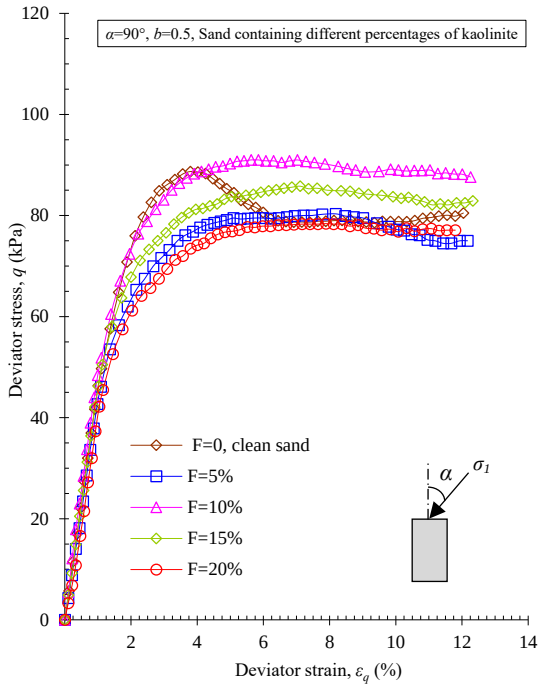

(a)

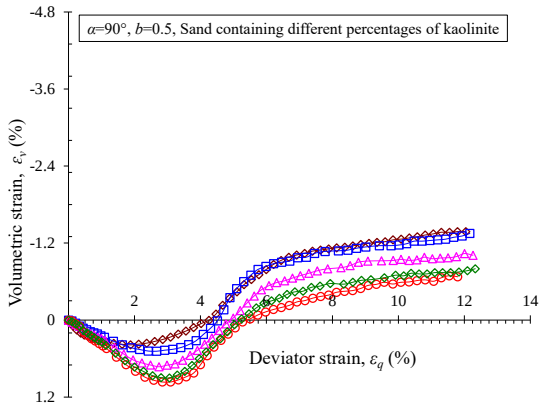

(b)

Figure 5.6 Relationships between (a) deviator stress and deviator strain; (b) volumetric strain and deviator strain (sand containing different clay contents, α = 90°)

Figure 5.7 shows the variation in peak deviator stress q_p versus fines content (clay) F. This variation can be discussed considering both the reduction in q_p corresponding to 5% clay and the increase in q_p associated with a 10% clay content. The abnormal decrease in q_p that occurred in sand when F = 5% is attributed to a small amount of fines acting as a lubricating layer between particles. It is well known that the shear strength of clean sand depends totally on the friction between particles and, thus, the presence of fines as inter-particle layers decreases friction and thereby stability. The particles can move and slide easily under shearing; and consequently, exhibit lower values of q_p. This is consistent with results of several researchers such Mollins, Stewart, and Cousens (1999), Naeini and Baziar (2004) and Carraro et al. (2009). Moreover, standard triaxial tests were carried out to determine the shear strength parameters of the sand mixed with various percentages of clay (Table 5.2). On the other hand, the increase in the deviator stress associated with F = 10% is related to the fact that such a percentage likely fills the voids between sand particles, which provides a certain amount of cohesion to the matrix that compensates for some of the decrease in friction that can occur due to the presence of fines between particles. This means that F = 10% is likely the optimum fines content. Indeed, both of the increasing and decreasing effects are likely to occur simultaneously and it is better to take them into consideration.

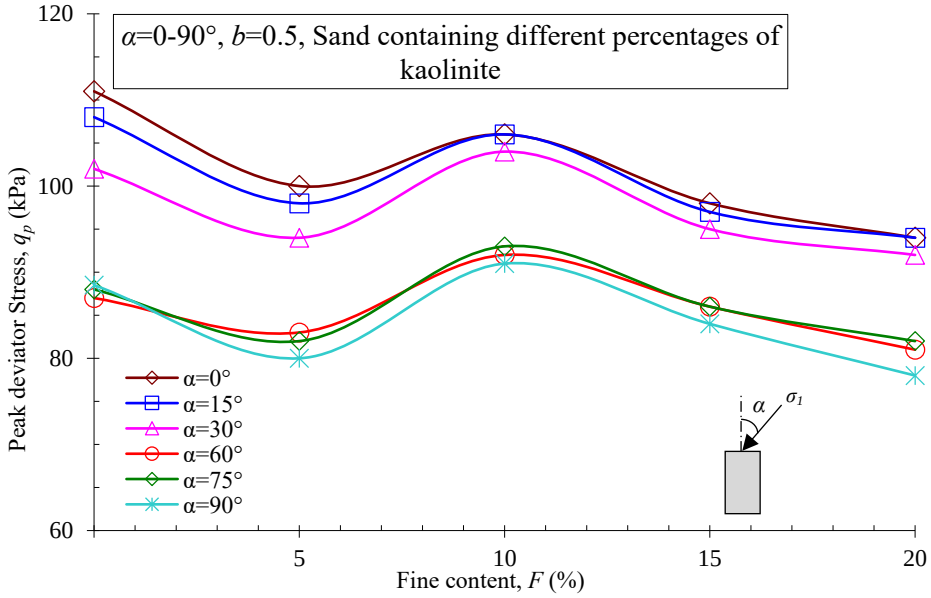

Figure 5.7 Variation of the peak deviator stress q_p with fines content under different directions of principal stress α.

Table 5.2 Shear strength parameters of sand mixed with various percentages of clay

	Fine content, F (%)				
Shear strength parameters	0	5	10	15	20
Cohesion, C (kPa)	0	10.3	14.2	22.6	27.1
Angle of internal friction, ϕ (°)	40.1	39.3	40.1	38.8	38.0

Figure 5.8 shows the variation of the peak deviator stress q_p along the direction of principal stress α. The combined results are presented as a three-dimensional (3D) surface in Figure 5.9. Increasing the clay contents caused significant decreases in directional dependence, particularly for $F \geq 10\%$, although there were still differences between the q_p values obtained at α = 0–30° and those at α = 60–90°. For example, for 10% fine content, the deviator stress remained constant at 106.2 kPa with increases in α from 0° to 15°, before decreasing slightly to 104.2 kPa at α = 30° and then decreasing to 92.0% when α = 60–90°, a difference ratio of about 13.3%. For the other fines contents of 15% and 20%, the difference ratios in peak deviator stress Δq were 12.3% and 14.8%, respectively. These differences in peaks deviator stress Δq were much less than that with clean sand (21.8%). In other words, the effect of principal stress direction α on the peak deviator stress q_p decreased by 37.1% by adding 10% kaolinite to sand. This reduction in directional dependence can be seen clearly through the failure surface presented in Figure 5.10, where the envelope for 10% clay was more symmetrical in shape than that for clean sand.

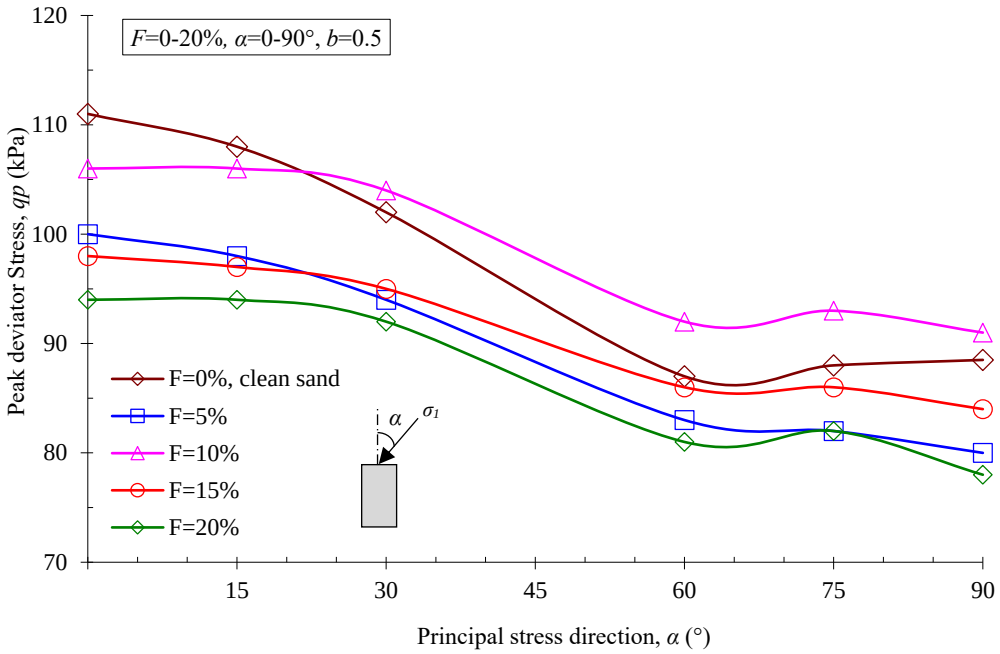

Figure 5.8 Variation in peak deviator stress q_p with principal stress direction α for different fines contents F

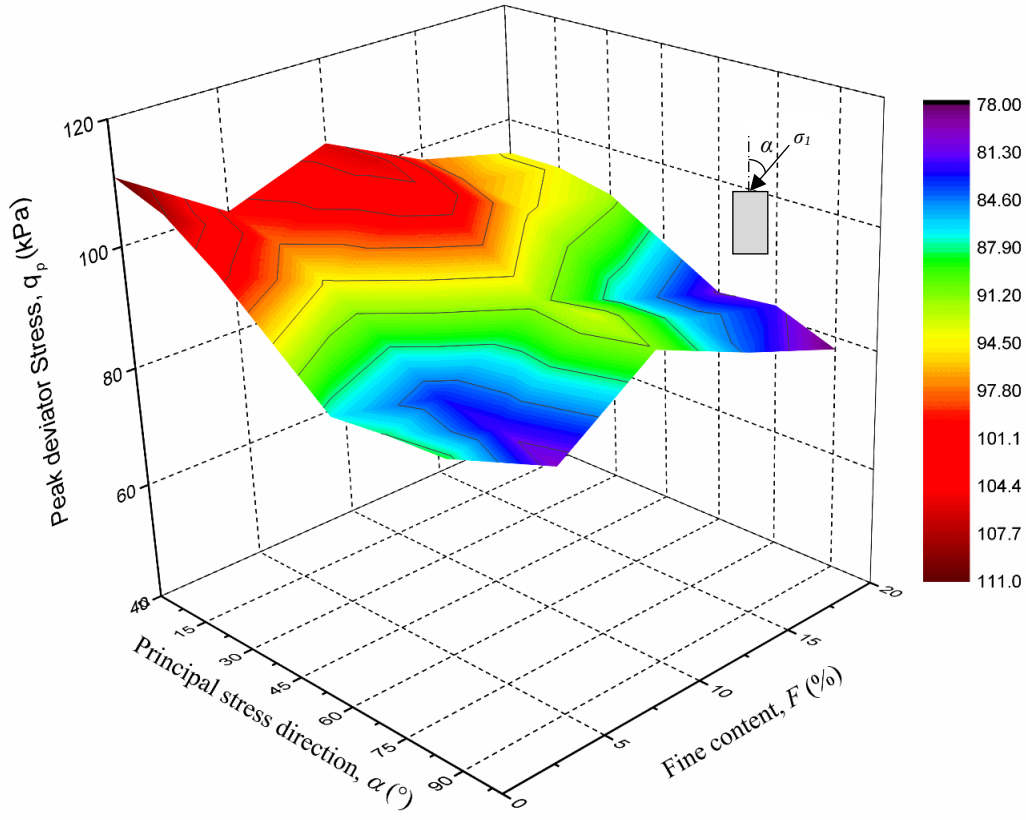

Figure 5.9 Composite α, F, q_p values of the 3D failure surface for sand-clay mixtures

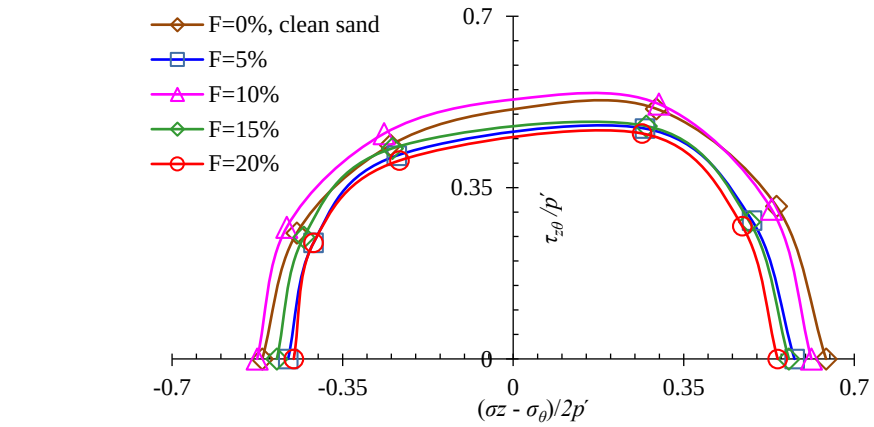

(a)

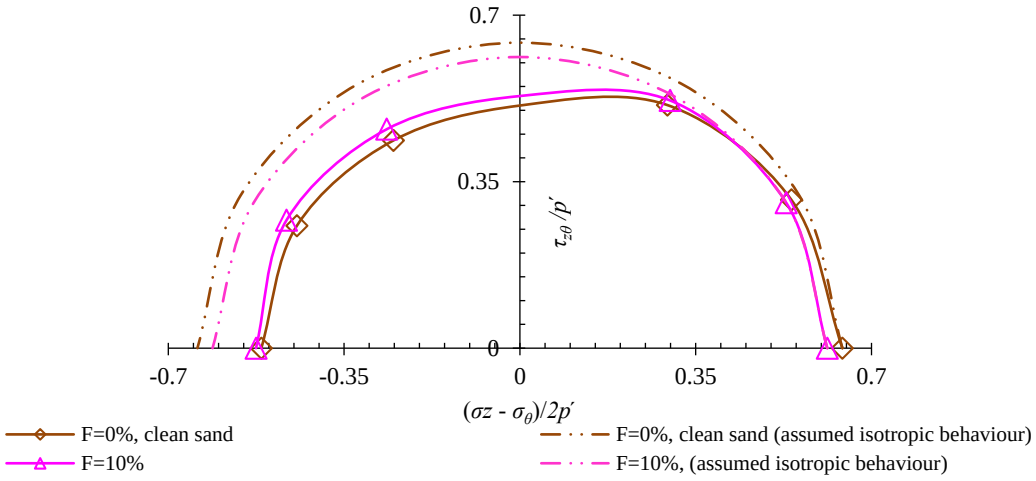

(b)

Figure 5.10: (a) Failure envelopes of sand containing different fines contents; (b) Comparison of the anisotropic failure envelopes and isotropic assumed envelopes of sand containing 0% and 10% fines

This reduction in the difference in peak deviator stress Δq is likely related to the effect of the clay in the matrix, and can be explained from two perspectives. Firstly, clay can occupy inter-particular voids to provide a cushioning effect (Thevanayagam et al., 2002) and improve the poor interlocking that occurs due to the preferential alignment of sand particles along the bedding plane. Therefore, such a cushioning effect decreases what likely occurs in clean sand samples in terms of easy sliding and rotation

of particles along the horizontal plane. On the other hand, the presence of fines and the mixing process could significantly decrease the preferred alignment of particles compared with clean sand. Further, decreasing the amount of sand particles in the matrix due to replacement by clay fines can also reduce the effect of preferred alignment. Despite this, the presence of fines cannot totally prevent the anisotropic behaviour of soil. This agrees with several researchers who have reported clear anisotropic characterisation of mixtures, such as Nakase and Kamei (1983), Kumruzzaman and Yin (2010b), Kumruzzaman and Yin (2010a) and Keyhani and Haeri (2013). A clay content of 10% gave maximum deviator stress associated with a significant decrease in anisotropy, and thus, this clay content was adopted for addition to reinforced sand in Sections 5.3–5.5.

5.2.2 Volumetric Strain Characteristics

This part presents and discusses the volumetric strain associated with deviator stress that was presented in the above section.

Figures 5.1b-5.6b show that, compared with clean sand, compression behaviour was dominant in mixtures until they developed large values of deviator strain ε_q. For example, compressive volumetric strain in matrices with F = 20% was induced from the beginning of shearing until the deviator strain ε_q achieved 4.0, 4.5, 4.6, 5.2, 5.0 and 5.4% at α = 0, 15, 30, 60, 75 and 90°, respectively, compared with ε_q = 2.75–4.25% for clean sand (depending on α, as discussed earlier). As the clay content increased, there was an increasing tendency for the sample volume to decrease. This increase is linked to the nature of clay, which has high compressibility compared with sand, and thus, any inclusion of clay between particles will cause greater compression strain. For example, the compression volumetric strain under α = 0° reached 0.23% with 5% fines, while with increasing fines contents of 10, 15 and 20%, compression volumetric strain increased to 0.32, 0.44 and 0.55%, respectively. The induced compressive strain varied depending on α where, for example, ε_v with F = 15% was 0.44, 0.58, 0.74, 0.91, 0.82 and 0.9% with α = 0, 15, 30, 60, 75 and 90°, respectively. Although the amounts of compressive strain were higher for sand-clay mixtures, as expected, the variation along the principal stress direction was less relative to clean sand. This lower variation is related to the cushioning effect provided by fines occupying the inter-granular voids.

Compared with clean sand, this cushioning effect contributes to better stability of the particles in the mixture. It reduces the tendency of particles to move and slide along the bedding plane, which can create poor interlocking planes (e.g., in clean sand) due to the preferred alignment of particles.

As mentioned previously, the volume of samples tended to expand when deviator strain reached a given value. In general, as fines content increased, dilative strain decreased. For example, dilative strain $(\varepsilon_v)_{dil}$ at ε_q = 12% for samples tested under α = 0° was 4.4% for clean sand while it decreased to 4.0, 3.4, 3.1, and 2.6% for F = 5, 10, 15 and 20%, respectively. Irrespective of the fines content, the matrix exhibited decreases in dilation strain with increases in the principal stress direction. For example, dilative strain at 12% deviator stress for a mixture with 15% clay content decreased from 3.1% at α = 0° to 2.405, 1.81, 0.914, 0.9023 and 0.77% for α = 15, 30, 60, 75 and 90°, respectively. Moreover, the combination of the largest fines content and largest principal stress direction resulted in the lowest dilative strain, and vice versa. This decrease in dilative strain occurring due to increasing α is related to the fact that soil has a greater tendency to compress along the horizontal direction and dilate along the vertical one.

5.3 Geogrid-reinforced Sand-clay Mixture

5.3.1 Strength Characteristics

In this part, three and six layers of geogrid were used to reinforce the selected sand-clay mixture, i.e. F = 10%. This percentage was selected as it gave the maximum strength and also decreased the anisotropic effect significantly. Such samples were tested considering different directions of principal stress (α = 0, 30, 60 and 90°) to investigate the stress-strain behaviour of the reinforced mixture under constant b of 0.5 and p' = 100 kPa (as illustrated in Table 5.1).

The curves illustrated in Figures 5.11a and 5.12a can be classified into two groups, α = 0 and 30°; and α = 60 and 90°, although there are some difference in each group. Deviator stress q developed with increasing deviator strain ε_q for different values of α, noting that the stiffness (slope) was lower for larger values of α. After reaching the peak, the post-peak loss was insignificant. For sand-clay mixtures reinforced with three layers of geogrid (Figure 5.11a), the deviator stress curves for α = 60 and 90° were very close to each other, and much less than those of α = 0 and 30°, where the peak deviator stress q_p was 186.7, 170.6, 124.8 and 126.4 kPa for α = 0, 30°, 60 and 90°, respectively. Figure 5.12a shows a similar trend for mixtures reinforced with six layers of geogrid. Here, q_p decreased insignificantly from 219.1 to 217.3 kPa as α changed from the vertical direction to 30°, followed by a rapid drop to 137.2 and 138.8 kPa as α increased to 60 and 90°, respectively. Figure 5.13 summarises the variation in peak deviator stress of geogrid-reinforced sand-clay mixtures along the direction of principal stress α, and compares it with reinforced clean sand. Further, the peak deviator stress q_p of the geogrid-reinforced sand-clay mixtures is depicted in Figure 5.14 as a 3D surface that considers α and N_{reinf}.

Compared with unreinforced mixtures, geogrid provided a large amount of improvement, as expected. The increasing ratios q_p of mixtures, due to three layers of geogrid inclusion, relative to the unreinforced mixture, were 76.1, 64.0, 35.6 and 35.9% for α = 0, 30, 60 and 90°, respectively. As the number of geogrid layers increased to six, this improvement becomes very significant, at 107.3, 108.5, 49.1 and 49.2%, respectively. However, it is clear that the improvement was not the same under

all directions of principal stress represented, and this is linked mainly to the fact that planar reinforcements exhibit directional dependence in shearing resistance (as discussed in Chapter 4).

Compared with results for geogrid-reinforced clean sand (discussed in Chapter 4), mixed sand reinforced with three and six layers exhibited slight to medium changes in deviator stress of 1.7–8.7% for α = 0° and 30°. However, under α = 60 and 90°, deviator stress improved significantly by 16.0–30.2%, respectively, compared with reinforced sand without clay. Therefore, it can be reported that although the anisotropic strength effect on reinforced mixtures is clear, it was significantly lower than that of reinforced clean sand (Figure 5.13). The difference in peak deviator stress Δq of geogrid-reinforced mixtures due to variation in α decreased to 33.1–37.3%, compared with 47.4–50.4% for reinforced clean sand. As discussed previously, this anisotropy can be attributed to the lower ability of reinforcement to resist horizontal principal stress than vertical stress. The anisotropic failure envelopes for sand-clay mixtures reinforced with geogrid are plotted in Figure 5.15, in addition to the envelopes for sand, mixed sand-clay, and reinforced sand.

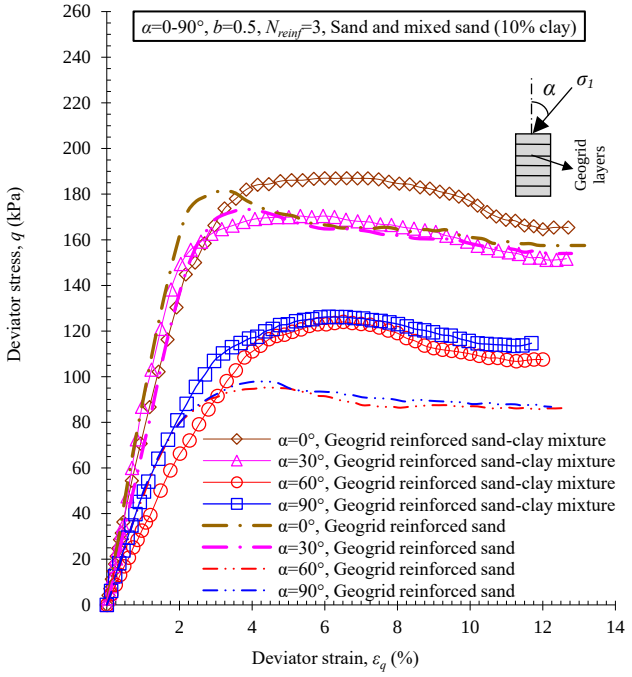

(a)

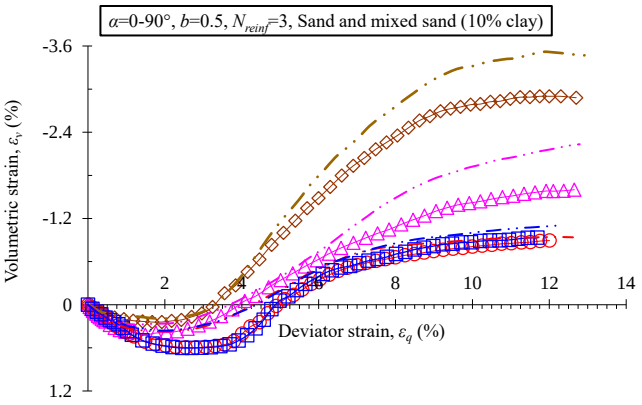

(b)

Figure 5.11 Relationships between (a) deviator stress and deviator strain; (b) volumetric strain and deviator strain for a sand-clay mixture (10% clay) reinforced with three layers of geogrid under different α

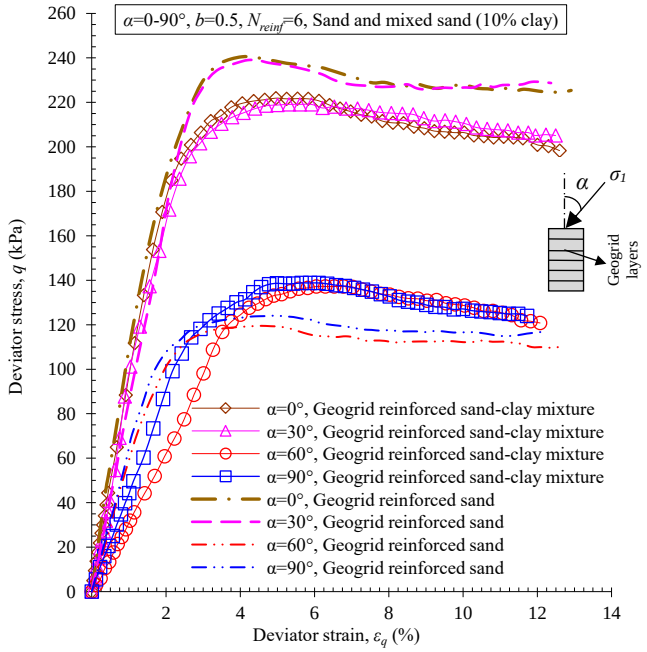

(a)

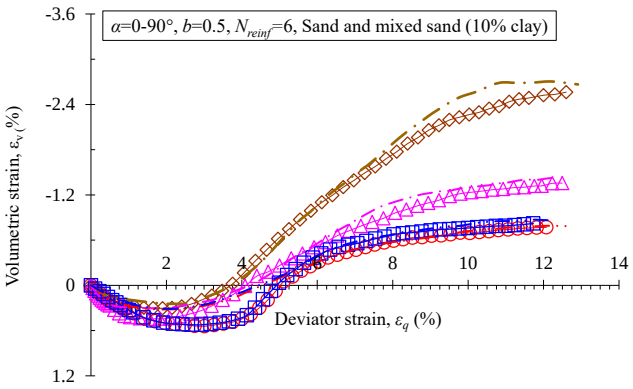

(b)

Figure 5.12 Relationships between (a) deviator stress and deviator strain; (b) volumetric strain and deviator strain for a sand-clay mixture (10% clay) reinforced with six layers of geogrid under different α.

The improvement in the reinforced mixture can be attributed to the roles of the reinforcement and the fines. The reinforcement contributes to confinement, passive resistance and the resistance of particles inside apertures. Moreover, 10% kaolinite inclusion significantly improves bonding and provides additional strength in terms of cohesion to the matrix.

The lower amount of anisotropy observed in the geogrid-reinforced mixture compared with the reinforced clean sand is related to the role of the added clay, which provides bonding between the geogrid and sand particles. This consequently improves the performance of geogrid layers, even under horizontal loading. This means that clay can act as a cementation material to improve the behaviour of geogrid-reinforced sand and make it act as a single mass. The lower anisotropy is also related to the cushioning effect provided by the fines occupying the inter-granular voids, which improves resistance to horizontal loading by decreasing the amount of sliding and rotation of particles along the bedding plane. Moreover, the mixing process of the sand-clay mixture reduces the tendency of particles to align horizontally, and consequently, decreases the anisotropic effect, although it is still present, as explained in the previous section and by many studies (e.g. Keyhani & Haeri, 2013; Kumruzzaman & Yin, 2010a, 2010b; Nakase & Kamei, 1983). In addition, inducing larger deformation to the mixed sand-clay than that of clean sand likely helps to put the reinforcement layers under a certain level of tension. For example, during the consolidation stage, larger axial strain could be induced in reinforced mixed sand-clay, as compared to reinforced clean sand, thereby mobilising the tensile strength of the geogrid, even before the shearing stage. As mentioned in Chapter 4, the improvement provided by reinforcement layers under horizontal loading is low compared with improvements to vertical loads. Therefore, the clearly observed improvement in reinforced mixtures under α = 60 and 90° could be a reflection to the aforementioned benefits of clay: 1) as a cement material that provides better bonding between geogrid and sand, and 2) the role of clay in mobilising the tensioned membrane to a certain level due to the associated larger induced deformation.

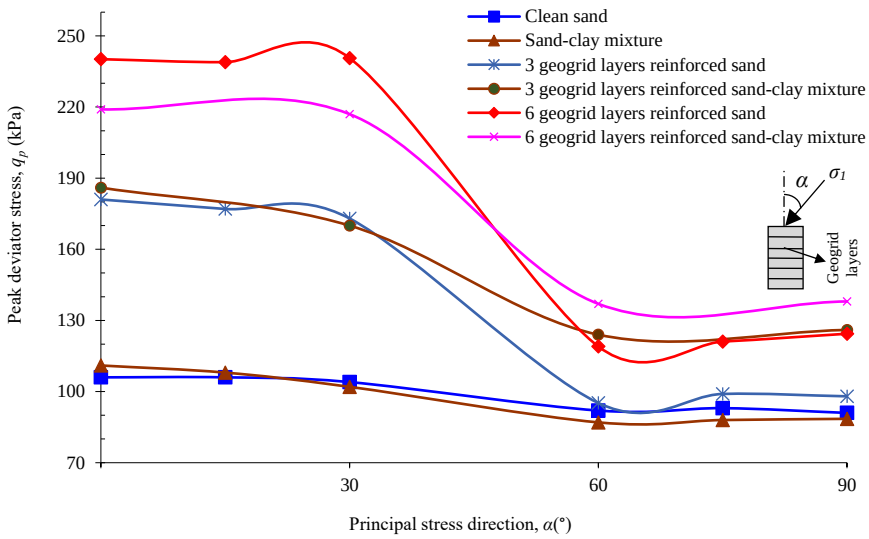

Figure 5.13 Comparison the variation of peak deviator stress q_p of three and six geogrid layer-reinforced sand containing 10% clay with those of unreinforced sand, unreinforced sand-clay and reinforced clean sand

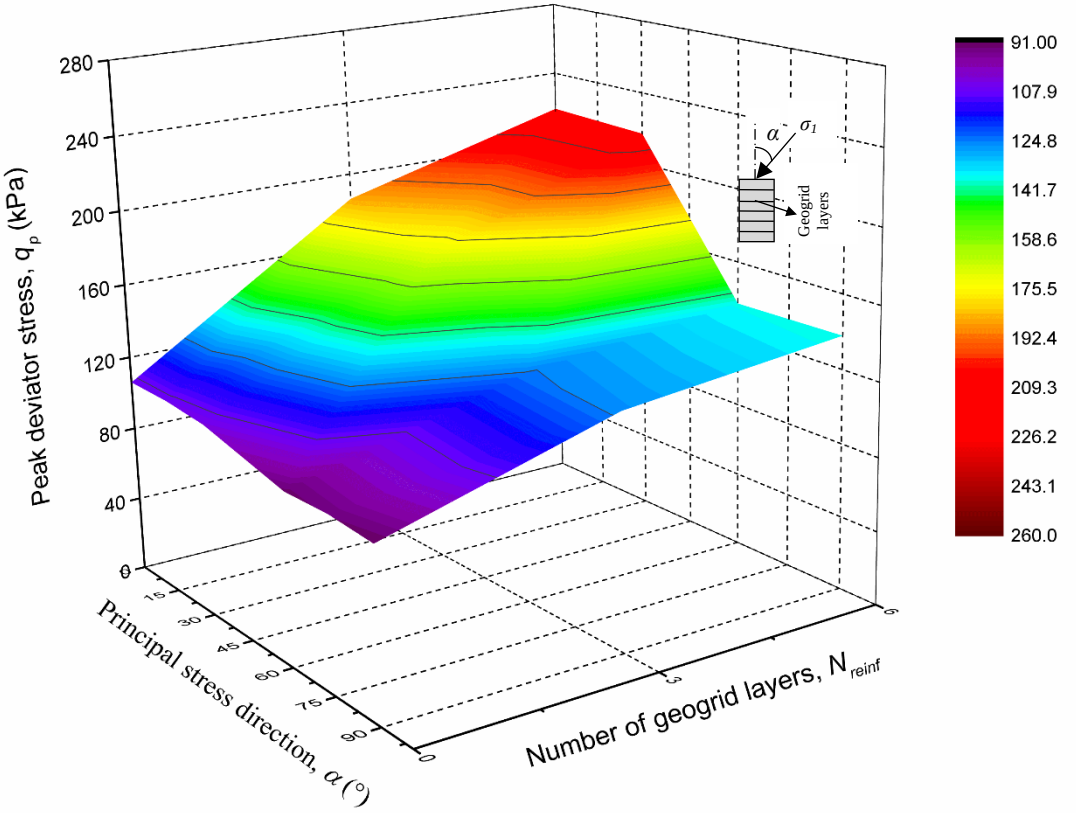

Figure 5.14 Composite α, N_{reinf}, q_p values of 3D failure surface for geogrid-reinforced sand-clay mixture

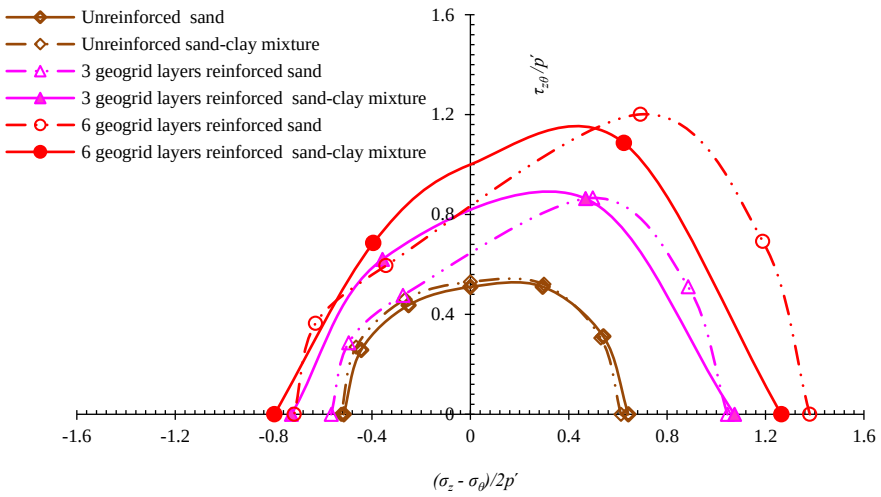

Figure 5.15 Comparison the failure envelopes of sand containing 10% clay and reinforced with three and six layers of geogrid, with those of sand, mixture, and reinforced sand

5.3.2 Volumetric Strain Characteristics

The volumetric strains of sand-10% clay mixtures reinforced with three and six layers of geogrid and sheared under different directions of principal stress (α = 0, 30, 60 and 90°) are illustrated in Figures 5.11b and 5.12b.

Discussion of these results will make comparisons with cases when geogrid was used with clean sand (Chapter 4) and also when mixtures were used without reinforcement (Section 5.2.2). Similar to the trends for unreinforced mixed sand-clay, and reinforced clean sand, the zero-volumetric change, at which transformation from initial contraction to dilation occurs, depends on the direction of principal stress α. For example, ε_v of samples reinforced with six layers of geogrid and sheared under vertical principal stress changed early to dilation, i.e., when ε_q reached 3.6%. As α increased to 15, 30 and 90°, the deviator strain ε_q required to start dilation increased to 4.0, 4.97 and 4.88%, respectively. These values are close to those of both unreinforced mixed sand and reinforced clean sand. This increase in the ε_q range is expected when we consider the role of reinforcement in restraining expansion strain, which extends the range in which compression dominates.

Moreover, the ultimate developed compressive volumetric strain $(\varepsilon_v)_{comp}$ of reinforced mixed sand also varies depending on the direction of principal stress α. For the six-layer-reinforced mixture, for example, it was a minimum of 0.30% under $\alpha = 0°$ and increased to 0.44, 0.54 and 0.52% for $\alpha = 30$, 60° and 90°. As expected, these values are larger than those of reinforced clean sand (0.25–0.32%) due to the compression nature of the clay. A similar trend was observed for the mixture reinforced with three layers.

On the other hand, the reinforced mixture exhibited a significant amount of dilation, particularly under $\alpha = 0°–30°$, compared with its compression strain. Dilative volumetric strain developed rapidly under $\alpha = 0°$, corresponding to deviator strain ε_q. This is in contrast to that under $\alpha = 60$ and 90°, where dilative strain developed at a low rate. For example, the dilative volumetric strains $(\varepsilon_v)_{dil}$ of the mixture reinforced with six geogrid layers at $\varepsilon_q = 12\%$ was 2.50, 1.33, 0.76 and 0.82% for $\alpha = 0$, 30, 60 and 90°, respectively. Dilative volumetric strains $(\varepsilon_v)_{dil}$ of the reinforced mixture were lower than those of the unreinforced mixture, where the reduction ratio ranged between 20.9 and 28.8% (depending on α) due to the confinement provided by the tensioned geogrid.

The effect of fines content on the dilative volumetric strains $(\varepsilon_v)_{dil}$ was determined by comparing these results with those of reinforced clean sand (represented by dashed lines in Figures 5.11b and 5.12b). It can be clearly observed that fines content decreased the amount of dilation by 5–8.2% (depending on α). This result is in line with studies conducted on conventional triaxial devices, such as Carraro et al. (2009). This reduction is likely related to what was previously explained regarding the role of clay as a cementation material. Clay provides cohesion to the matrix and enhances the bonding performance of samples, which in turn decreases the tendency of sand samples to expand under load. Adding clay and embedded geogrid decreases the dilation of sand significantly, by 43–48% under $\alpha = 0°$ and 30°, and 40% under $\alpha = 60°$ and 90°.

5.4 Geotextile-reinforced Sand-clay Mixtures

5.4.1 Strength Characteristics

The deviator stress-strain of mixtures containing 10% clay and reinforced with three and six layers of nonwoven geotextile are presented herein (Figures 5.16a and 5.17a) under various principal stress directions of 0–90°.

The deviator stress of sand-clay mixtures reinforced with three and six layers of geotextile increased with increases in deviator strain until peaking, after which insignificant post-peak decrease occurred for different values of α (Figures 5.16a and 5.17a). There were significant differences between the deviator stresses that developed under compression, i.e. α = 0–30°, compared to those under extension mode, i.e. α = 60–90°. The variation in peak deviator stresses along principal stress direction α (Figure 5.18) is typical to that reported previously, but with less variation. For three layers of geotextile, the largest q_p of 212.3 kPa occurred with a vertical principal stress, while it reduced to 194.7, 145.0 and 144.6 kPa when α was rotated to 30, 60 and 90°, respectively, constituting a maximum difference ratio Δq_p of 31.7%. A similar trend was observed for six layers of reinforcement, where the q_p decreased by 29.4% as α changed to 60–90°, compared with the 258.1 kPa observed at α = 0°. Figure 5.19 shows a 3D surface of the results of testing the geotextile-reinforced sand-clay mixture.

To better understand the effect of clay on reinforced sand, the results for reinforced mixed sand were compared with those of reinforced clean sand. To facilitate comparison, the curves for reinforced sand and reinforced mixed sand were plotted in Figures 5.16a and 5.17a. The difference between the peak deviator stress of reinforced mixed sand and that of reinforced clean sand was slight under α = 0–30° but significant when α = 60–90° (Figure 5.18). For example, the improvement in q_p due to the addition of 10% clay to sand reinforced with three and six layers of geotextile was ≤ 2.8% under α = 0–30°, compared with 25.7–37.8% when α = 60–90°. This improvement in strength under α = 60–90° caused significant decreases in directional dependence in the geotextile-reinforced mixed sand; the difference in deviator stress Δq_p due to the variation of α was significantly lower at 29.4–31.7%, compared with 46.7–47.7% for

reinforced clean sand. On the other hand, the unreinforced mixture showed a significant improvement due to geotextile reinforcement. Three layers of nonwoven geotextile increased the q_p values of mixed sand by 87.1–100.3% and 55.4–57.6% for α = 0–30° and 60–90°, respectively. The improvement was greater when six layers of geotextile were used, being 143.2–143.5% for α = 0–30° and 95.6–97.8% for α = 60–90°. The relationship between $(\sigma_z - \sigma_\theta) / 2p'$ and $\tau_{z\theta} / p'$ at peak state for different values of α are depicted in Figure 5.20. It is apparent that the anisotropic effect is reduced with addition of clay to the reinforced sand.

Addition of clay plays a significant role in improving strength under α = 60–90°, and consequently, decreasing directional dependence. This role was explained in Section 5.3; in summary, clay may provide a cementation function to the composite, giving it a cushioning effect, better interlocking, increasing the stability of particles along the bedding plane, decreasing the tendency for particles to align, and inducing greater strain, which mobilises the tensile action of the geotextile. Despite this, the strength under α = 60–90° was still much lower than that under α = 0–30°. This is attributed to the horizontally-placed planar reinforcement, which gives better performance under a vertical principal stress direction than a horizontal one.

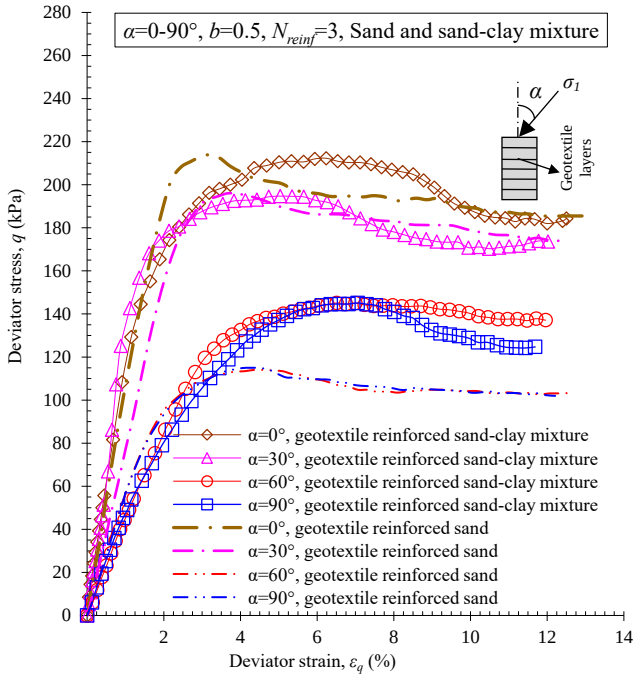

(a)

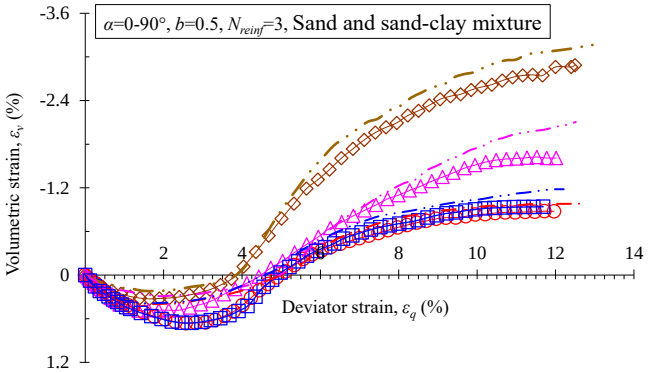

(b)

Figure 5.16 Relationships between (a) deviator stress and deviator strain; (b) volumetric strain and deviator strain for mixed sand (10% clay) reinforced with three layers of nonwoven geotextile under different values of α

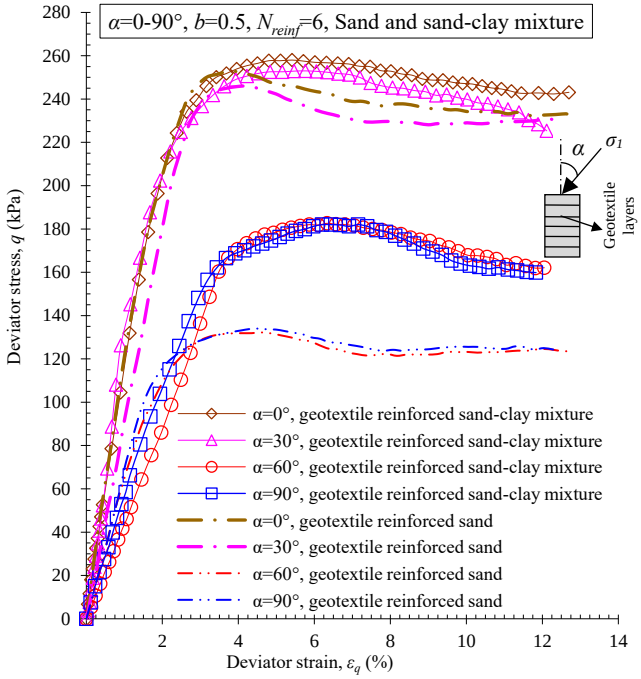

(a)

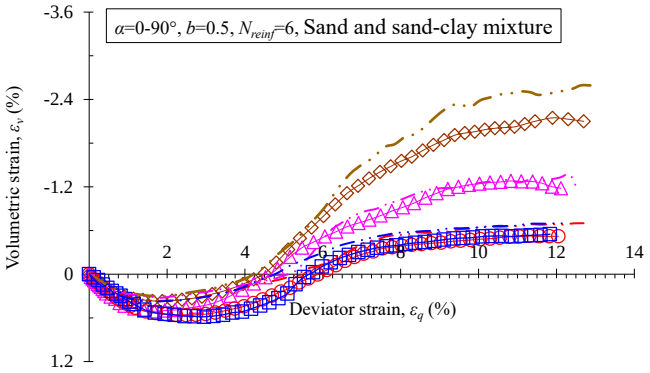

(b)

Figure 5.17 Relationships between (a) deviator stress and deviator strain; (b) volumetric strain and deviator strain for mixed sand (10% clay) reinforced with six layers of nonwoven geotextile under different values of α

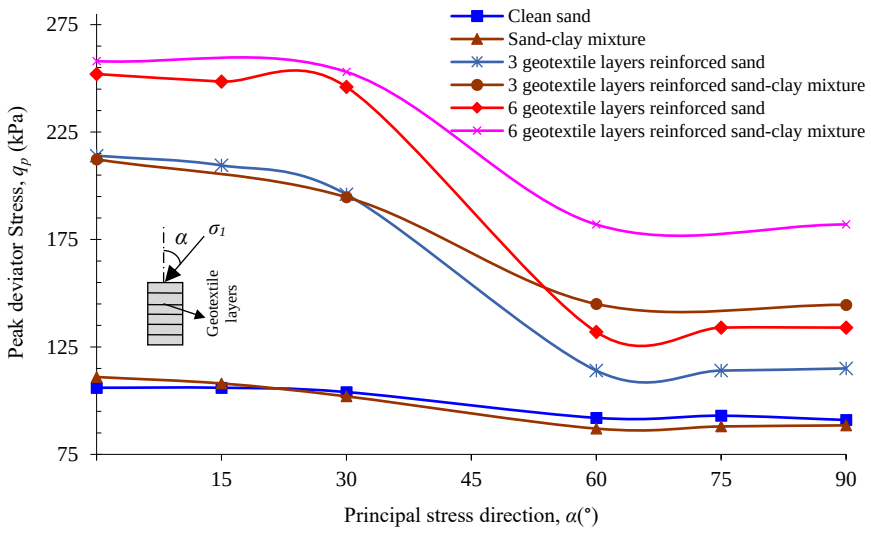

Figure 5.18 Comparison of variation in peak deviator stress q_p for sand containing 10% clay reinforced with three and six nonwoven geotextile layers, and those of sand, mixed sand, and reinforced sand

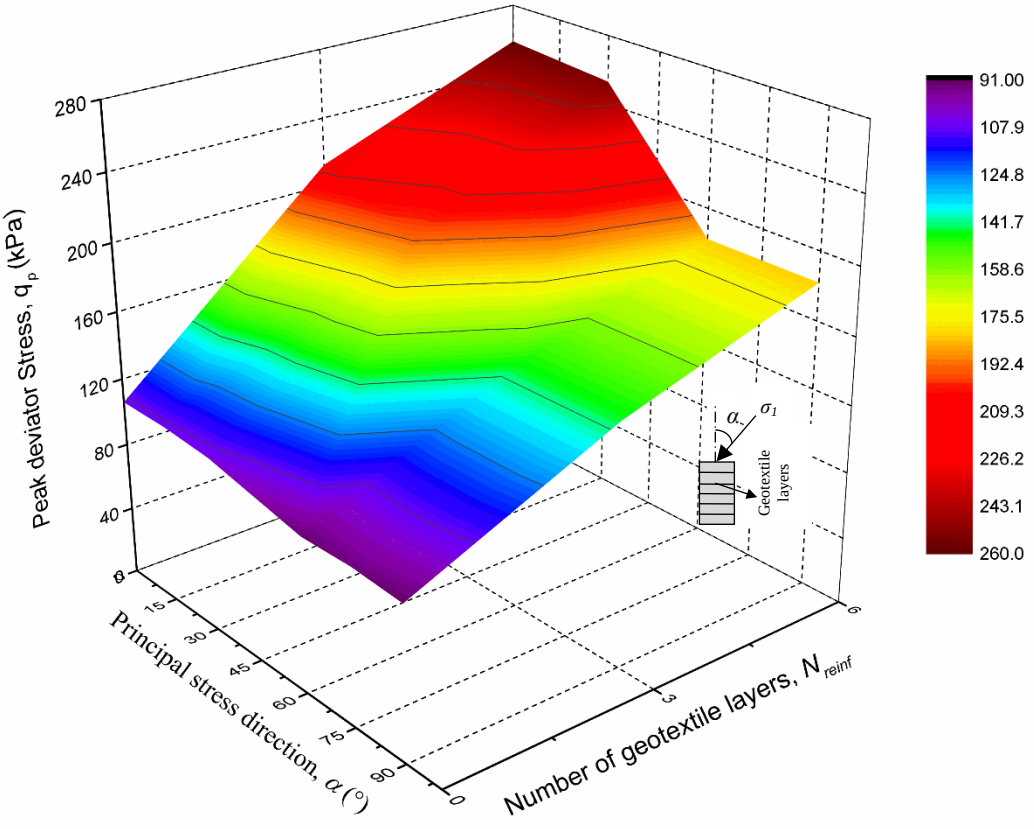

Figure 5.19 Composite α, N_{reinf}, q_p values of 3D failure surface for geotextile-reinforced sand-clay mixture

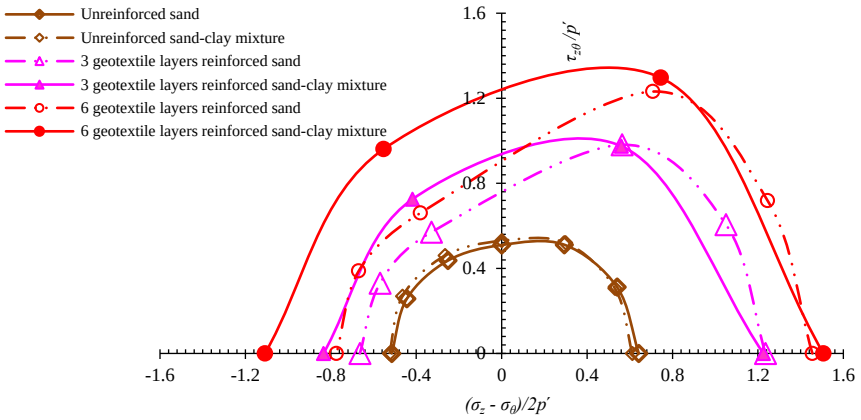

Figure 5.20 Comparison of the failure envelopes of mixed sand-clay reinforced with three and six layers of nonwoven geotextile with those of reinforced pure sand, unreinforced sand and unreinforced mixed sand-clay

5.4.2 Volumetric Strain Characteristics

Figures 5.16 and 5.17 shows the volumetric strain-deviator strain relationships of mixed sand reinforced with three and six layers of geotextile.

From the beginning of shearing until deviator strain ε_q reached 3.7–4.3% (for α = 0–30°) and 4.8–5.0% (for α = 60–90°), the volume of geotextile-reinforced mixtures tended to decrease. Maximum contractive strain $(\varepsilon_v)_{comp}$ of samples reinforced with six layers, for example, was 0.37, 0.51, 0.563 and 0.585% at α = 0, 30, 60 and 90°, respectively. Larger contractive strain at larger α values indicates that the horizontal plane still has a relatively high tendency to compress.

On the other hand, when ε_q exceed 3.7–5.0% (depending on α) geotextile-reinforced mixtures began to expand. The rate of accumulation of such expansion strain under α = 0 and 30° was greater than when α = 60–90°. Similar to unreinforced mixed sand, unreinforced sand or reinforced sand, the amount of this dilative volumetric strain $(\varepsilon_v)_{dil}$ was still dependent on the direction of principal stress α. For example, at ε_q = 12%, the six geotextile layer-reinforced mixture under α = 0° developed the largest $(\varepsilon_v)_{dil}$ value of 2.1% and this value decreased to 1.18, 0.52 and 0.55% as α increased to 30, 60 and 90°, respectively. This variation reflects the anisotropic effect, where the vertical direction exhibits a greater tendency for dilation than the horizontal one.

Compared with unreinforced mixed sand, the expansion strain $(\varepsilon_v)_{dil}$ of six layer-reinforced mixed sand under different values of α decreased by 34.4–46.7%. This decrease was expected and can be attributed to the confinement provided by tensioned geotextile. On the other hand, comparison with reinforced clean sand (six layers) implies that adding fines reduces dilation strain $(\varepsilon_v)_{dil}$ by 16.3–22.5% for α = 0–30° and 34.1–36.0% for α = 60–90°. This better performance, even under extension conditions (α = 60–90°), gives a good indication of the benefit of bonding between the geotextile and the sand caused by the cementation of the added clay, which provides greater interlocking and makes samples behave like a single composite. Inclusion of both clay and geotextile contributed to an approximate 51.8–59.7% reduction in dilation, compared with clean sand. A similar trend was observed for mixtures reinforced with three layers of geotextile, however, as expected, there was less improvement.

5.5 Geocell-reinforced Sand-clay Mixtures

5.5.1 Strength Characteristics

In this section, the results for a sand-10% clay mixture reinforced with a 3D geo-inclusion are presented (Figures 5.21-5.23).

The developed deviator of reinforced sand-clay mixture stress q at 0° was almost coincident with that at 30°, and a similar match was also observed between 60 and 90°. Adding 10% clay to the geocell-reinforced sand resulted in q_p increasing by approximately 10.9–12.1% under α = 60–90°. This can clearly be seen in Figure 5.22; q_p varied from 265.4–268.2 kPa for α = 0–30° to 224.2 kPa for α = 60–90°. This represents a Δq of only 16.4% compared with 25.3% for reinforced sand. This means that the variation of q_p decreased. This is an indication that adding fines can contribute to a relative decrease in the effects of principal stress direction, i.e. anisotropic effects on strength, to a certain degree.

On the other hand, a composite of sand, 10% clay and geocell reinforcement improved the peak deviator stresses q_p by 141.1, 160.0, 157.5 and 153.4% for α = 0, 30, 60 and 90°, respectively, compared with unreinforced clean sand, and by 153.1, 150.4, 143.6

and 146.5%, respectively, compared with unreinforced sand-clay mixture. This improvement in terms of increasing deviator stress and decreasing directional dependence is related to the roles of geocell (as explained in Chapter 4) and the roles of fines (as explained in the previous two sections). The main roles of geocell include: all-around confinement provided by the tensioned wall, bending resistance provided by the formed stiff composite, and friction between the particles and walls. Fines content provides a cushioning effect, improves interlocking, increases bonding and decreases preferential alignment. The combination of fines and geocell changes the bulk of individual particles, which is likely unstable along the weakest horizontal plane, into a well-bonded composite material. Although this composite still exhibits directional dependence, it is significantly lower than that observed for unreinforced samples, as well as geogrid and geotextile-reinforced samples.

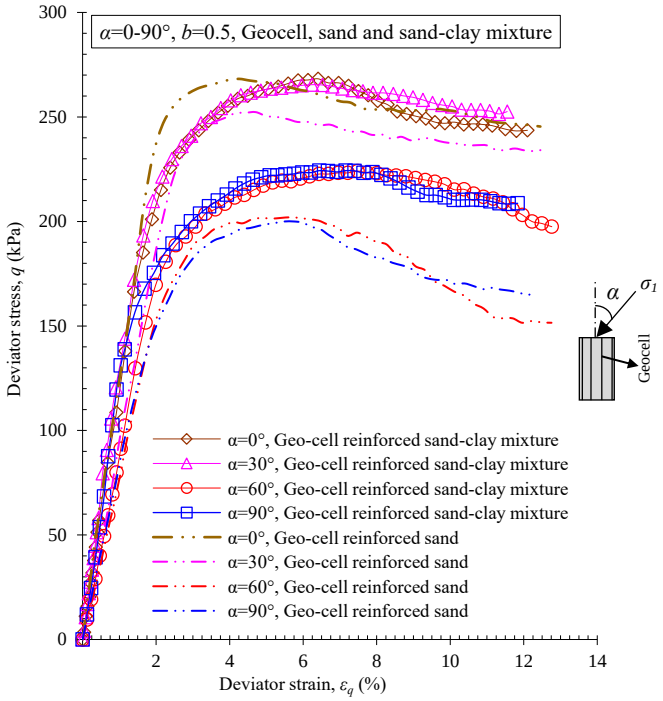

(a)

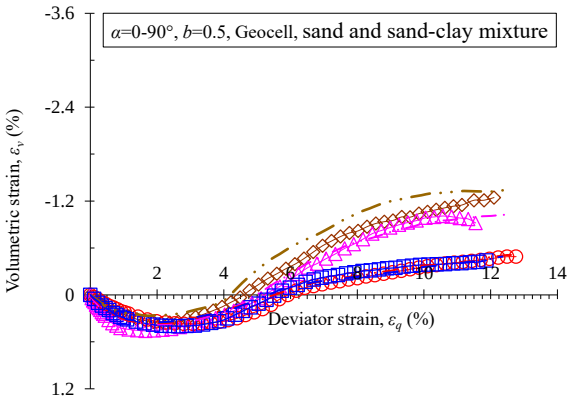

(b)

Figure 5.21 Relationships between (a) deviator stress and deviator strain; (b) volumetric strain and deviator strain for mixed sand (10% clay) reinforced with geocell under different α

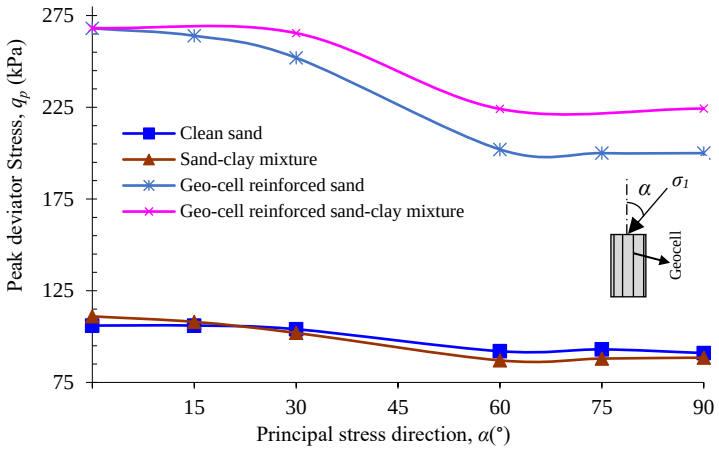

Figure 5.22 Comparison of the variation in peak deviator stress q_p with principal stress direction α for geocell-reinforced sand containing 10% clay and unreinforced sand, unreinforced mixed sand, and reinforced sand

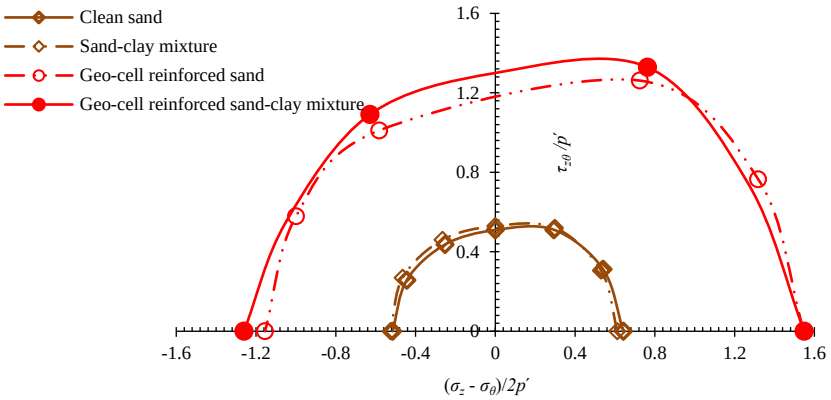

Figure 5.23 Comparison of the failure envelopes of geocell-reinforced sand containing 10% clay and samples of unreinforced sand, unreinforced mixed sand, and reinforced sand

5.5.2 Volumetric Strain Characteristics

The induced volumetric strains of the sand-clay mixture reinforced with geocell are presented in Figure 21b.

Reinforced mixtures exhibited contractive volumetric strains of 0.37–0.46% for α = 0–90°. Compared with reinforced sand, there was an increase in the contractive volumetric strain $(\varepsilon_v)_{comp}$ of 35–39%. This owes to the compressibility of the clay and also to the development of larger deviator stresses. On the other hand, the reinforced mixture under α = 60–90° exhibited a decrease in $(\varepsilon_v)_{comp}$ by approximately 35.3% compared with unreinforced mixtures. This decrease is related to horizontal confinement, friction between particles and the geocell walls, and the bonding between the cells and sand provided by the clay.

After deviator strain ε_q reached 4.5–5.9% (depending on α), dilative strain dominated the deformation behaviour. Dilative strain $(\varepsilon_v)_{dil}$ increased steadily with shearing and reached 1.21% at ε_q = 12% with principal stress in the vertical direction, compared with 0.92, 0.47 and 0.44% for α = 30, 60 and 90°, respectively. These amounts were lower by 57.8–72.5% (depending on α) than those of unreinforced clean sand, and 52.6–64.4% lower compared with unreinforced mixed sand. This decrease is attributed to the combination of geocell reinforcement and clay, which both provide restraint. The geocell provides all-around restraint to the sample and limits lateral deformation, consequently decreasing expansion of the sand's volume. Moreover, the presence of fines gives the matrix greater stability by providing bonding and cohesion of sand particles, which decreases their tendency to flow laterally.

5.6 Comparative performance of sand-clay mixtures reinforced with different types of geosynthetics

Adding up to 20% clay to sand samples generally decreased the anisotropy and deviator stress of the mixture. An exception was for samples containing 10% clay, where some increase in deviator stress was observed. The low anisotropy is related to the cushioning effect of clay, which increases the resistance of the bedding plane to horizontal shearing. Moreover, the cementation effect causes sand to behave as a single mass, while the mixing process decreases the tendency of particles to align. Table 5.3 shows the peak deviator stresses of sand samples mixed with various percentages of clay and tested under various directions of principal stress.

Inclusion of 10% clay improved the performance of sand reinforced with different types of geosynthetics. This improvement is attributed to clay providing bonding between the reinforcement and the sand particles. Therefore, the low ability of geogrid and geotextile to sustain horizontal principal stress (as explained in Chapter 4) is improved considerably by the cementation action of clay. Table 5.4 shows the peak deviator stresses for sand-clay mixtures reinforced with geogrid, geotextile and geocell and tested under various directions of principal stress.

For geogrid-reinforced sand, clay addition resulted in decreases in peak deviator stress under conditions of α = 0–30°, while clear increases occurred when α = 60–90°. However, clay inclusion generally increases the peak deviator stress of geotextile- and geocell-reinforced sand across the full range of α, i.e. 0–90°.The Difference in the peak deviator stress caused by changing α were 50.4, 47.7 and 25.3% for geogrid-, geotextile- and geocell-reinforced sand, respectively. These decreased to 37.3, 29.4 and 16.4% when 10% clay was added.

Table 5.3 Summary of the peak deviator stress of sand-clay mixtures obtained under various α

Direction of principal stress, α (°)	Clay content, F (%)				
	0	5	10	15	20
	Peak deviator stress, q_p (kPa)				
0	111.3	100.6	106.2	98.4	94.2
15	108.0	98.6	106.0	97.2	94.2
30	102.2	94.4	104.2	95.2	92.1
60	87.0	83.1	92.3	86.0	81.0
75	88.0	82.8	93.1	86.3	82.5
90	88.5	80	91.0	84.0	78.1

Table 5.4 Summary of the peak deviator stresses of reinforced sand-clay mixtures obtained under various α

Direction of principal stress, α (°)	Unreinforced sand-clay mixture	Geogrid reinforced sand-clay mixture		Geotextile reinforced sand-clay mixture		Geocell reinforced sand-clay mixture
		3 layers	6 layers	3 layers	6 layers	
	Peak deviator stress, q_p (kPa)					
0	106.2	186.7	219.1	212.3	258.1	268.2
30	104.2	170.6	217.3	194.7	253.1	265.4
60	92.3	124.8	137.2	145.0	182.0	224.1
90	91.0	126.4	138.8	144.6	182.3	224.3
	Difference in peak deviator stress, Δq_p (%)					
	13.3	33.1	37.3	31.7	29.4	16.4

Chapter 6

Effect of the Intermediate Principal Stress Parameter on the Stress-strain Characteristics of Reinforced Samples under Various Directions of Principal Stress

6.1 Introduction

This chapter presents and discusses the results of a comprehensive set of tests on sand and sand-clay mixtures, both unreinforced and reinforced with geosynthetics. These were conducted to investigate the influence of the intermediate principal stress parameter *b* on the characteristics of anisotropic stress-strain and volumetric change in sand samples. The samples were 100% sand, or a sand-clay mixture (10% clay), and were either unreinforced or reinforced with geogrid, geotextile or geocell. These samples were subjected to various values of *b* (0.2, 0.5 and 1.0) and principal stress α (0, 30, 60 and 90°). This chapter also demonstrates the extent to which clay fines and different types of geosynthetic reinforcement decrease the effect of *b*. Table 6.1 summarises the test program.

Section 6.2 will be devoted to reviewing and discussing the effect of *b* on the stress and strain characteristics of sand and a sand-clay mixture. The following sections will be dedicated to the characteristics of sand and mixed sand-clay reinforced with six layers of geogrid (Section 6.3), six layers of geotextile (Section 6.4) and geocell (Section 6.5). Finally, a summary and comparison the effect of *b* on sand and mixed sand-clay reinforced with planar and cellular inclusions will be made in Section 6.6.

Table 6.1 Summary of the conditions and parameters of the tests presented in this chapter

Test Series		Plastic Fine content, F (%)	Relative density, D_r (%)	Mean effective stress, p'(kPa)	Intermediate principal stress parameter, b	Principal stress direction, α (°)
Series I Unreinforced clean sand		0	69.4–70.1	100	0.2	0, 30, 60 & 90
		0	70.1–70.7	100	0.5	0, 30, 60 & 90
		0	70.1–70.3	100	1.0	0, 30, 60 & 90
Series II Unreinforced sand-clay mixture		10	69.8–70.4	100	0.2	0, 30, 60 & 90
		10	70.1-70.2	100	0.5	0, 30, 60 & 90
		10	69.3–70.2	100	1.0	0, 30, 60 & 90
Series III Reinforced clean sand	6 layers-Geogrid	0	69.1–69.8	100	0.2	0, 30, 60 & 90
		0	69.9–70.4	100	0.5	0, 30, 60 & 90
		0	69.2–70.4	100	1.0	0, 30, 60 & 90
	6 layers-Geotextile	0	69.6–70.4	100	0.2	0, 30, 60 & 90
		0	70.2–70.3	100	0.5	0, 30, 60 & 90
		0	68.8–69.7	100	1.0	0, 30, 60 & 90
	Geocell	0	68.8–70.1	100	0.2	0, 30, 60 & 90
		0	69.3–70.6	100	0.5	0, 30, 60 & 90
		0	69.2–70.5	100	1.0	0, 30, 60 & 90
Series IV Reinforced sand-clay mixture	6 layers-Geogrid	10	70.4–70.7	100	0.2	0, 30, 60 & 90
		10	69.8–70.1	100	0.5	0, 30, 60 & 90
		10	70.1-70.4	100	1.0	0, 30, 60 & 90
	6 layers-Geotextile	10	70.3–71.2	100	0.2	0, 30, 60 & 90
		10	70.1–70.2	100	0.5	0, 30, 60 & 90
		10	70.3–70.9	100	1.0	0, 30, 60 & 90
	Geocell	10	68.8–70.4	100	0.2	0, 30, 60 & 90
		10	69.9–70.1	100	0.5	0, 30, 60 & 90
		10	69.4-–71.4	100	1.0	0, 30, 60 & 90

6.2 Effect of *b* on Sand and Sand with 10% Clay

6.2.1 Strength Characteristics

The effect of the intermediate principal stress parameter b on the stress-strain characteristics of sand and mixed sand-clay under different directions of principal stress α is illustrated in Figures 6.1a-6.4a. Note that the results obtained under b = 0.5 were presented in Chapters 4 and 5 in the discussion of the effect of α on sand and mixed sand-clay. In this chapter, the results of tests under b = 0.2, 1.0 and 0.5 will be presented to investigate the effect of b on sand and mixed sand-clay.

In clean (100%) sand, irrespective of the principal stress direction α, the peak deviator stress q_p decreases with increasing b values. At α = 0°, deviator stress develops rapidly with increasing strain and there is no significant difference in q_p at different values of b (0.2, 0.5 and 1.0), until deviator stress approaches a peak, when a clear difference occurs. This difference in q_p due to the variation in b occurs earlier for larger directions of principal stress α. The relationship between the peaks of deviator stress q_p and intermediate principal stress parameter b for different directions of principal stress α is depicted in Figure 6.5. Peak deviator stresses q_p were largest under b = 0.2, at 120.5, 110.4, 99.0 and 100.2 kPa for α = 0, 30, 60 and 90° respectively. They then decreased by approximately 7.6–12.1% as b increased to 0.5 and by 12.6–17.0% with further increases of b to 1.0. It is noteworthy to mention that the combination of a large direction of principal stress α and large intermediate principal stress parameter b caused the lowest strength. For example, among the different values of b and α tested, the combination of α = 60–90° and b = 1.0 resulted in the minimum peak deviator stress q_p of 83.1–85.4 kPa. This is an approximately 30.0% reduction compared with the conditions of α = 0° and b = 0.2, which resulted in the greatest strength. The 3D surface of peak deviator stresses, obtained from different intermediate principal stresses b and directions of principal stress α, are presented in Figure 6.6a.

Figure 6.7 shows the variation in q_p along α for different values of b. Peak deviator stress under b = 0.2 decreased from a maximum value of 120.5 kPa under α = 0° by 8.3, 17.8 and 16.8% as α increased to 30, 60 and 90°, respectively. Larger difference in deviator stress Δq_p was observed when b increased to unity (b = 1.0), where q_p

decreased from 105.2 kPa, at α = 0°, by 12.1, 18.8 and 21.0%, corresponding to increases in α to 30, 60 and 90°, respectively.

In sand containing 10% kaolinite, the trend was generally similar to that of clean sand (Figures 6.1a-6.4a), but the anisotropic effect was significantly lower (Figures 6.1a-6.4a; Figures 6.5-6.7). For example, the q_p of the mixture tested under α = 0° decreased from 114.7 kPa under b = 0.2 to 106.2 and 102.3 kPa under b = 0.5 and 1.0, respectively, consisting of a decreasing ratio of 10.4%. For inclined principal stresses, i.e. α = 30, 60 and 90°, the decreasing ratio of q_p due to increasing of b to 1.0 was in the range 11.2–12.6%. It is noteworthy that the minimum q_p value obtained under b = 0.2, which occurred at α = 60–90°, was close to the maximum q_p obtained under b = 1.0, which occurred at α = 0°. The variation of q_p with b and α is presented in Figures 6.5-6.7. From these figures, the effect of b on q_p can be easily recognised and compared between clean sand and mixed sand-clay. Compared with clean sand, mixed sand-clay exhibited a significantly lower degree of anisotropy, as represented by the difference in deviator stresses Δq_p implied in the figures. For a given direction of principal stress α, the reductions in q_p occurring due to increases of b from 0.2 to 1.0 were 12.6–17.0% for sand and 10.4–12.6% sand-clay (Figures 6.5-6.7). Moreover, the reduction in q_p due to the variation of α from 0–90° decreased from 17.8, 21.8 and 21.0% for clean sand under b = 0.2, 0.5 and 1.0, respectively, to 9.8, 13.0 and 12.0%, respectively, for mixed sand-clay. The failure surfaces obtained from torsional tests on clean sand and sand-clay are presented in the $(\sigma_z - \sigma_\theta) / 2p'$ and $\tau_{z\theta} / p'$ spaces (Figures 6.8) to give a simple and clear description of the stress states of the samples. The effect of the anisotropic response is clear and can be seen at the point where the shapes of the failure envelopes are asymmetrical.

The effect of b can be explained based on the induced anisotropy and the definition of b. Particles are packed together in such a way that the majority are aligned horizontally, and thus, the bedding plane has poor interlocking and low strength. To sustain the applied load, column-like microstructures are formed by stacking particles primarily along the direction of principal stress α, i.e., the applied stress. As explained in Chapter 4, these columns have the largest width under α = 0° and the smallest width under α = 90°. Accordingly, the columnar structures under α = 90° exhibit the least

stability. Consequently, increasing load along the horizontal plane, i.e. $\alpha = 90°$, results in less peak deviator stress. In the hollow cylinder apparatus HCA, the radial stress σ_r is equal to the intermediate principal stress σ_2, and thus, b reflects the variation in σ_r, where the condition of $b = 0$ means that $\sigma_2 = \sigma_3 = \sigma_r$, while under $b = 1.0$, the condition changes to $\sigma_2 = \sigma_1 = \sigma_r$. Furthermore, σ_1 is the largest developed stress among the other principal stresses observed during the tests. Therefore, this means that stress along the horizontal plane in the second condition of $b = 1.0$, ($\sigma_1 = \sigma_r$), is larger than that when $b = 0$, ($\sigma_3 = \sigma_r$), and thus, a smaller peak deviator stress is likely to develop under $b = 1.0$. Under conditions of $\alpha = 90°$, σ_1 will turn to the horizontal plane, and thus, the combined condition of $b = 1$, i.e. $\sigma_r = \sigma_1$, and $\alpha = 90°$ results in the largest stresses along the horizontal plane. On the other hand, the reduction in the anisotropic effect, in terms of b and α, in mixed sand-clay is attributed to the role of clay, which occupies the inter-particle voids, as discussed in Chapter 5. This fine material provides very good bonding and cohesion in addition to a cushioning effect that improves particle interlocking and increases resistance against lateral or inclined loading.

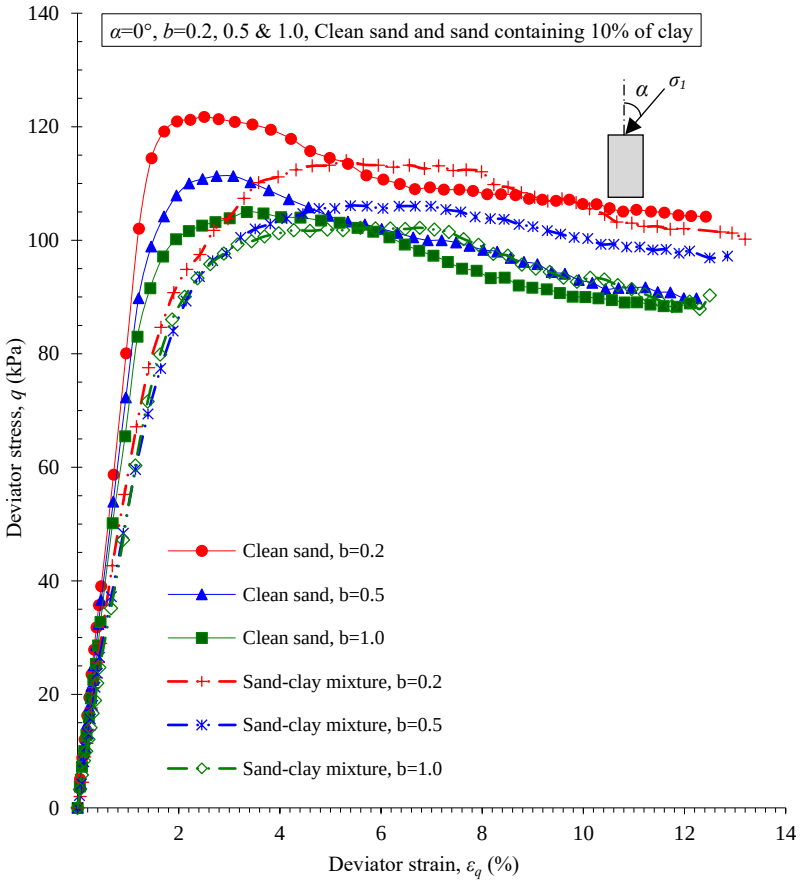

(a)

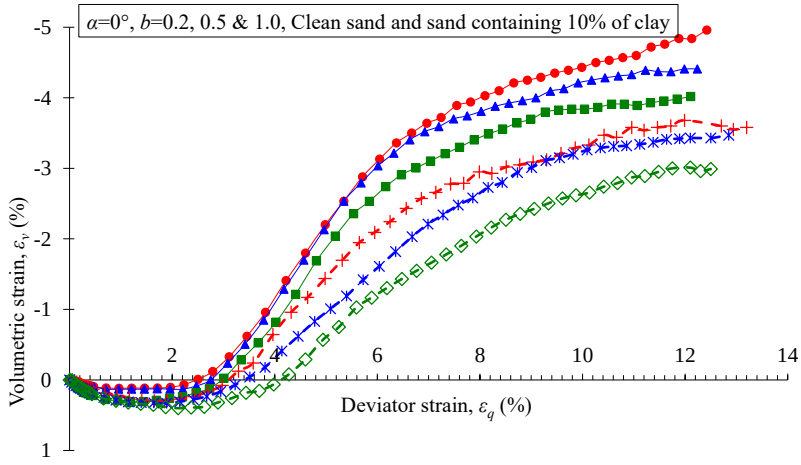

(b)

Figure 6.1 Relationships between (a) deviator stress and deviator strain; (b) volumetric strain and deviator strain of clean sand, and sand containing different clay contents, under different values of b (α = 0°)

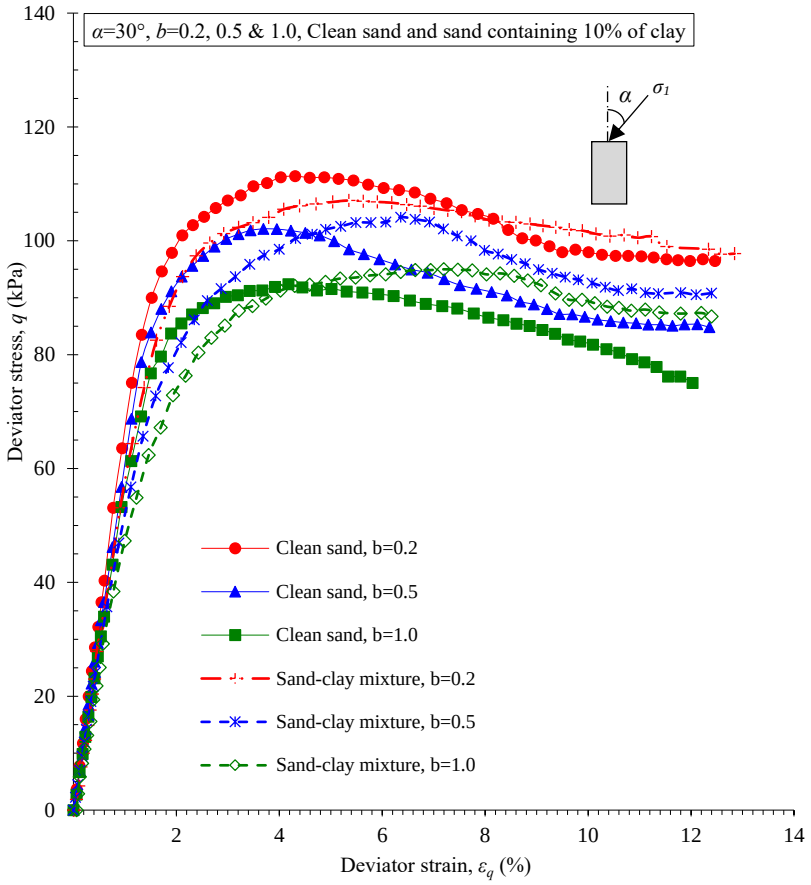

(a)

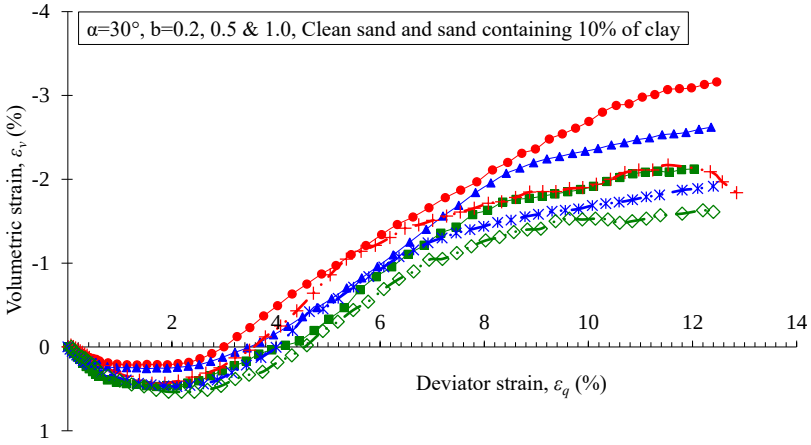

(b)

Figure 6.2 Relationships between (a) deviator stress and deviator strain; (b) volumetric strain and deviator strain of clean sand, and sand containing different clay contents, under different values of b (α = 30°)

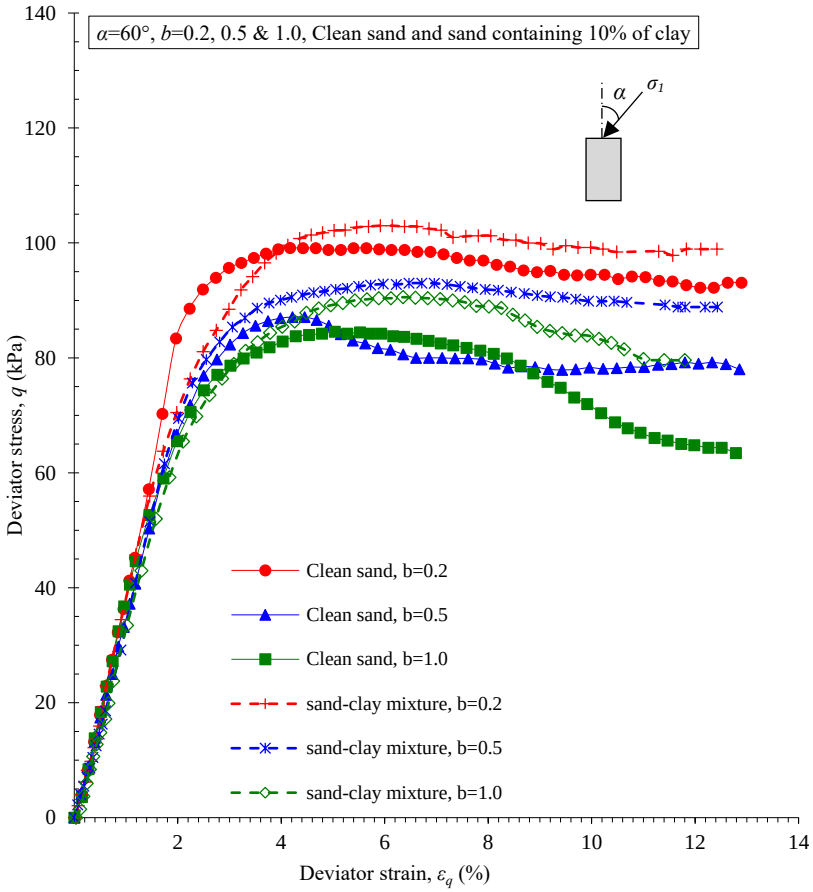

(a)

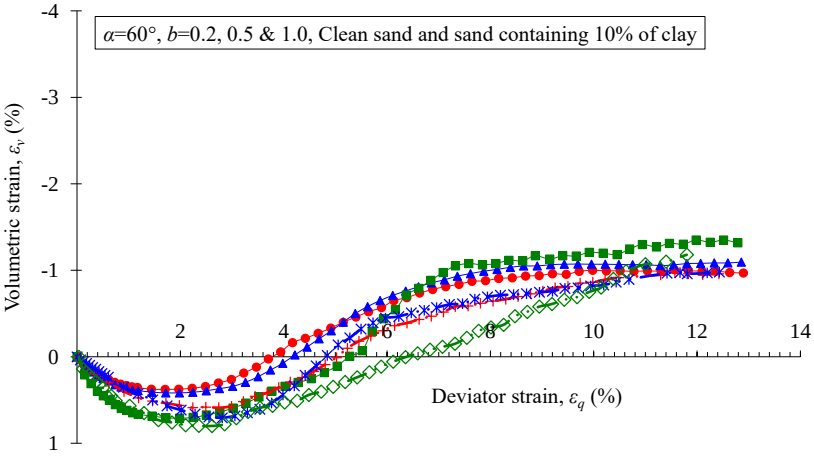

(b)

Figure 6.3 Relationships between (a) deviator stress and deviator strain; (b) volumetric strain and deviator strain of clean sand, and sand containing different clay contents, under different values of b (α = 60°)

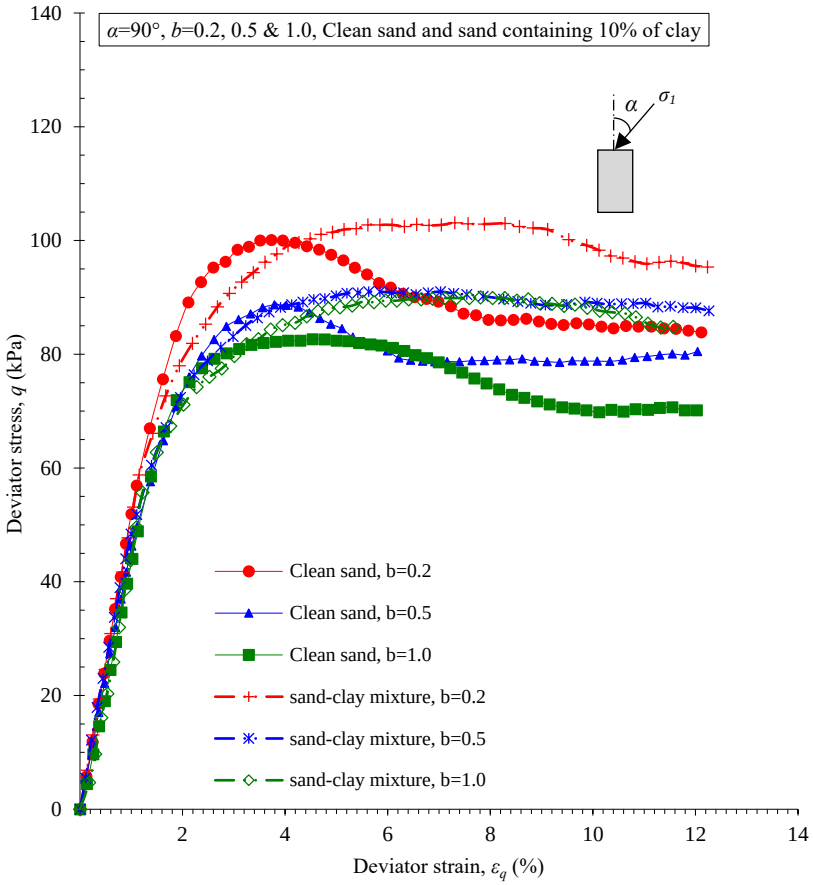

(a)

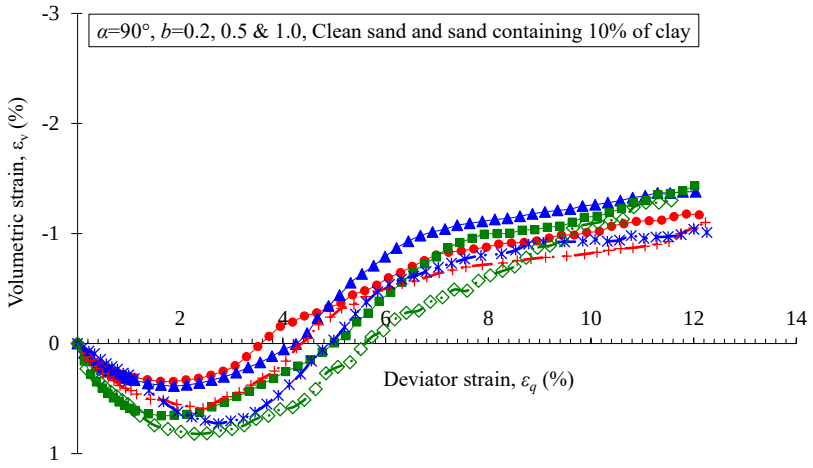

(b)

Figure 6.4 Relationships between (a) deviator stress and deviator strain; (b) volumetric strain and deviator strain of clean sand, and sand containing different clay contents, under different values of b (α = 90°)

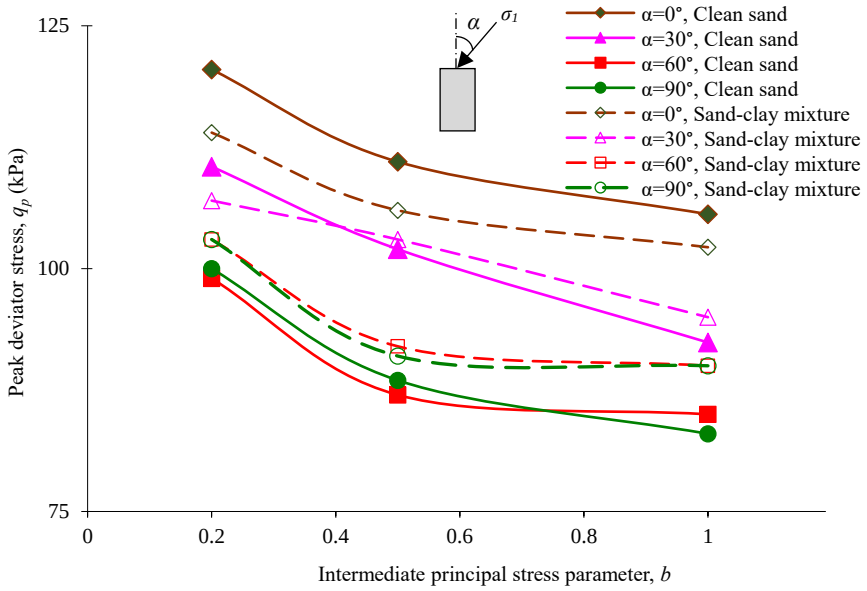

Figure 6.5 Variation of the peak deviator stress q_p of clean sand and sand containing 10% of clay against intermediate principal stress parameter b under different directions of the principal stress α

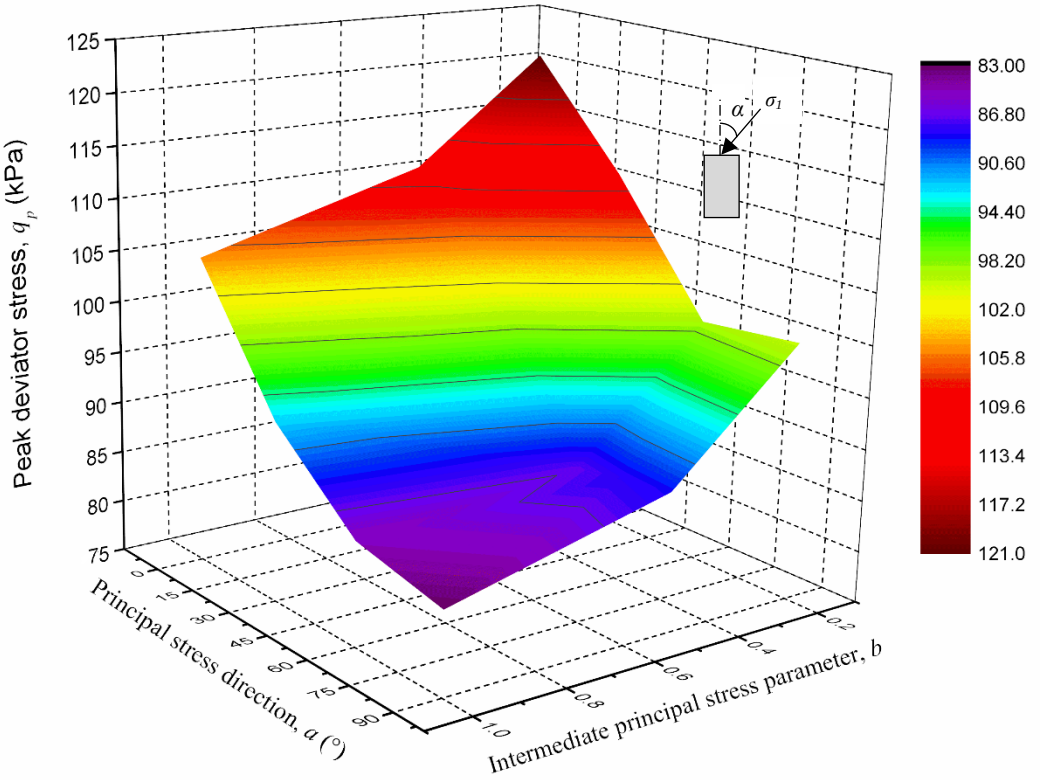

(a)

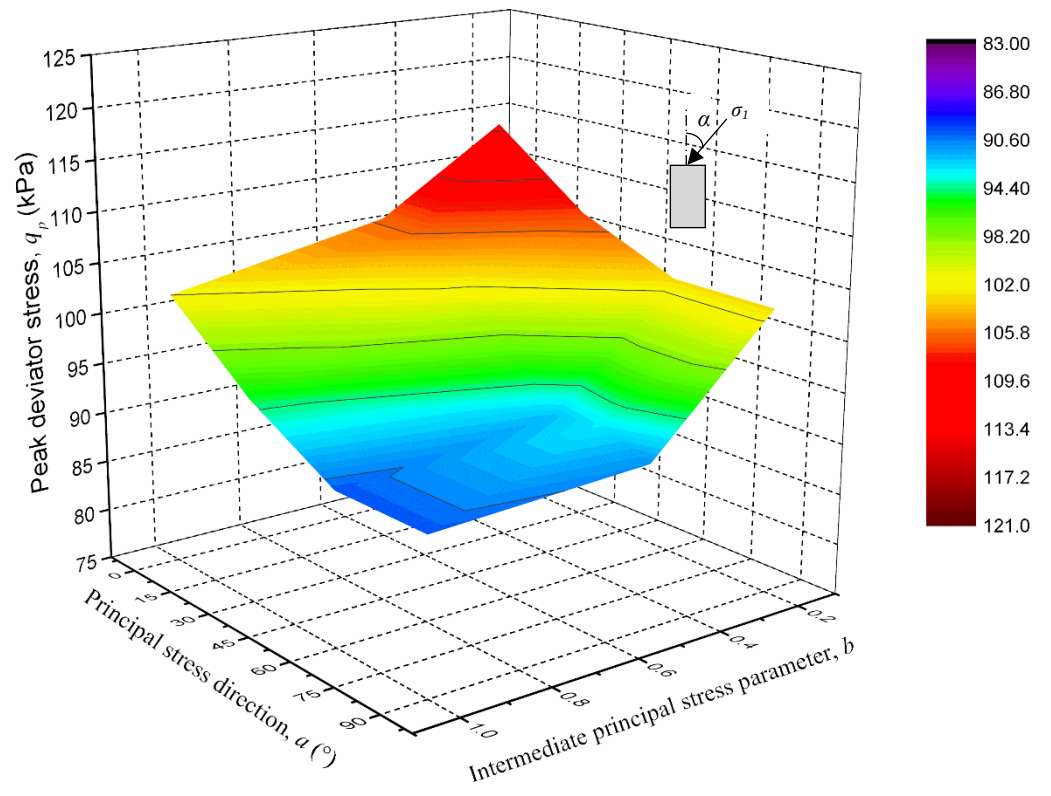

(b)

Figure 6.6 Composite *b*, *α*, q_p diagram of the 3D failure surface for (a) clean sand and (b) mixed sand-clay

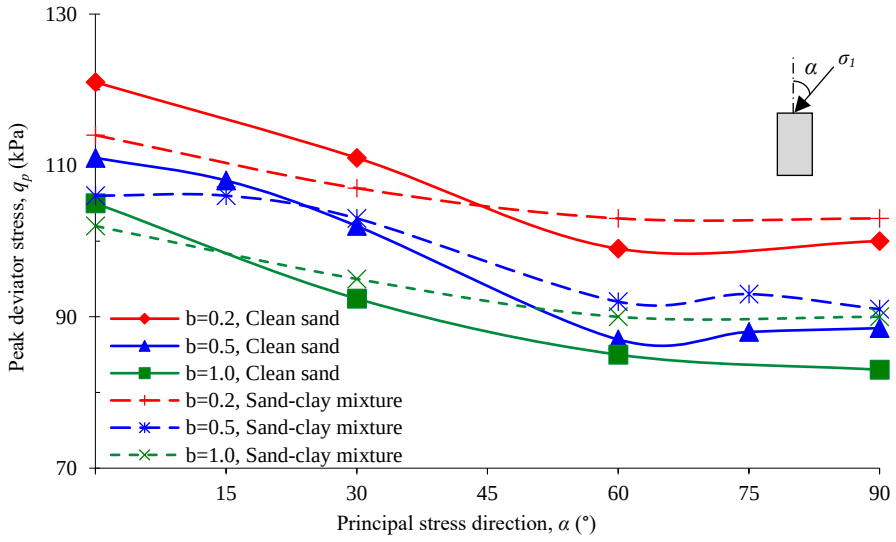

Figure 6.7 Variation of the peak deviator stress q_p of sand and sand containing 10% of clay against the direction of the principal stress *α* for different values of intermediate principal stress parameter *b*

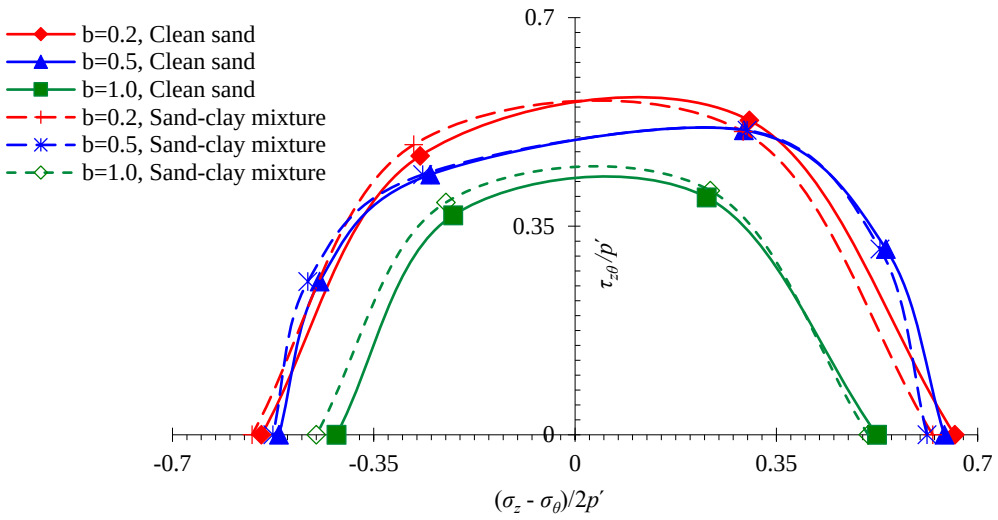

Figure 6.8 Failure envelopes of sand and sand containing 10% clay under different values of the intermediate principal stress parameter *b*

6.2.2 Volumetric Strain Characteristics

The volumetric strain characteristics of sand and mixed sand-clay, tested under different values of *b*, are illustrated in Figures 6.1b-6.4b.

Regarding the compression strain of sand, it is clear that the amount of compression strain increased with increases in *b*, particularly at b = 1.0 where the maximum compression $(\varepsilon_v)_{comp}$ of samples tested under α = 0° increased from 0.11 to 0.13 and 0.31% with increases in *b* from 0.2 to 0.5 and 1.0, respectively. A similar trend was observed for the rest of the values of α, but with larger developed compression strains. For example, when α = 60°, the compression strain increased to 0.37, 0.42 and 0.70 for b = 0.2, 0.5 and 1.0, respectively. This indicates that the decreases in the volumes of samples were larger under a combination of larger values of principal stress direction α and intermediate principal stress parameter *b*.

A similar trend was observed for mixed sand-clay, in which increases in *b* resulted in increases in compression strain $(\varepsilon_v)_{comp}$ depending on the direction of principal stress α. However, for all *b* values, the mixture exhibited larger values of $(\varepsilon_v)_{comp}$ than those of clean sand. However, the effect of *b* on the compression volumetric strain of mixed sand-clay was less than that of clean sand. For example, the $(\varepsilon_v)_{comp}$ values for mixed

sand-clay only increased by 37.7–43.8%, compared with 86.8–87.1% for clean sand, as b increased from 0.2 to 1.0 under α = 60–90°. This implies that the clay fines fill voids in the sand to improve cohesion, bonding and interlocking of the bedding plane. Therefore, increasing the horizontal stresses associated with increasing b to 1.0, resulted in a lesser effect in mixed than clean sand.

For both clean and mixed sand, it can be observed that the deviator strain ε_q corresponding to zero volumetric strain (i.e., the point of transformation from compression to expansion behaviour), was larger for larger b values, irrespective of the direction of principal stress α. Moreover, for all b values, the ε_q value required to start dilation increased as α increased. For example, for clean sand, the change from dilative to compressive strain behaviour under vertical principal stress (α = 0°) occurred at ε_q = 2.5% when b was 0.2, and increased to 2.7 and 3.0% as b increased to 0.5 and 1.0, respectively. Meanwhile, in mixed sand-clay, it occurred at ε_q = 3.0, 3.3 and 4.0% for b = 0.2, 0.5 and 1.0, respectively. With increases of α to 60°, for example, these ε_q values increased to 3.8, 4.1 and 5.2% for sand and to 4.9, 4.8 and 6.4% for mixed sand-clay at b = 0.2, 0.5 and 1.0, respectively.

Regarding expansion strain, samples tested under α = 0–30° showed larger dilative volumetric strain $(\varepsilon_v)_{dil}$ when b was 0.2, compared with conditions of b = 0.5 or 1.0. The expansion strain of sand and sand-clay mixture under α = 0° developed to 4.8% and 3.7%, respectively, at ε_q = 12% when b was 0.2, and as b increased to 1.0, these values decreased to 4.0% (for sand) and 3.0% (for mixture). However, samples under conditions of α = 60–90° showed increases in expansion strain with increasing b values, indicating that such extension conditions ($\sigma_z < \sigma_r$) combined with larger horizontal stress (b = 1.0) expands the volume of samples vertically. For example, when α was 90° the $(\varepsilon_v)_{exp}$ value of sand increased from 1.1 to 1.4%, corresponding to increases in b from 0.2 to 1.0. Similar reductions were observed for mixed sand-clay but at a lower amount, where $(\varepsilon_v)_{exp}$ increased from 1.0% to 1.3% as b increased from 0.2 to 1.0. This means that increasing b to 1.0 results in decreases in the expansion strain of sand and mixed sand-clay of 16.9–31.6% when α = 0–30°, while it increases by 22.6–33.3% for α = 60–90°. Under all b values, expansion volumetric strain $(\varepsilon_v)_{dil}$ decreased as α increased and the reduction ratio was in the range of 60.6–79.5%.

The explanation for this behaviour is linked to the mechanism described in the section above (6.2.1). The preferred alignment of soil particles produces soil that is stiff in the vertical direction due to both the high interlocking of particles and the high stability provided by columnar microstructures. Meanwhile, in the horizontal direction, soil particles exhibit poor interlocking and produce low-stability columns. Therefore, sample anisotropy is characterised by high dilation in the vertical direction and high compressive strain along the horizontal direction. This means that any increase in stress along the horizontal plane will result in increases in compression, where particles easily rotate and slide along this poorly-interlocking plane. Consequently, increasing b to 1.0, which is associated with increasing horizontal stress, i.e. $\sigma_r = \sigma_1$, causes larger contractive deformation. The largest compressive volumetric strain takes place when α rotates to 90° and b increases to 1.0. However, the horizontal stress under b = 0.2 is relatively small, and thus, it produces high dilation and low compression.

6.3 Effect of *b* on Geogrid-reinforced Sand and Sand Containing 10% Clay

6.3.1 Strength Characteristics

Chapters 4 and 5 were dedicated to the effect of α on sand and a sand-clay mixture (10% clay) reinforced with various layers of geogrid. In this section, the effects of three different values of intermediate principal stress parameter b (0.2, 0.5 and 1.0) on clean and mixed sand reinforced with six layers of geogrid are presented under constant p' of 100 kPa and α = 0, 30, 60 and 90°.

It can be seen that b has a clear effect on the stress-strain relationship of the reinforced samples, as shown in Figures 6.9a-6.12a. For all directions of principal stress α, samples under b = 0.2 exhibited the greatest strength, while minimum strength occurred when b was 1.0. For example, the peak deviator stress q_p of samples that sheared under α = 0° decreased from 257.8 kPa for b = 0.2 to 240.1 and 218.7 kPa when b increased to 0.5 and 1.0, respectively. This consists of reduction ratios of 6.9 and 15.2%, respectively. This decreasing ratio of q_p due to increases in b from 0.2 to 1.0 becomes 16.2, 19.7 and 22.6% when α = 30, 60 and 90°, respectively. The variations in peak deviator stress q_p along b and along α for different values of b are

depicted in Figures 6.13 and 6.14, respectively. This data is also combined into the 3D surface shown in Figure 6.15. Although different b values exhibited different peaks of deviator stress q_p, the trend for the variation of q_p along the principal stress direction α was similar for all b values. Here, q_p decreased at a slight or moderate rate as α increased from 0 to 30°, then dropped sharply with further increases in α to 60 and 90° (Figures 6.14). This indicates the significant directional dependence represented by the 45.1–50.4% difference in peak deviator stress Δq_p.

The reduction in q_p occurring with increasing value of b is related to the lesser ability of geogrid to resist horizontal stresses, as its tensile strength cannot be mobilised to a level similar to that attained under vertical loading. Such horizontal stress, as explained previously in Section 6.2, increases with increasing b, where the intermediate principal stress σ_2 (i.e. σ_r) becomes equal to the major principal stress σ_1 when b = 1.0. This means that under b = 1.0, the stress applied horizontally becomes the largest, and thus, the geogrid layers provide less improvement.

Despite the fact that b still influenced the strength of the geogrid reinforced sand-clay mixture, the added clay content made this effect lower than in reinforced clean sand (Figures 6.9a-6.12a). Under vertical major principal stress, the q_p of reinforced mixed sand decreased from a maximum of 247.4 kPa (when b = 0.2) to 219.8 and 213.1 kPa (as b increased to 0.5 and 1.0, respectively), resulting a decreasing ratio of 13.9% (Figure 6.13). For shearing under α, 30–90°, the decreasing ratio of q_p in reinforced mixed sand due to increasing b from 0.2 to 1.0 became 10.7–17.2%. These reduction ratios of q_p are lower than those of reinforced sand, which were 15.2–22.6%. Moreover, under each of the three considered b values, deviator stress q_p varied considerably along α (Figures 6.14). Under b = 0.2, the q_p of reinforced mixed sand decreased from its largest value of 247.4 kPa at 0° to 229.3, 159.1 and 160.7 kPa at α = 30, 60 and 90°, respectively, consisting of a 35.6% difference ratio between $(q_p)_{max}$ and $(q_p)_{min}$. This differences in q_p due to changing the principal stress direction α became 37.6 and 37.5% for b = 0.5 and 1.0, respectively. Although these difference ratios are significant, they are lower than those of reinforced sand, which were 45.1–50.4%. It should be mentioned that under b = 1.0, the minimum strength occurred when the sample sheared under α = 90°, instead of 60°, as when b = 0.2 and 0.5. This

is likely related to the combination of conditions (i.e., α = 90° and b = 1.0) which causes horizontal stress to dominate the behaviour of the sample. The failure envelopes, in the $(\sigma_z - \sigma_\theta) / 2p'$ vs. $\tau_{z\theta} / p'$ space, of sand and mixed sand-clay reinforced with six layers of geogrid, for different b values, are shown in Figure 6.16. Such envelopes refer to the anisotropic strengths of reinforced clean and mixed sand for all considered values of the intermediate principal stress parameter b.

The lesser effect of b on reinforced mixed sand compared with reinforced clean sand is attributed to the clay content acting as a cementation agent. The clay occupies inter-particular voids, which increases particle interlocking along the bedding plane, provides cohesion to the mass of sand, and improves bonding between the geogrid and sand particles. Despite this improvement in the performance of reinforced samples under increasing horizontal stress, the difference in q_p remained clear.

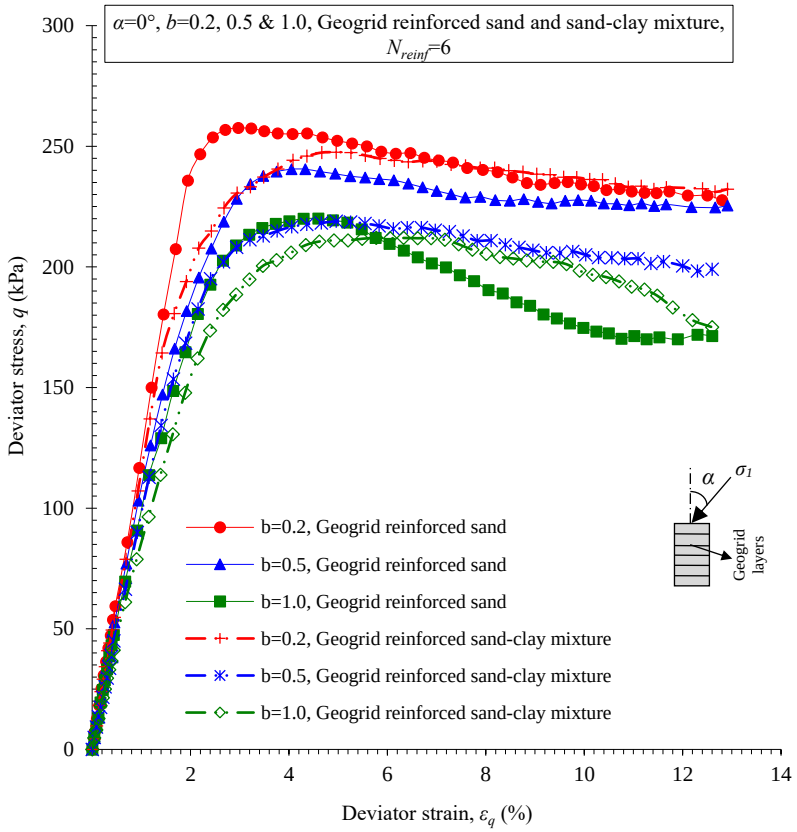

(a)

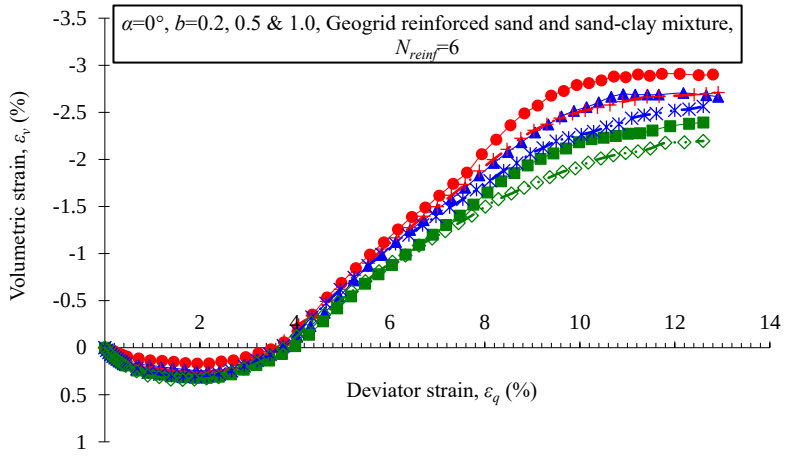

(b)

Figure 6.9 Relationships between (a) deviator stress and deviator strain; (b) volumetric strain and deviator strain of clean sand and mixed sand-clay reinforced with 6 layers of geogrid under different values of b (α = 0°)

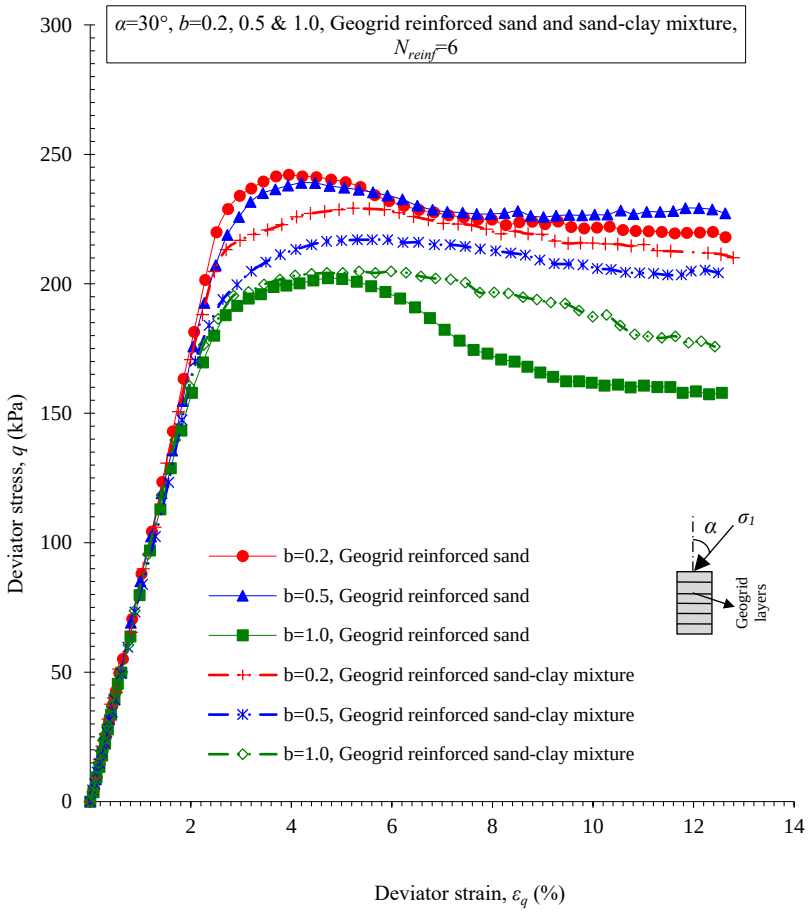

(a)

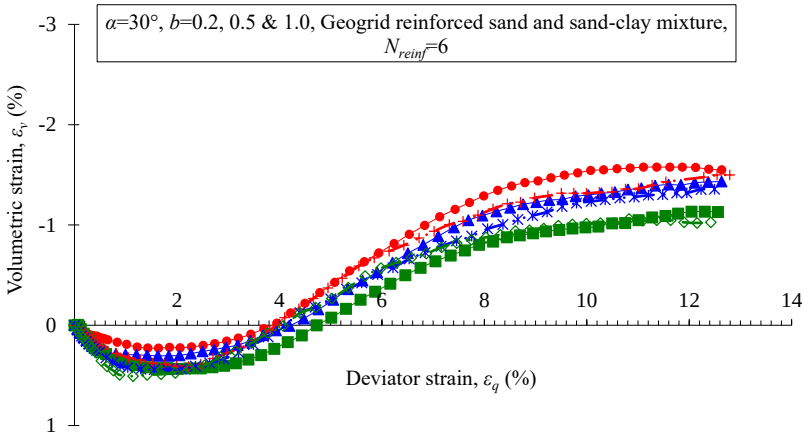

(b)

Figure 6.10 Relationships between (a) deviator stress and deviator strain; (b) volumetric strain and deviator strain of clean sand and mixed sand-clay reinforced with 6 layers of geogrid under different values of b (α = 30°)

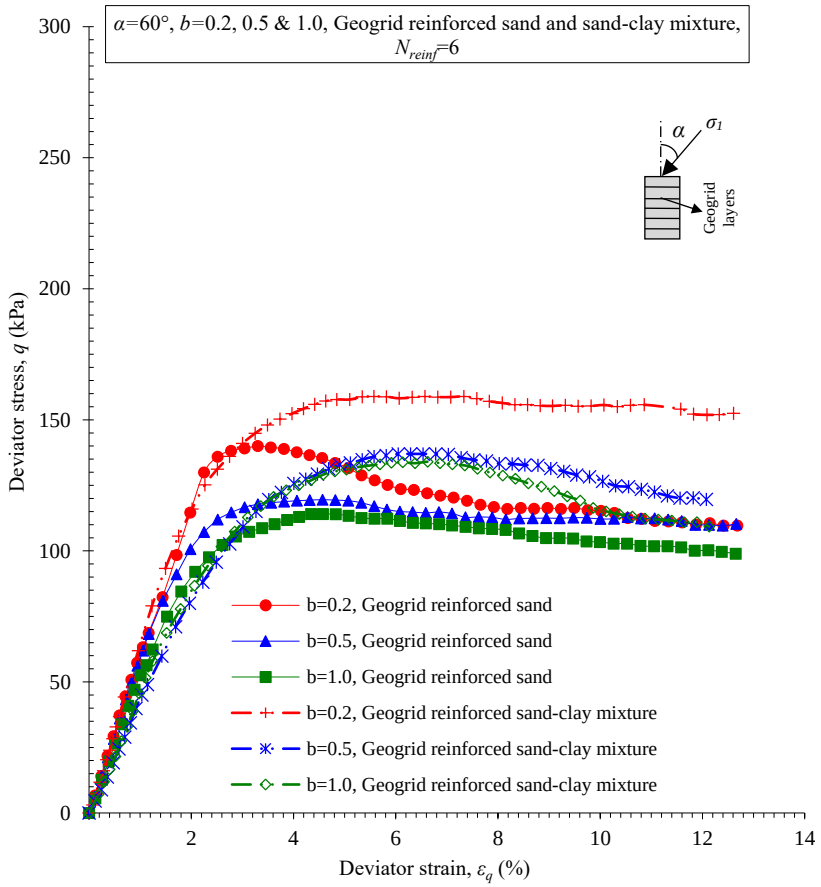

(a)

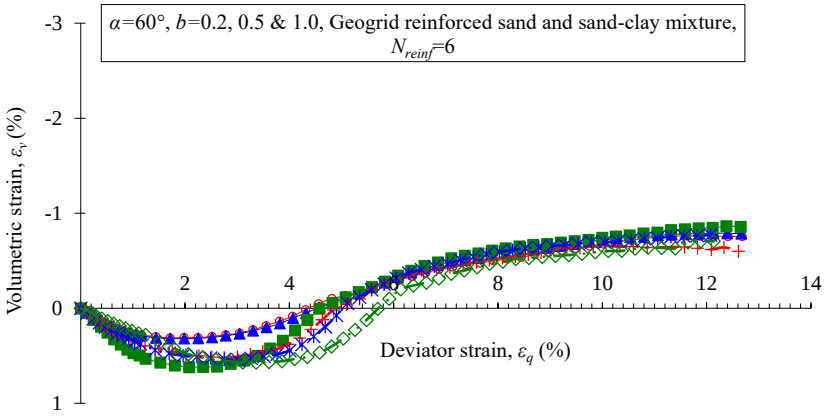

(b)

Figure 6.11 Relationships between (a) deviator stress and deviator strain; (b) volumetric strain and deviator strain of clean sand and mixed sand-clay reinforced with 6 layers of geogrid under different values of b (α = 60°)

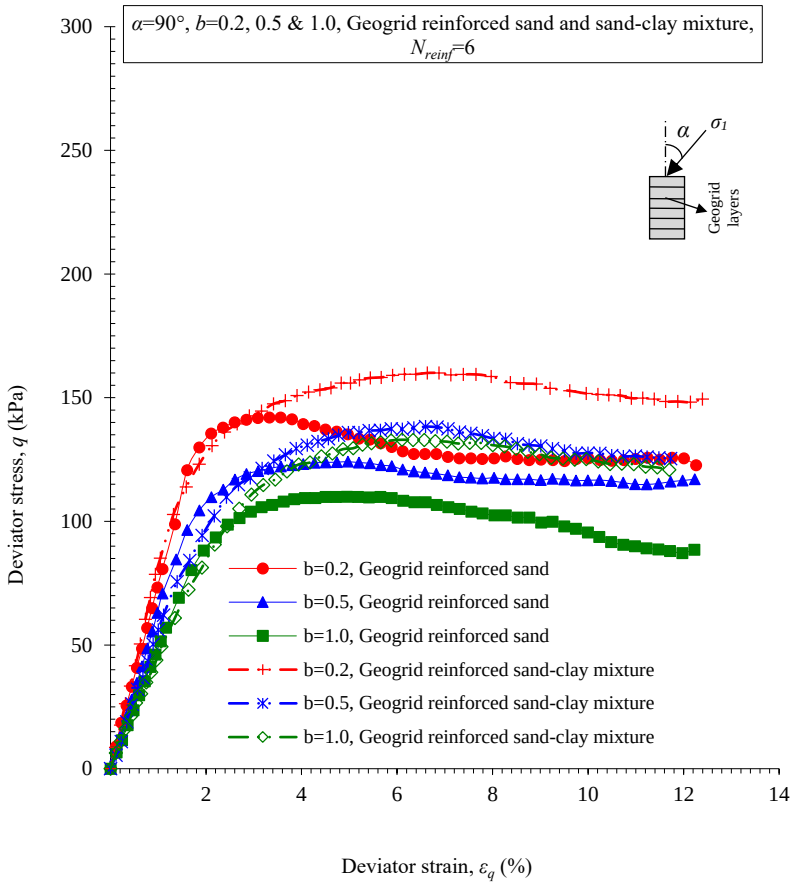

(a)

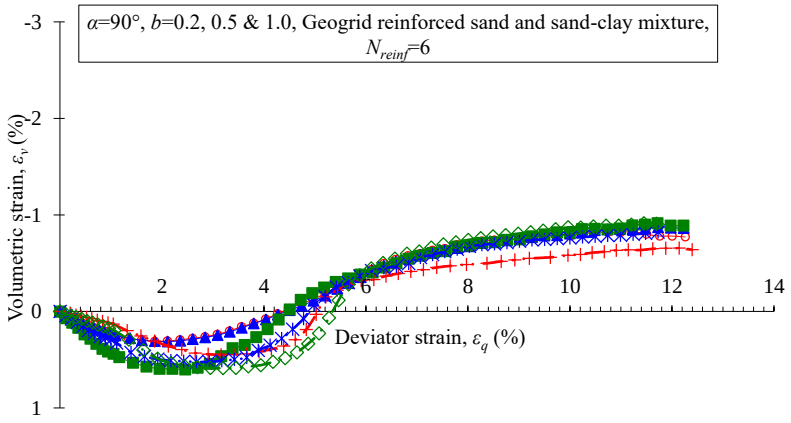

(b)

Figure 6.12 Relationships between (a) deviator stress and deviator strain; (b) volumetric strain and deviator strain of clean sand and mixed sand-clay reinforced with 6 layers of geogrid under different values of b (α = 90°)

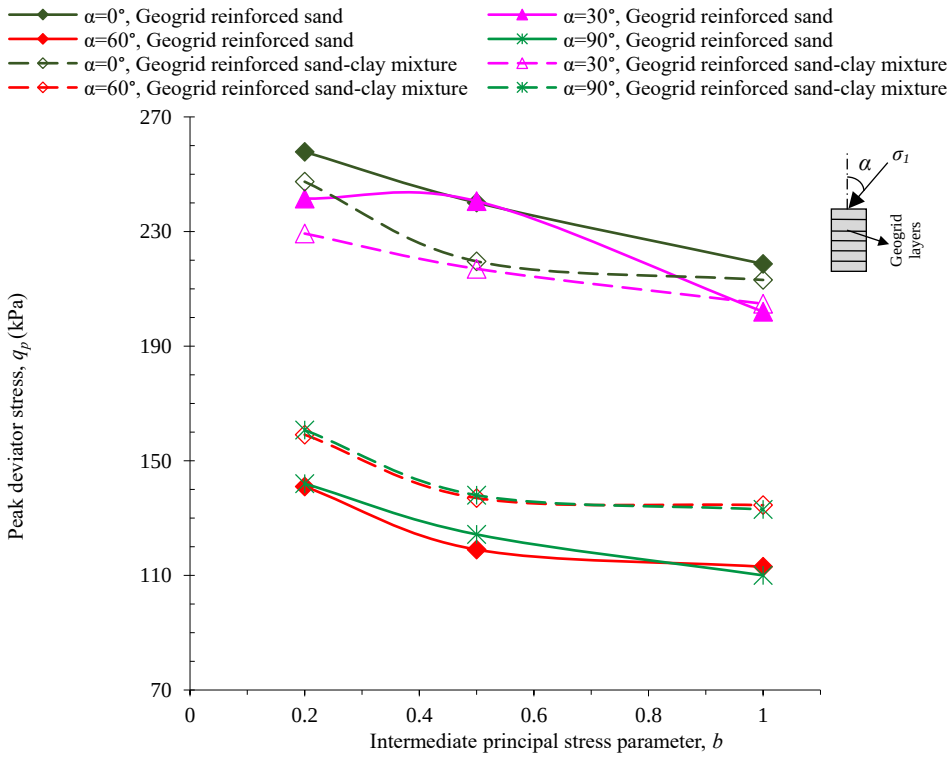

Figure 6.13 Variation of the peak deviator stress q_p of clean sand and mixed sand-clay reinforced with 6 layers of geogrid against intermediate principal stress parameter b under different directions of the principal stress α

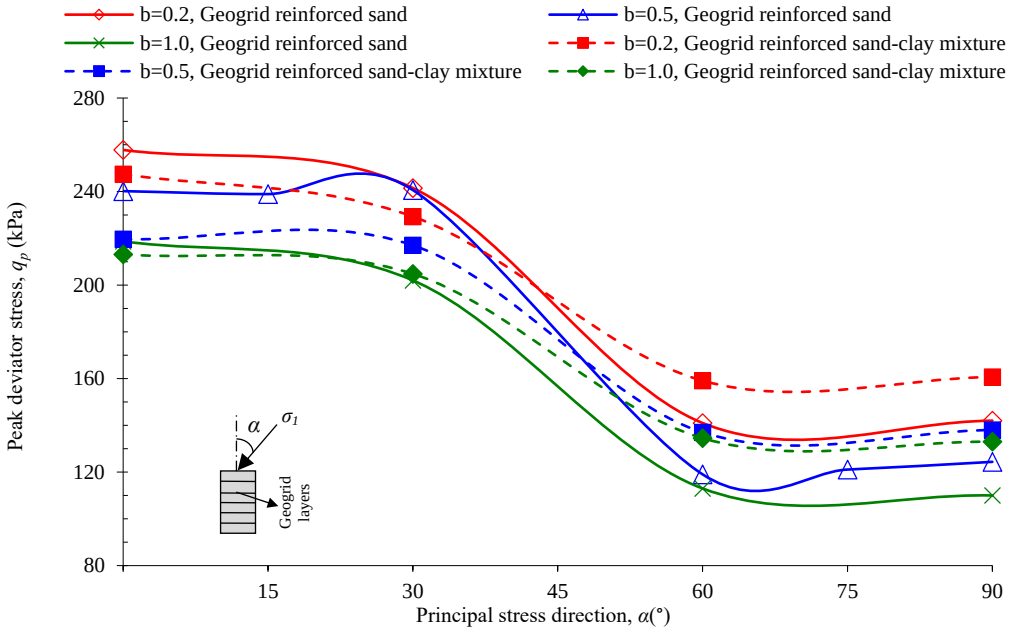

Figure 6.14 Variation of the peak deviator stress q_p of clean sand and mixed sand-clay reinforced with 6 layers of geogrid against the direction of the principal stress α for different values of the intermediate principal stress parameter b

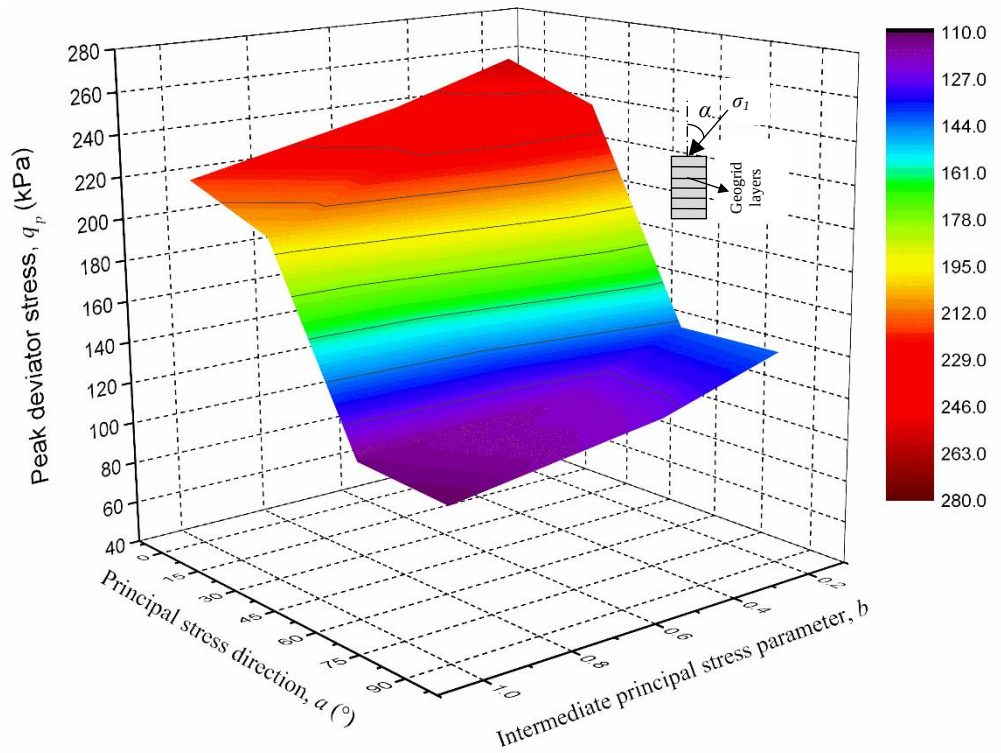

(a)

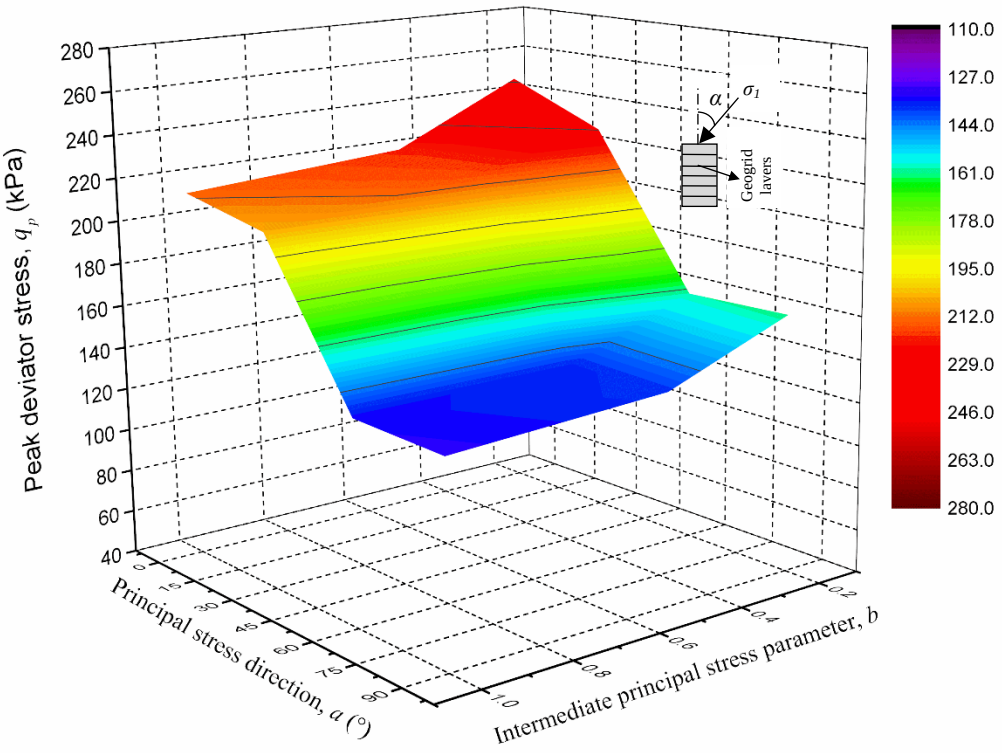

(b)

Figure 6.15 Composite b-α-q_p diagram of the 3D failure surface for 6 geogrid layer-reinforced (a) clean sand, and (b) mixed sand-clay

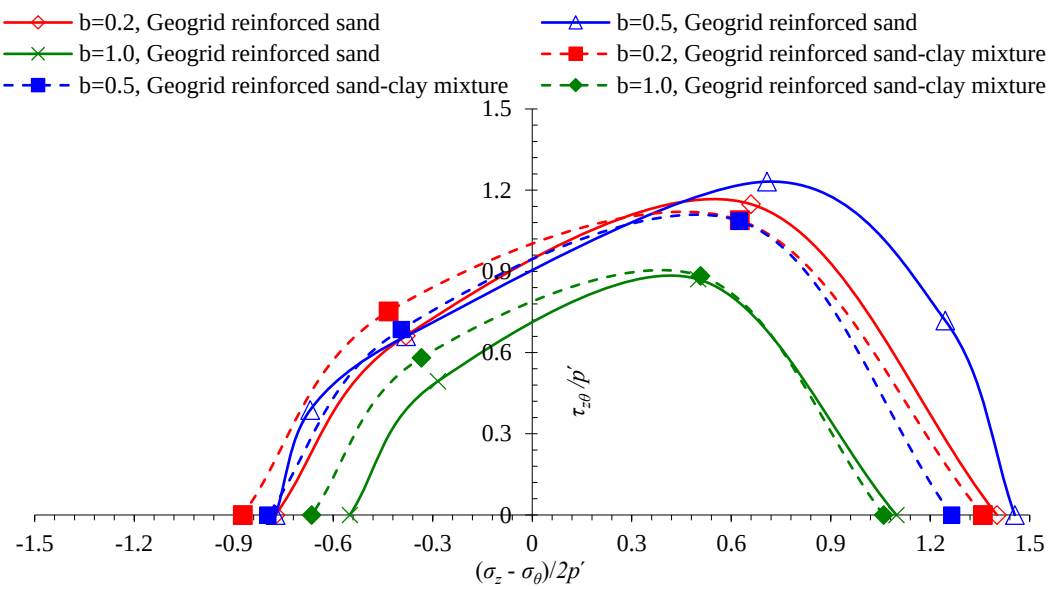

Figure 6.16 Comparison the failure envelopes of clean sand and mixed sand-clay (containing 10% clay) reinforced with 6 layers of geogrid for different values of *b*

6.3.2 Volumetric Strain Characteristics

The effects of varying *b* between 0.2, 0.5 and 1.0 on the volumetric strain of sand and mixed sand-clay (10% clay) reinforced with six layers of geogrid and sheared under α = 0, 30, 60 and 90° are depicted in Figures 6.9b-6.12b.

Samples initially experienced decreases in volume; the compression strain $(\varepsilon_v)_{comp}$ was 0.17, 0.23, 0.32 and 0.31% for α = 0, 30, 60 and 90°, respectively, under *b* = 0.2. These amounts of strains increased by 86.9–93.7% with increases of *b* to 1.0. A similar trend was observed for reinforced mixed sand-clay where, for example, increasing *b* from 0.2 to 0.5 and 1.0 under α = 0° resulted in increases in $(\varepsilon_v)_{comp.}$ from 0.26 to 0.33 and 0.34%, respectively.

When deviator strain ε_q reached 2.6–4.0% for reinforced sand and 3.2–6.1% for the reinforced mixture, samples started showing expansion strain irrespective of the value of *b*. With increasing *b*, the tendency of geogrid-reinforced sand and mixed sand-clay to expand decreased clearly under α = 0–30°, while it increased when α rotated to 60–90°. For example, the expansion volumetric strain $(\varepsilon_v)_{dil}$ of reinforced sand under *b* =

0.2 was 2.9, 1.5, 0.76 and 0.78% at ε_q = 12% for α = 0, 30, 60 and 90°, respectively. Increasing b to 1.0 resulted in decreases in this strain by 20.0–27.8% when α = 0–30°, while for α = 60–90° $(\varepsilon_v)_{dil}$ increased by 11.4–14.1%. Under combined conditions of b = 0.2 and α = 0–30°, horizontal stress is least, indicating that reinforced sand and mixed sand-clay tends to exhibit large expansion laterally, while samples under b = 1.0 and α = 60–90° tend to expand vertically where the horizontal stress is largest. Although the trend is similar, reinforced mixed sand-clay under different values of b exhibited less expansion strain than that of reinforced clean sand, reflecting the role of fines as cementation agents for better interlocking, interaction and bonding between particles and between particles and the geogrid.

These effects of b are related to the explanation presented in Section 6.2. Large horizontal stresses, such as those caused by increasing b, can confine and decrease the likely expansion strain, which occurs primarily under α = 0–30°, and increase the compression strain, which occurs primarily horizontally when α = 60–90°.

6.4 Effect of *b* on Geotextile-reinforced Sand and Sand Containing 10% Clay

6.4.1 Strength Characteristics

In this section, the effects of b on the stress behaviour of sand and mixed sand-clay reinforced with six layers of geotextile are presented.

The effect of b on the deviator stress q of nonwoven geotextile-reinforced sand is clear under all of the considered directions of principal stress α (Figures 6.17a-6.20a). For b = 0.2, q_p of reinforced sand varied significantly along α and was 274.1, 257.4, 160.1 and 160.7 kPa for α = 0, 30, 60 and 90°, respectively, constituting a maximum reduction ratio Δq_p of 41.5%. When b increased to 1.0, these values decreased by 14.9–24.0% while the reduction ratio Δq_p increased to 47.6%. Figures 6.21 and 6.22 depict the variation in peak deviator stress q_p along b and α, respectively.

The anisotropic response of geotextile-reinforced sand mixed with 10% clay to variation in the intermediate principal stress parameter b was similar to that observed in reinforced clean sand. Adding clay content provided a certain level of increased strength for reinforced samples, particularly under α = 60–90°. The difference in q_p between reinforced sand and reinforced mixed sand-clay for all values of b under α = 0–30° was slight (≤ 3.0%). However, under α = 60–90°, the reinforced mixture exhibited larger q_p values than those of reinforced sand, by 18.6–19.4% for b = 0.2 and 32.7–37.8% for both b = 0.5 and 1.0. Accordingly, difference in peak deviator stress due to increasing b to 1.0 was 12.1–15.5% (for all α values) for reinforced mixed sand-clay, compared with 14.9–24.0% for reinforced clean sand. Furthermore, Clay decreased the anisotropic difference in peak deviator stress Δq_p (due to variation of α), to 29.4–32.3% (for all b values), compared with 41.5–47.7% for reinforced clean sand. The variations in q_p of reinforced sand and mixed sand-clay along b and α are shown clearly in the 3D surface presented in Figure 6.23. The largest reduction of q_p occurred at α = 90° when b=1.0. This is attributed to the combination of the larger b and larger α values, which resulted in the maximum stresses being applied horizontally and, consequently, their being less ability to mobilise the geotextile's tensile strength.

The anisotropic failure envelopes are plotted in Figure 6.24. Each of these curves represents the failure surface, $(\sigma_z - \sigma_\theta)/2p'$ versus $\tau_{z\theta}/p'$, of reinforced sand and mixed sand-clay under different values of intermediate principal stress parameter b. Although all failure envelopes do not have the symmetrical shapes that indicate anisotropic behaviour, clay inclusion contributed to decreased directional dependence in geotextile-reinforced sand.

Compared with unreinforced samples (presented in Section 6.2), inclusion of six layers of geotextile (tested under various values of b) increased the peak deviator stress q_p of unreinforced sand by 44.3–133.1% and that of unreinforced mixed sand-clay by 80.4–143.0%. The increase in strength is related, as explained in Chapters Four and Five, to the confinement of tensioned members and the cementation function of the added clay. However, anisotropic behaviour due to increases in b or/and increases in α is caused by increased horizontal stress, at expense of vertical stress, which decreases the soil pressure on planar layers, and consequently, decreases mobilisation of the tensile strength of the geotextile.

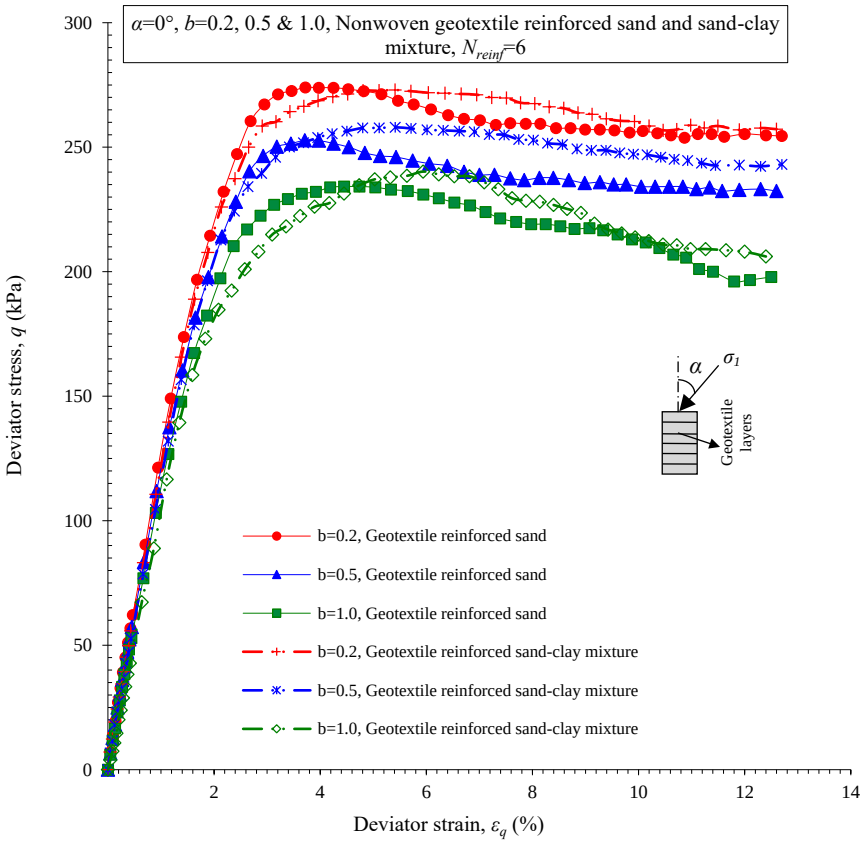

(a)

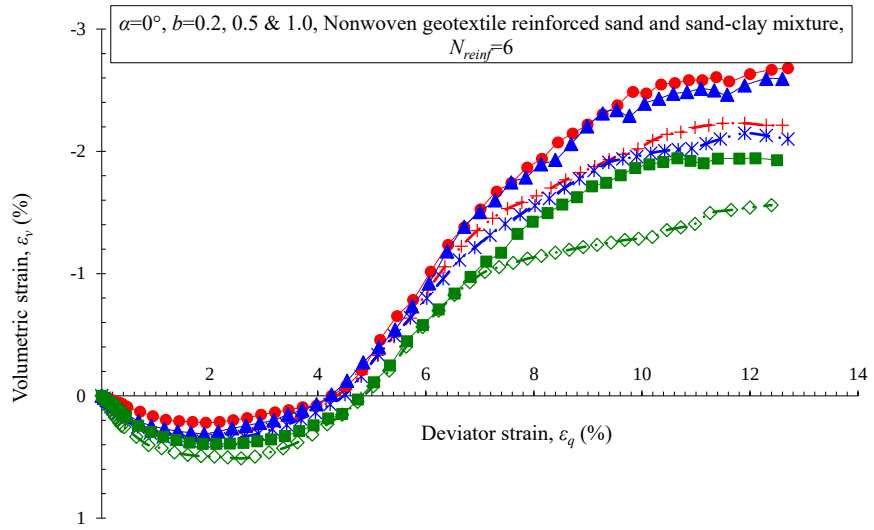

(b)

Figure 6.17 Relationships between (a) deviator stress and deviator strain; (b) volumetric strain and deviator strain for clean sand and mixed sand-clay reinforced with 6 layers of geotextile under different values of b (α = 0°)

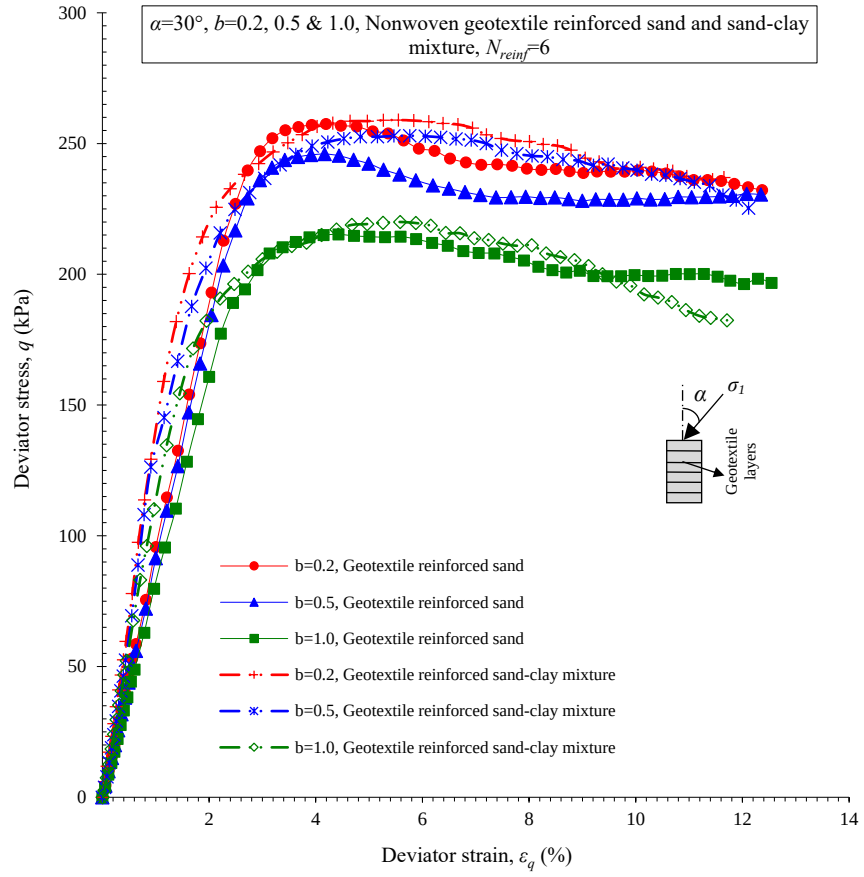

(a)

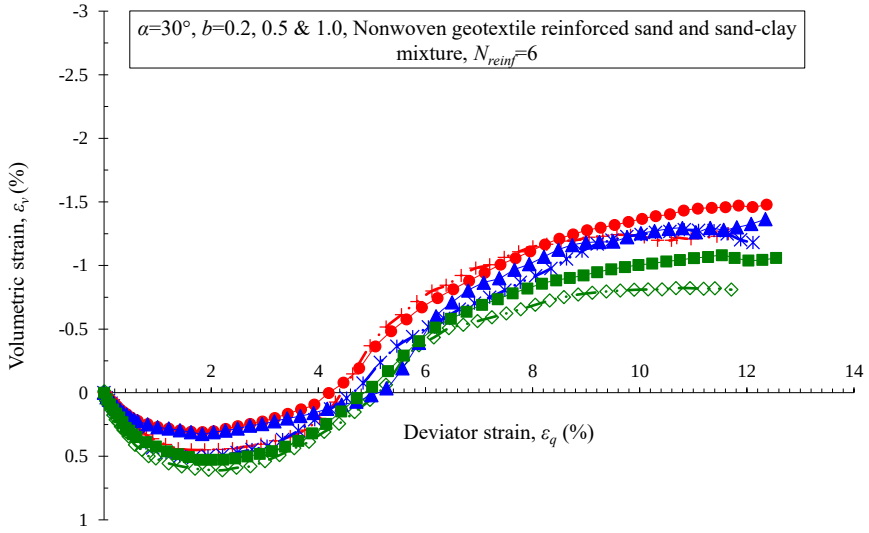

(b)

Figure 6.18 Relationships between (a) deviator stress and deviator strain; (b) volumetric strain and deviator strain for clean sand and mixed sand-clay reinforced with 6 layers of geotextile under different values of b (α = 30°)

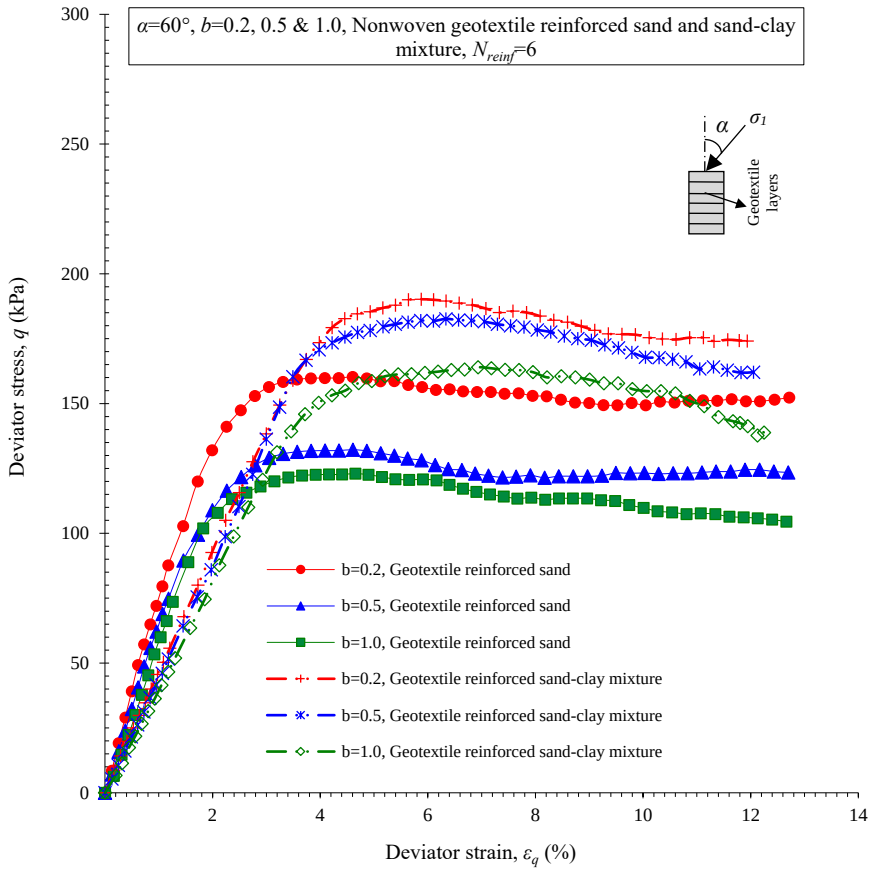

(a)

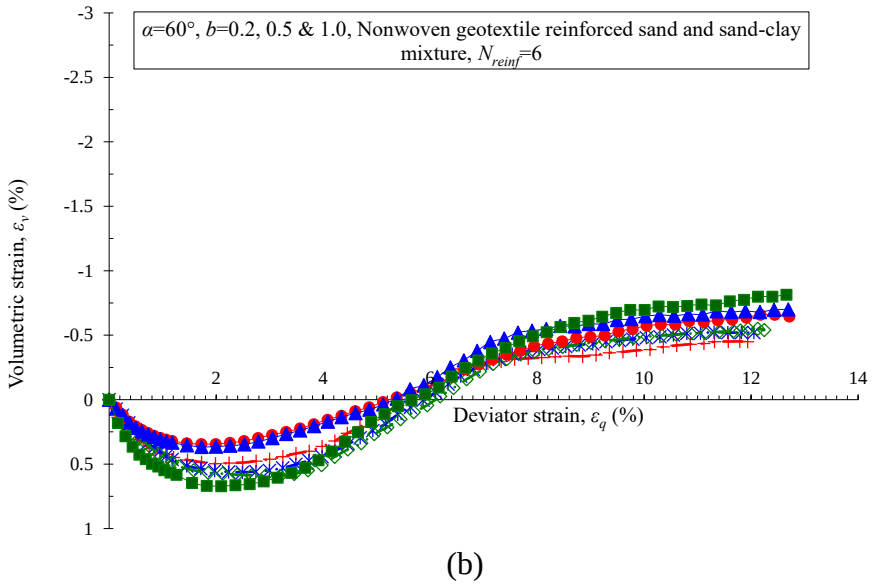

(b)

Figure 6.19 Relationships between (a) deviator stress and deviator strain; (b) volumetric strain and deviator strain for clean sand and mixed sand-clay reinforced with 6 layers of geotextile under different values of b (α = 60°)

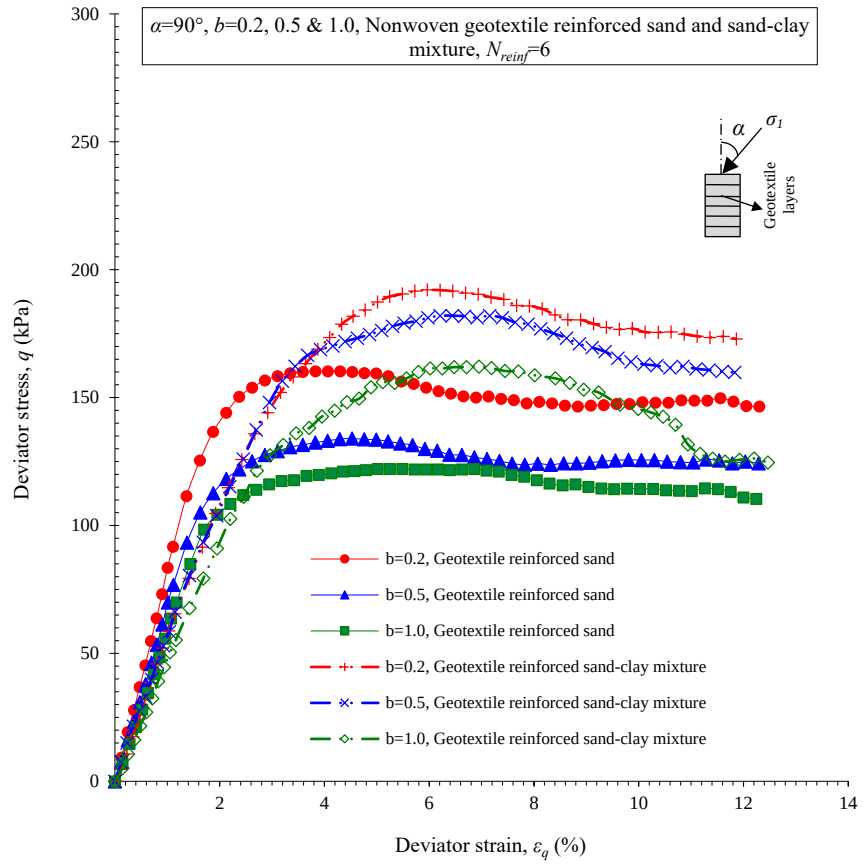

(a)

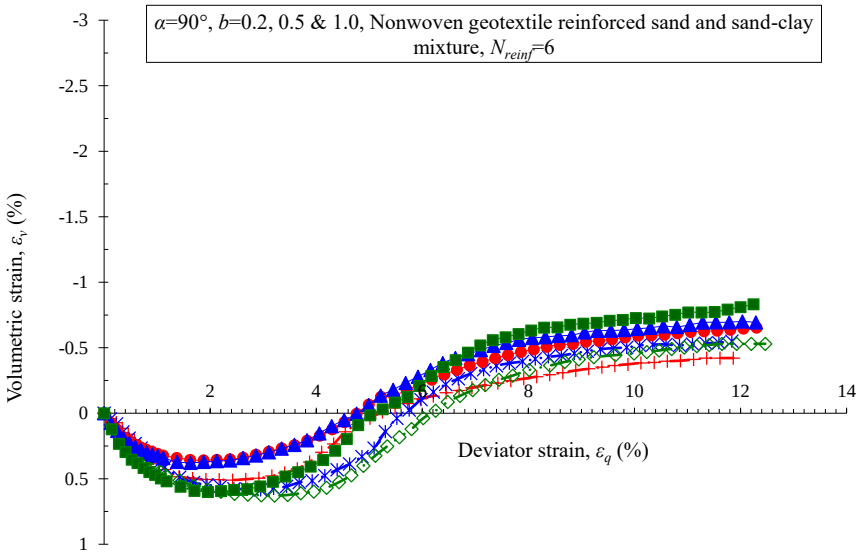

(b)

Figure 6.20 Relationships between (a) deviator stress and deviator strain; (b) volumetric strain and deviator strain for clean sand and mixed sand-clay reinforced with 6 layers of geotextile under different values of b (α = 90°)

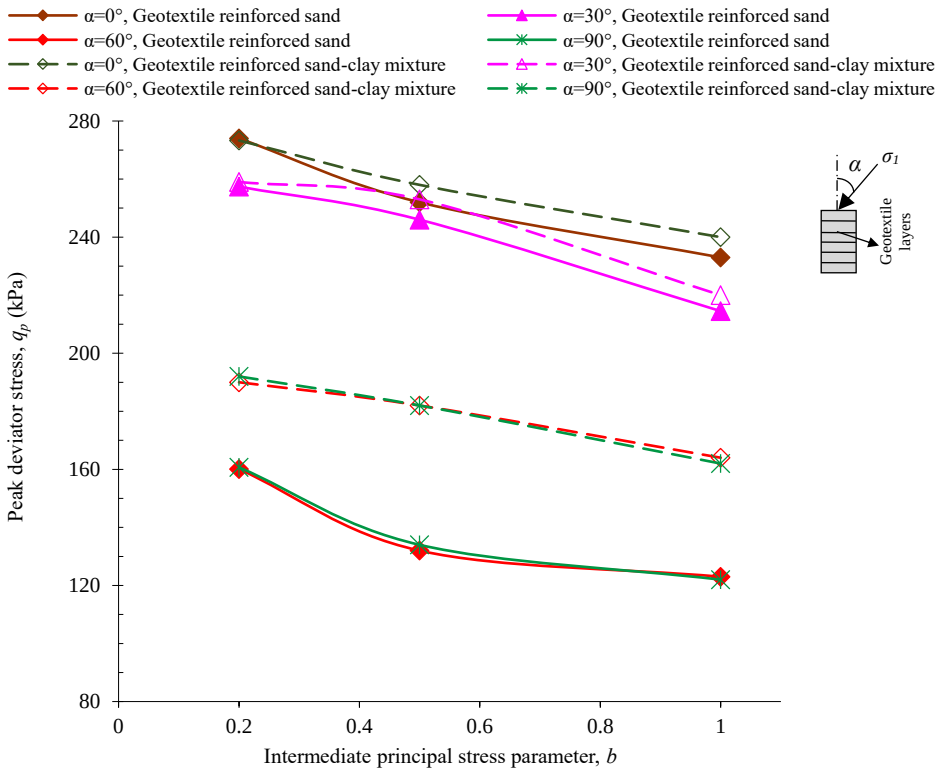

Figure 6.21 Variation of the peak deviator stress q_p of clean sand and mixed sand-clay reinforced with 6-layers of geotextile against intermediate principal stress parameter b under different directions of the principal stress α

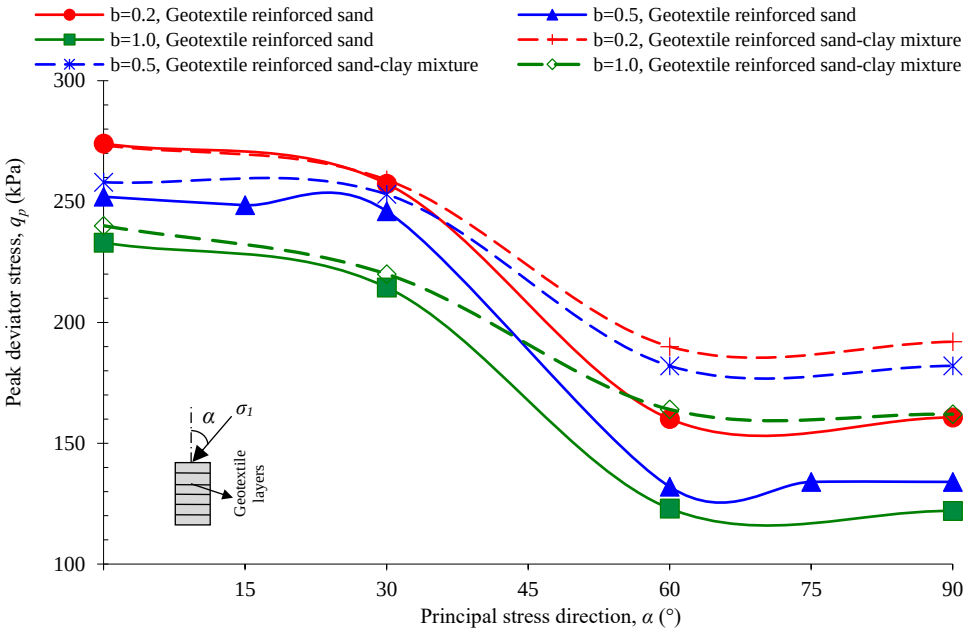

Figure 6.22 Variation of the peak deviator stress q_p of clean sand and mixed sand-clay reinforced with 6 layers of geotextile against the direction of the principal stress α for different values of the intermediate principal stress parameter b

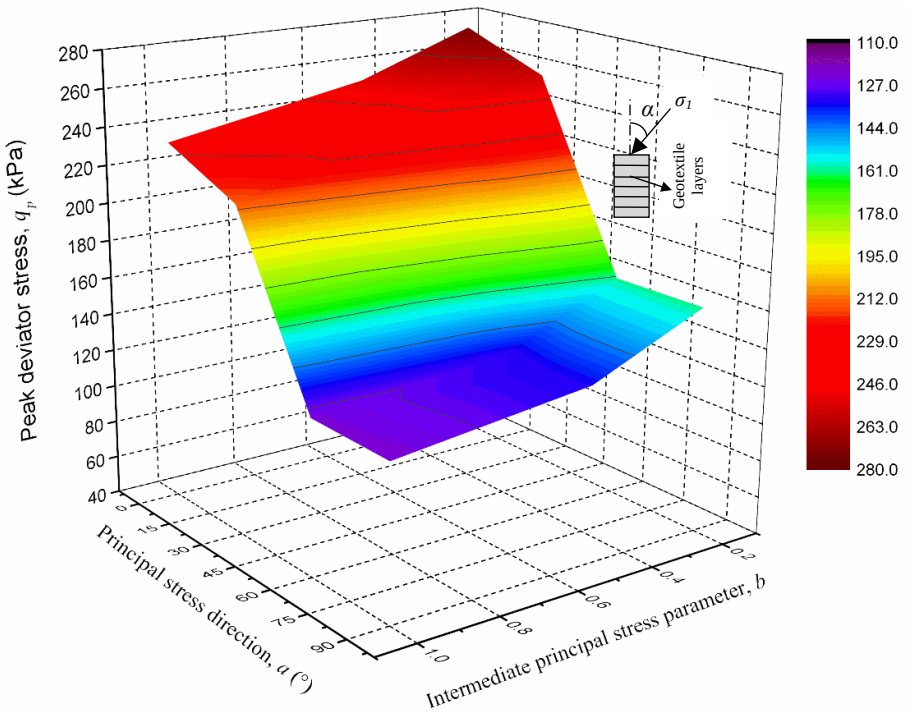

(a)

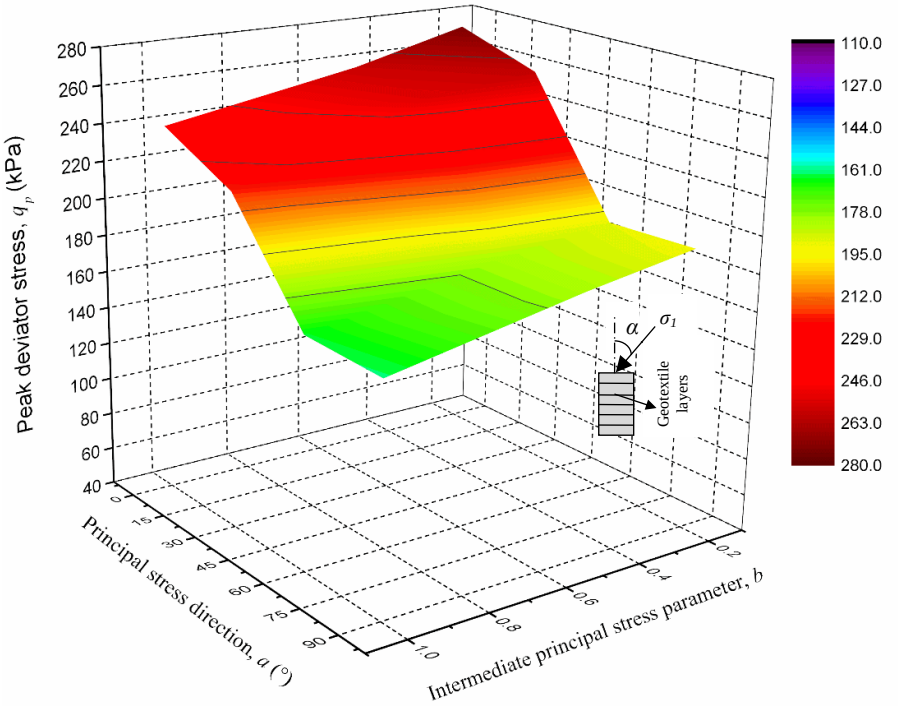

(b)

Figure 6.23 Composite b-α-q_p diagram of 3D failure surface for (a) 6 nonwoven geotextile layer-reinforced clean sand, and (b) 6 nonwoven geotextile layer-reinforced mixed sand-clay

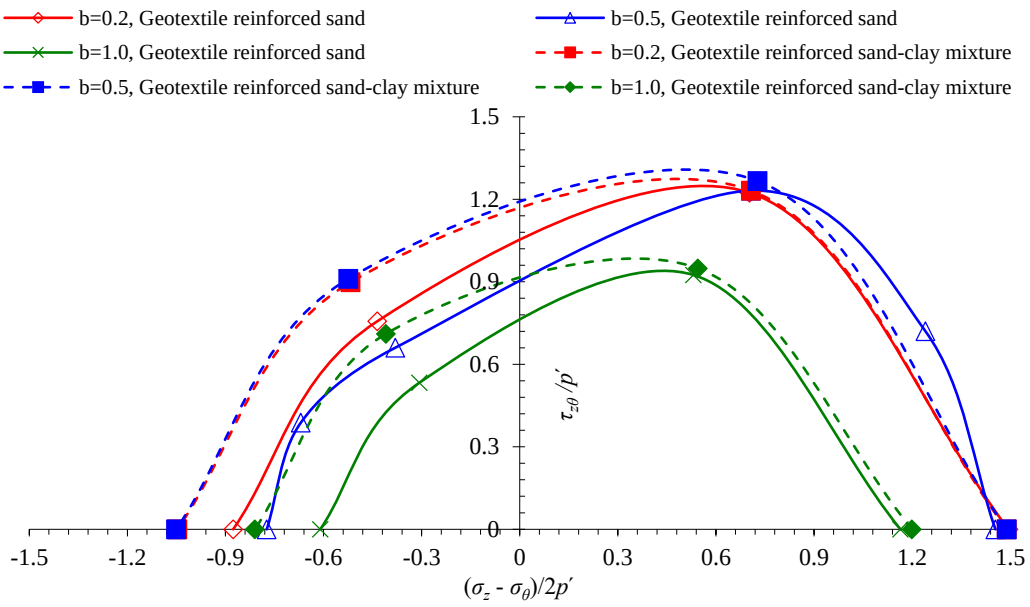

Figure 6.24 Comparison of the failure envelopes of clean sand and mixed sand-clay (containing 10% clay) reinforced with 6 layers of nonwoven geotextile at different values of *b*

6.4.2 Volumetric Strain Characteristics

The compression strain of reinforced sand increased initially and continued until ε_q reached 4.4–5.6% under different values of *b* and α. The peak compression strain of sand reinforced with six layers of geotextile changed from 0.22% to 0.39% under α = 0°, and from 0.35 to 0.60% under α = 90°, corresponding to an increase in *b* from 0.2 to 1.0 (Figures 6.15a-6.18a). A similar trend was observed for geotextile-reinforced mixed sand-clay containing 10% clay.

Regarding expansion strain, increasing horizontal stress, i.e. increasing *b*, can confine the lateral strain induced by the principal stress at angles close to vertical, i.e. α = 0–30°. However, under α = 60–90°, increasing *b* is likely to result in some increase in expansion toward vertical as the horizontal stresses become larger than the vertical ones. For example, expansive volumetric strain $(\varepsilon_v)_{dil}$ of geotextile-reinforced sand at ε_q = 12% and under α = 0° decreased from 2.6% to 1.94% with increases of *b* from 0.2 to 1.0, while it increased under α = 90° from 0.65% to 0.81%. Moreover, for all values of *b*, the dilative strain varied significantly depending on the direction of principal stress α. Sand containing 10% clay and reinforced with geotextile exhibited a similar

trend but with a lesser amount of expansion; when α = 0°, $(\varepsilon_v)_{dil}$ decreased from 2.22 to 1.51%, while it increased at α = 90° from 0.43 to 0.53%. Irrespective of the value of *b*, geotextile reinforcement significantly decreased dilation in sand and mixed sand-clay.

6.5 Effect of *b* on Geocell-reinforced Sand and Sand Containing 10% Clay

6.5.1 Strength Characteristics

In this section, the deviator stress characteristics of clean sand and mixed sand-clay reinforced with geocell tested under three different values of *b* (0.2, 0.5 and 1.0) are presented.

The general trends are similar to those of samples with other types of reinforcement, where increases in *b* are associated with decreases in peak deviator stress q_p, as shown in Figures 6.25a-6.28a and 6.29-6.31. Under *b* = 0.2, the q_p values of geocell-reinforced sand were 278.3, 260.0, 209.3 and 209.1 kPa for α = 0, 30, 60 and 90°, respectively. These amounts decreased insignificantly by 2.7–4.1% as *b* increased to 0.5, and by 5.2–10.3% when *b* reached 1.0. The anisotropic difference in q_p due to the variation of α from 0 to 90° was 24.7, 25.3 and 22.8 for *b* = 0.2, 0.5 and 1.0, respectively. This means that the difference in q_p due to the variation of α under a given *b* value was larger than the difference due to the variation of *b* under a given α value (Figures 6.29- 6.31).

Addition of fines to the geocell-reinforced sand resulted in slight differences in peak deviator stress q_p under α = 0° for all values of *b*, while under α = 30–90°, the geocell-reinforced mixed sand-clay exhibited deviator stress that was greater than that of reinforced sand, by 3.4–12.1% (depending on *b* and α). Furthermore, geocell-reinforced mixed sand-clay showed a lower influence of the *b* value on the peak deviator stress q_p. The difference in q_p due to increasing *b* to 1.0 was 3.5–6.2% (depending on α), compared with 5.2–10.3% for geocell-reinforced sand. Moreover, variations in q_p along the principal stress direction α were 15.7, 16.4 and 15.1% for *b* = 0.2, 0.5 and 1.0, respectively, which is smaller than for geocell-reinforced sand.

Compared with unreinforced clean sand, inclusion of both geocell and 10% clay improved q_p by 125.8–143.7, 141.0–159.7 and 142.4–174.4% under b = 0.2, 0.5 and 1.0, respectively.

Within the considered full range of b and α values, the lowest q_p of 196.0 kPa (for reinforced clean sand) and 216.4 (for reinforced mixed sand-clay) occurred when samples were subjected to conditions of b = 1.0 and α = 90°. Meanwhile, the maximum value of 278.3kPa (for reinforced clean sand) and 272.2 kPa (for reinforced mixed sand-clay) occurred under conditions of b = 0.2 and α = 0° (Figures 6.29-6.31). The variations in q_p between these two conditions were about 29.5% and 20.4% for reinforced sand and mixed sand-clay, respectively. The anisotropic response can be also identified in the failure surfaces when plotting the space of $(\sigma_z - \sigma_\theta) / 2p'$ versus $\tau_{z\theta} / p'$ (Figure 6.32), although the performance of samples reinforced with geocell was better than those reinforced with planar geosynthetics.

The significant improvement in q_p and the small effect of b observed is related to the 3D cellular confinement provided by geocell. It provides more effective confinement than planar reinforcement that is placed horizontally, even under horizontal loading, in addition to providing friction along the wall and bending resistance. The 10% clay added as a cementation material provides significant bonding to the sand and the geo-inclusion, improving the performance of the composite.

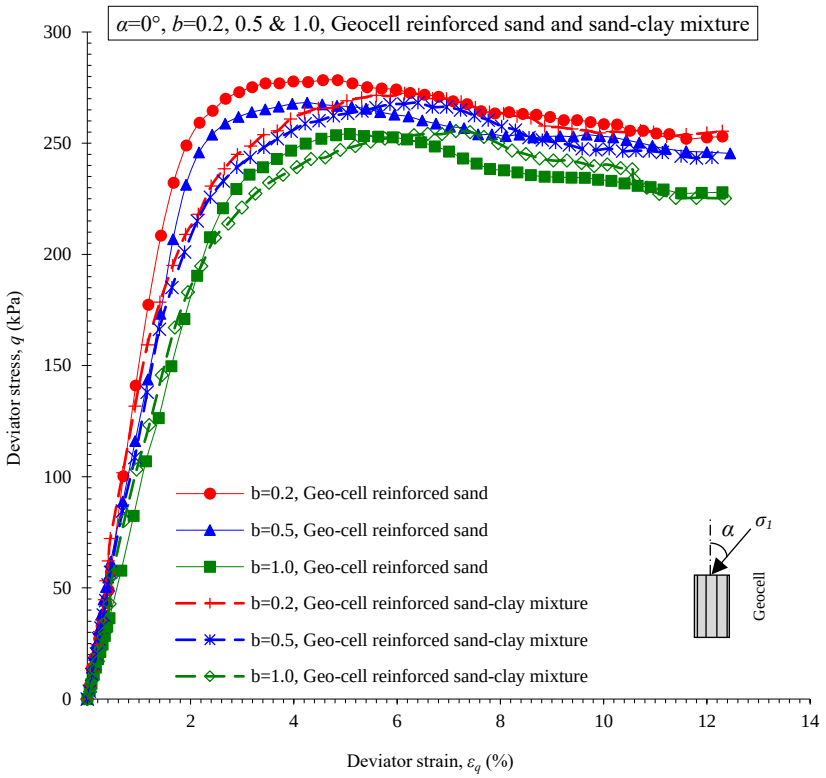

(a)

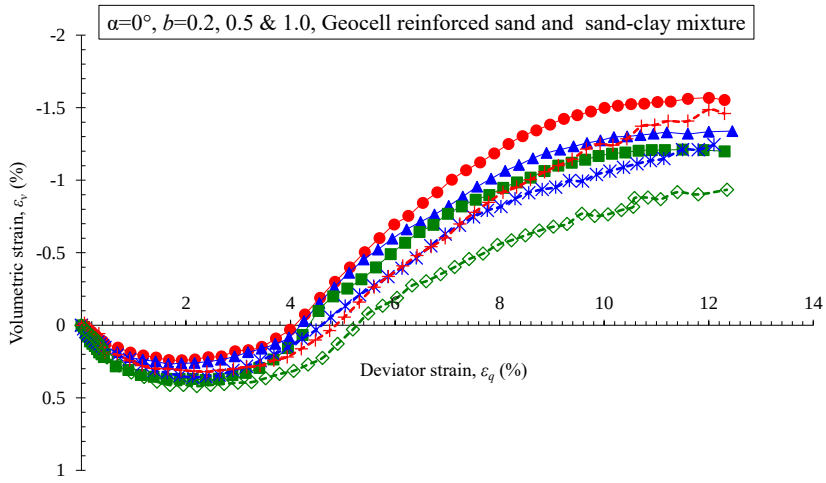

(b)

Figure 6.25 Relationships between (a) deviator stress and deviator strain; (b) volumetric strain and deviator strain of clean sand and mixed sand-clay reinforced with geocell under different values of b (α = 0°)

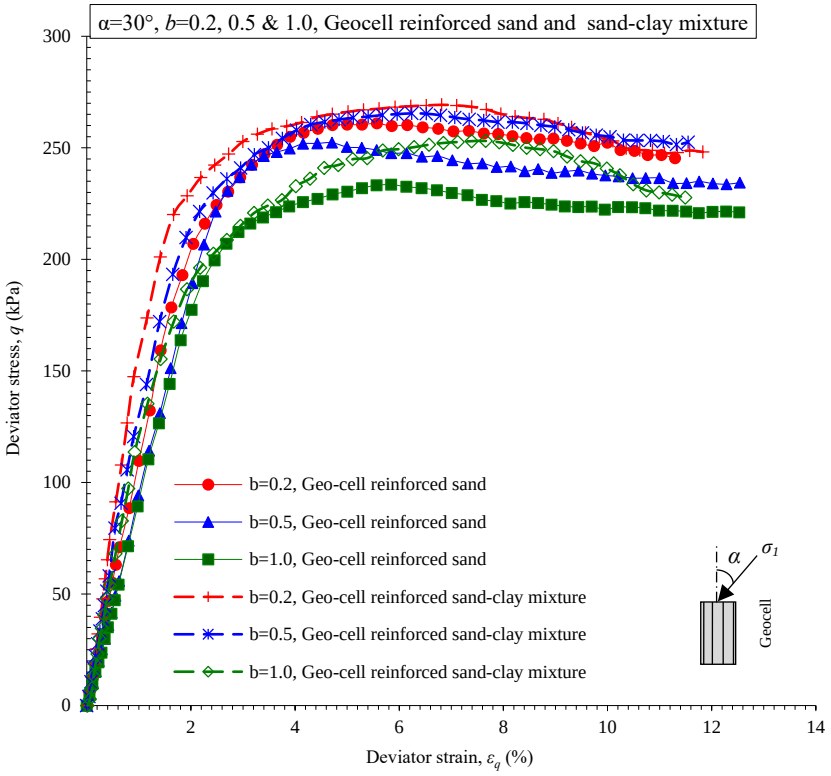

(a)

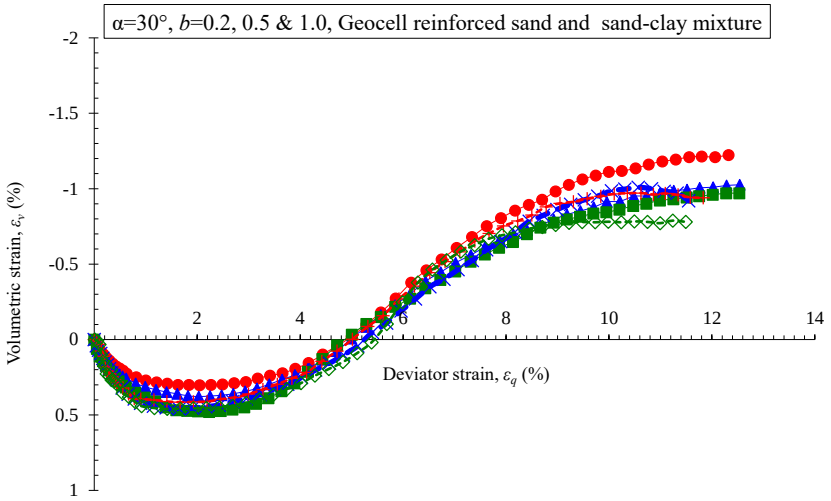

(b)

Figure 6.26 Relationships between (a) deviator stress and deviator strain; (b) volumetric strain and deviator strain of clean sand and mixed sand-clay reinforced with geocell under different values of b (α = 30°)

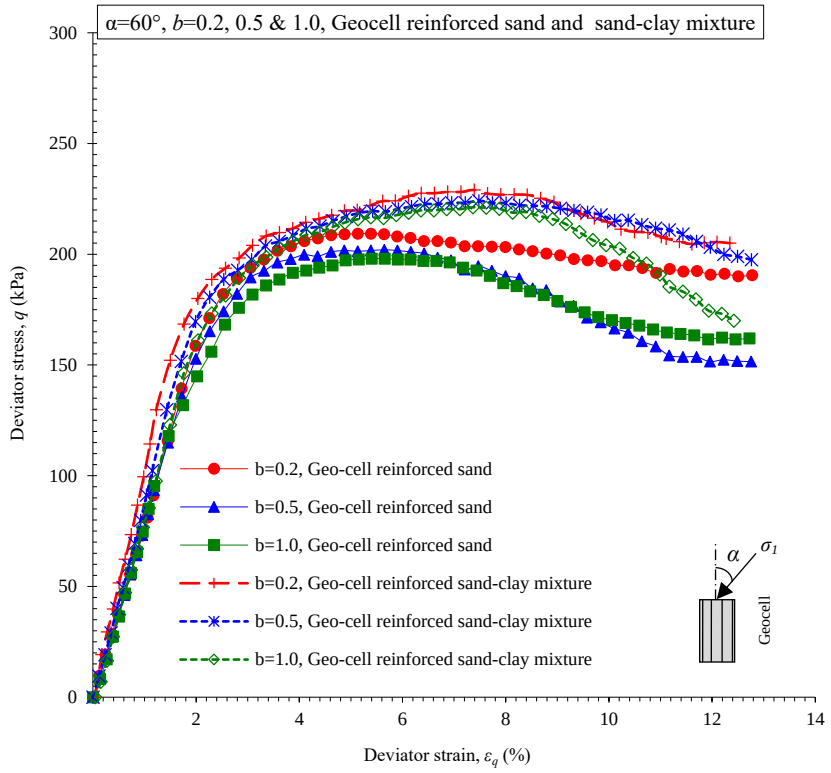

(a)

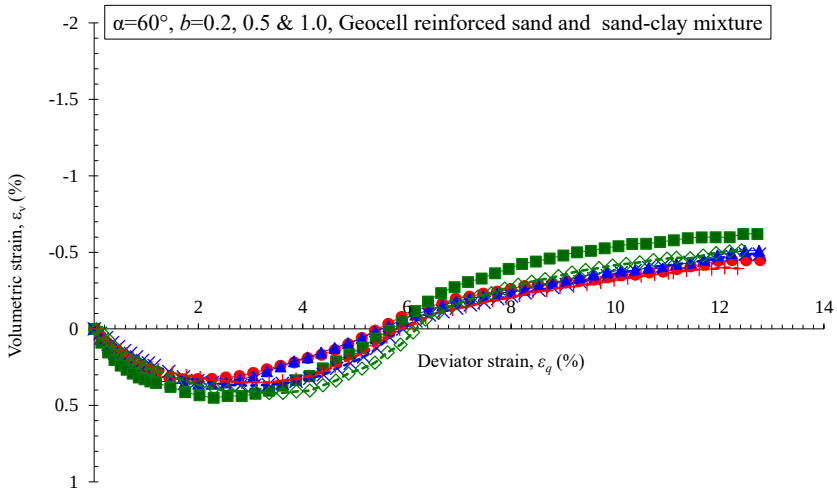

(b)

Figure 6.27 Relationships between (a) deviator stress and deviator strain; (b) volumetric strain and deviator strain of clean sand and mixed sand-clay reinforced with geocell under different values of b (α = 60°)

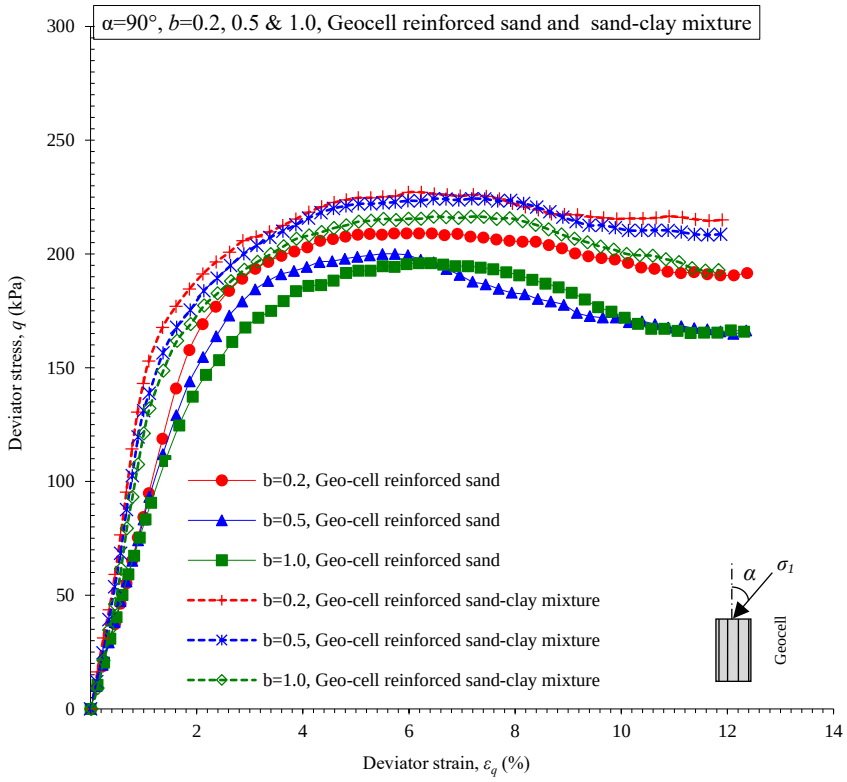

(a)

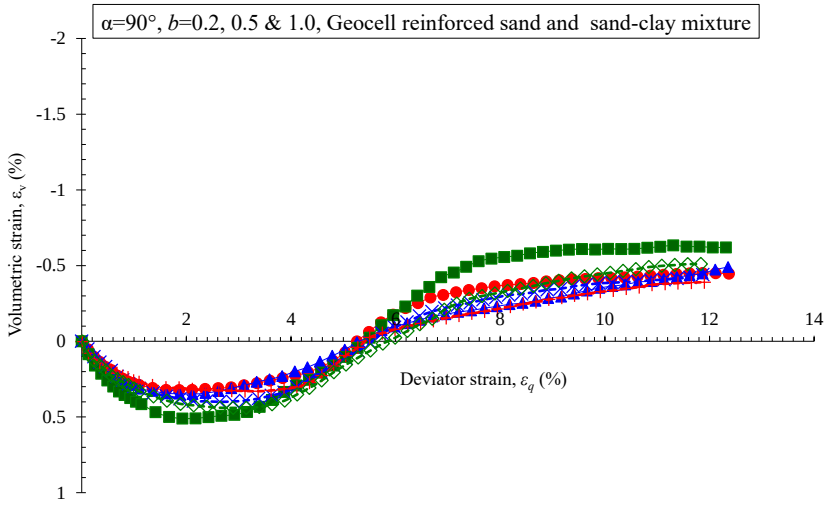

(b)

Figure 6.28 Relationships between (a) deviator stress and deviator strain; (b) volumetric strain and deviator strain of clean sand and mixed sand-clay reinforced with geocell under different values of b (α = 90°)

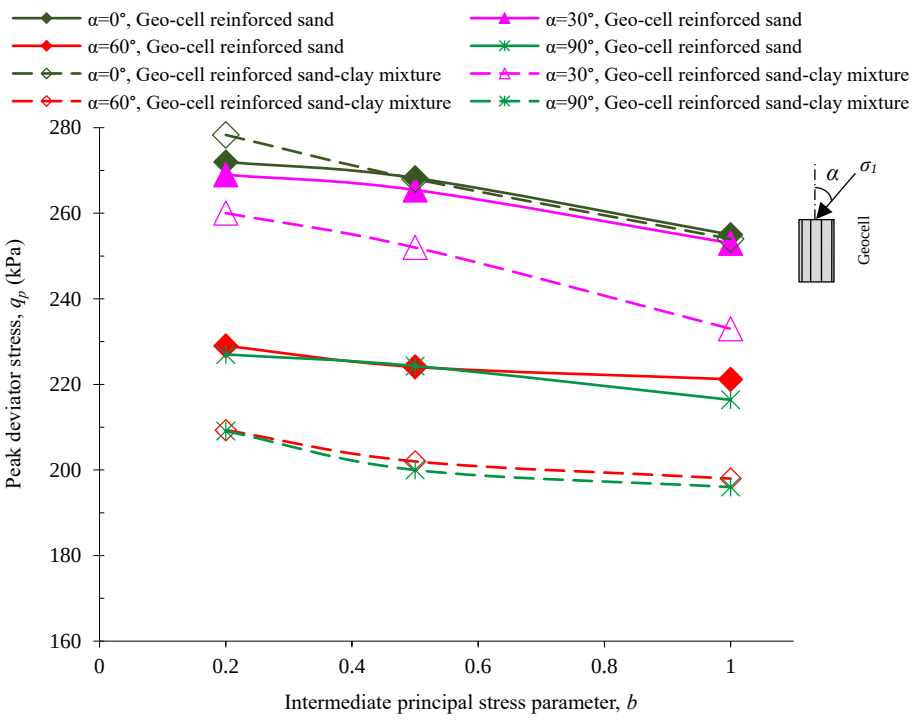

Figure 6.29 Variation of the peak deviator stress q_p of clean sand and mixed sand-clay reinforced with geocell against intermediate principal stress parameter b under different directions of the principal stress α

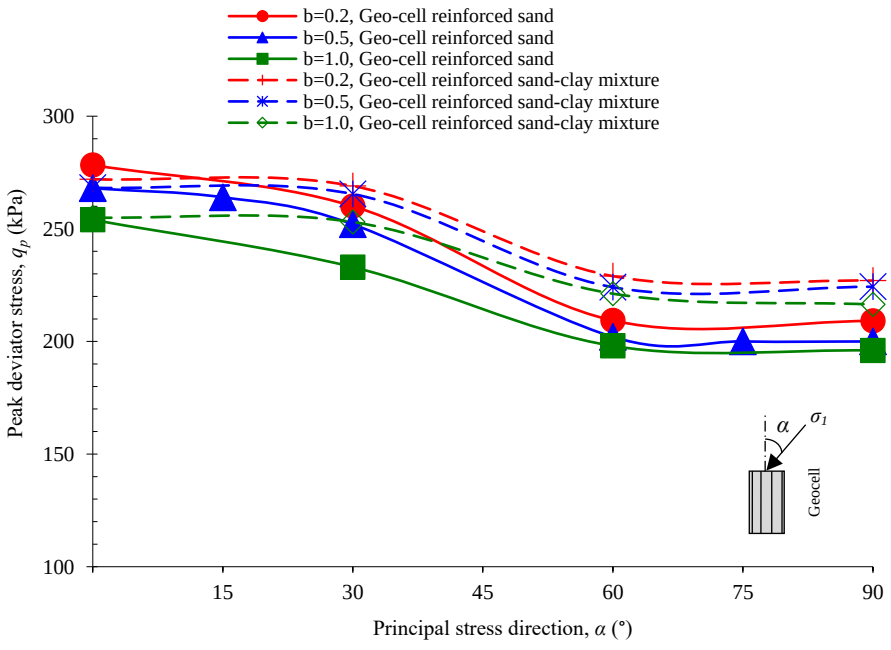

Figure 6.30 Variation of the peak deviator stress q_p of clean sand and mixed sand-clay reinforced with geocell against the direction of the principal stress α for different values of the intermediate principal stress parameter b

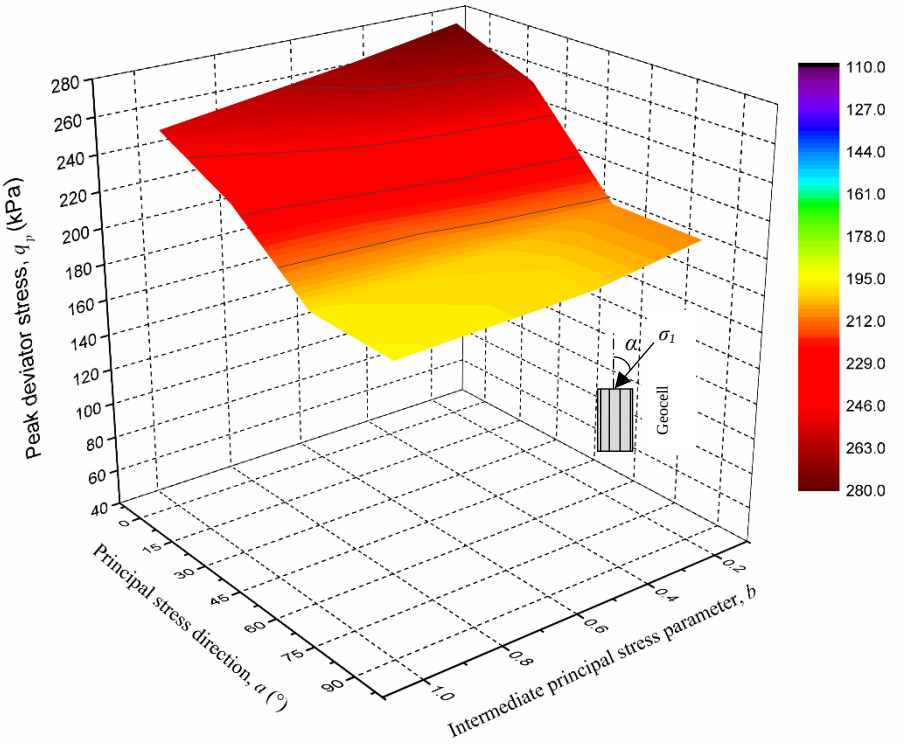

(a)

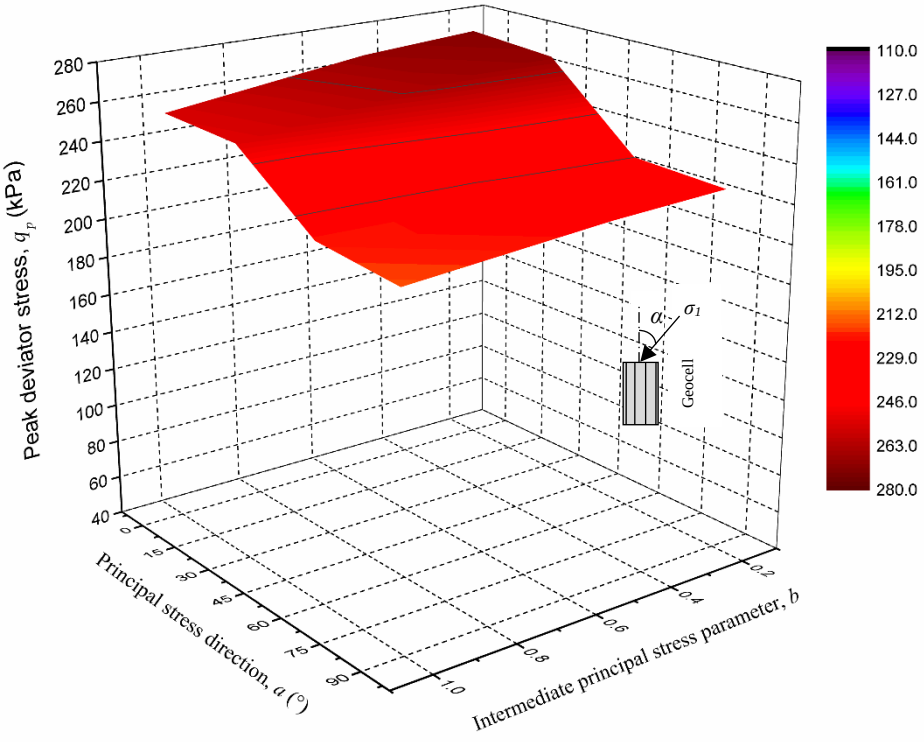

(b)

Figure 6.31 Composite b-α-q_p diagram of the 3D failure surface for geocell-reinforced (a) clean sand, and (b) mixed sand-clay

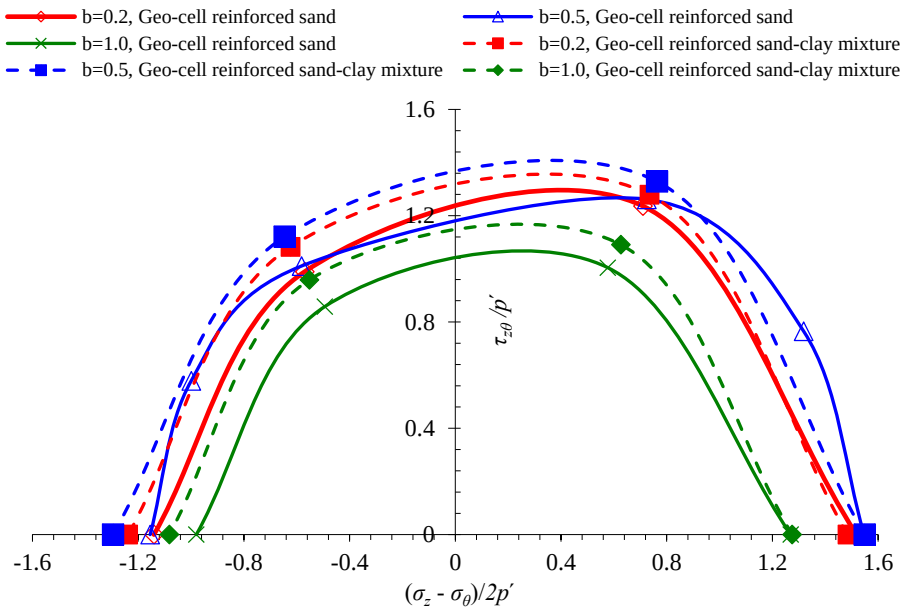

Figure 6.32 Comparison the failure envelopes of clean sand and mixed sand-clay (containing 10% clay) reinforced with geocell for different values of *b*

6.5.2 Volumetric Strain Characteristics

The volumetric strain ε_v characteristics of cellular-reinforced sand and sand containing 10% clay under different *b* and α values are presented herein and in Figures 6.25b-6.28b.

It is clear that the volumetric deformation of geocell-reinforced samples was less than that of samples with other types of reinforcement. Increasing *b* from 0.2 to 1.0 under α = 0° resulted in an increase in compression volumetric strain $(\varepsilon_v)_{com}$ from 0.24 to 0.37% for reinforced sand and from 0.32 to 0.42% for reinforced mixed sand-clay. Under α = 90°, $(\varepsilon_v)_{comp}$ increased from 0.32 to 0.51% for reinforced sand and from 0.33 to 0.45 for reinforced mixed sand-clay as *b* increased to 1.0. Although the reinforced mixed sand-clay exhibited larger peak deviator stress than reinforced sand, particularly under α = 60–90°, the associated compression strain $(\varepsilon_v)_{comp}$ of reinforced mixed sand-clay was lower. This indicates the cushioning effect of clay and its role as a cementation material that improves bonding.

The dilation behaviour of reinforced sand and reinforced mixed sand-clay was restricted significantly; it decreased to 1.56–0.45% (for reinforced sand) and 1.41–

0.39% (for reinforced mixed sand-clay) under b = 0.2 (depending on α) compared with 4.8–1.0% for unreinforced sand. The restraint increased as b increased under α = 0–30° due to increases in lateral stress. Increasing b from 0.2 to 1.0 under α = 0°, for example, led to decreases in expansion strain $(\varepsilon_v)_{dil}$ from 1.56% and 1.41% for reinforced sand and reinforced mixed sand-clay, respectively, to 1.19% and 0.91%. When α was 60–90°, however, horizontal stress became the major stress while the vertical stress became the minor stress, and consequently, increasing b to 1.0 resulted in increasing expansion toward vertical from 0.4–0.45 to 0.5–0.62%.

6.6 Comparison of the Effect of *b* on Samples Reinforced with Different Geosynthetics

This section presents a summary and comparison the effect of b on clean sand and mixed sand-clay reinforced with planar inclusions (geogrid and geotextile) and cellular inclusions (geocell) (Figures 6.33-6.35).

Under all directions of principal stress α, cellular reinforcement resulted in the minimum effect of b on the peak deviator stress q_p. Increasing b from 0.2 to 1.0 resulted in a decrease in the deviator stress of planar (geogrid/geotextile)-reinforced sand by 14.9–24.0%, compared with only 5.2–10.3% when geocell was used. The anisotropic difference due to variation of α under all three values of b was also a minimum when geocell was used, compared with using other reinforcements. The differences in the deviator stresses of geocell-reinforced sand along α were 24.7, 25.3 and 22.8% for b = 0.2, 0.5 and 1.0, respectively, compared with for example, 45.1, 50.4 and 49.6%, respectively, for geogrid-reinforced sand. This lesser effect of anisotropy on the deviator stress of geocell-reinforced samples is linked to the maximal improvement in strength, particularly under α = 60–90°, provided by the 3D geocell inclusion. In comparison, planar reinforcements have a lesser ability to resist horizontal loading. For example, geogrid or geotextile inclusion increased the minimum deviator stress of sand, that occurred at α = 60–90° when b=1.0, by only 32.5–42.4% compared with 136.1% with geocell. Tables 6.2 and 6.3 show the peak deviator stresses for clean sand and sand-clay mixtures reinforced with geogrid, geotextile and geocell and tested under various values of b and α.

Adding 10% clay to the reinforced sand resulted in clear increases in deviator stress under α = 60–90° and for all values of b, noting that when b = 1.0, the increasing ratio of deviator stress was largest. Inclusion of fines improved performance in geotextile-reinforced samples more than when other types of reinforcement were used, although the amount of deviator stress of geocell-reinforced mixed sand-clay was still the largest. Under b = 0.2 and α = 90°, for example, the deviator stresses of geocell-, geogrid- and geotextile-reinforced sand increased by 10.4, 20.9 and 33.1%, respectively, when 10% clay was added.

These benefits of geocell and fines inclusion were reflected in the lesser amount of compressive volumetric strain occurring under b = 1.0 and α = 90°, despite the larger associated deviator stress. For all reinforcement types, increasing b resulted in decreased dilation strain in reinforced samples. Geocell-reinforced sand and mixed sand-clay had the lowest amounts of dilative strain, while geogrid-reinforced samples had the greatest. For example, increasing b from 0.2 to 1.0 under α = 0° resulted in a decrease in dilation strain from 2.9 to 2.3% for geogrid-reinforced sand, from 2.60 to 1.94% for geotextile-reinforced sand, and from 1.55 to 1.19% for geocell-reinforced sand.

The increase in the b value refers to an increase the intermediate principal stress σ_2 that is equal, in hollow cylinder samples, to the radial stress σ_r. Increasing b to 1.0 means that σ_r becomes equal to σ_1 and, thus, the stresses applied horizontally increase. Under such conditions, the tensile strength of the planar layers of geogrid and geotextile (which are placed horizontally) is not sufficiently mobilised to resist the horizontal stress. However, the 3D form of geo-inclusion (geocell) acts on the entire perimeter of the sample due to the confinement of its mobilised, tensioned wall, and thus, it provides greater improvement, even under b = 1.0 and/or α = 60 and 90°.

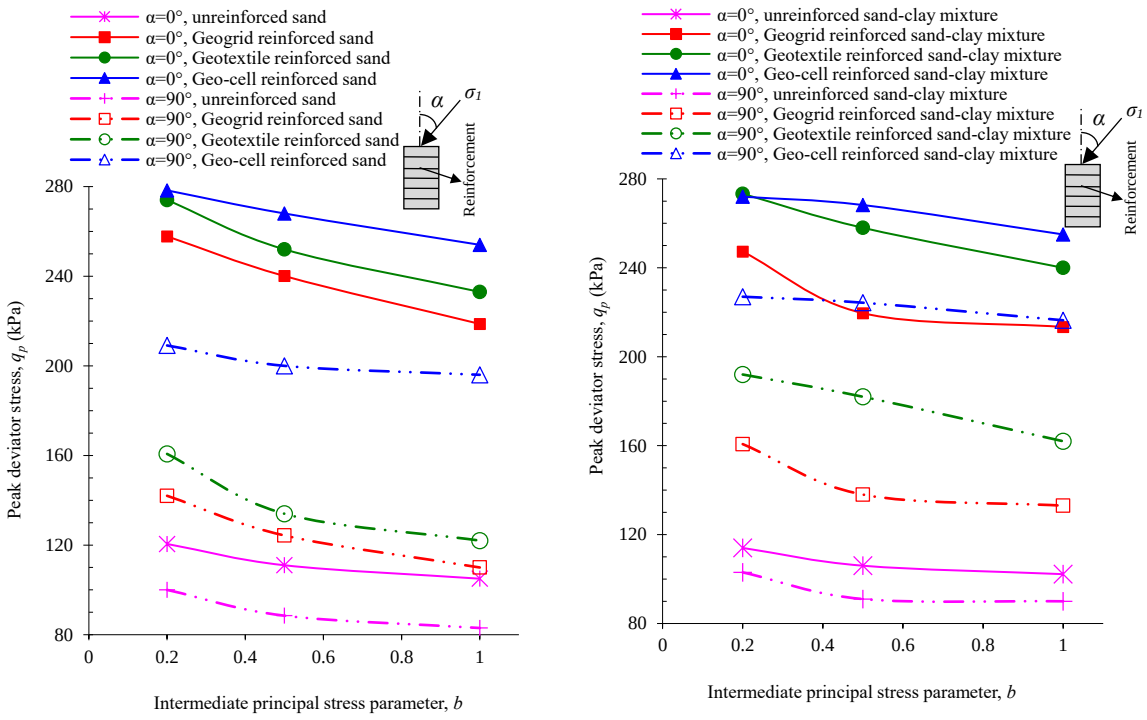

(a) (b)

Figure 6.33 Comparison the variation of peak deviator stress q_p against b of (a) clean sand and (b) mixed sand-clay reinforced with different geosynthetics

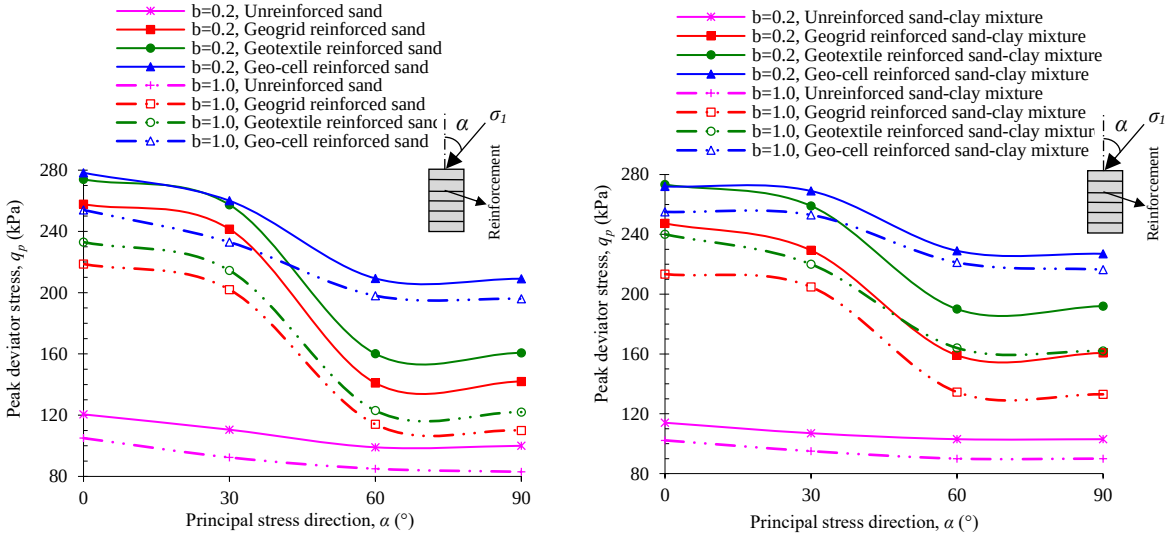

(a) (b)

Figure 6.34 Comparison the effects of b on the variations of peak deviator stress q_p along α of (a) clean sand and (b) mixed sand-clay reinforced with different geosynthetics

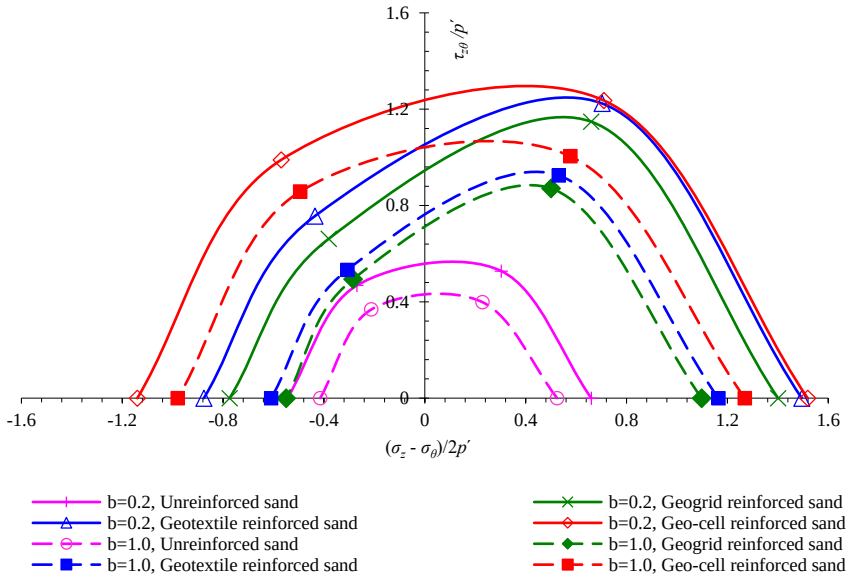

(a)

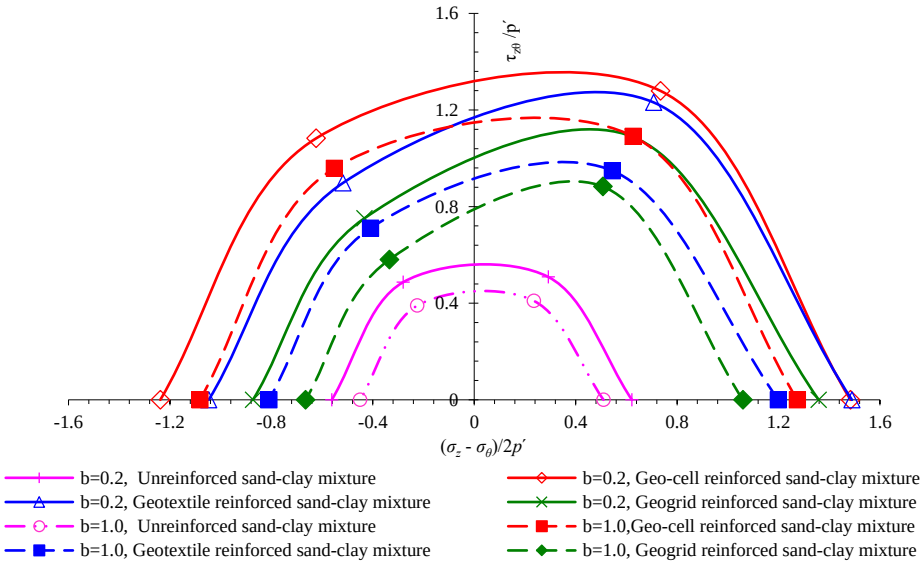

(b)

Figure 6.35 Comparison of the effects of *b* on the failure envelopes of (a) clean sand and (b) mixed sand-clay reinforced with different geosynthetics

Table 6.2 Summary of the peak deviator stress of reinforced clean sand obtained under various values of b and α

Direction of principal stress, α (°)	Unreinforced sand			Geogrid reinforced sand			Geotextile reinforced sand			Geocell reinforced sand		
				6 layers			6 layers					
	Intermediate principal stress, b											
	0.2	0.5	1.0	0.2	0.5	1.0	0.2	0.5	1.0	0.2	0.5	1.0
	Peak deviator stress, q_p (kPa)											
0	120.5	111.3	105.2	257.8	240.1	218.7	274.1	252.7	233.2	278.3	268.0	254.2
30	110.4	102.2	92.4	241.5	240.6	202.4	257.4	246..0	214.5	260.0	252.8	233.1
60	99.0	87.0	85.4	141.3	119.0	113.5	160.1	132.1	123.3	209.3	202.3	198.3
90	100.2	88.5	83.1	142.2	124.3	110.1	160.7	134.8	122.0	209.1	200.1	196.0
	Difference in peak deviator stress, Δq_p (%)											
	17.8	21.8	21.0	45.1	50.4	49.6	41.5	47.7	47.6	24.7	25.3	22.8

Table 6.3 Summary of the peak deviator stress of reinforced sand-clay mixtures obtained under various values of b and α

Direction of principal stress, α (°)	Unreinforced sand-clay mixture			Geogrid reinforced sand-clay mixture			Geotextile reinforced sand-clay mixture			Geocell reinforced sand-clay mixture		
				6 layers			6 layers					
	Intermediate principal stress, b											
	0.2	0.5	1.0	0.2	0.5	1.0	0.2	0.5	1.0	0.2	0.5	1.0
	Peak deviator stress, q_p (kPa)											
0	114.7	106.2	102.3	247.4	219.8	213.1	273.3	258.1	240.2	272.2	268.2	255.1
30	107.1	104.2	95.2	229.3	217.3	204.8	258.8	253.1	220.1	269.1	265.4	253.6
60	103.6	92.3	90.4	159.1	137.2	134.5	190.1	182.0	164.3	229.4	224.1	221.2
90	103.4	91.0	90.0	160.7	138.8	133.0	192.3	182.3	162.4	227.3	224.3	216.4
	Difference in peak deviator stress, Δq_p (%)											
	9.8	13.3	12.0	35.6	37.6	37.5	30.4	29.4	32.3	15.7	16.4	15.1

Chapter 7

Cyclic Deformation of Reinforced Clean Sand and Mixed Sand-clay under Cyclic Rotation of Principal Stress Direction

7.1 Introduction

In the previous chapters, the principal stress direction was kept constant at a specific angle during the tests; however, in this chapter, the direction of principal stress was rotated cyclically during the tests. Thus, this chapter aimed to investigate the cyclic deformation of unreinforced and geosynthetic-reinforced sand and mixed sand-clay under the anisotropic condition of cyclic rotation of the principal stress direction. The effects of three different cyclic ratios on the behaviour of sand and sand reinforced with three and six layers of geogrid were investigated. Moreover, the behaviour of samples (sand and mixed sand-clay) reinforced with six layers of nonwoven geotextile and geocell under rotational conditions was investigated for selected cyclic ratios. The axial, radial, circumferential, shear and volumetric strains, and the shear moduli and damping ratios of unreinforced and reinforced samples, are presented and discussed. Details of the tests performed are summarised in Table 7.1.

Sections 7.2 and 7.3 will be devoted to reviewing and discussing the effect of cyclic rotation of the direction of principal stress on the characterisation of sand and sand reinforced with various numbers of geogrid layers. Section 7.4 will discuss the dynamic characterisation of sand and reinforced sand under cyclic rotation. The following section will be dedicated to the effect of different stress ratios q/p' on the characteristics of sand reinforced with three and six geogrid layers (Section 7.5). Section 7.6 will discuss the characterisation of sand reinforced with six layers of nonwoven geotextile and geocell under cyclic rotation of principal stress. Finally, the effect of cyclic rotation of principal stress on mixed sand-clay (10% clay) reinforced with six layers of geogrid, nonwoven geotextile and geocell are presented in Section 7.7.

Table 7.1 Summary of the conditions and parameters of the tests performed in this chapter

Test Series			Plastic fines content, F (%)	Relative density, D_r (%)	Mean effective stress, p' (kPa)	Intermediate principal stress parameter, b	Stress ratio, q/p'
Series I Unreinforced clean sand			0	70.8	100	0.5	0.69
			0	70.2			0.9
			0	69.8			1.1
Series II Reinforced clean sand	Geogrid	2 layers	0	70.1	100	0.5	0.69
		3 layers	0	70.3			0.69
		4 layers	0	71.0			0.69
		5 layers	0	69.3			0.69
		6 layers	0	69.7			0.69
	Geogrid	3 layers	0	70.4	100	0.5	0.9
		6 layers	0	69.8			1.1
	Nonwoven geotextile	6 layers	0	70.1	100	0.5	1.1
	Geocell	----	0	69.4	100	0.5	1.1
Series III Unreinforced sand-clay mixture			10	69.5	100	0.5	1.1
Series IV Reinforced sand-clay mixture	Geogrid	6 layers	10	71.1	100	0.5	1.1
	Nonwoven geotextile	6 layers	10	70.8	100	0.5	1.1
	Geocell	----	10	69.6	100	0.5	1.1

7.2 Sand Response to Cyclic Rotation of Principal Stress Direction

In this section, the deformation behaviour of unreinforced clean sand is presented. Deviator stress q and mean effective stress were constant at approximately 69 kPa and 100 kPa, respectively, during these tests (Figure 7.1a), i.e., the stress ratio $q/p' = 0.69$, while the direction of principal stress α rotated continuously (Figure 7.1b).

A typical stress path followed in the rotational shear test with $q/p' = 0.69$ is shown in Figure 7.2. Here, the direction of principal stress α was rotated counter-clockwise from 0° to 180° following the circular cyclic path from A to B, C, D and then A. Sixty cycles in total were performed, and during these cycles of rotation of the principal stress direction, axial stress σ_z, circumferential stress σ_θ and shear stress $\tau_{z\theta}$ varied with oscillation mode, while the radial stress σ_r, mean effective stress p', deviator stress q, intermediate principal stress ratio b, major principal stress σ_1, intermediate principal stress σ_2 and minor principal stress σ_3 were kept unchanged (Figure 7.3).

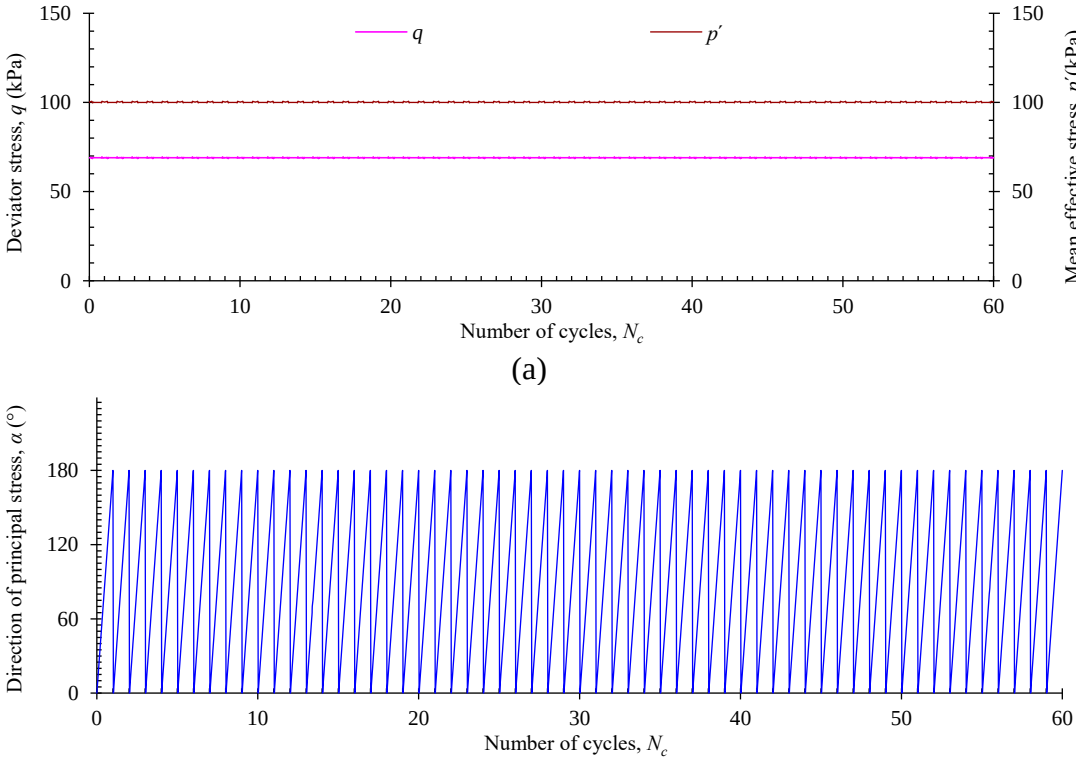

Figure 7.1 Typical variation of (a) deviator stress q and mean effective stress p', and (b) the direction of principal stress α over 60 cycles in rotational shear under (q/p' = 0.69).

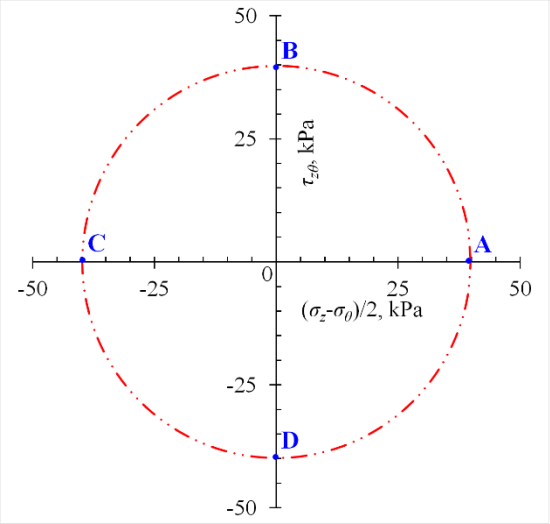

Figure 7.2 Typical stress path of cyclic rotation test under q/p' = 0.69.

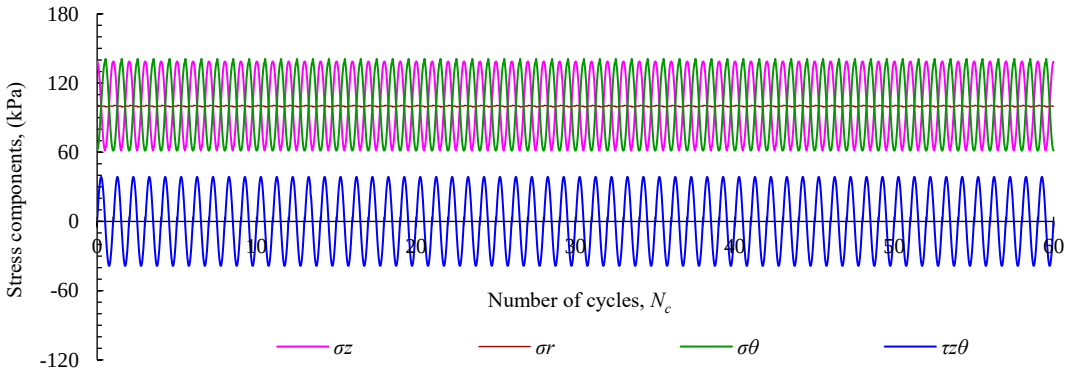

(a)

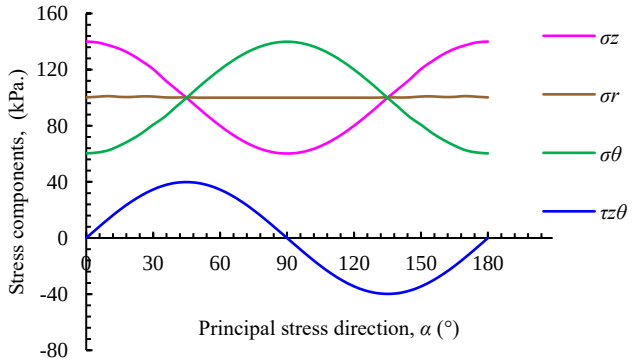

(b)

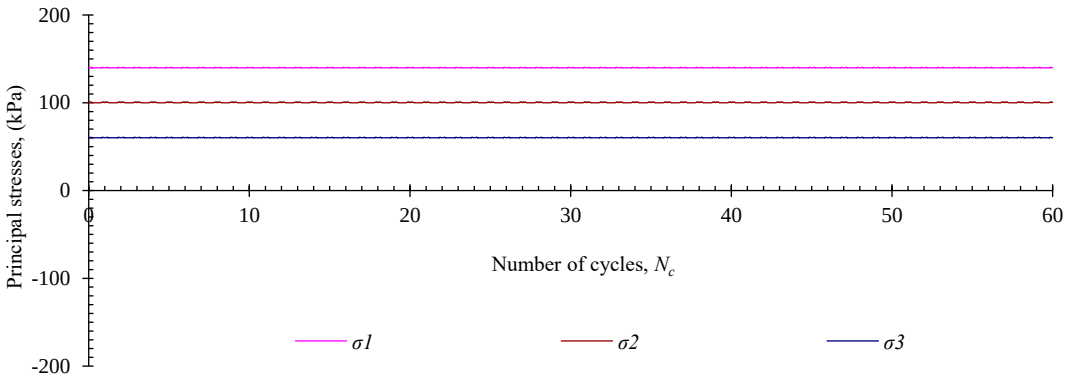

(c)

Figure 7.3 Typical variation of stress components (axial σ_z, radial σ_r, circumferential σ_θ and shear stresses $\tau_{z\theta}$) in (a) rotational shear over 60 cycles; (b) rotational shear during the first cycle, and (c) principal stresses (major σ_1, intermediate σ_2 and minor σ_3 stresses) over 60 cycles in rotational shear

Figure 7.4a shows the variation in the strain components according to the number of cycles N_c and during rotation of the principal stress direction. Positive and negative signs indicate compression and dilation, respectively. It is evident that although the deviator stress q was kept constant during the test, significant vertical ε_z, radial ε_r, circumferential ε_θ and shear $\gamma_{z\theta}$ strains were generated, indicating a significant effect of the rotation of the principal stress direction on the deformation behaviour of the unreinforced clean sand.

In Figure 7.4b, an increase of the shear strain $\gamma_{z\theta}$ can be observed from the beginning of rotation, reaching a maximum value at $\alpha = 73°$ then decreasing to zero as α increases to 115°. Further increases of α result in the shear strain reaching its lowest value at around 137° and then increasing slightly until the end of the cycle. However, it does not return to the initial value before rotation. The circumferential strain ε_θ increased slightly with rotation. However, when α approached 40°, ε_θ began to increase significantly with its maximum value occurring at $\alpha = 105°$, before it decreased and remained in the compression side. A similar trend is observed for ε_r, however, its variation along α is less than that of ε_θ along α. For the axial strain ε_z, clear dilation

behaviour was recorded where ε_z increased slightly from the beginning of rotation until α = 30–40° when a dramatic increase of dilation began, reaching its maximum value at α = 105° before decreasing steadily until the end of the cycle (α = 180°) and remaining dilated.

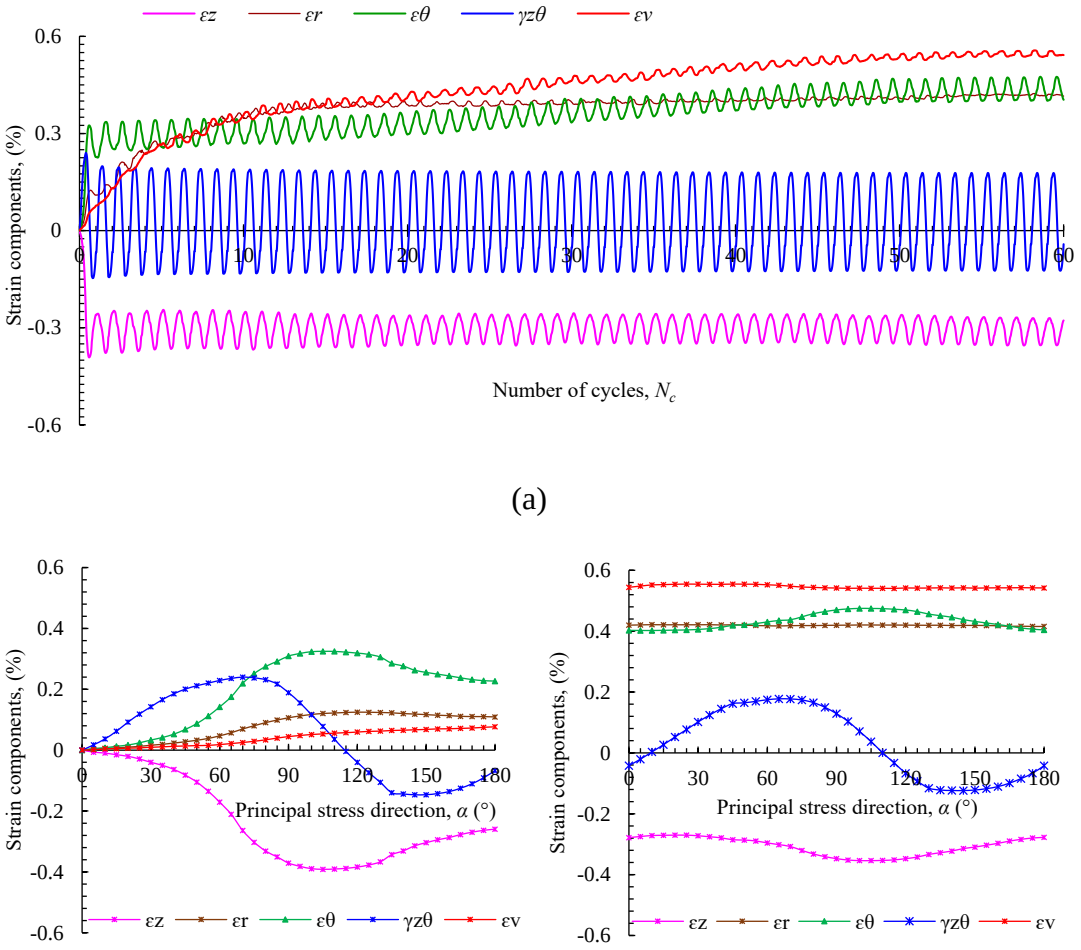

Figure 7.4 Variation of strain components (axial ε_z, radial ε_r, circumferential ε_θ, shear $\gamma_{z\theta}$ and volumetric ε_v strains) in rotational shear over (a) 60 cycles; (b) the direction of principal stress α during the first cycle; and (c) the direction of principal stress α during the 60th cycle.

All strain components at the end of the cycle (Figure 7.4b) did not return to their initial values before starting the rotation, although the stress components did return to their initial state (Figures 7.3a and b). This shows that plastic strains occur and lead to irrecoverable deformation (Figure 7.4). This plastic strain can also be seen in the spiral curve of the strain path in the deviator strain space ($\varepsilon_z - \varepsilon_\theta$) vs. $\gamma_{z\theta}$ (Figure 7.5). In this strain path, when plastic deformation occurs, the strain trajectory forms an open space and the vector from the start point to the end point of each single cycle represents the amount of irrecoverable strain (X. Li et al., 2016; Yu et al., 2016). The largest plastic strain can be observed in the first cycle. However, with continuous rotation, the open space tends to become closed, indicating development of a small amount of plastic deformation.

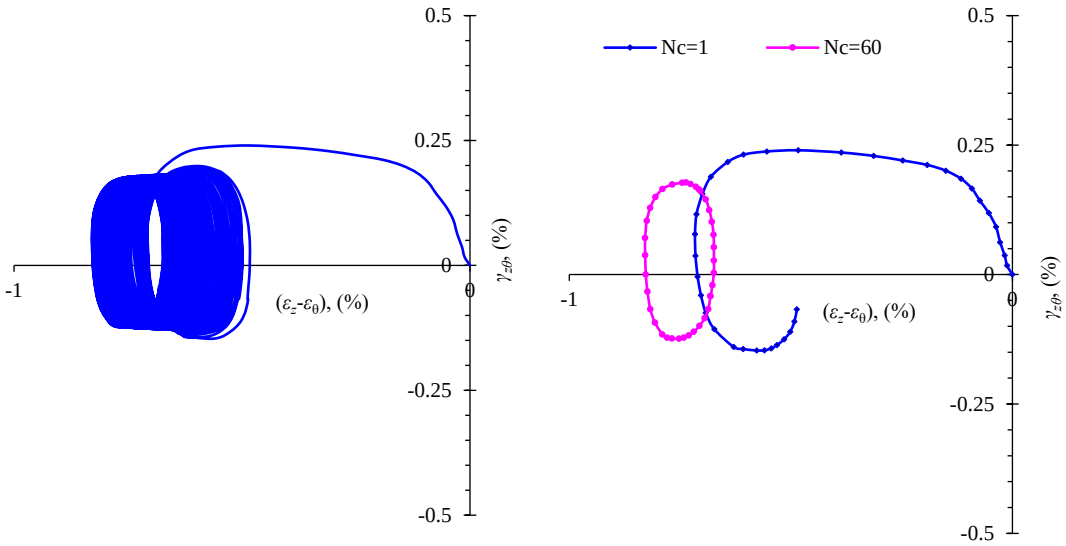

(a) (b)

Figure 7.5 Strain paths of unreinforced sand in deviator strain space for (a) cyclic rotation and (b) the first and 60th cycles.

By comparing subsequent cycles of rotation of the principal stress direction, it can be observed that most of the strains are produced during the first cycle (Figure 7.4). Subsequently, ε_z reduces moderately within the first five cycles, followed by a slight decrease as the number of cycles N_c increases. The circumferential strain ε_θ increases

slightly as the number of cycles increases, but ε_r increases significantly until N_c = 20, and then the rate of increase decreases. For example, the axial strain ε_z increases to -0.39% after the first rotation cycle and then decreases to -0.347% and -0.345% after 30 and 60 cycles, respectively. Circumferential strain ε_θ reached 0.322% during the first cycle and increased to 0.4% and 0.46% as N_c increased to 30 and 60 cycles, respectively. This is consistent with Tong et al. (2008); Tong et al. (2010), Xiong et al. (2016) and Yu et al. (2016).

These variations in strain components can be explained in relation to the variation in the stress state; where the sample, with inherent anisotropy due to the preferred orientation of particles, is subjected to axial stress vertically before starting rotation, in which axial stress σ_z and circumferential stress σ_θ are the major and minor principal stresses, respectively (Yan et al., 2015; L. Yang, 2013). This results in the sample having higher compressibility and lower dilation in the horizontal direction than in the vertical direction (Yan et al., 2015; L. Yang, 2013). Once the rotation begins, σ_z decreases while σ_θ increases (Figure 7.3). The resulting deformation is in the form of contraction along the circumferential direction, i.e. the plane that is most susceptible to deformation. Sand subjected to cyclic rotation will develop an anisotropic structure due to the capability of the granular material to rearrange its internal structure and achieve mechanical stability when sheared. This anisotropic fabric will rotate continuously in the direction of the principal stress (with a few degrees of lag), consequently resulting in accumulated strains that have varied oscillation characteristics (X. Li & Yu, 2010; Yu et al., 2016).

The volumetric strains are presented in Figures 7.6 and 7.7, where positive values indicate compressive behaviour. Volumetric strain accumulates as the number of cycles increases, although the deviator stress ratio q/p' is constant at 0.69 throughout the cyclic rotation and most of the induced ε_v occurs during the first cycle, after which the accumulation rate tends to reduce (Figure 7.6). A similar trend was observed by Tong et al. (2008) and Yu et al. (2016). During the first five cycles, the volumetric strain is contractive along α. With increasing numbers of cycles, the variation of ε_v along α becomes smaller with some dilation (Figure 7.7). This dilation is likely attributed to the densification of samples that occurred during previous cycles of

rotation. Although both contraction and dilation occur in the samples during individual cycles, contractive behaviour is dominant in the accumulated volumetric strain at the end of each cyclic rotation. This agrees with the findings of Xiong et al. (2016), who reported that sand became 12% denser after 20 cycles of rotation.

This indicates that fabric anisotropy can considerably affect the deformation behaviour of sand, particularly in the first cycle of rotation of the principal stress direction. However, in subsequent cycles, the development and oscillation of the accumulated strain components tends to decrease significantly (Figures 7.4-7.7). This may be attributed to the property of soil, which can achieve some structural stability after the continuous orientation, realignment and rearrangement of particles that occurs with increasing amounts of cyclic rotation. This is consistent with the anisotropic critical state (ACS) proposed by X. Li and Dafalias (2011), where soil becomes independent of initial fabric anisotropy unless severe particle breakage occurs. Similar observations in terms of this critical state and destruction of the initial anisotropic fabric were reported by Oda and Koishikawa (1979), Sazzad and Suzuki (2010), Fu and Dafalias (2011), Fonseca et al. (2013) and Tong et al. (2014). This destruction of initial anisotropy was also recognised by Seyedi Hosseininia (2012a), who observed a significant drop in the frequency of particles oriented along a specific angle α after samples were subjected to loading.

This reduction in the development and oscillation of the accumulated strain components also corresponds to a process of loss and creation of contacts in the anisotropic fabric. This occurs as the number of cycles increases, where the occurrence of plastic strain results in the loss of existing fabric contacts and generates new contacts which, consequently, leads to continuous change in the contact fabric. This change in the fabric is linked to the fabric anisotropy of granular material which can be recognised from the orientation of the normal contact distribution (Sazzad & Suzuki, 2010). In the inherent anisotropic structure, the elongated particles prefer to align horizontally and thus exhibit the greatest stability under vertical stress and less stability under inclined stress. Therefore, particles tend to rotate to support the rotation of the principal stress direction, which rotates continuously. Consequently, more normal contacts will be lost during cycles of rotation while the preferred direction of

the contact anisotropy tends to rotate towards the principal direction. The change in fabric anisotropy is significant during the first few cycles and then becomes steady, indicating that the fabric might approach a critical state after many cycles of accumulated changes and reorientations of the contact fabric.

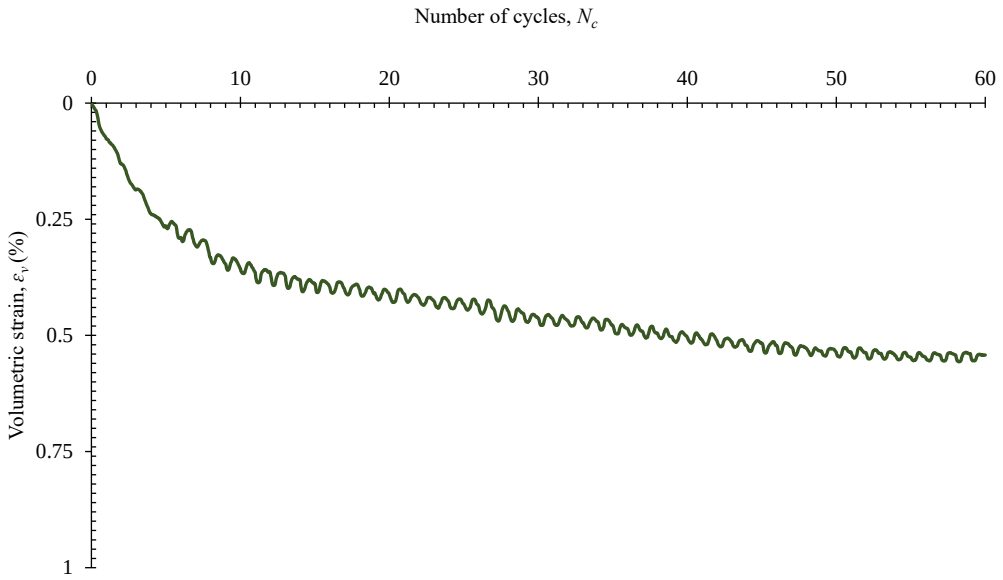

Figure 7.6 Variation of volumetric strain ε_v in rotational shear over 60 cycles

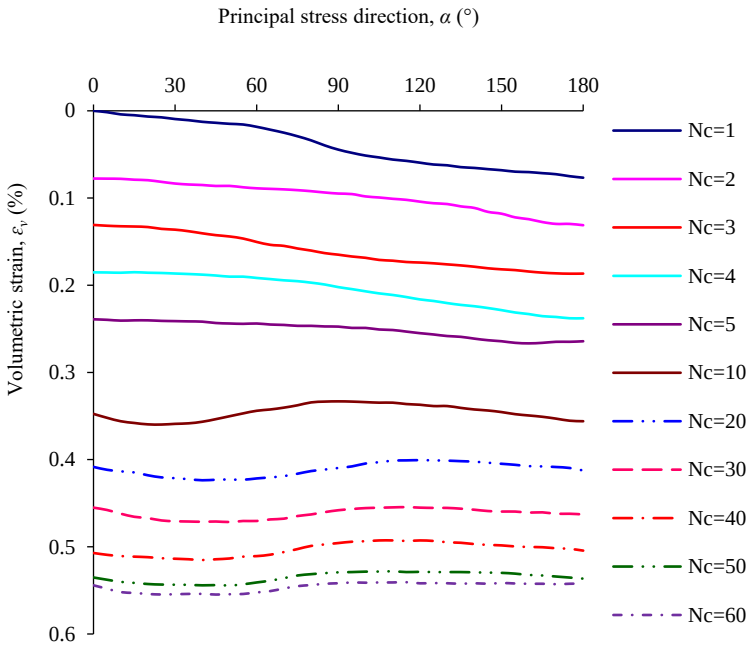

Figure 7.7 Variation of volumetric strain ε_v in rotational shear along the direction of principal stress α for various numbers of cycles

7.3 Response of Geogrid-reinforced Sand to Cyclic Rotation of Principal Stress Direction

Figures 7.8-7.12 show the deformation behaviour of sand reinforced with different numbers of geogrid layers under cyclic rotation. It is clear that the geogrid reinforcement plays a significant role in decreasing all four strain components. Circumferential ε_θ and radial ε_r strains decreased clearly when 3–6 layers of geogrid were used. However, such decreases were slight to moderate in the axial ε_z and shear $\gamma_{z\theta}$ strains. Volumetric strain ε_v accumulated as the number of cycles increased, although most was induced during the first cycle, after which it accumulated at a low rate (Figures 7.13 and 7.14). During the first five cycles, the volumetric strain was contractive along α. With subsequent cycles, a slight dilation occurred and the variation of ε_v along α became insignificant (Figures 7.13 and 7.14). It can be observed, for example, that the amount of volumetric strain and its variation along α was much lower in sand reinforced with six layers compared with unreinforced sand. However, reinforcement with two layers did not show a significant effect.

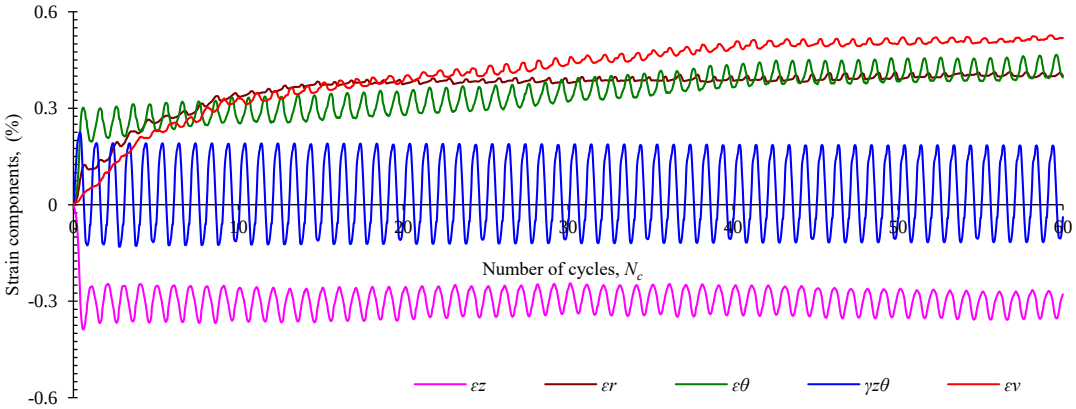

(a)

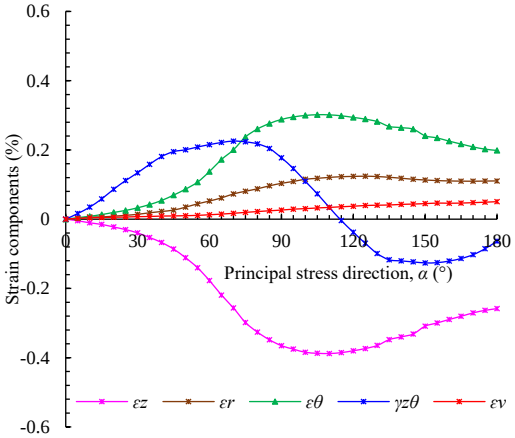

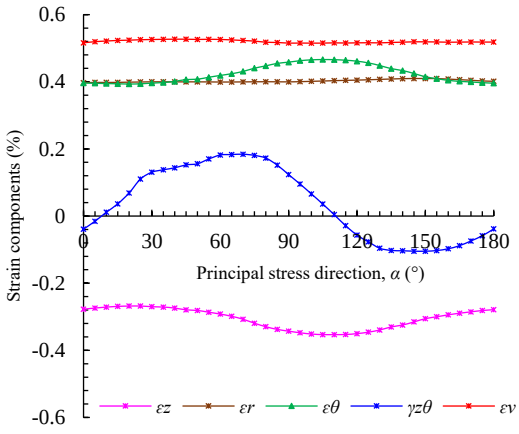

(b) (c)

Figure 7.8 Variation of strain components in 2-geogrid layer-reinforced sand (axial ε_z, radial ε_r, circumferential ε_θ, shear $\gamma_{z\theta}$ and volumetric ε_v strains) in rotational shear along: (a) 60 cycles; (b) the direction of principal stress α during the first cycle; and (c) the direction of principal stress α during the 60th cycle

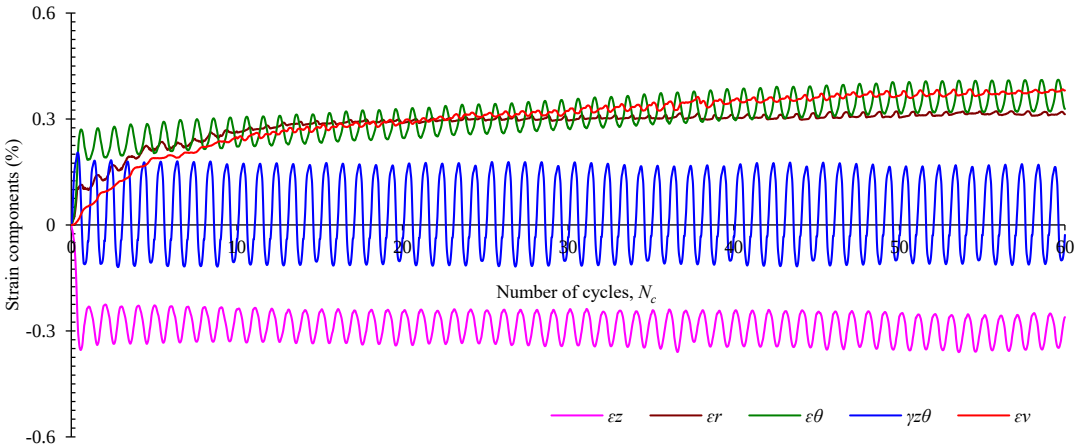

(a)

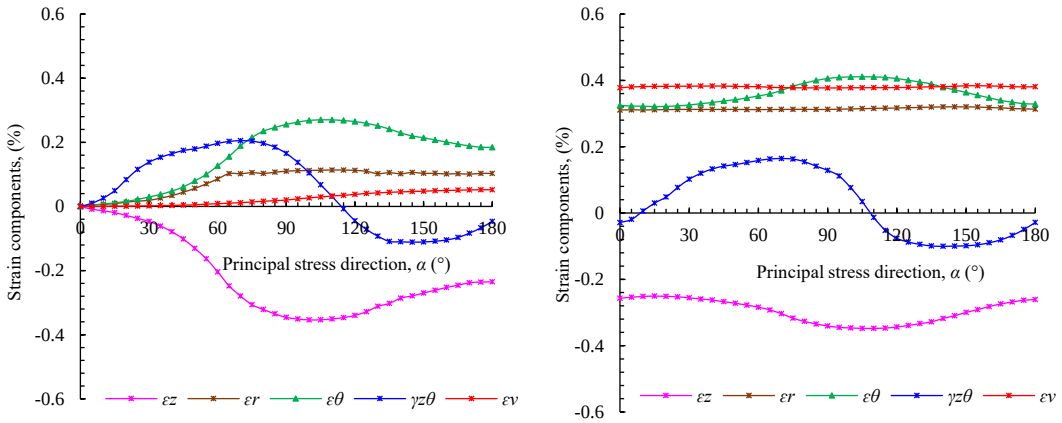

(b)

(c)

Figure 7.9 Variation of strain components of 3-geogrid layer-reinforced sand (axial ε_z, radial ε_r, circumferential ε_θ, shear $\gamma_{z\theta}$ and volumetric ε_v strains) in rotational shear along: (a) 60 cycles; (b) the direction of principal stress α during the first cycle; and (c) the direction of principal stress α during the 60th cycle

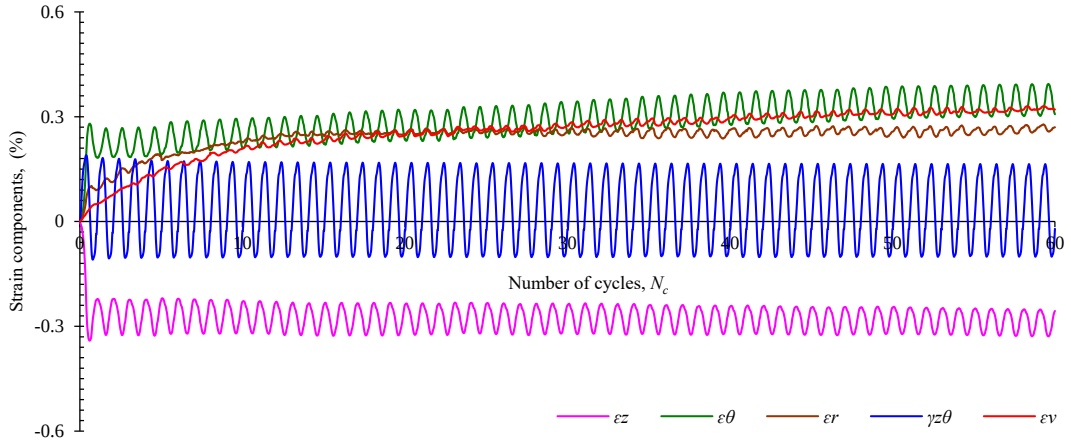

(a)

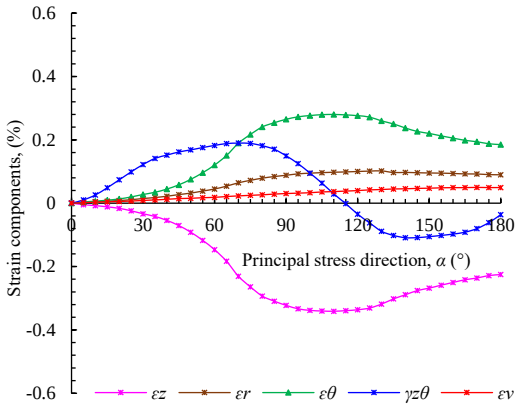

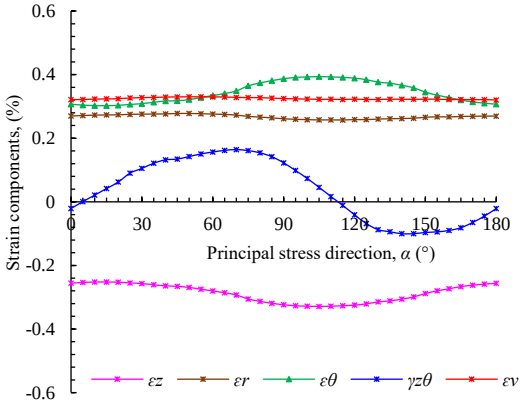

(b) (c)

Figure 7.10 Variation of strain components of 4-geogrid layer-reinforced sand (axial ε_z, radial ε_r, circumferential ε_θ, shear $\gamma_{z\theta}$ and volumetric ε_v strains) in rotational shear along: (a) 60 cycles; (b) the direction of principal stress α during the first cycle; and (c) the direction of principal stress α during the 60th cycle

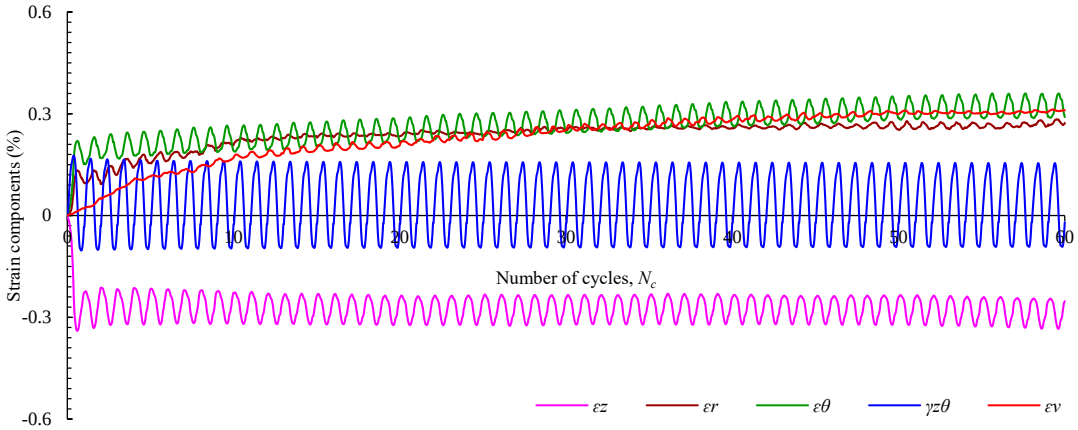

(a)

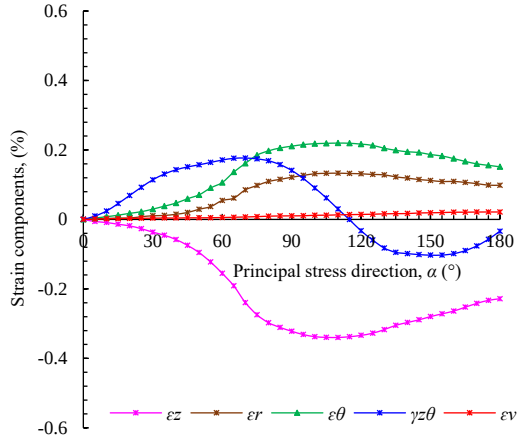

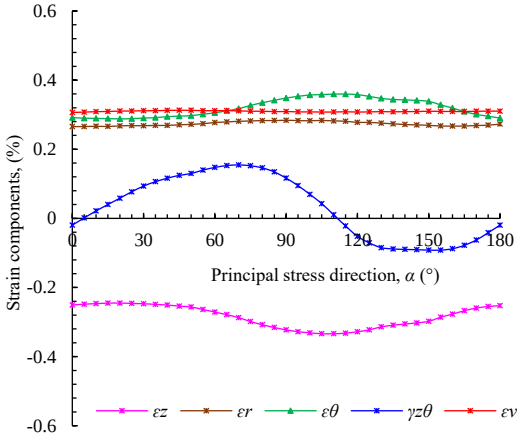

(b) (c)

Figure 7.11 Variation of strain components of 5-geogrid layer-reinforced sand (axial ε_z, radial ε_r, circumferential ε_θ, shear $\gamma_{z\theta}$ and volumetric ε_v strains) in rotational shear along: (a) 60 cycles; (b) the direction of principal stress α during the first cycle; and (c) the direction of principal stress α during the 60th cycle

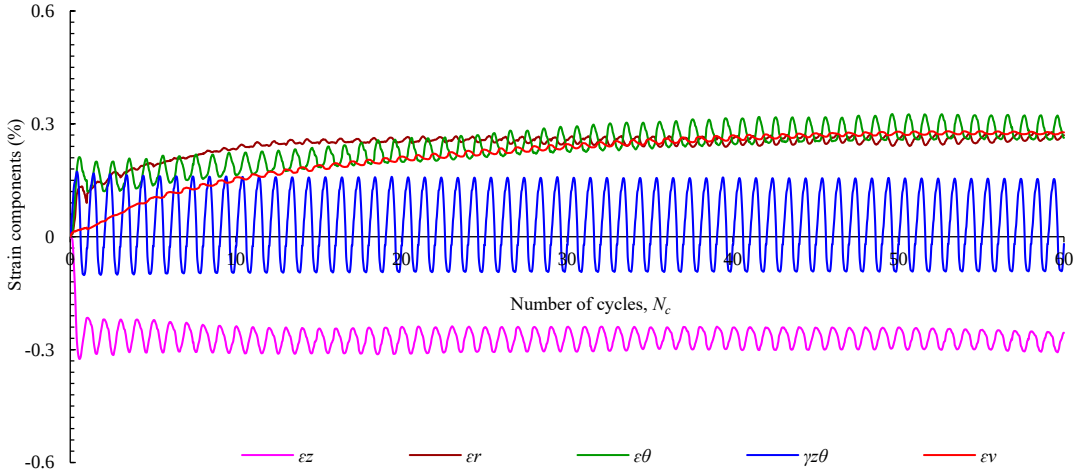

(a)

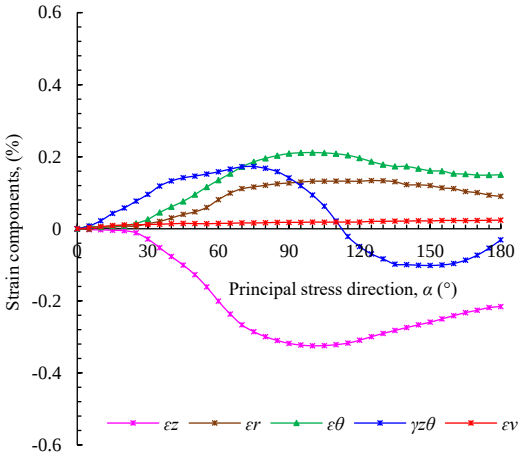

(b)

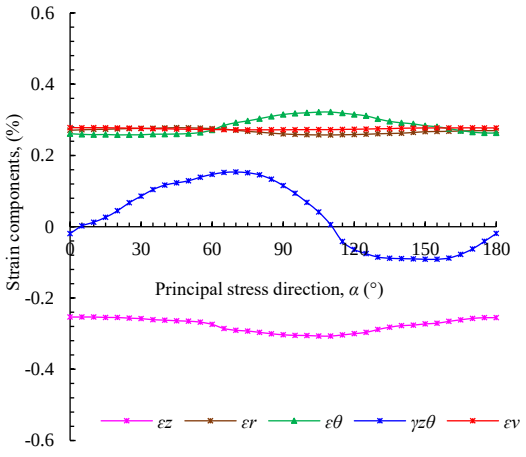

(c)

Figure 7.12 Variation of strain components of 6-geogrid layer-reinforced sand (axial ε_z, radial ε_r, circumferential ε_θ, shear $\gamma_{z\theta}$ and volumetric ε_v strains) in rotational shear along: (a) 60 cycles; (b) the direction of principal stress α during the first cycle; and (c) the direction of principal stress α during the 60th cycle

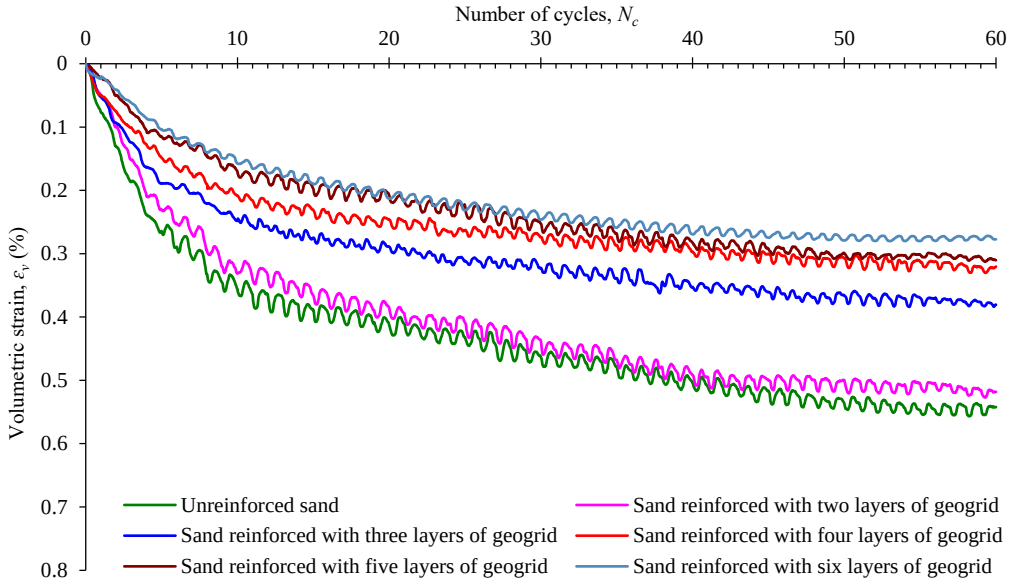

Figure 7.13 Variation of volumetric strain ε_v in sand reinforced with different numbers of geogrid layers in rotational shear along 60 cycles

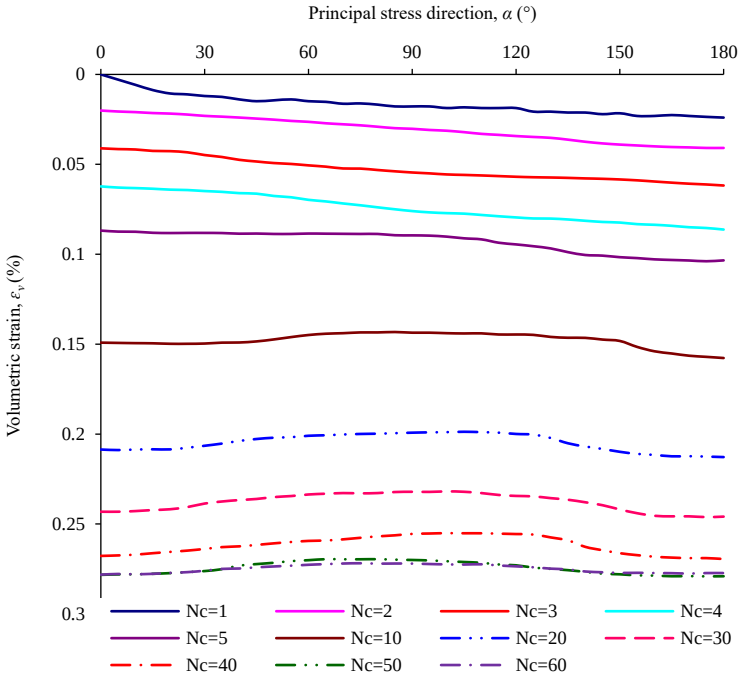

Figure 7.14 Variation of volumetric strain ε_v of sand reinforced with 6 layers of geogrid in rotational shear along the direction of principal stress α for different numbers of cycles

The oscillation characteristics of strains are linked to the variation of the applied stresses, while the observed reduction in the induced strains is attributed to the mechanism of the geogrid reinforcement, which provides internal confinement. This confinement varies depending on the tensile strength of the geogrid, the friction between the sand and geogrid at the interface, and the induced stress of sand confined in the geogrid apertures due to the passive resistance provided by the reinforcement.

Before rotation, the sample is under an axial stress, resulting in an axial deformation and, subsequently, increasing the interaction between the geogrid and the sand. This mobilises radial strength in the geogrid that resists the lateral deformation generated in the sample. The variation in the strain components is likely to be related to the variation in the stresses (Figures 7.3a and b). For rotation in the range α = 0–45°, σ_z remains greater than σ_θ, although σ_z starts to decrease and σ_θ increases, resulting in dilation in the vertical direction and slight contraction in the circumferential direction. Within this range, the applied vertical stress contributes to greater interaction between the sand and the geogrid, resulting in a restriction of the lateral strain. With continued rotation in the range α = 45–90°, σ_z decreases further while σ_θ increases and the condition changes to $\sigma_\theta > \sigma_z$. Consequently, the interaction becomes reduced, resulting in clear lateral contraction. However, this contraction was less than that of unreinforced sand. The subsequent rotation (α = 90–135°) shows that σ_z and σ_θ increase and decrease, respectively, noting that σ_θ remains larger than σ_z and this increase in σ_z provides greater interaction between the geogrid and the sand. This can restrain the contractive lateral deformation and decrease dilation in the vertical direction. For the remaining range of rotation (α > 135°), σ_z becomes larger than σ_θ, resulting in greater interaction and, consequently, higher restraint.

Although the cyclic rotation still induces clear deformation, reinforcement can restrict the radial and circumferential strains. This restraint becomes more evident in the subsequent cycles due to densification and stress history, which lead to advanced interaction between the sand particles and geogrid layers. It should be mentioned that sand reinforced with two layers of geogrid shows insignificant resistance to cyclic rotation. The improvement of deformation behaviour can be explained based on the sand-geogrid interaction, which may include the mechanisms of ***(a)*** shear resistance

between the sand and the surfaces of the geogrid ribs and surrounding soil, and ***(b)*** internal shear resistance of particles inside the geogrid apertures (Liu, Zornberg, Chen, Ho, & Lin, 2009). Moreover, the normal stress on reinforced sand results in an increase in the frictional resistance. Therefore, the observed lower levels of lateral strain (radial and circumferential) in reinforced sand can be explained by the fact that, during cyclic rotation, particularly when materials become subjected to rotations of α = 0–45° and 135–180° (conditions of $\sigma_z > \sigma_\theta$), lateral deformation is likely to develop in alignment with the direction of the reinforcement layers. The inclusion of a geogrid will result in shear interaction and interlocking forces between particles and the reinforcement layer, as mentioned in the above mechanism. Induced shear stresses will be transmitted from the sand particles to the geogrid, which will come under tension where tensile strain is induced, resulting in a tensile stress along the reinforcement. The geogrid will resist this induced tensile stress and strain by mobilising tensile strength, confinement, and interaction of the geogrid reinforcement with the surrounding soil. This will consequently restrict the development of lateral tensile strains (lateral expansion), induced in the sand adjacent to the geogrid layer. This restriction will decrease the level of dilation motivation and increase the strength. As the reinforcement layers increase, there will be greater confinement and interaction and, thus, greater resistance to lateral deformation occurs. This is consistent with the findings of Higuchi et al. (1998), Peng et al. (2000), Nazzal et al. (2007) and Liu et al. (2014).

However, when α rotates along 45–135°, i.e. when $\sigma_\theta > \sigma_z$, the performance of the reinforcement becomes very low. This can be related to samples entering an extension-like mode throughout this range, where the axial stress σ_z becomes smaller than the circumferential stress σ_θ. As explained in Chapter Four, the improvement provided by planar reinforcement depends mainly on its tensile strain, which should be mobilised by lateral expansion strains. However, in this range, the applied vertical stress was the least, resulting in a very slight development of the lateral expansion strain that is required to transmit and mobilise the tensile strength of the geogrid. Therefore, the ability of geogrid layers to provide confinement that resists shearing and induced strain under the conditions of α = 45–135° was at a minimum.

The induced strain in the reinforced sand caused by rotation in the range of 45–135^{o} can also be linked to the relative approach between mobilized plane and the horizontal plane, characterised as the weakest plane. This weakness of the horizontal bedding plane is due to the fact that particles tends to align themselves horizontally, resulting in poor interlocking and easy sliding and, consequently, maximum deformation and minimum strength. The potential mobilised plane makes an angle of ($45^{o} - \phi/2$) on both sides of the principal stress. Therefore, the rotation in the range of 45–135^{o} moves the mobilised plane closer to the weakened horizontal plane where the geogrid lies, resulting in less effective reinforcement. Similar trends in the response of reinforced sand to the principal stress direction were reported by Habibi et al. (2014).

The spiral curve of the strain path (Figure 7.15) shows that there is an induced plastic strain, particularly during the first cycle in which the space is open, followed by a smaller amount of irrecoverable deformation in which the space of each cycle tends to be closed. Although this is similar to the trend of unreinforced sand described in the previous section, the induced plastic strain of reinforced sand is much lower than that of unreinforced sand, as illustrated in Figure 7.16.

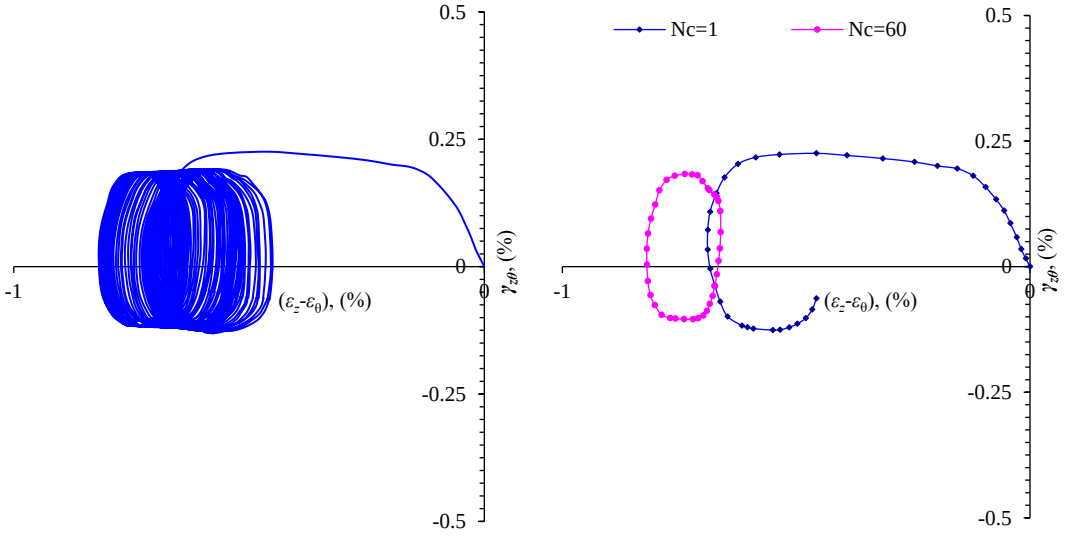

(i) (ii)

(a) 2-Geogrid layer-reinforced sand

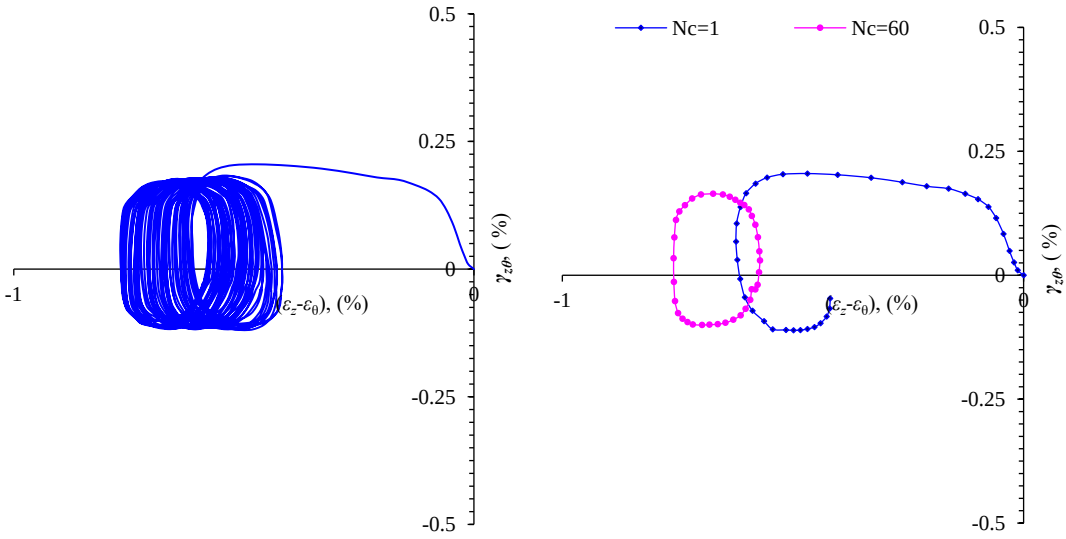

(i) (ii)

(b) 3-Geogrid layer-reinforced sand

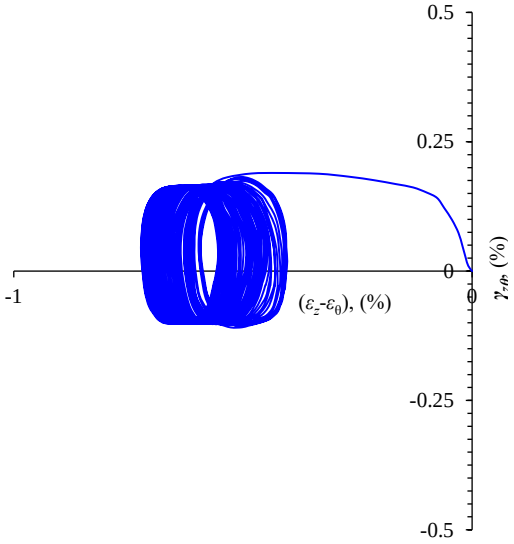

(i)

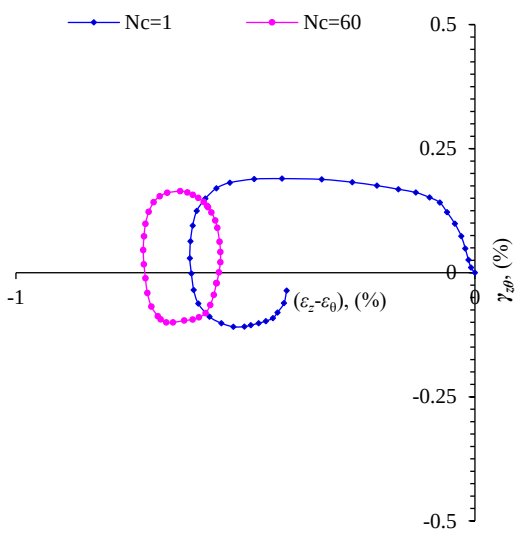

(ii)

(c) 4-Geogrid layer-reinforced sand

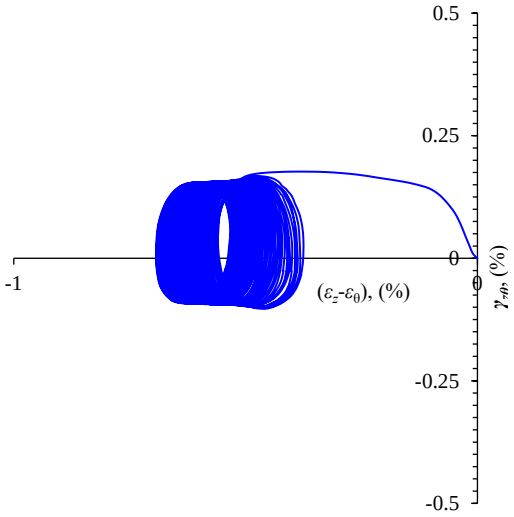

(i)

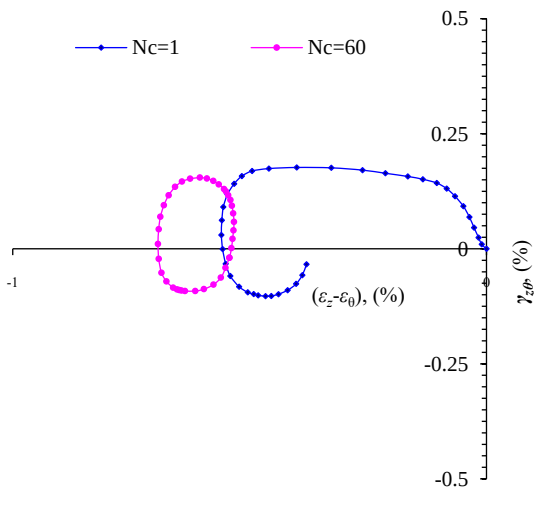

(ii)

(d) 5-Geogrid layer-reinforced sand

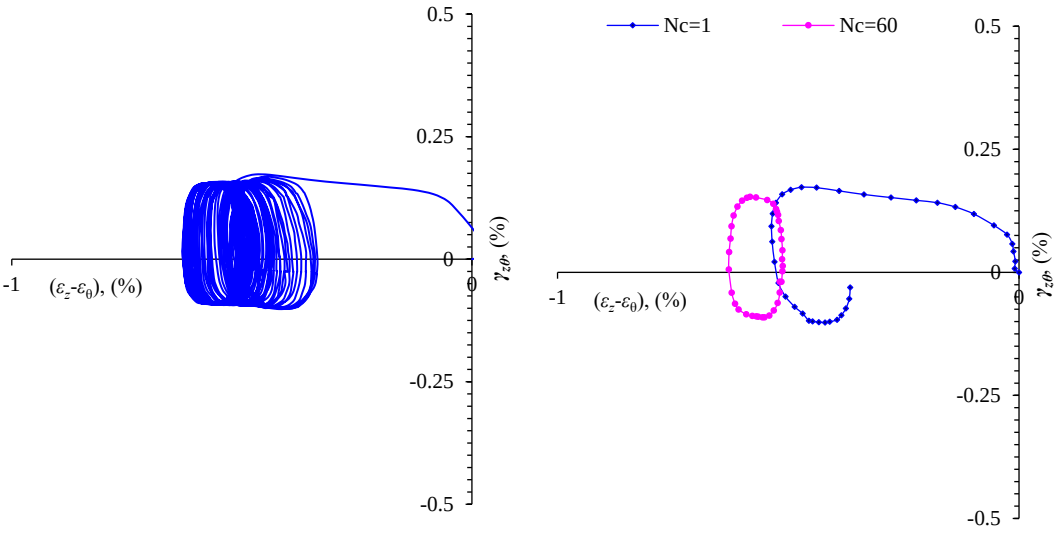

(i) (ii)

(e) 6-Geogrid layer-reinforced sand

Figure 7.15 Strain paths of sand reinforced with different numbers of geogrid layers in deviator strain space for (i) cyclic rotation and (ii) the first and 60th cycles

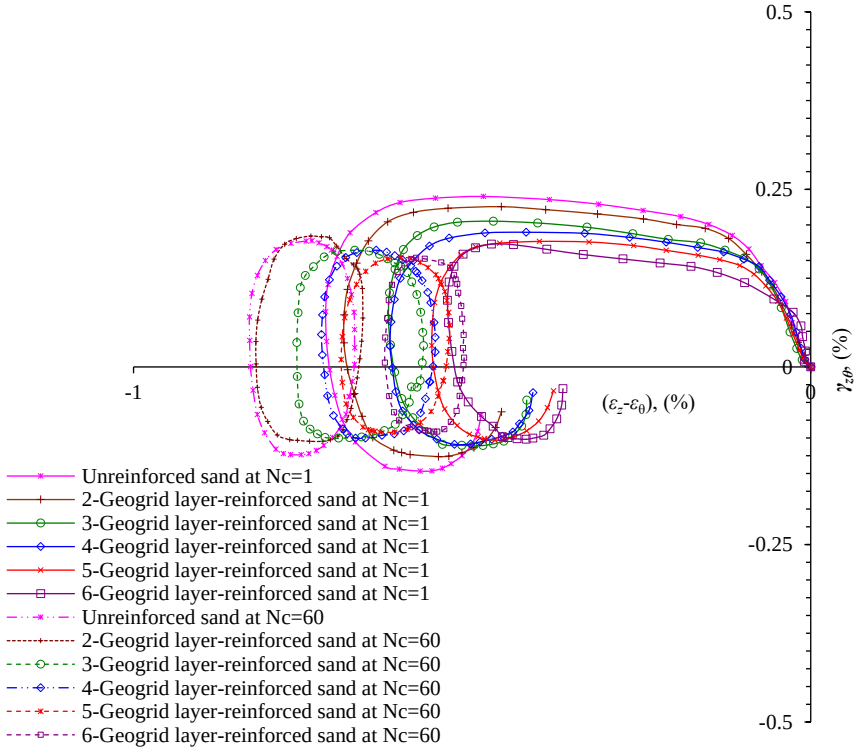

Figure 7.16 Comparisons of the strain paths in deviator strain space of the first and 60th cycles in unreinforced sand and sand reinforced with various numbers of geogrid layers

Although the aim of these tests was to study the anisotropic deformation and dynamic properties of reinforced sand as a composite material subjected to cyclic rotation of the principal stress direction, an attempt has been made to investigate the mobilised stress of the reinforcement. However, measuring the deformation of reinforcement inside a triaxial apparatus is very complex, and only Chandrasekaran et al. (1989), Nguyen et al. (2013) and Liu et al. (2014) have tried to do so. We followed a method similar to Nguyen et al. (2013) to compute the mobilised stress in reinforcement, which depends on measuring the plastic deformation that can be induced in it. During the tests, significant amounts of strains were induced in the reinforced samples (acting as composite materials), as previously presented. However, even after 60 cycles of rotation (by the end of the test), the residual deformation (residual strain) occurring in the geogrid reinforcement is negligible and, thus, we could not compute the mobilized stress of the reinforcement. This negligible residual strain can be attributed to the nature of soil that deformed easily compared to geogrid reinforcement. It can also be attributed to the nature of the cyclic testing conducted to investigate the induced strain of reinforced sand *en masse* (as a composite material) under continuous rotation of principal stress direction while the deviator stress was kept constant. In other words, constant deviator stress results in a slight amount of plastic strain in the reinforcement that is too small to measure. This means that only elastic strain can be mobilised in the reinforcement, which then returns to its original state a certain number of cycles after loading is removed.

7.4 Shear Modulus and Damping Ratio of Sand and Geogrid-reinforced Sand Subjected to Cyclic Rotation of Principal Stress Direction

Shear modulus (G) is defined as the secant slope connecting the extreme points on a hysteresis loop (Maheshwari, Kale, & Kaynia, 2012). Figure 7.17 shows that the hysteresis loops incline toward vertical as the number of cycles increases. The largest incline occurs during the first few cycles and then decreases. Geogrid reinforcement results in a clear increase in the shear modulus, which, in the first cycle, increases from 22.2 MPa for unreinforced sand to 24.6, 27.1, 29, 31.4 and 32.1 MPa for sand reinforced with two, three, four, five and six layers of geogrid, respectively, as shown

in Figure 7.18. This means that reinforcement with two layers provides a slight increase in shear modulus of 10.8% compared with 22.1, 30.1, 41.4 and 44.5% for samples reinforced with three, four, five and six layers, respectively. This increase in shear modulus is linked to the restraint and confinement of the geogrid that eliminates induced shear strain.

The ratio of shear modulus G_n/G_1 is plotted in Figure 7.19. It is common practice to normalize G_n (obtained from subsequent cycles), by dividing it by G_1 (shear modulus during the first cycle). It is clear that the shear modulus ratio G_n/G_1 of unreinforced sand increases by approximately 6.5% during the second cycle, by 10.6% during the 5^{th} cycle, and then has a lesser rate of increase, reaching approximately by 17.8% and 23.2% after 30 and 60 cycles, respectively. This agrees with the studies of Yan et al. (2015) and Tong et al. (2010) and can be explained by the densification that occurs in the sand during cyclic rotation and also by its shear history, as mentioned in Section 7.2.

The shear modulus of reinforced sand exhibited a similar trend, i.e., the shear modulus clearly increases over the first few cycles and then increases at a lower, stable rate over subsequent cycles. After 60 cycles, the shear modulus of sand reinforced with two, three, four, five and six layers of geogrid increased by 22.0, 18.2, 15.3, 15.2 and 13.4%, respectively, relative to the first cycle (Figure 7.19). Although the rate of increase in the shear modulus of clean sand with increasing numbers of cycles was less than that of reinforced sand, the value of the latter was still larger. For example, the shear modulus for six layer-reinforced sand was 32.1 MPa at the first cycle and increased by 13.4% to 36.4 MPa after 60 cycles, compared with 22.19 and 27.11 MPa for unreinforced sand at the first and 60^{th} cycles, respectively (a 23.2% increase).

The damping ratio (λ) refers to the energy dissipated by soil during cyclic loading (Chen et al., 2016), and can be calculated directly from each hysteresis loop of the shear strain-shear stress relationship (as shown in Figure 2.17 in Chapter 2) using the following equation:

$$\lambda = \Delta W / 4\pi W \tag{7.1}$$

where ΔW represents the energy dissipated in a single cycle while W is the largest strain energy stored during that cycle (Zhang, Andrus, & Juang, 2005).

It was found that the damping ratio λ calculated at the first cycle remained constant at about 31% and did not change significantly, in both unreinforced and reinforced sands (Figure 7.18). This insignificant variation is related to the fact that the damping ratio of soil is a function of the loading velocity represented by the frequency of cyclic loading (Naeini & Gholampoor, 2014; Ravishankar et al., 2005). In this study, the frequency of cyclic rotation was constant, and thus, the variation in damping ratio λ was very slight. This is consistent with the report of Naeini and Gholampoor (2014). However, with increasing numbers of cycles, the damping ratio tended to decrease. For example, the λ of unreinforced sand decreased from 31.1% during the first cycle to 27.6% after 60 cycles, whereas for six-layer geogrid-reinforced sand, it decreased slightly from 31.2% to 29.7% (Figure 7.20). This decrease is linked to the densification that occurs due to cyclic rotation, where the void ratio decreases with increasing cycles and dissipates lower amounts of energy during the cyclic rotation. This is in agreement with the results reported by Uthayakumar (1992) and Kirar and Maheshwari (2013), who demonstrated that decreases in damping ratio and increases in shear modulus are related to increases in density.

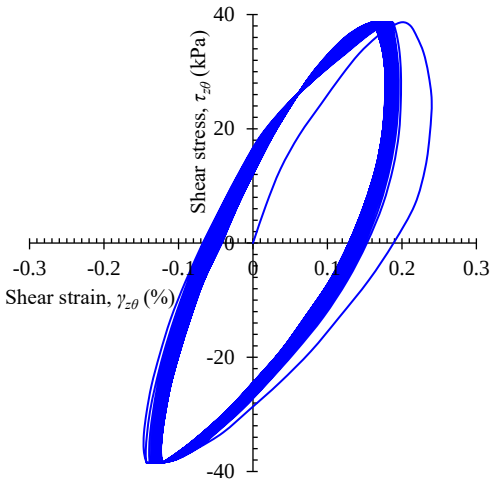

(a) Unreinforced sand

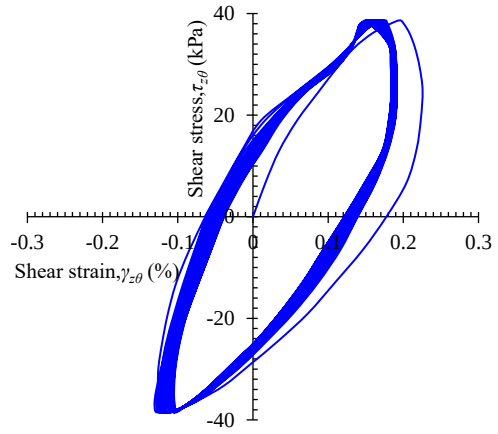

(b) 2-Geogrid layer-reinforced sand

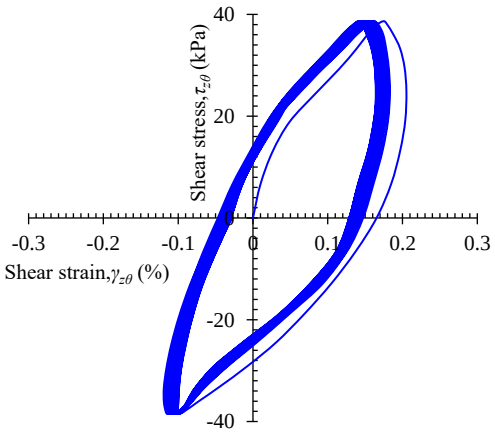

(c) 3-Geogrid layer-reinforced sand

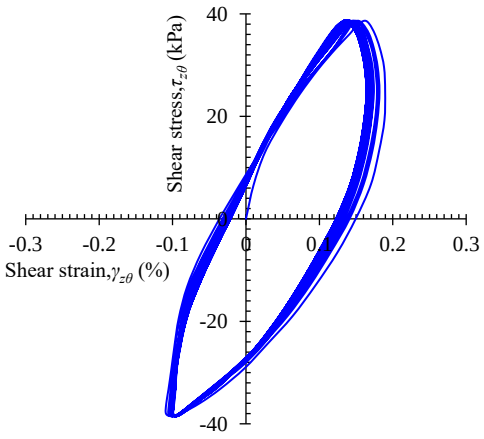

(d) 4-geogrid layer-reinforced sand

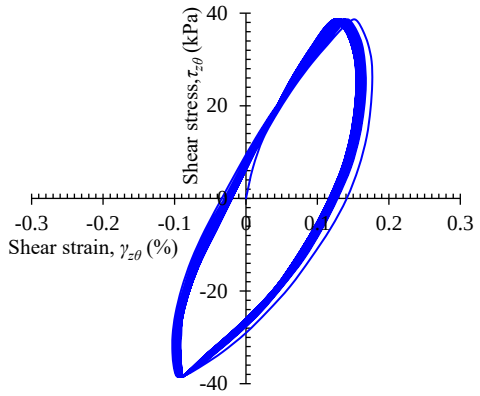

(e) 5-geogrid layer-reinforced sand

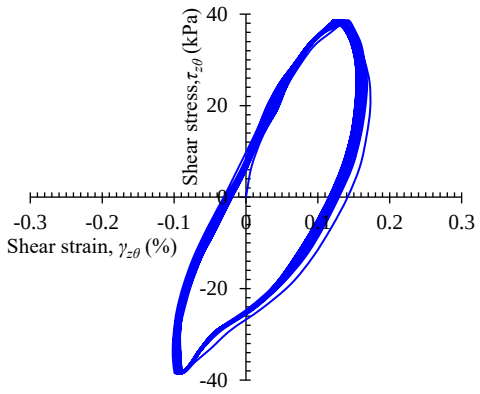

(f) 6-Geogrid layer-reinforced sand

Figure 7.17 Hysteretic shear stress-strain relationships for sand reinforced with different numbers of geogrid layers

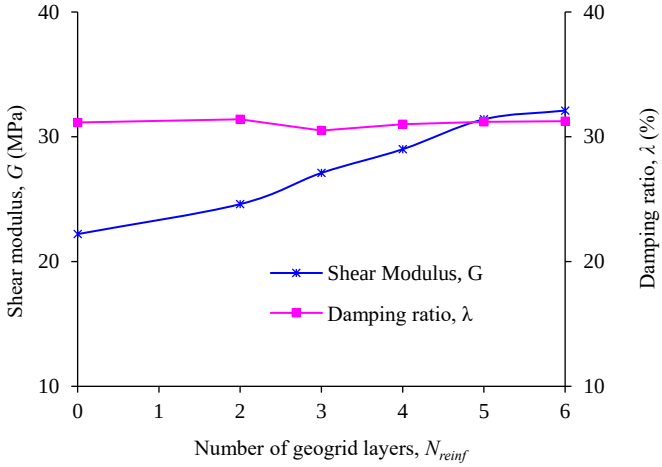

Figure 7.18 Variations of shear modulus G and damping ratio λ at the first cycle with various numbers of geogrid layers (under q/p'= 0.69)

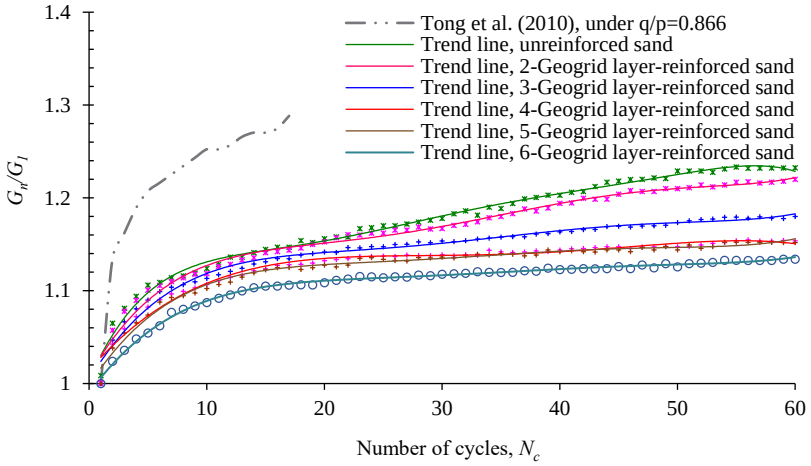

Figure 7.19 Variations in the shear modulus ratio (G_n/G_1) of unreinforced and reinforced sands under cyclic rotation of the principal stress direction (under q/p'= 0.69)

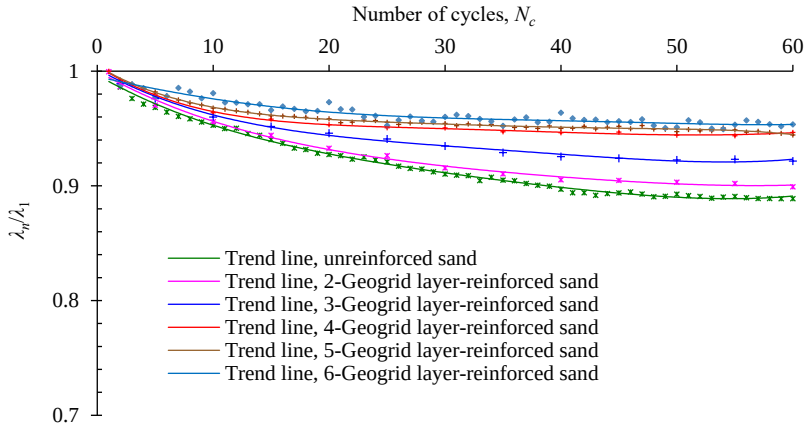

Figure 7.20 Variations in the normalised damping ratio (λ_n/λ_1) of unreinforced and reinforced sands under cyclic rotation of the principal stress direction (under q/p'= 0.69)

7.5 Effect of Varying the Stress Ratio *q/p′* on the Characterisation of Sand and Geogrid-reinforced Sand under Cyclic Rotation

In this section, the effect of cyclic rotation under different stress ratios *q/p′* of 0.69, 0.9 and 1.1 on the characterisation of sand and sand reinforced with three and six layers of geogrid will be presented. Figures 7.21-7.26 show the typical variation of deviator stress *q*, mean effective stress *p′*, direction of principal stress *α*, components and principals of the applied stresses, and the stress path during cyclic rotation tests considering *q/p′* = 0.9 and 1.1, noting that the stress variation of tests under *q/p′* = 0.69 was presented previously in Section 7.2 and Figures 7.1-7.3.

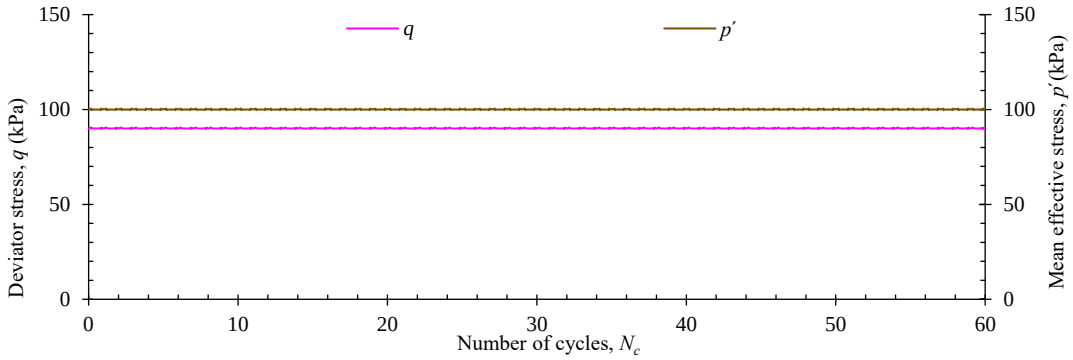

(a)

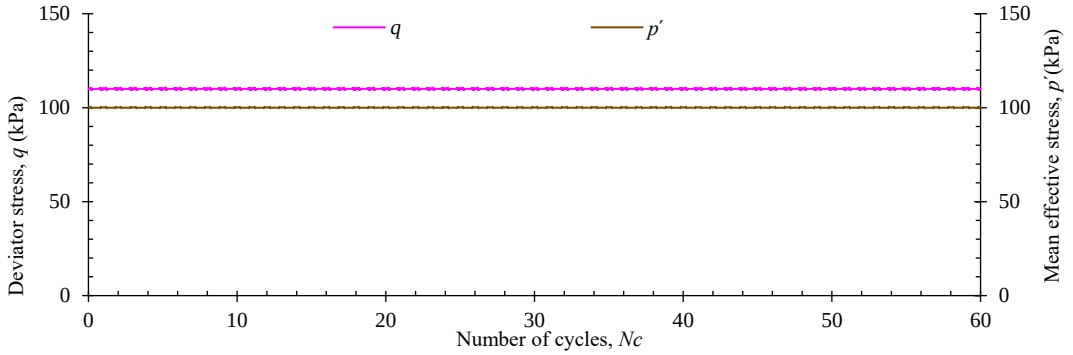

(b)

Figure 7.21 Typical variation of deviator stress *q* and mean effective stress *p′* under (a) *q/p′* = 0.9 and (b) *q/p′* = 1.1

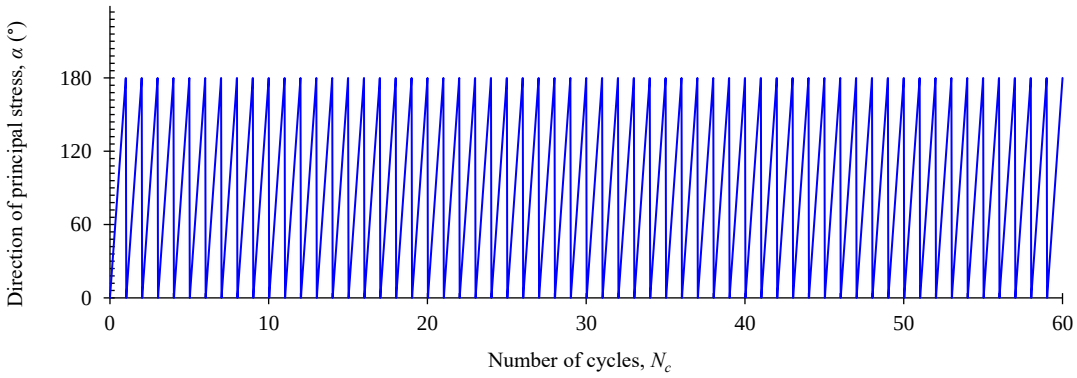

(a)

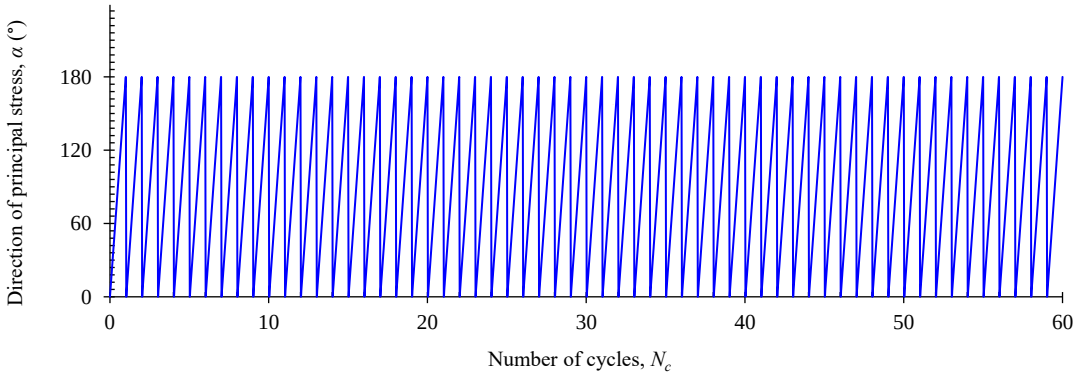

(b)

Figure 7.22 Typical variation of the direction of principal stress α during 60 cycles of rotational shear under (a) q/p' = 0.9 and (b) q/p' = 1.1

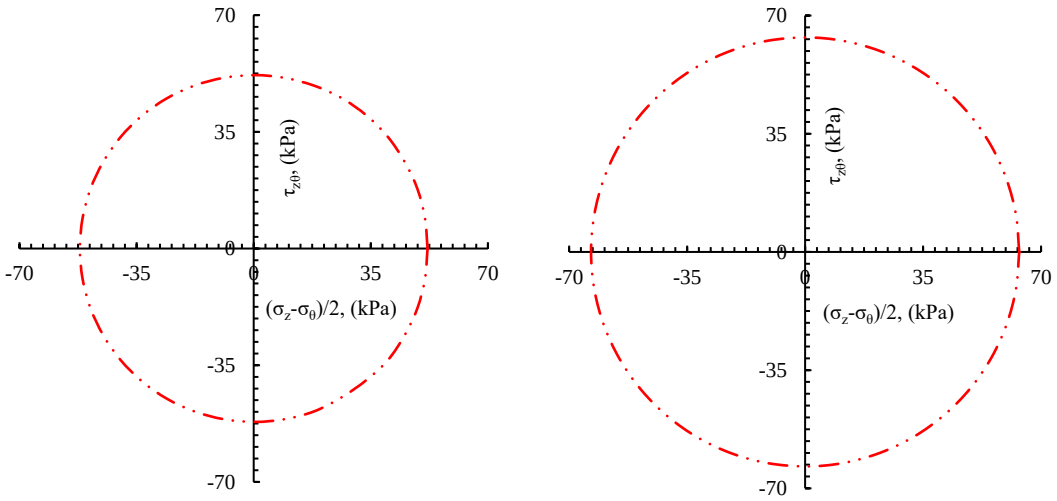

(a) (b)

Figure 7.23 Typical stress path obtained from cyclic rotation testing under (a) q/p' = 0.9 and (b) q/p' = 1.1

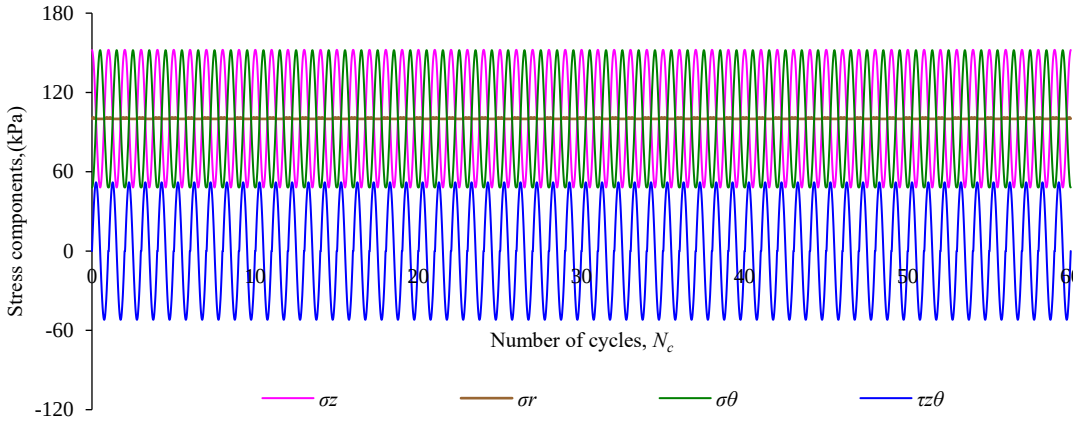

(a)

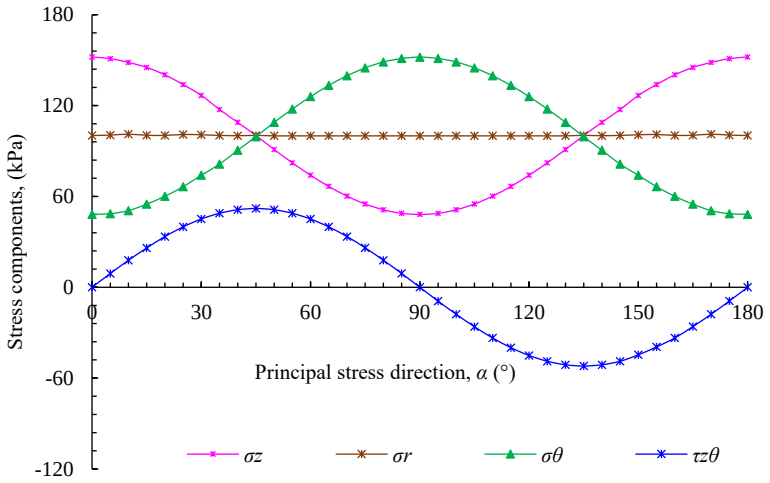

(b)

Figure 7.24 Variation of stress components (σ_z, σ_r, σ_θ and $\tau_{z\theta}$) under $q/p' = 0.9$ in rotational shear (a) over 60 cycles; (b) along the direction of principal stress α during the first cycle

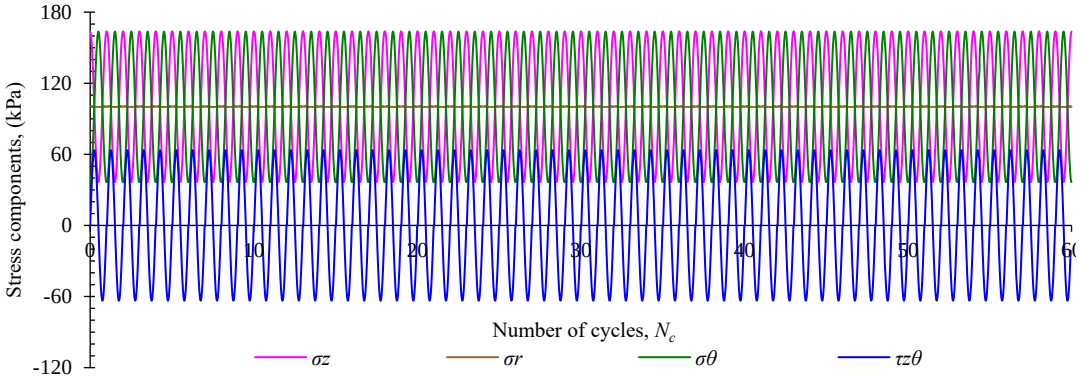

(a)

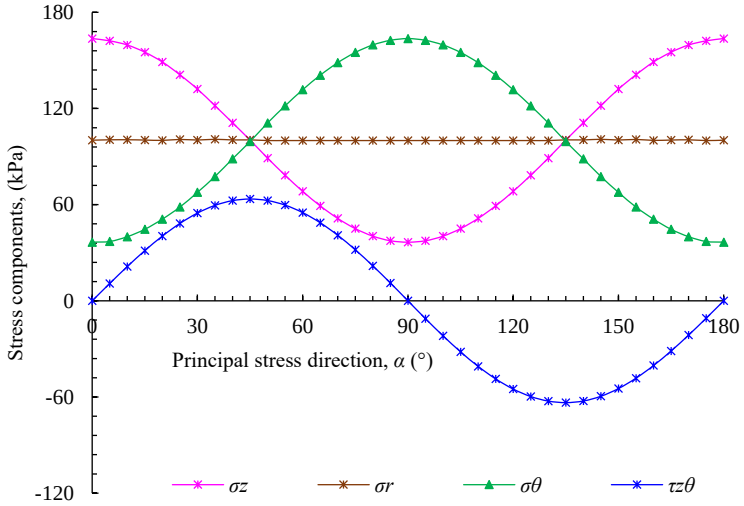

(b)

Figure 7.25 Variation of stress components (σ_z, σ_r, σ_θ and $\tau_{z\theta}$) under q/p' = 1.1 in rotational shear (a) over 60 cycles; (b) along the direction of principal stress α during the first cycle

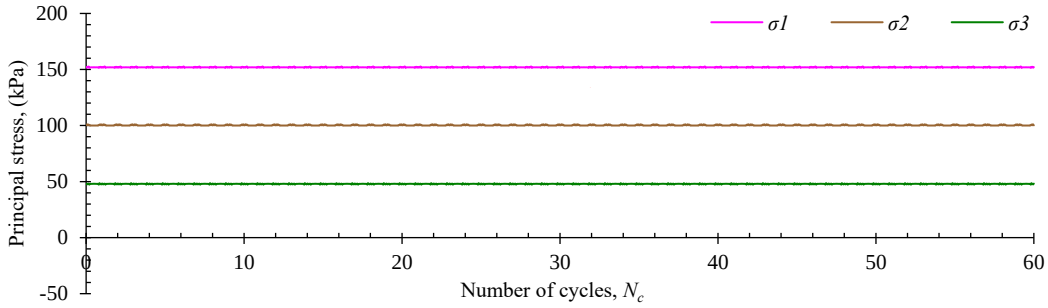

(a)

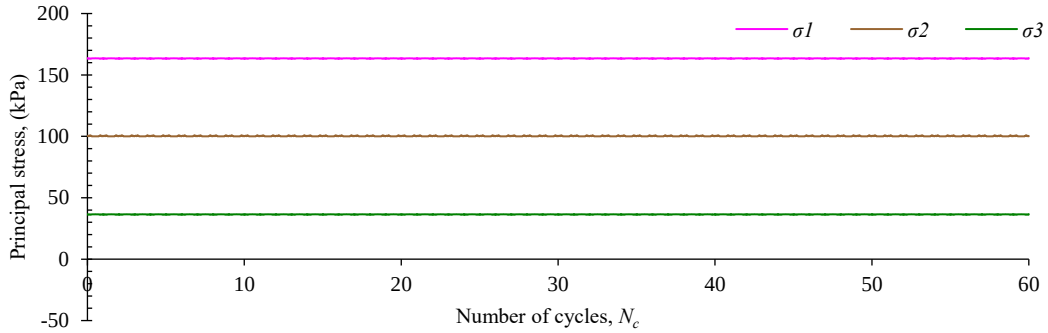

(b)

Figure 7.26 Variation of principal stresses (major σ_1, intermediate σ_2 and minor σ_3 stresses) along 60 cycles in rotational shear under (a) q/p' = 0.9 and (b) q/p' = 1.1

Dramatic strains were induced in the unreinforced sand during the first cycle under q/p' = 0.9 and 1.1, resulting in failure of the sample at α = 50°, as shown in Figure 7.27. Sand reinforced with three layers of geogrid also failed at α = 60° under both of the stress ratios (Figure 7.28). However, six-geogrid layer-reinforced sand clearly sustained the 60 cycles of the rotation under all of the three considered cyclic ratios (q/p' = 0.69, 0.9 and 1.1), although with considerable induced strains. In general, the trends of strain variation along the direction of principal stress were similar for all values of the cyclic stress ratio. The axial strain ε_z was induced in an expansive form (- sign) while both the radial ε_r and circumferential ε_θ strains were induced as contractive (+ sign). Figures 7.29 and 7.30 show the variations of the strain components under q/p' = 0.9 and 1.1, respectively. Note that the results for reinforced sand under q/p' = 0.69 were presented in Section 7.3.

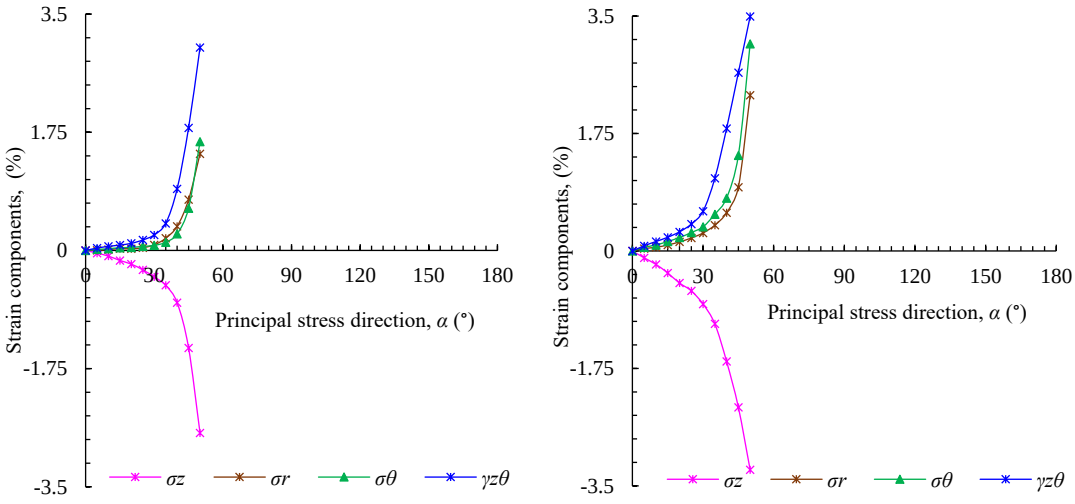

(a) (b)

Figure 7.27 Variation of the developed strain components (axial ε_z, radial ε_r, circumferential ε_θ and shear strains $\gamma_{z\theta}$) of unreinforced sand under (a) q/p' = 0.9 and (b) q/p' = 1.1

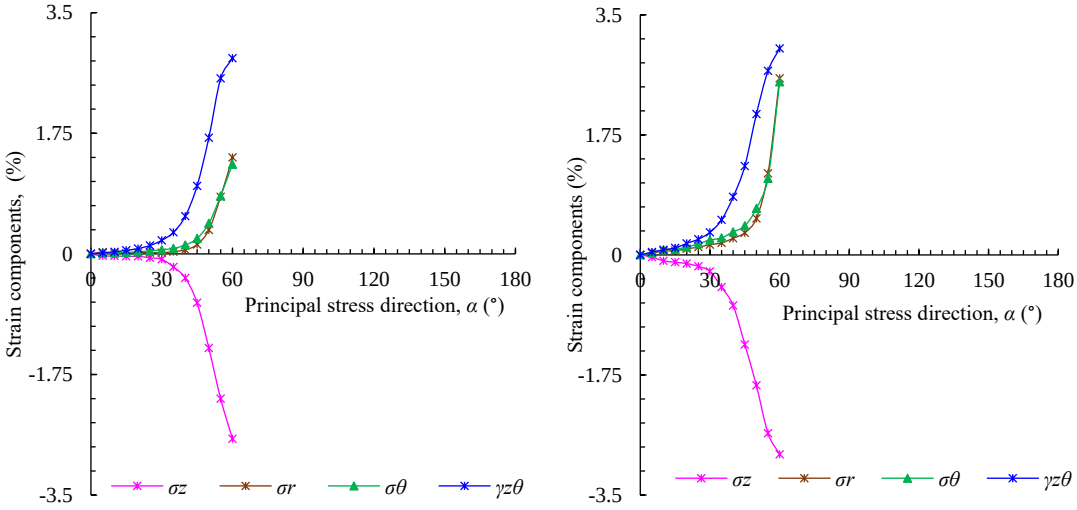

(a) (b)

Figure 7.28 Variation of the developed strain components (axial ε_z, radial ε_r, circumferential ε_θ and shear strains $\gamma_{z\theta}$) of sand reinforced with three geogrid layers under (a) q/p' = 0.9 and (b) q/p' = 1.1

Regarding axial strain ε_z, increasing the stress ratio q/p' from 0.69 to 0.9 and then 1.1 resulted in increases in the maximum axial strain ε_z during the first cycle, from 0.34 to 1.42 and 2.3%, respectively. During the first cycle, the maximum axial strain occurred at α = 107.5° under a stress ratio q/p' of 0.69, while it occurred slightly earlier at 105.5° and 100° for q/p' = 0.9 and 1.1, respectively. After that, axial strain decreased but did not return to zero at the end of the first cycle, i.e. at α = 180°. Both of the radial ε_r and circumferential ε_θ strains accumulated at a slight rate until α reached 30° for q/p' = 0.9 and 1.1, compared with 60° for q/p' = 0.69. Then, they increased dramatically to maximum values, which occurred at α values similar to those where the maximum ε_z values occurred. As q/p' increased from 0.69 to 1.1, maximum radial strain increased from 0.13 to 0.70%, while maximum circumferential strain increased from 0.22 to 1.65%. Radial and circumferential strains started decreasing from their maximum values as α increased, but did not reach zero at the end of the first cycle, indicating the occurrence of plastic strains. Regarding shear strain $\gamma_{z\theta}$, its maximum value occurred at α = 65–75° under all cyclic stress ratios. The amplitude of shear strain $\gamma_{z\theta}$ at the first cycle increased from 0.26 to 1.61 and then 2.22% as q/p' increased from 0.69 to 0.9 and then 1.1, respectively.

At the end of the first cycle, all strains were irrecoverable although the applied stresses returned to their initial values, indicating plastic occurrence. As the stress ratio q/p' increased, the amounts of plastic axial, circumferential and radial strains and shear increased. The induced plastic strains and the effect of q/p' on them can also be observed in the strain paths of geogrid-reinforced sand shown in Figure 7.15e (in Section 7.3 for sand reinforced with six layers of geogrid under q/p' = 0.69) and Figure 7.31 (for sand reinforced with six layers of geogrid under q/p' = 0.9 and 1.1). A comparison between strain paths, at the first cycle, of geogrid-reinforced sand tested under different values of q/p' is shown in Figure 7.32. It can be observed that as q/p' increased, the gap between the beginning of the path and its end became larger where (ε_z - ε_θ) increased from -0.37 to -1.273% as q/p' increased from 0.69 to 1.1.

It can also be observed that at the first few cycles under q/p' = 0.9 and 1.1, there was significant induced axial strain in the form of expansion and, after that, this strain

decreased with further rotation of α. This is linked to the densification that occurs in sand, and also to the high interaction between the dense sand and the geogrid. Moreover, planar reinforcements can become curved under loading and, thus, provide better performance against horizontal loading during subsequent cycles. A similar trend was also observed regarding shear strain.

At the 60th cycle (Figures 7.29c-7.30c), the variation in all strains, i.e. ε_z, ε_θ and ε_r, along α became very small under all stress ratios q/p' compared with those that occurred during the first cycle. This means that at this advanced stage of cycling, most strains were plastic without significant elasticity, which led to the observed variations during the first few cycles. Regarding shear strain $\gamma_{z\theta}$, its amplitude decreased significantly with increasing numbers of cycles for all values of q/p', but it remained clearly present. For example, $\gamma_{z\theta}$ of sand reinforced with six layers of geogrid (under q/p' = 1.1) changed cyclically along α from 1.51 to -0.71% at N_c = 1, compared with variation from 0.33 to -0.24% when N_c = 60.

Volumetric strain ε_v in sand reinforced with six layers of geogrid accumulated significantly with increases in q/p', as shown in Figure 7.33. At the end of the first cycle (N_c = 1), ε_v increased from 0.02 to 0.07 and then 0.15% as q/p' increased from 0.69 to 0.9 and then 1.1, respectively. After thirty cycles (N_c = 30), ε_v increased from 0.26 to 0.58 and then 1.08%, respectively. Under q/p' = 0.69, the amplitude of volumetric strain ε_v, i.e. the oscillation of ε_v along α, was small and decreased with increasing numbers of rotation cycles. It was 0.018 and 0.01% at N_c = 30 and 60, respectively. However, with increases of q/p' to 1.1, there was a clear increase in the amplitude to 0.068% at N_c = 30, and this amplitude remained almost same even at the 60th cycle. Irrespective of the value of the stress ratio, q/p', most of the volumetric strain occurred during the first few cycles, where about 40% of the total volumetric strain ε_v accumulated after 10 cycles.

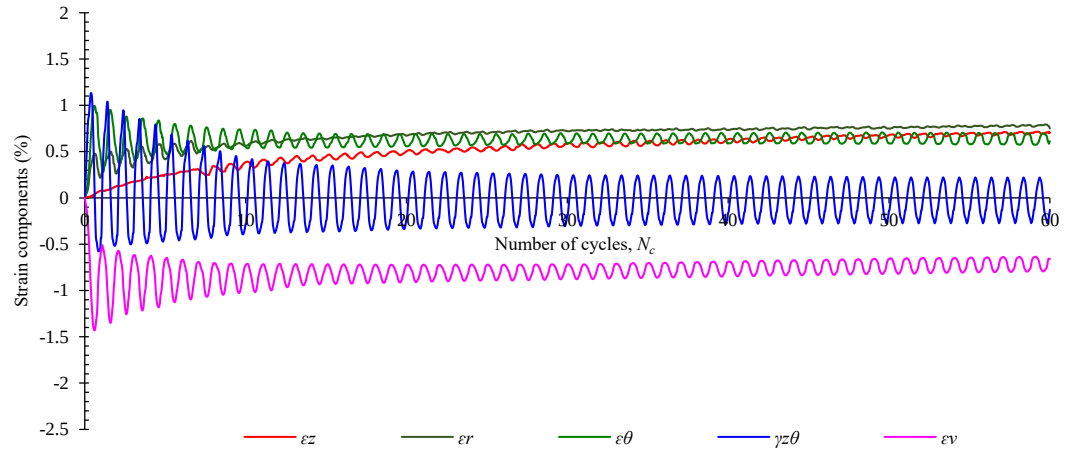

(a)

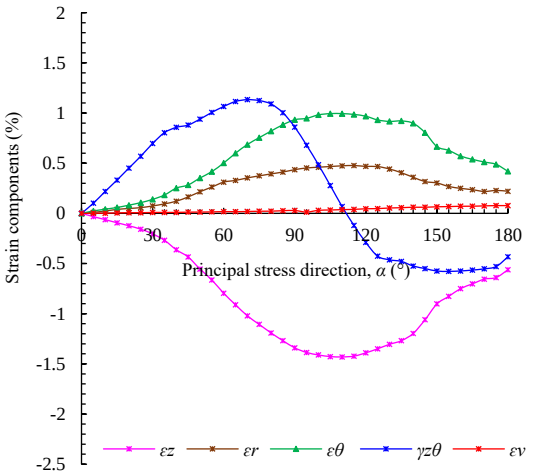

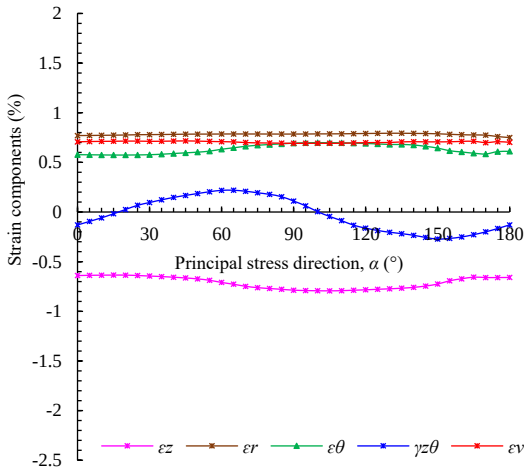

(b) (c)

Figure 7.29 Variation of strain components in 6-geogrid layer-reinforced sand under $q/p' = 0.9$ (ε_z, ε_r, ε_θ, $\gamma_{z\theta}$ and ε_v) in rotational shear (a) over 60 cycles; (b) along the direction of principal stress α during the first cycle; and (c) along the direction of principal stress α during the 60th cycle

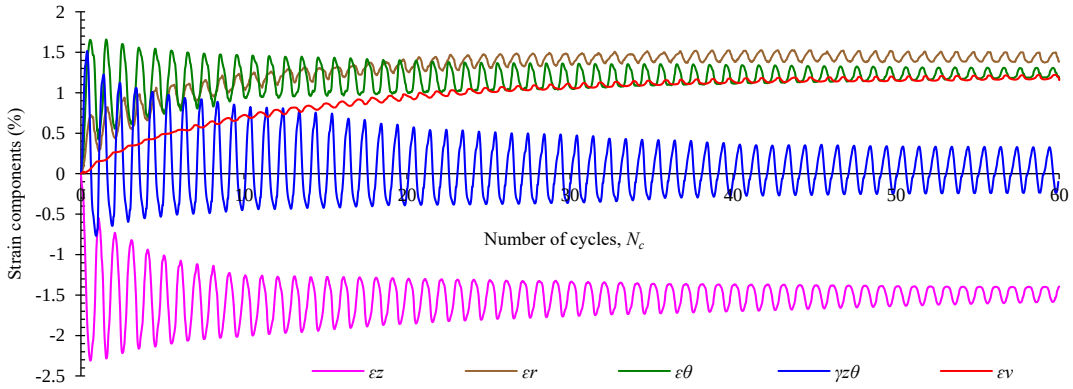

(a)

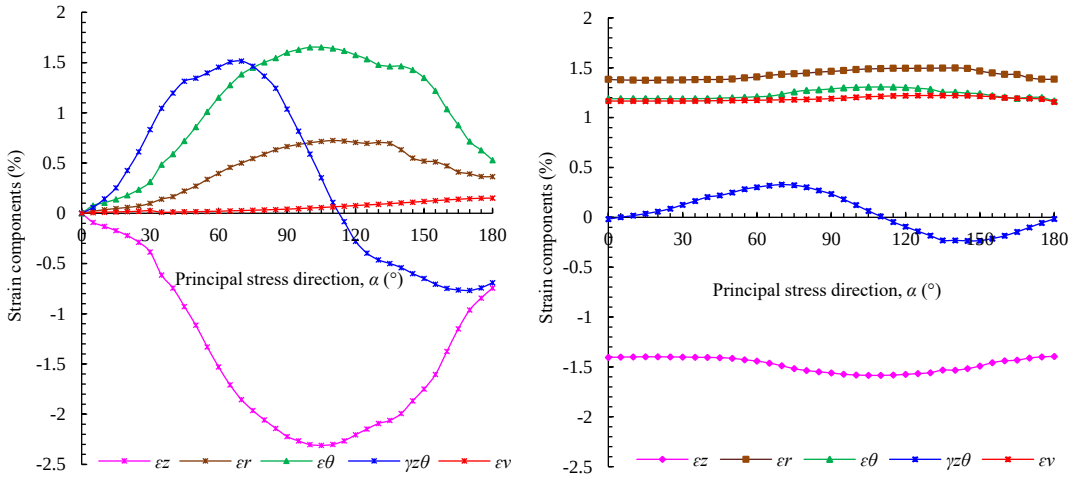

(b) (c)

Figure 7.30 Variation of strain components of 6-geogrid layer-reinforced sand under $q/p' = 1.1$ (ε_z, ε_r, ε_θ, $\gamma_{z\theta}$ and ε_v) in rotational shear (a) during 60 cycles; (b) along the direction of principal stress α during the first cycle; and (c) along the direction of principal stress α during the 60th cycle

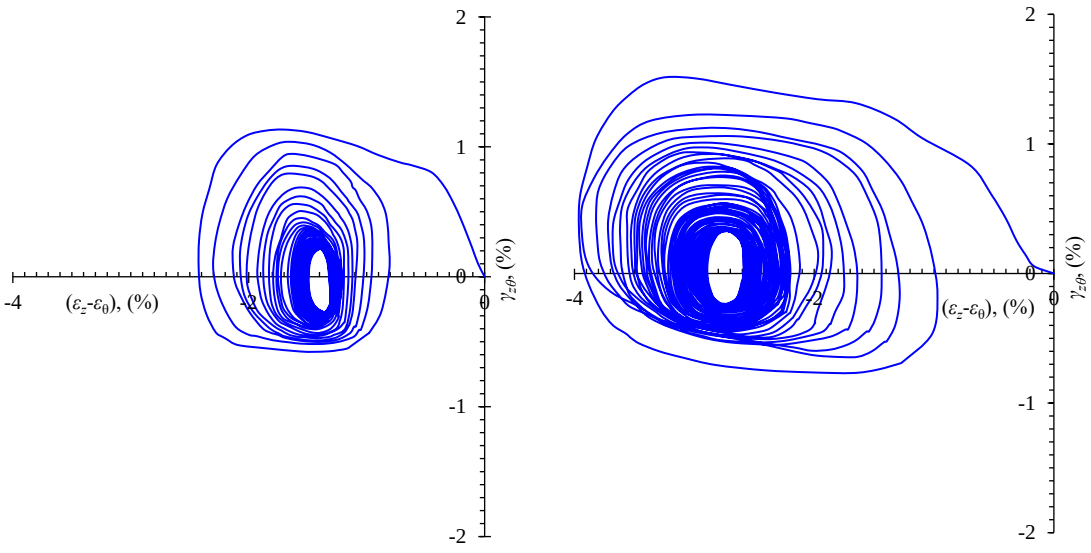

(a) (b)

Figure 7.31 Strain paths of sand reinforced with 6 layers of geogrid in the deviator strain space under (a) q/p' = 0.9 and (b) q/p' = 1.1

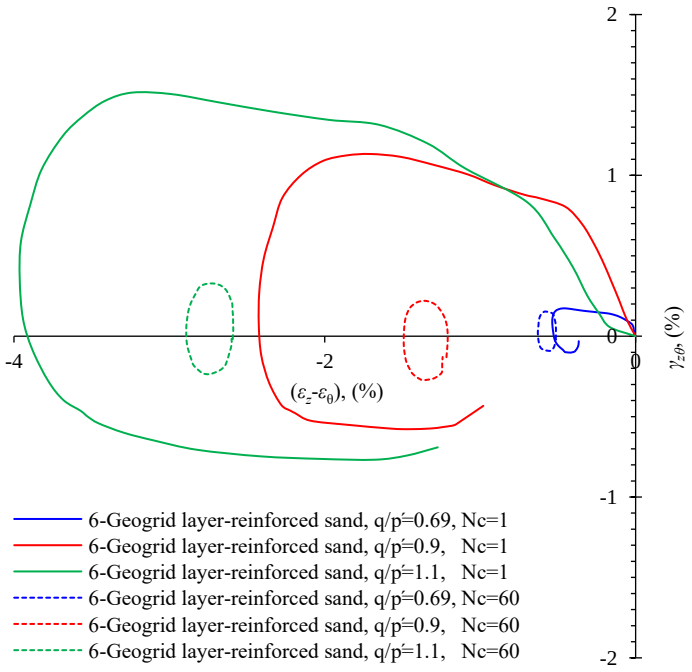

Figure 7.32 Comparisons of the strain paths of sand reinforced with six layers of geogrid in the deviatoric strain space of the first and 60th cycles under stress ratios q/p' = 0.69, 0.9 and 1.1

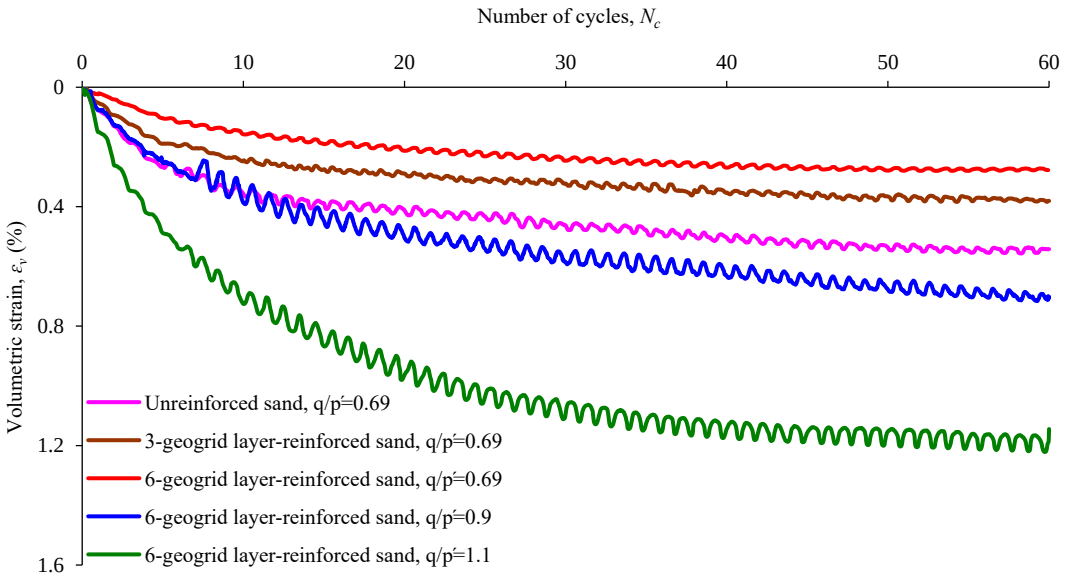

Figure 7.33 Variation in the volumetric strain ε_v of sand and reinforced sand (three and six layers of geogrid) in rotational shear over 60 cycles and under different stress ratios

Regarding the effect of q/p' on the dynamic characterisation of six-geogrid layer-reinforced sand under cyclic rotation of principal stress, the hysteretic shear stress-strain relationships are plotted in Figure 7.34 (for cyclic rotation under q/p' = 0.9 and 1.1) and also in Figure 7.17f (in Section 7.4 for cyclic rotation under q/p' = 0.69). The shear moduli computed at N_c = 1 under q/p' = 0.9 and 1.1 were small compared to that when q/p' = 0.69, as shown in Figure 7.35. This is related to the largest shear strain induced, which corresponded to the much larger stress ratio. However, increasing the number of rotation cycles increased the shear modulus, as shown in Figure 7.36, which illustrates the ratio of G_n/G_1. This ratio was larger, in general, for larger stress ratios q/p'(Figure 7.36) due to the densification that occurs under such large applied stresses. On the other hand, the damping ratio increased only by 10–13.4% as q/p' increased from 0.69 to 0.9–1.1 (Figure 7.35). This increase is related to the largest deformation that occurred initially and resulted in a disturbed sand state. As N_c increased, λ_n/λ_1 for all values of q/p' decreased slightly (Figure 7.37).

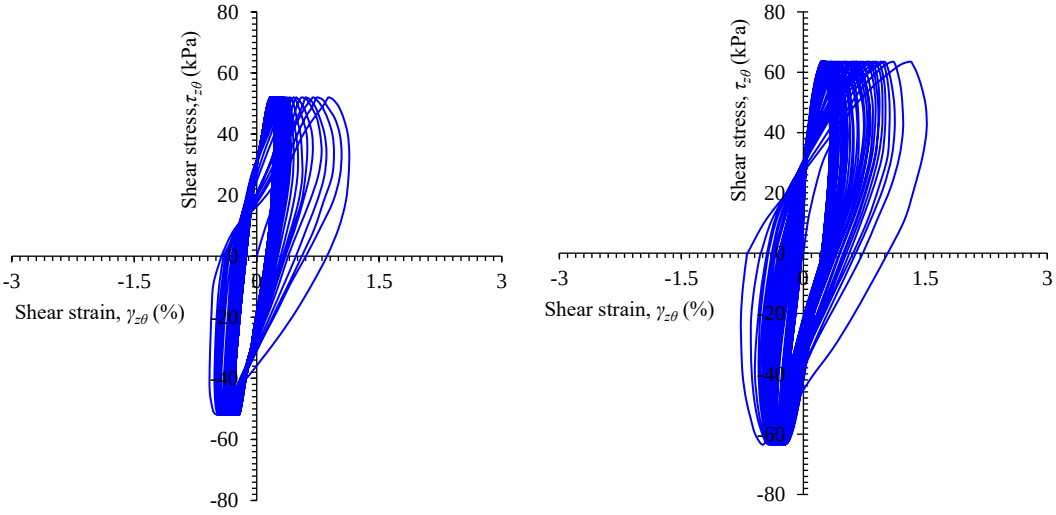

(a) (b)

Figure 7.34 Hysteretic shear stress-strain relationships for sand reinforced with six layers of geogrid under (a) q/p' = 0.9 and (b) q/p' = 1.1

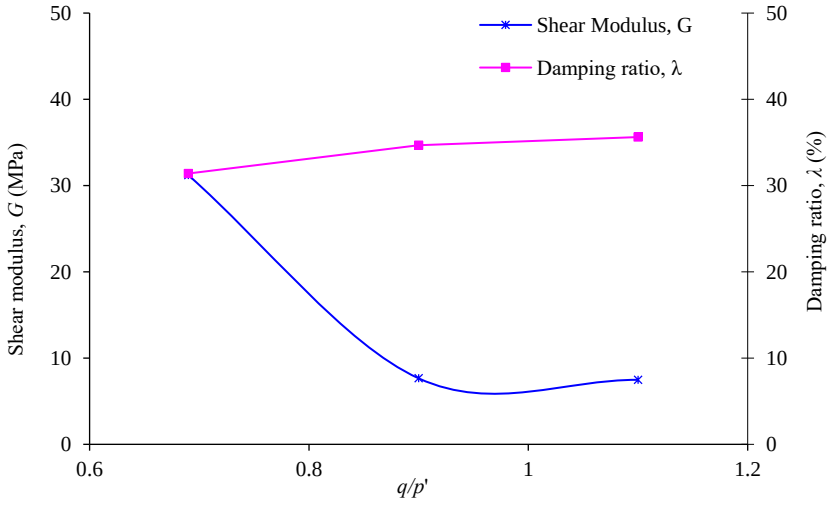

Figure 7.35 Variations of shear modulus and damping ratio of sand reinforced with six layers of geogrid at the first cycle N_c against stress ratio q/p'

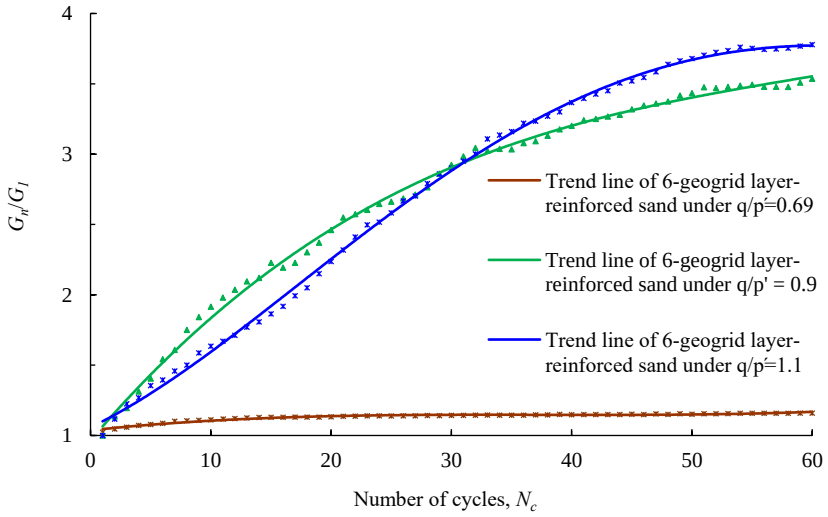

Figure 7.36 Variations in the ratio of shear modulus (G_n/G_1) of 6-geogrid layer-reinforced sand under different stress ratios q/p'

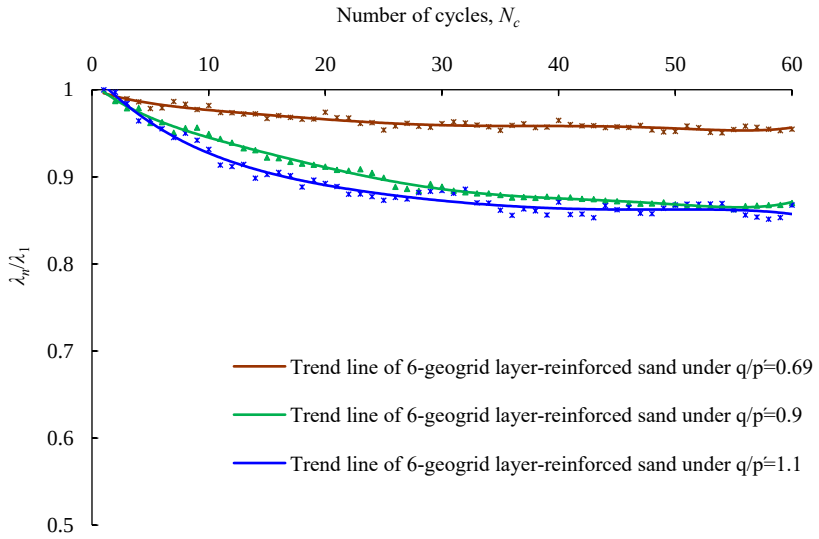

Figure 7.37 Variations in the normalised damping ratio (λ_n/λ_1) of 6-geogrid layer-reinforced sand under different stress ratios q/p'

7.6 Response of Sand Reinforced with Nonwoven Geotextile and Geocell to Cyclic Rotation of Principal Stress Direction

In this section, the effect of cyclic rotation, with a q/p' value of 1.1, on the characterisation of sand reinforced with six layers of nonwoven geotextile and geocell will be presented. These results will be compared with those of six-geogrid layer-reinforcement under $q/p' = 1.1$, which were presented in Section 7.5.

Figures 7.38 and 7.39 show the variation of induced strains in nonwoven geotextile- and geocell-reinforced sand under cyclic rotation q/p' of 1.1. Geocell and nonwoven geotextile exhibited smaller strains compared with those of geogrid. The axial strain ε_z of geocell- and geotextile-reinforced sand at the first cycle was approximately 1.6%, compared with 2.3% for geogrid-reinforced samples. At 60 cycles of rotation, the axial strain of geocell-reinforced sand decreased to 0.94%, while it was 1.0 and 1.58% when geotextile and geogrid were used, respectively. After that, the rate of decrease became slight. Furthermore, the amplitude of axial strain for all geo-inclusion types (geogrid, geotextile and geocell) decreased significantly with increasing numbers of cycles.

The radial strain ε_r in geotextile and geocell reinforced sand at the first cycle was approximately similar to that when geogrid was used (0.70–0.74%), while with increases in N_c to 60, the ε_r of geogrid-reinforced sand accumulated to 1.49%, compared with 1.2 and 0.77% for geotextile and geocell reinforced sand respectively. The circumferential strain ε_θ of geocell- and geotextile-reinforced sand at the first cycle was approximately 0.93%, compared with 1.65% for geogrid-reinforced samples. After 60 cycles of rotation, ε_θ was 0.77, 1.0 and 1.31 for geocell, geotextile and geogrid respectively.

The shear strain $\gamma_{z\theta}$ for the three types of geo-inclusions varied from positive to negative values, and its amplitudes decreased with increasing numbers of cycles of rotation. For example, during the first cycle, the shear strain amplitudes of geogrid, nonwoven geotextile and geocell were 2.22, 1.75 and 1.64% respectively, indicating that geogrid induced the largest amount of shear strain. The smaller induced shear strain of geocell resulted in a larger shear modulus (which will be discussed later), where the hysteretic shear stress-strain relationships of reinforced sand indicated that

the loops tended to converge when geocell, but not planar, reinforcement was used. As the number of cycles increased, however, these amplitudes decreased to approximately similar strains of 0.57%.

Sand reinforced with different geo-inclusions exhibited plastic strain, particularly at the first few cycles, as shown in Figures 7.38 and 7.39. Moreover, the strain paths (Figure 7.40 for geotextile and geocell reinforced sand and Figure 7.31b in Section 7.5 for geogrid-reinforced sand) indicated that all reinforcement types had similar plastic strains, as represented by the open part of the hysteretic loops in the first cycle. However, during subsequent cycles, the strain path ended at almost the same point as its beginning, indicating that insignificant plastic strain was induced during later cycles and most of it accumulated during the first few cycles. Figure 7.41 shows a comparison of strain paths in the deviatoric strain space of the 1st and 60th cycles of sand reinforced with different geo-inclusions. It can be observed that the strain paths of geotextile-and geocell-reinforced sand at the first cycle were close to each other, with a plastic strain, i.e. (ε_z - ε_θ), of 0.76%, while that of geogrid-reinforced sand was wider and characterised by a larger plastic strain of 1.27%.

Figure 7.42 illustrates clear differences in the volumetric strain accumulated under cyclic rotation between the 2D geo-inclusions (geogrid and geotextile) and the 3D geocell. Geocell provided better performance in terms of decreasing volumetric change in reinforced sand, which accumulated to 0.61% after 60 cycles, compared with 1.1 and 1.21% for geotextile and geogrid samples, respectively. Similar to what was observed in the previous sections, most of the volumetric strain occurred during the first few cycles; approximate 37–42% of the total volumetric change was induced during the first ten cycles.

Figure 7.43 shows the hysteretic loops of the shear stress-strain relationships for sand reinforced with different geo-inclusions. Figure 7.44 shows a clear increase in the subsequent shear modulus of reinforced sand relative to that at the first cycle. Moreover, geogrid reinforcement resulted in a larger normalised shear modulus G_n/G_1, which was 3.8 at N_c = 60 compared with 3.3 and 2.9 for geotextile- and geocell-reinforced sand, respectively. This is a reflection of the larger strains accumulated in the geogrid-reinforced sand compared with other types, which resulted in densified

sand with increased interaction with the geogrid. However, the shear modulus of sand reinforced with geocell was still larger than that of sand reinforced with geogrid, even after 60 cycles, where it was 28.2, 29.3 and 31.1 MPa for geogrid-, geotextile- and geocell-reinforced sand, respectively. The damping ratio λ decreased at a small rate with increasing numbers of cycles of rotation. After 60 cycles, the damping ratio λ of sand reinforced with different geo-inclusions decreased by approximately 11.0–14.0% relative to the initial values at the first cycle (Figure 7.45). This decrease is linked to the densification that occurred in the samples during the cycles of rotation.

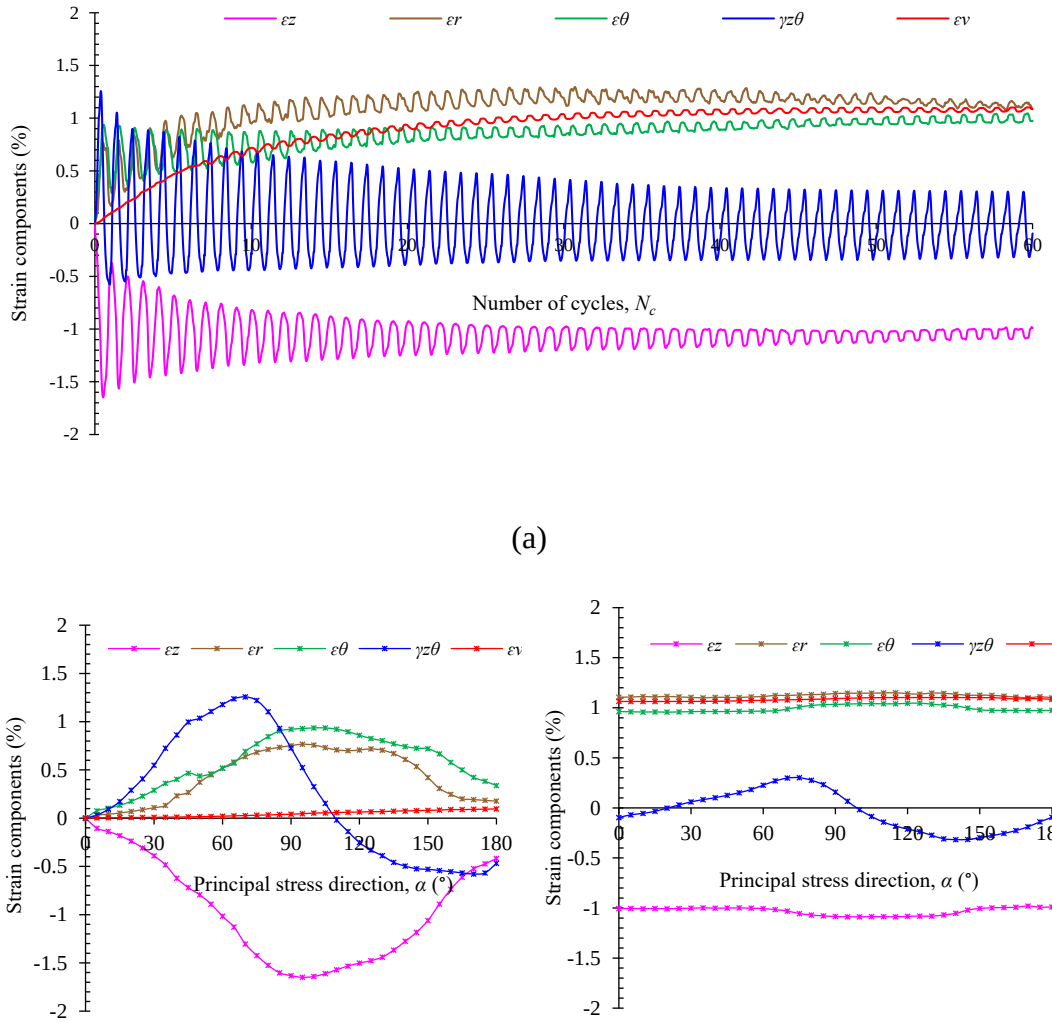

Figure 7.38 Variation of strain components in 6-layer nonwoven geotextile-reinforced sand under q/p' = 1.1 (ε_z, ε_r, ε_θ, $\gamma_{z\theta}$ and ε_v) in rotational shear: (a) over sixty cycles; (b) along the direction of principal stress α during the first cycle; and (c) along the direction of principal stress α during the 60th cycle

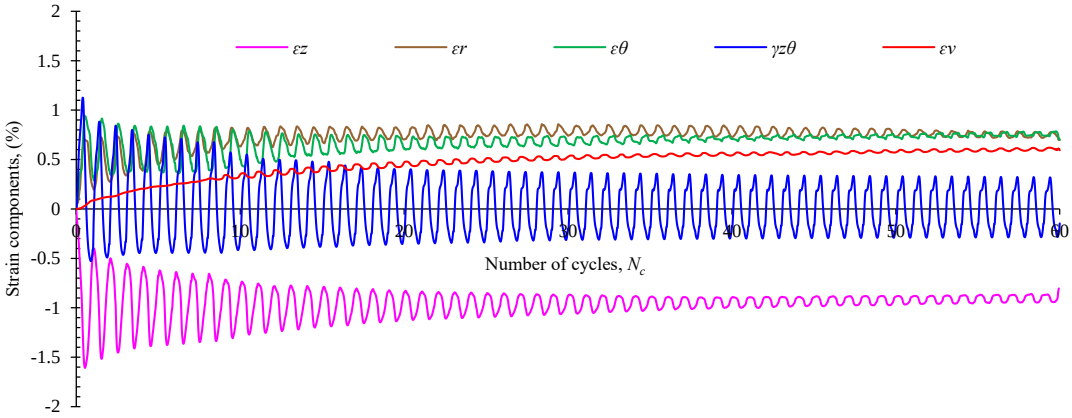

(a)

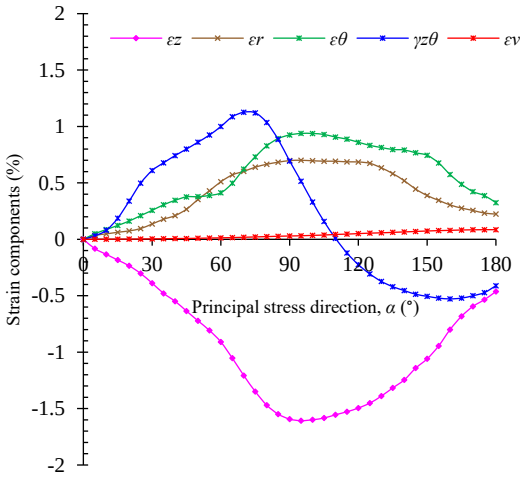

(b)

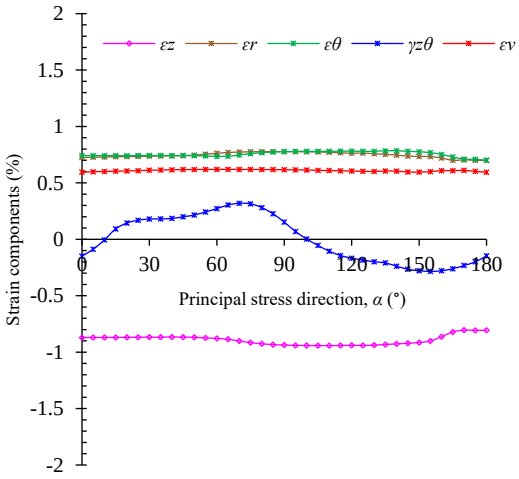

(c)

Figure 7.39 Variation of strain components of geocell-reinforced sand under q/p' = 1.1 (ε_z, ε_r, ε_θ, $\gamma_{z\theta}$ and ε_v) in rotational shear: (a) over 60 cycles; (b) along the direction of principal stress α during the first cycle; and (c) along the direction of principal stress α during the 60th cycle

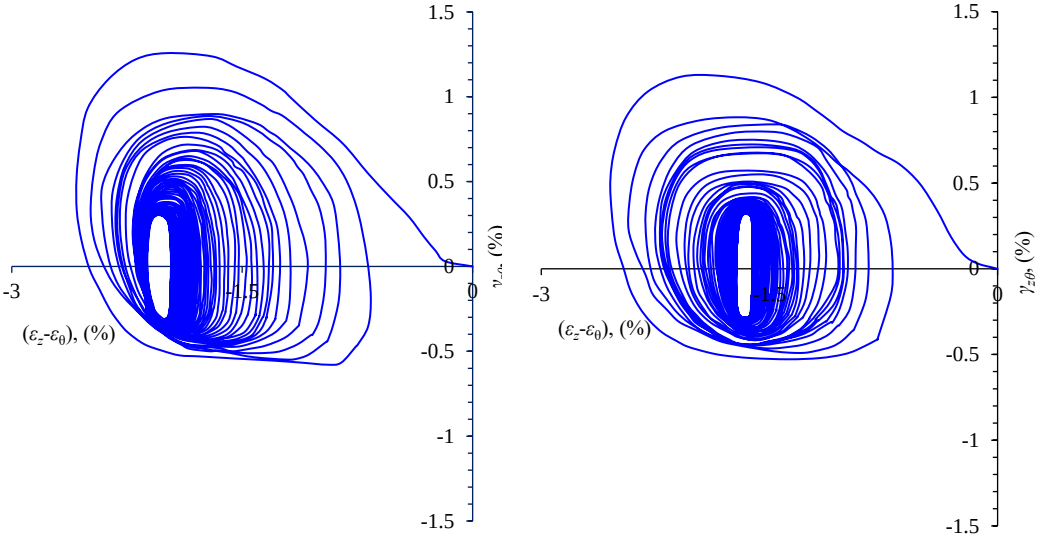

(a) (b)

Figure 7.40 Strain paths of sand reinforced with (a) nonwoven geotextile (6 layers) and (b) geocell under q/p' = 1.1

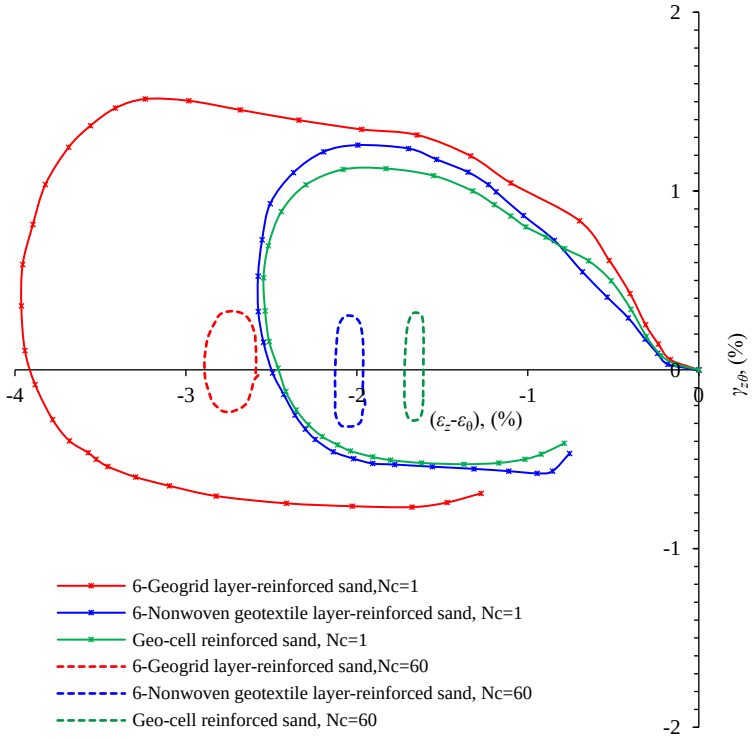

Figure 7.41 Comparisons of the strain paths of sand reinforced with geogrid (6 layers), nonwoven geotextile (6 layers) and geocell at the first and 60th cycles under q/p' = 1.1

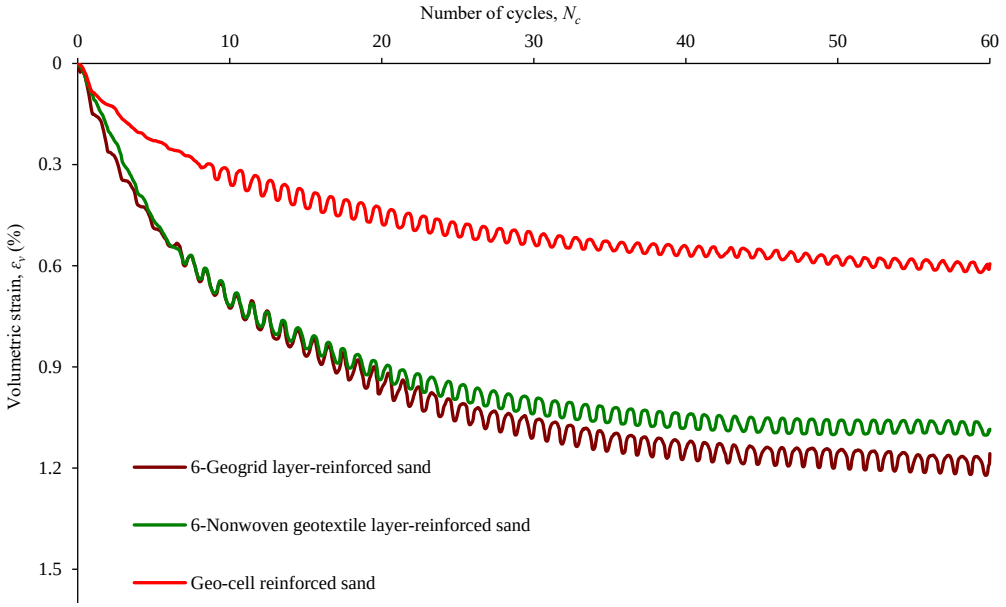

Figure 7.42 Variation of volumetric strain ε_v of sand reinforced with geogrid (6 layers), nonwoven geotextile (6 layers) and geocell in rotational shear over 60 cycles under q/p' = 1.1

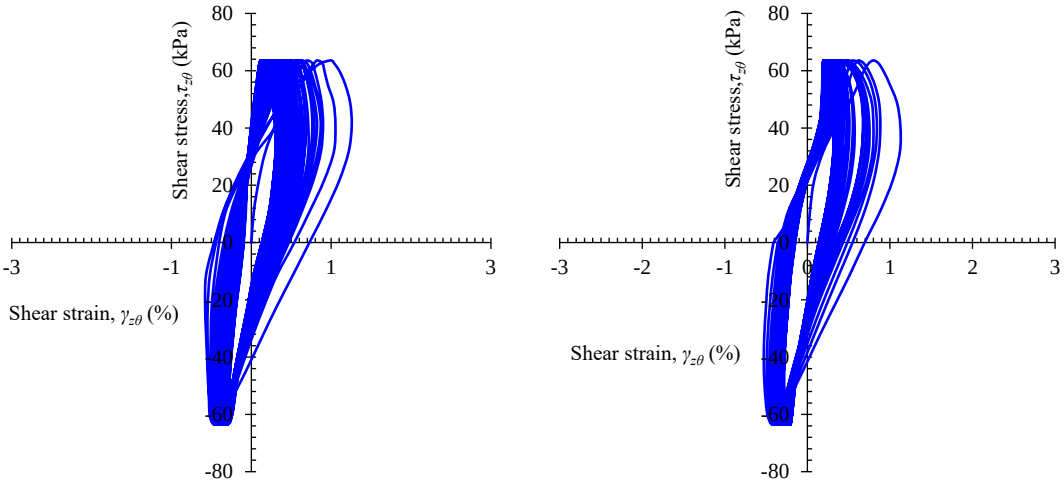

(a) (b)

Figure 7.43 Hysteretic shear stress-strain relationships for sand reinforced with (a) nonwoven geotextile (6 layers) and (b) geocell under q/p' = 1.1

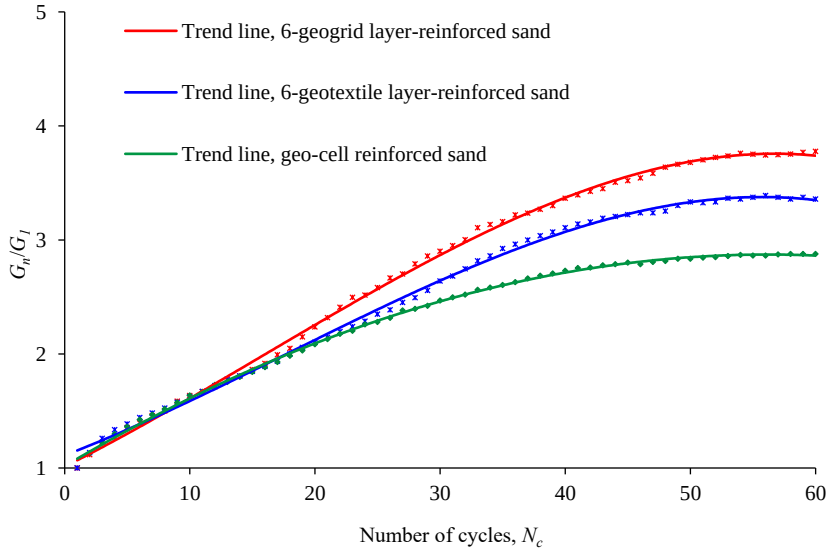

Figure 7.44 Variations in the shear modulus ratio (G_n/G_1) of sand reinforced with geogrid (6 layers), nonwoven geotextile (6 layers) and geocell under q/p' = 1.1

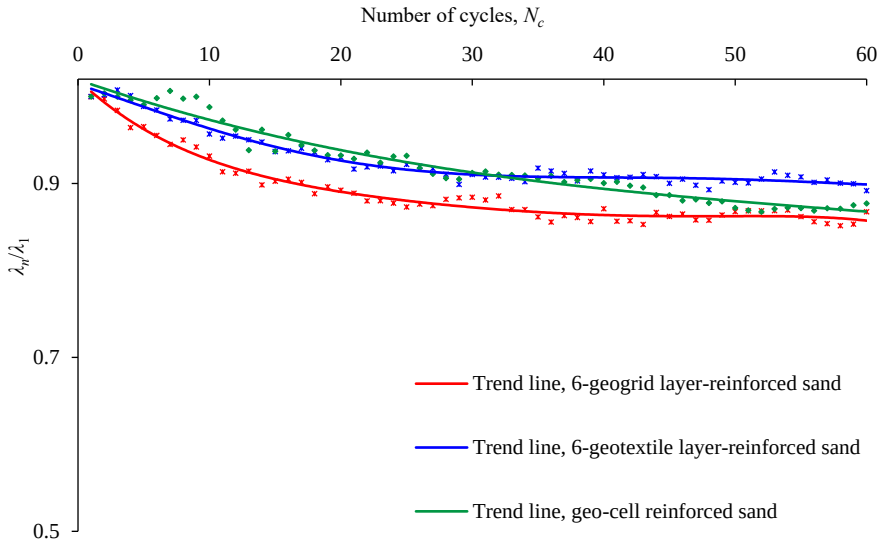

Figure 7.45 Variations in the normalised damping ratio (λ_n/λ_1) of sand reinforced with geogrid (6 layers), nonwoven geotextile (6 layers) and geocell under q/p' = 1.1

7.7 Effect of Clay Content on the Response of Reinforced Sand to Cyclic Rotation of the Principal Stress Direction

In this section, the effect of adding 10% clay to the sand samples (reinforced with six layers of geogrid, six layers of nonwoven geotextile or geocell) is investigated.

Figure 7.46a shows the variation in the strain components of mixed sand-clay reinforced with geogrid according to the number of cycles. Moreover, the variations of these strains along α for the first and last cycles are presented in Figure 7.47a and compared with those of geogrid-reinforced clean sand. The general trend is similar; however, adding clay to reinforced sand resulted in decreased axial ε_z and circumferential ε_θ strains at N_c = 1, of 1.93% and 1.27%, respectively, compared with ε_z = 2.3% and ε_θ = 1.65% for geogrid-reinforced clean sand (Figure 7.47a). As the number of cycles increased, the amplitudes of these strains decreased significantly. On the other hand, the radial strain ε_r of reinforced mixed sand-clay at the cycle was close to that of reinforced clean sand (at 0.70%). At N_c = 60, it accumulated to 1.28%, which is less than that of reinforced clean sand, i.e. 1.49%. The amplitude shear strain $\gamma_{z\theta}$ of reinforced mixed sand-clay developed to 2.38% at N_c = 1, which is slightly larger than that of reinforced sand.

The effect of adding clay to the sand samples reinforced with six layers of nonwoven geotextile was similar to that of adding clay to the geogrid-reinforced samples, as shown in Figures 7.46b and 7.47b. The axial, radial and circumferential strains of reinforced mixed sand-clay exhibited slight differences compared with those of reinforced clean sand. However, the shear strain $\gamma_{z\theta}$ that developed at the first cycle in the geotextile-reinforced mixture was larger than that of reinforced clean sand. For example, the amplitude of $\gamma_{z\theta}$ of the geotextile-reinforced mixture was 2.36%, compared with 1.75% in geotextile-reinforced sand.

Compared to mixed sand-clay with planar reinforcement, mixtures with geocell had lower strain components and amplitudes (Figures 7.46c and 7.47c). Furthermore, the developed strains, except for the axial strain, were lower than when geocell was used with clean sand. For example, after 60 cycles, the ε_z, ε_r and ε_θ values of reinforced

mixtures reached 0.69, 0.50, and 0.84%, respectively, compared with 0.94, 0.77 and 0.77% for reinforced clean sand.

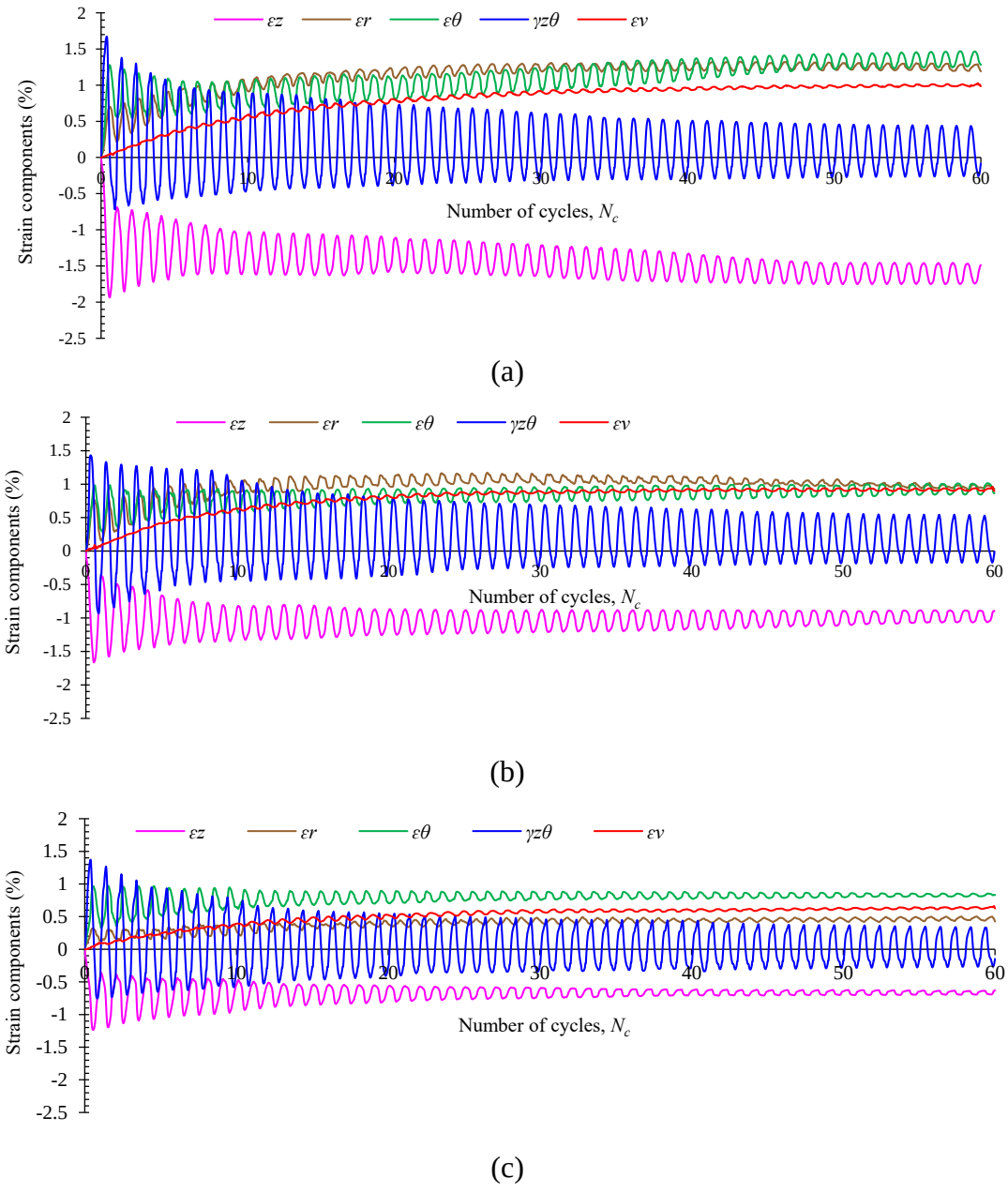

Figure 7.46 Variation of strain components in reinforced mixed sand-clay (10% clay) under q/p'= 1.1 (ε_z, ε_r, ε_θ, $\gamma_{z\theta}$ and ε_v) in rotational shear over 60 cycles: (a) geogrid (6 layers), (b) nonwoven geotextile (6 layers) and (c) geocell

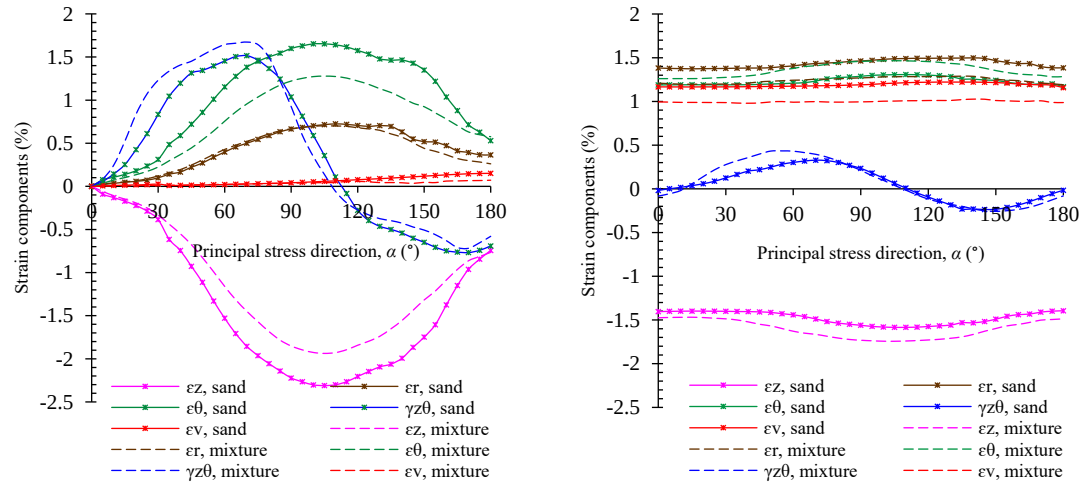

(i) N_c = 1 (ii) N_c = 60

(a)

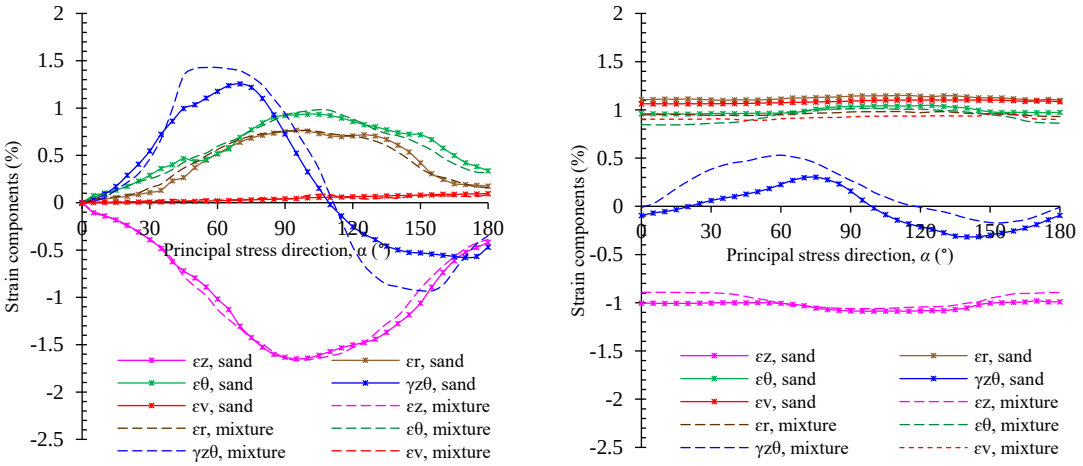

(i) N_c = 1 (ii) N_c = 60

(b)

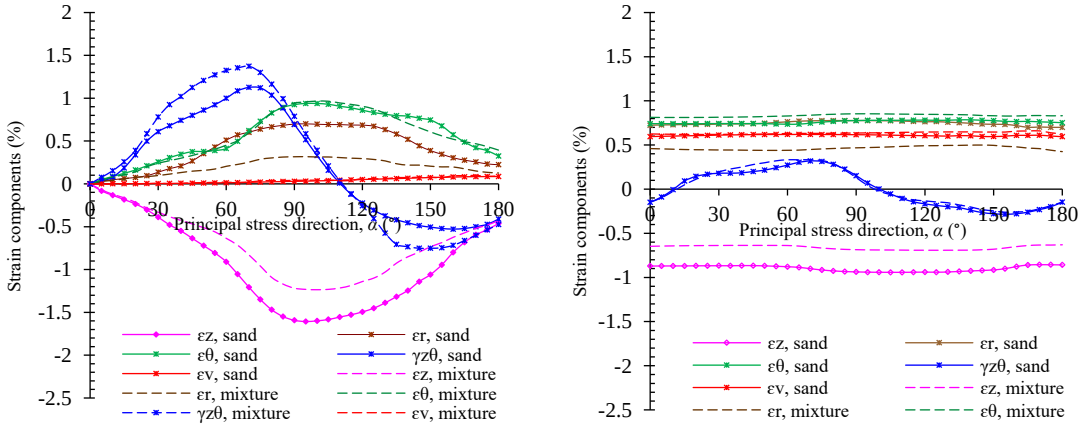

(i) N_c = 1 (ii) N_c = 60

(c)

Figure 7.47 Comparison between the variation of strain components of sand and mixed sand-clay reinforced with (a) 6 layers of geogrid (b) 6 layers of geotextile and (c) geocell

Figure 7.48 shows the strain path of mixed sand-clay reinforced with geogrid, geotextile and geocell. The strain trajectories at the first and 60th cycles of rotation are plotted together in Figure 7.49 and compared with those of reinforced clean sand. The general trend is similar, where these trajectories appear to be opened at N_c = 1, while when reinforced mixtures are continuously subjected to rotation, the evolution of the strain paths appear as spirals.

Volumetric strain ε_v is presented in Figure 7.50. It is clear that the addition of clay resulted in lower volumetric strain for both geogrid- and geotextile-reinforced samples. Moreover, geocell-reinforced mixed sand-clay showed a significant decrease in ε_v. At the first few cycles, the volumetric strain ε_v increased dramatically, then the rate of increase became lower as N_c increased. After 60 cycles of rotation, the volumetric strain reached about 1.01, 0.93 and 0.64% for mixtures reinforced with geogrid, geotextile and geocell, respectively, compared with 1.21, 1.1 and 0.61% for reinforced clean sand.

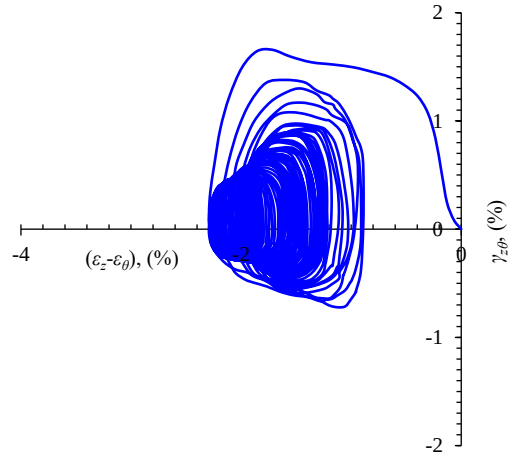

(a)

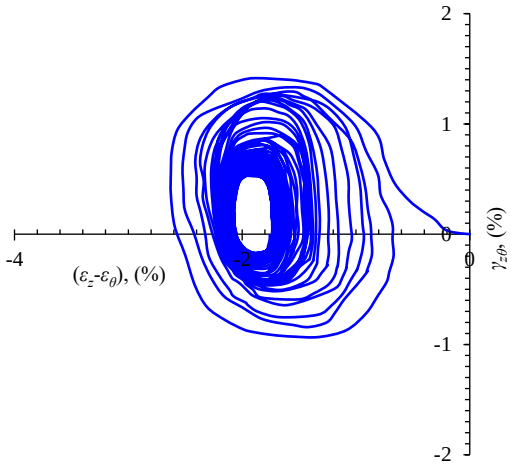

(b)

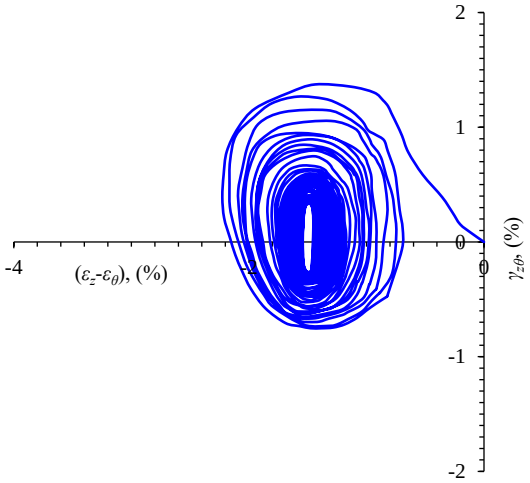

(c)

Figure 7.48 Strain paths of mixed sand-clay reinforced with (a) geogrid (6 layers), (b) nonwoven geotextile (6 layers) and (c) geocell in deviator strain space under $q/p' = 1.1$

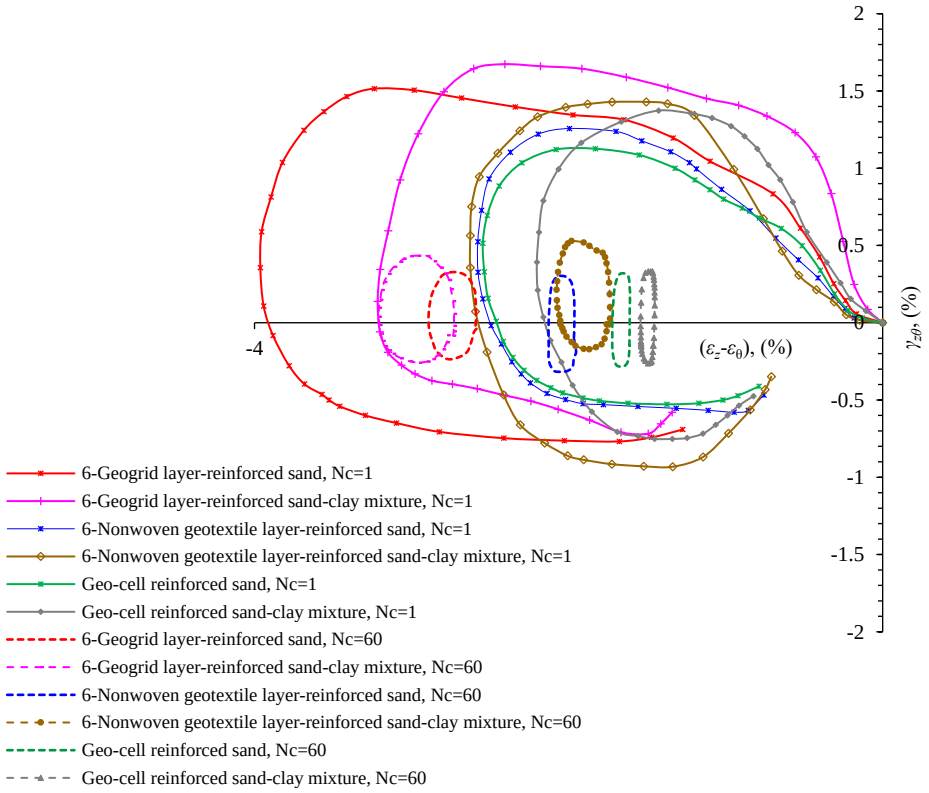

Figure 7.49 Comparison strain paths of mixed sand-clay and pure sand reinforced with geogrid (6 layers), nonwoven geotextile (6 layers) and geocell, in deviator strain space under $q/p' = 1.1$

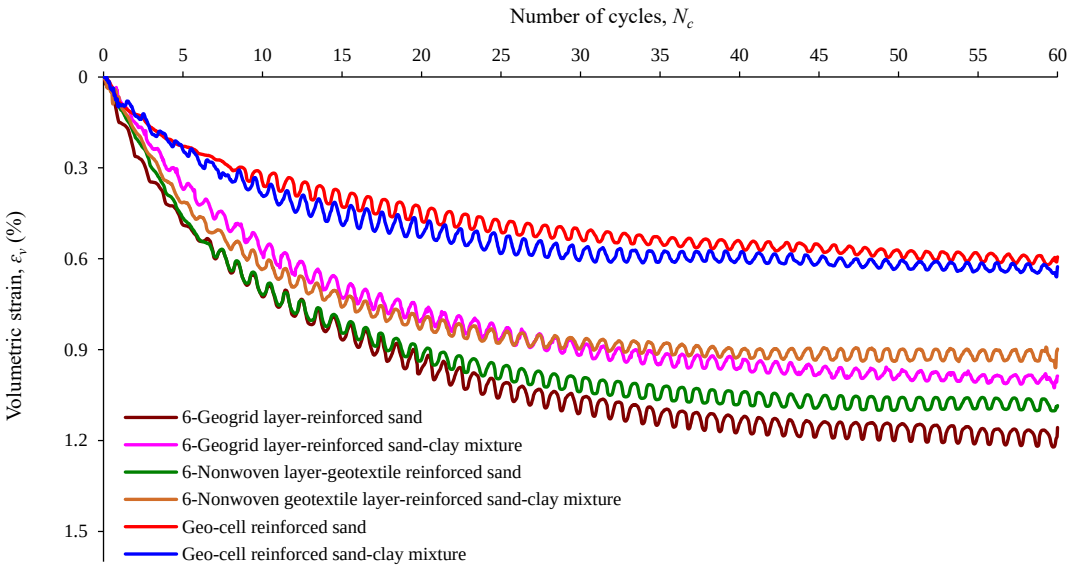

Figure 7.50 Variation of volumetric strain ε_v of sand and mixed sand-clay reinforced with geogrid (6 layers), nonwoven geotextile (6 layers) and geocell under $q/p' = 1.1$

The hysteresis loops of the shear strain-stress relationships are depicted in Figure 7.51. From each single loop, the shear modulus and damping ratio was computed and is presented in the forms of G_n/G_1 and λ_n/λ_1 (Figures 7.52 and 7.53). Adding clay (10%) resulted in decreases in the shear moduli G of all types of reinforced samples. As the number of cycles of rotation N_c increased, G increased but was still less than that of reinforced clean sand after the same number of cycles. For example, mixed sand-clay reinforced with geogrid, geotextile and geocell exhibited shear moduli of 6.8, 5.7 and 6.9 MPa, respectively, at the first cycle and 21.2, 22.8 and 27.7 MPa at the 60th cycle. This means that adding 10% clay reduced the shear moduli at N_c = 60 by 24.9, 22.1 and 10.6% for geogrid-, geotextile- and geocell-reinforced sand, respectively. The damping ratio λ was approximately similar at the first cycle for mixed sand-clay reinforced with planar and three-dimensional geo-inclusions, at 28.4. However, when the number of cycles increased to 60, the λ value of mixed sand-clay reinforced with geo-inclusions decreased by 8.0–11.0%. This general trend was quite similar to that of reinforced pure sand, but the damping ratio of reinforced mixed sand-clay was smaller than that of reinforced pure sand (Figure 7.53).

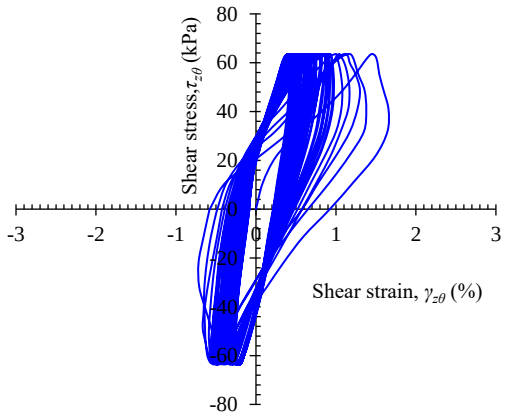

(a)

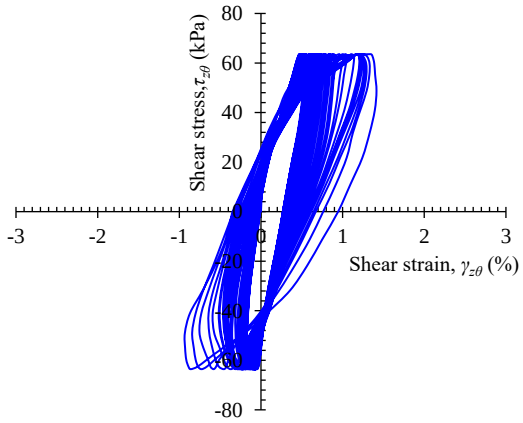

(b)

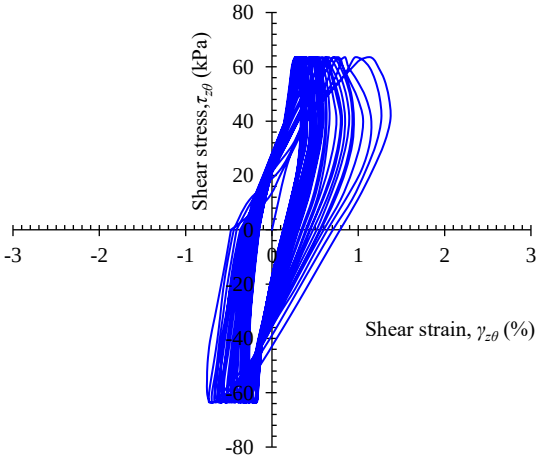

(c)

Figure 7.51 Hysteretic shear stress-strain relationships for mixed sand-clay reinforced with (a) geogrid (6 layers), (b) nonwoven geotextile (6 layers) and (c) geocell in deviator strain space under $q/p' = 1.1$

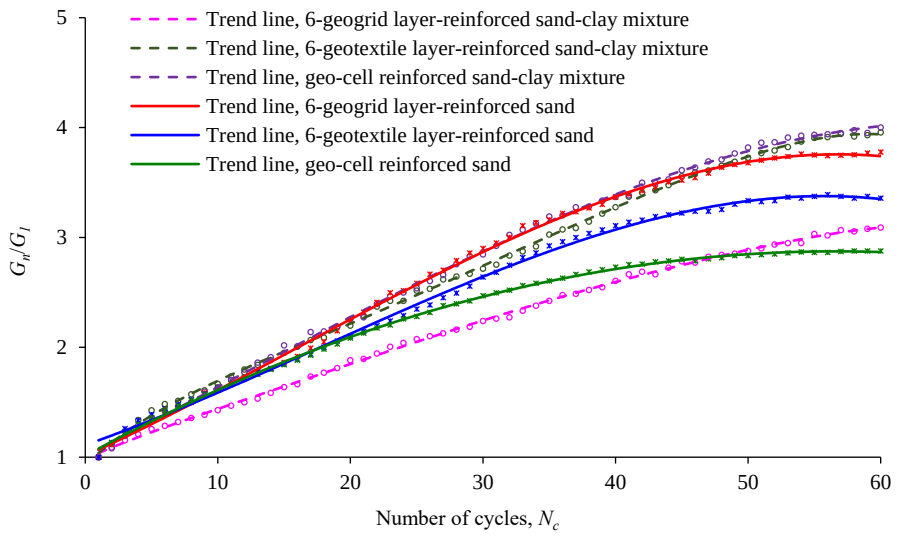

Figure 7.52 Variations in the ratio of shear modulus (G_n/G_1) of sand and mixed sand-clay reinforced with geogrid (6 layers), nonwoven geotextile (6 layers) and geocell under $q/p' = 1.1$

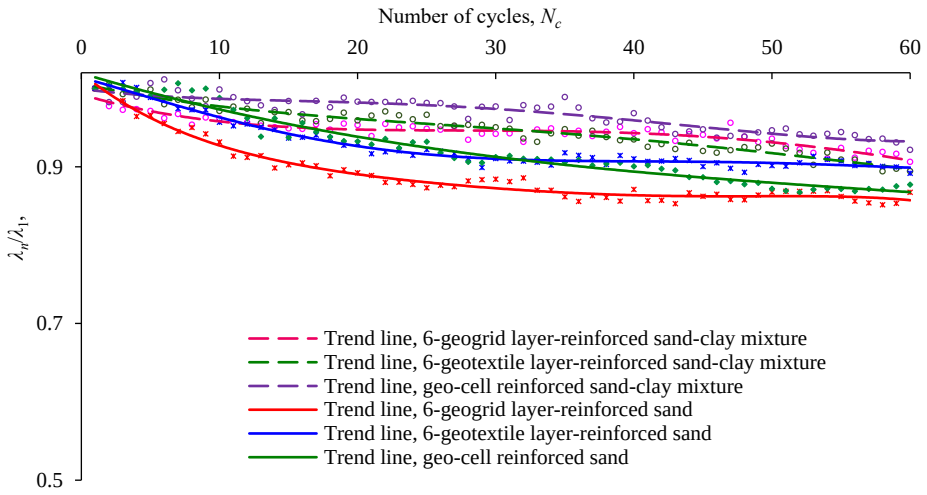

Figure 7.53 Variations in the normalised damping ratio (λ_n/λ_1) of sand and mixed sand-clay reinforced with geogrid (6 layers), nonwoven geotextile (6 layers) and geocell under $q/p' = 1.1$

7.8 Comparative Performance of Samples Reinforced with Different Types of Geosynthetics under Cyclic Rotation

Rotation of the principal stress direction under a constant q/p' value of 1.1 caused failure in unreinforced sand and mixed sand-clay during the first test cycle. Samples reinforced with geogrid, geotextile and geocell sustained 60 cycles of rotation, although significant strains were induced. These strains varied with oscillation mode due to variation in the applied stresses, subsequently changing from extension to compression and leading to variation in the performance of the planar reinforcement. Table 7.2 summarises the induced strains, shear modulus and damping ratios of sand reinforced with different reinforcements.

Similar trends were observed after the addition of 10% clay to reinforced sand. A comparison of the induced strains of clean sand and sand-clay mixtures containing different reinforcements is plotted in Figure 7.47. For example, the volumetric strains of reinforced mixed sand-clay were slightly less than those of reinforced sand. These lower strains can be attributed to the clay, which improves bonding between the reinforcement and the sand particles. Table 7.3 summarises the induced strains, shear modulus and damping ratios of reinforced sand-clay mixtures.

Cyclic rotation had a lesser effect on the deformation characteristics of samples reinforced with geocell than samples reinforced with other geosynthetics. For example, the volumetric strain after 60 cycles of rotation was 0.61% for geocell-reinforced sand, while it reached 1.1 and 1.21% for geotextile- and geogrid-reinforced sand, respectively. Figure 7.50 compares the volumetric strains of samples reinforced with different types of geosynthetics. The difference in the induced strains of the different reinforcements is related to the fact that planar-type reinforcements (geogrid and geotextile), cannot be mobilised under extension conditions when the principal stress rotates towards the horizontal. However, geocell has walls that provide all-round confinement even under horizontal principal stress.

Irrespective of the reinforcement type, the amplitudes of the strains of reinforced samples decreased significantly with increasing numbers of cycles. Significant

amounts of induced strain, particularly at the first cycle, are plastic. A comparison of the strain paths, at the first cycle, of sand with planar and 3D reinforcements, is presented in Figure 7.49. The gaps between the beginnings and ends of the paths indicate the induced plastic strains, which are almost same for the different reinforcements.

At the first cycle, the shear modulus of sand reinforced with geocell was larger than for samples containing other reinforcements. With increasing numbers of cycles, the shear modulus of sand reinforced with different geo-inclusions increased significantly and, at N_c = 60, approached the same value. The damping ratio was approximately constant for all reinforced samples and decreased by 10–15 with increasing numbers of cycles.

Table 7.2 Summary of the induced strains, shear modulus and damping ratios of reinforced clean sand (q/p' = 1.1)

	ε_z, (%) (-)*		ε_θ, (%) (+)*		ε_r, (%) (+)*		$\gamma_{z\theta}$, (%)		ε_v, (%) (+)* N_c=60	G, (MPa)		λ	
	N_c=1	N_c=60	N_c=1	N_c=60	N_c=1	N_c=60	N_c=1	N_c=60		N_c=1	N_c=60	N_c=1	N_c=60
Sand	It failed during the first cycle												
6-geogrid layers-reinforced sand	2.3	1.58	1.65	1.31	0.70	1.49	1.51 to -0.71	0.33 to -0.24	1.21	7.4	28.2	35.6	30.9
6-geotextile layers-reinforced sand	1.60	1.0	0.93	1.0	0.74	1.2	1.22 to -0.53	0.27 to -0.30	1.1	8.7	29.3	33.7	30.1
Geocell reinforced sand	1.60	0.94	0.93	0.77	0.70	0.77	1.12 to -0.52	0.31 to -0.26	0.61	10.7	31.1	35.9	31.5

NOTE: Positive and negative signs indicate compression and dilation, respectively.

Table 7.3 Summary of the induced strains, shear modulus and damping ratios of reinforced sand-clay mixtures (q/p' = 1.1)

	ε_z, (%) (-)*		ε_θ, (%) (+)*		ε_r, (%) (+)*		$\gamma_{z\theta}$, (%)		ε_v, (%) (+)* N_c=60	G, (MPa)		λ	
	N_c=1	N_c=60	N_c=1	N_c=60	N_c=1	N_c=60	N_c=1	N_c=1		N_c=1	N_c=60	N_c=1	N_c=60
Sand-clay mixture	It failed during the first cycle												
6-geogrid layers-reinforced sand-clay mixture	1.93	1.74	1.27	1.46	0.7	1.28	1.68 to -0.70	0.43 to -0.23	1.01	6.8	21.26	28.2	25.6
6-geotextile layers-reinforced sand-clay mixture	1.64	1.05	0.98	1.0	0.76	0.91	1.42 to -0.94	0.53 to -0.15	0.93	5.7	22.8	28.6	25.4
Geocell reinforced sand-clay mixture	1.23	0.69	0.96	0.84	0.307	0.5	1.37 to -0.74	0.33 to -0.26	0.64	6.9	27.7	28.8	25.7

NOTE: Positive and negative signs indicate compression and dilation, respectively.

Chapter 8

Bearing Pressure and Deformation Characterisation of Cemented Sand

8.1 Introduction

Reinforcement of sand with cement is a technique common to many geotechnical applications. Furthermore, many cities in the world lie on geological deposits that exhibit crossbedding with different levels of cementation. For example, Perth, Australia, is located on the Swan Coastal Plain, which is covered by superficial cemented formations such as the Bassendean and Safety Bay sands. Therefore, the aim of this study was to investigate the bearing pressure and deformation characterisations of sand and sand reinforced with different proportions of Portland cement by conducting a series of loading tests using laboratory models. Description of the tests performed is provided in Table 8.1.

Section 8.2 presents the bearing pressure-settlement characterisations of sand and sand reinforced with 3, 5 and 7% cement under monotonic loading tests. The deformation characteristics of clean and cemented sands tested under cyclic loadings of various amplitudes are presented in Section 8.3. Finally, a discussion and summary of this chapter are made in Section 8.4.

Table 8.1 Summary of the model test program

Test Series	Cement content, (%)	Relative density, D_r (%)	Inclination angle, α (°)	Loading amplitude, $q_c/(q_b)_u^*$ (%)
Series I Monotonic loading tests	0	70.1–71.2	0, 15, 30, 45, 60, 75 and 90	---
	3	69.3–70.7	0, 15, 30, 45, 60, 75 and 90	---
	5	69.1–70.9	0, 15, 30, 45, 60, 75 and 90	---
	7	69.6–71.1	0, 15, 30, 45, 60, 75 and 90	---
Series II Cyclic loading tests	0	69.8–70.7	0, 15, 30, 45, 60, 75 and 90	10, 20 & 30
	3	69.6–71.4	0, 15, 30, 45, 60, 75 and 90	10, 20 & 30
	5	70.1–70.7	0, 15, 30, 45, 60, 75 and 90	10, 20 & 30
	7	69.7–70.5	0, 15, 30, 45, 60, 75 and 90	10, 20 and 30

$^*q_c$: cyclic loading.
$(q_b)_u$: ultimate bearing pressure obtained by monotonic loading tests.

8.2 Bearing Pressure and Deformation of Sand and Cemented Sand under Static Loading

8.2.1 Uncemented Sand

Typical curves of bearing pressure q_b versus settlement ratio S/B (settlement/footing width) for the model footing tests are presented in Figure 8.1. This figure shows that the curves were strongly affected by the initial anisotropy induced by different inclinations of the bedding plane α. The largest ultimate bearing pressure $(q_b)_u$ and stiffest response in sand was obtained with loading in the deposition direction, i.e. $\alpha = 0^o$. After which a slight decrease in $(q_b)_u$ was observed with increasing α, followed by a sharp drop to its minimum value at $\alpha = 75^o$, before reverting slightly, with a reduction in bearing pressure of 29.4%. Figure 8.2 demonstrates the reduction ratio in the bearing capacity at different values of α relative to that when $\alpha = 0^o$. This trend agrees with the results obtained in the triaxial tests using hollow cylinder samples that were presented in the previous chapters. These findings are also consistent with studies such as Miura et al. (1986). It can be explained using the plane of maximum obliquity (Matsuoka, 1974), which suggests that the lowest resistance to loading occurs when the mobilised plane and bedding plane are almost aligned. The mobilised plane makes an angle of $45 - Ø°/2$ with the direction of major stress, where $Ø$ is the angle of internal friction of the material used. Therefore, the coincidence occurs when the inclination of the bedding plane is 60–75^o, which consequently produces the maximum deformation and minimum strength.

The ultimate bearing capacity $(q_b)_u$ of sand occurred at different settlement ratios depending on α. For example, peaks occurred at settlement ratios of around 9–11% for $\alpha = 0–45^o$, while they occurred at settlement ratios ranging from 12.5–14% when $\alpha \geq 60^o$. This indicates that the sliding and rotation of particles tended to occur more easily as the inclination of the bedding plane became closer to the load direction.

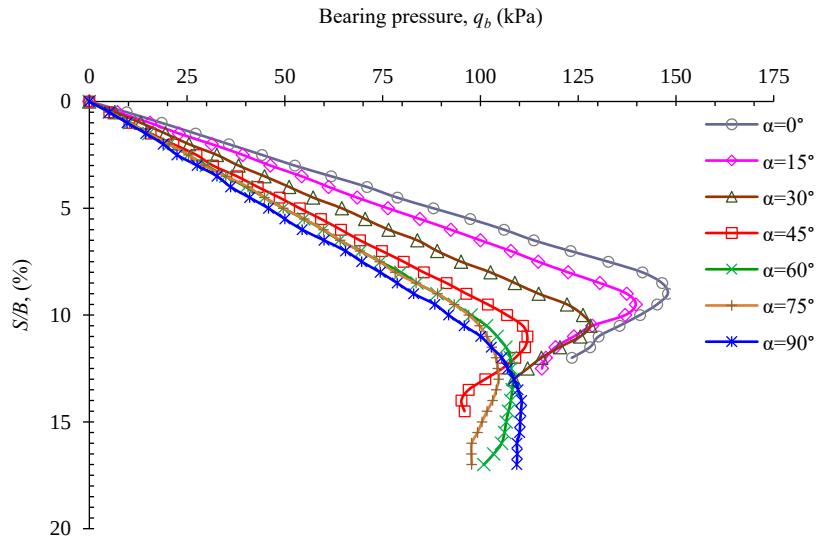

Figures 8.1 Bearing pressure-settlement of sand for various inclinations of bedding plane α

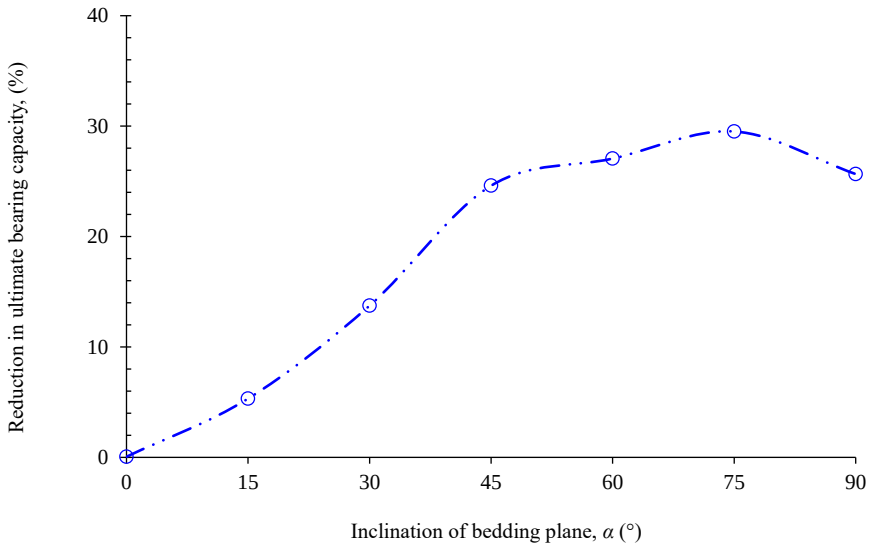

Figures 8.2 Reduction in the ultimate bearing pressure $(q_b)_u$ of sand

8.2.2 Cemented sand

The variations in bearing pressure with the settlement of cemented sand, and at different inclination angles α, are presented in this section.

From Figure 8.3, it can be observed that, in general, cement improves the characteristics of sand and reduces the anisotropic effect. This improvement depends on the cement content and inclination angle α. The ultimate bearing pressure $(q_b)_u$, when $\alpha = 0^o$, increased from 147.9 kPa for uncemented sand to 811.2 kPa for 3% cemented sand (Figure 8.3a). This ultimate bearing pressure $(q_b)_u$ did not change significantly over the range $\alpha = 0–30^o$, in which the reduction ratio did not exceed 2.5% (Figure 8.4); however, beyond this range of α, the ultimate bearing capacity clearly dropped, achieving a reduction of 18.4% at 75^o and 90^o tilting angles. By increasing the cement content to 5% and 7%, the ultimate bearing pressures $(q_b)_u$ under $\alpha = 0^o$ increased to 1096.3 kPa and 1901.8 kPa, respectively (Figures 8.3b and c), and remained relatively constant with α, with a reduction of less than 2.8% for $\alpha = 15–45^o$ and 8.1–12.1% for $\alpha = 60–90^o$. These results suggest that a cement content of 7% delivers the minimum influence of anisotropy on the ultimate bearing capacity.

For $\alpha \leq 45^o$, the ultimate bearing pressure $(q_b)_u$ of sand treated with 3% and 5% cement contents occurred in the settlement ratio range of 6.3–8.4%, compared with 4.8–5.7% when a 7% cement content was used. As the tilting angle α increased, i.e. $\alpha \geq 60^o$, the settlement ratio corresponding to ultimate bearing pressure increased to the ranges of 7.0–9.6% for 3% and 5% cement contents; and 5.4–6.6% for 7% cement content.

The interpretation and discussion of these results, and the results of the next cyclic section are presented in Section 8.4.

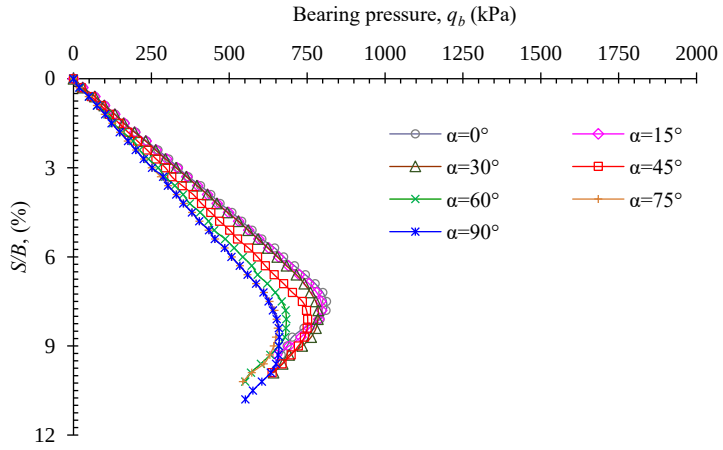

(a)

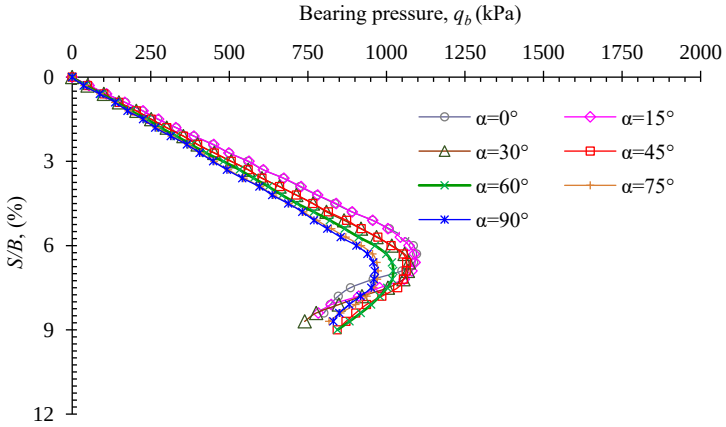

(b)

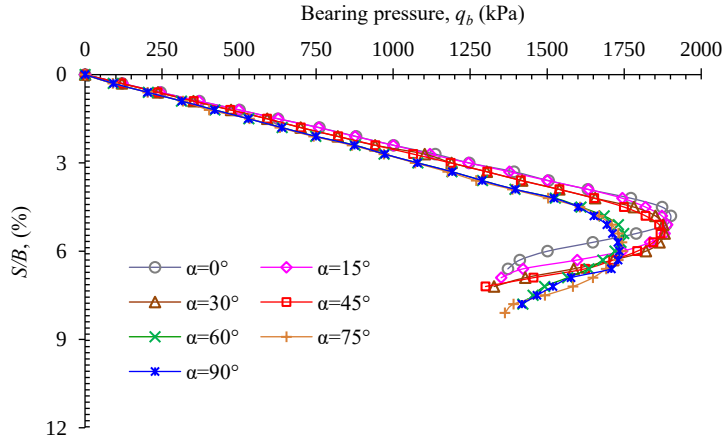

(c)

Figure 8.3 Bearing pressure-settlement of sand reinforced with cement contents of (a) 3%; (b) 5% and (c) 7%

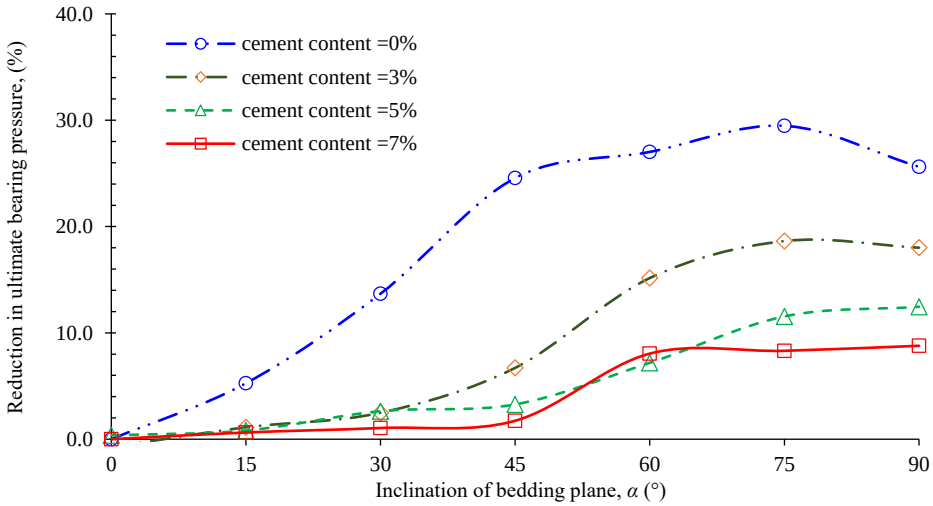

Figure 8.4 Reduction in the ultimate bearing pressure $(q_b)_u$ of cemented sand versus α

8.3 Cyclic Settlement of Sand and Cemented Sand under Various Loading Amplitudes and Inclinations of Bedding Plane α

8.3.1 Uncemented Sand

The results of samples prepared with different inclinations of bedding plane α and tested under different loading amplitudes $q_c/(q_b)_u$ are presented here in order to describe their macroscale deformation characteristics. It should be mentioned that these results pertain to soils that have experienced cyclic settlement after the application of different amplitudes of cyclic load.

The macroscale responses of tested samples shows that the orientation of the bedding plane α of samples had a clear effect on the sand's deformation. The settlement that developed with increasing numbers of cycles is plotted in Figure 8.5. For clarity, the variation in settlement along α for selected numbers of cycles is presented in Figure 8.6. For each inclination angle α, footing settlement increased significantly when the amplitude of the cyclic load $q_c/(q_b)_u$ was increased, as shown in Figures 8.5-8.7.

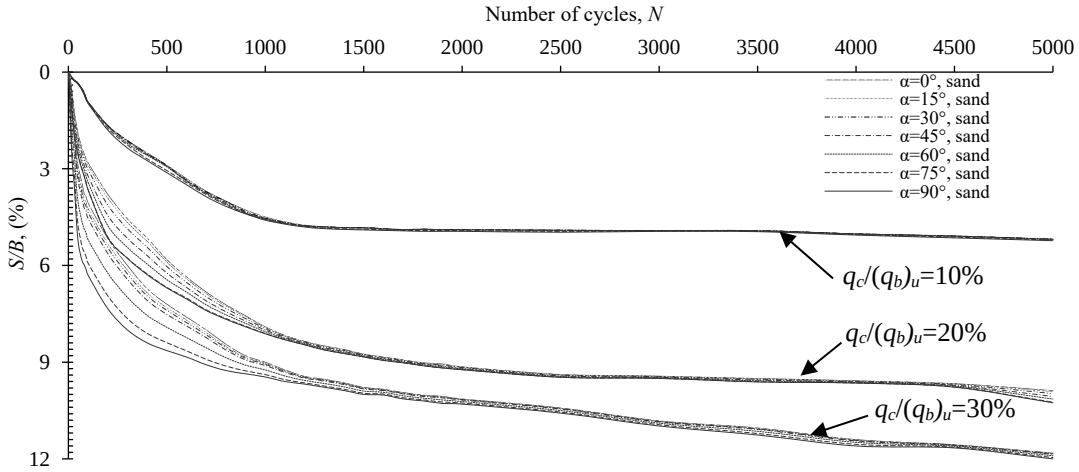

Figure 8.5 Variation of the *S/B* of sand with number of load cycles *N*

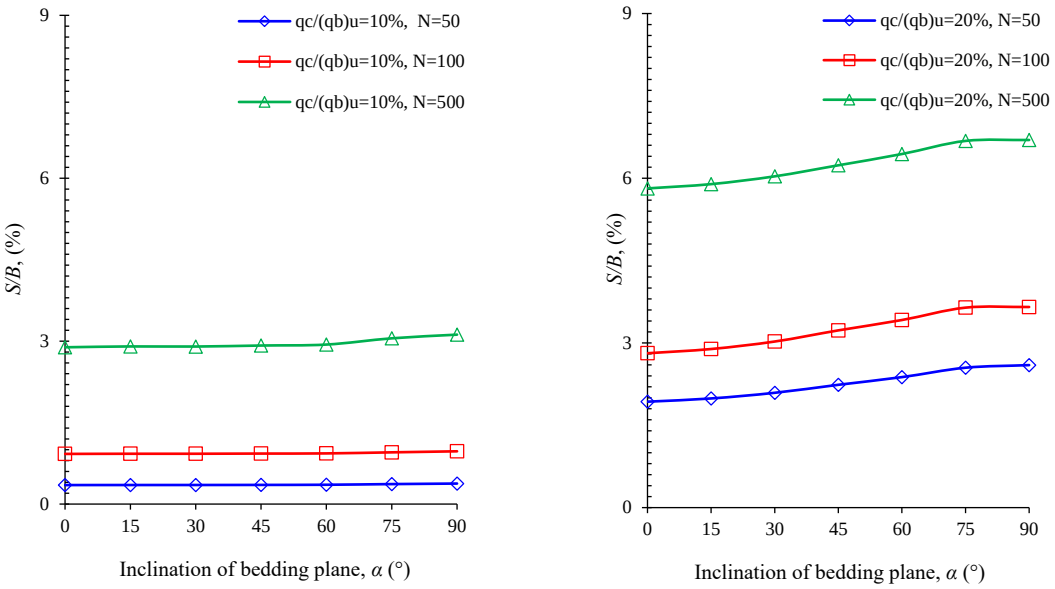

(a)

(b)

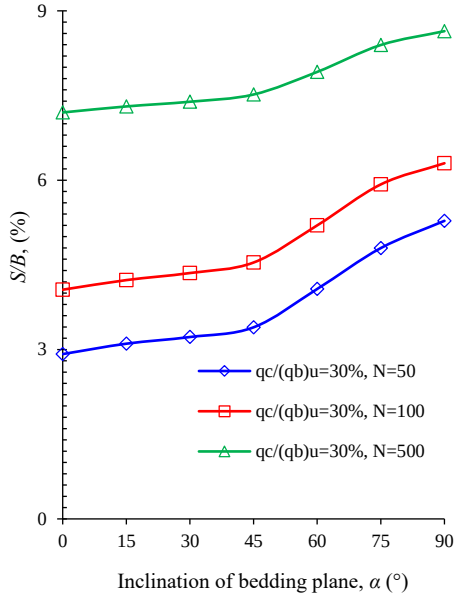

(c)

Figure 8.6 Variation of *S/B* of sand along angle of bedding plane α at selected numbers of load cycles *N* under (a) $q_c/(q_b)_u$=10%, (b) $q_c/(q_b)_u$=20% and (c) $q_c/(q_b)_u$=30%.

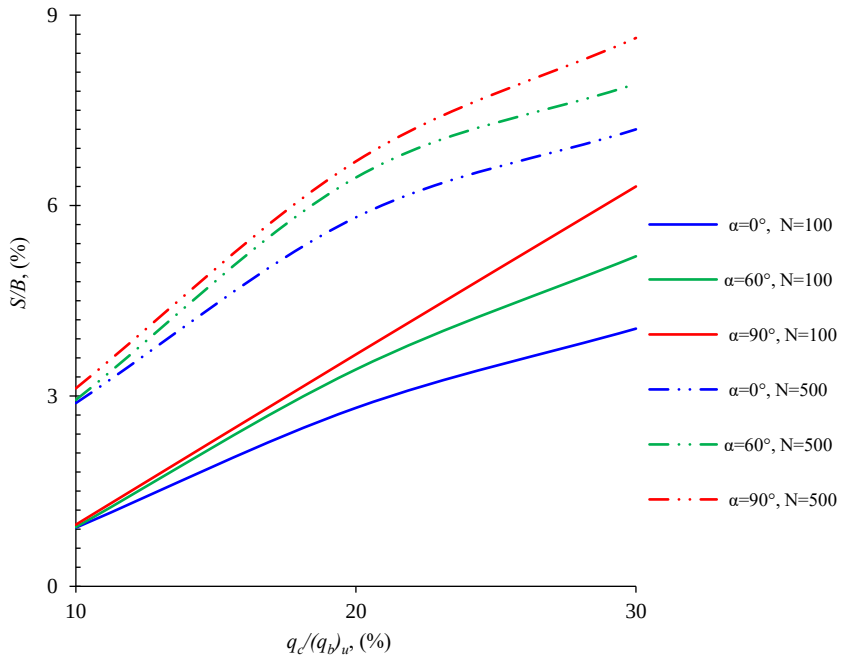

Figure 8.7 Variation of sand *S/B* with loading amplitude $q_c/(q_b)_u$ for α = 0, 60 and 90° at *N* = 100 and 500

The cyclic tests lasted for 5000 cycles, and it can be seen from Figure 8.5 that the settlement ratio *S/B* increased at a diminishing rate with continued cycling, irrespective of bedding plane inclination α. The number of cycles required to achieve 50% settlement decreased with increasing inclination angle α. For example, for samples prepared at $\alpha \leq 45°$, some 50% of the ultimate settlement occurred after *N* = 450, 350 and 300 for $q_c/(q_b)_u$ = 10, 20 and 30%, respectively. With further increases in the number of cycles, settlement still occurred, but at a lower rate. However, for α = 60–90°, similar percentages of settlement, i.e. 50%, occurred after fewer cycles of load, i.e. 350, 200 and 100 for $q_c/(q_b)_u$ = 10, 20 and 30%, respectively.

The variation of *S/B* under $q_c/(q_b)_u$ = 10% was very slight and the curves for different inclinations α were coincident on each other, as shown in Figure 8.5. For instance, the settlement ratio *S/B* at *N* = 100 was almost same, at 0.92–0.97, with variation of α from 0–90° (Figure 8.6a). For larger amplitudes of $q_c/(q_b)_u$ of 20% and 30%, settlement was not constant but varied clearly with inclination angle α. From Figures 8.6b and c, it can be observed that the settlement ratio *S/B* of sand under $q_c/(q_b)_u$ = 20% and 30% increased moderately for inclinations of α = 0–45°, followed by a rapid increase until

reaching the maximum value at α = 90°. When $q_c/(q_b)_u$ = 30%, for example, *S/B* increased from 4.06% at α = 0° to 4.23, 4.35, 4.54, 5.2, 5.92 and 6.3% for α = 15, 30, 45, 60, 75 and 90°, respectively. This clearly indicates that increases in the amplitude of cyclic loading lead to an increase in the effects of directional dependence, i.e. anisotropy. The difference ratio between $(S/B)_{0°}$ and $(S/B)_{90°}$ relative to that of $(S/B)_{0°}$ after 100 cycles increased rapidly from 5.2% to 55% as $q_c/(q_b)_u$ increased from 10% to 30%.

This effect of loading amplitude on the directional dependence of settlement is depicted in Figure 8.7. It is clear that the settlement ratio increased with increasing loading amplitudes irrespective of the inclination angle and that the rate of settlement ratio increase was larger when $q_c/(q_b)_u$ increased from 10% to 20% than from 20% to 30%. Note that the combined conditions of $q_c/(q_b)_u$ = 30% and α = 75–90° delivered maximum footing settlement after applying cyclic loading. As mentioned previously, there is a lack of data on cyclic settelement in anisotropic sand; however, irrespective of the anisotropic condition, the trend of increasing settlement with increasing amplitude is consistent with existing studies such as Yeo, Yen, Puri, Das, and Wright (1993), Vinod, Indraratna, and Moghaddam (2011) and Tafreshi and Dawson (2012).

As mentioned above, footing settlement was strongly affected by the inclination of the bedding plane during cyclic sinusoidal loading at most loading amplitudes. However, there was no variation in settlement ratio (*S/B*) due to changes in the inclination angle after the number of cycles reached 900, 1000 and 1300 for $q_c/(q_b)_u$ = 10, 20 and 30%, respectively. Although there is a lack of data comparing directional dependence and cyclic settlement, this trend of no variation in deformation is consistent with that observed by Tong et al. (2010), who found that variations in the volumetric strain of sand become slight after eight cycles of rotation of α. Furthermore, this trend is in line with that observed in Chapter Seven. This means that sand behaviour becomes independent of inclination, and accordingly, soil reaches the same settlement irrespective of bedding inclination angle α. For example, after a given number of cycles, samples prepared at α = 0−90° and subjected to $q_c/(q_b)_u$ = 30% reached similar settlement ratios of 9.8%, with less than 2% deviation for different values of α. This independence of settlement and inclination after 900, 1000 and 1300 load cycles is

probably attributable to the distortion of the initial fabric and the rearrangement of soil particles due to induced shear deformation within the soil.

8.3.2 Cemented Sand

The macroscale observations show that although reinforcement with Portland cement generally improves the deformation characteristics of sand, there is some variation associated with variation in the bedding plane inclination α, as shown in Figures 8.8-8.15. This effect is strongly dependent on loading amplitude and cement content.

The development of settlement according to the number of cycles and α are presented in Figures 8.8 and 8.9 for 3% cemented sand, in Figures 8.10 and 8.11 for 5% cemented sand and in Figures 8.12 and 8.13 for 7% cemented sand. Variation in the settlement ratio S/B of cemented sand according to loading amplitude $q_c/(q_b)_u$ at α = 0° and 90° and N = 100 and 500 are also plotted in Figure 8.14. From all these figures, it can be seen that cyclic loading amplitude and bedding plane orientation have lesser effects on the deformation of cemented sand than uncemented sand.

Figures 8.8, 8.9 and 8.14a show that sand with 3% cement subjected to $q_c/(q_b)_u$ = 10% exhibited low variation in S/B due to fabric anisotropy, while this variation became clear when q_c/q_u increased to 30%. For example, the settlement ratio S/B increased from 1.96% at α = 0° to 2.4% at α = 90° after 500 cycles of $q_c/(q_b)_u$ = 30%, which constitutes a difference ratio of approximately 22% between $(S/B)_{0°}$ and $(S/B)_{90°}$. Under lower amplitudes $q_c/(q_b)_u$ of 10%, the difference ratio in S/B was insignificant.

Increasing the cement content reduced the effect of α on the variation in settlement ratio. For 7% cement, the settlement and its variation with α became slight under all amplitudes (Figures 8.12, 8.13 and 8.14c). This marginal variation was also observed with 5% cement, but only for $q_c/(q_b)_u$ = 10% and 20%. Figure 8.15 clearly shows how the gap between settlement at α = 0° and that at 90° decreased and diminished with increasing cement content.

Most of the settlement (i.e., 50% of final settlement) occurred after a number of cycles that was less dependent on α. For example, for 3% cemented sand, 50% settlement occurred after N = 450–600 when q_c/q_u = 30%, and after N = 550–700 for both $q_c/(q_b)_u$

= 10 and 20%. After most of the settlement occurred, the variation in settlement versus α decreased with further cycles, and the differences between $(S/B)_{0^\circ}$ and $(S/B)_{90^\circ}$ become slight. The settlement of samples at different inclinations (0°, 15°, 30°, 45°, 60°, 75° and 90°) converged after a certain number of cycles.

As mentioned previously in this chapter and in Chapter Two, it is difficult to find relevant data on cyclic settlement, especially when considering directional dependence or fabric. This lack of data regarding the combination of fabric and bonding was also mentioned by Gao and Zhao (2012). However, some studies have been performed on cemented sand using triaxial, unconfined or numerical methods, such as those by Salehzadeh et al. (2008), Gao and Zhao (2012), Salehzadeh et al. (2008) and Eghbali and Fakharian (2014). These studies have found clear directional dependence in sand response that is similar to that of the present study.

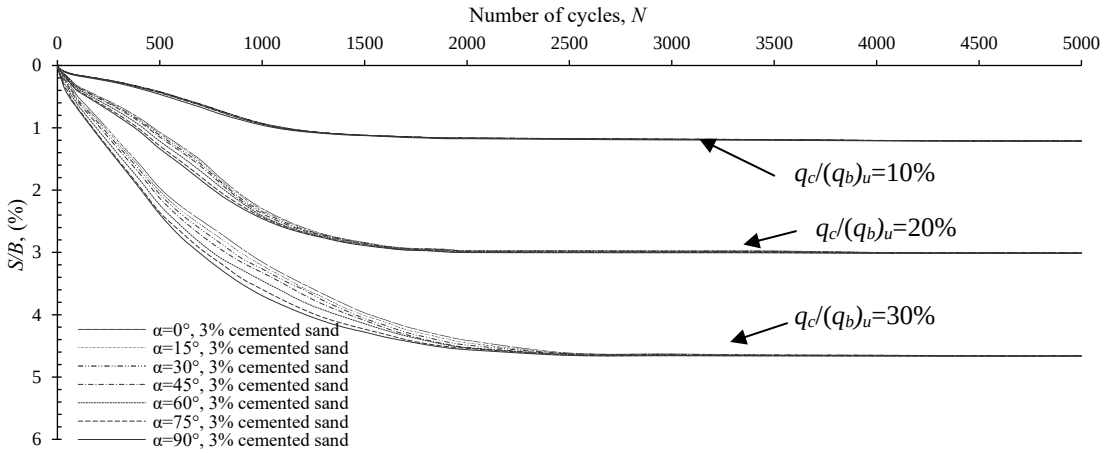

Figure 8.8 Variation of the *S/B* of cemented sand (3%) with number of load cycles *N*

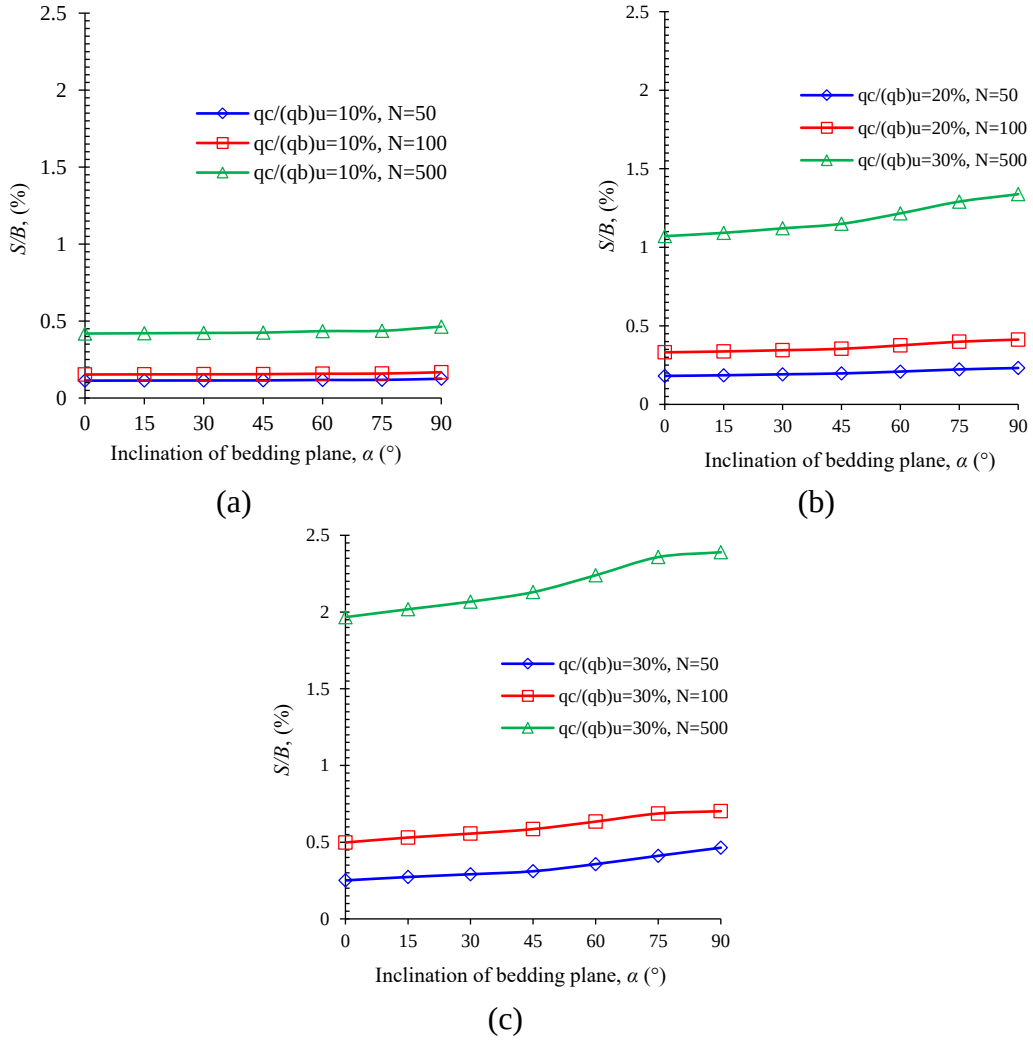

Figure 8.9 Variation of the *S/B* of cemented sand (3%) with α at selected numbers of load cycles *N* under $q_c/(q_b)_u$ = (a) 10%, (b) 20% and (c) 30%

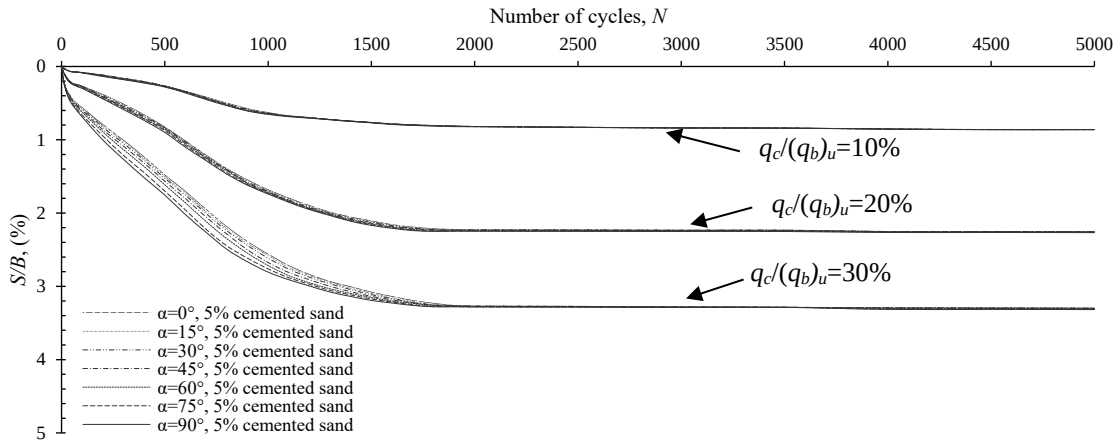

Figure 8.10 Variation of the *S/B* of cemented sand (5%) with number of load cycles *N*

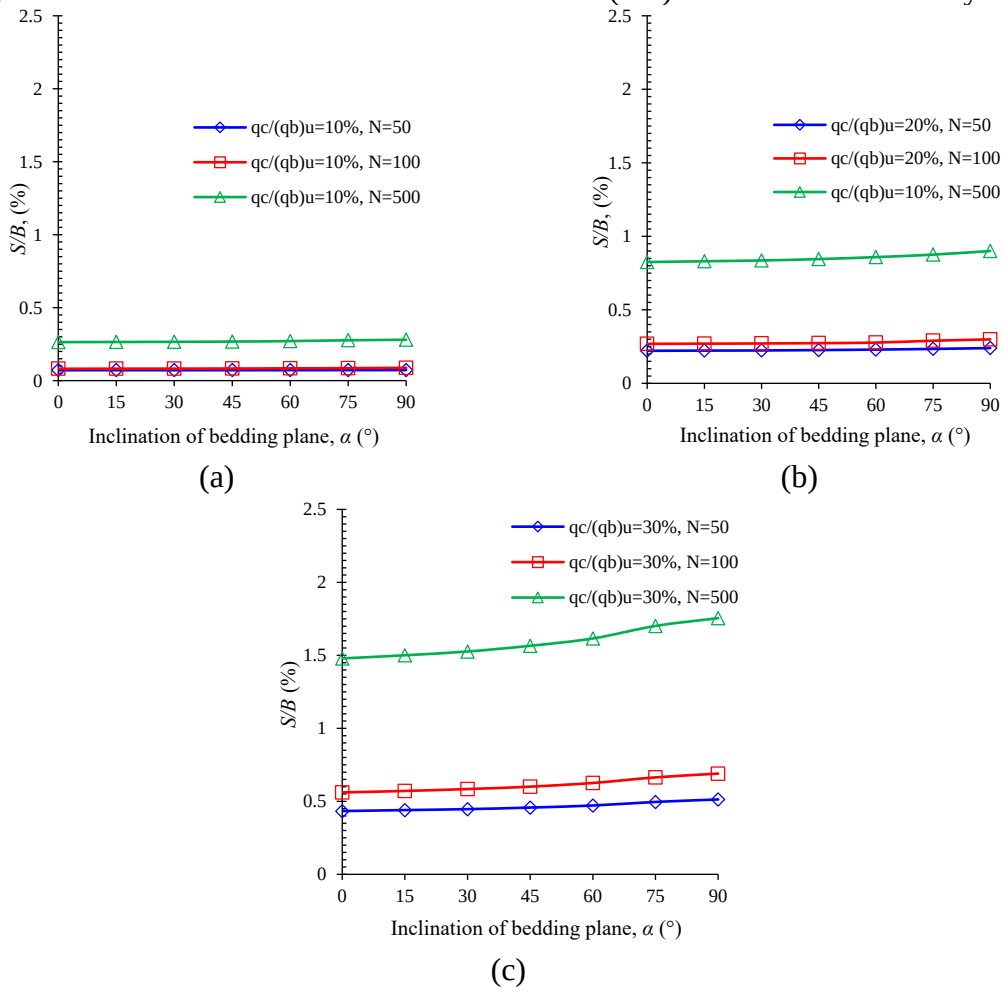

Figure 8.11 Variation of the *S/B* of cemented sand (5%) along *α* at selected numbers of load cycles *N* under $q_c/(q_b)_u$ = (a) 10%, (b) 20% and (c) 30%

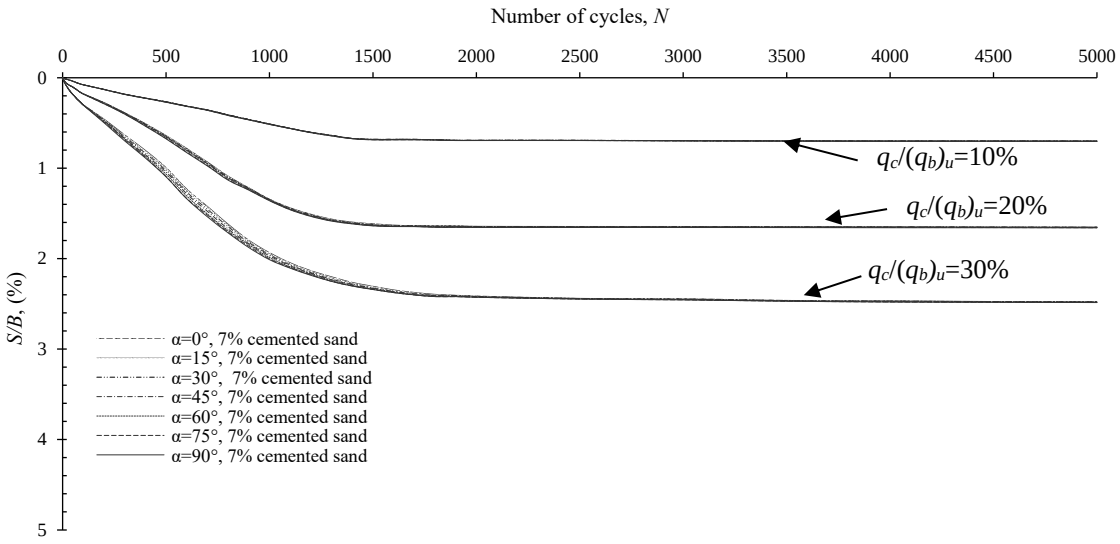

Figure 8.12: Variation of the *S/B* of cemented sand (7%) with number of load cycles *N*

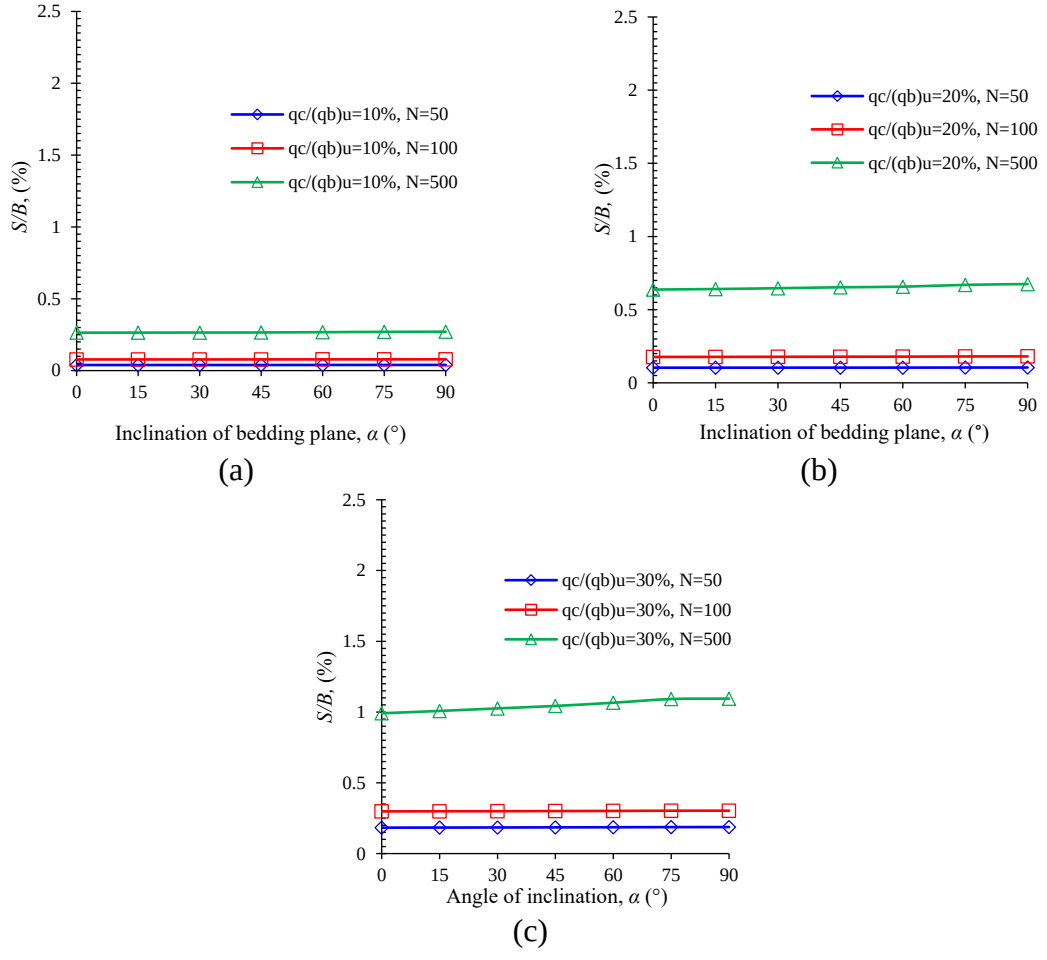

Figure 8.13: Variation of the *S/B* of cemented sand (7%) along α at selected numbers of load cycles *N* under $q_c/(q_b)_u$ = (a) 10%, (b) 20% and (c) 30%

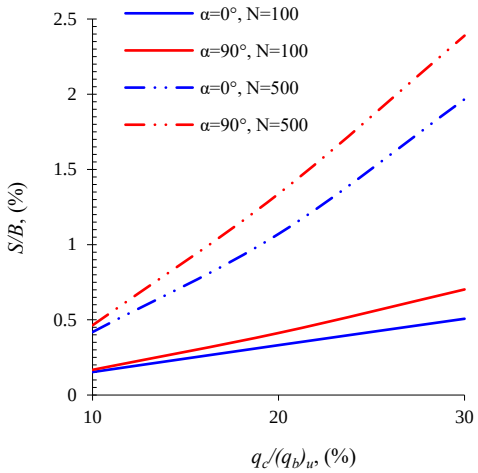

(a)

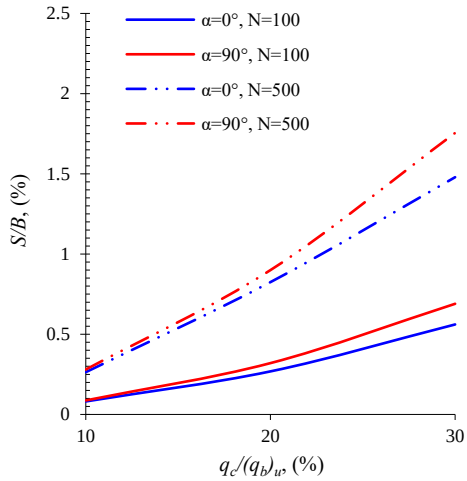

(b)

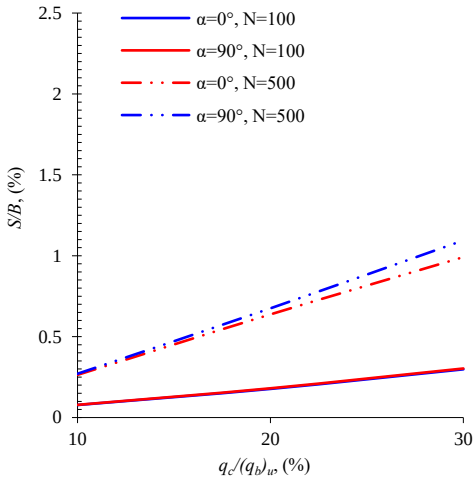

(c)

Figure 8.14 Variation of the *S/B* of cemented sand along loading amplitude $q_c/(q_b)_u$ for α = 0° and 90° at *N* = 100 and 500 and cement contents of (a) 3%, (b) 5% and (c) 7%

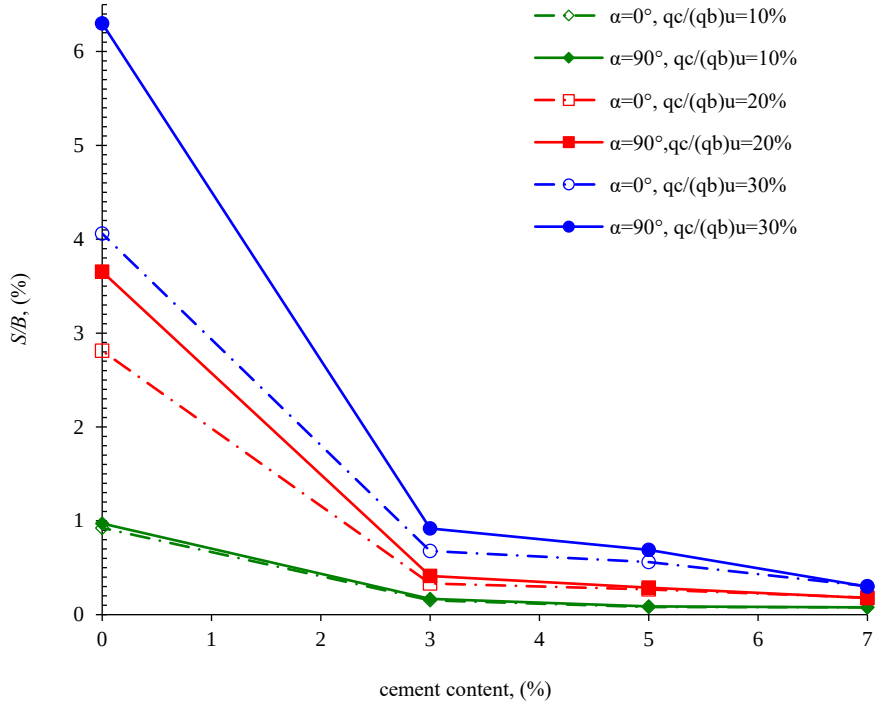

Figure 8.15 Variation of *S/B* with cement content

8.4 Discussion and Comparison of Performance of Uncemented and Cemented sand

This study aimed to investigate the macro-scale characteristics of sand strength and settlement at various bedding plane inclinations α, amplitudes of cyclic loading $q_c/(q_b)_u$, and cement contents. Although micro-scale behaviour is beyond the scope of this study, some discussion of it is included in the interpretation of the results. The ultimate bearing pressure of uncemented and cemented sand were summarised in Table 4.2.

8.4.1 Uncemented Sand

Sand with an inclination of $\alpha > 0°$ exhibited less bearing pressure and larger settlement than those when $\alpha = 0$. This is because the particles can rotate more easily due to the lower stability of the inclined fabric. Such instability has been reported by Sazzad and Suzuki (2010) and Seyedi Hosseininia (2012b). Once loading has begun, columnar

microstructures are formed of stacked particles along the load direction to withstand and transmit the applied stress (Oda et al., 1998; Seyedi Hosseininia, 2012b). These columnar microstructures are induced vertically due to the fact that loading tests were performed, as mentioned before, by applying a vertical load on an inclined bedding plane. Therefore, the widest columns occurred when α = 0° and resulted in the most stable state. However, with increases in the bedding plane angle, column width and, consequently, strength and stability, became lower as particles could more easily rotate due to the torque produced by the eccentricities of forces (Seyedi Hosseininia, 2012b). Further, the bedding plane has poor interlocking and, thus, when it was parallel to the load direction, reductions in strength and increases in settlement were observed. The variation in settlement is also attributable to the tremendous difference in the evolution of contact normal of particles during loading; many studies have found that a greater number of contacts occurs when α = 0° than at other inclinations (Fonseca et al., 2013; Seyedi Hosseininia, 2012b, 2013).

After a specific number of load cycles, the settlement curves of soils with different initial anisotropies converged. This can be attributed to the continuous orientation, realignment and rearrangement of sand particles as loading progresses or the number of load cycles increases, eventually resulting in a stable structure. This is consistent with Fonseca et al. (2013), who mentioned that anisotropic effects decrease during loading. This is related to the anisotropic critical state (ACS) proposed by Li and Dafalias (2012), where soil becomes independent of its initial fabric anisotropy unless severe particle breakage occurs. This critical state of anisotropy has been observed by Fu and Dafalias (2011b), Tong et al. (2014), Oda and Koishikawa (1979) and Sazzad and Suzuki (2010), who observed no changes in residual bearing capacity and internal friction due to the initial anisotropic fabric being destroyed by severe shear deformation along the failure zone. Seyedi Hosseininia (2012a) confirmed such destruction of initial anisotropy by reporting that there is a clear reduction in the frequency of particles oriented along a specific angle, α, compared with the initial pre-loading state. This reduction corresponds to a process of loss and creation of contacts in the anisotropic fabric during loading cycles. Sazzad and Suzuki (2010) and Sazzad (2014) reported significant breakage of contacts in the horizontal axis and generation

of new contacts in the vertical axis when α = 0°, while the reverse response occurs during unloading. For inclined bedding planes, particles tend to rotate in order to align horizontally and support the vertical load. This results in a loss of horizontal contacts and the creation of new vertical ones. In other words, more contacts are likely to occur in the vertical direction, leading to reduced fabric anisotropy at the end of loading. The opposite response occurs at the end of unloading, indicating that changes in the contact fabric reduce with increasing numbers of cycles due to particle reorientation and rearrangement. Consequently, variation in settlement is eliminated after a specific number of cycles which, in this study, was 1700 cycles.

Table 8.2 Summary of the ultimate bearing pressure of uncemented and cemented sand obtained under various α

Inclination of bedding plane, α (°)	Ultimate bearing pressure $(q_b)_u$, (kPa)			
	Uncemented sand	Cemented sand		
		3%	5%	7%
0	147.9	811.2	1096.3	1901.8
15	140.1	796.4	1091.8	1889.9
30	127.6	785.6	1071	1881.5
45	111.5	751.2	1064.3	1868.3
60	107.9	683.1	1021	1748.1
75	104.3	656.4	973.9	1743.7
90	110.0	660.0	963.1	1734.4
	Difference in ultimate bearing pressure, (%)			
	29.4	18.4	12.1	8.8

8.4.2 Cemented Sand

The behaviour of cemented sand is rather complex due to the combination of both cementation and the effect of fabric. Cementation occurs when cement particles gather around sand particles that are in contact with each other (Figure 8.16), resulting in parallel interparticle bonding. This phenomenon depends on many parameters, such as soil fabric, void ratio, and the cement type and content. These bonds contribute to stabilising the overall sand structure, making it more like a single block. The particles change from being loosely arranged to being cemented together and, as a consequence, the soil behavior is less dependent on particle properties such as angularity, shape, orientation and alignment. Interparticle bonding creates a stable structure that can sustain applied stresses as a single mass and reduces the susceptibility of the substance to behave as a granulate, i.e., anisotropic, material. When cemented sand is subjected to loading, all particles in the bonded network contribute to carrying the applied stress, resulting in a force chain that is distributed in a webbed pattern (Y. Wang & Leung, 2008). This makes soil more stable and eliminates dependence on individual particles.

In uncemented sand, directional dependence is related to differences in the stability of the columnar microstructures that are generated and the evolution of the contact normals in the direction of loading. With cementation, the bonding between particles stacked in columnar structures gives cemented blocks high stability. There is less variation in stability due to the inclination angle α and, as a consequence, the tendency of individual particles to rotate and/or collapse is reduced. Moreover, all particles in the bonding network share the applied load as a webbed force chain (Y. Wang & Leung, 2008) and, therefore, the evolution of the contact normals in the load direction is reduced. Moreover, mixing sand with cement contributes toward eliminating the tendency of particles to align horizontally.

As the loading, amplitude and/or number of cycles increases, however, stress concentrates inside the force chain and, consequently, value degradation may occur, initiating cracks (Figure 8.17) bond breakages and weak points (Lo, Lade, & Wardani, 2003; Saxena & Lastrico, 1978). Interparticle bonding is weakened due to elastic deformation, then debonding associated with plastic deformation occurs. This

breakage of bonds is initially slight, so that the bonding network is still intact, resulting in induced settlement even with the presence of cement. After that, bond destruction accelerates, particularly under high amplitudes, low cement contents and high cycle numbers, as reported by Saxena and Lastrico (1978) and Lo et al. (2003). Increases in load, stress or strain change the force chain into a columnar pattern due to concentrations of stress inside it, and the columns become subject to collapse (Y. Wang & Leung, 2008). The observed remaining directional dependence, even with cementation, may be attributed to this weakening and breakage of bonds. Stress becomes concentrated at particular locations in the force chain, resulting in lower stability. Accordingly, samples with high cement contents and subjected to low amplitude loadings exhibited insignificant anisotropic responses.

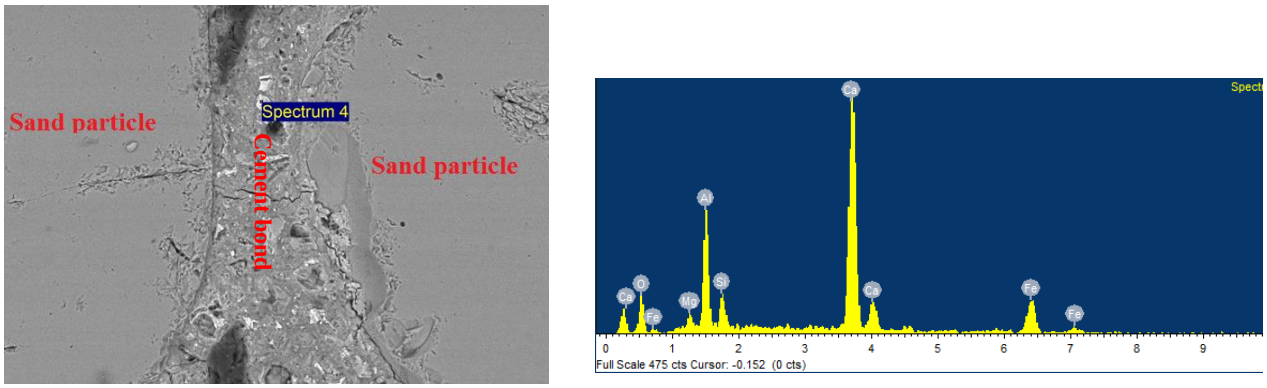

Figure 8.16: SEM image and the EDS showing cement bonding between sand particles (5% cement content)

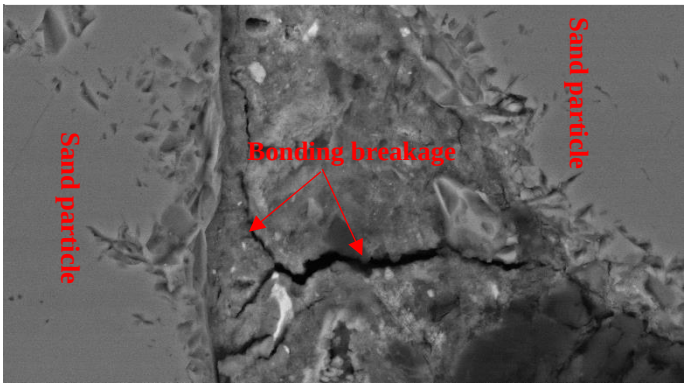

Figure 8.17: SEM image showing breakage in cementation bonds after shearing (5% cement content)

It is worth mentioning that although some bonding remained during the breakage process, properly-sized clusters and decemented particles became detached from the bonding network (Y. Wang & Leung, 2008). These detached, bonded clusters and cemented particles may also have roles in reducing directional dependency, as they act as fine materials that fill voids and alter the way the particles are packed. Moreover, broken cementation remains stuck to particles after breakage, giving them rough surfaces, and consequently, reducing the weakness in the plane that is caused by their preferential alignment.

Chapter 9

Conclusions and Recommendations

9.1 Introduction

Soil reinforcement is widely used in many geo-structures that induce complex anisotropic conditions, i.e. principal stresses with different directions α, different intermediate principal stress parameters b and/or cyclic rotation of the principal stress direction. However, the effect of anisotropy on the characterisation of reinforced sand has not yet been addressed. Therefore, investigation of the response of reinforced sand to such conditions is imperative.

This thesis focused on hollow cylinder torsional testing of reinforced sand in monotonic and cyclic rotation tests in order to better understand the characterisation of reinforced sand under anisotropic conditions. A fully-automated hollow torsional shear apparatus was the primary equipment used for this objective. This is the only type of device that provides independent control of four stress parameters, three principal stresses and the direction of principal stress. Thus, it can simulate shearing conditions under various values of α and b. Furthermore, it has the ability to rotate the direction of principal stress while the deviator stress and principal stresses are held constant.

The motivations behind this study were as follows:

1) Characterisation of reinforced sand via investigation of anisotropic effects related to variation in ***i)*** the direction of principal stress and ***ii)*** the intermediate principal stress parameter. Tested samples were reinforced with various layers of planar geosynthetics (geogrid and geotextile) and 3D geo-inclusion (geocell). The effects of adding clay to sand and reinforced sand were also investigated to show the extent to which it can reduce directional dependence.

2) Investigation of the effect of cyclic rotation of the principal stress direction on the characterisation of reinforced samples. During these tests, the magnitude of deviator stress was held constant while the direction of principal stress rotated continuously.

The effect of rotation was investigated under a constant value of q/p' = 1.1 for sand and mixed sand-clay samples, both unreinforced and reinforced with geogrid, geotextile and geocell. Furthermore, the effects of cyclic rotation of the principal stress direction at three different stress ratios (q/p' = 0.69, 0.9 and 1.1) were investigated for sand and geogrid-reinforced sand.

3) Investigation of the bearing pressure and settlement characterisation of sand cemented with Portland cement as a function of the angle of bedding plane α to the horizontal. The effect of the anisotropic bed was investigated under monotonic and cyclic tests.

The response of reinforced soil to such anisotropic stress states should be taken into account, particularly as anisotropy may be the reason for significant differences between the calculated and experimentally-modelled strengths and deformations that are often observed. These conditions result in significant differences in soil characteristics and can lead to significant uncertainties and problems in geotechnical constructions, if ignored. Thus, it is inappropriate to generalise a particular shear strength across multiple positions because this can lead to over- or under-estimation of bearing capacity. An approximate bearing capacity theory including such anisotropic effects is, therefore, very important to be considered in design, in order to avoid potential future problems. Moreover, anisotropy resulted in a significant amount of plastic deformation under continuous rotation of α. This should be considered in most geotechnical applications, particularly pavement to control rutting, where settlement and movement are major design considerations. It is clear that present results provide important guidance on the effects of anisotropy on strength/deformation properties, which has clear implications for design. Therefore, introducing the parameters of α, b and cyclic rotation of α into geotechnical engineering models of the performance of reinforced soils is a crucial step toward improving design guidelines and guaranteeing the safe design of geostructures. In conclusion, this study can provide a basis for further efforts to investigate anisotropic effects on reinforced sand to achieve solid designs and analysis of reinforced geostructures.

9.2 Conclusions

9.2.1 Effect of Principal Stress Direction on Geosynthetic-reinforced Sand/Sand-clay Mixtures

1. Sand reinforced with different types of geosynthetics exhibited larger peak deviator stress q_p under all directions of principal stress α compared with unreinforced clean sand. The largest improvement was achieved when geocell was used, while geogrid provided the minimum benefit. The peak deviator stress of sand at $\alpha = 0°$ increased by 141.4% when geocell was used for reinforcement, compared with 127.6% and 116.3% for six layers of geotextile and geogrid reinforcement, respectively.

2. The performance of reinforced sand varied significantly according to the direction of principal stress α. This variation can be divided into two ranges, $\alpha = 0–30°$ and $\alpha = 60–90°$. The improvement was significant for $\alpha \leq 30°$ and the anisotropic effect was minimal. However, there was a different trend for $\alpha \geq 60°$, where less improvement in strength was observed, corresponding with significant anisotropic effects. Reinforcement with the 3D geo-inclusion, i.e. geocell, resulted in significant improvement, even under conditions of $\alpha = 60–90°$. For instance, sand reinforced with six layers of planar reinforcement (geogrid and geotextile) showed increases in deviator stress of only 36.7–51.5% with $\alpha \geq 60°$, compared with 116.1–141.7% under $\alpha \leq 30°$. Meanwhile, geocell increased the deviator stress by 141.4–147.8% at $\alpha \leq 30°$ and 126.0–132.2% for $\alpha \geq 60°$.

3. Under all α values, q_p decreased as the clay fines content increased to 5%, then increased with 10% fines, before decreasing again with further fines addition. The developed peaks of deviator stress for mixed sand were less than those of clean sand, except for sand with 10% clay under $\alpha = 30–90°$, where larger peak deviator stress was observed. All sand-clay mixtures exhibited lower anisotropy than clean sand.

4. Adding 10% clay to geosynthetic-reinforced sand improved its performance, particularly under conditions of $\alpha = 60–90°$, and consequently, decreased the anisotropic effect on strength. The variation in deviator stress dropped to 29.4–37.3%

for planar-reinforced mixed sand-clay, compared with 47.7–50.4% for planar-reinforced clean sand, while for geocell-reinforced mixtures, it decreased to 16.4%, compared with 25.3% for geocell-reinforced clean sand.

5. All geo-inclusions effectively restrained volumetric strain under all directions of principal stress α, and geocell provided the largest restraint. However, as α increased, the volumetric strains for reinforced sand and reinforced mixed sand-clay approached each other. Moreover, the combination of the largest clay content and shearing under the largest direction of principal stress resulted in a significant decrease in the dilative volumetric strain, and vice versa. The dilative volumetric strain of reinforced sand-clay mixtures was lower than those of reinforced clean sand samples.

6. The improvements provided by planar reinforcements (geotextile and geogrid) can be primarily attributed to the confinement provided by the interfacial interaction, in addition to the internal shear resistance of soil particles inside the geogrid apertures, and the passive resistance that occurs along the transverse ribs of geogrid. However, with geocell reinforcement, the reinforcing action is primarily attributed to the all-around confinement provided by the 3D structure of the geocell. As mentioned in point 2 above, two trends were observed according to the value of α.

a. Shearing under α = 0–30° deforms sand particles laterally, inducing a shear interaction and interlocking of particles and the geo-inclusions, as mentioned in the above mechanism. These shear stresses are transmitted from the sand particles to the reinforcement layers, which become tensioned membranes. The induced lateral deformation of sand imposes an active pressure on the wall of the geocell, and thus, circumferential strain can develop on the membrane wall. Accordingly, the tensile strength of the planar layers and the curved geocell is mobilised, providing extra confinement. This additional confinement can bring sand particles closer to each other along with increase bonding between sand particles and the reinforcement. This induces frictional forces that likely contribute to arresting the lateral spread of the sand and increasing its strength. As a consequence, the lateral stability of reinforced samples increases, creating a stiff composite material.

b. However, the range of α = 60–90° corresponded with a clear anisotropic effect. This can be attributed to the fact that the ability of planar reinforcement layers (i.e. geogrid and geotextile), which are laid horizontally, to resist shearing decreases as the direction of principal stress approaches the horizontal bedding plane. Furthermore, within this range of α = 60–90°, the plane of maximum stress obliquity coincides with the horizontal bedding plane (the weakest plane). Moreover, it is worth noting that when $\alpha \geq 60°$, samples were sheared in an extension-like mode in which the radial stress σ_r became greater than the axial stress σ_z. Therefore, under such conditions, planar reinforcement does not provide as much resistance as when it is under compression. As consequence of the above-mentioned factors, geotextile and geogrid layers cannot be tensioned enough to provide the expected confinement of sand.

The significant decrease in anisotropy that occurs when geocell is used, compared with other reinforcements, is attributed to the fact that geocell is placed vertically in a way that surrounds the soil, rather than horizontally as with geogrid and geotextile. Therefore, confinement, friction and better interlocking between particles can be induced, even under inclined principal stresses. Moreover, by virtue of geocell's 3D structure that encloses the soil, the geocell walls contribute to resisting and delaying the possible initiation of the shear band, and intercept the failure planes under all directions of principal stress.

7. The lesser effect of α on unreinforced and reinforced sand-clay mixtures is attributed to the role of clay in occupying inter-particular voids in the sand. This fine material provides very good bonding between sand particles, and between sand and the planar reinforcement, in addition to providing a cushioning effect that improves interlocking and increases resistance to lateral or inclined loading. Furthermore, the presence of fines and a mixing process could significantly decrease the preferred alignment of particles compared with clean sand.

9.2.2 Effect of the Intermediate Principal Stress Parameter on Geosynthetic-reinforced Sand and Sand-clay Mixtures

1. Increasing the value of b decreased the peak deviator stress q_p irrespective of the principal stress direction α. Under all b values, there was clear variation in q_p along α. This decrease and variation in q_p was lower for sand containing 10% clay. As b increased from 0.2 to 1.0, q_p decreased in the range of 12.6–17.0% (depending on α) for sand and 10.4–12.6% for the sand-clay mixture. Regarding the compressive strain of sand, it is clear that the amount of compression strain increased with increasing b, particularly at b = 1.0. Samples tested under α = 0–30° showed less dilative volumetric strain $(\varepsilon_v)_{dil}$ when b was 1.0, compared with conditions of b = 0.2 or 0.5. However, samples under conditions of α = 60–90° showed increases in expansion strain with increasing b values,

2. The effect of b on the characterisation of reinforced sand was similar to the trend mentioned in point 1. Furthermore, adding 10% clay to reinforced sand resulted in a lesser effect of b on q_p. Minimum deviator stress generally occurred at α = 60° under b = 0.2 and 0.5, while it occurred at α = 90° under b = 1.0. The deviator stress q_p of sand with planar reinforcement decreased by 14.9–24.0% as b increased from 0.2 to 1.0 for different directions of principal stress, while it became 10.7 –17.2% when 10% clay was added. However, geocell-reinforced samples exhibited the least effect of b– the decrease in q_p was in the range 5.2–10.3% for geocell-reinforced sand and 3.5–6.2% for the geocell-reinforced sand-clay mixture.

It is noteworthy that the combination of a large direction of principal stress (α = 60–90°) and large intermediate principal stress parameter (b = 1.0) resulted in the lowest strength, while conditions of α = 0° and b = 0.2 produced the greatest strength.

3. This behaviour is attributed to the fact that b reflects the variation in radial stress σ_r, which is equal to σ_2 in the HCA. Accordingly, for b = 1.0, $\sigma_2 = \sigma_1 = \sigma_r$, while when b = 0.0, $\sigma_2 = \sigma_3 = \sigma_r$, and thus, the former case causes larger stresses along the horizontal plane than the latter case. Therefore, applying this largest horizontal stress along the horizontal direction of samples, which is characterised by poor interlocking and lower

stability of the columnar microstructures that form due to the preferred alignment of particles, causes lower deviator stress and larger compressive strain. As a consequence, the conditions b = 1.0 and α = 90° lead to the lowest resistance against the applied load. The lesser effect of b on unreinforced and reinforced sand after addition of clay is attributed to what was mentioned in point 7 in Section 9.2.1.

Under such conditions of increasing horizontal stress at the expense of vertical stress, soil pressure on horizontally-placed planar reinforcement decreases, resulting in less ability to mobilise the tensile strength of the planar geo-inclusions. However, the 3D type of reinforcement (geocell) acts on the entire perimeter of the sample due to the confinement provided by its mobilised tensioned wall, and thus, it provides larger improvement, even under b = 1.0.

9.2.3 Effect of Cyclic Rotation of Principal Stress Direction on Geosynthetic-reinforced Sand/Sand-clay Mixture

1. Unreinforced and reinforced sand exhibited significant strain that was induced by the rotation of the principal stress direction, although deviator stress was constant. Geocell provided better performance than geotextile and geogrid in terms of decreasing the induced strain components and the volumetric change of reinforced sand. In general, shear strain $\gamma_{z\theta}$ varied with oscillation mode, reaching its maximum contractive value at $\alpha \approx$ 65–70° and maximum expansive value at around 140–160°. The circumferential ε_θ and radial ε_r strains significantly increased in contractive form after α = 30–60°, and reached a maximum value at α = 105° before decreasing. However, dramatic increases in dilative axial strain ε_z occurred after α = 30–40° and reached a maximum value at α = 100–107°, followed by a steady decrease.

2. Plastic strains are induced mostly during the first few cycles of rotation despite the fact that stress states do return to their initial values (i.e., before rotation) at the end of each single cycle. These plastic strains in reinforced sand are much lower than those in unreinforced sand.

3. During cyclic rotation under q/p' = 0.69, induced volumetric strain and its variation along α decreased with increases in the number of geogrid layers. However, rotation

under q/p' = 0.9 and 1.1, caused failure in unreinforced sand and sand reinforced with three layers of geogrid at α = 50–60°. Samples reinforced with geocell, six layers of geotextile or geogrid sustained rotation under q/p' = 1.1 for 60 cycles, although with considerable induced strains. Adding clay to sand reinforced with geosynthetics reduced the induced volumetric strain.

4. The lower induced strains in reinforced samples can be attributed to the reinforcing mechanism explained in Section 9.2.1. Furthermore, the oscillatory characteristics of strains are linked to the variation in the applied stresses that lead to variation in the performance of the planar reinforcement. Before rotation, the sample is under an axial stress, resulting in an axial deformation that increases the interaction between the reinforcement and the sand, and mobilises the tensile strength of the reinforcement. Accordingly, reinforced samples exhibited better performance during rotation from α = 0° to α = 45°, in which $\sigma_z > \sigma_\theta$. However, during the rotation from α = 45° to α = 135°, the state changed to $\sigma_\theta > \sigma_z$, although σ_θ and σ_z decreased and increased, respectively, in the range α = 90–135°. Therefore, planar reinforcements was under-performed due to the fact that reinforced samples entered an extension mode that provides minimum interaction between the planar reinforcement and the sand particles. For the remaining range of rotation (α >135°), σ_z becomes larger than σ_θ, resulting in greater interaction and restraint. Restraint becomes more evident in subsequent cycles due to the densification and stress history that leads to advanced interaction between the layers and walls of the geo-inclusions and the sand particles.

5. A clear increase in the shear modulus was observed during the first few cycles of rotation due to the sand densification that occurs during cyclic rotation and also due to the shear history. Note that the rate of increase becomes smaller and more stable during subsequent cycles. Increasing the number of reinforcement layers results in significant increases in the shear modulus. The damping ratio λ calculated from the first cycle remains almost constant for both unreinforced and reinforced sands, due to the fact that the damping ratio of the soil is a function of the loading velocity represented by the frequency of loading during cycles. However, with increasing numbers of cycles, the damping ratio tends to decrease due to sand densification, where an associated decrease in the void ratio dissipates a lower amount of energy

during rotation. Increasing the stress ratio on the geogrid-reinforced sand resulted in a decrease in the shear modulus and damping ratio.

Adding 10% clay to sand resulted in a decrease in the shear modulus G for all types of geo-inclusion-reinforced samples. The damping ratio λ was approximately the same for all geo-inclusion-reinforced sand-10% clay mixtures.

9.2.4 Anisotropic Bearing Pressure and Settlement under Monotonic and Cyclic Tests

1. Bearing pressure-settlement ratio relationships were strongly affected by the initial anisotropy induced by different tilting angles of the bedding plane α. The difference between the maximum and minimum peak bearing capacity of clean sand due to anisotropy was about 29.4%. Furthermore, the settlement ratio, corresponding to peak bearing capacity, increased as α increased. This difference in the peak bearing pressure decreased significantly when cement was added to the sand, and was 18.4, 12.1 and 8.8% with cement contents of 3, 5 and 7%.

2. Under cyclic loading, the settlement of uncemented sand varied clearly with inclination angle α under larger amplitudes of $q_c/(q_b)_u$ of 20% and 30%. Furthermore, the number of cycles required to achieve 50% settlement decreased with increasing inclination angle α and with increasing amplitudes. Note that the combined conditions of $q_c/(q_b)_u$ = 30% and α = 75–90° delivered maximum footing settlement after applying cyclic loading. The variation in settlement that occurred due to α became insignificant after 900–1300 cycles (depending on the cyclic amplitudes).

On the other hand, the gap between settlement at α = 0° and that at 90° decreased when cement was added to the sand. Sand with 7% cement exhibited a small variation in induced settlement.

3. Directional dependence in uncemented sand is caused by differences in the stability of the columnar microstructures and the associated contact normals that evolve in the direction of loading. Adding cement promotes inter-particular bonding that creates a stable structure in which particles are transformed from being loosely arranged to

being cemented together. Consequently, there is reduced susceptibility to behaving as a granulate, i.e. anisotropic, material. This means that there is decreased dependence on particle characteristics such as shape, angularity, orientation and alignment. Furthermore, the mixing process inhibits the preferred alignment of sand particles.

However, as the amplitude and/or number of cycles increases, stress concentrates inside the force chain, and consequently, value degradation may occur, initiating cracks, bond breakages and weak points. Such breakage is initially slight, so that the bonding network is still intact, and induces elastic settlement even with the presence of cement. After that, the destruction of bonds accelerates, particularly under high amplitudes, low cement contents and high numbers of cycles.

It is worth mentioning that some properly-sized clusters and decemented particles become detached from the bonding network. These detached bonded clusters and cemented particles may also have roles in reducing directional dependency, as they act as fine materials that fill voids and form a different type of particle packing. Moreover, the broken cementing that remains stuck around particles after breakage creates rough surfaces, and consequently, contributes to preventing weakness in any plane due to the preferential alignment of particles.

9.3 Recommendations for Future Research

The current research has provided some understanding of the anisotropic characterisation of reinforced sand. However, due to limited time and other constraints, there are a number of aspects that require further research. The following topics are recommended for future study.

1. Evaluation of anisotropically-induced stresses and strains in reinforcements embedded in the field, under monotonic loading and cyclic rotation.
2. Extension of similar research to other soil types and/or other types of reinforcements.
3. Evaluation of the characterisation of reinforced sand under simultaneous changes in b and anisotropic consolidation.
4. A systematic investigation of the effects of particle shape, particle size, sand density (medium to loose state) on the anisotropic behavior of sand is recommended.
5. Evaluation of the effects of α, b and cyclic rotation on sand cemented with Portland cement under drained and undrained conditions.
6. Numerical modelling of reinforced sand based on experimental results could be undertaken using the discrete element method (DEM) or other methods. This method can study behavior at the micro scale, in addition to validating and further extending the anisotropic characterisation of reinforced sand.

References

Abdi, M., Sadrnejad, A., & Arjomand, M. (2009). Strength enhancement of clay by encapsulating geogrids in thin layers of sand. *Geotextiles and Geomembranes, 27*(6), 447-455.

Abu-Farsakh, M., & Chen, Q. (2011). Evaluation of geogrid base reinforcement in flexible pavement using cyclic plate load testing. *International Journal of Pavement Engineering, 12*(03), 275-288.

Abu-Farsakh, M., Souci, G., Voyiadjis, G. Z., & Chen, Q. (2011). Evaluation of factors affecting the performance of geogrid-reinforced granular base material using repeated load triaxial tests. *Journal of Materials in Civil Engineering, 24*(1), 72-83.

Acar, Y. B., & El-Tahir, E.-T. A. (1986). Low strain dynamic properties of artificially cemented sand. *Journal of Geotechnical Engineering, 112*(11), 1001-1015.

Afzali-Nejad, A., Lashkari, A., & Shourijeh, P. T. (2017). Influence of particle shape on the shear strength and dilation of sand-woven geotextile interfaces. *Geotextiles and Geomembranes, 45*(1), 54-66.

Aghajani, H. F., & Salehzadeh, H. (2015). Anisotropic behavior of the Bushehr carbonate sand in the Persian Gulf. *Arabian Journal of Geosciences, 8*(10), 8197-8217.

Al-Qadi, I., Brandon, T., & Bhutta, S. (1997). *Geosynthetics stabilized flexible pavements*. Paper presented at the Proceedings of Geosynthetics '97, IFAI, Long Beach, California,USA.

Al Hattamleh, O., Muhunthan, B., & Shalabi, F. (2009). Numerical simulation of fabric anisotropy and strain localization of sand under simple shear. *International Journal for Numerical and Analytical Methods in Geomechanics, 33*(9), 1255-1275.

Anubhav, & Basudhar, P. (2013). Interface behavior of woven geotextile with rounded and angular particle sand. *Journal of Materials in Civil Engineering, 25*(12), 1970-1974.

Arthur, J., & Assadi, A. (1977). *Ruptured sand sheared in plane strain.* Paper presented at the Proceedings of 9th international conference Soil Mechanics and Foundation Engineering, Tokyo.

Arthur, J., Chua, K., & Dunstan, T. (1977). Induced anisotropy in a sand. *Geotechnique, 27*(1), 13-30.

Arthur, J., & Menzies, B. (1972). Inherent anisotropy in a sand. *Geotechnique, 22*(1), 115-128.

Arthur, J., & Phillips, A. (1975). Homogeneous and layered sand in triaxial compression. *Geotechnique, 25*(4), 799-815.

ASTM D4253. (2016). Standard Test Methods for Maximum Index Density and Unit Weight of Soils Using a Vibratory Table. from ASTM International www.astm.org

ASTM D4318. (2017). Standard Test Methods for Liquid Limit, Plastic Limit, and Plasticity Index of Soils. from ASTM International www.astm.org

ASTM D6637/D6637M. (2015). Standard Test Method for Determining Tensile Properties of Geogrids by the Single or Multi-Rib Tensile Method. from ASTM International www.astm.org

ASTM D422. (2007). Standard Test Method for Particle-Size Analysis of Soils In. ASTM International, West Conshohocken, PA, 2007.
ASTM D854. (2014). Standard Test Method For Specific Gravity Of Soil Solids By Water Pycnometer. from ASTM International www.astm.org
ASTM D4254. (2016). Standard Test Methods for Minimum Index Density and Unit Weight of Soils and Calculation of Relative Density. from ASTM International www.astm.org
ASTM D4595. (2017). Standard Test Method for Tensile Properties of Geotextiles by the Wide-Width Strip Method. from ASTM International www.astm.org
Azami, A., Pietruszczak, S., & Guo, P. (2010). Bearing capacity of shallow foundations in transversely isotropic granular media. *International Journal for Numerical and Analytical Methods in Geomechanics, 34*(8), 771-793.
Bahadori, H., Ghalandarzadeh, A., & Towhata, I. (2008). Effect of non plastic silt on the anisotropic behavior of sand. *Soils and foundations, 48*(4), 531-545.
Bathurst, R. J., & Karpurapu, R. (1993). Large-scale triaxial compression testing of geocell-reinforced granular soils. *ASTM Geotechnical Testing Journal, 16*(3), 296-303.
Bergado, D., Chai, J., Abiera, H., Alfaro, M., & Balasubramaniam, A. (1993). Interaction between cohesive-frictional soil and various grid reinforcements. *Geotextiles and Geomembranes, 12*(4), 327-349.
Cabalar, A. F. (2011). The effects of fines on the behaviour of a sand mixture. *Geotechnical and Geological Engineering, 29*(1), 91-100.
Çabalar, A. F., & Mustafa, W. S. (2015). Fall cone tests on clay–sand mixtures. *Engineering Geology, 192*, 154-165.
Cai, Y. (2010). *An experimental study of non-coaxial soil behaviour using hollow cylinder testing.* University of Nottingham,
Cai, Y., Yu, H.-S., Wanatowski, D., & Li, X. (2012). Noncoaxial behavior of sand under various stress paths. *Journal of Geotechnical and Geoenvironmental Engineering, 139*(8), 1381-1395.
Cancelli, A., & Montanelli, F. (1999). *In-ground test for geosynthetic reinforced flexible paved roads.* Paper presented at the Proceedings of Geosynthetics Boston, USA.
Cancelli, A., Rimoldi, P., & Montanelli, F. (1993). Index and performance tests for geocells in different applications. In J. Cheng (Ed.), *Geosynthetic Soil Reinforcement Testing Procedures* (pp. 64-75): ASTM International.
Carraro, J. A. H., Prezzi, M., & Salgado, R. (2009). Shear strength and stiffness of sands containing plastic or nonplastic fines. *Journal of Geotechnical and Geoenvironmental Engineering, 135*(9), 1167-1178.
Casagrande, A. (1944). Shear failure of anisotropic materials. *Proc. Boston Soc. Civ. Engineers, 31*, 74-87.
Chandrasekaran, B., Broms, B. B., & Wong, K. S. (1989). Strength of fabric reinforced sand under axisymmetric loading. *Geotextiles and Geomembranes, 8*(4), 293-310.
Chen, H., & Wan, J. P. (2004). The effect of orientation and shape distribution of gravel on slope angles in central Taiwan. *Engineering Geology, 72*(1), 19-31.
Chen, Q., & Abu-Farsakh, M. (2010). Field Rutting Performance of Various Base and Subbase Materials Under Two Types of Loading. *Transportation Research Record: Journal of the Transportation Research Board*(2186), 90-100.

Chen, R., Huang, Y., & Huang, F. (2013). Confinement effect of geocells on sand samples under triaxial compression. *Geotextiles and Geomembranes, 37*, 35-44.

Chen, X., Jia, Y., & Zhang, J. (2017). Geogrid-reinforcement and the critical state of graded aggregates used in heavy-haul railway transition subgrade. *Transportation Geotechnics, 11*, 27-40.

Clough, G. W., Iwabuchi, J., Rad, N. S., & Kuppusamy, T. (1989). Influence of cementation on liquefaction of sands. *Journal of Geotechnical Engineering, 115*(8), 1102-1117.

Clough, G. W., Kuck, W. M., & Kasali, G. (1979). Silicate-stabilized sands. *Journal of Geotechnical and Geoenvironmental Engineering, 105*(1), 65–82.

Clough, G. W., Sitar, N., Bachus, R. C., & Rad, N. S. (1981). Cemented sands under static loading. *Journal of Geotechnical Engineering Division, 107*(6), 799–817.

Coli, N., Boldini, D., Bandini, A., & Lopes, D. (2012). *Modeling of complex geological rock mixtures under triaxial testing conditions.* Paper presented at the ISRM International Symposium-EUROCK 2012, Stockholm, Sweden.

Consoli, N. C., Cruz, R. C., Floss, M. F., & Festugato, L. (2010). Parameters controlling tensile and compressive strength of artificially cemented sand. *Journal of Geotechnical and Geoenvironmental Engineering, 136*(5), 759-763.

Consoli, N. C., Montardo, J. P., Prietto, P. D. M., & Pasa, G. S. (2002). Engineering behavior of a sand reinforced with plastic waste. *Journal of Geotechnical and Geoenvironmental Engineering, 128*(6), 462-472.

Consoli, N. C., Rotta, G., & Prietto, P. (2006). Yielding-compressibility-strength relationship for an artificially cemented soil cured under stress. *Geotechnique, 56*(1), 69-72.

Consoli, N. C., Vendruscolo, M. A., Fonini, A., & Dalla Rosa, F. (2009). Fiber reinforcement effects on sand considering a wide cementation range. *Geotextiles and Geomembranes, 27*(3), 196-203.

Consoli, N. C., Vendruscolo, M. A., & Prietto, P. D. M. (2003). Behavior of plate load tests on soil layers improved with cement and fiber. *Journal of Geotechnical and Geoenvironmental Engineering, 129*(1), 96-101.

Coop, M., & Atkinson, J. (1993). The mechanics of cemented carbonate sands. *Geotechnique, 43*(1), 53-67.

Da Fonseca, A. V., Rios, S., Amaral, M., & Panico, F. (2013). Fatigue cyclic tests on artificially cemented soil. *Geotechnical testing journal, 36*(2), 227-235.

Dafalla, M. A. (2013). Effects of clay and moisture content on direct shear tests for clay-sand mixtures. *Advances in Materials Science and Engineering, 2013*, 1-8.

Das, B. M., & Omar, M. (1994). The effects of foundation width on model tests for the bearing capacity of sand with geogrid reinforcement. *Geotechnical & Geological Engineering, 12*(2), 133-141.

Das, B. M., & Sobhan, K. (2013). *Principles of geotechnical engineering*: Cengage Learning.

Dash, S. K. (2010). Influence of relative density of soil on performance of geocell-reinforced sand foundations. *Journal of Materials in Civil Engineering, 22*(5), 533-538.

Dash, S. K., Krishnaswamy, N., & Rajagopal, K. (2001). Bearing capacity of strip footings supported on geocell-reinforced sand. *Geotextiles and Geomembranes, 19*(4), 235-256.

Dos Santos, A. S., Consoli, N. C., & Baudet, B. (2010). The mechanics of fibre-reinforced sand. *Geotechnique, 60*(10), 791-799.

Eghbali, A., & Fakharian, K. (2014). Effect of principal stress rotation in cement-treated sands using triaxial and simple shear tests. *International Journal of Civil Engineering, 12*(1), 1-14.

Espinoza, R., & Bray, J. (1995). An integrated approach to evaluating single-layer reinforced soils. *Geosynthetics International, 2*(4), 723-739.

Fei, K. (2016). Experimental study of the mechanical behavior of clay–aggregate mixtures. *Engineering Geology, 210*, 1-9.

Fonseca, J., O'Sullivan, C., Coop, M., & Lee, P. (2013). Quantifying the evolution of soil fabric during shearing using scalar parameters. *Geotechnique, 63*(10), 818-829.

Fu, P., & Dafalias, Y. F. (2011). Study of anisotropic shear strength of granular materials using DEM simulation. *International Journal for Numerical and Analytical Methods in Geomechanics, 35*(10), 1098-1126.

Futaki, M., Suzuki, H., & Yamato, S. (1990). *Super Large Triaxial Compression Tests on Reinforced Sand with High-Strength Geogrid.* Paper presented at the Proceedings of the 4th International Conference on Geotextiles, Geomembranes and Related Products, The Hague, The Netherlands.

Gao, Z., & Zhao, J. (2012). Constitutive modeling of artificially cemented sand by considering fabric anisotropy. *Computers and Geotechnics, 41*, 57-69.

GCTS. (2016). HCA-600 Large Scale Dynamic Hollow Cylinder Testing System. Retrived from www.gcts.com.

Georgiannou, V. N. (1988). *The behaviour of clayey sands under monotonic and cyclic loading.* Imperial College London (University of London),

Georgiannou, V. N., Burland, J., & Hight, D. (1990). The undrained behaviour of clayey sands in triaxial compression and extension. *Geotechnique, 40*(3), 431-449.

Giroud, J. P., & Han, J. (2004). Design method for geogrid-reinforced unpaved roads. I. Development of design method. *Journal of Geotechnical and Geoenvironmental Engineering, 130*(8), 775-786.

Gray, D. H., & Al-Refeai, T. (1986). Behavior of fabric-versus fiber-reinforced sand. *Journal of Geotechnical Engineering, 112*(8), 804-820.

Guo, L., Chen, J., Wang, J., Cai, Y., & Deng, P. (2016). Influences of stress magnitude and loading frequency on cyclic behavior of K 0-consolidated marine clay involving principal stress rotation. *Soil Dynamics and Earthquake Engineering, 84*, 94-107.

Guo, P. (2008). Modified direct shear test for anisotropic strength of sand. *Journal of Geotechnical and Geoenvironmental Engineering, 134*(9), 1311-1318.

Guo, P., & Stolle, D. F. E. (2005). On the failure of granular materials with fabric effects. *Soils and foundations, 45*(4), 1-12.

Gurbuz, A., & Mertol, H. C. (2012). Interaction between assembled 3D honeycomb cells produced from high density polyethylene and a cohesionless soil. *Journal of Reinforced Plastics and Composites, 31*(12), 828-836.

Habibi, M., Shafiee, A., & Jafari, M. (2014). Monotonic Behavior of Geotextile Reinforced Soils under Discrete Rotation of Principal Stresses. *Iranian Journal of Science and Technology. Transactions of Civil Engineering, 38*, 325-335.

Haeri, S., Noorzad, R., & Oskoorouchi, A. (2000). Effect of geotextile reinforcement on the mechanical behavior of sand. *Geotextiles and Geomembranes, 18*(6), 385-402.

Hamidi, A., & Haeri, S. M. (2008). Stiffness and deformation characteristics of a cemented gravely sand. *International Journal of Civil Engineering, 6*(3), 159-173.

Han, J., Yang, X., Leshchinsky, D., & Parsons, R. (2008). Behavior of geocell-reinforced sand under a vertical load. *Transportation Research Record: Journal of the Transportation Research Board*(2045), 95-101.

Haruyama, M. (1981). Anisotropic deformation-strength characteristics of an assembly of spherical particles under three dimensional stresses. *Soils and foundations, 21*(4), 41-55.

Hight, D., Gens, A., & Symes, M. (1983). The development of a new hollow cylinder apparatus for investigating the effects of principal stress rotation in soils. *Geotechnique, 33*(4), 355-383.

Higuchi, T., Ishihara, K., Tsukamoto, Y., & Masuo, T. (1998). Deformation and strength of geogrid-reinforced granular soil at plane strain conditions. *Soils and foundations, 38*(1), 221-227.

Hryciw, R. D., Zheng, J., & Shetler, K. (2016). Particle roundness and sphericity from images of assemblies by chart estimates and computer methods. *Journal of Geotechnical and Geoenvironmental Engineering, 142*(9), 04016038.

Hsiao, D.-H., Phan, V. T.-A., Hsieh, Y.-T., & Kuo, H.-Y. (2015). Engineering behavior and correlated parameters from obtained results of sand–silt mixtures. *Soil Dynamics and Earthquake Engineering, 77*, 137-151.

Huang, C., & Tatsuoka, F. (1990). Bearing Capacity of Reinforced Horizontal Sandy Ground. *Geotextiles and Geomembranes, 9*(1), 51-82.

Huang, J., & Airey, D. (1998). Properties of artificially cemented carbonate sand. *Journal of Geotechnical and Geoenvironmental Engineering, 124*(6), 492-499.

Infante, D. J. U., Martinez, G. M. A., Arrua, P. A., & Eberhardt, M. (2016). Shear Strength Behavior of Different Geosynthetic Reinforced Soil Structure from Direct Shear Test. *International Journal of Geosynthetics and Ground Engineering, 2*(2), 1-16.

Iwasaki, T., & Tatsuoka, F. (1977). Effects of grain size and grading on dynamic shear moduli of sands. *Soils and foundations, 17*(3), 19-35.

Jewell, R. (1990). Reinforcement bond capacity. *Geotechnique, 40*(3), 513-518.

Jewell, R. (1996). *Soil reinforcement with geotextiles*: Construction Industry Research and Information Association.

Jewell, R., & Wroth, C. (1987). Direct shear tests on reinforced sand. *Geotechnique, 37*(1), 53-68.

Jiang, M., Li, L., & Yang, Q. (2013). Experimental investigation on deformation behavior of TJ-1 lunar soil simulant subjected to principal stress rotation. *Advances in Space Research, 52*(1), 136-146.

Jiang, X., Cui, P., & Ge, Y. (2015). Effects of fines on the strength characteristics of mixtures. *Engineering Geology, 198*, 78-86.

Juran, I., Knochenmus, G., Acar, Y., & Arman, A. (1988). Pull-out response of geotextiles and geogrids (synthesis of available experimental data). In R. D. Holtz (Ed.), *Geotechnical Special Publication* (pp. 92-111). New York, USA: ASCE.

Juran, I., & Riccobono, O. (1991). Reinforcing soft soils with artificially cemented compacted-sand columns. *Journal of Geotechnical Engineering, 117*(7), 1042-1060.

Kallstenius, T., & Bergau, W. (1961). *Research on the texture of granular masses.* Paper presented at the Proceedings of the 5th international conference on soil mechanics and foundation engineering.

Kandasami, R. K., & Murthy, T. G. (2014). Effect of intermediate principal stress on the mechanical behavior of angular sand. In *Soil Behavior and Geomechanics* (pp. 406-415).

Kandasami, R. K., & Murthy, T. G. (2015). Experimental studies on the influence of intermediate principal stress and inclination on the mechanical behaviour of angular sands. *Granular Matter, 17*(2), 217-230.

Kawamura, S., & Miura, S. (2014). Bearing capacity improvement of anisotropic sand ground. *Proceedings of the Institution of Civil Engineers-Ground Improvement, 167*(3), 192-205.

Kawamura, S., Miura, S., & Yokohama, S. (2010). Mechanical behavior of anisotropic sand ground beneath structures subjected to cyclic loading such as wave loading. *Soils and foundations, 50*(5), 645-657.

Keyhani, R., & Haeri, S. M. (2013). Evaluation of the effect of anisotropic consolidation and principle stress rotation on undrained behavior of silty sands. *Scientia Iranica. Transaction A, Civil Engineering, 20*(6), 1637.

Khedkar, M., & Mandal, J. (2009). Behaviour of cellular reinforced sand under triaxial loading conditions. *Geotechnical and Geological Engineering, 27*(5), 645-658.

Kim, Y.-S., Oh, S.-W., & Cho, D.-S. (2010). Effect of non-woven geotextile reinforcement on mechanical behavior of sand. *Journal of the Korean Geosynthetic Society, 9*(4), 39-45.

Kinney, T., Abbott, J., & Schuler, J. (1998). Benefits of using geogrids for base reinforcement with regard to rutting. *Transportation Research Record: Journal of the Transportation Research Board*(1611), 86-96.

Kirar, B., & Maheshwari, B. (2013). *Effects of Silt Content on Dynamic Properties of Solani Sand.* Paper presented at the Proceeding of 7th International Conferences on Case Histories in Geotechnical Engineering, Chicago.

Koerner, R. (1986). Designing wiih Geosynthetics. In: Prentice-Hall, Eaglewood Cliffs, New Jersey.

Kumar, G., & Wood, D. M. (1999). Fall cone and compression tests on clay±gravel mixtures. *Geotechnique, 49*(6), 727-739.

Kumruzzaman, M., & Yin, J.-H. (2010a). Influence of principal stress direction on the stress-strain-strength behaviour of completely decomposed granite. *Facta universitatis-series: Architecture and Civil Engineering, 8*(1), 79-97.

Kumruzzaman, M., & Yin, J.-H. (2010b). Influences of principal stress direction and intermediate principal stress on the stress–strain–strength behaviour of

completely decomposed granite. *Canadian Geotechnical Journal, 47*(2), 164-179.

Lade, P. V., & Duncan, J. M. (1973). Cubical triaxial tests on cohesionless soil. *Journal of Soil Mechanics & Foundations Div, 99*(10), 793–811.

Lade, P. V., Liggio, C., & Yamamuro, J. A. (1998). Effects of non-plastic fines on minimum and maximum void ratios of sand. *Geotechnical testing journal, 21*(4), 336-347.

Lade, P. V., Rodriguez, N. M., & Van Dyck, E. J. (2014). Effects of principal stress directions on 3D failure conditions in cross-anisotropic sand. *Journal of Geotechnical and Geoenvironmental Engineering, 140*(2), 04013001.

Lal, D., Sankar, N., & Chandrakaran, S. (2017). Effect of reinforcement form on the behaviour of coir geotextile-reinforced sand through laboratory triaxial compression tests. *International Journal of Geotechnical Engineering*, 1-7.

Latha, M. G., & Murthy, V. S. (2006). Investigations on sand reinforced with different geosynthetics. *Geotechnical testing journal, 29*(6), 474–481.

Latha, M. G., & Murthy, V. S. (2007). Effects of reinforcement form on the behavior of geosynthetic reinforced sand. *Geotextiles and Geomembranes, 25*(1), 23-32.

Lee, M.-J., Hong, S.-J., Choi, Y.-M., & Lee, W. (2010). Evaluation of deformation modulus of cemented sand using CPT and DMT. *Engineering Geology, 115*(1), 28-35.

Lekarp, F., & Dawson, A. (1998). Modelling permanent deformation behaviour of unbound granular materials. *Construction and building materials, 12*(1), 9-18.

Leroueil, S., & Hight, D. (2003). Behaviour and properties of natural soils and soft rocks. In T. S. Tan, K. K. Phoon, D. W. Hight, & S. Leroueil (Eds.), *Characterisation and engineering properties of natural soils* (Vol. 1, pp. 29-254).

Leshchinsky, B., & Ling, H. (2012). Effects of geocell confinement on strength and deformation behavior of gravel. *Journal of Geotechnical and Geoenvironmental Engineering, 139*(2), 340-352.

Li, X., & Dafalias, Y. F. (2002). Constitutive modeling of inherently anisotropic sand behavior. *Journal of Geotechnical and Geoenvironmental Engineering, 128*(10), 868-880.

Li, X., & Dafalias, Y. F. (2004). A constitutive framework for anisotropic sand including non-proportional loading. *Geotechnique, 54*(1), 41-55.

Li, X., & Dafalias, Y. F. (2011). Anisotropic critical state theory: role of fabric. *Journal of Engineering Mechanics, 138*(3), 263-275.

Li, X., Yang, D., & Yu, H.-S. (2016). Macro deformation and micro structure of 3D granular assemblies subjected to rotation of principal stress axes. *Granular Matter, 18*(3), 1-20.

Li, X., & Yu, H.-S. (2009). Influence of loading direction on the behavior of anisotropic granular materials. *International Journal of Engineering Science, 47*(11), 1284-1296.

Li, X., & Yu, H.-S. (2010). Numerical investigation of granular material behaviour under rotational shear. *Geotechnique, 60*(5), 381-394.

Li, Y., Huang, R., Chan, L. S., & Chen, J. (2013). Effects of particle shape on shear strength of clay-gravel mixture. *KSCE Journal of Civil Engineering, 17*(4), 712-717.

Lindquist, E., & Goodman, R. (1994). Strength and deformation properties of a physical model melange. In L. S. Nelson PP (Ed.), *1st North American Rock Mechanics Symposium* (pp. 843–850). Balkema, Rotterdam: American Rock Mechanics Association.

Ling, H. I. (2003). Civil and Environmental Applications of Geosynthetics. In H. I. Ling, D. Leshchinsky, & F. Tatsuoka (Eds.), *Reinforced Soil Engineering: Advances in Research and Practice* (pp. 1). New York: Marcel Dekker, INC.

Liu, C.-N., Yang, K.-H., & Nguyen, M. D. (2014). Behavior of geogrid–reinforced sand and effect of reinforcement anchorage in large-scale plane strain compression. *Geotextiles and Geomembranes, 42*(5), 479-493.

Liu, C.-N., Zornberg, J. G., Chen, T.-C., Ho, Y.-H., & Lin, B.-H. (2009). Behavior of geogrid-sand interface in direct shear mode. *Journal of Geotechnical and Geoenvironmental Engineering, 135*(12), 1863-1871.

Lo, S.-C., Lade, P. V., & Wardani, S. (2003). An experimental study of the mechanics of two weakly cemented soils. *Geotechnical testing journal, 26*(3), 328-341.

Lopes, M.-L. (2002). Soil-geosynthetic interaction. In K. S. Sanjay (Ed.), *Geosynthetics and Their Applications* (pp. 55-78): Thomas Telford, London.

Maheshwari, B., Kale, S., & Kaynia, A. (2012). Dynamic properties of Solani sand at large strains: a parametric study. *International Journal of Geotechnical Engineering, 6*(3), 353-358.

Mahmood, A., & Mitchell, J. (1974). Fabric-property relationships in fine granular materials. *Clays and Clay minerals, 22*(516), 397-408.

Mali, S., & Singh, B. (2015). Influence of Geocell and Fibre Reinforcement on Strength Behaviour of a Sandy Soil. *Journal of Civil Engineering and Environmental Technology, 2*(3), 228-233

Marri, A., Uddin, S., & Wanatowski, D. (2014). Sample Preparation Technique for Fiber Reinforced Cemented Soils. *Procedia Engineering, 77*, 140-147.

Marri, A., Wanatowski, D., & Yu, H. (2012). Drained behaviour of cemented sand in high pressure triaxial compression tests. *Geomechanics and Geoengineering, 7*(3), 159-174.

Matsuoka, H. (1974). Stress-strain relationships of sands based on the mobilized plane. *Soils and foundations, 14*(2), 47-61.

Matsuoka, H., & Geka, H. (1983). A stress-strain model for granular materials considering mechanism of fabric change. *Soils and foundations, 23*(2), 83-97.

Maurer, D. A., & Malasheskie, G. J. (1989). Field performance of fabrics and fibers to retard reflective cracking. *Geotextiles and Geomembranes, 8*(3), 239-267.

Medley, E. (2004). Observations on tortuous failure surfaces in bimrocks. *Felsbau Rock Soil Eng-J Eng Geol Geomech Tunnell, 5*, 35-43.

Medley, E., & Lindquist, E. S. (1995). *The engineering significance of the scale-independence of some Franciscan melanges in California, USA.* Paper presented at the The 35th US Symposium on Rock Mechanics (USRMS), Rotterdam.

Menéndez, B., Zhu, W., & Wong, T.-F. (1996). Micromechanics of brittle faulting and cataclastic flow in Berea sandstone. *Journal of structural geology, 18*(1), 1-16.

Michalowski, R. L., & Čermák, J. (2003). Triaxial compression of sand reinforced with fibers. *Journal of Geotechnical and Geoenvironmental Engineering, 129*(2), 125-136.

Milligan, G., Earl, R., & Bush, D. (1990). *Observations of photo-elastic pullout tests on geotextiles and geogrids.* Paper presented at the 4th International Conference on Geotextiles, Geomembranes and Related Products, The Hague, The Netherlands.

Miura, K., Miura, S., & Toki, S. (1986). Deformation behavior of anisotropic dense sand under principal stress axes rotation. *Soils and foundations, 26*(1), 36-52.

Moghaddas-Nejad, F., & Small, J. C. (1996). Effect of geogrid reinforcement in model track tests on pavements. *Journal of transportation engineering, 122*(6), 468-474.

Mollins, L. H. (1996). *The design of bentonite-sand mixtures.* University of Leeds,

Mollins, L. H., Stewart, D., & Cousens, T. (1999). The drained strength of bentonite enhanced sand. *Geotechnique, 49*(4), 523-528.

Montanelli, F., Zhao, A., & Rimoldi, P. (1997). *Geosynthetic-reinforced pavement system: testing and design.* Paper presented at the Proceeding of Geosynthetics, Long Beach, California.

Mounes, S. M., Karim, M. R., Mahrez, A., & Khodaii, A. (2011). An overview on the use of geosynthetics in pavement structures. *Scientific Research and Essays, 6*(11), 2234-22418.

Naeini, S., & Baziar, M. (2004). Effect of fines content on steady-state strength of mixed and layered samples of a sand. *Soil Dynamics and Earthquake Engineering, 24*(3), 181-187.

Naeini, S., & Gholampoor, N. (2014). Cyclic behaviour of dry silty sand reinforced with a geotextile. *Geotextiles and Geomembranes, 42*(6), 611-619.

Naeini, S., Khalaj, M., & Izadi, E. (2013). Interfacial shear strength of silty sand–geogrid composite. *Proceedings of the Institution of Civil Engineers-Geotechnical Engineering, 166*(1), 67-75.

Nakase, A., & Kamei, T. (1983). Undrained shear strength anisotropy of normally consolidated cohesive soils. *Soils and foundations, 23*(1), 91-101.

Nakata, Y., Hyodo, M., Murata, H., & Yasufuku, N. (1998). Flow deformation of sands subjected to principal stress rotation. *Soils and foundations, 38*(2), 115-128.

Naughton, P. J., & O'Kelly, B. C. (2001). *An overview of the University College Dublin hollow cylinder apparatus.* Paper presented at the Proceedings of the 14th Young European Geotechnical Engineer's Conference, Sofia, Bulgaria.

Nazzal, M., Abu-Farsakh, M., & Mohammad, L. (2007). Laboratory characterization of reinforced crushed limestone under monotonic and cyclic loading. *Journal of Materials in Civil Engineering, 19*(9), 772-783.

Nemat-Nasser, S. (1980). On behavior of granular materials in simple shear. *Soils and foundations, 20*(3), 59-73.

Nemat-Nasser, S. (2000). A micromechanically-based constitutive model for frictional deformation of granular materials. *Journal of the Mechanics and Physics of Solids, 48*(6), 1541-1563.

Nguyen, M., Yang, K., Lee, S., Wu, C., & Tsai, M. (2013). Behavior of nonwoven-geotextile-reinforced sand and mobilization of reinforcement strain under triaxial compression. *Geosynthetics International, 20*(3), 207-225.

Nishimura, S., Minh, N., & Jardine, R. (2007). Shear strength anisotropy of natural London Clay. *Geotechnique, 57*(1), 49-62.

Nouri, S., Nechnech, A., Lamri, B., & Lopes, M. L. (2016). Triaxial test of drained sand reinforced with plastic layers. *Arabian Journal of Geosciences, 9*(1), 53.
O'Kelly, B. C., & Naughton, P. J. (2005). Development of a new hollow cylinder apparatus for stress path measurements over a wide strain range. *Geotechnical testing journal, 28*(4), 345-354.
O'Rourke, T., & Crespo, E. (1988). Geotechnical properties of cemented volcanic soil. *Journal of Geotechnical Engineering, 114*(10), 1126-1147.
Oda, M. (1972a). Deformation mechanism of sand in triaxial compression tests. *Soils and foundations, 12*(4), 45-63.
Oda, M. (1972b). Initial fabrics and their relations to mechanical properties of granular material. *Soils and foundations, 12*(1), 17-36.
Oda, M. (1993). Inherent and induced anisotropy in plasticity theory of granular soils. *Mechanics of materials, 16*(1-2), 35-45.
Oda, M., & Iwashita, K. (1999). *Mechanics of granular materials: an introduction*: CRC Press.
Oda, M., Kazama, H., & Konishi, J. (1998). Effects of induced anisotropy on the development of shear bands in granular materials. *Mechanics of materials, 28*(1), 103-111.
Oda, M., & Koishikawa, I. (1979). Effect of strength anisotropy on bearing capacity of shallow footing in a dense sand. *Soils and foundations, 19*(3), 15-28.
Oda, M., Koishikawa, I., & Higuchi, T. (1978). Experimental study of anisotropic shear strength of sand by plane strain test. *Soils and foundations, 18*(1), 25-38.
Palmeira, E. M. (2004). Bearing force mobilisation in pull-out tests on geogrids. *Geotextiles and Geomembranes, 22*(6), 481-509.
Parkin, A., Gerrard, C., & Willoughby, D. (1968). Discussion on deformation of sand in shear. *Journal of the Soil Mechanics and Foundations Division, 94*(1), 336-340.
Peng, F., Kotake, N., Tatsuoka, F., Hirakawa, D., & Tanaka, T. (2000). Plane strain compression behaviour of geogrid-reinforced sand and its numerical analysis. *Soils and foundations, 40*(3), 55-74.
Phan, V. T.-A., Hsiao, D.-H., & Nguyen, P. T.-L. (2016). Effects of Fines Contents on Engineering Properties of Sand-Fines Mixtures. *Procedia Engineering, 142*, 213-220.
Pokharel, S. K., Han, J., Leshchinsky, D., Parsons, R. L., & Halahmi, I. (2010). Investigation of factors influencing behavior of single geocell-reinforced bases under static loading. *Geotextiles and Geomembranes, 28*(6), 570-578.
Qian, Y., Han, J., Pokharel, S. K., & Parsons, R. L. (2010). Experimental study on triaxial geogrid-reinforced bases over weak subgrade under cyclic loading. In *GeoFlorida 2010: Advances in Analysis, Modeling & Design* (pp. 1208-1216).
Rad, N. S., & Tumay, M. T. (1986). Effect of cementation on the cone penetration resistance of sand: A model study. *Geotechnical testing journal, 9*(3), 117-125.
Radjai, F., & Azéma, E. (2009). Shear strength of granular materials. *European Journal of Environmental and Civil Engineering, 13*(2), 203-218.
Rajagopal, K., Krishnaswamy, N., & Latha, G. M. (1999). Behaviour of sand confined with single and multiple geocells. *Geotextiles and Geomembranes, 17*(3), 171-184.

Ram Rathan Lal, B., & Mandal, J. (2013). Study of cellular reinforced fly ash under triaxial loading conditions. *International Journal of Geotechnical Engineering, 7*(1), 91-104.

Ravishankar, B., Sitharam, T., & Govindaraju, L. (2005). *Dynamic properties of Ahmedabad sands at large strains.* Paper presented at the Proceedings, Indian Geotechnical Conference-2005, Ahmedabad, India.

Razeghi, H. R., & Romiani, H. M. (2015). Experimental investigation on the inherent and initial induced anisotropy of sand. *KSCE Journal of Civil Engineering, 19*(3), 583-591.

Rios, S., Da Fonseca, A. V., & Baudet, B. A. (2014). On the shearing behaviour of an artificially cemented soil. *Acta Geotechnica, 9*(2), 215-226.

Rios, S., Ramos, C., Da Fonseca, A. V., Cruz, N., & Rodrigues, C. (2017). Mechanical and durability properties of a soil stabilised with an alkali-activated cement. *European Journal of Environmental and Civil Engineering*, 1-23.

Romiani, H. M., Razeghi, H. R., & Keykha, H. A. (2015). Effect of Intermediate Stress Ratio on The Anisotropic Behavior of Sand. *Electronic Journal of Geotechnical Engineering, 11*.

Rothenburg, L., & Bathurst, R. (1989). Analytical study of induced anisotropy in idealized granular materials. *Geotechnique, 39*(4), 601-614.

Saada, A. S. (1970). Testing of anisotropic clay soils. *Journal of the Soil Mechanics and Foundations Division, 96*(5), 1847-1852.

Salehzadeh, H., Hassanlourad, M., Procter, D., & Merrifield, C. (2008). Compression and extension monotonic loading of a carbonate sand. *International Journal of Civil Engineering, 6*(4), 266-274.

Salgado, R., Bandini, P., & Karim, A. (2000). Shear strength and stiffness of silty sand. *Journal of Geotechnical and Geoenvironmental Engineering, 126*(5), 451-462.

Sariosseiri, F., & Muhunthan, B. (2009). Effect of cement treatment on geotechnical properties of some Washington State soils. *Engineering Geology, 104*(1), 119-125.

Saxena, S. K., & Lastrico, R. M. (1978). Static properties of lightly cemented sand. *Journal of the Geotechnical Engineering Division, GT12*, 1449–1464.

Sayao, A. (1989). *Behaviour of sand under general stress paths in the hollow cylinder torsional device.* University of British Columbia,

Sayao, A., & Vaid, Y. (1996). Effect of intermediate principal stress on the deformation response of sand. *Canadian Geotechnical Journal, 33*(5), 822-828.

Sazzad, M. M. (2014). Micro-scale behavior of granular materials during cyclic loading. *Particuology, 16*, 132-141.

Sazzad, M. M., & Suzuki, K. (2010). Micromechanical behavior of granular materials with inherent anisotropy under cyclic loading using 2D DEM. *Granular Matter, 12*(6), 597-605.

Schnaid, F., Prietto, P. D., & Consoli, N. C. (2001). Characterization of cemented sand in triaxial compression. *Journal of Geotechnical and Geoenvironmental Engineering, 127*(10), 857-868.

Seyedi Hosseininia, E. (2012a). Discrete element modeling of inherently anisotropic granular assemblies with polygonal particles. *Particuology, 10*(5), 542-552.

Seyedi Hosseininia, E. (2012b). Investigating the micromechanical evolutions within inherently anisotropic granular materials using discrete element method. *Granular Matter, 14*(4), 483-503.
Seyedi Hosseininia, E. (2013). Stress–force–fabric relationship for planar granular materials. *Geotechnique, 63*(10), 830-841.
Shafiee, A., Tavakoli, H., & Jafari, M. (2008). Undrained behavior of compacted sand-clay mixtures under monotonic loading paths. *Journal of Applied Sciences, 8*(18), 3108-3118.
Shi, W.-c., Zhu, J.-g., Chiu, C.-f., & Liu, H.-l. (2010). Strength and deformation behaviour of coarse-grained soil by true triaxial tests. *Journal of Central South University of Technology, 17*(5), 1095-1102.
Shukla, S. (2002). Shallow foundations. In S. Shukla (Ed.), *Geosynthetics and Their Applications* (pp. 123). London: Thomas Telford.
Shukla, S. (2012). Fundamentals of geosynthetics. In *Handbook of Geosynthetic Engineering: Geosynthetics and their applications* (pp. 1-44): ICE Publishing.
Shukla, S. (2016). *An introduction to geosynthetic engineering*: CRC Press.
Shukla, S., Sivakugan, N., & Das, B. (2009). Fundamental concepts of soil reinforcement—an overview. *International Journal of Geotechnical Engineering, 3*(3), 329-342.
Shukla, S., & Yin, J.-H. (2006). *Fundamentals of geosynthetic engineering*: Taylor & Francis.
Siddiquee, M., Tatsuoka, F., Tanaka, T., Tani, K., Yoshida, K., & Morimoto, T. (2001). Model tests and FEM simulation of some factors affecting the bearing capacity of a footing on sand. *Soils and foundations, 41*(2), 53-76.
Sireesh, S., Sitharam, T., & Dash, S. K. (2009). Bearing capacity of circular footing on geocell–sand mattress overlying clay bed with void. *Geotextiles and Geomembranes, 27*(2), 89-98.
Skempton, A. W. (1985). Residual strength of clays in landslides, folded strata and the laboratory. *Geotechnique, 35*(1), 3-18.
Sridharan, A., Murthy, B. S., Bindumadhava, & Revanasiddappa, K. (1991). Technique for using fine-grained soil in reinforced earth. *Journal of Geotechnical Engineering, 117*(8), 1174-1190.
Swan Cement Material Safety Data Sheets (2012). Product Data AS3972 General Purpose Cement Type GP Retrieved from http://swancement.com.au/wp-content/uploads/sites/2/2014/03/Kwinana-Grey-GP-24May12.pdf
Symes, M., Gens, A., & Hight, D. (1988). Drained principal stress rotation in saturated sand. *Geotechnique, 38*(1), 59-81.
Tafreshi, S. M., & Asakereh, A. (2007). Strength evaluation of wet reinforced silty sand by triaxial test. *International Journal of Civil Engineering, 5*(4), 274-283.
Tafreshi, S. M., & Dawson, A. (2010a). Behaviour of footings on reinforced sand subjected to repeated loading–Comparing use of 3D and planar geotextile. *Geotextiles and Geomembranes, 28*(5), 434-447.
Tafreshi, S. M., & Dawson, A. (2010b). Comparison of bearing capacity of a strip footing on sand with geocell and with planar forms of geotextile reinforcement. *Geotextiles and Geomembranes, 28*(1), 72-84.
Tafreshi, S. M., & Dawson, A. (2012). A comparison of static and cyclic loading responses of foundations on geocell-reinforced sand. *Geotextiles and Geomembranes, 32*, 55-68.

Tastan, E. O. (2009). *Effects of principal stress rotation and intermediate principal stress changes on the drained monotonic and undrained cyclic behavior of clean and nonplastic silty Ottawa sands formed underwater*: Colorado State University.

Thevanayagam, S., Shenthan, T., Mohan, S., & Liang, J. (2002). Undrained fragility of clean sands, silty sands, and sandy silts. *Journal of Geotechnical and Geoenvironmental Engineering, 128*(10), 849-859.

Tong, Z., Fu, P., Zhou, S., & Dafalias, Y. F. (2014). Experimental investigation of shear strength of sands with inherent fabric anisotropy. *Acta Geotechnica, 9*(2), 257-275.

Tong, Z., Yu, Y.-L., Zhang, J.-M., & Zhang, G. (2008). Deformation behavior of sands subjected to cyclic rotation of principal stress axes. *Chinese Journal of Geotechnical Engineering, 30*(8), 1196-1202.

Tong, Z., Zhang, J.-M., Yu, Y.-L., & Zhang, G. (2010). Drained deformation behavior of anisotropic sands during cyclic rotation of principal stress axes. *Journal of Geotechnical and Geoenvironmental Engineering, 136*(11), 1509-1518.

Touahamia, M., Sivakumar, V., & McKelvey, D. (2002). Shear strength of reinforced-recycled material. *Construction and building materials, 16*(6), 331-339.

Tuna, S., & Altun, S. (2012). Mechanical behaviour of sand-geotextile interface. *Scientia Iranica, 19*(4), 1044-1051.

Uthayakumar, M. (1992). *Dynamic properties of sands under cyclic torsional shear.* University of British Columbia,

Uthayakumar, M. (1996). *Liquefaction of sands under multi-axial loading.* University of British Columbia,

Vallejo, L. E. (2001). Interpretation of the limits in shear strength in binary granular mixtures. *Canadian Geotechnical Journal, 38*(5), 1097-1104.

Vallejo, L. E., & Mawby, R. (2000). Porosity influence on the shear strength of granular material–clay mixtures. *Engineering Geology, 58*(2), 125-136.

Vinod, J., Indraratna, B., & Moghaddam, A. (2011). *Behaviour of geocell reinforced foundation under cyclic loading.* Paper presented at the Proceedings of Indian Geotechnical Conference, Kochi, Indian

Wan, R. G., & Guo, P. J. (2004). Stress dilatancy and fabric dependencies on sand behavior. *Journal of Engineering Mechanics, 130*(6), 635-645.

Wang, Y., & Leung, S. (2008). Characterization of cemented sand by experimental and numerical investigations. *Journal of Geotechnical and Geoenvironmental Engineering, 134*(7), 992-1004.

Wang, Z., Jacobs, F., Ziegler, M., & Yang, G. (2017). *Experimental and DEM Investigation of Geogrid Reinforcement Effects under Plane Strain Conditions.* Paper presented at the International Conference on Transportation Infrastructure and Materials.

Wen-Jie, X., Qiang, X., & Rui-Lin, H. (2011). Study on the shear strength of soil–rock mixture by large scale direct shear test. *International Journal of Rock Mechanics and Mining Sciences, 48*(8), 1235-1247.

Wijewickreme, D. (1990). *Behaviour of sand under simultaneous increase in stress ratio and rotation of principal stresses.* University of British Columbia,

Wijewickreme, D., & Vaid, Y. P. (1993). Behaviour of loose sand under simultaneous increase in stress ratio and principal stress rotation. *Canadian Geotechnical Journal, 30*(6), 953-964.

Wrzesiński, G., & Lechowicz, Z. (2013). Influence of the rotation of principal stress directions on undrained shear strength. *The Journal of Warsaw University of Life Sciences, 45*(2), 183-192.

Xiong, H., Guo, L., Cai, Y., & Yang, Z. (2016). Experimental study of drained anisotropy of granular soils involving rotation of principal stress direction. *European Journal of Environmental and Civil Engineering, 20*(4), 431-454.

Xu, W.-J., Hu, R.-L., & Tan, R.-J. (2007). Some geomechanical properties of soil–rock mixtures in the Hutiao Gorge area, China. *Geotechnique, 57*(3), 255-264.

Yadav, M., Agnihotri, A. K., Priyadarshee, A., & Dhane, G. (2014). Application of Geocells in Reinforcement of Soil: A Review. *Journal of Civil Engineering and Environmental Technology*, 60-64.

Yamada, Y., & Ishihara, K. (1979). Anisotropic deformation characteristics of sand under three dimensional stress conditions. *Soils and foundations, 19*(2), 79-94.

Yamada, Y., & Ishihara, K. (1981). Undrained deformation characteristics of loose sand under three-dimensional stress conditions. *Soils and foundations, 21*(1), 97-107.

Yan, J.-j., Zhou, J., Gong, X.-n., & Cao, Y. (2015). Undrained response of reconstituted clay to cyclic pure principal stress rotation. *Journal of Central South University, 22*(1), 280-289.

Yang, D. (2014). *Microscopic study of granular material behaviours under general stress paths.* University of Nottingham,

Yang, L. (2013). *Experimental study of soil anisotropy using hollow cylinder testing.* University of Nottingham,

Yang, L., Li, X., Yu, H.-S., & Wanatowski, D. (2016). A laboratory study of anisotropic geomaterials incorporating recent micromechanical understanding. *Acta Geotechnica, 11*(5), 1111-1129.

Yang, X., Han, J., Pokharel, S. K., Manandhar, C., Parsons, R. L., Leshchinsky, D., & Halahmi, I. (2012). Accelerated pavement testing of unpaved roads with geocell-reinforced sand bases. *Geotextiles and Geomembranes, 32*, 95-103.

Yang, Y., Fei, W., Yu, H.-S., Ooi, J., & Rotter, M. (2015). Experimental study of anisotropy and non-coaxiality of granular solids. *Granular Matter, 17*(2), 189-196.

Yang, Z., Li, X. S., & Yang, J. (2008). Quantifying and modelling fabric anisotropy of granular soils. *Geotechnique, 58*(4), 237-248.

Yang, Z., Lit, X., & Yang, J. (2008). Quantifying and modelling fabric anisotropy of granular soils. *Geotechnique*.

Yeo, B., Yen, S., Puri, V., Das, B., & Wright, M. (1993). A laboratory investigation into the settlement of a foundation on geogrid-reinforced sand due to cyclic load. *Geotechnical and Geological Engineering, 11*(1), 1-14.

Yetimoglu, T., Wu, J. T., & Saglamer, A. (1994). Bearing capacity of rectangular footings on geogrid-reinforced sand. *Journal of Geotechnical Engineering, 120*(12), 2083-2099.

Yoon, Y. W., Heo, S. B., & Kim, K. S. (2008). Geotechnical performance of waste tires for soil reinforcement from chamber tests. *Geotextiles and Geomembranes, 26*(1), 100-107.

Yoshimine, M., & Ishihara, K. (1998). Flow potential of sand during liquefaction. *Soils and foundations, 38*(3), 189-198.

Yoshimine, M., Ishihara, K., & Vargas, W. (1998). Effects of principal stress direction and intermediate principal stress on undrained shear behavior of sand. *Soils and foundations, 38*(3), 179-188.

Yoshimine, M., Ozay, R., Sezen, A., & Ansal, A. (1999). Undrained plane strain shear tests on saturated sand using a hollow cylinder torsional shear apparatus. *Soils and foundations, 39*(2), 131-136.

Yu, H.-S., Yang, L.-T., Li, X., & Wanatowski, D. (2016). Experimental investigation on the deformation characteristics of granular materials under drained rotational shear. *Geomechanics and Geoengineering, 11*(1), 47-63.

Zeghal, M., & Tsigginos, C. (2015). A micromechanical analysis of the effect of fabric on low-strain stiffness of granular soils. *Soil Dynamics and Earthquake Engineering, 70*, 153-165.

Zhang, J., Andrus, R. D., & Juang, C. H. (2005). Normalized shear modulus and material damping ratio relationships. *Journal of Geotechnical and Geoenvironmental Engineering, 131*(4), 453-464.

Zheng, J., & Hryciw, R. (2015). Traditional soil particle sphericity, roundness and surface roughness by computational geometry. *Geotechnique, 65*(6), 494-506.

Zhou, H., & Wen, X. (2008). Model studies on geogrid-or geocell-reinforced sand cushion on soft soil. *Geotextiles and Geomembranes, 26*(3), 231-238.